

Nuclear Structure and Reactions  
superfluidity in nuclei with Cooper pair transfer

G. Potel and R. A. Broglia

December 2, 2016



# Preface

The elementary modes of nuclear excitation are vibrations and rotations, single-particle (quasiparticle) motion, and pairing vibrations and rotations. The specific reactions probing these modes are inelastic, single- and two- particle transfer processes respectively. Within this context one can posit that nuclear structure (bound) and reactions (continuum) are but two aspects of the same physics. This is the reason why they can be treated on equal footing in terms of elementary modes of excitation, within the framework of nuclear field theory (NFT). This theory provides the rules to diagonalize in a compact and economic way the nuclear Hamiltonian for both bound and continuum states correcting for overcompleteness of the basis (particle-vibration coupling (structure), non-orthogonality (reaction)), and for Pauli principle violation.

Pairing vibrations and rotations, closely connected with nuclear superfluidity are, arguably, paradigms of quantal nuclear phenomena. They thus play an important role within the field of nuclear structure. It is only natural that two-nucleon transfer plays a similar role concerning direct nuclear reactions. In fact, this is the central subject of the present monograph.

At the basis of fermionic pairing phenomena one finds Cooper pairs, weakly bound, extended, strongly overlapping (quasi-) bosonic entities, made out of pairs of nucleons dressed by collective vibrations and interacting through the exchange of these vibrations as well as through the bare  $NN$ -interaction, eventually corrected by  $3N$  contributions. Cooper pairs not only change the statistics of the nuclear stuff around the Fermi surface and, condensing, the properties of nuclei close to their ground state. They also display a rather remarkable mechanism of tunnelling between target and projectile in direct two-nucleon transfer reaction. In fact, being weakly bound ( $\ll \epsilon_F$ , Fermi energy) they display correlations over distances (correlation length) much larger than nuclear dimensions ( $\gg R$ , nuclear radius). On the other hand, Cooper pairs are forced to be confined within such dimensions by the action of the average potential, which can be viewed as an external field as far as these pairs are concerned.

The correlation length paradigm comes into evidence, for example, when two nuclei are set into weak contact in a direct reaction. In this case, each of the partner nucleons of a Cooper pair has a finite probability to be confined within the mean field of each of the two nuclei. It is then natural that a Cooper pair can tunnel, equally well correlated, between target and projectile, through simultaneous

than through successive transfer processes. Consequently, although one does not expects supercurrents in nuclei, one can study long-range pairing correlations in terms of individual quantal state. The above mentioned weak coupling Cooper pair tunnelling reminds the tunnelling mechanism of electronic Cooper pairs across a barrier (e.g. a dioxide layer) separating two superconductors, known as Josephson junction. The main difference is that, as a rule, in the nuclear time dependent junction efimerely established in direct two-nucleon transfer process, only one or even none of the two weakly interacting nuclei are superfluid (or superconducting). Now, in nuclei, paradigmatic example of fermionic finite many-body system, zero point fluctuations (ZPF) in general, and those associated with pair addition and pair subtraction modes known as pairing vibrations in particular, are much stronger than in condensed matter. Consequently, and in keeping with the fact that pairing vibrations are the nuclear embodiment of Cooper pairs in nuclei, pairing correlations based on even a single Cooper pair can lead to clearly observable effects in two-nucleon transfer processes.

Nucleonic Cooper pair tunnelling has played and is playing a central role in the probing of these subtle quantal phenomena, both in the case of exotic nuclei as well as of nuclei lying along the stability valley, and have been instrumental in shedding light on the subject of pairing in nuclei at large, and on nuclear superfluidity in particular. Consequently, the subject of two-nucleon transfer occupies a central place in the present monograph both concerning the conceptual and the computational aspects of the description of nuclear pairing, as well as regarding the quantitative confrontation of the results and predictions with the experimental findings.

Because of the central role the interweaving of the variety of elementary modes of nuclear excitation, namely single particle motion and collective vibrations play in nuclear superfluidity, the study of Cooper pair tunnelling in nuclei aside from requiring a consistent description of nuclear structure in terms of dressed quasiparticles and vibrations resulting from both bare and induced interactions, also involves the description of one-nucleon transfer as well as knock out processes. Consequently, in the present monograph the general physical arguments and technical computational details concerning the calculation of absolute one-and two nucleon transfer cross sections, making use of state of the art nuclear structure information, are discussed in detail. As a consequence, theoretical and experimental nuclear practitioners, as well as fourth year and PhD students can use the present monograph at profit. To make simpler this use, the basic nuclear structure formalism, in particular that associated with pairing and with collectives modes in nuclei, is economically introduced through general physical arguments. This is also in keeping with the availability in the current literature, of detailed discussions of such material.

Within this context, the monographs *Nuclear Superfluidity* by Brink and Broglia and *Oscillations in Finite Quantum Systems* by Bertsch and Broglia, published also by Cambridge University Press can be considered companion volumes to the present one.

Concerning the notation, we have divided each chapter into sections. Each subsection may in turn be broken down into subsections. Equations and Figures are identified by the number of the chapter and that of the section. Thus (6.1.33) labels the thirtythird equation of section 1 of chapter 6. Similarly, Fig. 6.1.2 labels the second figure of section 1 of chapter 6. Concerning the Appendices, they are labelled by the chapter number and by a Latin letter in alphabetical order, e.g. App. 6.A, App. 6.B, etc. Concerning equations and Figures, a sequential number is added. Thus (6.E.15) labels the fifteenth equation of Appendix E of chapter 6, while Fig. 6.F.1 labels the first figure of Appendix F of Chapter 6. References are referred to in terms of the author's surname and publication year and are found in alphabetic order in the bibliography.

Throughout, a number of footnotes are found. This is in keeping with the fact that footnotes can play a special role within the framework of an elaborated presentation. In particular, they allow one to emphasize relevant issues in an economic way. Being outside the main text, they give the possibility of stating eventual important results, without the need of elaborating on the proof. Within this context, in the paper Born (1926), introducing the probabilistic interpretation of Schrödinger's wavefunction, the fact that this probability is connected with its modulus squared and not with the wavefunction itself, is only explained in a footnote.

Most of the material contained in this monograph have been the subject of lectures of the four year course "Nuclear Structure Theory" which RAB delivered throughout the years at the Department of Physics of the University of Milan, as well as at the Niels Bohr Institute and at Stony Brook (State University of New York). It was also presented by the authors in the course Nuclear Reactions held in the academic year 2009 at the PhD School of Physics of the University of Milan.

RAB wants to acknowledge the central role the collaboration with Francisco Barranco and Enrico Vigezzi has played concerning the nuclear structure aspects of the present monograph. Its debt with the late Aage Winther regarding the reaction aspects of the present volume is difficult to express in words. The overall contributions of Daniel Bès, Ben Bayman and Pier Francesco Bortignon are only too explicitly evident throughout the text and constitute a daily source of inspiration.

Gregory Potel Aguilar  
Livermore

Ricardo A. Broglia  
Milano

## Bibliography

M. Born. Zur Quantenmechanik der Stoßvorgänge. *Zeitschr. f. Phys.*, 37:863, 1926.



# Contents

<b>1</b>	<b>Introduction</b>	<b>11</b>
1.1	Elementary modes of excitation . . . . .	11
1.2	Sum rules . . . . .	17
1.3	Particle–vibration coupling . . . . .	23
1.3.1	Fluctuation and damping . . . . .	25
1.3.2	Induced interaction . . . . .	31
1.4	Coupling between elementary modes . . . . .	34
1.5	Non–orthogonality . . . . .	36
1.6	Coupling between intrinsic and relative motion . . . . .	41
1.7	Nuclear Field Theory for pedestrians . . . . .	46
1.7.1	The concept of elementary modes of excitation . . . . .	49
1.7.2	NFT rules and applications . . . . .	51
1.7.3	Spurious states . . . . .	59
1.7.4	Applications . . . . .	66
1.8	Competition between ZPF . . . . .	73
1.9	Optical potential and transfer . . . . .	76
1.9.1	Bare particles and Hartree–Fock field . . . . .	76
1.9.2	Physical particles and optical potential . . . . .	77
1.9.3	$^3_3\text{Li}_8$ structure in a nutshell . . . . .	78
1.9.4	$^{11}\text{Li}(p, p)^{11}\text{Li}$ optical potential and transfer reaction channels	81
1.10	Summary . . . . .	87
1.A	Confronting theory with experiment . . . . .	88
1.A.1	One–particle transfer . . . . .	88
1.A.2	Two–particle transfer . . . . .	90
1.B	Inelastic Scattering . . . . .	91
1.B.1	$(\alpha, \alpha')$ –scattering . . . . .	91
1.C	Technical details NFT . . . . .	95
1.C.1	Graphical solution . . . . .	96
1.C.2	Overlap . . . . .	97
1.D	NFT and reactions . . . . .	98
1.D.1	Potential scattering . . . . .	100
1.D.2	Transfer . . . . .	101

<b>2 Pairing with transfer</b>	<b>113</b>
2.1 Nuclear Structure in a nutshell . . . . .	113
2.1.1 Two-nucleon modified formfactors . . . . .	123
2.2 Renormalization and spectroscopic amplitudes . . . . .	125
2.3 Quantality Parameter . . . . .	128
2.4 Cooper pairs . . . . .	130
2.4.1 independent-particle motion . . . . .	131
2.4.2 independent-pair motion . . . . .	136
2.5 Pair vibration spectroscopic amplitudes . . . . .	141
2.5.1 Pair removal mode . . . . .	144
2.5.2 Pair addition mode . . . . .	146
2.6 Halo pair addition mode and pygmy . . . . .	151
2.6.1 Cooper pair binding: a novel embodiment of the Axel-Brink hypothesis . . . . .	153
2.A Nuclear van der Waals Cooper pair . . . . .	161
2.B Renormalized coupling constants $^{11}\text{Li}$ : resumé . . . . .	162
2.C Lindemann criterion and connection with quantality parameter . .	164
2.D The van der Waals interaction . . . . .	164
<b>3 Simultaneous versus successive transfer</b>	<b>177</b>
3.1 Simultaneous versus successive Cooper pair transfer in nuclei . . . . .	177
3.2 Transfer probabilities, enhancement factor . . . . .	178
3.2.1 Interplay between mean field and correlation length . . . . .	191
3.3 Correlations in Cooper pair tunneling . . . . .	193
3.4 Pair transfer . . . . .	196
3.4.1 Cooper pair dimensions . . . . .	197
3.5 Comments on the optical potential . . . . .	202
3.6 Weak link between superconductors . . . . .	206
3.7 Phase coherence . . . . .	210
3.8 Hindsight . . . . .	213
3.A Medium polarization effects and pairing . . . . .	216
3.A.1 Nuclei . . . . .	216
3.A.2 Metals . . . . .	226
3.A.3 Elementary theory of phonon dispersion relation . . . . .	228
3.A.4 Pairing condensation (correlation) energy beyond level density . . . . .	232
3.A.5 Hindsight . . . . .	233
3.B Cooper pair: radial dependence . . . . .	235
3.B.1 Number of overlapping pairs . . . . .	239
3.B.2 Coherence length and quantality parameter for ( $ph$ ) vibrations . . . . .	241
3.B.3 tunneling probabilities . . . . .	243
3.B.4 Nuclear correlation (condensation) energy . . . . .	245
3.B.5 Possible (dream?) experiment . . . . .	246

3.C	Absolute Cooper pair tunneling cross section . . . . .	248
3.C.1	Saturation density, spill out and halo . . . . .	250
<b>4</b>	<b>One-particle transfer</b>	<b>263</b>
4.1	General derivation . . . . .	264
4.1.1	Coordinates . . . . .	270
4.1.2	Zero-range approximation . . . . .	271
4.2	Examples and Applications . . . . .	271
4.2.1	$^{120}\text{Sn}(p, d)^{119}\text{Sn}$ and $^{120}\text{Sn}(d, p)^{121}\text{Sn}$ reactions. . . . .	272
4.2.2	Dressing of single-particle states: parity inversion in $^{11}\text{Li}$ . . . . .	276
4.A	Minimal mean field theory . . . . .	283
4.B	Single-particle strength function . . . . .	285
4.C	Vacuum and medium polarization . . . . .	288
4.D	The Lamb Shift . . . . .	290
4.E	Self-energy and vertex corrections . . . . .	290
4.F	Single-nucleon transfer for pedestrians . . . . .	292
4.F.1	Plane-wave limit . . . . .	295
4.G	One-particle knockout within DWBA . . . . .	296
4.G.1	Spinless particles . . . . .	296
4.G.2	Particles with spin . . . . .	304
4.G.3	One-particle transfer . . . . .	310
4.H	Modified formfactors . . . . .	313
4.H.1	Two-particle transfer . . . . .	313
4.H.2	One-particle transfer . . . . .	313
4.H.3	Inelastic scattering . . . . .	313
4.H.4	Elastic scattering . . . . .	313
4.I	Dynamical shell model in a nutshell . . . . .	313
<b>5</b>	<b>Two-particle transfer</b>	<b>323</b>
5.1	Summary of second order DWBA . . . . .	324
5.2	Detailed derivation of second order DWBA . . . . .	328
5.2.1	Simultaneous transfer: distorted waves . . . . .	328
5.2.2	matrix element for the transition amplitude . . . . .	329
5.2.3	Coordinates for the calculation of simultaneous transfer . . . . .	338
5.2.4	Matrix element for the transition amplitude (alternative derivation) . . . . .	341
5.2.5	Coordinates used to derive Eq. (5.2.89) . . . . .	343
5.2.6	Successive transfer . . . . .	346
5.2.7	Coordinates for the successive transfer . . . . .	351
5.2.8	Simplifying the vector coupling . . . . .	352
5.2.9	non-orthogonality term . . . . .	353
5.2.10	Arbitrary orbital momentum transfer . . . . .	354
5.2.11	Successive transfer contribution . . . . .	356
5.A	ZPF and Pauli principle . . . . .	360

5.B	Coherence and effective formfactors . . . . .	361
5.C	Succesive, simultaneous, non-orthogonality . . . . .	366
5.C.1	Independent particle limit . . . . .	373
5.C.2	Strong correlation (cluster) limit . . . . .	374
5.D	Spherical harmonics and angular momenta . . . . .	375
5.D.1	addition theorem . . . . .	375
5.D.2	expansion of the delta function . . . . .	376
5.D.3	coupling and complex conjugation . . . . .	376
5.D.4	angular momenta coupling . . . . .	377
5.D.5	integrals . . . . .	377
5.D.6	symmetry properties . . . . .	378
5.E	distorted waves . . . . .	379
5.F	hole states and time reversal . . . . .	380
5.G	Spectroscopic amplitudes in the BCS approximation . . . . .	382
5.H	Bayman's two-nucleon transfer amplitudes . . . . .	384
<b>6</b>	<b>Structure with two neutrons</b>	<b>389</b>
6.1	Evidence for phonon mediated pairing . . . . .	389
6.1.1	Structure . . . . .	393
6.1.2	Reaction . . . . .	394
6.2	Pairing rotational bands . . . . .	396
6.2.1	Fluctuations . . . . .	397
6.2.2	Pairing rotations . . . . .	398
6.2.3	Pairing vibrations in superfluid nuclei . . . . .	400
6.3	BCS-like correlation . . . . .	402
6.A	Bootstrap mechanism to break gauge invariance . . . . .	404
6.A.1	Gedanken eksperiment . . . . .	404
6.B	Table 1 PRL . . . . .	406
6.C	Formfactors for the reaction ${}^1\text{H}({}^{11}\text{Li}, {}^9\text{Li}){}^3\text{H}$ . . . . .	409
6.D	Software . . . . .	409
6.E	Articulo Belyaev Pairing vibrational band based on $N = 6$ . . . . .	413
6.F	Simple estimates revisited. . . . .	413
6.G	Statistics. . . . .	413
6.H	Correlation length and quantality parameter. . . . .	414
6.I	$k$ -mass in ${}^{11}\text{Li}$ and Pauli principle. . . . .	416

# Chapter 1

## Introduction

### 1.1 Elementary modes of excitation

Subject to external probes which couple weakly to the nucleus, that is in such a way that the system can be expressed in terms of the properties of the excitation in the absence of probes<sup>1</sup>, the nucleus reacts in terms of single-particle (-hole) motion (one-particle transfer), vibrations (surface, spin, etc.) and rotations (Coulomb excitation and inelastic scattering) and pairing vibrations and rotations (two-nucleon transfer reactions) (see Figs. 1.1.1, 1.1.2 and 1.1.3, also Sect. 1.7.1).

In the figures, a cartoon representation (color online) of elastic, inelastic, one- and two-particle direct transfer reactions induced by alpha and proton projectiles impinging on  $^{208}\text{Pb}$  are shown. In all cases a standard setup is used, in which a light projectile is aimed at a fixed target (thin foil made out of  $^{208}\text{Pb}$ ). The outgoing particles carrying the corresponding physical information, i.e. momentum, angular momentum, energy, etc. transferred to or from the target, are deflected by the electromagnetic fields of a spectrometer and eventually recorded at a given angle by particle detectors (points a,b... in magnet). Those events provide structural information as shown in the two dimensional strength function displayed below the cartoon laboratory setup.

These strength functions, recorded at a wide range of angles provide the absolute differential cross sections of each of the nuclear states populated in the process. They are typically measured in millibarns per steradian (mb/sr). To translate these quantities into nuclear structure information, a model of structure and of reactions is needed to calculate the absolute cross sections, to be compared with the data. The risks of using relative cross section is that of overlooking limitations in the description of the reaction mechanism or in that of the structure description of the states involved in the reaction under study. Or of both.

In this connection, it is of notice that either one sets equal weight in correctly calculating the mean field properties and the clothing of the single-particles (i.e. the physical nucleons (structure, see e.g. Figs. 1.2.1 and 1.3.2)) than in working

---

<sup>1</sup>Pines, D. and Nozières (1966),Bohr, A. and Mottelson (1975)

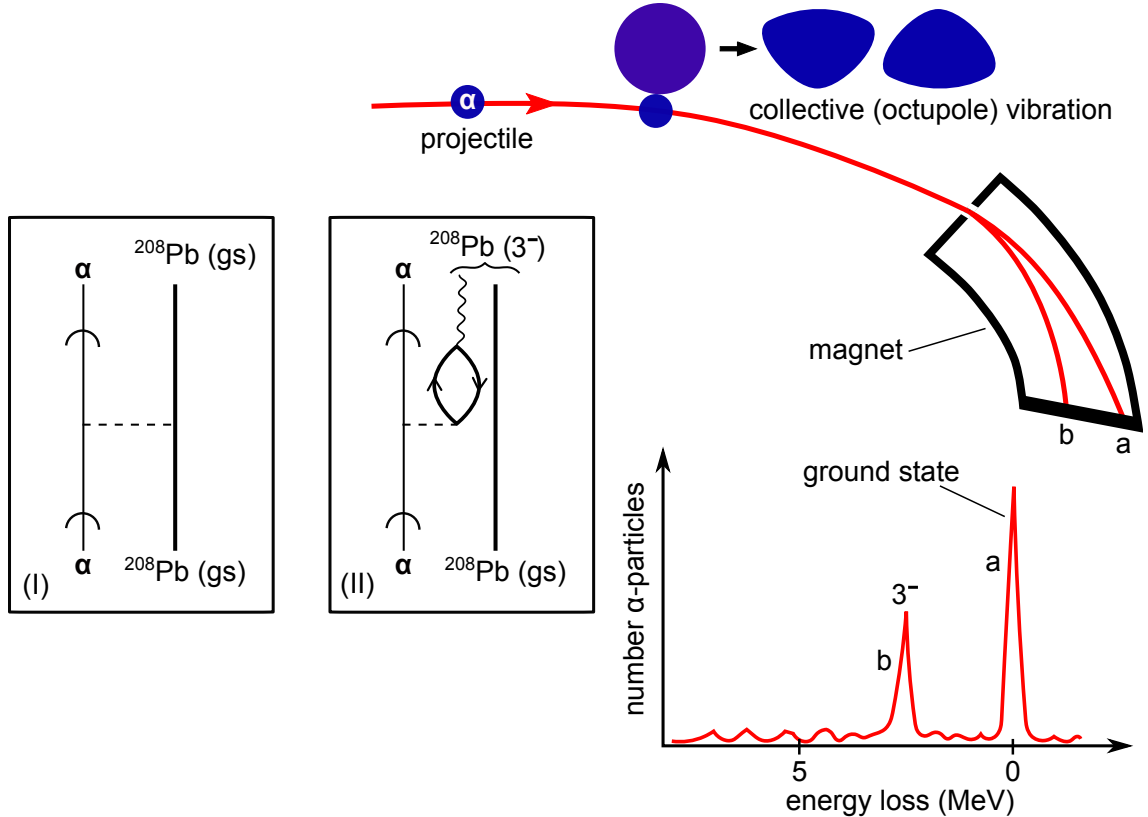


Figure 1.1.1: Schematic representation of: **a)** **elastic** (population of the ground state), and **inelastic b)** (population lowest octupole vibration 2.62 MeV) processes associated with the reaction  $^{208}\text{Pb}(\alpha, \alpha')^{208}\text{Pb}$  (for more details see Sect. 1.3). In the inset (II) one of the NFT(r+s) diagrams describing the excitation of the low-lying octupole vibration (wavy line), of  $^{208}\text{Pb}$  is given. A pointed (curved) arrow on a line indicates propagation of a nucleon in the target nucleus (in the continuum). The horizontal dashed line represents the action of the mean field (see Fig. 1.2.1) while the solid dot stands for the particle–vibration coupling vertex (Sect. 1.3). In the inset (I) a NFT(r+s) diagram describing the elastic process (potential scattering) is displayed. From the measurement of the differential cross section one can deduce the partial wave phase shifts (Appendix 1.D) Outgoing particles are deflected in a spectograph and recorded in a detector. The corresponding excitation function is given in the lowest part of the figure (after Mottelson (1976b)).

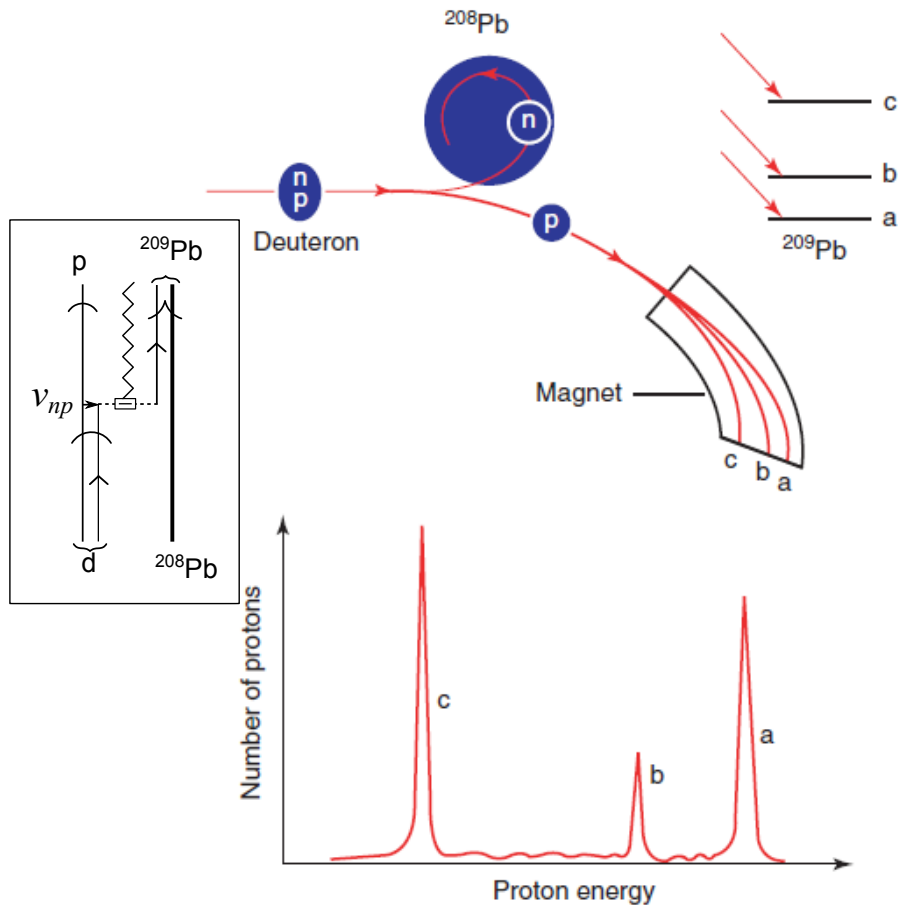


Figure 1.1.2: Schematic cartoon representation of the one-nucleon transfer reaction  $^{208}\text{Pb}(d, p)^{209}\text{Pb}$  populating the single-particle states of  $^{209}\text{Pb}$ . In the inset a NFT( $r+s$ ) diagram describing the process is shown. A standard (pointed) arrowed curve indicates the transferred nucleon, moving with the proton in the deuteron (double, curve arrowed, line), or around the (assumed, for simplicity, inert)  $^{208}\text{Pb}$  core. The energy of the outgoing proton reflects both the  $Q$ -value of the reaction and the excitation energy of the final state. In the inset, a NFT( $r+s$ ) diagram describing one of the possible transfer processes is schematically shown. An arrowed curve indicates the transferred nucleon. The jagged curve represents the recoil elementary mode which couples (dashed square) the relative motion (reaction) to the intrinsic nucleonic degrees of freedom (structure) through a Galilean operator transformation. For more details see caption to Fig. 1.1.1 and 1.9.2, see also Ch. 4 and Fig. 4.1.1 as well as App. 1.D and Sect. 5.C (after Mottelson (1976b)).

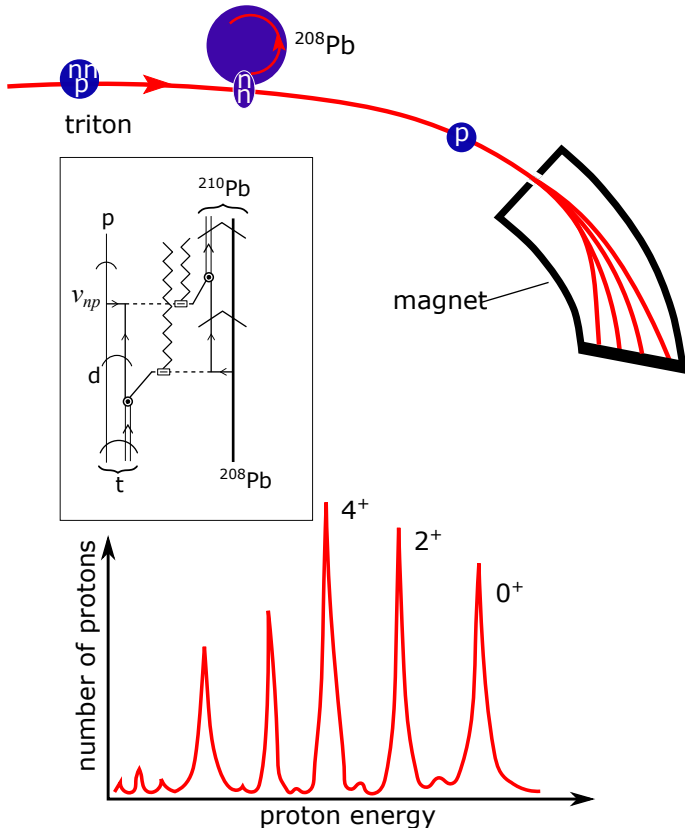


Figure 1.1.3: Schematic representation of the two–nucleon transfer reaction  $^{208}\text{Pb}(t, p)^{210}\text{Pb}$  populating the ground state  $0^+$ , and two particle excited states  $2^+$  and  $4^+$  (monopole, quadrupole and hexadecapole pair addition modes of  $^{208}\text{Pb}$ , i.e. multipole pariring vibrations, see Brink, D. and Broglia (2005) Sect. 5.3.1 p. 108, Broglia et al. (1974), Ragnarsson and Broglia (1976), Broglia, R. A. et al. (1971a), Broglia, R. A. et al. (1971b), Bès and Broglia (1971b), Bès and Broglia (1971a), Flynn, E.R. and Igo, G. and Barnes, P.D. and Kovar, D. and Bès, D. R. and Broglia, R.A. (1971), Bès et al. (1972), Broglia (1981), Bohr and Mottelson (1974), Flynn, E. R. et al. (1972), Bortignon et al. (1976); see also Kubo et al. (1970)). In the inset a NFT(r+s) diagram of the transfer process is displayed. In selecting it, it was assumed, as detailed calculations indicate, that the main contribution to the process arises from the successive transfer of the nucleons. The jagged curves represent the recoil mode coupling the intrinsic and the relative motion, thus accounting for the mass partition associated with the different channels and the change in scaling between entrance and exit channel distorted waves. The corresponding momentum mismatch being taken care by Galilean transformations (recoil effects) (see also caption to Fig. 1.1.2 and App. 1.D; also Ch. 5, in particular Figs. 5.C.1 and 5.C.2). As discussed in the following Chapters (see in particular Chs. 2 and 3), Cooper pairs are extended objects, the fermionic partners being correlated over distances much larger than nuclear dimensions (correlation length  $\xi \approx 36 \text{ fm} \gg 2R_0 \approx 14.2 \text{ fm}$  ( $A = 208$ )). Because the single particle potential acts on these pairs as a rather strong external field, this feature is not obvious in structure calculations, becoming apparent in reaction calculations. The dineutron moving in the triton and around the  $^{208}\text{Pb}$ , (assumed for simplicity to be inert) is represented by a double arrowed line. Each individual transferred neutron is indicated with a single arrowed line. The curved arrows on the triton and on the proton indicate motion in the continuum with outgoing and incoming asymptotic waves, respectively. The arrow encompassing the pair addition mode and the core  $^{208}\text{Pb}$ , indicate intrinsic (structure) motion (after Mottelson (1976b)).

out the reaction mechanism (see Ch. 4), or the confrontation between theoretical predictions and experimental observation would unlikely be fruitful<sup>2</sup>. Arguably, an example of such an approach is given in Sect. 1.10 of this Chapter.

Echoing Heisenberg's requirement<sup>3</sup> that no concept enters the quantal description of a physical system which has no direct relation to experiments, and Landau's result that any weakly excited state of a quantal many-body system may be regarded as a gas of weakly interacting elementary modes of excitation<sup>4</sup>, Bohr, Mottelson and coworkers<sup>5</sup> developed a unified field theoretical description of the nuclear structure (Nuclear Field Theory, NFT) in terms of quasiparticles, vibrations and rotations, both in 3D– as well as in gauge– and other “abstract” spaces, with close connections with direct nuclear reactions<sup>6</sup>. Within this context also given in Figs. 1.1.1–1.1.3 (insets) are *unified NFT diagrams of structure and reactions (NFT(s+r))*<sup>7</sup>, which microscopically describe the variety of processes in terms of elementary modes of excitation. That is, in the present case in which the target is a closed shell system, a particle–hole (inelastic scattering), one–particle (single-particle stripping) and two–particle (Cooper pair transfer) modes.

In keeping with the fact that all the nuclear degrees of freedom are exhausted by those of the nucleons, and that the different reactions, that is Coulomb, inelastic and one– and two– particle transfer reactions project particular, but somewhat overlapping components of the total wavefunction, the nuclear elementary modes of excitation give rise to an overcomplete, non orthogonal, Pauli principle violating basis, both concerning structure as well as reactions. The coupling between unperturbed fermionic and bosonic degrees of freedom is proportional to this overlap between single–particle and collective modes. Nuclear Field Theory<sup>8</sup>, provides the conserving sum rules protocol to diagonalize these couplings to any order of perturbation theory, also infinite if so required for specific processes. The clothed physical elementary modes resulting from the interweaving of the bare modes are orthogonal to each other, fulfill Pauli principle, and behave like a non interacting

---

<sup>2</sup>*Structure and Reactions.* Within this context one can ask how one understands what the correct elements are to describe a reaction process, if one does not know in detail the structure of the initial and final states? In a nutshell: how can one understand reaction without knowing structure (eyes without object)?

Vice versa, how can one understand what the elements needed for a correct description of the structure of levels is, if one does not know how to observe them, how to bring that information to the detector?. In other words, how can one understand structure without knowing reaction (object without eyes)? The answer to both questions is that you cannot. As simple as that.

<sup>3</sup>Heisenberg (1949).

<sup>4</sup>Landau (1941)).

<sup>5</sup>Bohr and Mottelson (1969), Bohr (1976), Mottelson (1976a), Bohr, A. and Mottelson (1975), Bohr et al. (1958), Belyaev (1959), Nilsson (1955), Bès, D. R. and Broglia (1966).

<sup>6</sup>Alder et al. (1956), Alder and Winther (1975), Broglia and Winther (2004), Austern (1970), Glendenning, N. K. (2004), Satchler (1980), Satchler (1983), see also Potel, G. et al. (2013).

<sup>7</sup>Broglia, R. A. (1979); Broglia and Winther (2004); Broglia et al. (2016)

<sup>8</sup>Bès et al. (1976b), Bès et al. (1976c), Bès et al. (1976a), Bès and Broglia (1975), Broglia et al. (1976), Bès, D. R. and Broglia, R. A. and Dussel, G. G. and Liotta (1975), Mottelson (1976a), Bès and Broglia (1977), Bortignon, P. F. et al. (1977), Bortignon, P. F. et al. (1978), Broglia and Winther (2004), Reinhardt (1975), Reinhardt (1978a), Reinhardt (1978b), Reinhardt (1980).

gas, providing a microscopic solution to the many–body nuclear problem. Its predictions, embodied in absolute cross sections and transition probabilities, can be directly compared with the observables whose values are obtained by studying the nuclear system with the variety of ever more precise and varied arsenal of experimental probes<sup>9</sup>.

At this point a proviso or two are in place. The original elementary modes of nuclear excitation melt together, due to their interweaving, into effective fields. Each of them display properties which reflects that of all the others, their individuality resulting from the actual relative importance of each one of them. What one calls physically a (clothed) particle is only partially to be associated with that particle field alone. It is also partially to be associated with the vibrational fields (surface, density, spin, pairing, etc.), because they are in interaction through the particle–vibration coupling vertices. And conversely, what one calls a nuclear vibration can couple to particle–hole (in the case of a surface vibration), two–particle (in the case of a pair addition) or a two–hole (in the case of a pair removal) configurations. The associated fermions can couple to other vibrational modes and, eventually in the course of time, recombine to reform the original vibration. The outcome of such processes, namely the dressed physical elementary modes of excitation, is closely connected with the renormalization program of quantum electrodynamics (QED)<sup>10</sup> implemented, in NFT, in terms of Feynman diagrams<sup>11</sup> and made operative in a number of cases in term of empirical renormalization prescription<sup>9</sup>. The specific experimental probes of the bare elementary modes of nuclear excitation reveal only one, in most cases likely the most important aspects of the physical (clothed) elementary modes. Renormalization (NFT program) reflects the physical unity of low–energy nuclear research requiring the melting not only of elementary modes of excitation but also of structure and reaction theory, let alone of the different experimental techniques developed to study the atomic nucleus (Within this context cf. Ch. Fig. 1.10.1).

As can be seen from the contents of the present monograph, the accent is set on relating theoretical prediction with experimental finding, through the unification of structure and reactions. In particular the unification of pairing and two–nucleon transfer, where the two subjects are blended together, which is what happens in nature. The theory of direct reaction for two–particle transfer is discussed in Ch. 5 (see summary Sect. 5.1). To be operative, two–nucleon spectroscopic amplitudes and optical potentials are needed. One–particle transfer processes are at the basis of the above derivations, and are summarized in Sect. ???. Once the NFT rules to work the variety of elements (spectroscopic and, with the help of them, reaction ampli-

---

<sup>9</sup>What NFT cannot do, is to solve problems regarding ill behaved bare forces, or the consequences of associated particle–vibration coupling vertices which eventually lead to divergences. Within this context, *empirical renormalization* has proved to be a powerful and physically consistent prescription to implement the NFT and to make connection with experimental data (see e.g. Sect. 4.2, see also Barranco et al. (2004) and Broglia et al. (2016), and refs. therein)

<sup>10</sup>Schwinger (2001).

<sup>11</sup>Feynman (1975).

tudes) have been laid out and/or the pertinent literature refer to, concrete embodiments are provided and eventual absolute cross sections calculated and confronted with the experimental data (for details see App. 1.A). Within this scenario, once the NFT renormalization program associated with a characterising set of observables, e.g. the energy ( $\hbar\omega_{2^+}$ ) and electromagnetic transition probability ( $B(E2)$ ) of the collective, low-lying quadrupole vibration of  $^{120}\text{Sn}$  has been carried out, a decision is to be taken. Unless one is not specifically studying such type of nuclear excitations, e.g. through inelastic scattering, but just using them to e.g. cloth single-particles, one turns to the *empirical renormalization* program<sup>12</sup>. Within the framework of the particular example, one calculates the  $\hbar\omega_{2^+}$  and  $B(E2)$  values making use of the harmonic approximation to diagonalize a separable quadrupole-quadrupole interaction adjusting its strength  $k_2$  so as to reproduce the experimental findings. As a rule, the resulting  $k_2$  has a value close to that required by self consistency<sup>13</sup> (see also Sect. 1.3). Within the properties mentioned, i.e. single-particle self energy, the final outcome differs little from that obtained from a full implementation of the NFT renormalization program. On the other hand, the use of the *empirical renormalization* program, aside from being an economic procedure for self consistency in phonon renormalization, allows to avoid difficulties associated with the zero-range character (ultraviolet divergences) and finite size instabilities of many effective interactions.

## 1.2 Sum rules

A quantitative measure of the overcompleteness mentioned above and concerning the elementary modes of excitation basis is provided by the use of exact and approximate sum rules that the observables (cross sections) associated with the variety of probes to which the nucleus is subject, have to fulfill. An example of the first type (exact) is provided by the Thomas–Reiche–Kuhn (TRK) sum rule. Of the second type (approximate) by some of the two–nucleon transfer (TNTR) sum rules<sup>14</sup>. Others, which relate one– with two–particle transfer processes<sup>15</sup> being exact. In both cases they embody particle (pair) number conservation. Charged particles in the first case (electrons in atoms and molecules, effective charges of neutrons and protons in nuclei). Number of Cooper pairs in nuclei in the second. Physically, they provide information concerning: 1) the maximum amount of energy which the quantal system can absorb from a beam of light ( $\gamma$ -rays) shined on it; 2) the total two–nucleon transfer cross section (ring area fraction of the total (geometrical) reaction cross section) exhausted by the final ( $A \pm 2$ ) states populated in the transfer process.

In other words, these sum rules provide: a quantitative measure of the single–

---

<sup>12</sup>Barranco, F. et al. (2001); Idini, A. et al. (2014); Idini et al. (2015); Broglia et al. (2016)

<sup>13</sup>Bohr, A. and Mottelson (1975)

<sup>14</sup>Broglia, R. A. et al. (1972)

<sup>15</sup>Bayman, B. F. and Clement (1972); Lanford (1977)

particle subspace the quantal system under study, in particular the nucleus, uses to correlate particle–hole excitations and thus induce the antenna–like motion of protons against neutrons or, to correlate pairs of nucleons moving in time reversal states around the Fermi energy, leading to a sigmoidal distribution of the associated level occupancy<sup>16</sup>.

The TRK sum rule can, in the nuclear case, be written as<sup>17</sup>

$$S(E1) = \sum_{\alpha} |\langle \alpha | F | \tilde{0} \rangle|^2 (E_{\alpha} - E_0) = \frac{9}{4\pi} \frac{\hbar^2 e^2}{2m} \frac{NZ}{A}, \quad (1.2.1)$$

where  $|\alpha\rangle$  labels the complete set of excited dipole states which can be reached operating with the dipole operator  $F$  on the initial correlated vacuum state  $|\tilde{0}\rangle$ . Within this context, each elementary mode of excitation, provides a specific contribution to the total zero point fluctuations of the ground state (ZPF, see Sect. 1.7), that is,

$$\langle \tilde{0} | F^2 | \tilde{0} \rangle = \frac{\hbar\omega}{2C_{\alpha}} = \frac{\hbar^2}{2D_{\alpha}} \frac{1}{\hbar\omega_{\alpha}}. \quad (1.2.2)$$

In other words, they perturb the static nucleon Fermi sea, that is the set of occupied levels of the mean field potential (Fig. 1.2.1)

$$U(r) = \int d\mathbf{r}' \rho(r') v(|\mathbf{r} - \mathbf{r}'|), \quad (1.2.3)$$

inducing virtual particle–hole excitations ( $k, i$ , i.e.  $\epsilon_i \leq \epsilon_F$  and  $\epsilon_k > \epsilon_F$ , see Eqs. (1.2.6) and (1.4.1) (see Fig. 1.2.2). In the above equation,  $\rho(r)$  is the nuclear density and  $v$  is the nuclear two–body interaction.

In Eq. (1.2.1), the quantity

$$F = e \sum_n \left( \left( \frac{N-Z}{2A} - t_z(n) \right) r_n Y_{1\mu}(\hat{r}_n) \right), \quad (1.2.4)$$

is the dipole operator acting both on the protons ( $t_z = -1/2$ ) and on the neutrons ( $t_z = 1/2$ ) of mass  $m$ , as indicated by the  $\alpha$ –sum over all nucleon states ( $A = N+Z$ , mass number).

Because  $|\langle \alpha | F | \tilde{0} \rangle|^2$  measures the probability with which the state  $|\alpha\rangle$  is populated, the  $\alpha$ –sum in (1.2.1) gives a measure of the maximum energy that the nucleus can absorb from the  $\gamma$ –beam, as can be seen by measuring  $|\langle \alpha | F | 0 \rangle|^2$  in single–particle (sp) units (Weisskopf (W) units)

$$\begin{aligned} B_{sp}(E1; j_1 \rightarrow j_2) &= \frac{3}{4} e_{E1}^2 \langle j_1 \frac{1}{2} 1 0 | j_2 \frac{1}{2} \rangle^2 \times \langle j_2 | r | j_1 \rangle^2, \\ &\approx \frac{1}{4\pi} A^{2/3} e_{E1}^2 \text{ fm}^2 = B_W(E1), \end{aligned} \quad (1.2.5)$$

---

<sup>16</sup>Within this context, the absolute two–nucleon transfer cross section populating the ground state of a superfluid nucleus is proportional to the number of Cooper pairs contributing to the nuclear condensate. This quantity is rather stable along a pairing rotational band, in keeping with the fact that the “intrinsic”  $|BCS\rangle$ –state of the deformed system in gauge space, is essentially the same for all members of the band. This fact is at the basis of an approximate, physically sum rule.

<sup>17</sup>Bohr, A. and Mottelson (1975); Bertsch and Broglia (2005); Bortignon, P. F. et al. (1998)

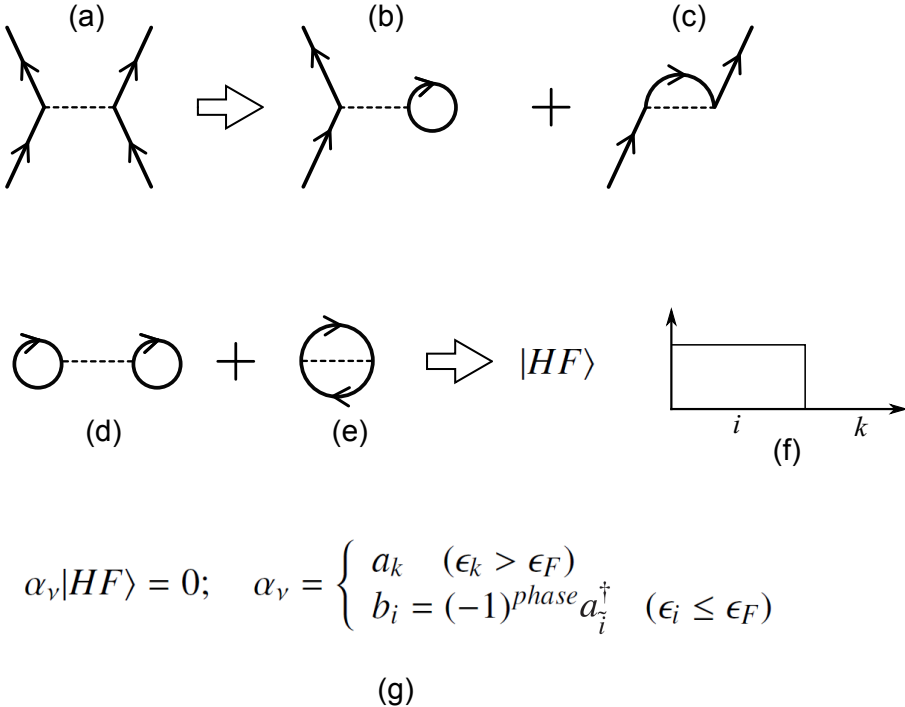


Figure 1.2.1: Schematic representation of the processes characterizing the Hartree–Fock ground state (single-particle vacuum), in terms of Feynman–NFT diagrams. (a) nucleon–nucleon interaction trough the bare (instantaneous)  $NN$ –potential. (b) Hartree mean field contribution. (c) Fock mean field contribution. (d,e) ground state correlations (ZPF) associated with the Hartree and Fock processes. (f) decoupling between occupied and empty states operated by the HF field. (g) This decoupling allows for the definition of two annihilation operators:  $a_k(b_i)$  particle (hole) annihilation operators, implying the existence of hole (antiparticle) states ( $b_i^\dagger |HF\rangle$ ) with quantum numbers time reversed to that of particle states, (for details see Brink, D. and Broglia (2005) App. A). In other words, the  $|HF\rangle$  ground (vacuum) state is filled to the rim ( $\epsilon_F$ ) with  $N$  nucleons. The system with  $(N - 1)$  nucleons can, within the language of (Feynman’s) field theory, be described in terms of the degrees of freedom of that of the missing nucleon (hole-, antiparticle state). Such a description is obviously considerably more economic than that corresponding to an antisymmetric wavefunction with  $(N - 1)$  spatial and spin coordinates  $(\mathbf{r}_i, \sigma_i)$ . Within the above scenario, a stripping reaction  $N(d, p)(N + 1)$  can be viewed as the creation of a particle state ( $a_k^\dagger |HF\rangle = |k\rangle$ ) and that of a pickup reaction  $N(p, d)(N - 1)$  as that of a hole state ( $b_i^\dagger |HF\rangle \equiv |k\rangle$ ).

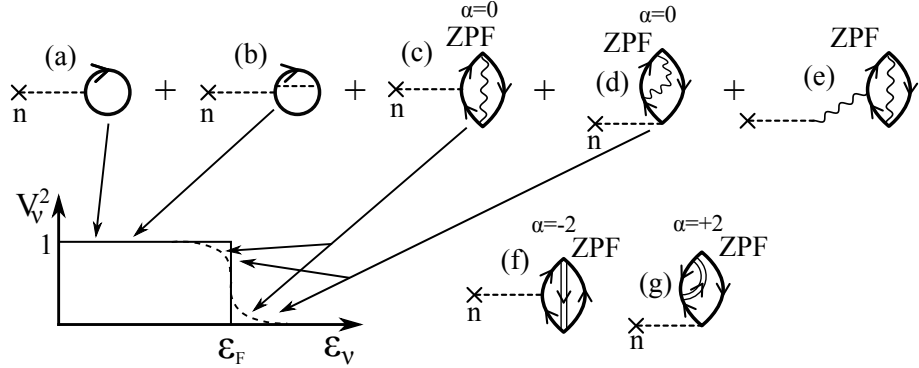


Figure 1.2.2: Schematic representation of the Fermi distribution. The sharp, heavy line drawn step function schematically represents the Hartree–Fock occupation numbers. The associated nuclear density measured with the help of an external field (cross attached to a dashed line) through processes of type (a) (Hartree: H) and (b) (Fock: F) is expected to display a diffusivity of the order of the strong force. Zero Point Fluctuations (ZPF) associated with collective particle–hole state, i.e. processes with transfer quantum number  $\alpha = 0$  and shown in (c), (d) and (e), and with pairing vibrations, i.e. pair addition (graph (f)) and pair removal (graph (g)), smooth the occupation numbers around the Fermi energy (dashed curve) and leads to a nuclear density of larger diffusivity than that associated with HF. One- and two-particle strengths which in this (mean field) approximation are found in a single  $A$ -mass system, are a result of ZPF ( $\alpha = 0, \pm 2$ ) distributed over a number of nuclei ( $A, A \pm 2$ ).

where  $(e)_{E1} = (N/A)e$  for neutrons and  $(e)_{E1} = -(Z/A)e$  for protons, in keeping with the fact that the motion of a nucleon is associated with a recoil of the rest of the nucleus, since the total center of mass remains at rest in an intrinsic excitation.

Within this context is that independent-particle motion in general and the existence of a mean field ((MF), Hartree–Fock (HF) solution) in particular can be viewed as the most collective of all nuclear phenomena<sup>18</sup>. It is then not surprising that

$$\begin{aligned} S(E1) &= \sum_n |\langle \alpha | F | \tilde{0} \rangle|^2 (E_\alpha - E_0) \\ &= \sum_{k,i} |\langle k, i | F | \text{gs(MF)} \rangle|^2 (\epsilon_k - \epsilon_i), \end{aligned} \quad (1.2.6)$$

provided  $|\tilde{0}\rangle$  contains the ground state correlations mentioned in connection with Eq. (1.2.2), and that  $|\text{gs(MF)}\rangle$  those associated with  $\Delta x \Delta p \geq \hbar$  (see Fig. 1.2.1). In other words, provided

$$|\text{HF}\rangle = |\text{gs(MF)}\rangle = \prod_{i \in \text{occup}} a_i^\dagger |0\rangle \quad (1.2.7)$$

---

<sup>18</sup>Mottelson (1962).

where  $|0\rangle$  is the particle vacuum ( $a_j|0\rangle = 0$ ), and  $\Gamma_\alpha|\tilde{0}\rangle = 0$ ,  $\Gamma_\alpha^\dagger$  being the creation operator of a dipole Random Phase Approximation (RPA-) correlated particle-hole like mode ( $\Gamma_\alpha^\dagger = \sum_{ki} X_{ki}^\alpha a_k^\dagger a_i + Y_{ki}^\alpha (a_k^\dagger a_i)^\dagger$ )<sup>19</sup>. Relation (1.2.6) is a consequence of the fact that  $S(E1)$  is proportional to the average value of the double commutator  $[[H, F], F]$  in the ground state of the system ( $|\tilde{0}\rangle$  or  $|HF\rangle$ ). Because  $F$  is a function of only the nucleon coordinates, and assuming  $v(|\mathbf{r} - \mathbf{r}'|)$  to be velocity independent, the only contribution to the double commutator arises from the (universal) kinetic energy term of the Hamiltonian. Thus, the value (1.2.1) is model independent. In other words, this value does not depend on the correlations acting among the nucleons, but on the number of them participating in the motion and on their mass (inertia) as testified by the fact that  $\sum_\alpha \hbar\omega_\alpha \left(\frac{\hbar\omega_\alpha}{2C_\alpha}\right) = \sum_\alpha \left(\frac{\hbar^2}{2D_\alpha}\right)$ . It is then not surprising that the TRK sum rule was used in the early stages of quantum mechanics, to determine the number of electrons in atoms.

Let us now go back to two-nucleon transfer (pairing) processes. The absolute cross sections associated with the population of the final states can be set essentially on equal footing with respect to each other concerning  $Q$ -value and recoil effects, with the help of empirically determined global functions<sup>20</sup>. In this way, the theoretical absolute cross section associated with e.g. the  $A(t, p)A + 2$  population (we assume  $N$  to be even) of the  $n$ th final state of spin  $J$  and parity  $(-1)^J$  can be written as

$$\sigma^{(n)}(J = L, Q_0) = \left| \sum_{j_1 \geq j_2} B(j_1 j_2; J_n) S(j_1 j_2; L, Q_0) \right|^2, \quad (1.2.8)$$

where

$$S^2(j_1 j_2; L, Q_0) = \sigma(j_1, j_2; L, Q_0), \quad (1.2.9)$$

while

$$B(j_1 j_2; J_n) = \left\langle \Phi_{J_n}(\xi_{A+2}) \left| \Phi_{J_i=0}(\xi_A) \frac{[a_{j_1}^\dagger a_{j_2}^\dagger]_J}{[1 + \delta(j_1, j_2)]^{1/2}} \right. \right\rangle, \quad (1.2.10)$$

is the two-nucleon spectroscopic amplitude,  $\Phi_{J_i=0}(\xi_A)$  being the wavefunction describing the ground state of the initial nucleus,  $\Phi_{J_n}(\xi_{A+2})$  that of the final state,  $\xi$  labeling the relative radial and spin intrinsic coordinates. Assuming  $A$  to be a closed shell system, and  $J = 0$ , one can write

$$|0_n^+\rangle = \sum_{j_1 \geq j_2} c^{(n)}(j, j; J = 0) |j, j; J = 0\rangle, \quad (1.2.11)$$

where  $n = 1, 2, 3, \dots$  labels the final nucleus states of spin and parity  $J^\pi = 0^+$  in increasing energy order. Making use of the completeness relation of the coefficients

---

<sup>19</sup>Bertsch and Broglia (2005).

<sup>20</sup>see Broglia, R. A. et al. (1972)

$c^{(n)}(j, j; J = 0)$  one obtains,

$$\sum_n \sigma^{(n)}(J = L = 0, Q_0) = \sum_j \sigma(j, j; L = 0, Q_0). \quad (1.2.12)$$

The above equation is rather similar to (1.2.6), aside from the fact that the  $Q$ -value effect can, in connection with (1.2.6), be analytically dealt with, while  $\sigma(\{Q\})$  is a functional of  $Q$ . Furthermore, the complete separation of the relative and intrinsic motion coordinates taking place in e.g. (1.2.6), is in keeping with the fact that in elastic and inelastic processes the mass partition is equal in both entrance and exit channels. Thus, the intrinsic (structure) and the relative motion (reaction) coordinates can be treated separately. This is not the case for transfer processes, both intrinsic and reaction coordinates being interweaved through the recoil process (particle–recoil mode coupling, see jagged curve Figs 1.1.2 and 1.1.3; see also Sect. 1.6).

A parallel with the discussion carried out in connection with (1.2.5) regarding the TRK sum rule, can be drawn defining two-particle units as,

$$\sigma_{2pu}^{\max}(A, L, Q_0) = \max [\sigma(j_1, j_2; L, Q_0)], \quad (1.2.13)$$

where  $\max[\ ]$  indicates that the largest two-particle absolute cross section in the single-particle subspace considered (hot orbital), is to be considered. In this way one can write the relation (1.2.12) in dimensionless units. Furthermore, one can define enhancement factors. Another quite useful two-particle transfer sum rule has been introduced in the literature<sup>21</sup>, which relates the differences between two-nucleon stripping and pick-up reactions cross sections, with single-particle transfer processes<sup>22</sup>.

The above arguments carried out for nuclei around closed shells, can be equally well be applied to the case of open shell nuclei, making use of the corresponding two-nucleon spectroscopic amplitudes<sup>23</sup>. In particular, in the case of independent pair motion, i.e. the BCS mean field solution of the pair problem, the pair transfer amplitude is given by

$$\begin{aligned} a'_0 &= \langle BCS(N+2) | P^\dagger | BCS(N) \rangle \\ &= \sum_j \frac{2j+1}{2} U'_j(N) V'_j(N+2) \end{aligned} \quad (1.2.14)$$

where

$$P^\dagger = \sum_{m>0} a_{jm}^\dagger a_{\overline{jm}}^\dagger, \quad (1.2.15)$$

creates two nucleons in time reversal states.

---

<sup>21</sup>Bayman, B. F. and Clement (1972)

<sup>22</sup>Lanford (1977)

<sup>23</sup>See App. 2, Broglia, R.A. et al. (1973).

Pairing, similar to ZPF (Fig. 1.2.2) smooth out the sharp HF Fermi surface. The number of pairs in each level participating in this smoothing is  $(2j+1)/2$  their occupancy being measured by the simultaneous, and apparently contradictory, property of being a particle (amplitude  $V'_j$ ) and a hole (amplitude  $U'_j$ ). In other words  $\alpha'_0$  measures the number of pairs of nucleons participating in the smoothing of the Fermi surface and thus can be viewed as the spectroscopic amplitude associated with the population of pairing rotational bands in two–nucleon transfer processes. It is expected that  $\alpha'_0$  does not depend on  $N$  and is about conserved along a pairing rotational band. Because  $d\sigma(gs(N) \rightarrow gs(N+2))/d\Omega \approx |\alpha'_0|$ , conservation is also expected for these absolute cross section. But in this case, it is a conservation of physical character, and not mathematical one. If one finds that at the angle where  $L = 0$  two–nucleon transfer cross sections have the first maximum, as a rule close to  $0^\circ$ , the two nucleon strength function is dominated by a single peak, that associated with the ground state, and this is so for a number of isotopes differing by two nucleons, one can conclude one is in presence of a pairing rotational band. This is why (1.2.14) can be properly viewed as the order parameter of the nuclear superfluid phase and, in keeping with (1.2.15), two–nucleon transfer reaction is the specific tool to probe pairing in nuclei.

### 1.3 Particle–vibration coupling

The Hamiltonian describing a system of independent particles and of collective surface vibrations can be written as<sup>24</sup>

$$H = H_M + H_{coupl} + H_{coll}, \quad (1.3.1)$$

where

$$H_M = T + U \quad (1.3.2)$$

is the mean field Hamiltonian, sum of the single–particle kinetic energy and of the self–consistent potential  $U = f(\rho_A)$ , functional of the density. That is,

$$U = U_H + U_x, \quad (1.3.3)$$

where

$$U_H = \int d\mathbf{r}' \rho(r') v(|\mathbf{r} - \mathbf{r}'|), \quad (1.3.4)$$

is the Hartree potential, and

$$U_x = - \sum_{i(\epsilon_i \leq \epsilon_F)} \varphi_i^*(\mathbf{r}') v(|\mathbf{r} - \mathbf{r}'|) \varphi_i^*(\mathbf{r}) \quad (1.3.5)$$

is the exchange (Fock) potential. It is well established that the nucleus can react collectively to external sollicitations. In particular the nuclear surface<sup>25</sup> can vibrate

---

<sup>24</sup>Bohr, A. and Mottelson (1975); Brink, D. and Broglia (2005)

<sup>25</sup>We consider in the present section only this type of collective modes

in certain normal modes which, in the harmonic approximation can be described as

$$H_{coll} = \frac{\hat{\Pi}_\alpha^2}{2D_\alpha} + \frac{C_\alpha}{2}\hat{\alpha}^2, \quad (1.3.6)$$

where

$$\hat{\alpha} = \sqrt{\frac{\hbar\omega_\alpha}{2C_\alpha}} (\Gamma_\alpha^\dagger + \Gamma_\alpha), \quad (1.3.7)$$

is the collective coordinate and  $\hat{\Pi}_\alpha$  being the correspondent conjugate momentum.  $\Gamma_\alpha^\dagger(\Gamma)$  is the creation (annihilation) operator of the corresponding quanta. Microscopically, these modes can be calculated in the RPA as correlated particle-hole excitations<sup>26</sup>.

The particle-vibration coupling Hamiltonian can be written as,

$$H_{coup} = \kappa\hat{\alpha}\hat{F}, \quad (1.3.8)$$

with

$$\hat{F} = \sum_{\nu_1\nu_2} \langle \nu_1 | F | \nu_2 \rangle a_{\nu_1}^\dagger a_{\nu_2}, \quad (1.3.9)$$

and

$$F = -\frac{1}{\kappa}R_0 \frac{\partial U(r)}{\partial r} Y_{LM}^*(\hat{r}). \quad (1.3.10)$$

It is of notice that  $\kappa$  characterizes the relationship between potential and density, of the mode considered. The self-consistent value is ( $\langle F \rangle = \alpha$  cf. Bohr, A. and Mottelson (1975)),

$$\kappa = \int R_0 \frac{\partial U}{\partial r} R_0 \frac{\partial \rho}{\partial r} r^2 dr. \quad (1.3.11)$$

Both the coupling constant and the potential  $U$  are negative, for attractive fields.  $H_{coup}$  embodies the coupling of the motion of a single-nucleons with the collective vibrations of the surface, with a matrix element (see Fig.1.3.1)

$$V_{\nu,\alpha'} = \langle n_\alpha = 1, \nu' | H_{coup} | \nu \rangle = \langle n_\alpha = 1, \nu \nu' | H_{coup} | 0 \rangle = \Lambda_\alpha \langle \nu' | F | \nu \rangle, \quad (1.3.12)$$

where

$$\Lambda_\alpha = \kappa \sqrt{\frac{\hbar\omega_\alpha}{2C_\alpha}} \sim \frac{\kappa\beta_\alpha}{\sqrt{2L_\alpha + 1}}, \quad (1.3.13)$$

is the particle-vibration coupling strength, while  $\beta_\alpha$  is the (dynamic) deformation parameter. Assuming  $\beta_L^2 \ll \beta_L$ , one can treat the particle-vibration coupling in the weak coupling approximation. Consequently  $H_{coup}$ , can be diagonalized perturbatively<sup>27</sup>.

---

<sup>26</sup>Bohm and Pines (1951); Pines and Bohm (1952); Bohm and Pines (1953); Bertsch and Broglia (2005).

<sup>27</sup>For more details we refer to Bohr, A. and Mottelson (1975); Brink, D. and Broglia (2005) and Bertsch and Broglia (2005), and refs. therein.

Making the ansatz that the physical (clothed) single-particle states results from the coupling to only surface vibrations, the Hamiltonian (1.3.1) can be regarded as being complete to describe the elementary modes of excitation and their couplings. Adding to (1.3.1) the terms describing the spin, spin-isospin, etc. particle-hole modes, as well as those associated with multipole pairing vibrations (see Sect. 2.5 as well as caption to Fig. 1.1.3), i.e. pair addition and pair subtraction modes (with  $\lambda^\pi = 0^+, 2^+, 4^+ \dots$ , and eventually  $1^-, 3^- \dots$ ), and the corresponding coupling terms, and diagonalizing perturbatively the resulting Hamiltonian, will lead to the physical single-particle states of spherical normal systems (nuclei around close shells). For spherical open-shell nuclei effects arising from the coupling to the condensate<sup>28</sup> will somewhat affect the actual value of the results, e.g. the energy of the two-quasiparticle phonon<sup>29</sup>.

### 1.3.1 Fluctuation and damping

To second order one finds<sup>30</sup>,

$$\begin{aligned} & \left( -\frac{\hbar^2}{2m} \nabla_r^2 + U_H(r) \right) \varphi_j(r) + \int d^3 r' U_x(\vec{r}, \vec{r}') \varphi_j(\vec{r}'), \\ & + (\Delta E_j + iW_j) \varphi_j(\vec{r}) \\ & \approx \left( -\frac{\hbar^2}{2m_k} \nabla_r^2 + U''_H(r) + \Delta E''_j + iW''_j \right) \varphi_j(\vec{r}), \\ & = \varepsilon_j \varphi_j(\vec{r}), \quad \left( U''_H = \frac{m}{m_k} U \text{ and similarly for } \Delta E'' \text{ and } W'' \right), \end{aligned} \quad (1.3.14)$$

where  $m_k = \left( 1 + \frac{m}{\hbar^2 k} \partial U_x / \partial k \right)^{-1} \approx 0.7m$  is the  $k$ -mass<sup>31</sup>, while

$$\Delta E_j^{(\omega)} = \text{Re} \sum_j (\omega) = \lim_{\Delta \rightarrow 0} \sum_{\alpha'} \frac{V_{\nu, \alpha'}^2 (\omega - E_{\alpha'})}{(\omega - E_{\alpha'})^2 + (\frac{\Delta}{2})^2}, \quad (1.3.15)$$

and

$$W_j^{(\omega)} = \text{Im} \sum_j (\omega) = \lim_{\Delta \rightarrow 0} \sum_{\alpha'} \frac{V_{\nu, \alpha'}^2}{(\omega - E_{\alpha'})^2 + (\frac{\Delta}{2})^2}, \quad (1.3.16)$$

are the real and imaginary contributions to the self-energy calculated in second order perturbation theory<sup>32</sup>. (see Fig. 1.3.2; note  $E_{\alpha'} = \epsilon_{\nu'} + \hbar\omega_\alpha$ ). and  $V_{\nu, \alpha'}$  have been defined in (1.3.12).

<sup>28</sup>see Bès, D. R. and Kurchan (1990)

<sup>29</sup>see Barranco et al. (2004)

<sup>30</sup>see e.g. Brink, D. and Broglia (2005), see also Mahaux, C. et al. (1985) and references therein.

<sup>31</sup>This is in keeping with the fact that the non-local component of the mean field can parametrized at profit as  $0.4E$ , where  $E = |\hbar^2 k^2 / 2m - \epsilon_F|$  (Perey and Buck (1962)) see also Sect. 1.9.

<sup>32</sup>Given a Hamiltonian  $H_{coupl}$ , the contribution to the energy in second order perturbation theory is

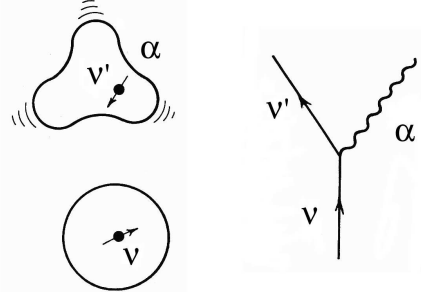


Figure 1.3.1: Schematic representation of the process by which a nucleon excites the vibrations of the surface.

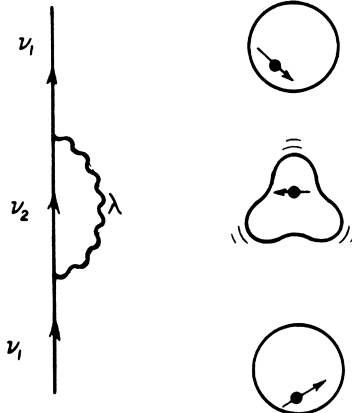


Figure 1.3.2: Self-energy (polarization, PO, see e.g. Fig. 4.2.4 and App. 4.I) graph renormalizing a single-particle.

$$\Sigma_\nu(\omega) = \sum_{\alpha'} \frac{V_{\nu,\alpha'}^2}{\omega - E_{\alpha'}},$$

where  $|\alpha'\rangle \equiv |n_\alpha = 1, \nu'\rangle$  are the intermediate states which can couple to the initial single-particle state  $\nu$ . Note that the expression above is not well defined, in that the energy denominator may vanish. As a rule, textbooks in quantum mechanics deal with such a situation by stating that accidental degeneracies are to be eliminated by diagonalization. Now, this is not a real solution of the problem, because it does not contemplate the case where there are many intermediate state with  $E_{\alpha'} \approx \omega$ . In other words, where the particle can decay into a more complicated (doorway-) state (Feshbach (1958)), starting in the single-particle level  $\nu$  of energy  $\omega$ , without changing its energy (real process). This is a typical dissipative (diffusion) process, and has to be solved by direct diagonalization (see Fig.1.3.5). Another way around, is to extend the function  $\Sigma_\nu(\omega)$  into the complex plane ( $E_{\alpha'} \rightarrow E_{\alpha'} + \frac{i\Delta}{2}$ ) thus *regularizing the divergence* through a coarse grain approximation, determining the finite contributions and then taking the limit for  $\Delta \rightarrow 0$  (Eqs.(1.3.15) and (1.3.16)). The resulting complex potential (*optical potential* from the *complex dielectric function* of optics), parametrizes in simple terms the shift of the centroid of the single-particle state and its finite lifetime.

For many purposes  $\Delta E$  can be treated in terms of an effective mass

$$m_\omega = m(1 + \lambda), \quad (1.3.17)$$

where

$$\lambda = -\frac{\partial \Delta E}{\partial \omega}, \quad (1.3.18)$$

is the *mass enhancement factor*, while

$$Z_\omega = m/m_\omega,$$

measures the single-particle content (discontinuity) at the Fermi energy.

Consequently, Eq.(1.3.14) can be rewritten as

$$\left( -\frac{\hbar^2}{2m^*} \nabla_r^2 + U'_H + iW(\omega) \right) \varphi_j(\vec{r}) = \varepsilon_j \varphi_j(\vec{r}), \quad (1.3.19)$$

with

$$m^* = \frac{m_k m_\omega}{m}. \quad (1.3.20)$$

and  $U'_H = (m/m^*)U$  and similarly for  $W'$ . Because  $\lambda \approx 0.4$  (i.e. the dressed single-particle  $m_\omega$  is heavier than the bare nucleon, as it has to carry a phonon along or, better, move in a cloud of phonons),  $m^* \approx 1$  and  $Z_\omega \approx 0.7$ . Furthermore, due to the fact that  $\hbar\omega_\alpha \approx 2 - 2.5\text{MeV}$ , the range of single-particle energy  $E = \varepsilon - \varepsilon_F$  over which the particle-vibration coupling process displayed in Fig.1.3.2 is effective is  $\approx \pm 2\hbar\omega_\alpha \approx 4 - 5$  around the Fermi energy (see Figs.1.3.3 and 1.3.4)

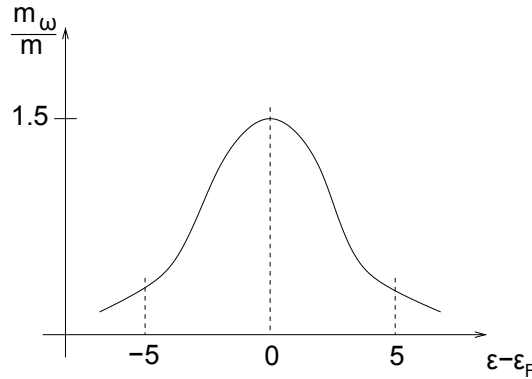


Figure 1.3.3: Schematic representation of the  $\omega$ -mass as a function of the single-particle energy.

It is of notice that  $\Delta E_j$  (Eq.(1.3.15)) indicates the shift of the centroid of the "dressed" single-particle state due to the coupling to the intermediate (more complex states) doorway states  $\alpha' \equiv (\nu', \alpha)$ , while  $\Gamma = 2W$  measures the energy range over which the single-particle state spreads due to the coupling (see Fig.1.3.5).

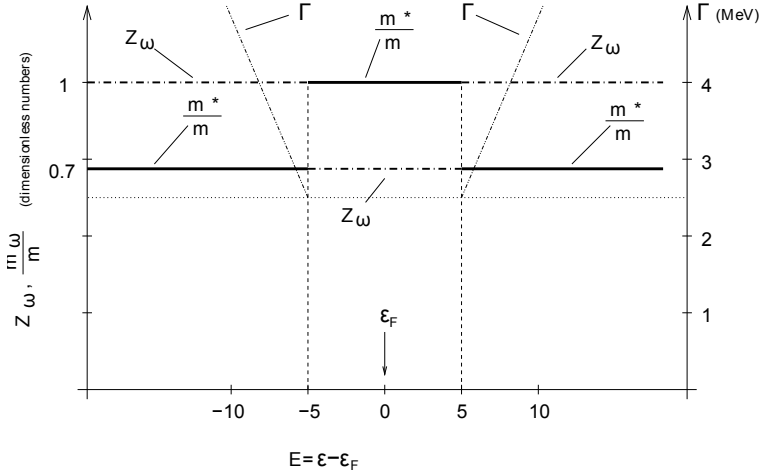


Figure 1.3.4: Schematic representation of the behaviour of  $m_\omega/m$ ,  $Z_\omega = (m_\omega/m)^{-1}$  and  $\Gamma$  as a function of  $E = \epsilon - \epsilon_F$ .

While all states contribute to  $\Delta E$  (“off-the-energy-shell process”, i.e. intermediate, virtual processes in which energy is not conserved), essentially only “on-the-energy-shell processes”, that is processes which conserve the energy, contribute to  $\Gamma$ . In fact

$$\lim_{\Delta \rightarrow 0} \frac{\Delta}{(\omega - E_{\alpha'})^2 + \left(\frac{\Delta}{2}\right)^2} = 2\pi\delta(\omega - E_{\alpha'}),$$

and

$$\Gamma(\omega) \approx 2\pi\bar{V}^2 n(\omega), \quad (1.3.21)$$

where  $\bar{V}^2$  is the average value of  $V_{\nu,\alpha'}^2$ , while

$$n(\omega) = \sum_{\alpha'} \delta(\omega - E_{\alpha'}), \quad (1.3.22)$$

is the density of energy-conserving states  $\alpha'$ . Eq.(1.3.21) is known as *the Golden rule*.

On the other hand, assuming the distribution of single-particle levels is symmetric with respect to the Fermi energy

$$\Delta E(\omega) = \lim_{\Delta \rightarrow 0} \sum_{\alpha'} \frac{V_{\nu,\alpha'}^2(\omega - E_{\alpha'})}{(\omega - E_{\alpha'})^2 + \left(\frac{\Delta}{2}\right)^2} = 0 \quad (1.3.23)$$

as there are equally many states pushing the state down than up (see Fig.1.3.5).

Quantum mechanically there cannot be imaginary potentials<sup>33</sup>, and the breaking of a stationary state into many, more complicate stationary states (Fig. 1.3.5(b))

---

<sup>33</sup>See however Caldeira and Leggett (1981), Caldeira and Leggett (1983) and refs. therein.

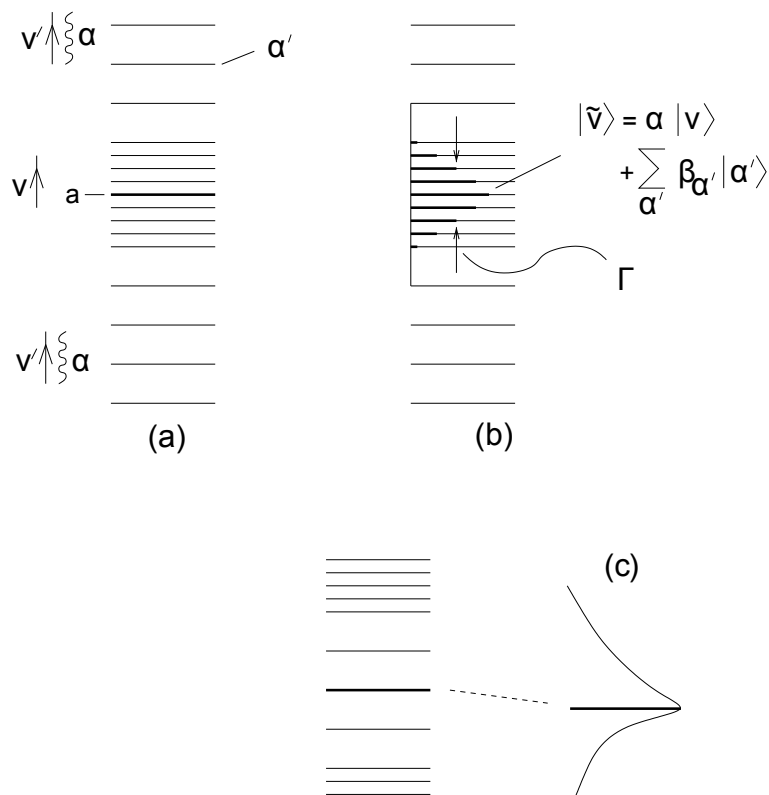


Figure 1.3.5: Schematic representation of the result of the diagonalization of  $H_{coul}$  in a basis consisting of the single-particle states  $|v\rangle$  and the  $|\alpha'\rangle = |v', \alpha\rangle$  doorway states (see Fig. 1.3.1). In (c) we show a situation where there are more states  $|\alpha'\rangle$  above  $|a\rangle$  than below.

is the only correct picture to describe the coupling of a nucleon moving in a single-particle state with more complicate configurations<sup>34</sup>. However, such a description is quite involved. On the other hand, to account for the change of the centroid energy and of its spreading width in terms of an *optical potential*  $\Delta E + iW$  is very economic and convenient. In any case  $\Gamma$  measures the range of energy over which the "pure" single-particle state  $|a\rangle$  spreads due to the coupling to the more complicated doorway states  $|\alpha'\rangle$ . In other words, a stationary state

$$\varphi_\nu(\vec{r}_i t) = e^{\frac{i\omega t}{\hbar}} \varphi_\nu(\vec{r}), \quad (1.3.24)$$

has a probability density

$$\int d^3 r |\varphi_\nu(\vec{r}_i t)|^2 = \int d^3 r |\varphi_\nu(\vec{r})|^2 = 1, \quad (1.3.25)$$

which does not depend on time. That is, if at  $t = 0$ , the probability that the particle is in a state  $\nu$  is 1, it will have this probability also at  $t = \infty$ , implying an infinite lifetime. If however,

$$\omega = \varepsilon_\nu^{(0)} + \Delta E_\nu(\omega) + i\frac{\Gamma}{2}\nu(\omega), \quad = \varepsilon_\nu + i\frac{\Gamma_\nu}{2}(\omega) \quad , (\varepsilon_\nu = \varepsilon_\nu^{(0)} + \Delta E_\nu)$$

then

$$\varphi_\nu(\vec{r}_i t) = e^{i\frac{\varepsilon_\nu t}{\hbar}} e^{-\frac{\Gamma_\nu t}{2\hbar}},$$

and

$$\int d^3 r |\varphi_\nu(\vec{r}_i t)|^2 = e^{-\frac{\Gamma_\nu t}{\hbar}}, \quad (1.3.26)$$

implying a lifetime of the single-particle state

$$\tau = \Gamma/\hbar. \quad (1.3.27)$$

One may ask, how it is possible that the coupling to complicate (but still simple) states like  $|\alpha'\rangle = |n_\alpha = 1, \nu'\rangle$  can explain the full damping of a single-particle state 8–10 MeV from the Fermi energy  $\varepsilon_F$ , where the density of levels of all types is very large. This is because the Hamiltonian given in Eq. (1.3.1) contains all the basic physics to describe the single-particle motion as far as surface modes are concerned (within this context see the discussion carried out following Eq. (1.3.13)). Any coupling to more complicated states will go through a hierarchy of couplings. In

---

<sup>34</sup>To be noted that if we spread the strength of a stationary quantal state in a number of doorway stationary states over an energy range  $\Gamma$ , and set all components in phase at  $t = 0$ , they will essentially be out of phase at  $t = \tau = \hbar/\Gamma$ . In other words, each component will behave independent of each other and the original correlated state, created at  $t = 0$  with probability 1 essentially ceases to exist at  $t = \tau$ . This does not imply that each of the incoherent members of the original coherent state cannot  $\gamma$ -decay at a much later stage. It is through such a process ( $\Gamma_\gamma \sim \hbar/10^{-15}$  sec) as well as through particle decay ( $\Gamma^\downarrow \sim \hbar/10^{-18}$  sec) that each (compound) state carrying a fraction of the giant resonance, e.g. the GDR, acquires a finite lifetime.

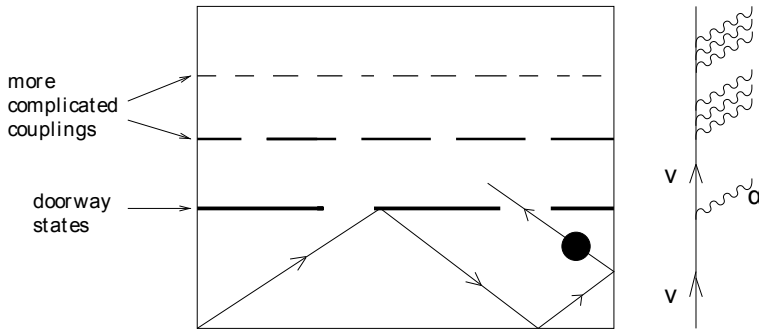


Figure 1.3.6: Schematic representation of the different levels of couplings leading to the damping of a single-particle state. It is essentially the first doorway coupling which controls the probability the ball (black dot) reflecting elastically on the walls of the box has to remain in the first compartment.

particular, all couplings, even the most complicate, should go through the coupling to states of type  $|v', \alpha'\rangle$ . In other words,  $|\alpha'\rangle$  is a doorway state (see Fig.1.3.6)<sup>35</sup>.

In the nuclear case, the *doorway coupling provides the basic breaking* of the single-particle motion, while higher-order couplings essentially only *fill in valleys* (see Fig.1.3.7). In other words, the quantity  $\Gamma$  (Eq.(1.3.27)), gives the range over which the single-particle state is spread due to all the couplings.

In the case of the  $1s_{1/2}$  orbital of  $^{40}Ca$  ( $\epsilon - \epsilon_F = -8$  MeV), simple estimates<sup>36</sup> lead to  $\bar{V}^2 \approx 0.3$  MeV for the coupling to an  $L = 2$  phonon, and  $n(\epsilon_F) \approx 2$  MeV $^{-1}$ . Consequently

$$\Gamma \approx 4\text{MeV}, \quad (1.3.28)$$

in overall agreement with the experimental findings (see Fig. 1.3.8).

The result given in Eq.(1.3.28) is a particular example of the general (empirical) result (see Fig. 1.3.4)<sup>37</sup>.

$$\Gamma_{sp}(E) = \begin{cases} 0.5E & E > 5 \text{ MeV}, \\ 0 & E \leq 5 \text{ MeV}, \end{cases} \quad (1.3.29)$$

where

$$E = |\epsilon - \epsilon_F|. \quad (1.3.30)$$

### 1.3.2 Induced interaction

A nucleon at the Fermi energy which creates, by bouncing inelastically off the nuclear surface a collective mode, has no other choices than to continue on such

<sup>35</sup>Feshbach (1958).

<sup>36</sup>Mahaux, C. et al. (1985)

<sup>37</sup>Bertsch et al. (1983)

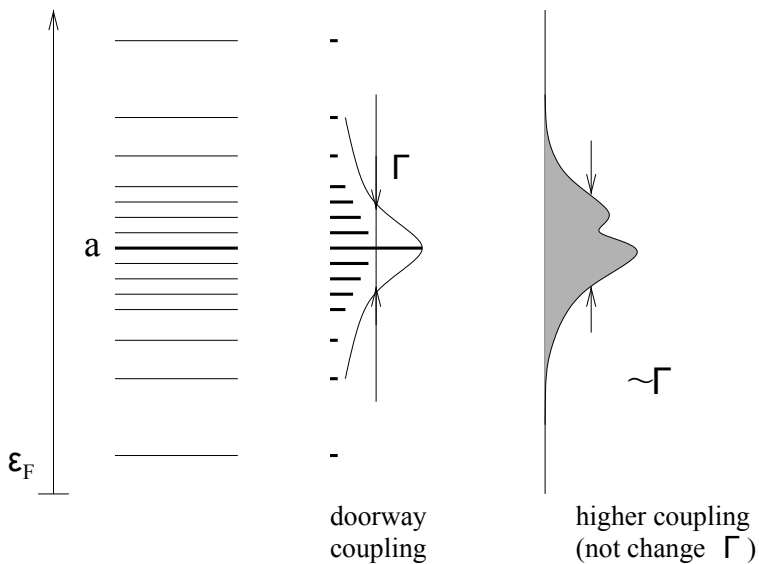


Figure 1.3.7: Schematic representation of the breaking of a single particle state  $|a\rangle$  (heavy black horizontal line) through the coupling to doorway states ( $|\alpha'\rangle = |\nu_2 \otimes \lambda'; \nu_1\rangle$ ; thin horizontal lines) and eventually to increasingly more complicated (many-particle)–(many-hole) configurations.

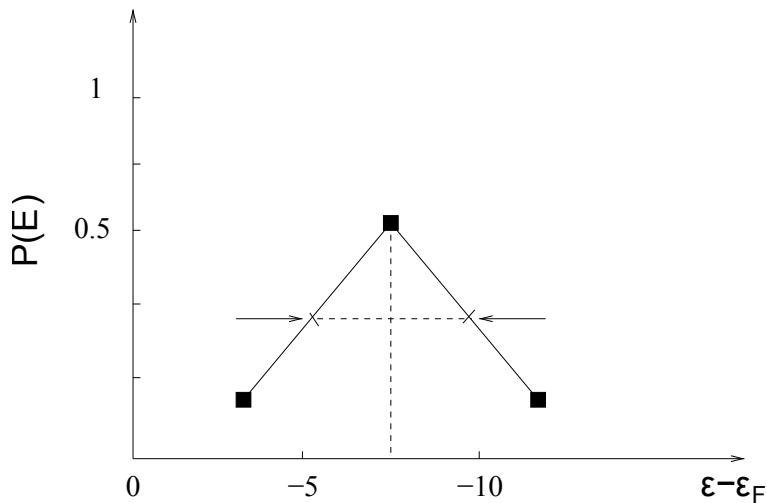


Figure 1.3.8: Schematic representation of the experimental strength function (solid squares) associated with the  $2s$  state of  $^{40}Ca$ . Also indicated is the full width at half maximum (FWHM) (after Mahaux, C. et al. (1985) Fig. 2.12).

a state, or to reabsorb the vibration at a later instant of time (virtual process, Fig. 1.3.2). In the presence of another nucleon, the vibration virtually excited by one nucleon may be absorbed by the second one (Fig. 1.3.9), the exchange of a vibration leading to an (induced) interaction.

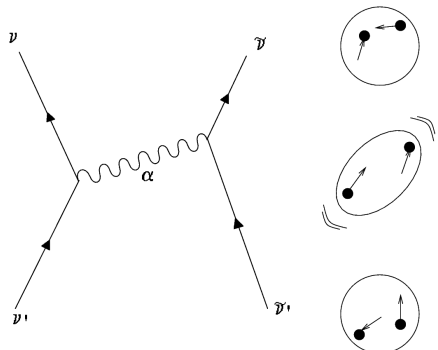


Figure 1.3.9: Schematic representation of the exchange of phonons between nucleons.

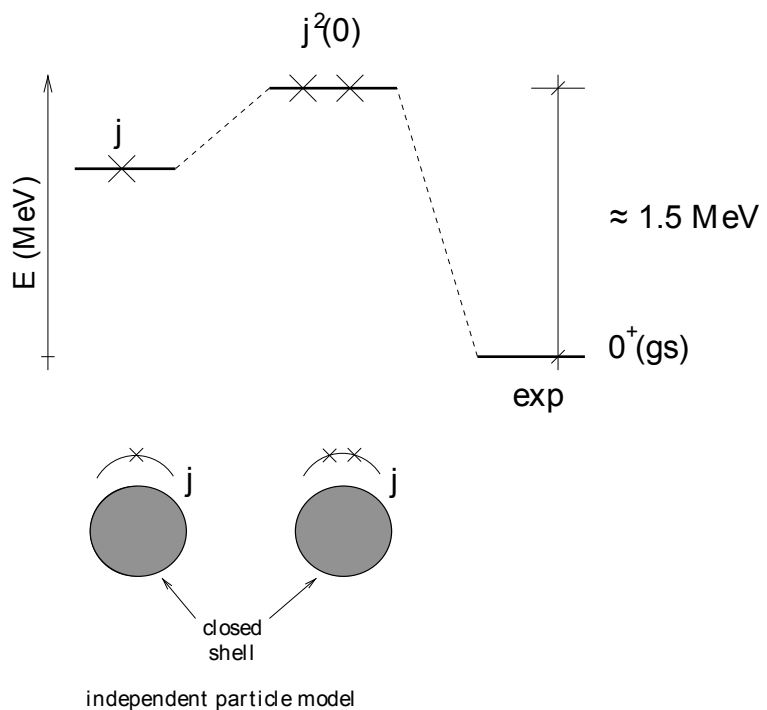


Figure 1.3.10: Schematic representation of the predictions of the independent particle model for one- and two-particles outside closed shell, in comparison with the experimental findings (e.g. for the case of  $^{210}\text{Pb}$ , where  $j = g_{9/2}$ ).

Simple estimates of this induced interaction leads, in the case of  $^{208}\text{Pb}$ , to values of the matrix element for pairs of particles coupled to angular momentum  $J^\pi = 0^+$  of  $-1.5\text{ MeV}$ , when summed over all the different multipolarities  $\alpha$  ( $L^\pi = 2^+, 3^-, 5^-$ , label  $\alpha$  in Fig. 1.3.9). The fact that one considers particles coupled to angular momentum zero is because the associated orbitals have maximum overlap, thus profiting at best from the (pairing) interaction<sup>38</sup>. In the case of two particles outside closed shell one would then expect the ground state to display, due to this mechanism, a correlation energy of about  $1.5 \text{ MeV}$  larger than that predicted by the independent particle model (see Fig. 1.3.10), and about half the value if one takes into account that  $Z_\omega \approx 0.7$  for each of the interacting particles. From this result one can conclude that the pairing interaction induced by the process depicted in Fig. 1.3.9, is likely to renormalize in an important way the bare,  $NN(^1S_0)$ —short range pairing interaction.

## 1.4 Coupling between elementary modes

Let us now return to the subject of the finite overlap existing between the elementary modes of nuclear excitation. That is, to the fact that one is working in a basis of states which contains already much of the physics one likes to describe, but which has the shortcoming of being overcomplete. An orthogonalization protocol, like a generalized Gram–Schmidt procedure, but leading to an effective field theory, where the different modes melt to some extent together, is called for (see Sect. 1.5).

A similar situation is found in the case of transfer processes in general, and of two-nucleon transfer in particular. One can work out the associated transfer amplitude by orthogonalizing, making use of second order perturbation theory, the single-particle wavefunctions of target and projectile. This can be done both within the semiclassical approximation (Sect. 5.C, see also Sect. 1.6) and DWBA (Sect. 3.2 and 5.2).

Because the coupling between elementary modes of excitation is proportional to their overlap, and in keeping with the fact that mean field theory is the natural starting point of nuclear structure calculations, overcompleteness of the basis is tantamount to the appearance of linear couplings between quasiparticles and collective modes (see Sect. 1.3 and App. 1.B in the case of surface modes and Sect. 1.7 in the case of surface and of pairing modes; see also Fig. 1.7.9), which in the case of reactions corresponds to the recoil modes (see e.g. Figs. 1.1.2 and 1.1.3, 5.C.1 and 5.C.2; see Fig. 4.1.1 in the case of one-particle transfer).

Basis orthogonalization thus implies the diagonalization of the associated particle-vibration coupling Hamiltonian  $H_c$ . The rules to do so have been cast into a graphical effective field theory, namely the Nuclear Field Theory (NFT, see Sect. 1.7). In it, the free fields are to be calculated in the HF (HFB) approximation (particle (quasiparticle)) and in the RPA (QRPA) (vibrations). These elementary modes of excitation interact through the particle–vibration coupling vertices, while particles

---

<sup>38</sup>Note that quadrupole pairing correlations are also important.

can also interact through four-point vertices ( $NN$ -bare interaction) (Figs. 1.7.9 (a) and (b)).

The NFT rules for evaluating the effect of these couplings between fermions and bosons involve a number of restrictions concerning initial and intermediate states as compared with the usual rules of perturbation theory that are to be used in evaluating the effect of the original (bare) nucleon–nucleon interaction properly renormalized by the exchange of vibrations between nucleons. This is in keeping with the fact that the collective modes contain, from the start, the correlations arising from forwards and backwards going particle–hole ( $\beta = 0$ ) as well as particle–particle ( $\beta = +2$ ) and hole–hole ( $\beta = -2$ ) bubbles. Furthermore, this is because these (quasi) bosons are not elementary but composite fields, made out of pairs of fermions, and thus subject to the Pauli principle (see Sect. 1.8).

The general validity of NFT rules have been demonstrated by proving the equivalence existing, to each order of perturbation theory, between the many-body finite nuclear system propagator calculated in terms of Feynman diagrams involving only the fermionic degrees of freedom i.e. explicitly respecting Pauli in a complete and not overcomplete basis, and the propagator constructed in terms of Feynman diagrams involving fermion and phonon degrees of freedom (NFT Feynman diagrams) in the case of a general two-body interaction and an arbitrary distribution of single-particle levels<sup>39</sup>.

Concerning the actual embodiment of NFT one can recognize the practical difficulties of respecting the corresponding rules. This is in keeping with the fact that there is not a single bare, well behaved, low- $k$   $NN$ -force (eventually with  $3N$  and higher order corrections) with which it is possible to generate a mean field (Eq. (1.2.3), also Fock potential see Fig. 1.2.1 (c)) to determine the single-particle states and, by introducing a periodic time-dependence with the constrain

$$\delta U(r) = \int d\mathbf{r} \delta\rho(r') v(|\mathbf{r} - \mathbf{r}'|), \quad (1.4.1)$$

calculate the collective modes associated with the variety of particle–hole ( $\beta = 0$ ; density, spin, isospin, etc.) and pairing ( $\beta = \pm 2$ ; monopole and multipole pair addition and pair subtraction) modes. If this was possible, one could then diagonalize, within the framework of NFT and to the desired order of perturbation, also infinite order, the resulting particle–vibration couplings, and thus obtain renormalized quantities which can be directly compared with the data. In other words, a real physical *ab initio* calculation could be done, resulting in a single, common ground state which, corrected with the corresponding homogeneous ZPF lead eventually to the “exact” ground state as well as to properly dressed modes and pairing interaction (see Sect. 1.7).

On the other hand, empirical implementation of the NFT rules (empirical renormalization)<sup>40</sup> have been carried out, making use of the bare Argonne  $v_{14}$  poten-

---

<sup>39</sup>(Bès and Broglia (1975); see also Baranger (1969)) and the lecture notes of McFarlane (1969)

<sup>40</sup>Broglia et al. (2016).

tial, and of Skyrme like SLy4<sup>41</sup> forces (or Saxon–Woods parametrizations and  $m_k \approx 0.7m$ ) to determine the mean field and spin vibrational channels, and of multipole–multipole forces with self–consistent coupling constants for the variety of density vibrational channels.

The resulting predictions are, as a rule, able to provide, together with the specific reaction software, in particular COOPER and SINGLE, an overall account of “complete” sets of experimental data, obtained with the help of Coulomb, inelastic and one– and two–nucleon transfer data, able to map out the nuclear structure and reaction landscape<sup>42</sup>. Summing up, the nuclear structure description given by the elementary modes of nuclear excitation approach within the framework of NFT, provides a unified description of the variety of observables. At the same time, each cross section or transition probability is connected to essentially all others. This is the reason why 5, brings together pair (as well as one–particle) transfer with the rest of the observables both for open–shell nuclei along the stability valley, as well as for exotic closed shell nuclei, to demonstrate that: 1) it is possible to predict, with few (4–5) parameters, most of them strongly constrained by empirical input, the experimental findings within a 10% level of accuracy; 2) that the nuclear landscape, as it emerges from NFT based on elementary modes of excitation and of their interweaving through the particle–vibration coupling, is well funneled (Fig. 1.4.1), its minimum essentially coinciding with the global minimum resulting from the empirical renormalization choice of basic quantities ( $m_k$ , strength bare pairing, properties of few low–lying collective modes ( $p - h$ ) and pairing vibrations) An important proviso concerning the above parlance is that one considers a group of homogeneous nuclei like e.g. open shell spherical superfluid nuclei (like the Sn isotopes), or nuclei around closed shells (like  $^{208}\text{Pb}$ ,  $^{12}\text{Be}$ ,  $^{11}\text{Li}$ , etc.), for details see Sect. ??.

## 1.5 Non–orthogonality

The ground state of  $^{210}_{84}\text{Po}_{126}$  can be viewed as the proton pair addition mode of the doubly closed shell nucleus  $^{208}_{82}\text{Pb}_{126}$ , mode displaying  $J^\pi = 0^+$  and  $\beta = +2$  (transfer–) quantum numbers. Within this framework  $^{209}_{83}\text{Bi}_{126}$  is expected to be a *bona fide* proton single–particle system ( $\beta = +1$ ), in which the  $g_{7/2}$ ,  $d_{5/2}$ ,  $h_{11/2}$ ,  $d_{3/2}$  and  $s_{1/2}$  valence orbitals are occupied, the odd proton occupying, in the ground state, a substate of the  $h_{9/2}$  orbital.

This picture can be specifically probed through one–proton stripping and pick up reactions, e.g. with the help of  $^{210}\text{Po}(t, \alpha)^{209}\text{Bi}$  and  $^{208}\text{Pb}({^3\text{He}}, d)^{209}\text{Bi}$  transfer processes<sup>43</sup>. The pick–up reaction cross section is, in the case of e.g. the states

---

<sup>41</sup>Chabanat et al. (1997)

<sup>42</sup>Idini et al. (2015); Idini, A. et al. (2014); Potel, G. et al. (2013).

<sup>43</sup>It is of notice that in the present case, as well as in Sect. 1.7, and at variance with the rest of the monograph, use will be made, for the sake of being didactic, of spectroscopic factors, see end of Sect. 2.1.

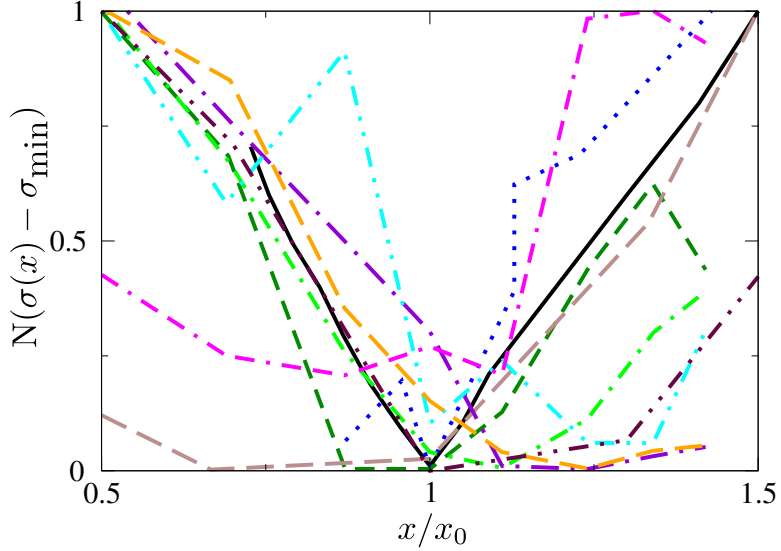


Figure 1.4.1: Root mean square deviations  $\sigma(x)$  (see Table 1) between theoretical predictions and experimental values of the different structural properties which “completely” characterise the open-shell nucleus  $^{120}\text{Sn}$  and involve the island of superfluid nuclei  $^{118,119,120,121,122}\text{Sn}$ , calculated as a function of  $G$  (referred to  $G_0 = 0.22\text{MeV}$ ),  $m_k$  ( $(m_k)_0 = 0.7m$ ), and  $\beta_2$  ( $(\beta_2)_0 = 0.13$ ) and in general to  $x$  ( $x_0$ ), measured with respect to the minimum value  $\sigma_{\min} = \sigma(x_{\min})$ , displayed in the interval  $0.5 \leq x/x_0 \leq 1.5$  and normalized according to  $0 \leq N(\sigma(x) - \sigma_{\min}) \leq 1$ . The curves represent: the deviation of the pairing gap associated with the  $h_{11/2}$  orbital ( $\Delta_{h_{11/2}}(G/G_0)$ ) (solid black curve);  $\Delta_{h_{11/2}}(m_k/(m_k)_0)$  (dotted blue curve);  $\Delta_{h_{11/2}}(\beta_2/(\beta_2)_0)$  (dashed green curve)); the deviation of the quasiparticle spectrum ( $E_{qp}(G/G_0)$  (dashed brown curve);  $E_{qp}(\beta_2/(\beta_2)_0)$  (dash-dotted green curve)); the deviation of the  $h_{11/2} \otimes 2^+$  multiplet splitting  $E_{h_{11/2} \otimes 2^+}(\beta_2/(\beta_2)_0)$  (dash-dotted purple curve); the deviation of the centroid position of the  $d_{5/2}$  strength function  $S_{d_{5/2}}(\beta_2/(\beta_2)_0)$  (dash-dotted cyan curve); the deviation of the width of the  $d_{5/2}$  strength function  $S_{d_{5/2}}(\beta_2/(\beta_2)_0)$  (dash-dotted pink curve); the deviation of the quadrupole transition strength  $B(E2)(\beta_2/(\beta_2)_0)$  (dashed orange curve). For details see Idini et al. (2015). The remarkable feature of the present figure is the fact that, in spite of the fluctuations of the results typical of finite many-body systems, clearly defines a funnel in which all minima fall within a narrow window of  $x/x_0$  values ( $1 \pm 0.2$ ). This is a novel and unexpected result, which can be considered as an emergent property of a description of structure and reactions carried out in a basis of elementary modes of excitations, interacting through the PVC vertices according to the NFT rules.

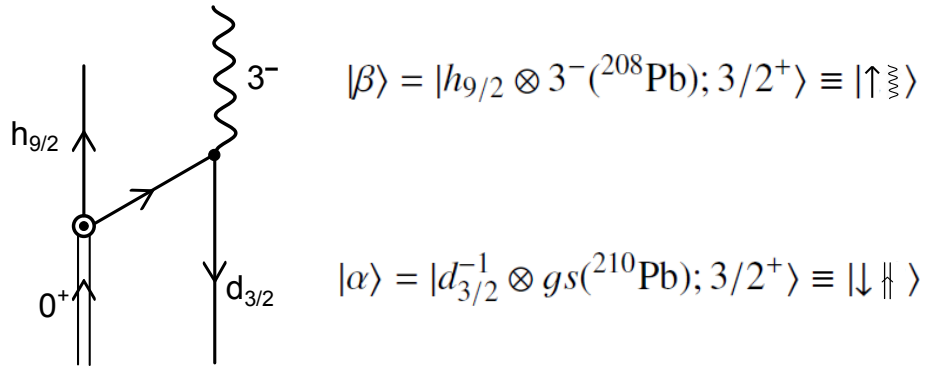


Figure 1.5.1: NFT diagram describing one of the most important processes coupling the  $2p - 1h$  states  $|\alpha\rangle$  and  $|\beta\rangle$  (see Eqs. (1.5.1) and (1.5.2)), product of bare elementary modes of excitation consisting in the  $^{208}\text{Pb}$ ,  $0^+$  pair addition mode and the  $d_{3/2}$  proton hole state, and of the lowest octupole vibration of  $^{208}\text{Pb}$  and of a proton moving in the  $h_{9/2}$  orbital.

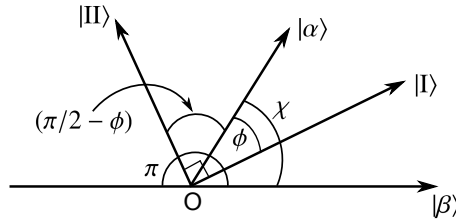


Figure 1.5.2: Schematic representation of the  $3/2^+$  states entering the NFT calculation of the process displayed in Fig. 1.5.1. The basis state  $|\alpha\rangle$  carries the full ( $t, \alpha$ ) transfer strength ( $tr$ )  $\sigma^{tr}$ , while the basis state  $|\beta\rangle$  the full octupole ( $oct$ ) strength  $\sigma^{oct}$  (see Tables 1.5.1–1.5.3). The overlap between these states is  $\cos \chi$ . The physical states obtained through the (Feynman) diagrammatic “orthogonalization process” are denoted  $|I\rangle$  and  $|II\rangle$  (see Eqs. (1.5.3) and (1.5.4)).

$1/2^+(s_{1/2})$  and  $11/2^-(h_{11/2})$ , essentially consistent with a single peak displaying full  $(2j + 1)$  occupancy. On the other hand, two  $3/2^+$  states with essentially equal strength and exhausting the associated  $(2j + 1 (= 4))$  strength are observed. Furthermore, the four peaks mentioned above are essentially not excited in the stripping process (see Table 1.5.1). In an attempt to further clarify the structure of the two  $3/2^+$ , recur is made to the inelastic process  $^{209}\text{Bi}(d, d')$ . Both states are excited in the inelastic process, the associated angular distributions revealing the octupole character of such excitation (Tables 1.5.2 and 1.5.3).

In keeping with the fact that the same experiment reveals a multiplet (septuplet) of states with centroid around 2.6 MeV and with summed  $L = 3$  inelastic cross section consistent with that of the lowest collective (2.615 MeV,  $B(E3)/B_{sp} \approx 32$ ) octupole vibration of  $^{208}\text{Pb}$ , one can posit that the two  $3/2^+$  states are a linear combination of the unperturbed (two particles)–(one hole)  $(2p-1h)$  states (see Fig.

	$E_x(\text{MeV})$	$S(t, \alpha)(2j + 1)$	$S(^3\text{He}, d)$
$3/2^+$	2.49	$1.8 \pm 0.3 (4)$	$< 0.01$
$3/2^+$	2.95	$2.2 \pm 0.3 (4)$	$< 0.01$
$1/2^+$	2.43	$1.8 (2)$	$< 0.02$
$11/2^-$	3.69	$10 (12)$	$< 0.05$

Table 1.5.1: Single-particle strength associated with the single-particle transfer reactions  $^{210}\text{Po}(t, \alpha)^{209}\text{Bi}$  and  $^{208}\text{Pb}(^3\text{He}, d)^{209}\text{Bi}$  (see Bortignon, P. F. et al. (1977)).

1.5.1),

$$|\alpha\rangle = |d_{3/2}^{-1} \otimes gs(^{210}\text{Pb}); 3/2^+\rangle, \quad (1.5.1)$$

and

$$|\beta\rangle = |h_{9/2} \otimes 3^-(^{208}\text{Pb}); 3/2^+\rangle. \quad (1.5.2)$$

Because these states lie very close in energy they mix. According to NFT, the most important contribution to this mixing arises from the process given in Fig. 1.5.1. The resulting physical (mixed) states can be written as,

$$|I\rangle = -0.53|\alpha\rangle + 0.76|\beta\rangle, \quad (1.5.3)$$

and

$$|II\rangle = 1.02|\alpha\rangle + 0.80|\beta\rangle, \quad (1.5.4)$$

as resulting from the calculation of the diagram displayed in Fig. 1.5.1 to all orders of perturbation, with the help of Brillouin–Wigner perturbation theory (diagonalization of the corresponding effective Hamiltonian<sup>44</sup>. Let us now calculate the overlap  $O = \langle \alpha | \beta \rangle$  between the basis states  $|\alpha\rangle$  and  $|\beta\rangle$ , that is  $O = \cos \chi$  (see Fig. 1.5.2). Following this figure one can write,

$$\sqrt{\sigma_I^{tr}} = \cos \phi; \quad \sqrt{\sigma_{II}^{tr}} = \cos \left( \frac{\pi}{2} - \phi \right) = \sin \phi, \quad (1.5.5)$$

where

$$\sigma^{tr} = \sigma_I^{tr} + \sigma_{II}^{tr} = 1, \quad (1.5.6)$$

in keeping with the fact that the absolute cross sections of the states  $|I\rangle$  and  $|II\rangle$  are normalized in terms of the total cross section (see caption to Fig. 1.5.2).

In the same way

$$\sqrt{\sigma_I^{oct}} = \cos(\chi - \phi) = \cos \chi \cos \phi + \sin \chi \sin \phi, \quad (1.5.7)$$

---

<sup>44</sup>See p. 316 Bortignon, P. F. et al. (1977) and references therein.

		$\frac{\sigma(^{209}\text{Bi}(9/2^-;gs) \rightarrow ^{209}\text{Bi}(3/2^+;E))}{\sigma(^{208}\text{Pb}(gs) \rightarrow (3^-;2.615 \text{ MeV}))}$
3/2	2.49	$0.041 \pm 0.003$
3/2	2.95	$0.011 \pm 0.002$

Table 1.5.2: The total inelastic cross section  $\sigma^{oct}$  associated with the lowest octupole vibrational state of  $^{208}\text{Pb}$  can be written in terms of that associated with a single magnetic substate  $\sigma'$  as  $\sigma_{3^-}^{oct} = 7\sigma'$ . That associated with the multiplet  $(h_{9/2} \otimes 3^-)_{J^+}(J = 3/2 - 15/2)$  as  $\sigma_{3^-}^{oct} = 70\sigma'$ , in keeping with the fact that the  $h_{9/2}$  state has 10 magnetic substates. Thus, the strength associated with the 3/2 channel is  $4/70=0.057$  to be compared with the observed summed (percentage) strength  $0.053 \pm 0.005 (= (0.042 \pm 0.003) + (0.011 \pm 0.002))$  associated with the 2.45 MeV and the 2.95 MeV 3/2<sup>+</sup> states; see Bortignon, P. F. et al. (1977).

	$E_n(\text{MeV})$		$\frac{\sigma(h_{9/2} \rightarrow 3/2^+)}{\sigma(0^+ \rightarrow 3^-)} (\%)$		$S(t, \alpha)$		$S(^3\text{He}, d)$	
	Theory	Exp	Theory	Exp	Theory	Exp	Theory	Exp
3/2	2.480	2.494	3.76	$4.2 \pm 0.3$	1.83	$1.8 \pm 0.3$	0.02	$< 0.01$
3/2	3.125	2.95	1.56	$1.1 \pm 0.2$	2.25	$2.2 \pm 0.3$	$10^{-5}$	$< 0.01$

Table 1.5.3: Summary of NFT predictions concerning the structure of the two lowest 3/2<sup>+</sup> state of  $^{209}\text{Bi}$ , in comparison with the experimental data (see Table 4.7 of Bortignon, P. F. et al. (1977)).

and

$$\sqrt{\sigma_{II}^{oct}} = \cos\left(\pi - \left(\frac{\pi}{2} - \phi + \chi\right)\right) = -\cos\left(\frac{\pi}{2} + (\phi - \chi)\right) = \sin\phi \cos\chi + \sin\chi \cos\phi. \quad (1.5.8)$$

Thus

$$\sqrt{\sigma_I^{oct}} = \cos\chi \sqrt{\sigma_I^{tr}} + \sin\chi \sqrt{\sigma_{II}^{tr}}, \quad (1.5.9)$$

and

$$\sqrt{\sigma_{II}^{oct}} = -\cos\chi \sqrt{\sigma_{II}^{tr}} + \sin\chi \sqrt{\sigma_I^{tr}}. \quad (1.5.10)$$

Multiplying the above relations by  $\sqrt{\sigma_I^{tr}}$  and  $\sqrt{\sigma_{II}^{tr}}$  respectively one obtains,

$$\sqrt{\sigma_I^{tr} \sigma_I^{oct}} = \cos\chi \sigma_I^{tr} + \sin\chi \sqrt{\sigma_I^{tr} \sigma_{II}^{tr}}, \quad (1.5.11)$$

and

$$\sqrt{\sigma_{II}^{tr} \sigma_{II}^{oct}} = -\cos\chi \sigma_{II}^{tr} + \sin\chi \sqrt{\sigma_I^{tr} \sigma_{II}^{tr}}, \quad (1.5.12)$$

which, upon subtraction leads to the expression of the overlap

$$\cos \chi = \frac{\sqrt{\sigma_I^{tr} \sigma_I^{oct}} - \sqrt{\sigma_{II}^{tr} \sigma_{II}^{oct}}}{\sigma_I^t + \sigma_{II}^t}. \quad (1.5.13)$$

Making use of the values of Tables 1.5.1–1.5.3 (see also Fig. 1.7.10 (e) last column labeled *experiment*)<sup>45</sup> one obtains

$$\cos \chi = \frac{\sqrt{1.8 \times 4.2} - \sqrt{2.2 \times 1.1}}{4} = 0.298 \quad (1.5.14)$$

Simple estimates of the NFT prediction can be made making use of the relations<sup>46</sup>.

$$\begin{aligned} \langle I|I \rangle &= (-0.53)^2 + (0.76)^2 - 2 \times 0.53 \times 0.75 \mathcal{O} = 1, \\ \langle II|II \rangle &= (1.02)^2 + (0.80)^2 + 2 \times 1.02 \times 0.80 \mathcal{O} = 1, \end{aligned}$$

and  $\langle I|II \rangle = -0.53 \times 1.02 + 0.76 \times 0.80 + (-0.53 \times 0.80 + 0.76 \times 1.02) \mathcal{O} = 0$  leading to  $\mathcal{O} = -0.18, -0.42$  and  $-0.19$  respectively and, thus, to the average value of  $-0.26$ . Of course, one can hardly expect to obtain the sign to agree with that of the NFT expression, as it is associated with a free choice of the axis of references (Fig. 1.5.2) (note also the fact that the quantities  $\sigma$  appearing above are well defined, while  $\sqrt{\sigma}$  is undetermined by an overall sign).

## 1.6 Coupling between intrinsic and relative motion

In what follows, we consider the reaction



within the framework of the semiclassical approximation<sup>47</sup>. In the center-of-mass system, the local Hamiltonian may be written

$$H = T_{aA} + H_a + H_A + V_{aA} = T_{bB} + H_b + H_B + V_{bA}, \quad (1.6.2)$$

in keeping with energy conservation. Within this context other, mixed, representations are possible.

One then solves the time-dependent Schrödinger equation

$$i\hbar \frac{\partial \Psi}{\partial t} = H\Psi, \quad (1.6.3)$$

with the initial conditions that the nuclei  $a$  and  $A$  are in their ground states, and where the relative motion is described by a narrow wavepacket of rather well defined impact parameter and velocity.

---

<sup>45</sup>See Table 4.7 of Bortignon, P. F. et al. (1977).

<sup>46</sup>see Table 4.6 Bortignon, P. F. et al. (1977).

<sup>47</sup>Broglio and Winther (2004) and references therein.

We expand  $\Psi$  on (stationary) channel wavefunctions

$$\Psi = \sum_{\beta} c_{\beta} (\mathbf{r}_{\beta} - R_{\beta}) \Psi_{\beta} e^{-iE_{\beta}t/\hbar}, \quad (1.6.4)$$

where

$$\Psi_{\beta}(t) = \Psi_m^b(\xi_b) \Psi_n^B(\xi_B) \exp(i\delta_{\beta}). \quad (1.6.5)$$

The index  $\beta$  labels both the partition of nuclei ( $b, B$ ) as well as the quantal states of the two nucleons ( $m, n$ ).

The phase  $\delta_{\beta}$  is defined as

$$\delta_{\beta} = \frac{1}{\hbar} \left\{ m_{\beta} \mathbf{v}_{\beta}(t) \cdot (\mathbf{r}_{\beta} - \mathbf{R}_{\beta}(t)) - \int_0^t \left( U_{\beta}(R_{\beta}(t')) - \frac{1}{2} m_{\beta} \mathbf{v}_{\beta}(t')^2 \right) dt' \right\}. \quad (1.6.6)$$

Where an extra phase has been added to eliminate, as far as possible, the diagonal matrix elements in the coupled equations. The phase factor  $\exp(i\delta_{\beta})$  acting on the channel wavefunction is essentially a Galilean transformation (see jagged “phonon” in the NFT reaction diagrams displayed in Figs. 4.1.1 (one-particle transfer) and 5.C.1 and 5.C.2 (two-particle transfer); see also Figs. 1.1.2 and 1.1.3).

The function  $c_{\beta}$  can be expressed as

$$c_{\beta} = a_{\beta}(t) \chi_{\beta}(\mathbf{r}_{\beta} - \mathbf{R}_{\beta}(t), t) \quad (1.6.7)$$

product of an amplitude  $a_{\beta}$  of asymptotic values ( $t = \pm\infty, 0$  or  $1$ ), and a normalized shape (wavepacket) function,  $R_{\beta}(t)$  being the relative motion elastic trajectory.

Properly combining the above quantities and making use of the time-dependent Schrödinger equation one obtains

$$i\hbar \sum_{\beta} \dot{a}_{\beta}(t) \langle \Psi_{\xi} | \Psi_{\beta} \rangle_{\mathbf{R}_{\xi\gamma}} e^{iE_{\beta}t/\hbar} = \sum_{\gamma} \langle \Psi_{\xi} | V_{\gamma} - U_{\gamma}(r_{\gamma}) | \Psi_{\gamma} \rangle_{\mathbf{R}_{\xi\gamma}} a_{\gamma}(t) e^{iE_{\beta}t/\hbar}, \quad (1.6.8)$$

where

$$f(\mathbf{R}) = \langle \Psi_{\xi} | V_{\gamma} - U_{\gamma}(r_{\gamma}) | \Psi_{\gamma} \rangle_{\mathbf{R}} \quad (1.6.9)$$

are the formfactors, and

$$g(\mathbf{R}) = \langle \Psi_{\xi} | \Psi_{\beta} \rangle_{\mathbf{R}} \quad (1.6.10)$$

the overlaps between the intrinsic channel wavefunctions.

The coupled equations can be written in a more compact form by introducing the adjoint channel wavefunction

$$\omega_{\xi} = \sum_{\gamma} g_{\xi\gamma}^{-1} \Psi_{\gamma}, \quad (1.6.11)$$

where  $g^{-1}$  is the reciprocal of the overlap matrix

$$g_{\xi\gamma} = \langle \Psi_\xi | \Psi_\gamma \rangle. \quad (1.6.12)$$

Thus

$$(\omega_\xi, \Psi_\beta) = \delta(\xi, \beta), \quad (1.6.13)$$

and

$$i\hbar \dot{a}_\beta(t) = \sum_\gamma \langle \omega_\beta | V_\gamma - U_\gamma | \Psi_\gamma \rangle_{\mathbf{R}_{\beta\gamma}} e^{(E_\beta - E_\gamma)t/\hbar} a_\gamma(t). \quad (1.6.14)$$

Consequently, the proper tunneling Hamiltonian is obtained by a basis orthogonalization process. These coupled equations, being first order in time, can be solved knowing the initial conditions at time  $t = -\infty$ ,

$$a_\gamma(-\infty) = \delta(\gamma, \alpha), \quad (1.6.15)$$

where  $\alpha$  labels the entrance channel, that is, the nuclei  $a$  and  $A$  in their ground state. The cross section for the reaction  $\alpha \rightarrow \beta$  is

$$\left( \frac{d\sigma}{d\Omega} \right)_{\alpha \rightarrow \beta} \sim |a_\beta(t = +\infty)|^2, \quad (1.6.16)$$

Let us now solve the coupled equations in first order perturbation theory. For this purpose we insert  $\delta(\gamma, \alpha)$  at the place of  $a_\gamma(t)$  obtaining

$$\begin{aligned} a_\beta(t) &= \frac{1}{i\hbar} \int_{-\infty}^t \langle \omega_\beta | V_\alpha - U_\alpha | \Psi_\alpha \rangle_{\mathbf{R}_{\beta\alpha}(t)} \exp^{i(E_\beta - E_\alpha)t'/\hbar} dt' \\ &= \frac{1}{i\hbar} \int_{-\infty}^t dt' \langle \Psi_\beta | V_\alpha - U_\alpha | \Psi_\alpha \rangle_{\mathbf{R}_{\beta\alpha}(t)} \exp^{i(E_\beta - E_\alpha)t'/\hbar} \end{aligned} \quad (1.6.17)$$

where the expansion,

$$\omega_\beta = \Psi_\beta - \langle \Psi_\alpha | \Psi_\beta \rangle_{\mathbf{R}_{\beta\alpha}(t)} \quad (1.6.18)$$

has been used, and the ansatz made, that the global optical potentials ( $U$ : real part), and standard nucleon–nucleon interactions  $V$  fulfill the relation

$$\langle \Psi_\alpha | V_\alpha - U_\alpha | \Psi_\alpha \rangle = 0. \quad (1.6.19)$$

It is of notice that the overlap appearing in Eq. (1.6.18) can, in the case of a two-particle transfer reaction

$$\alpha \equiv a (= b + 2) + A \rightarrow b + B (= A + 2) \equiv \beta, \quad (1.6.20)$$

contribute with an amplitude  $\langle \Psi_\beta | \mathbb{1} | \Psi_\gamma \rangle \langle \Psi_\gamma | V_\alpha - U_\alpha | \Psi_\alpha \rangle$ , where  $\mathbb{1}$  is the unit operator, while  $\gamma \equiv f (= b + 1) + F (= A + 1)$ , denotes the mass partition of the

intermediate channel. The above expression strongly suggests that a consistent description of two-transfer reactions in a non-orthogonal basis involves, at least, three strongly interweaved reaction channels (as testified by the fact that they can be shifted around by changing representation, that is post-post, prior-prior, and prior-post, see e.g. Eq. (1.6.2) as well as Fig. 5.C.2), namely  $\alpha$ ,  $\gamma$  and  $\beta$  and consequently has to be calculated, at least, to second order of perturbation theory, that is, including simultaneous and successive transfer and non-orthogonality corrections.

Let us now return to the sum-rule subject considering, for simplicity, the simultaneous transfer amplitude (1.6.17) (see also Sect. 5.C Eq. 5.C.4). That is,

$$\begin{aligned} a^{(1)}(t = +\infty) &= \frac{1}{i\hbar} \int_{-\infty}^{\infty} dt \exp\left[\frac{i}{\hbar}(E^{bB} - E^{aA})t + \gamma_{\beta\alpha}(t)\right] \\ &\times \langle \phi^{B(A)}(\mathbf{r}_{1A}, \mathbf{r}_{2A}) | U(r_{1b}) | e^{\sigma_{\beta\alpha}} \phi^{a(b)}(\mathbf{r}_{1b}, \mathbf{r}_{2b}) \rangle_{\mathbf{R}_{\alpha\beta}(t)}, \end{aligned} \quad (1.6.21)$$

where

$$\sigma_{\beta\alpha} = \frac{1}{\hbar} \frac{m_n}{m_A} (m_{aA} \mathbf{v}_{aA}(t) + m_{bB} \mathbf{v}_{bB}(t)) \cdot (\mathbf{r}_\alpha - \mathbf{r}_\beta), \quad (1.6.22)$$

takes care of recoil effects, the phase factor  $e^{\sigma_{\beta\alpha}}$  being a generalized Galilean transformation associated with the mismatch between entrance and exit channels, while the phase

$$\begin{aligned} \gamma_{\beta\alpha}(t) &= \int_0^t dt' \left\{ U_\beta(\mathbf{R}_\beta(t')) - \frac{1}{2} m_\beta v_\beta^2(t') - U_\alpha(\mathbf{R}_\alpha(t')) + \frac{1}{2} m_\alpha v_\alpha^2(t') \right\} \\ &+ \frac{1}{2\hbar} (m_\alpha \mathbf{v}_\alpha(t) + m_\beta \mathbf{v}_\beta(t)) \cdot (\mathbf{R}_\beta(t) - \mathbf{R}_\alpha(t)), \end{aligned} \quad (1.6.23)$$

is related to the effective  $Q$ -value of the reaction.

The rate of change of the formfactor  $\langle \phi^{B(A)}, U(r_{1b}) e^{i\sigma_{\beta\alpha}} \phi^{a(b)} \rangle$  with time is slow, being completely overshadowed by the rapidly varying phase factor  $\exp\left[\frac{i}{\hbar}(E^{bB} - E^{aA})t + \gamma_{\beta\alpha}(t)\right]$ . Similar relations concerning recoil and  $Q$ -value effects can be obtained from the amplitudes associated to successive and to non-orthogonality terms i.e.  $a^{(2)}(\infty)$  and  $a^{(NO)}$  (see Ch. 5, Sect. 5.C).

Summing up, to compare two-nucleon transfer cross sections on equal structural footing, one has to eliminate the kinematical oscillating phase which can completely distort the “intrinsic” (reduced matrix element) value of the two-nucleon cross section. And for that, one has to work on each of the three amplitudes to extract at best the phases which couple relative and intrinsic motion.

Let us make a parallel with the sum rule associated with electromagnetic decay (Coulomb excitation,  $\gamma$ -decay). The absolute transition probability for absorption (emission) of a photon from nuclear dipole states is measured in  $\text{sec}^{-1}$  by (Bohr and Mottelson (1969))

$$T(E1) = (1.59 \times 10^{15}) \times (E)^3 \times B(E1), \quad (1.6.24)$$

where  $E$  is the energy of the transition and  $B(E1)$  the reduced transition probability. It is this quantity that enters the TRK-sum rule,

$$S(E1) = \langle 0 | [[H, \mathcal{M}(E1)], \mathcal{M}(E1)] | 0 \rangle / 2, \quad (1.6.25)$$

and not  $T(E1)$ . Now, in this particular case the  $Q$ -value dependence of the observed absolute transition probabilities can be eliminated analitically ( $E^3$  dependence), as well as the overall factor ( $1.59 \times 10^{15}$ ), in keeping with the fact that the mass partition ( $a + A \rightarrow a + A^*$ ) as well as the overall factor does not change between entrance and exit channels or, equivalently, the coordinate of relative motion  $\mathbf{R}_{\alpha\alpha'}(t)$  is always that describing the relative center of mass position of target and projectile. This fact allows for a complete separation between structure and reaction (kinematics), explicit in the general expression of  $T(E\lambda)$ , that is,

$$T(E\lambda; I_1 \rightarrow I_2) = \left( \frac{8\pi(\lambda+1)}{\lambda[(2\lambda+1)!!]^2} \frac{1}{\hbar} q^{2\lambda+1} \right) (B(E\lambda; I_1 \rightarrow I_2)), \quad (1.6.26)$$

where  $\mathbf{q}$  is the momentum of the photon, and

$$B(E\lambda; I_1 \rightarrow I_2) = \frac{\langle I_2 | \mathcal{M}(E\lambda) | I_1 \rangle}{\sqrt{2I_1 + 1}}, \quad (1.6.27)$$

the reduced transition probability. Thus, the first factor in the expression of  $T(E\lambda)$  contains all the kinematics (reaction) of the process, the second one the nuclear structure part of it. In the above relation, the multipole tensor is defined as,

$$\mathcal{M}(E\lambda, \mu) = \int \rho(\mathbf{r}) r^\lambda Y_{\lambda\mu}(\hat{\mathbf{r}}) d\mathbf{r}. \quad (1.6.28)$$

It is of notice that the non-diagonal elements (transition moments) are involved in electric  $\rho_e$  and nuclear ( $\rho$ ) multipole processes ( $\gamma$ -decay, Coulomb excitation, inelastic scattering, etc.).

Returning to the expression of the first order (simultaneous) two-nucleon transfer amplitude  $a^{(1)}(t = +\infty)$  one can only devise empirical protocols to try to extract the  $\gamma$ - and  $\sigma$ -phase dependence (see Eqs. (1.6.21)–(1.6.23)) from it and set all absolute two-nucleon transfer cross sections  $d\sigma/d\Omega \sim |a|^2$  on equal footing regarding kinematics, so as to allow to compare the intrinsic, reduced transition probabilities (structure). In other words, extract the structure information contained in, e.g.,

$$\phi^{B(A)}(\mathbf{r}_{1A}, \mathbf{r}_{2A}) = \langle \mathbf{r}_{1A}, \mathbf{r}_{2A} | \Gamma_1^\dagger(\beta = +2) | \tilde{0} \rangle, \quad (1.6.29)$$

where

$$\Gamma_n^\dagger(\beta = +2) = \sum_k X_k^n [a_k^\dagger a_k^\dagger]_0 - \sum_i Y_i^n [a_i a_i]_0, \quad (1.6.30)$$

is the pair creation addition mode acting on of a closed shell system  $|\tilde{0}\rangle$ , as well as in

$$\phi^{B(A)}(\mathbf{r}_{1A}, \mathbf{r}_{2A}) = \langle \mathbf{r}_{1A}, \mathbf{r}_{2A} | [a_k^\dagger a_k^\dagger]_0 | 0 \rangle, \quad (1.6.31)$$

that is, in the pure two-particle configuration  $|j_k^2(0)\rangle$  describing two nucleons moving in time reversal states of the close shell system  $|0\rangle$ . If one was able to disentangle the  $\gamma$  and  $\sigma$  dependence of  $a^{(1)}$  (as well as that of  $a^{(2)}$  and  $a^{(NO)}$ , see above) from its formfactor dependence, the comparison between the quantities  $\sum_n |c^{(n)}|^2$ ,  $\sum_k |X_k^{(n)}|^2$  and  $\sum_i |Y_i^{(n)}|^2$  could eventually be phrased in terms of exact sum rules. This not being the case, one has to deal with approximate TNTR sum rules. With this proviso in mind, TNTR sum rules are nonetheless quite useful.

## 1.7 Nuclear Field Theory for pedestrians

Nuclear Field Theory (NFT) was tailored after Feynman's graphical version of quantum electrodynamics (QED). It is then natural that in discussing NFT analogies with QED will be recurrent. Pairing is important in atomic nuclei, and Cooper pairs play a central role both in open and in closed shell nuclei. In the first case through condensation and superfluidity, closely connected with the observation of pairing rotational bands. In the second case, through collective pairing vibrations which change particle number in two<sup>48</sup>. It is then also natural that references to BCS and Cooper condensation and tunneling are widely used in this monograph<sup>49</sup>. Arguably, as a consequence of special relativity which put an end to the concept of ether, the field-free and matter-free vacuum was rightly considered as *bona fide* empty space. The advent of quantum mechanics changed this situation, the vacuum becoming populated. In quantum mechanics an oscillator, for example, cannot be at rest. The oscillatory nature of the radiation field requires zero point fluctuations (ZPF) of the electromagnetic fields in the vacuum state of lower energy. The occupation of the negative kinetic energy electron states and the subsequent calculation of the cross section for pair creation by photons in the Coulomb field of atomic nuclei, (the nuclear particle-hole excitations), contribute another step in the understanding of the QED vacuum.

When the fields are expressed in terms of creation and annihilation operators, the fermion and boson fields in its simple form consists on the product of two fermion creation or destruction operator  $a^\dagger$  or  $a$  and one boson operator  $\Gamma^\dagger$  or  $\Gamma$ : e.g.  $a_\nu^\dagger a_\nu \Gamma_a^\dagger$ , (see Fig. 1.7.1). That is, bilinear in the fermion fields and linear in the boson fields.

---

<sup>48</sup>For details concerning pairing rotations and vibrations we refer to Bès and Broglia (1977) and Brink, D. and Broglia (2005) Chs. 4 and 5 respectively, and refs. therein.

<sup>49</sup>Within this context see Broglia, R. A. and Zelevinsky, V. (2013)

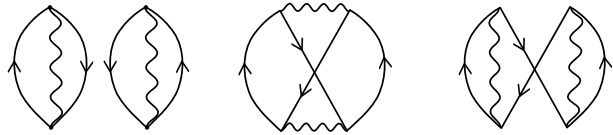


Figure 1.7.1: Oyster diagrams describing the correlation of the nuclear ground state associated with the ZPF of a collective particle–hole excitation is built, and Pauli principle correction processes in which fermions are exchanged.

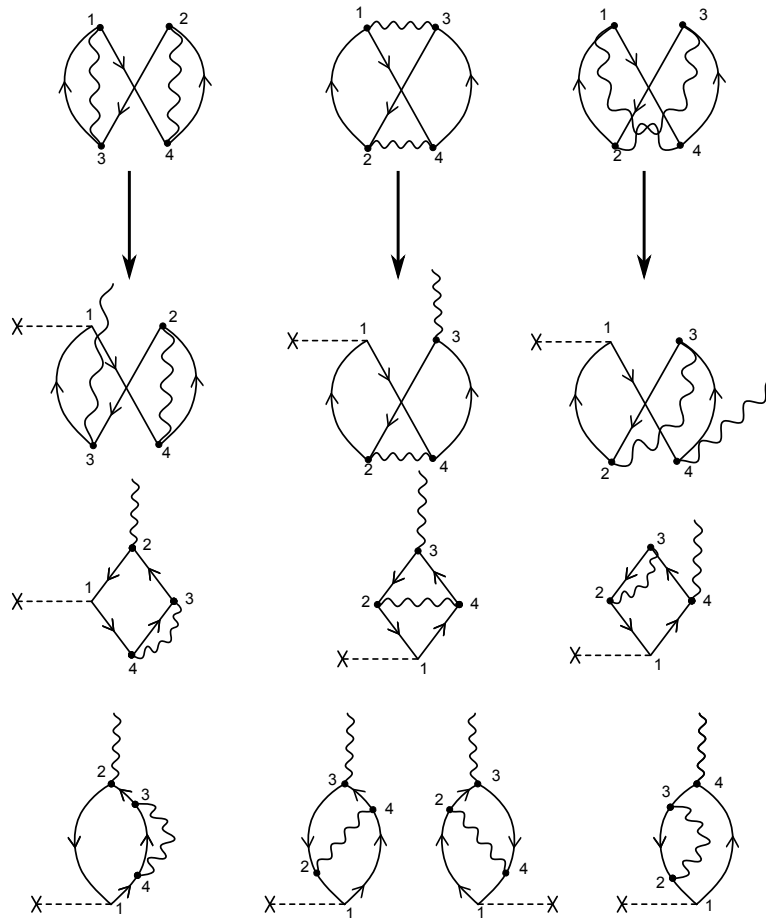


Figure 1.7.2: Some of the possible outcomes resulting from acting with a single-particle field, e.g. that associated with inelastic processes (represented by a horizontal dashed line starting with a  $\times$ ), on the Pauli corrected ZPF oyster diagrams associated with collective ( $p - h$ ) excitations of the nuclear vacuum (see also Fig. 1.7.1). It is of notice the care with which the contribution of the collective states have to be selected, only ones which can be accurately calculated. Within this context one returns to the question of empirical renormalization mentioned in the text (see Sect. 1.4, cf. also Idini et al. (2015), Broglia et al. (2016)).

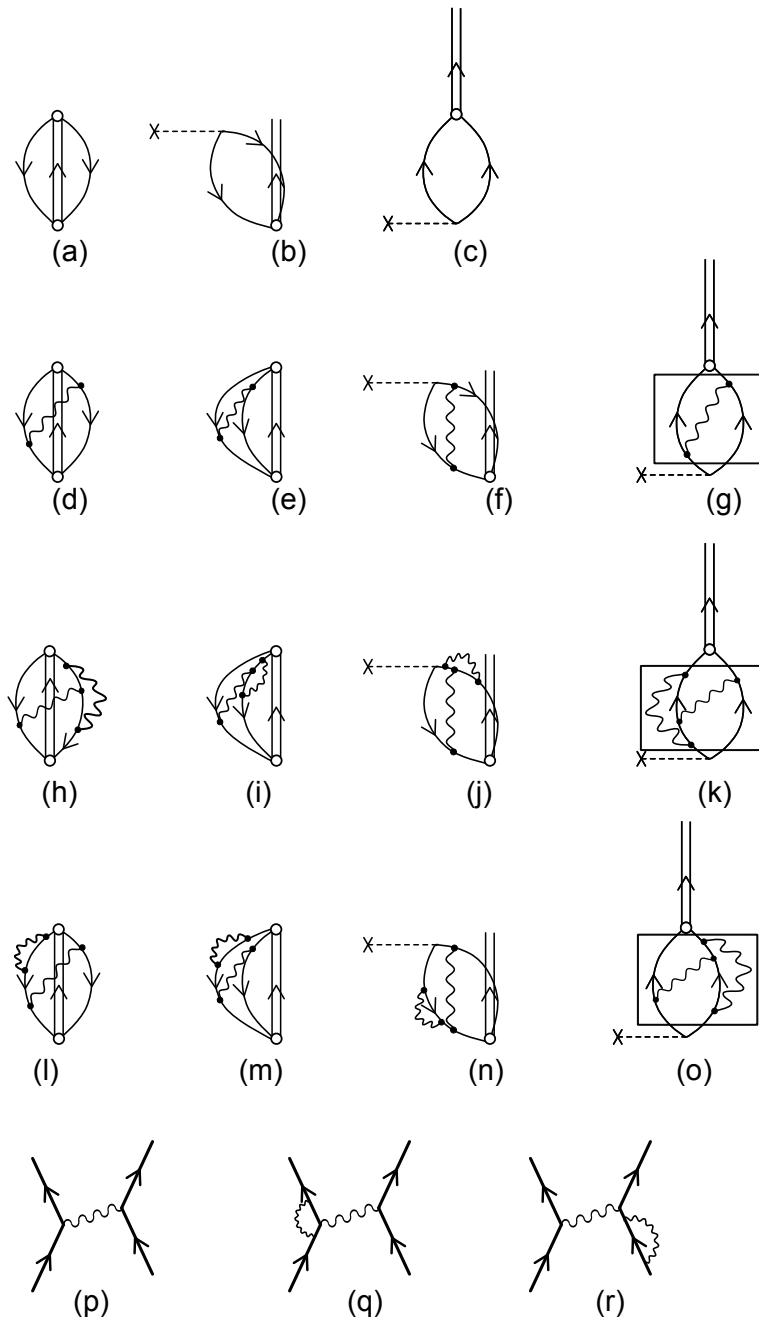


Figure 1.7.3: ZPF associated with the pair addition mode taking into account the interweaving of nucleons with density modes. The processes boxed in (g), (k) and (o), are associated with the induced pairing interaction (medium polarization effects; (p), (q), (r)) resulting from the exchange of density modes between nucleons moving in time reversal states. The two-nucleon stripping and pickup external field is labeled by a dashed horizontal line which starts with a  $\times$ .

A detailed graphical NFT treatment of the vacuum has an important consequence concerning the probing of nuclear structure with reactions. By intervening it with an external field one will excite the modes whose properties can be eventually compared with experiment without further ado.

In other words, if one is in doubt of which are the properly dressed elementary, physical modes of excitation, do not study them, or calculate them and then compare the results with the experimental data. This comes after. One should first find out how to specifically excite the mode in question, by acting with an external field on the ZPF of the vacuum. That is, by carrying out a *gedanken*, NFT-like *experiment* as in Fig. 1.7.2 for  $p - h$ -vibrations and in Fig. 1.7.3 regarding pairing vibrations. Because the corresponding processes deal with physical states, they translate with ease into a laboratory setup. In keeping with the fact that the vacuum contains all the information (right physical degrees of freedom) of the quantal system under study, forcing virtual processes associated with vacuum ZPF to become real, one is guaranteed to get, in each instance, the real, dressed, physical particle. Of course, once the *gedanken eksperiment* has provided this information, one should use such properly renormalized modes, in all the rest of the calculations, at the risk of neglecting relevant physics.

Let us now provide a short introduction of NFT for pedestrians and see how the above considerations become concretely implemented<sup>50</sup>

### 1.7.1 The concept of elementary modes of excitation<sup>51</sup>

The Hamiltonian of a many-body system of noninteracting particles, bosons or fermions, can be written as

$$H = \sum_i H_i, \quad (1.7.1)$$

where the summation is over all the particles of the system and where each  $H_i$  depends only on the variables of the  $i$ -th particle. The single-particle Schrödinger equation is

$$H_i \psi_k(\mathbf{r}_i) = \epsilon_k \psi_k(\mathbf{r}_i), \quad (1.7.2)$$

where  $\epsilon_k$  is the single-particle energy eigenvalue and

$$\psi_k(\mathbf{r}_i) \equiv \langle \mathbf{r}_i | a_k^\dagger | 0 \rangle \quad (1.7.3)$$

is the corresponding wave function. The operator  $a_k^\dagger$  creates a particle in the state  $k$  when acting in the vacuum state  $|0\rangle$ . The energy levels of the system are given by the equation

$$E_n = \sum_k n_k \epsilon_k, \quad (1.7.4)$$

---

<sup>50</sup>For details we refer to Bortignon, P. F. et al. (1977) and refs. therein.

<sup>51</sup>Bès and Broglia (1977)

the corresponding eigenstates being

$$|n\rangle = \prod_k \frac{(a_k^\dagger)^{n_k}}{\sqrt{n_k!}} |0\rangle, \quad (1.7.5)$$

where  $n_k = 0$  or  $1$  in the case of fermions and  $n_k = 0, 1, 2, \dots$  in the case of bosons.

Now we consider a system of interacting particles. The Hamiltonian will in this case be

$$H = \sum_i H_i + \frac{1}{2} \sum_{i,j} H_{ij}, \quad (1.7.6)$$

where  $i, j$  label the co-ordinates of the  $i$ -th and  $j$ -th particle.

In some cases it is possible to recast the two-body Hamiltonian in the form

$$H = \sum_r H'_r, \quad (1.7.7)$$

with the associated Schrödinger equation

$$H'_r \psi_r(\zeta) = \epsilon_r \psi_r(\zeta), \quad (1.7.8)$$

$\zeta$  representing a general variable (e.g. the single-particle co-ordinate, the gap parameter, the shape of the nucleus, etc.). The wave function  $\psi_r(\zeta)$  is the  $\zeta$ -co-ordinate representation of the eigenstate  $a_\tau^\dagger |\tilde{0}\rangle$ . The operator  $a_\tau^\dagger$  creates an excitation with the quantum number  $\tau$  when acting in the state  $|\tilde{0}\rangle$ , the vacuum of all the excitations  $\tau$ .

The energy of the levels of the system, or at any rate of the most important ones to determine the physical response of it to external probes, can be written in the form

$$E_m = \sum_\tau n_\tau \epsilon_\tau \quad (1.7.9)$$

The corresponding eigenstate can be written in the same way as before, *i.e.*

$$|n\rangle = \prod_\tau \frac{(a_\tau^\dagger)^{n_\tau}}{\sqrt{n_\tau!}} |\tilde{0}\rangle. \quad (1.7.10)$$

Additivity features similar to (1.7.9) hold for other physical quantities, *i.e.*

$$\langle n|O|m\rangle = \sum_\tau A_\tau \sqrt{n_\tau} \delta(n_\tau, m_\tau + 1), \quad (1.7.11)$$

where

$$O = \sum_\tau A_\tau a_\tau^\dagger \quad (1.7.12)$$

is the operator which specifically excites the eigenstates described by  $\psi_\tau(\xi)$ . Because the excitation energies  $E_m$  and observables  $|\langle m' | O | m \rangle|^2$  (e.g. two-particle transfer cross-section, electromagnetic-transition probabilities, etc.) are linear combinations of  $\epsilon_\tau$  and  $A_\tau$ , respectively, the eigenstates with energy  $\epsilon_\tau$  and associated observable  $A_\tau$  are called the *elementary excitations of the system*.

There lie thus two ideas behind the concept of elementary excitations<sup>52</sup>. First, there is the idea that the total binding energy, although an important quantity by itself, does not have much to do with the behaviour of the physical system. Thus, the state  $|\tilde{0}\rangle$  is assumed to exist but to act only as a background whose detailed intrinsic structure one does not need to know to describe the behaviour of the system. What is important is the behaviour of the lower excited states relative to the ground state. The second idea is that the low-lying states often are of a particular simple character, and are amenable to a simple and rigorous mathematical treatment. With the help of experimental probes which couple weakly to the nucleus, i.e. in such a way that the system can be expressed in terms of the properties of the excitation in the absence of probes, it has been possible to identify the following' elementary excitations in systems around closed shells<sup>53</sup>:

- a) single particle and holes,
- b) shape vibrations,
- c) spin and isospin vibrations and charge exchange modes,
- d) pairing vibrations.

Away from closed shells one has to add to the above modes:

- e) rotations in 3D-space (e.g. quadrupole rotations)
- f) rotations in gauge space (pairing rotations).

Different probes have been utilized in the process of the identification of the different modes. In particular two-neutron transfer reactions induced by tritons and protons have played a central role in unraveling the basic features of the pairing modes.

### 1.7.2 NFT rules and applications

A field theory can be formulated in which the nuclear elementary modes of excitation play the role of the free fields and in which their mutual interweaving

---

<sup>52</sup>This concept was first introduced ,by Landau (Landau, 1941) to describe the spectrum of HeII. It was subsequently utilized in nuclear physics by Bohr and Mottelson Bohr and Mottelson (1969); Bohr, A. and Mottelson (1975) to obtain a unified description of the nuclear spectrum.

<sup>53</sup>The restriction to closed shell nuclei is made to simplify the discussion. The concept of elementary modes of excitation applies equally well to open-shell nuclei.

takes place through the particle–vibration coupling vertices<sup>54</sup>. This theory provides a graphical perturbative approach to obtain the exact solution of the many-body nuclear-structure problem in the product basis  $\psi_\tau(\zeta)\psi_\eta(\Delta)\dots\psi_\gamma(\Gamma)$

Note that the nuclear bosonic fields are built out by utilizing those degrees of freedom (particles and holes) which already exhaust all the nuclear degrees of freedom. It is thus an essential feature of the product basis to be over-complete and to violate the Pauli principle. On the other hand, this basis is directly related to observables of the system. The different experiments project out only one or two of its components.

In what follows we state and apply the nuclear-field-theory rules, to calculate the interactions between the nuclear free fields and the reaction processes between the resulting physical states. This is done for a system with one particle outside closed shells and which displays collective vibrations, in the framework of a two-level model.

### Schematic model

The model considered consists of two single-particle levels, each with degeneracy<sup>55</sup>  $\Omega$  and with a schematic monopole particle–hole interaction coupling the particles in the two levels.

The total Hamiltonian is equal to

$$H = H_{sp} + H_{TB} \quad (1.7.13)$$

where

$$H_{sp} = \frac{\epsilon}{2} N_0, \quad N_0 = \sum_{\sigma=\pm 1, m} \sigma a_{m,\sigma}^\dagger a_{m,\sigma}, \quad (1.7.14)$$

and

$$H_{TB} = -\frac{V}{2} (A^\dagger A + AA^\dagger), \quad A^\dagger = \sum_m a_{m,1}^\dagger a_{m,-1}. \quad (1.7.15)$$

The index  $\sigma$  labels the two levels, while  $m$  labels the degenerate states within each level. The strength of the monopole coupling is denoted by  $V$  and the energy difference between the two levels is  $\epsilon$ . The matrix element of (1.7.15) is given by

$$\langle m, 1; m', -1 | H_{TB} | m'', 1; m''', -1 \rangle = -V \delta(m, m') \delta(m'', m'''). \quad (1.7.16)$$

---

<sup>54</sup>Bohr, A. and Mottelson (1975); Bès et al. (1974); Broglia et al. (1976).

<sup>55</sup>It is of notice the difference of a factor of 2 in the degeneracy of each level as compared to Sect. 2 of Bortignon, P. F. et al. (1977) in which case it is  $2\Omega$ . This is in keeping with the fact that, as a rule,  $\Omega = (2j+1)/2$ .



Figure 1.7.4: Graphical representation of the amplitude of the collective phonon (wavy line) on a given particle–hole excitation  $((m, 1), (m, m - 1))$ . This amplitude can be written in terms of the interaction vertex denoted by  $\Lambda_i$ , and the energy denominator  $\omega_i - \epsilon'$ . The particles (holes) are depicted by upward (downward) going arrowed lines.

### Field-theoretical solutions

The free nuclear and fermion fields are the elementary modes of excitation comprising surface vibrations and single particles, respectively. The boson fields are defined through the random–phase approximation, in terms of particle-hole excitations. The basis utilized to describe the nuclear systems is a product of the different free fields. The closed-shell system of the schematic model under consideration corresponds to the lowest ( $\sigma = -1$ ) level filled with  $\Omega$  particles, While the upper ( $\sigma = 1$ ) level remains empty. The basis particle and hole states are obtained by adding or removing a single particle to/from this closed-shell configuration. The corresponding wave functions and energies, which should include the Hartree–Fock corrections (see Fig. 1.2.1 (a)–(c)) generated by the residual interaction<sup>56</sup>, are

$$\begin{cases} |m, 1\rangle = a_{m,1}^\dagger |0\rangle, & E(m, 1) = \frac{1}{2}(\epsilon + V), \\ |m, -1\rangle = a_{m,-1}^\dagger |0\rangle, & E(m, -1) = \frac{1}{2}(\epsilon + V). \end{cases} \quad (1.7.17)$$

Thus the unperturbed energy for producing a particle-hole excitation with respect to the ground state is

$$\epsilon' = E(m, 1) + E(m, -1) = \epsilon + V. \quad (1.7.18)$$

The contribution  $V$  in (1.7.17) is the Hartree–Fock: contribution to the particle–hole excitation.

---

<sup>56</sup>The Hartree–Fock energy associated with the Hamiltonian (1.7.13) can be obtained from the linearization relation  $[H, a_{\sigma,m}^\dagger] = E(m, \sigma)a_{\sigma,m}^\dagger$  acting on the Hartree–Fock vacuum, which in this case coincides with the single-particle vacuum defined by  $a_{m,-1}^\dagger |0\rangle = a_{m,1} |0\rangle = 0$

If we define the creation operator of the normal modes as

$$\beta_\nu^\dagger = \sum_m \lambda_m^\nu a_{m,1}^\dagger a_{m,-1}, \quad (1.7.19)$$

the linearization equation

$$[H, \beta_\nu^\dagger] = \omega_\nu \beta_\nu^\dagger \quad (1.7.20)$$

yields

$$\begin{cases} \omega_1 = \epsilon' - V\Omega, \\ \omega_\nu = \epsilon' \quad (\nu = 2, 3, \dots, \Omega). \end{cases} \quad (1.7.21)$$

Utilizing (1.7.20) and the normalization condition

$$[\beta_\nu, \beta_{\nu'}] = \delta(\nu, \nu'), \quad (1.7.22)$$

we obtain for the amplitudes associated with the lowest mode

$$\lambda_m^1 = \frac{1}{\sqrt{\Omega}}. \quad (1.7.23)$$

One can also write this amplitude as the ratio between a coupling matrix element and an energy denominator, i.e.

$$\lambda_m^1 = \frac{\Lambda_1}{\omega_1 - \epsilon'} \quad (1.7.24)$$

From (1.7.21), (1.7.23) and (1.7.24) We obtain

$$\Lambda_1 = -V\sqrt{\Omega} \quad (1.7.25)$$

which is the strength with which a particle hole excitation  $(m, 1; m, -1)$  couples to the collective phonon (see Fig. 1.7.4). This can also be seen by calculating the matrix element of the interaction Hamiltonian (1.7.15) between the normal modes and the single particle-hole state

$$\Lambda_\nu = \langle n_\nu = 1 | H_{TB} | m, 1; m', -1 \rangle = -V\sqrt{\Omega}\delta(m, m')\delta(\nu, 1). \quad (1.7.26)$$

Note that the particle–vibration coupling strengths associated with the other normal modes lying at an energy  $\epsilon'$  are equal to zero. As shown in ref. [Bès et al. (1974); Broglia et al. (1976)], the exact solution of (1.7.13) is reproduced by utilizing as the basic degrees of freedom both the vibrations (see (1.7.21)) and the particles (see (1.7.17)) coupled through the interactions (1.7.16) (four–point vertex) and (1.7.26) (particle–vibration coupling). A significant part of the original interaction has already been included in generating the collective mode (1.7.21). This implies that the rules for evaluating the effect of the couplings (1.7.16) and (1.7.26) between fermions and bosons involve a number of restrictions as compared with the usual rules of perturbation theory that are to be utilized in evaluating the effect of the original interaction (1.7.15) acting in a fermion space. They read as follows:

- I) In initial and final states, proper diagrams involve collective modes and particle modes, but not any particle configuration that can be replaced by a combination of collective modes. This restriction permits an initial state comprising the configuration  $(n_v = 1; m)$ , but excludes  $(m, 1; m : m', 1)$ .
- II) The couplings (1.7.16) and (1.7.26) are allowed to act in all orders to generate the different diagrams of perturbation theory; the restriction I) does not apply to internal lines of these diagrams.
- III) The internal lines of diagrams are, however, restricted by the exclusion of diagrams in which a particle-hole pair is created and subsequently annihilated without having participated in subsequent interactions.
- IV) The energies of the uncoupled particle and phonon fields are to be calculated by utilizing the Hartree-Fock approximation (see eq. (1.7.17)) and the RPA (see eq. (1.7.21)), respectively. The contributions of all allowed diagrams are evaluated by the usual rules of perturbation theory.

We note that the external fields acting on the system are allowed to create any state which may generate the different diagrams of perturbation theory. The corresponding matrix elements should be weighted with the amplitude of the component through which the final state is excited. The above rules are also valid for those situations which cannot be treated in perturbation theory and where a full diagonalization is called for. Thus, *e.g.*, when the system displays a spurious state (see sect. 1.7.3). In what follows we discuss the energy of the  $2p - 1h$ -like excitations. We distinguish between two types of states, namely

$$|n_i = 1; m, 1\rangle, \quad \begin{cases} \omega_1 = \epsilon' - V\Omega, & \Lambda_1 = -\sqrt{\Omega}V \\ & (i = 1; m = 1, 2, \dots, \Omega), \\ \omega_i = \epsilon', & \Lambda_i = 0 \\ & (i = 2, \dots, \Omega; m = 1, 2, \dots, \Omega), \end{cases} \quad (1.7.27)$$

and<sup>57</sup>

$$|m, 1; m, -1; m', 1\rangle, \quad \epsilon' \quad (m, m' = 1, 2, \dots, \Omega). \quad (1.7.28)$$

The physical states are to be written as

$$|qm\rangle = \sum \xi_{iqm} |n_1 = 1; m, 1\rangle, \quad (1.7.29)$$

as (1.7.28) cannot be basis states according to rule I), but only intermediate states. The quantities  $\xi_{iqm}$  are the amplitudes of the physical state in the different components of the product basis of elementary excitations. The model space contains  $\Omega^2$  states, While the correct number is  $\Omega - 1$ . Thus the basis  $|n_1 = 1; m, 1\rangle$  contains  $\Omega$

---

<sup>57</sup>Since the states (1.7.28) are restricted to be intermediate states of the perturbation expansion, the configuration  $(m, 1; m, -1; m', 1)$  is allowed.

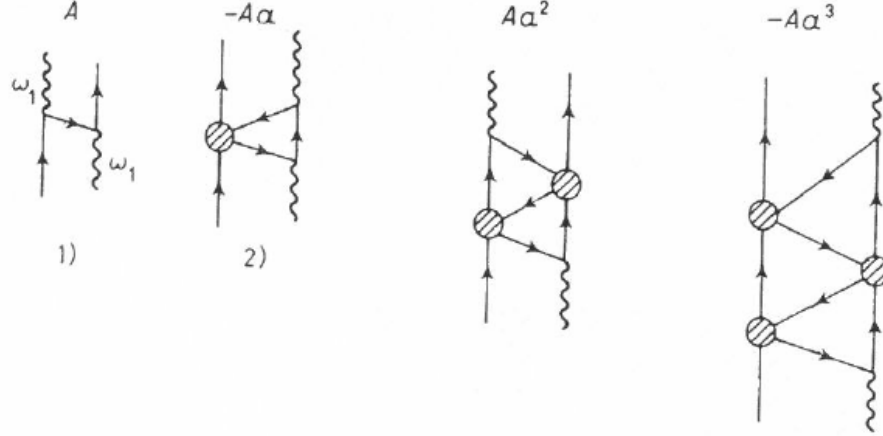


Figure 1.7.5: Contributions to the interaction of a fermion and a collective boson  $\omega_i$  to order  $1/\Omega^4$ . The secular equation  $E - E^{(0)} = A \sum_n a^n (-1)^n$  is given in terms of the quantities  $A = 4\Omega V 23/(3\epsilon' - 2E)$  and  $a = 2V/(3\epsilon' - 2E)$ .

spurious states. Its origin can be traced back to the violation of the Pauli principle (see also sect. 1.7.3). To obtain the energy of  $|qm\rangle$  we have to allow the states  $|n_1 = 1; m, 1\rangle$  to interact through the vertices (1.7.16) and (1.7.26) and generate all the different perturbation theory diagrams (see rule II)) except those containing bubbles (see rule III)).

The different graphical contributions calculated in the framework of the Brillouin–Wigner perturbation theory are displayed in fig. 1.7.5. There is only one (diagonal) matrix element given by a single summation, which can be carried to all orders in the interaction vertices, and can be written as

$$X_{ii'} = A \sum_n (-1)^n a^n \delta(i, i') = \quad (1.7.30)$$

$$= \frac{A}{1 + a} \delta(i, i') \delta(n, 1) = -K(E) (\sqrt{\Omega} V)^2 \delta(i, i') \delta(i, 1), \quad (1.7.31)$$

where  $a$  and  $A$  are defined in the caption to the figure and

$$K(E) = \left(\frac{3}{2}\epsilon' - E + V\right)^{-1} \quad (1.7.32)$$

is the effective coupling strength. The associated secular equation

$$|(\omega_i - E)\delta(i, i') + X_{ii'}| = 0 \quad (1.7.33)$$

is equivalent to the dispersion relation

$$\frac{1}{K(E)} = \sum_i \frac{(\sqrt{\Omega} V)^2}{\omega_i - E} \delta(i, 1). \quad (1.7.34)$$

Thus the energies of the system are determined by the equation

$$E = \omega_1 + \frac{\Omega V^2}{\frac{3}{2}\epsilon' - E + V}. \quad (1.7.35)$$

It admits the two solutions

$$E_{qm} = \begin{cases} \frac{3}{2}\epsilon', \\ \frac{1}{2}\epsilon' + \omega_1 + V = \frac{3}{2}\epsilon' - \Omega V + V, \end{cases} \quad (1.7.36)$$

and agree with the exact value<sup>58</sup>.

Because  $A = 0$  for  $i \neq 1$ , there is no summation in (1.7.29) and

$$|qm\rangle = N_{qm}^2 |n_1 = 1; m, 1\rangle, \quad (1.7.37)$$

Where

$$1 = N_{qm}^2 \left( 1 - \frac{\partial X_{11}}{\partial E} \right) = N_{qm}^2 \left( 1 - \frac{\Omega V^2}{\left( \frac{3}{2}\epsilon' - E + V \right)^2} \right) \quad (1.7.38)$$

For  $E_{qm} = \frac{1}{2}\epsilon' + \omega_1 + V$  we obtain

$$N_{qm}^2 = \frac{\Omega}{\Omega - 1}, \quad (1.7.39)$$

while for  $E_{qm} = \frac{3}{2}\epsilon'$  the state is nonnormalizable as the quantity in parentheses in (1.7.38) is either negative ( $\Omega > 1$ ) or zero ( $\Omega = 1$ ). The state defined by

$$|q, m\rangle = \sqrt{\frac{\Omega}{\Omega - 1}} |n_1 = 1; m, 1\rangle \quad (1.7.40)$$

and

$$E_{qm} = \frac{1}{2}\epsilon' + \omega_1 + V = \frac{3}{2}\epsilon' - V(\Omega - 1) \quad (1.7.41)$$

exhausts the inelastic sum rule in agreement with the exact results. Note that (1.7.40) is specifically excited in inelastic processes, as can be seen by direct inspection. The external inelastic field can act in two ways, exciting either a particle-hole pair or a phonon, with amplitudes

$$\langle m, 1; m', -1 | A_1^\dagger | 0 \rangle = \delta(m, m') \quad (1.7.42)$$

and

$$\langle n_i = 1 | A_1^\dagger | 0 \rangle = \sqrt{\Omega} \delta(i, 1) \quad (1.7.43)$$

---

<sup>58</sup>The exact solutions can be easily obtained by noting that the operators  $A^\dagger, A$  and  $\frac{1}{2}N_0$  are generators of the  $SU_2$  group (see Bortignon, P. F. et al. (1977)).

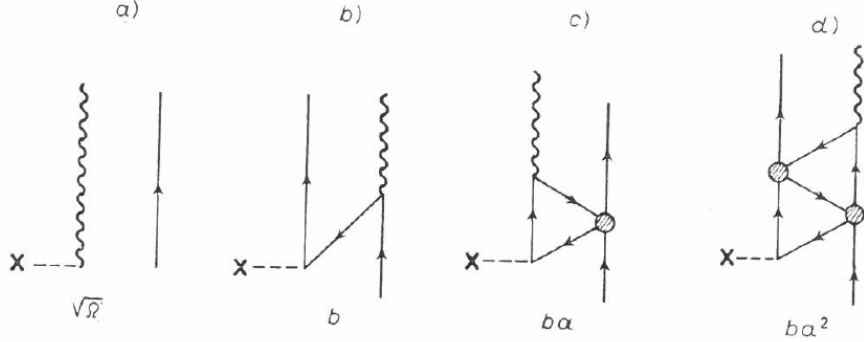


Figure 1.7.6: Grapical representation of the different terms contributing to the matrix element of the transfer operator  $\sqrt{\Omega}A_1^\dagger$  up to order  $1/\Omega^3$ . Note that the different contributions b),c), etc. have a one-to-one correspondence with the different contributions to  $E$  (see fig 1.7.5).  $a = -2V/(3\epsilon' - 2E)$ ,  $b = 2\Lambda_1/(3\epsilon' - 2E)$ .

respectively. The different graphical contributions to the inelastic-scattering process are displayed in Fig. 20, and can again be summed to all orders in the interaction vertices giving

$$\langle n_1 = 1; m, 1 | A_1^\dagger | m, 1 \rangle = \sqrt{\Omega} + \frac{\Lambda_1}{\frac{3}{2}\epsilon' - E_{qm} + V}. \quad (1.7.44)$$

For  $E_{qm} = \frac{3}{2}\epsilon'$  this quantity is equal to zero. Thus, the corresponding states do not carry any inelastic strength, a feature which is closely related to the fact that they cannot be normalized and that they do not display any correlation energy<sup>59</sup>. On the other hand, the matrix element associated with (1.7.40) is

$$\langle qm | A_1^\dagger | m, 1 \rangle = \sqrt{\frac{\Omega}{\Omega - 1}} \frac{\Omega - 1}{\sqrt{\Omega}} = \sqrt{\Omega - 1} \quad (1.7.45)$$

which agrees with the exact answer. The results (1.7.41) and (1.7.45) can be traced down to Pauli-principle corrections. In fact, the state  $|n_i = 1; m, 1\rangle$  has a nonvanishing matrix element, implying a single particle-vibration coupling vertex, with the state  $|m, 1; m, -1; m, 1\rangle$ . This component, which is spurious, is removed by the different graphs displayed in fig. 1.7.5 and 1.7.6. The presence of the odd particle  $(m, 1)$  blocks the particle-hole excitation  $(m, 1; m, -1)$  which was present in the uncoupled system. Thus the system increases its energy by a quantity  $V$ . The reduction of the inelastic amplitude from  $\sqrt{\Omega}$  to  $\sqrt{\Omega - 1}$  also indicates that there is one less particle-hole excitation responding to the external probe.

---

<sup>59</sup>Note that, even if  $N(E_{qm} = \epsilon_m) \rightarrow \infty$ , the matrix elements associated with the different transitions tend to zero more rapidly and the final result converges and is equal to zero as expected.

### 1.7.3 Spurious states

While the model space product of elementary modes of excitation discussed in the last section contains  $\Omega^2$  states, only  $\Omega(\Omega - 1)$  are physically possible, the number of spurious states being  $\Omega$ . On the other hand, the agreement between the exact and the nuclear-field-theoretical results shows that the effects of those spurious states are eliminated from all the matrix elements associated with physical observables.

In what follows we show that, in fact, the spurious states are isolated in an explicit way in the nuclear field theory<sup>60</sup>. Their energy coincides with the initial unperturbed energy, while all physical operators have zero off-diagonal matrix elements between any physical state and a spurious state, in particular the unit operator, which measures the overlap of the two types of states. For this purpose we use again a schematic model consisting in a number,  $\Omega$ , of single-particle levels in which particles interact by means of a “monopole” force,

$$H = H_{sp} + H_{int}, \quad (1.7.46)$$

where

$$H_{sp} = \frac{1}{2} \sum_{m=1}^{\Omega} \epsilon_m (a_{m,1}^\dagger a_{m,1} - a_{m,-1}^\dagger a_{m,-1}), \quad (1.7.47)$$

and

$$H_{int} = -VA^\dagger A, \quad (1.7.48)$$

with

$$a^\dagger = \sum_{m=1}^{\Omega} a_{m,1}^\dagger a_{m,1}. \quad (1.7.49)$$

The energy of the  $i$ -th phonon is determined by the RPA dispersion relation (see rule IV))

$$\sum_{m=1}^{\Omega} \frac{1}{\epsilon_m - \omega_i} = \frac{1}{V}. \quad (1.7.50)$$

The eigenfunction corresponding to the different modes is

$$|n_i = 1\rangle = \sum_m \frac{\Lambda_i}{\epsilon_m - \omega_i} a_{m,1}^\dagger a_{m,-1} |0\rangle. \quad (1.7.51)$$

The particle-vibration coupling constant is given by

$$\Lambda_i = -\langle n_i = 1 | H_{int} | m, 1; m', -1 \rangle = \left[ \sum_m \frac{1}{(\epsilon_m - \omega_i)^2} \right]^{-\frac{1}{2}} \delta(n, n'), \quad (1.7.52)$$

---

<sup>60</sup>Broglio et al. (1976)

where  $|n_i = 1\rangle$  denotes a state containing one phonon, while  $|m, 1; m, -1\rangle$  is the eigenstate associated with particle-hole excitation. The other interaction to be included (rule II)) is the four-point vertex which has the value

$$\langle m, 1; m', -1 | H_{int} | m'', 1; m', -1 \rangle = -V\delta(m, m')\delta(m'', m''). \quad (1.7.53)$$

The single-particle energies to be used in calculating the different graphs are  $\frac{1}{2}\epsilon_m$ , as the Hartree-Fock contribution (see rule IV)) of  $H_{int}$  is zero.

Similarly to  $H_{int}$  the “inelastic operator” has two different matrix elements, namely

$$\langle n_i = 1 | a_{m',1}^\dagger a_{m',-1} | 0 \rangle = \frac{\Lambda_i}{\epsilon_{m'} - \omega_i} \quad (1.7.54)$$

and

$$\langle m', 1; m'', -1 | a_{m,1}^\dagger a_{m,-1} | 0 \rangle = \delta(m, m')\delta(m', m''). \quad (1.7.55)$$

In what follows we discuss again the system comprising an odd particle, in the orbit  $(m, 1)$ , in addition to a single phonon excitation of the vacuum. According to rule I) initial and final states may involve both collective mode and particle modes, but not any particle configuration that can be replaced by a combination of collective modes. The exclusion of the states  $|m, 1; m', 1; m', -1\rangle$  eliminates most of the double counting of two-particle, one-hole states. The  $\Omega$  “proper” states of the form  $|n_i = 1; m, 1\rangle$  are allowed. However, there are only  $\Omega - 1$  (two-particle, one-hole) states in which the odd particle is in the state  $(m, 1)$ . Therefore, a spurious state remains in the spectrum of the elementary modes of excitation.

If we displace the zero-point energy of the odd system to  $\frac{1}{2}\epsilon_m$  the unperturbed energy of the basis state  $|n_i = 1; m, 1\rangle$  is  $\omega_i$ .

The lower-order corrections to this energy which do not contain bubbles are drawn in fig. 1.7.7 (I). Iterating these processes to infinite order we obtain the secular equation

$$|(\omega_i - E)\delta(i, i') + X_{ii'}(E)| = 0, \quad (1.7.56)$$

where

$$X_{ii'} = -\frac{\Lambda_i \Lambda_{i'}}{E - \epsilon_m - V} \quad (1.7.57)$$

The different contributions calculated in the framework of the Brillouin-Wigner perturbation theory are energy dependent, and take into account renormalization effects of the states not explicitly included in the calculations. The dispersion relation fixing the energies  $E_m$  of the physical states (see App. 1.C)

$$E - \epsilon_m - V = \sum_{i=1}^{\Omega} \frac{\Lambda_i^2}{\omega_i - E} = F(E) \quad (1.7.58)$$

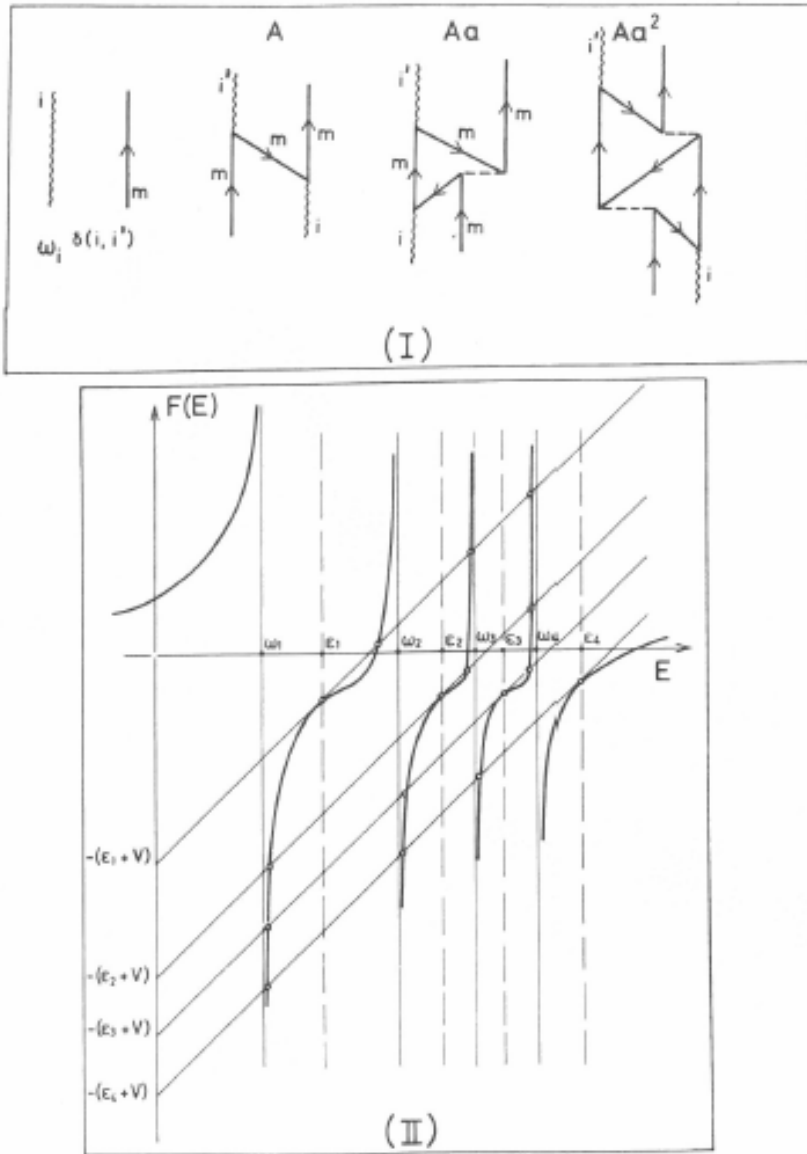


Figure 1.7.7: Lower order contributions to the energy matrix element between the basis states  $|n_i = 1; m, 1\rangle$ . The dashed line stands for the model bare interaction (see eq. 1.7.53). The quantity  $X_{ii'}(E) = A \sum_n a^n = -\Lambda_i \Lambda'_i / (E - \epsilon_m - V)$ , where  $A = -\Lambda_i \Lambda'_i / (E - \epsilon_m)$  and  $a = V / (E - \epsilon_m)$ , is the matrix element iterated to all orders in  $1/\Omega$ . The secular equation of the problem is  $|\omega_i \delta(i, i') + X_{ii'}| = 0$ , and is equivalent to the dispersion relation (1.7.58). II) Graphical solution of the dispersion relation (1.7.58), for the case  $\Omega = 4$ . The function  $F(E) = \sum_i \Lambda_i^2 / (\omega_i - E)$  is displayed as a continuous thick line, while the parallel lines  $E - \epsilon_m - V$  have been drawn as thin continuous lines intersecting the ordinates axis at  $-(\epsilon_m + V)$ . The intersections between the two functions give the eigenvalues of the secular equation. For each value of  $\epsilon_m$  there are  $\Omega + 1$  roots, the root at  $E = \epsilon_m$  being double.

There is one equation for each single-particle level because the monopole force cannot change the m-state of the odd particle. The relation (1.7.58) can be solved graphically as shown in Fig. 1.7.7 (II). The energy  $E = \epsilon_m$  is always a root of (1.7.58), in fact a double root since

$$\left[ \frac{dF(E)}{dE} \right]_{E=\epsilon_m} = \sum_i \frac{\Lambda_i^2}{(\omega_i - \epsilon_m)^2} = 1 \quad (1.7.59)$$

and the line  $E - \epsilon_m - V$  is at  $45^\circ$ . The remaining intersections of this line and the function  $F(E)$  give rise to  $\Omega - 1$  additional roots denoted by  $(qm)$ , whose energy  $E_{qm}$  agrees with the physical eigenvalues obtained from the exact solution of the model. The eigenvectors associated with the physical states  $(qm)$  are

$$|qm\rangle_F = \sum_i \xi_{iqm} |i; m, 1\rangle, \quad (1.7.60)$$

where

$$\xi_{iqm} = -N_{qm} \frac{\Lambda_i}{\omega_i - E_{qm}} = \langle i; m, 1 | qm \rangle_F. \quad (1.7.61)$$

The normalization condition which determines  $N_{qm}$  is

$$\begin{aligned} {}_F\langle qm | qm \rangle_F &= 1 = \sum_{i,i'} \left( \delta(i, i') - \frac{\partial X_{ii'}}{\partial E} \right) \xi_{iqm}^* \xi_{i'qm} = \\ &= N_{qm}^2 \left[ \sum_i \frac{\Lambda_i^2}{(\omega_i - E_{qm})^2} - \frac{1}{(E_{qm} - \epsilon_m - V)^2} \sum_{i,i'} \frac{\Lambda_i^2 \Lambda_{i'}^2}{(\omega_i - E_{qm})(\omega_{i'} - E_{qm})} \right] = \\ &= N_{qm}^2 \left[ \sum_i \frac{\Lambda_i^2}{(\omega_i - E_{qm})^2} - 1 \right], \end{aligned} \quad (1.7.62)$$

where the dispersion relation (1.7.58) has been utilized, and where  $X_{ii'}$  is the matrix element appearing in (1.7.56). For  $E_{qm} = \epsilon_m$  the factor multiplying  $N_{qm}^2$  is zero (see eq. (1.7.59)). Thus, there are only  $\Omega - 1$  states which can be normalized when solving the Hamiltonian (1.7.46) in the framework of the nuclear field theory. The full spuriousity of the elementary-mode product basis is concentrated in a single state<sup>61</sup>.

The subscript  $F$  has been utilized in (1.7.60) to indicate that we are dealing with the nuclear-field solution of the Hamiltonian (1.7.46) (for simplicity it will not be used in the following). Note that these eigenvectors are expressed in terms of only the allowed initial or final states (see rule I)

$$|i; m, 1\rangle \equiv a_{m,1}^\dagger |i\rangle, \quad (1.7.63)$$

---

<sup>61</sup>Note that the mathematical relation  $N^2 f(E) = 1, N^2$ , being the norm of the state with energy  $E$ , implies that such state is spurious if  $f(E) = 0$  or  $f(E) < 0$  (see eq. (1.7.38) and subsequent discussion).

which are assumed to form an orthonormal basis, in particular in deriving the relation (1.7.62). This is equivalent to the basic assumption of the nuclear field theory of the independence of the different modes of excitation, i.e., in the present case,

$$[\Gamma_i, a_{m,1}^\dagger] = 0. \quad (1.7.64)$$

Rules I–IV) discussed in the last section give the proper mathematical framework to this ansatz, which has played a basic role in developing a unified theory of nuclear structure. The above discussion can be illuminated by utilizing a conventional treatment of the residual interaction. Expanding the states  $|n_i = 1; m, 1\rangle$  in terms of particle and hole state, we can write, with the help of (1.7.51)

$$a_{m,1}^\dagger |n_i = 1\rangle = a_{m,1}^\dagger \sum_{m' \neq m} \frac{\Lambda_i}{\epsilon' - \omega_i} a_{m',1}^\dagger |0\rangle \quad (1.7.65)$$

The overlap between the states  $|n_i = 1; m, 1\rangle$  is thus given by

$$\begin{aligned} Z(i, i') &= \langle i' | a_{m,i} a_{m,1}^\dagger \rangle = \\ &= \sum_{m' \neq m} \frac{\Lambda_i \Lambda_{i'}}{(\epsilon_{m'} - \omega_i)(\epsilon_{m'} - \omega_{i'})} = \delta(i, i') - \frac{\Lambda_i \Lambda_{i'}}{(\epsilon_m - \omega_i)(\epsilon_m - \omega_{i'})}, \end{aligned} \quad (1.7.66)$$

where the orthogonality relation

$$\sum_{m'} \frac{\Lambda_i \Lambda_{i'}}{(\epsilon_{m'} - \omega_i)(\epsilon_{m'} - \omega_{i'})} = \delta(i, i') \quad (1.7.67)$$

of the RPA solutions in the even system has been utilized. Because of the nonorthogonality of the basis, the eigenvalues of the system are determined by the relation

$$|Z(E)(H - E)| = 0. \quad (1.7.68)$$

This is fulfilled for

$$|H - E| = 0 \quad (1.7.69)$$

which yields the  $\Omega - 1$  physical roots, as well as for

$$|Z(E)| = 0. \quad (1.7.70)$$

This solution corresponds to the spurious root  $E_{qm} = \epsilon_m$ . In fact,

$$\begin{aligned} \lim_{\delta \rightarrow 0} \sum_i \xi_{iqm}(E_{qm} = \epsilon_m + \delta) Z_{ii'} &= \lim_{\delta \rightarrow 0} N_{qm}(E_{qm} = \epsilon_m + \delta) \\ &\times \sum_i \frac{\Lambda_i}{\omega_i - (\epsilon_m + \delta)} \sum_{m' \neq m} \frac{\Lambda_i \Lambda_{i'}}{(\epsilon_{m'} - \omega_i)(\epsilon_{m'} - \omega_{i'})} = 0, \end{aligned} \quad (1.7.71)$$

since

$$\sum_{m \neq m'} \frac{\Lambda_i \Lambda_{i'}}{(\epsilon_{m'} - \omega_i)(\epsilon_{m'} - \omega_{i'})} = \delta(m, m'). \quad (1.7.72)$$

Note that this solution in terms of the overlap  $Z$  gives the exact answer in the present ease, because of the simplicity of the model. In a general case which includes ground-state correlations this may not be true any longer.

Before discussing the consequences of the above discussion in connection with reaction matrix elements (one-particle transfer amplitudes), let us return to (1.7.62).

The physical amplitudes  $\xi_{iqm}$  are connected to  $\tilde{\xi}_{iqm}$  by the relation

$$\xi_{iqm} = \frac{\tilde{\xi}_{iqm}}{\sqrt{N_{qm}}}. \quad (1.7.73)$$

Thus,

$$N_{qm} = \sum_{i,i'} \left( \delta(i, i') - \frac{\partial X_{ii'}}{\partial E} \right) \tilde{\xi}_{qm}^* \tilde{\xi}_{qm} = \sum_{i,i'} \tilde{M}_{ii'}^{mm} \xi_{qm}^* \xi_{qm} \quad (1.7.74)$$

In usual perturbation theory

$$\frac{\partial X_{ii'}}{\partial E} \xi_{qm}^* \xi_{qm} < 0, \quad (1.7.75)$$

and  $N_{qm}$  is always  $> 1$ . In the present case, however, because the matrix elements of the effective Hamiltonian have to be calculated excluding the contributions containing bubbles, the quantity

$$\sum_{ii'} \frac{\partial X_{ii'}}{\partial E} \xi_{qm}^* \xi_{qm}, \quad (1.7.76)$$

can be either positive, or negative. From the above discussion it can be concluded that  $N_{qm}$  can vanish for certain states, eliminating the redundant degrees of freedom. Examples are discussed in Sect. 1.7.4.

We now calculate the one-particle stripping process leading to the odd system. This calculation illustrates the explicit concentration of the whole spuriousity into a single state which has zero correlation energy<sup>62</sup> and zero amplitude for the different physical processes exciting the  $\Omega - 1$  physical states.

One has first to calculate the amplitude for the transition to a basis component  $(n, = l; m, 1)$  including only those graphs in which all intermediate states are excluded from appearing as initial or final states. reflects the fact that the diagonalization procedure has included all interaction effects that link these allowed states. The final amplitude for the transition to the state  $(qm)$  is obtained by summing

---

<sup>62</sup>This is because the spurious state has zero phase space to correlate.

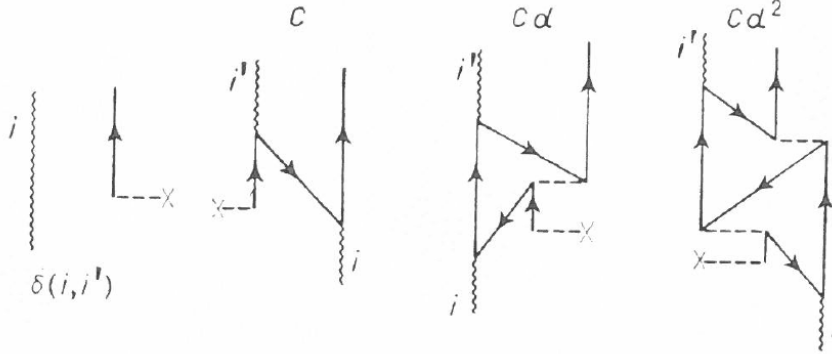


Figure 1.7.8: Lower order contributions to the one-particle transfer reaction induced by  $a_{m,1}^\dagger$ . The result of iterating the different contributions to all orders in  $1/\Omega$  is equal to  $T_{qm}(ii') = C \sum_n d^n = -\Lambda_i \Lambda_{i'} / (\omega_i - \epsilon_m)(E_{qm} - \epsilon_m - V)$ ,  $C = -\Lambda_i \Lambda_{i'} / (\omega_i - \epsilon_m)(E_{qm} - \epsilon_m)$ ,  $d = |V/(E_{qm} - \epsilon_m)|$ .

the amplitudes to  $n = 1; m, 1$  each weighted by the amplitude  $\xi_{iqm}$  given by eq. (1.7.61).

The lower-order contributions to the one-particle transfer amplitude between the state  $|n_i = 1\rangle$  and the state  $|qm\rangle$  are displayed in Fig. 1.7.8. They can be summed up to all orders of  $1/\Omega$ , the result being equal to

$$\begin{aligned}
 & \langle qm | a_{m,1}^\dagger | n_i = 1 \rangle \\
 &= \sum_{i'} \xi_{i'qm} \left\{ \delta(i, i') - \frac{\Lambda_i \Lambda_{i'}}{(\omega_i - \epsilon_m)(E_{qm} - \epsilon_m)} \left[ \frac{1}{1 - V/(E_{qm} - \epsilon_m)} \right] \right\} \\
 &= \sum_{i'} \xi_{i'qm} \{ \delta(i, i') - T_{qm}(i, i') \} = \\
 &= -N_{qm} \left[ \frac{\Lambda_i}{\omega_i - E_{qm}} - \frac{\Lambda_i}{(\omega_i - \epsilon_m)(E_{qm} - \epsilon_m - V)} \sum_{i'} \frac{\Lambda_{i'}^2}{\omega_{i'} - E_{qm}} \right] \\
 &= \frac{N_{qm}(E_{qm} - \epsilon_m)\Lambda_i}{(E_{qm} - \omega_i)(\omega_i - \epsilon_m)}. \tag{1.7.77}
 \end{aligned}$$

This quantity is zero for the spurious roots (*i.e.*  $E_{qm} = \epsilon_m$ ) and agrees with the exact result for the  $\Omega - 1$  remaining physical roots.

Utilizing the relations

$$\frac{1}{V} = \sum_m \frac{1}{\epsilon_m - \omega_i}, \tag{1.7.78}$$

and

$$\frac{1}{V} = \sum_{m \neq m'} \frac{1}{\epsilon_{m'} - E_{qm}}, \tag{1.7.79}$$

we obtain

$$\sum_{m \neq m'} \frac{1}{(\epsilon_{m'} - E_{qm})(\epsilon_{m'} - \omega_i)} = \frac{1}{(E_{qm} - \omega_i)(\epsilon_m - \omega_i)}. \quad (1.7.80)$$

Utilizing this relation we can derive the *one-particle transfer sum rule*. Note that (1.7.78) is the dispersion relation for the free phonon field. The second relation is, however, alien to the field theory results. Nevertheless, one can show that the solutions  $E_{qm}$  of (1.7.79) and of the nuclear–field–theory dispersion relation (1.7.58) are identical, except for the root  $E_{qm} = \epsilon_m$ . One can, therefore, utilize (1.7.79) as a mathematical relation without further justifications in the present context. One obtains

$$\begin{aligned} \sum_{qm} \left| \langle qm | a_{m,1}^\dagger | n_i = 1 \rangle \right|^2 &= \sum_{qm} \Lambda_{qm}^2 \Lambda_i^2 \sum_{m \neq m'} \frac{1}{(\epsilon_{m'} - E_{qm})(\epsilon_{m'} - \omega_i)} \\ &\times \sum_{m \neq m'} \frac{1}{(\epsilon_{m'} - E_{qm})(\epsilon_{m'} - \omega_i)}, \end{aligned} \quad (1.7.81)$$

where

$$\Lambda_{qm} = -N_{qm}(E_{qm} - \epsilon_m) = \left[ \sum_{m \neq m'} \frac{1}{(\epsilon_{m'} - E_{qm})} \right]^{-\frac{1}{2}}. \quad (1.7.82)$$

Thus

$$\sum_{qm} \left| \langle qm | a_{m,1}^\dagger | n_i = 1 \rangle \right|^2 = \Lambda_i^2 \sum_{m \neq m'} \frac{1}{(\epsilon_{m'} - \omega_i)^2} = 1 - \frac{\Lambda_i^2}{(\epsilon_m - \omega_i)^2} \quad (1.7.83)$$

where use has been made of the orthogonality relation

$$\sum_{m \neq m'} \frac{1}{(\epsilon_{m'} - E_{qm})(\epsilon_{m'} - E_{qm})} = \delta(m', m'') \quad (m', m'' \neq m). \quad (1.7.84)$$

The result (1.7.83) coincides with the exact result. Physically it means that the single-particle orbital  $(m, 1)$  is blocked by the amount  $\Lambda_i^2 / (\epsilon_m - \omega_i)^2$ , which is the probability that the phonon ( $n_i = 1$ ) is in the particle-hole configuration  $(m, 1; m, -1)$ , i.e. with its particle in the orbital  $(m, 1)$ .

#### 1.7.4 Applications

In what follows we discuss some aspects of the low-lying spectrum of the nucleus  $^{209}\text{Bi}$  in terms of fermions, surface ( $\beta^\dagger(0\lambda)$ ) and pairing ( $\beta^\dagger(2\lambda)$ ) modes.

The unperturbed states of the closed–shell–plus–one–particle system can be written in terms of the free fields as

$$|n2\lambda, j; IM\rangle = [\beta_n^\dagger(2\lambda)a_j]_{IM}|0\rangle, \quad (1.7.85)$$

and

$$|n0\lambda, j; IM\rangle = [\beta_n^\dagger(0\lambda)a_j^\dagger]_{IM}|0\rangle. \quad (1.7.86)$$

This constitutes the basis set of states  $\{\alpha_i\}$ . All other states give rise to the complementary Hilbert space  $\{a_i\}$ .

The elementary modes of excitation interact through the particle-vibration and four-point vertices displayed in Fig. 1.7.9 giving rise to the matrix elements

$$M_1(nj, n'j') \equiv \langle [\beta_n^\dagger(0\lambda)a_{j'}^\dagger]_{IM} | h_{eff}(E) | [\beta_n^\dagger(0\lambda)a_j^\dagger]_{IM} \rangle, \quad (1.7.87)$$

$$M_2(nj, n'j') \equiv \langle [\beta_{n'}^\dagger(2\lambda)a_{j'}^\dagger]_{IM} | h_{eff}(E) | [\beta_n^\dagger(2\lambda)a_j^\dagger]_{IM} \rangle, \quad (1.7.88)$$

and

$$M_3(nj, n'j') \equiv \langle [\beta_{n'}^\dagger(2\lambda)a_{j'}^\dagger]_{IM} | h_{eff}(E) | [\beta_n^\dagger(0\lambda)a_j^\dagger]_{IM} \rangle. \quad (1.7.89)$$

They are to be calculated by utilizing the graphical techniques of perturbation theory and the rules discussed in sect. 1.7.2. There are two parameters on which to expand upon in carrying out a perturbative calculation. The first one is the strength of the interaction vertices measured in terms of the average distance between single-particle levels. The second is  $1/\Omega$ , where  $\Omega = \sum_j(j + \frac{1}{2})$  is the effective degeneracy of the valence shells. These two parameters are in general connected through involved expressions. In the schematic model discussed in sect. 1.7.2, however, their relation is explicit and can be expressed as

$$\epsilon = O(1), \quad \Lambda = O\left(\frac{1}{\sqrt{\Omega}}\right) \quad \text{and} \quad V = O\left(\frac{1}{\Omega}\right) \quad (1.7.90)$$

Another feature which determines the family of diagrams to select to a given order of perturbation is the number of internal lines which can be freely summed up. Each of these summations introduces a multiplicative factor  $\Omega$ . Because most of the present knowledge on the applicability of the field theoretical techniques rests upon schematic models, we utilize  $1/\Omega$  as the expansion parameter, and assume the relations (1.7.90) to be valid for more general situations. The nucleus  $^{209}\text{Bi}$  has been investigated by means of high-resolution anelastic process<sup>63</sup>. Through these experiments a septuplet of states around 2.6 MeV of excitation was identified, with spins ranging from  $\frac{3}{2}^+$  to  $\frac{15}{2}^+$ .

In zeroth order these states can be interpreted in terms of a proton moving in the  $h_{9/2}$  orbital coupled to the lowest octupole vibration of  $^{208}\text{Pb}$ . The  $\frac{3}{2}^+$  of this multiplet displays also a large parentage based on the proton pair addition and proton hole moving in the  $d_{3/2}$  orbital, as revealed by the  $(t, \alpha)$  reaction on  $^{210}\text{Po}$ <sup>64</sup>.

---

<sup>63</sup>Ungrin et al. (1971), Broglia, R. A. et al. (1970).

<sup>64</sup>Barnes, P. et al. (1972).

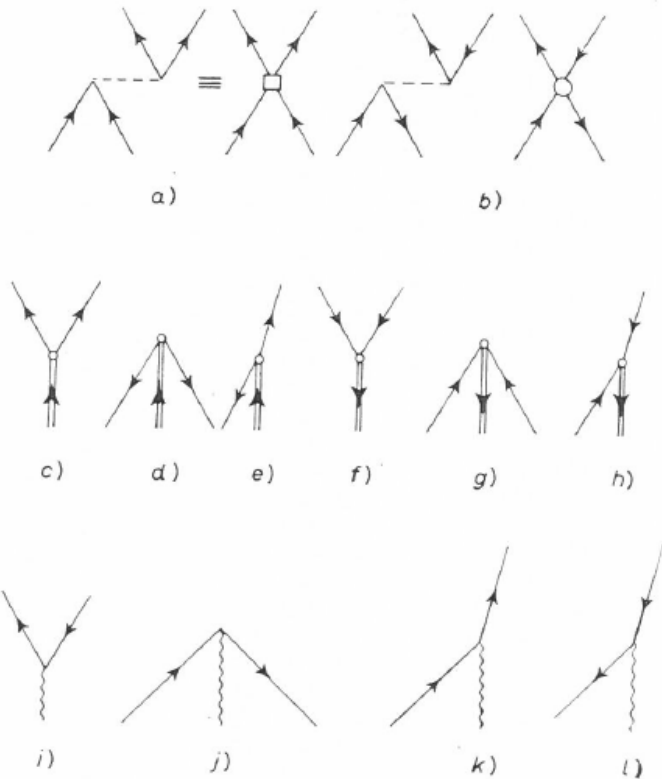


Figure 1.7.9: Interactions coupling the fermion fields with the pairing and surface vibrations. The different fermion and boson free fields are particle, hole, pairing vibration ( $\alpha = 2$ ), pairing vibration ( $\alpha = -2$ ), surface vibration ( $\alpha = 0$ ). The two possible four-point vertices are given in a) and b). They correspond to the pairing and particle-hole model bare interactions. In graphs c)–h) all possible couplings between the fermion fields (arrowed lines) and the pairing vibrational fields (double lines arrowed) are displayed. Graphs i)–l) are all the coupling vertices between the surface vibrations (wavy line) and the fermion fields. Note that there is no direct coupling between the two boson fields, as the field theory we are dealing with is linear in the different field coordinates.

The above results indicate that the (two-particle, one-hole) type of states in  $^{209}\text{Bi}$  are amenable to a simple description in term of the basis states

$$|2\lambda, j_1^{-1}; IM\rangle \equiv |j_1^{-1} \otimes \lambda^\pi(^{210}\text{Po}); IM\rangle \quad (\lambda^\pi = 0^+, 2^+, 4^+) \quad (1.7.91)$$

and

$$|0\lambda, j_2; IM\rangle \equiv |j_2 \otimes \lambda^\pi(^{208}\text{Pb}); IM\rangle \quad (\lambda^\pi = 3^-) \quad (1.7.92)$$

Only the lowest states of each spin and parity  $\lambda^\pi$  are included in the basis states, while all the RPA solutions are included in the intermediate states. The quadrupole surface vibration modes were allowed only as intermediate states. The single hole and particle states  $j_1^{-1}$  and  $j_2$ , respectively, correspond to experimentally known levels around the  $Z = 82$  shell closure. In what follows we discuss the different properties of the states generated by the basis spanned by the eigenvectors  $|2\lambda, j_1^{-1}; IM\rangle$  and  $|0\lambda, j_2; IM\rangle$ . We have divided the discussion in two parts. In the first part the two  $\frac{3}{2}^+$  states built out of the  $|d_{3/2}^{-1} \otimes gs(^{210}\text{Po})\rangle$  and  $|h_{9/2} \otimes 3^-(^{208}\text{Pb})\rangle$  configurations are studied in this space. This two-state system provides a rich laboratory to study the interplay of surface and pairing modes. In the second part the properties of the entire multiplet and of those states strongly excited in either the  $(t, \alpha)$  or  $(d, d')$  reactions are studied, in the complete configuration space.

a) *The  $\frac{3}{2}^+$  states* The two states

$$|1\rangle \equiv |d_{3/2}^{-1} \otimes gs(^{210}\text{Po}); 3/2^+\rangle \quad (1.7.93)$$

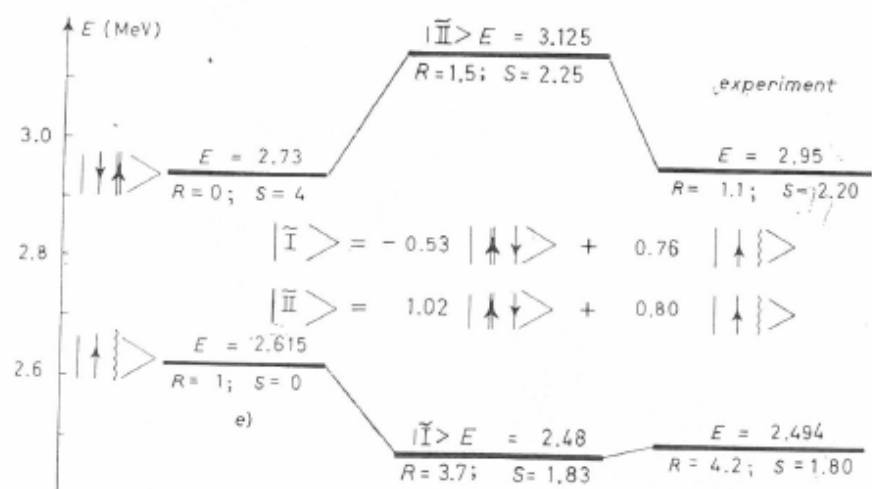
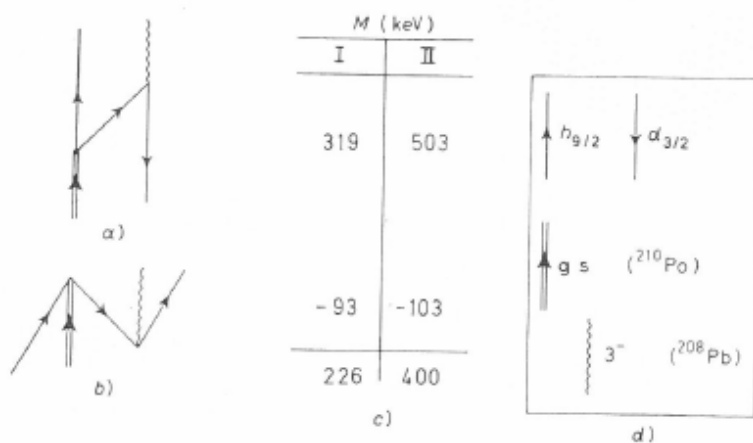
and

$$|2\rangle \equiv |h_{9/2} \otimes 3^-(^{208}\text{Pb}); 3/2^+\rangle \quad (1.7.94)$$

are 118 keV apart. They mix strongly through the couplings depicted by the graphs a) and b) of fig. 1.7.10. Because of the energy dependence of  $h_{eff}$  there is a different matrix element for each final state. The diagonalization of the matrices was carried out self-consistently, *i.e.* the energy denominators of the different graphs are to be calculated by utilizing the exact energies<sup>65</sup>. The corresponding graphical contributions to the spectroscopic factor and inelastic cross-sections are also collected in fig. 1.7.10. To be noted is the very different ratio of the  $(d, d')$  and  $(t, \alpha)$  cross sections. While  $R_1 = B(E3; (\frac{3}{2})_1)/B(E3; (\frac{3}{2})_2)$  is approximately equal to 1, the ratio  $R_2 = \sigma((t, \alpha); (\frac{3}{2})_2)/\sigma((t, \alpha); (\frac{3}{2})_1)$  is close to one. Because the component  $|2\rangle$  carries the inelastic-scattering strength, while the  $(t, \alpha)$  reaction proceeds mainly through the component of type  $|1\rangle$ , the difference between  $R_1$  and  $R_2$  can be traced back to the over-completeness of the basis which give rise to rather different normalizations of the two physical states. (see sect. 1.7.3).

---

<sup>65</sup>for more details, see ref. Bortignon, P. F. et al. (1977).



$$\begin{aligned} & \left\{ -0.53 \begin{bmatrix} \text{---} \\ \text{---} \\ \text{---} \end{bmatrix} + 1.02 \begin{bmatrix} \text{---} \\ \text{---} \\ \text{---} \end{bmatrix} \right\}^2 = 2 \times 10^{-2} \\ & \quad -0.103 \qquad \qquad \qquad 0.135 \\ & \quad -0.103 \qquad \qquad \qquad 0.135 \end{aligned}$$

f)

$$\begin{aligned} & 4 \times \left\{ -0.53 \begin{bmatrix} \text{---} \\ \text{---} \\ \text{---} \end{bmatrix} + 1.02 \begin{bmatrix} \text{---} \\ \text{---} \\ \text{---} \end{bmatrix} \right\}^2 = 1.12 \\ & \quad 1.12 \\ & \quad 4.16 \\ & 4 \times \left\{ -0.53 \begin{bmatrix} \text{---} \\ \text{---} \\ \text{---} \end{bmatrix} + 1.02 \begin{bmatrix} \text{---} \\ \text{---} \\ \text{---} \end{bmatrix} + -0.010 \begin{bmatrix} \text{---} \\ \text{---} \\ \text{---} \end{bmatrix} + -0.011 \begin{bmatrix} \text{---} \\ \text{---} \\ \text{---} \end{bmatrix} \right\}^2 = 1.82 \\ & \quad 1.82 \\ & \quad 2.27 \\ & \quad -0.211 \qquad \qquad \qquad 0.014 \\ & \quad -0.333 \qquad \qquad \qquad 0.015 \end{aligned}$$

g)  
h)

$$\frac{1}{10} \left\{ 0.76 \begin{bmatrix} \text{---} \\ \text{---} \\ \text{---} \end{bmatrix} + 0.80 \begin{bmatrix} \text{---} \\ \text{---} \\ \text{---} \end{bmatrix} \right\}^2 = \frac{1.92 \times 10^{-2}}{2.13 \times 10^{-2}} \quad e^2 b^3$$

( 3.3 % )  
i) ( 3.6 % )

= 0.577

$$\begin{aligned}
& \frac{1}{10} \left[ -0.53 \left[ \begin{array}{c} \text{Diagram 1} \\ \text{Diagram 2} \end{array} \right] + \left[ \begin{array}{c} \text{Diagram 3} \\ \text{Diagram 4} \end{array} \right] \right] + \\
& + \left[ \begin{array}{c} \text{Diagram 5} \\ \text{Diagram 6} \\ \text{Diagram 7} \\ \text{Diagram 8} \\ \text{Diagram 9} \\ \text{Diagram 10} \end{array} \right] + \left[ \begin{array}{c} \text{Diagram 11} \\ \text{Diagram 12} \\ \text{Diagram 13} \\ \text{Diagram 14} \\ \text{Diagram 15} \\ \text{Diagram 16} \end{array} \right] = \\
& = \frac{0.0216}{(e^2 b^3)} \quad (3.7\%) \\
& \quad \quad \quad j) \quad (1.5\%)
\end{aligned}$$

Figure 1.7.10: In a), b) and c) we give the two contributions to the matrix element  $M(E) = \langle d_{3/2}^{-1} \otimes gs(^{210}\text{Po}) | h_{eff}(E) | h_{9/2} \otimes 3^-(^{208}\text{Pb}); 3/2 \rangle$  in lowest order in  $1/\Omega$ . The resulting wave functions  $|I\rangle$  and  $|II\rangle$  are displayed in c) normalized according to (??). In e) we also give the unperturbed, theoretical energies of the levels. The  $(t, \alpha)$  spectroscopic factor corresponding to the reaction  $^{210}\text{Po}(t, \alpha)^{209}\text{Bi}$  is denoted by  $S$ , while

$$R = \frac{d\sigma(h_{9/2} \rightarrow J)}{d\sigma(gs(^{208}\text{Pb}) \rightarrow 3^-(^{208}\text{Pb}))}.$$

is the ratio of inelastic cross sections. In d) we display the free fields. The zeroth and order  $1/\Omega$  contributions to the electromagnetic excitations are collected in i) and j). The value  $0.58e^2b^3$  is the  $B(E3; 0 \rightarrow 3)$  value associated with the 2.615 MeV state in  $^{208}\text{Pb}$ . In g) and h) we give the zeroth and order  $1/\Omega$  contributions to the spectroscopic factor associated with the  $^{210}\text{Po}(t, \alpha)^{209}\text{Bi}$  reaction. Finally in f) we display the lowest contribution to the spectroscopic factor associated with the  $^{208}\text{Pb}(^3\text{He}, d)$  reaction, which gives a measure of the ground state correlations of  $^{208}\text{Pb}$  associated with the existence of an octupole and a pairing vibration.

## 1.8 Competition between the variety of ZPF, in particular those associated with density ( $\beta = 0$ ) and pairing ( $\beta = \pm 2$ )

Particle-hole like vibrations, as e.g. collective surface quadrupole vibrations, induce dynamical distortions of the mean field which virtually break the  $(2j + 1)$  magnetic degeneracy of levels into two-fold (Kramer's) degenerate (Nilsson-like) levels, thus effectively reducing the density of states (DOS) around the Fermi energy. In Fig. 1.8.1 is given a schematic representation of the subtle effects the interweaving of single-particle motion and collective vibrations has on pairing correlations.

Pairing vibrations smooth out the sharp discontinuity of occupancy taking place at the Fermi energy displayed by closed shell systems, thus effectively concentrating into an effective, single  $j$ -shell, through dynamical  $(U_j V_j)$  weighting factors, the global degeneracy of levels in the energy region  $\epsilon_F \pm E_{corr}(\beta = \pm 2)$  (see Fig. 1.8.1 (g)).

Zero point fluctuations induced by particle-hole like and by pairing modes compete with each other for phase space, through Pauli principle (see Fig. 1.8.2), thus eventually leading to a single ground state containing all of the dressed renormalized ZPF (see Sect. 1.7). The Pauli principle NFT diagrams displayed in Figs. 1.8.2 (b) and 1.8.2 (d) are at the basis of the stabilization of the ground state in general and of the competition between (as a rule quadrupole) deformations in 3D space which breaks single-particle degeneracy (Nilsson potential), and in gauge space which thrives on large degeneracies<sup>66</sup>. It is also the reason why single open shell nuclei are usually spherical. When tidal-like polarization effects in doubly open shell nuclei become overwhelming, the nucleus makes use of a Jahn-Teller mechanism. This to profit at best and simultaneously, of the quadrupole-quadrupole (alignment) and of the pairing (independent pair motion in Kramers degenerate levels) interactions. In other words, of potential energy (quadrupole deformation, localization) and of pairs of nucleons solidly anchored to each other (localization), over distances  $\xi(\gg R_0)$  resulting in strongly overlapping entities and thus little sensitive to the orientation of the quadrupole deformed field (small moment of inertia), effect weakened in turn because of low spatial degeneracy. The fact that the moment of inertia  $\mathcal{J}$  of e.g. quadrupole deformed nuclei is found to be appreciably smaller (by about a factor of 2) than the rigid moment of inertia testifies to the role correlations play in nuclei. The fact that  $\mathcal{J}$  is considerably larger than the irrotational moment of inertia (by a factor of 5 cf. Bohr, A. and Mottelson (1975) p. 75) testifies to the subtle effects that spatial quantization, medium polarization effects, let alone the  $NN^{-1} S_0$  potential, eventually corrected by the three-body effects, have in Cooper pair binding.

---

<sup>66</sup>Bayman (1961); Bès and Sorensen (1969); Mottelson (1962); Bohr, A. and Mottelson (1975).

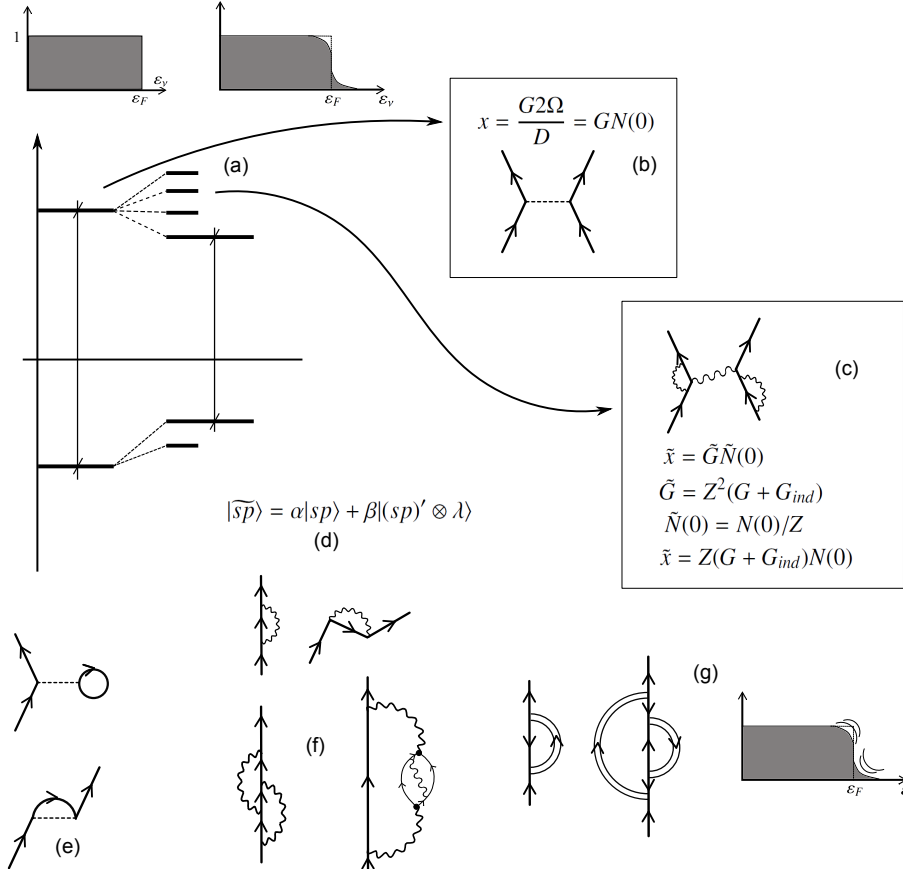


Figure 1.8.1: Schematic representation of some of the consequences the interweaving of the elementary modes of excitation with varied transfer quantum number ( $\beta = 0, \pm 1, \pm 2$ ; **(f)**, **(g)**) have in the (mainly single-particle) nuclear spectrum **(a)** (**e**), in particular pair correlations **(b, c)**, as measured by the (two-level) dimensionless parameter  $x = G2\Omega/D = GN(0)$ , product of the bare coupling constant  $G$  and the density of states (DOS) at the Fermi energy (ratio of the single-particle degeneracy  $2\Omega = (2j+1)$ , and the single-particle energy separation). Coupling with surface modes **(f)** reduce the effective value of  $D$  leading to an increase of  $N(0)$  as measured by  $1/Z$  but, at the same time decreases, through the breaking of the single-particle strength, the single-particle content **(d)** of each level (as measured by  $Z$ ; see e.g. Barranco et al. (2005) and refs. therein). The eventual increase of  $x$ , as reflected by  $\tilde{x}$ , results from a delicate balance of the two effects eventually overwhelmed by the induced pairing interaction resulting from the exchange of collective ( $\beta = 0$ ) vibration between pair of nucleons moving in time reversal states close to the Fermi energy, and by the dynamical smoothing of the Fermi energy by the coupling of single-particle states to  $\beta \pm 2$  pairing vibration **(g)**.

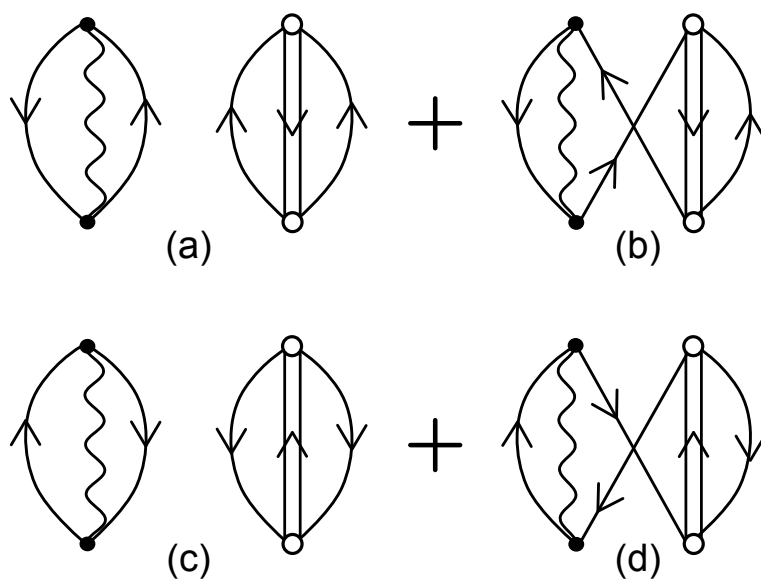


Figure 1.8.2: (a) (c) ZPF associated with  $p-h$  and pairing vibrations (pair subtraction and pair addition modes) make use of the same nucleon degrees of freedom to simultaneously, and independently, correlate  $p-h$ ,  $p-p$  and  $h-h$  excitations, thus violating Pauli principle (harmonic approximation). The NFT processes (b) and (d), which contribute to the correlation energy of the nucleus with opposite sign to that contributed by (a) and (d) (each unavoidable crossing of fermion lines contributes a minus sign), remove Pauli violating contributions to the corresponding order of perturbation.

## 1.9 Optical potential and transfer

### 1.9.1 Bare particles and Hartree–Fock field

Nucleon elastic scattering experiments at energies of tens of MeV can be accurately described in terms of an optical potential in which the real component is parametrized according to the (Woods–Saxon) potential<sup>67</sup>,

$$U(r) = Uf(r), \quad (1.9.1)$$

$f(r)$  being a Fermi (sigmoidal) function, of radius  $R_0 = r_0 A^{1/3}$  ( $r_0 = 1.27$  fm), diffusivity  $a = 0.57$  fm, and strength

$$U = U_0 + 0.4E \quad (1.9.2)$$

where

$$U_0 = \left( -51 + 33 \frac{N-Z}{A} \right) \text{ MeV}, \quad (1.9.3)$$

while  $E$  is the energy of the scattered particle  $\epsilon_k = \hbar^2 k^2 / 2m$ , measured from the Fermi energy. In the case of  ${}^3_3\text{Li}_8$ ,  $U_0 = 42$  MeV. One can replace the  $k$ –dependence in (1.9.2) by the so–called  $k$ –mass<sup>68</sup>

$$m_k = m \left( 1 + \frac{m}{\hbar^2 k} \frac{dU}{dk} \right)^{-1}, \quad (1.9.4)$$

where the energy independent Woods–Saxon potential has a depth given by  $\left(\frac{m}{m_k}\right) U_0 = U'_0$ <sup>69</sup>. For the nucleon of the core, i.e. of  ${}^9\text{Li}$ ,  $m_k = m(1+0.4)^{-1} \approx 0.7m$ . For the halo neutron<sup>70</sup>  $m_k = (1 + \mathcal{O} \times 0.4)^{-1}$ , where  $\mathcal{O} (= (R_0/R)^3)$  is the overlap between the core and the halo nucleons. From the  $R_0 = 2.69$  fm and  $R = 3.6$  fm one obtains  $m_k \approx 0.93 m$ .

---

<sup>67</sup>cf. e.g. Bohr and Mottelson (1969) and refs. therein.

<sup>68</sup>What in nuclear matter is called the  $k$ –mass and is a well defined quantity, in finite systems like the atomic nucleus, in which linear momentum is not a conserved quantity, is introduced to provide a measure of the non-locality of the mean field, and is defined for each state as the expectation value of the quantity inside the parenthesis in Eq. (1.9.4), calculated making use of the corresponding single-particle wavefunction (see e.g. ref. Bernard and Giai (1981), in which case  $m_k$  is referred to as the non-locality effective mass)

<sup>69</sup>See e.g. Fig. 2.14 Mahaux, C. et al. (1985).

<sup>70</sup>Assuming a velocity independent  $v$ , the dependence of the mean field stems from the exchange (Fock) potential  $U_x(\mathbf{r}, \mathbf{r}') = -\sum_i \varphi_i^*(\mathbf{r}') v(|\mathbf{r} - \mathbf{r}'|) \varphi_i(\mathbf{r})$  (linear in  $\mathcal{O}$ ), while the central potential is written as  $U(r) = \sum_i \int d\mathbf{r}' |\varphi_i(\mathbf{r}')|^2 v(|\mathbf{r} - \mathbf{r}'|)$ , (independent of  $\mathcal{O}$ ). Of notice that the coupling between e.g. the quadrupole vibration of the core ( ${}^8\text{He}$ ) and a halo neutron is also linear in  $\mathcal{O}$ , i.e.  $\langle H_c \rangle_{2^+(core), n(halo)} = \beta_2 \left( \frac{R_0}{\sqrt{5}} \frac{\partial U}{\partial r} \right) \mathcal{O}$  (see Sect. 1.9.2).

### 1.9.2 Physical particles and optical potential

Within the framework of the above scenario, each nucleon moves independently in the average field created by all the other nucleons<sup>71</sup> feeling their pushings and pullings only when trying to leave the nucleus, the summed effect being to be forced to scatter elastically off the nuclear surface. Schematically, the full complexity of the many-body nuclear Hamiltonian

$$H = T + v, \quad (1.9.5)$$

has been reduced to

$$H_{HF} = T + U(r) + U_x(\mathbf{r}, \mathbf{r}'). \quad (1.9.6)$$

In other words, and making use of the expression,

$$H = T + v(|\mathbf{r} - \mathbf{r}'|) = H_{HF} + (v(|\mathbf{r} - \mathbf{r}'|) - (U(r) + U_x(|\mathbf{r} - \mathbf{r}'|))) \quad (1.9.7)$$

the full many-body nuclear Hamiltonian (first expression) has been approximated by the Hartree–Fock Hamiltonian by neglecting the term in parenthesis. That is, by assuming that the sum of the direct and exchange potential gives a sensible approximation to the full two-body interaction  $v$ . This approximation (adding appropriate spin-orbit potential), although providing a number of important insights into the nuclear structure and reactions as the sequence of single-particle levels<sup>72</sup> (and associated magic numbers), and sensible nucleon–nucleus, elastic phase shifts, disagrees with experiment on a number of points. In particular, leading to a too low level density at the Fermi energy, to an infinite mean free path, also for nucleons moving in states (e.g. deep hole states) far removed from the Fermi energy, let alone the lack of collective electromagnetic transitions and the large value of the elastic cross section.

To move further, one has to go beyond independent particle as well as from potential scattering motion. That is, to allow the particles (both bound and projectile nucleons) to interact among themselves (four point vertices; see e.g. (1.7.16)) aside to interact with the nuclear as well as with the Fermi surfaces, as well as with spin, spin-isospin, etc. modes (particle vibration coupling, which in the case of surface modes has been introduced in (1.7.26)). In other words, to allow the elementary modes of excitation to interact according to the NFT rules. In the case in which one nucleon moves with asymptotic waves for  $r = -\infty$  (projectile), the interaction in parentheses in (1.9.7) open reaction channels. In particular, one- and two-particle transfer channels, in which the mass partition changes between entrance and exit channels.

Let us exemplify the consequences of the interaction between elementary modes of excitation in the case of  $^{11}\text{Li} + p$ .

---

<sup>71</sup>Pauli principle (Fock potential) having taken care not to count the contribution of a nucleon on itself.

<sup>72</sup>Mayer and Jensen (1955).

### 1.9.3 $^{11}_3\text{Li}_8$ structure in a nutshell

The sequence of single-particle levels for the  $^{10}_3\text{Li}_7$  associated with the mean field potential (1.9.3) implies that the distance between the last occupied neutron state  $0p_{1/2}(\epsilon_{1/2^-} = -1.2 \text{ MeV})$  and the first empty one,  $1s_{1/2}(\epsilon_{1/2^+} = 1.5 \text{ MeV})$  is 2.7 MeV (see Fig. 1.9.1). In other words, in  $^{10}\text{Li}$  the  $0s_{1/2}, 0p_{3/2}$  neutron orbitals are fully occupied, while  $0p_{1/2}$  carries three neutrons (one-hole state), making  $^{11}\text{Li}$  a single closed shell system.

There is clear experimental evidence which testifies to the fact that the first unoccupied states of  $^{10}\text{Li}$  are a virtual  $1/2^+$  ( $\epsilon_{1/2^+} = 0.2 \text{ MeV}$ ) and a resonant  $1/2^-$  ( $\epsilon_{1/2^-} = 0.5 \text{ MeV}$ ) state. According to NFT, this is a consequence of the self-energy renormalization of the bare  $1/2^+$  state and of the  $1/2^-$  state through a mainly PO (polarization) and CO (correlation) process respectively (Fig. 1.9.1). Thus parity inversion and the melting of the  $N = 8$  closed shell in favor of the new magic number  $N = 6$ . While  $^{10}\text{Li}$  is not bound,  $^{11}\text{Li}$  displays a two-neutron separation energy  $S_{2n} \approx 400 \text{ keV}$ . According to NFT this value of the two-neutron binding energy is the result of a subtle bootstrap mechanism. Being at threshold and essentially not feeling a centrifugal barrier, the  $1/2^+$  and  $1/2^-$  states, are essentially not available for the short range bare  $NN$ -pairing interaction, requiring a Cooper pair binding mechanism mediated by the exchange of long wavelength collective modes. This is the natural scenario of a very low-lying collective dipole mode for two main reasons. First, the presence of a dipole particle-hole transition  $1/2^+ \rightarrow 1/2^-$ , with energy about 0.3 MeV. The second one is related to the fact that the neutron halo in  $^{11}\text{Li}$  displays a very large radius, as compared to that of the closed shell core  $^9\text{Li}_6$ , and thus a small overlap with it. This single-particle controlled phenomenon<sup>73</sup> has a three-fold consequence: i) to screen the bare  $NN^{-1}S_0$  short range pairing interaction making it subcritical, ii) to screen the (repulsive) symmetry interaction, and (consequently), iii) to allow to bring at low energies a consistent fraction of the TRK-sum rule associated with the GDR at  $\approx 36 \text{ MeV}$ . In fact, a  $1^-$  resonance carrying  $\approx 8\%$  of the TRK sum rule and with centroid at an energy  $\lesssim 1 \text{ MeV}$  have been observed. Thus, the connotation of giant dipole pygmy resonance (GDPR). Exchanged between the heavily dressed neutrons moving in the parity inverted states, it provides, together with an almost negligible contribution of the bare  $NN$ -pairing interaction, the glue needed to bind the neutron halo Cooper pair to the  $^9\text{Li}$  core (Fig. 1.9.1). With little experimental input, NFT allows

---

<sup>73</sup>Within this context one is essentially forced to make a subtle extension of the statement according to which the single-particle motion is the most collective of all nuclear motions (Mottelson (1962)), emerging from the same properties of the nuclear interaction (both bare and induced) as collective motion does, and in turn at the basis of the detailed properties of each collective mode, acting as scaffolds and filters of the variety of embodiments. In fact, one has to add the characterisation of “physical” to “single-particle motion” (i.e. clothed) to englobe in the above statement also the present situation (parity inversion). In other words, while the bare  $s_{1/2}$  and  $p_{1/2}$  orbitals could never lead to a low-lying dipole strength, the corresponding clothed, physical states do so in a straightforward manner. Consequently: “physical, clothed single-particle motion, is one of the most collective of nuclear motions”, seems to be the right statement.

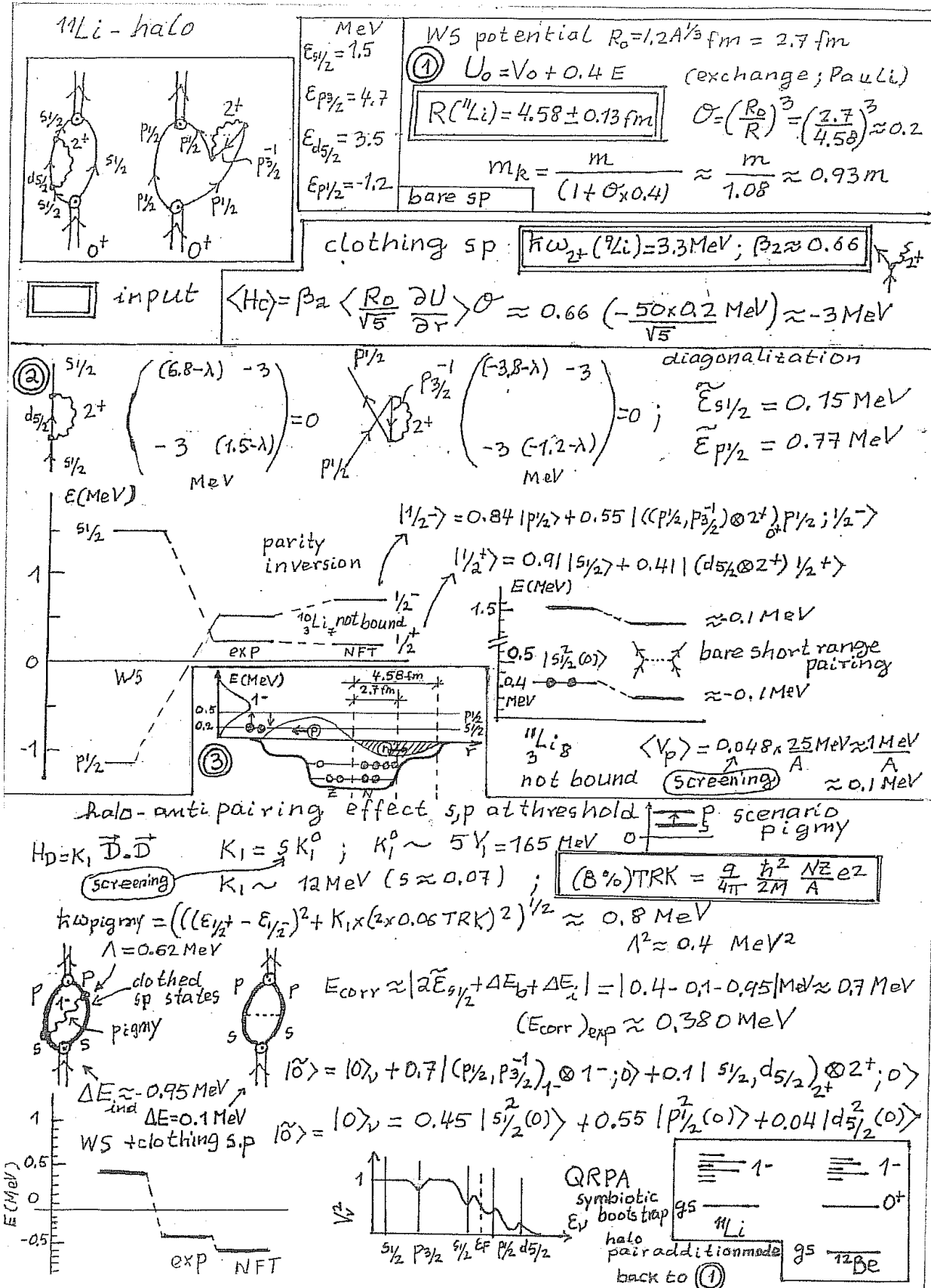


Figure 1.9.1

accurately and economically to propagates renormalization effects which not only renormalizes mean field, but overwhelms it providing a simple explanation of the experimental finding.

### Caption Fig 1.9.1

**1** Starting with well defined elements: Woods–Saxon (WS) potential, and the parameters characterizing the low–lying quadrupole vibration of the core (**input**), calculate the single–particle levels and collective vibration (separable interaction) and determine the corresponding scattering vertices (strength and form factors). From the ratio of the WS radius ( $R_0$ ) and of the observed one ( $R(^{11}\text{Li})$ ) **input**) determine the overlap  $\mathcal{O}$ . Because  $\mathcal{O} \ll 1$ , the contribution of the exchange (Fock) potential to the empirical WS potential is small (energy ( $k$ ) dependent term  $U \approx -50 \text{ MeV} + \mathcal{O}U_x$ ,  $U_x = 0.4E(\hbar^2k^2/2m)$ ,  $m_k/m = (1 + \mathcal{O}(m/\hbar^2k)\partial U_x/\partial k)^{-1}$ ) concerning the halo neutrons, essentially blurring the emergent new Pauli quantum number one (single occupancy) closely related to the many–body Dirac interpretation of the stability of the fully occupied vacuum (Pauli, Dirac, Nobel lectures). Consequently the neutron halo  $k$ –mass  $m_k$  has a value close to the bare mass  $m$ .

**2** Making use of the above elements one can cloth the bare single–particle states, in particular the  $s_{1/2}$  and  $p_{1/2}$  states. Parity inversion ensues, with  $1/2^+$  and  $1/2^-$  at threshold. As a consequence the  $N = 8$  shell closure melts away,  $N = 6$  becoming a new magic number, testifying to the fact that large amplitude fluctuations are as important or even more important than static mean field effects. As a result  ${}^3_3\text{Li}_7$  is not bound. Adding one more neutron and switching on the bare pairing interaction (e.g. a contact force  $V_p$  with constant matrix element  $G = 1.2 \text{ fm}^{-3}V_0/A \approx (28/A) \text{ MeV}$ , Brink, D. and Broglia (2005), pp 40-42), the screening resulting from the ratio  $r = \frac{(M_j)_{\text{halo}}}{(M_j)_{\text{core}}} \approx \frac{2}{2j+1} \left(\frac{R_0}{R}\right)^3 \approx 0.048$  makes  $(G)_{\text{scr}} = rG$  subcritical, resulting in an unbound system.

**3** Considering the sloshing back and forth of the halo neutron (with a small contribution from the core neutrons) against the core protons, leads to a dipole mode feeling a strongly screened (repulsive) symmetry potential  $s = \mathcal{O}(R_0/R)^2 \approx 0.07$  in keeping with the fact  $\kappa_1 \sim 1/R^2$ . In other words, while the price to pay to separate protons from neutrons in the core is  $5V_1 = 5 \times 33 \text{ MeV} = 165 \text{ MeV}$ , when referring to halo neutrons this price is reduced to  $5 \times 5V = 11.6 \text{ MeV}$  ( $V_1 = 0.07 \times 33 \text{ MeV} = 2.3 \text{ MeV}$ ) for halo neutrons. This fact is at the basis that  $\approx 8\%$  of the Thomas–Reiche–Kuhn sum rule (**input**) gets down to  $\approx 0.6 \text{ MeV}$ . Another way to say the same thing is that  $(V_1)_{\text{screened}} = sV_1$  is at the basis of the fact that the  $E1$  transition  $s_{1/2} \rightarrow p_{1/2}$  ( $\Delta\epsilon \approx 0.3 \text{ MeV}$ ) is only increased by a modest value ( $\hbar\omega_{\text{pygmy}} \approx 0.6 \text{ MeV}; \approx 10^{21} \text{ Hz}$ ), while the  $E1$  single–particle strength remains essentially unchanged (typical values in the case of stable nuclei being  $\approx 10^{-4}B_{sp}(E1)$  for pure low–energy ( $\lesssim 1 \text{ MeV}$ ) single–particle transitions). Now, the two halo neutrons dressed by the vibrations of the core (heavy arrowed lines) and interacting through the bare  $NN$ –pairing force are not bound. Consequently, the pygmy resonance will fade away almost as soon as it is generated (essentially lasting the neutron transversal time

$\approx 10^{21}$  s), unless... Unless it is exchanged between the two neutron configuration  $s_{1/2}^2(0)$  at threshold ( $2\epsilon_{s_{1/2}} \approx 0.4$  MeV) making it jump into the  $p_{1/2}^2(0)$ , also close to threshold ( $2\epsilon_{p_{1/2}} \approx 1$  MeV). As an intermediate boson, the pygmy resonance which couples to the halo neutron with a strength  $\Lambda \approx 0.62$  MeV (QRPA calculation), contributes to the gluing of the neutron halo Cooper pair with about 1 MeV binding. The corresponding correlation energy  $E_{corr} \approx 0.7$  MeV being mainly due to the pygmy exchange process. The symbiotic halo pair addition mode–pygmy DR of  $^{11}\text{Li}$  can, in principle be used as a building block of the nuclear spectrum, which can be moved around. A possible candidate being the first excited  $0^+$  state of  $^{12}\text{Be}$ , together with the associate dipole state. Because to calculate the giant dipole pygmy resonance (GDR) of  $^{11}\text{Li}$  one needs to know the ground state of this nucleus (halo–pair addition mode) so as to be able to determine microscopically the occupations factor the  $1s_{1/2}, 1p_{3/2}, s_{1/2}, p_{1/2}, d_{5/2}, \dots$ , etc. states to carry out a QRPA calculation of the mode, but to do so one needs to know the pygmy, once arrived to this point, one needs to go back to 1 and repeat the whole procedure so as to eventually reach convergence.

#### 1.9.4 $^{11}\text{Li}(p, p)^{11}\text{Li}$ optical potential and transfer reaction channels

NFT is based on elementary modes of excitation, modes which carry a large fraction of the nuclear correlation. Because its rules have no limitations concerning whether the excitations studied lie or not in the continuum, or whether the single-particle motion displays asymptotic conditions, it allows for a unified description of structure and reactions. An example of the above statement is provided by Fig. 1.9.2. Graph (a) is a NFT-diagram describing one of the processes contributing to the elastic reaction  $^{11}\text{Li}(p, p)^{11}\text{Li}$  as the system propagates in time (polarization contribution to the global (mean field) optical potential describing proton elastic scattering off  $^9\text{Li}$ ). Processes taking place between  $t_1$ – $t_7$ : the halo pair addition mode  $|0_v^+\rangle$  couples at time  $t_1$  with a pure bare configuration and its binding to the  $^9\text{Li}$  core results from parity inversion where the  $s_{1/2}$  continuum orbital is lowered to threshold through clothing with mainly quadrupole vibrational modes and the  $p_{1/2}$  bound state suffers a strong repulsion into a resonant state by Pauli principle with particles participating in the quadrupole mode. The resulting dressed neutron states get bound mainly through the exchange of the  $1^-$  giant dipole pygmy resonance (GDPR), represented for simplicity, as a correlated particle–hole excitation, with a small contribution from the bare pairing interaction. At time  $t_8$ , one of the neutrons of the halo Cooper pair is transferred (particle–recoil coupling vertex, see App. 1.D), to the incoming proton projectile through the proton–neutron interaction  $v_{np}$  (prior representation), leading to a deuteron. This neutron is, at time  $t_9$  transferred back (to a virtual  $^{10}\text{Li}$ ) through  $v_{np}$  acting a second time (post representation), with the simultaneous absorption of the recoil mode. Eventually, at time  $t_{10}$  the two neutrons merge, through the particle-pair vibrational coupling, into the halo pair addition mode  $|0_v\rangle$ . The real part of the diagram contributes to  $U_{opt}$  while the imaginary one to  $W_{opt}$ , corresponding to the real and imaginary (absorptive)

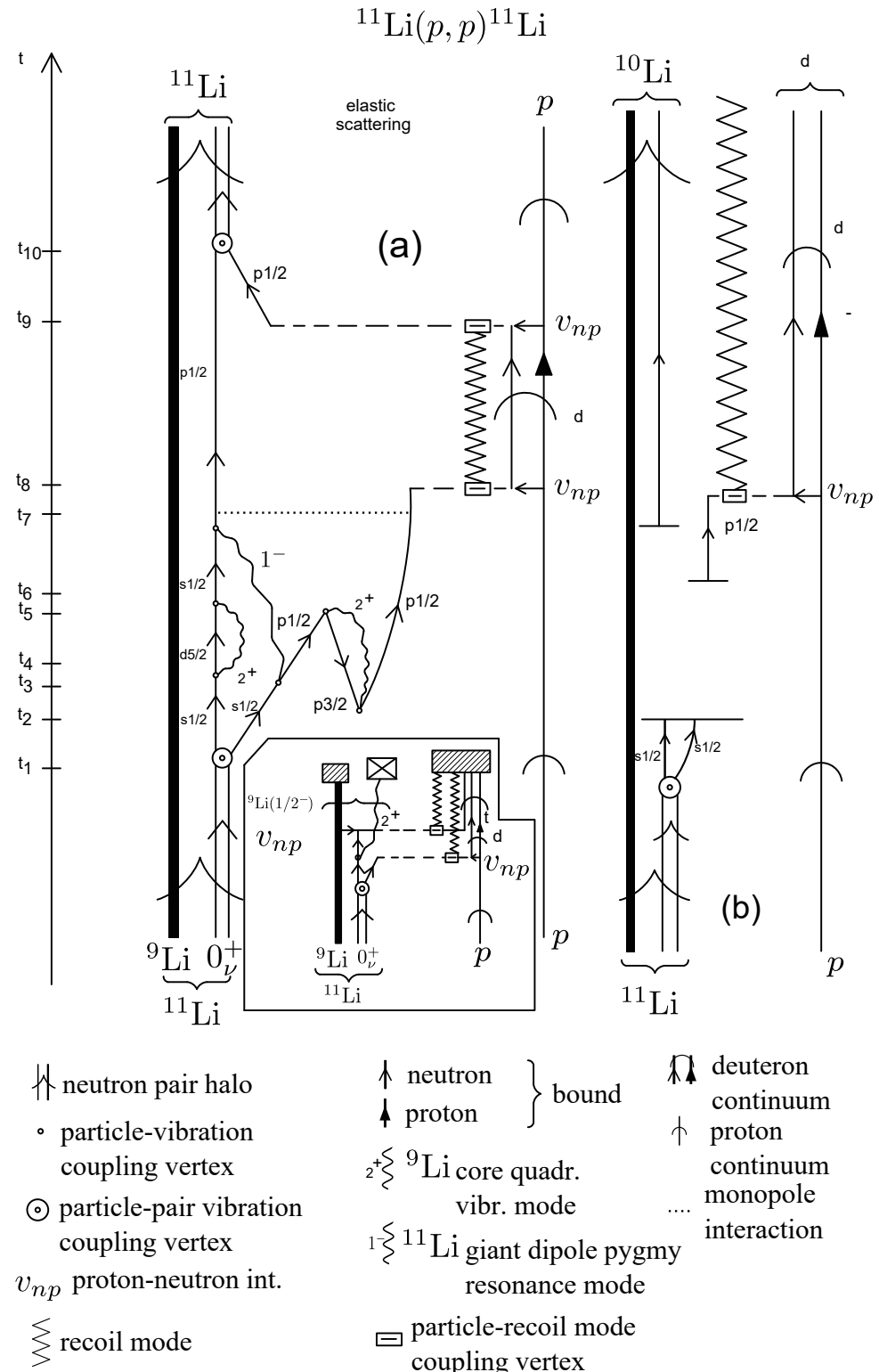


Figure 1.9.2: NFT diagram describing (a) one of the processes contributing to the elastic reaction  $^{11}\text{Li}(p, p)^{11}\text{Li}$  and (b) to the  $^{11}\text{Li}(p, d)^{10}\text{Li}$  process.

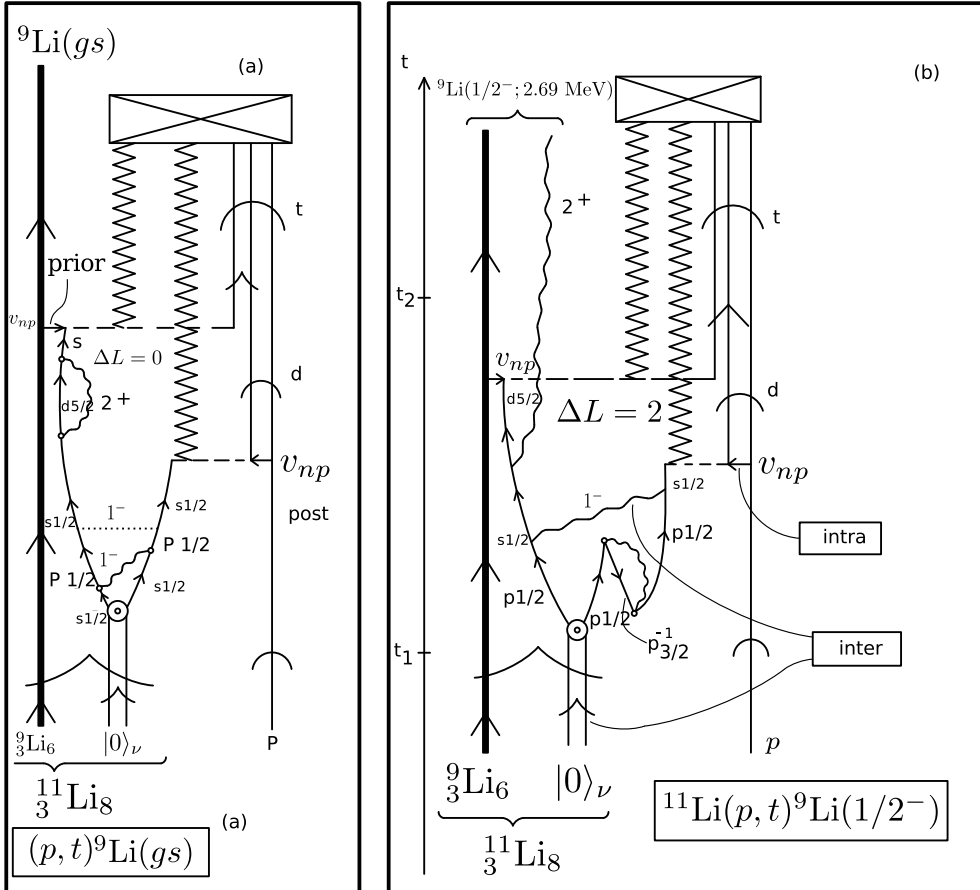


Figure 1.9.3: NFT-graphical representation of contributions to (a)  $^{11}\text{Li}(p, t)^9\text{Li}(\text{gs})$  and (b)  $^{11}\text{Li}(p, t)^9\text{Li}(1/2^-)$  reactions. The dotted horizontal line in (a) represents the  $NN$ -symmetry potential. The boxed labels in (b) indicate the bare ( $v_{np}$ ) and phonon mediated interactions which bind the Cooper pair to the core  $^9\text{Li}$  (intra), and those acting between target and projectile (eventually) also outgoing particle (inter). For more details see text. Time is assumed to run upwards. A single arrowed line represents a fermion (proton) (p) or neutron (n). A double arrowed line two correlated nucleons. In the present case two correlated (halo) neutrons (halo-neutron pair addition mode  $|0\rangle_\nu$ ). A heavy arrowed line represents the core system  $^9\text{Li}(\text{gs})$ . A standard pointed arrow refers to structure, while "round" arrows refer to reaction, regardless whether they are in the continuum or less. A wavy line represents (particle-hole) collective vibrations, like the low-lying quadrupole mode of  $^9\text{Li}$ , or the more involved dipole pigmy resonant state which, together with the bare pairing interaction (horizontal dotted line) binds the neutron halo Cooper pair to the core. A short horizontal arrow labels the proton-neutron interaction  $v_{np}$  responsible for the single-particle transfer processes, represented by an horizontal dashed line. The jaggy curve represents the (collective) recoil effect resulting from the mismatch between the relative centre of mass coordinates associated with the mass partitions  $^{11}\text{Li} + \text{p}$ ,  $^{10}\text{Li} + \text{d}$  (virtual), and  $^9\text{Li} + \text{t}$ .

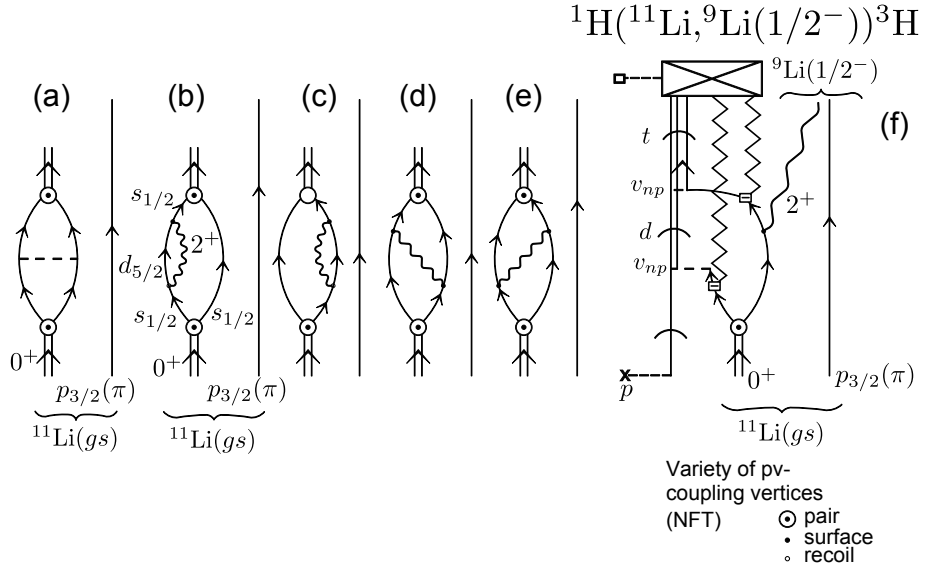


Figure 1.9.4: Lowest order, NFT diagrams associated with the processes contributing to the binding of the neutron halo Cooper pair (double arrowed line) of  $^{11}\text{Li}$  to the core  $^9\text{Li}$  through the exchange of the core quadrupole phonon (wavy line). Single arrowed lines describe the nucleon independent-particle motion of neutrons ( $s_{1/2}$ ,  $d_{5/2}$ , etc.) as well as of protons ( $p_{3/2}(\pi)$ ). (a) Bare interaction, four-point vertex (horizontal dashed line); (b, c) self energy, effective mass process dressing the  $s_{1/2}(v)$  single-particle state; (d, e) vertex correction (induced interaction) renormalizing the pair addition mode coupling vertex with which it couples to the fermion (dotted open circle); (f) NFT diagrams describing the reaction  $^1\text{H}(^{11}\text{Li}, ^9\text{Li}(1/2^-; 2.69 \text{ MeV})) ^3\text{H}$  populating the first excited state of  $^9\text{Li}$ . The jagged line represents the recoil mode carrying asymptotically to the detector the momentum mismatch associated with the transfer process (recoil). In this case of successive transfer, one for each transferred neutron ( $^{11}\text{Li}(\text{gs})+p \rightarrow ^{10}\text{Li}+d \rightarrow ^9\text{Li}(1/2^+) + t$ ). For details see Sect. (2.6) as well as Sect. (6.1).

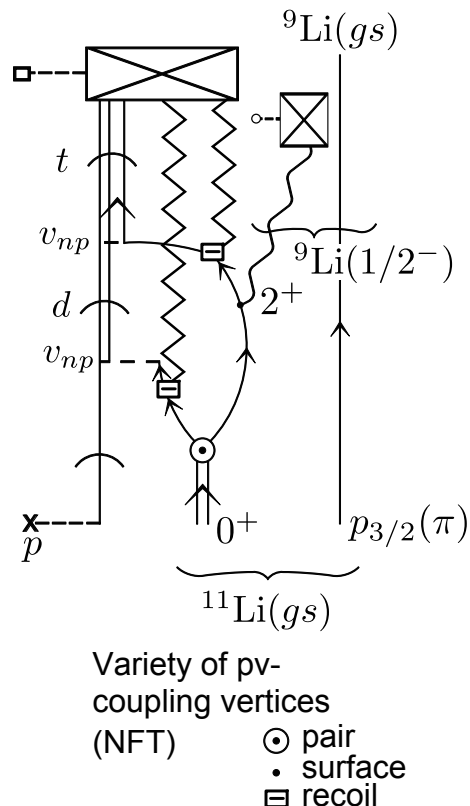


Figure 1.9.5: Gedanken  $\gamma$ -ray coincidence experiment  $^1\text{H}(^{11}\text{Li}, ^9\text{Li})^3\text{H}$  and  $^9\text{Li}(\text{gs}) + \gamma(E2; 2.69 \text{ MeV})$ . In this case, the virtual quadrupole phonon associated with self-energy and vertex correction processes becomes real through the action of the  $(p, t)$  external field. Thus, it is not only the recoil modes measured by particle detectors which have asymptotic wavefunction, but also the quadrupole vibration, which is measured by the  $\gamma$ -detector. For details see Caption Fig. 1.9.4.

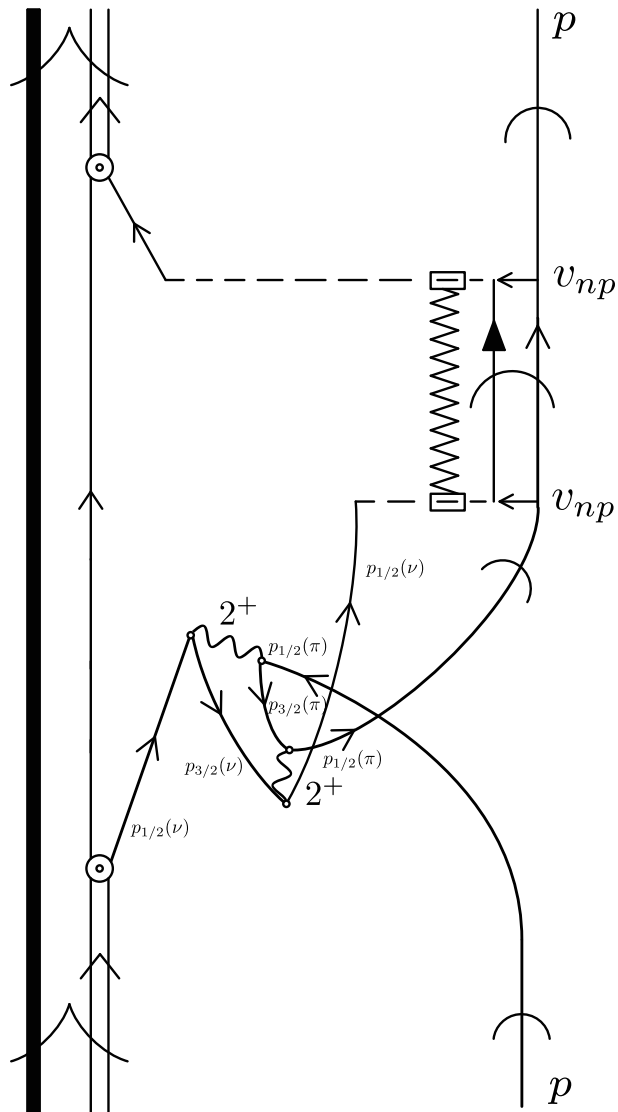


Figure 1.9.6: In keeping with standard direct reaction praxis, neither in Fig. 1.9.2 nor in 1.9.3 antisymmetrization is carried out between the impinging proton and the protons of  $^{11}\text{Li}$ . Within the present discussion  $(^{11}\text{Li}(p, p)^{11}\text{Li})$  (see Fig. 1.9.3), an example of such processes corresponds to the exchange of a proton participation in the quadrupole vibration of the core, with the projectile, as shown in the figure. Such a process will not only be two orders higher in perturbation in the particle-vibration coupling vertex. It will be strongly reduced by the square of the overlap between a proton moving in the continuum, and a  $p_{1/2}$  proton of the  $^9\text{Li}$  core bound by about 10 MeV.

component of the polarization contribution to the optical potential, to be added to the experimental determined (global)  ${}^9\text{Li}+p$  elastic scattering optical potential. It is of notice that this diagram exemplifies the elements needed to extend and formalize NFT rules of structure so as to be able to deal also with reactions. In Fig. 1.9.2 (b) one assumes the same processes to take place as in (a) up to time  $t_8$  (reason for which no details are repeated between  $t_2$  and  $t_8$ ). From there on the deuteron continues to propagate to the detector, and the effect of the particle–recoil coupling vertex is to be worked out and the corresponding outgoing distorted waves modified accordingly. Likely, the neutron in  ${}^{10}\text{Li}$  will break up before it can be recorded by the particle detector. Summing up, in the center of mass reference frame both  $p$  and  ${}^{11}\text{Li}$  display asymptotic states in entrance as well as in exit channels in case (a), and only in the entrance channel in case (b), while in the exit channel only  ${}^{10}\text{Li}({}^9\text{Li}+n)$  and the deuteron do so.

Another examples of the NFT diagrams of structure and reactions are given in Fig. 1.9.3. In (a) one contribution associated with the reaction  ${}^{11}\text{Li}(p,t){}^9\text{Li}(\text{gs})$  is shown, while in (b) one associated with the population of the first excited  $1/2^-$  (2.69 MeV) state of  ${}^9\text{Li}$ . Within this context we refer to Figs. 1.9.4 and 1.9.5 for a compact graphical representation of this last process. The importance of this process is that it provided, for the first time, direct evidence of phonon mediated pairing interaction in nuclei as theoretically predicted<sup>74</sup>.

Returning to the process displayed in Fig. 1.9.2 concerning the question of Pauli principle (also essential in the case of structure NFT) in this case not between e.g. the two halo neutrons, but between the incoming proton and the collective modes of the core ( ${}^9\text{Li}$ ) we refer to Fig. 1.9.6. It is of notice that making use of global optical potentials to describe the elastic channel, or mean field optical potentials to which to add polarization contribution like those displayed in Fig. 1.9.2 (a), the effect of Pauli principle between a nucleon projectile and the nucleons of the target is considered through the energy ( $k$ -dependent strength, so called Perey-Buck potential<sup>75</sup> (intimately connected with the  $k$ -mass)).

## 1.10 Summary

In Fig. 1.10.1 the results of a “complete” NFT(r+s) description of the open shell superfluid nucleus  ${}^{120}\text{Sn}$  in terms of the  ${}^{120}\text{Sn}(p,t){}^{118}\text{Sn}(\text{gs})$ ,  ${}^{122}\text{Sn}(p,t){}^{120}\text{Sn}(\text{gs})$ ,  ${}^{120}\text{Sn}(p,d){}^{119}\text{Sn}$ ,  ${}^{121}\text{Sn}(p,d){}^{120}\text{Sn}$ ,  ${}^{119}\text{Sn}(\alpha,\alpha'){}^{119}\text{Sn}$  ( $\gamma$ -decay) cross sections, energies and transition probabilities are displayed in comparison with the experimental findings. Arbitrarily forcing the PVC strength, the strength of the bare pairing force and the value of the  $k$ -mass to depart from their “physical” values, one can test the robustness of the NFT(r+s) picture of  ${}^{120}\text{Sn}$  given, and of the well funneled character of the associated nuclear structure and reaction landscape (Idini et al.

---

<sup>74</sup>Barranco, F. et al. (2001) Tanihata, I. et al. (2008); Potel et al. (2010); Tanihata et al. (2013); Beceiro–Novo et al. (2015).

<sup>75</sup>Perey and Buck (1962)

(2015), see also Fig. 1.4.1).

*In a very real sense this, namely the results collected in Fig. 1.10.1 is a nucleus. That is, the summed experimental and theoretical structural information accessed through (optical potential) asymptotic states, outcome of simultaneously probing the system with a complete array of experiments (elastic, anelastic and one- and two-nucleon transfer reactions), and of calculating the corresponding observables with an equally ample array of theoretical tools, as provided e.g. by NFT( $r+s$ ).*

## Appendix 1.A Confronting theory with experiment: absolute cross sections

In this appendix we provide a road map concerning the connection between theory and experiment<sup>76</sup> to be found in the present monograph, and in closely connected references.

### 1.A.1 One-particle transfer

#### Nuclei along the stability valley

Spectroscopic amplitudes

- $^{120}\text{Sn}(p, d)^{119}\text{Sn}(7/2^+)$ : Table 4.2.1
- $^{120}\text{Sn}(d, p)^{121}\text{Sn}(j^\pi)(j^\pi = 11/2^-, 3/2^+, 1/2^+, 5/2^+, 7/2^+)$ : Table ??
- $^{120}\text{Sn}(p, d)^{119}\text{Sn}((5/2^+); E_x \leq 2 \text{ MeV})$ : Table ??

#### Optical potentials

Dickey, S. A. et al. (1982); Bechara, M. J. and Dietzsch (1975)<sup>77</sup>.

#### Absolute differential cross sections: theory–experiment

Fig. 4.2.2 and 4.2.3.

#### Halo nuclei

- a)  $^9\text{Li}(d, p)^{10}\text{Li}(1/2^+)$
- b)  $^9\text{Li}(d, p)^{10}\text{Li}(1/2^-)$
- c)  $^{10}\text{Be}(d, p)^{11}\text{Be}$

---

<sup>76</sup>Physics is an experimental science: it is concerned only with those statements which in some sense can be verified by experiment (Schwinger (2001)).

<sup>77</sup>It is to be noted that, while no big differences are found, in all the transfer calculations involving medium heavy nuclei, the optical potentials collected in Table 6.2.2 were employed (Potel, G. et al. (2013)).

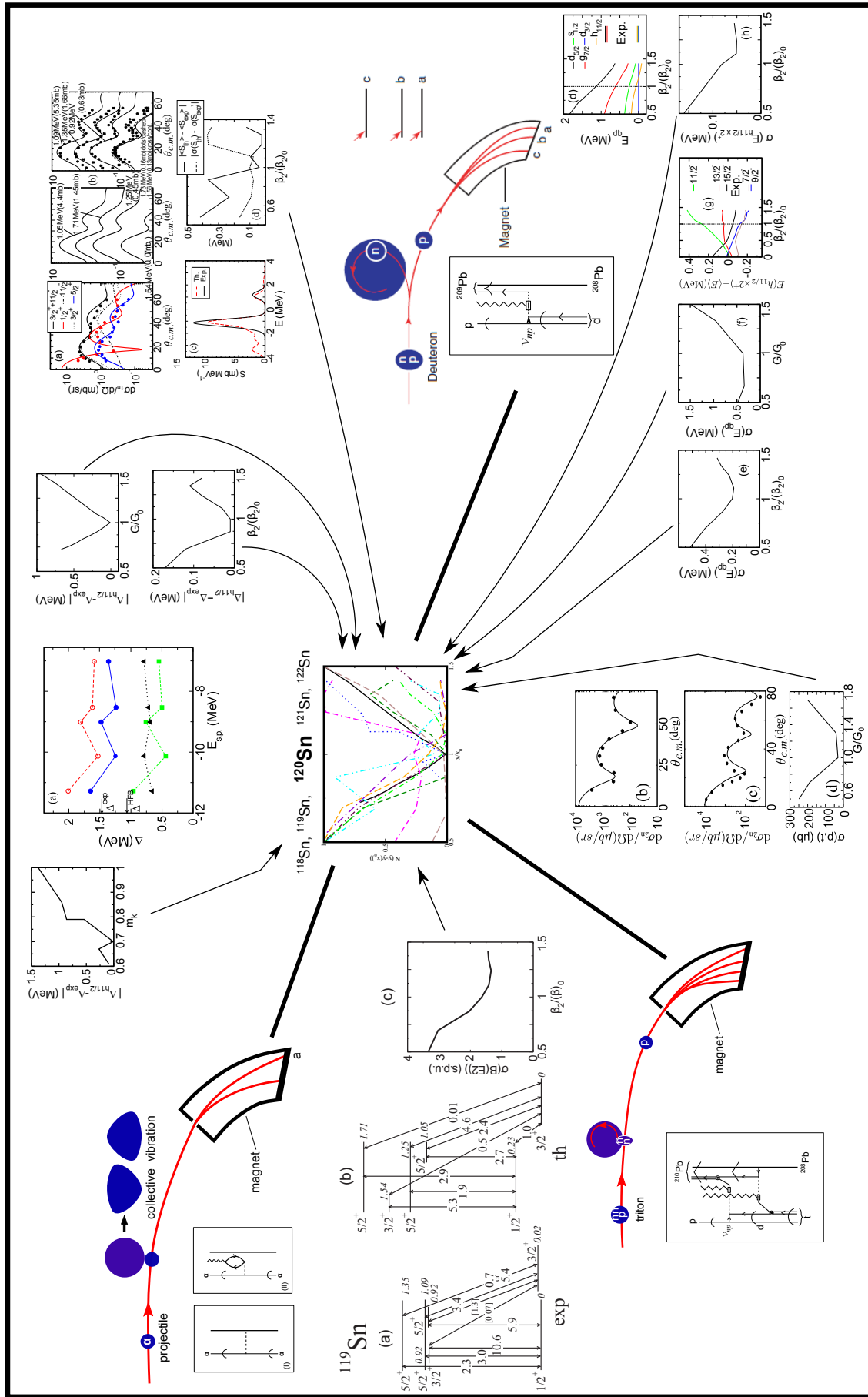
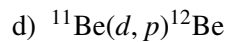


Figure 1.10.1



### **Optical potentials**

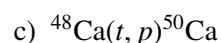
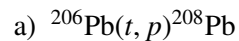
Orrigo and Lenske

#### **1.A.2 Two-particle transfer**

**Nuclei along the stability valley**

**Closed shell nuclei**

Spectroscopic amplitudes



### **Optical potentials**

**Absolute differential cross sections: theory-experiment**

Fig. 6.1.5

### **Open shell nuclei**



### **Spectroscopic amplitudes**

Table 6.2.1

### **Optical potentials**

Table 6.2.2

**Absolute differential cross sections: theory-experiment**

Fig. 6.2.1

**Nuclei around  $N = 6$  closed shell**

Spectroscopic amplitudes

- a)  ${}^1\text{H}({}^{11}\text{Li}, {}^9\text{Li}){}^3\text{H}$   
Eqs. (6.1.1)–(6.1.3)
- b)  ${}^7\text{Li}(t, p){}^9\text{Li}$
- c)  ${}^{10}\text{Be}(t, p){}^{12}\text{Be}$

**Optical potentials**

- a) Table 6.1.1
- b) ref
- c) ref

**Absolute differential cross sections: theory–experiment**

- a) Fig. 6.1.3
- b) Fig. 6.1.5
- c) Fig. 6.1.5

## Appendix 1.B Inelastic Scattering

In this Appendix we briefly discuss how to extract values of the effective deformation parameter  $\beta_L$  from inelastic scattering absolute differential cross sections in the most simple and straightforward way, ignoring all the complications associated with the spin carried by the particles, the spin–orbit dependence of the optical model potential  $\bar{U}(r_\beta)$  etc. The deformation parameter  $\beta_L$  enter e.g. the particle–vibration coupling Hamiltonian (Eqs. (1.3.8–1.3.13)).

### 1.B.1 $(\alpha, \alpha')$ -scattering

We start assuming that the interaction  $V'_\beta$  is equal to  $V'_\beta = V'_\beta(\xi_\beta, r_\beta)$ , which is usually called the stripping approximation. We can then write the differential cross section in the Distorted Wave Born Approximation (DWBA) as (see e.g. App 5.E) as,

$$\frac{d\sigma}{d\Omega} = \frac{k_\beta}{k_\alpha} \frac{\mu_\alpha \mu_\beta}{(2\pi\hbar^2)} |\langle \psi_\beta(\xi_\beta) \chi^{(-)}(k_\beta, \vec{r}_\beta), V'_\beta(\xi_\beta, r_\beta) \psi_\alpha(\xi_\alpha) \chi^{(+)}(k_\alpha, \vec{r}_\alpha) \rangle|^2. \quad (1.B.1)$$

For the case of inelastic scattering  $\xi_\alpha = \xi_\beta = \xi$ , thus

$$\psi_\beta(\xi_\beta) = \psi_{M_{I\beta}}^{I_\beta}(\xi) \quad (1.B.2a)$$

$$\psi_\alpha(\xi_\alpha) = \psi_{M_{I\alpha}}^{I_\alpha}(\xi) \quad (1.B.2b)$$

$$\vec{r}_\alpha = \vec{r}_\beta \quad \mu_\alpha = \mu_\beta, \quad (1.B.2c)$$

i.e we are always in the mass partition of the entrance channel.

Equation (1.B.1) can now be rewritten as

$$\frac{d\sigma}{d\Omega} = \frac{k_\beta}{k_\alpha} \frac{m_\alpha^2}{(2\pi\hbar^2)^2} \frac{1}{2I_\alpha + 1} \sum_{M_\alpha M_\beta} |\langle \chi^{(-)}(k_\beta, \vec{r}_\beta), V_{eff}(\vec{r}) \chi^{(+)}(k_\alpha, \vec{r}_\alpha) \rangle|^2, \quad (1.B.3)$$

where

$$\begin{aligned} V_{eff} &= \int d\xi \psi_{M_{I\beta}}^{I_\beta^*}(\xi) V'_\beta(\xi, \vec{r}) \psi_{M_{I\alpha}}^{I_\alpha}(\xi) \\ &= \int d\xi \psi_{M_{I\beta}}^{I_\beta^*}(\xi) V_\beta(\xi, \vec{r}) \psi_{M_{I\alpha}}^{I_\alpha}(\xi) \end{aligned} \quad (1.B.4)$$

as  $\psi^{I_\beta}$  and  $\psi^{I_\alpha}$  are orthogonal (remember  $V'_\beta = V_\beta - \bar{U}(r)$ ). We now expand the interaction in spherical harmonics, i.e.

$$\begin{aligned} V_\beta(\xi, \vec{r}) &= \sum_{LM} V_M^L(\xi, r) Y_M^L(\hat{r}) \\ &= \sum_{LM} V_M^L(\xi, \vec{r}). \end{aligned} \quad (1.B.5)$$

Defining

$$\int d\xi \psi_{M_{I\beta}}^{I_\beta^*}(\xi) [V_M^L(\xi, r) \psi^{I_\alpha}(\xi)]_{M_{I\beta}}^{I_\beta} = F_L(r), \quad (1.B.6)$$

we can write eq.(1.B.4) as

$$V_{eff}(\vec{r}) = \sum_{LM} (LMI_\alpha M_\alpha | I_\beta M_\beta) F_L(r) Y_M^L(\hat{r}). \quad (1.B.7)$$

Inserting (1.B.7) into (1.B.3) we obtain

$$\begin{aligned} \frac{d\sigma}{d\Omega} &= \frac{k_\beta}{k_\alpha} \frac{m_\alpha^2}{(2\pi\hbar^2)^2} \frac{1}{2I_\alpha + 1} \sum_{M_\alpha M_\beta} \left| \sum_{LM} (LMI_\alpha M_\alpha | I_\beta M_\beta) \right. \\ &\quad \times \left. \int d\vec{r} \chi^{(-)*}(k_\beta, \vec{r}_\beta) F_L(r) Y_M^{L*}(\hat{r}) \chi^{(+)}(k_\beta, \vec{r}_\beta) \right|^2 \\ &= \frac{k_\beta}{k_\alpha} \frac{m_\alpha^2}{(2\pi\hbar^2)^2} \frac{2I_\beta + 1}{2I_\alpha + 1} \\ &\quad \times \sum_{LM} \frac{1}{2L + 1} \left| \int d\vec{r} \chi^{(-)*}(k_\beta, \vec{r}_\beta) F_L(r) Y_M^{L*}(\hat{r}) \chi^{(+)}(k_\beta, \vec{r}_\beta) \right|^2, \end{aligned} \quad (1.B.8)$$

where we have used the orthogonality relation between Clebsch-Gordan coefficients

$$\begin{aligned} & \sum_{M_\alpha M_\beta} (LMI_\alpha M_\alpha | I_\beta M_\beta) (L'MI_\alpha M_\alpha | I_\beta M_\beta) \\ &= \sqrt{\frac{(2I_\beta + 1)^2}{(2L + 1)(2L' + 1)}} \sum_{M_\alpha M_\beta} (I_\beta - M_\beta I_\alpha M_\alpha | L - M) \\ & \quad \times (I_\beta - M_\beta I_\alpha M_\alpha | L' - M) = \frac{2I_\beta + 1}{2L + 1} \delta_{LL'} \\ & \quad (\text{fixed } M) \end{aligned} \quad (1.B.9)$$

Let us now discuss the case of inelastic scattering of even spherical nuclei.

The macroscopic Hamiltonian describing the dynamics of the multipole surface vibrations in such nuclei can be written, in the harmonic approximation as

$$H = \sum_{L,M} \left\{ \frac{B_L}{2} |\dot{\alpha}_M^L|^2 + \frac{C_L}{2} |\alpha_M^L|^2 \right\}, \quad (1.B.10)$$

where the collective coordinate  $\alpha_M^L$  is defined through the equation of the radius

$$R(\hat{r}) = R_0 \left[ 1 + \sum_{L,M} \alpha_M^L Y_M^{L*}(\hat{r}) \right], \quad (1.B.11)$$

and where  $R_0 = r_0 A^{1/3}$  fm.

The collective mode is generated from the interaction of the multipole field carried by each particle and the field of the rest of the particles. In turn this coupling modifies the single-particle motion. In particular the incoming projectile would feel this coupling. The potential  $V'_\beta$  is equal to

$$\begin{aligned} V'_\beta(\xi, \vec{r}) &= U(r - R(\hat{r})) \\ &= U(r - R_0 - R_0 \sum_{L,M} \alpha_M^L Y_M^{L*}(\hat{r})) \\ &= U(r - R_0) - R_0 \sum_{L,M} \alpha_M^L Y_M^{L*}(\hat{r}) \frac{dU(r - R_0)}{dr} \\ &= V_\beta(\xi, r) - \bar{U}_\beta(r) \end{aligned} \quad (1.B.12)$$

$$\begin{aligned} \bar{U}_\beta(r) &= -U(r - R_0) \\ V_\beta(\xi, \vec{r}) &= R_0 \frac{d\bar{U}_\beta(r)}{dr} \sum_{L,M} \alpha_M^L Y_M^{L*}(\hat{r}) \end{aligned} \quad (1.B.13)$$

Comparing with eq. (1.B.5) we obtain

$$V_M^L(\alpha, r) = R_0 \frac{d\bar{U}_\beta(r)}{dr} \alpha_{+M}^L \quad (1.B.14)$$

Note that  $H$  defined in Eq. (1.B.10) is the Hamiltonian of an  $L$ -dimensional harmonic oscillator, and that  $\alpha_M^L$  is a classical variable. One can quantize this Hamiltonian in the standard way,

$$\alpha_M^L = \sqrt{\frac{\hbar\omega_L}{2C_L}}(a_M^L - a_{-M}^{+L}), \quad (1.B.15)$$

where  $\hbar\omega_L$  is the energy of the vibration, and  $a_M^{+L}$  is the creation operator of a phonon. For an even nucleus

$$\begin{aligned} |\Psi_{M_\alpha}^{I_\alpha}\rangle &= |0\rangle \quad (I_\alpha = M_\alpha = 0), \\ |0\rangle &: \text{ ground (vacuum) state.} \end{aligned} \quad (1.B.16)$$

The one-phonon state can be written as,

$$\begin{aligned} |\Psi_{M_\alpha}^{I_\alpha}\rangle &= |I; LM\rangle = a_M^{+L}|0\rangle, \\ (I_\beta &= L; M_{I_\beta} = M). \end{aligned} \quad (1.B.17)$$

We can now calculate the matrix element of the operator (1.B.14), which connects states which differ in one phonon. Starting from the ground state we obtain

$$\begin{aligned} \langle I; LM | V_M^L(\alpha, r) | 0 \rangle &= (-1)^{L-M} R_0 \frac{d\bar{U}_\beta(r)}{dr} \sqrt{\frac{\hbar\omega_L}{2C_L}} \langle 0 | (a_M^L - a_{-M}^{+L}) | 0 \rangle \\ &= R_0 \frac{d\bar{U}_\beta(r)}{dr} \sqrt{\frac{\hbar\omega_L}{2C_L}} = -\frac{R_0}{\sqrt{2L+1}} \frac{d\bar{U}_\beta(r)}{dr} \beta_L \end{aligned} \quad (1.B.18)$$

where

$$\beta_L = \sqrt{\frac{(2L+1)\hbar\omega_L}{2C_L}}. \quad (1.B.19)$$

Substituting (1.B.18) into eq. (1.B.8) and making use of eqs. (1.B.16) and (1.B.17) we get

$$\begin{aligned} \frac{d\sigma}{d\Omega} &= \frac{k_\beta}{k_\alpha} \frac{\mu_\alpha^2}{(2\pi\hbar^2)^2} (\beta_L R_0)^2 \\ &\times \sum_M \frac{1}{2L+1} \left| \int d\vec{r} \chi^{(-)*}(k_\beta, \vec{r}) \frac{dU(r)}{dr} Y_M^{L*}(\hat{r}) \chi^{(+)}(k_\alpha, \vec{r}_\beta) \right|^2. \end{aligned} \quad (1.B.20)$$

Let us now assume that the nucleus has a permanent quadrupole ( $L = 2$ ) axially-symmetric deformation. For a  $K = 0$  band, the nuclear wave function has the form<sup>78</sup>

$$\Psi_{IMK=0} = \sqrt{\frac{2I+1}{8\pi^2}} \mathcal{D}_{M0}^I(\omega) \chi_{K=0} \quad (\text{intrinsic}), \quad (1.B.21)$$

---

<sup>78</sup>see e.g. Bohr, A. and Mottelson (1975) and refs. therein.

where we have used  $(\omega) = (\theta, \phi, \psi)$  to label the Eulerian angles which serve as orientation parameters.

In the intrinsic frame (which we take to coincide with the space-fixed axis when  $\theta = \phi = \psi = 0$ ) the nuclear surface has the shape

$$R(\hat{r}) = R_0 \left[ 1 + \sum_L b_L Y_0^L(\hat{r}) \right], \quad (1.B.22)$$

where the  $b_L$  introduced here is  $a_0^L$  in the intrinsic frame. When the nucleus has orientation  $\omega$ , this shape is rotated into

$$\hat{R}_\omega R(\hat{r}) = R_0 \left[ 1 + \sum_L b_L \mathcal{D}_{M0}^L(\omega) Y_0^L(\hat{r}) \right]. \quad (1.B.23)$$

One can then write,

$$W(r - R(\hat{r})) = W(r - R_0) - R_0 \frac{dW(r - R_0)}{dr} \sum_L b_L \mathcal{D}_{M0}^L(\omega) Y_0^L(\hat{r}), \quad (1.B.24)$$

which is the equivalent to Eq. (1.B.12) for the case of deformed nuclei. Then

$$V_M^L(b, r; \omega) = -\frac{d\bar{U}_\beta(r - R_0)}{dr} b_L \mathcal{D}_{M0}^L(\omega). \quad (1.B.25)$$

The effective interaction is now equal to

$$\begin{aligned} \langle \Psi_{IMK=0}, V_M^L(b, r; \omega) \Psi_{000} \rangle &= \\ &- R_0 \frac{d\bar{U}(r - R_0)}{dr} b_L \sqrt{\frac{(2L+1)^2}{8\pi^2}} \int d\omega \mathcal{D}_{M0}^{L*}(\omega) \mathcal{D}_{M0}^L(\omega) = \\ &- R_0 \frac{d\bar{U}(r - R_0)}{dr} b_L = -\frac{R_0}{\sqrt{(2L+1)}} \frac{d\bar{U}(r - R_0)}{dr} \beta_L = F_L(r) \\ &(\beta_L = \sqrt{(2L+1)} b_L) \end{aligned} \quad (1.B.26)$$

in complete analogy to (1.B.18). Thus the same formfactor is used for both types of collective excitation. Within the above simple scheme of structure and reaction, the normalization factor  $(\beta_L R_0)^2$  is the only free parameter that can be obtained from the comparison of the experimental and theoretical (DWBA) differential cross section. The quantity  $\beta_L$  is known as the multipole deformation (dynamic or static) parameter, and gives a direct measure of the coupling of the projectile to the vibrational field. The value of  $\beta_L$  can also be obtained from the  $B(EL)$  reduced transition probability, in which case one has a measure of the electric moment, instead of the mass moment.

## Appendix 1.C Technical details NFT

In this Appendix we briefly discuss two technical aspects related to the overcompleteness of the basis used in NFT.

### 1.C.1 Graphical solution

The dispersion relation (1.7.58), which is central in the discussion concerning spurious states in the overcomplete basis of elementary modes of excitation used to develop NFT, is solved numerically in Sect. 1.7 (Fig. 1.7.7 (II)). The technical details of the corresponding implementation emerges natural by making a parallel with the dispersion relation associated with the Cooper pair problem, taking into account the energy separation existing in nuclei between single-particle levels due to the fact that it is a finite system (spatial quantization). In this case, the wavefunction of the two-particle system can be written as

$$|0^+\rangle = \frac{1}{\sqrt{2}} \sum_j \alpha_j [a_j^\dagger a_j^\dagger]_0^0 |0\rangle, \quad (1.C.1)$$

where  $|0\rangle$  is the vacuum state and  $a_j^\dagger$  creates a particle in the orbital  $j$  with time-reversal properties  $\tau a_{jm}^\dagger \tau^{-1} = (-1)^{j-m} a_{j-m}^\dagger$ . The amplitudes  $\alpha_j$  are determined by the secular equation

$$(2\epsilon_j - E)\alpha_j = \sum_{j'} (j + 1/2)^{1/2} (j' + 1/2)^{1/2} G(j', j', j, j) \alpha_j. \quad (1.C.2)$$

If one replaces the radial integrals  $G(j', j', j, j) = -(V_0/4\pi) \int u_j^2(r) u_{j'}^2(r) r^2 dr$  (assuming the pairing force to be a contact interaction) by an average value  $G$ , the eigenvalues  $E$  are determined by the secular equation,

$$\frac{1}{G} = \sum_j \frac{(j + 1/2)}{2\epsilon_j - E} = \sum_j \sum_{m>0} \frac{1}{2\epsilon_j - E} = F(E). \quad (1.C.3)$$

The nature of the solution is illustrated in Fig. 1.C.1. When  $E$  goes from a value smaller to a value larger than  $2\epsilon_j$ ,  $F(E)$  decreases from  $+\infty$  to  $-\infty$  going through zero. The eigenvalues  $E$  are given by the intersection of  $F(E)$  with the line  $G^{-1}$ . While all other eigenvalues than the lowest one, are trapped between the unperturbed energies  $2\epsilon_j$ , the ground state correlation can freely increase as  $G$  increases.

Making use of the correspondence

$$\sqrt{j + 1/2} \leftrightarrow \Lambda_1 \quad (1.C.4)$$

and

$$G \leftrightarrow (E - \epsilon_m - V)^{-1}, \quad (1.C.5)$$

one can transform (1.C.3) into (1.7.58). Consequently, the graphical solution shown in Fig. 1.C.1 can be used for this dispersion relation (Fig. 1.7.7).

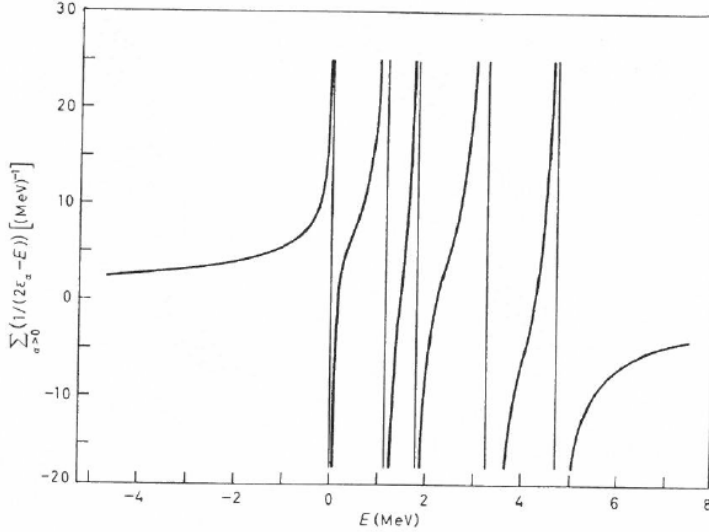


Figure 1.C.1: Dispersion relation for  $^{206}\text{Pb}$ . The single-hole states available to the two neutrons are  $p_{1/2}(0)$ ,  $f_{5/2}(0.57)$ ,  $p_{3/2}(0.89)$ ,  $i_{13/2}(1.63)$ ,  $f_{7/2}(2.34)$ . The label  $\alpha$  denotes the quantum numbers  $(j, m)$ .

### 1.C.2 Overlap

The states  $|\alpha\rangle$  and  $|\beta\rangle$  mix strongly through the couplings depicted by the graphs (a) and (b) of Fig. 1.7.10. Because of the energy dependence of the effective Hamiltonian (see (1.7.56), (1.7.57)) there is one matrix element for each state. The eigenvectors resulting from the diagonalization procedure were normalized according to (1.7.74). The corresponding amplitudes  $\xi_{iqm}$  (1.7.61) are displayed in Fig. 1.7.10 (e).

The normalization matrices  $\tilde{M}_{ii'}^{mm}$  associated with the two  $3/2^+$  states discussed in Sect. 1.5 and 1.7, are given in Table 1.C.1. Details concerning the off-diagonal matrix elements are collected in Table 1.C.2.

It is of notice that in a conventional two-state model calculation implying a single matrix one would obtain

$$|I\rangle = A|\alpha\rangle + B|\beta\rangle$$

and

$$|II\rangle = -B|\alpha\rangle + A|\beta\rangle, \quad (1.C.6)$$

with  $A^2 + B^2 = 1$ . This model would predict the value  $R = (\alpha/\beta)^2$  for the  $(t, \alpha)$  ratio  $R(t, \alpha) = \sigma_I^{tr}/\sigma_{II}^{tr}$  and  $1/R$  for the  $(\alpha, \alpha')$  ratio  $R(\alpha, \alpha') = \sigma_I^{oct}/\sigma_{II}^{oct}$  (see Sect. 1.7.4). The ratio  $R_{th}(t, \alpha) = 1.83/2.25 = 0.81$  (against  $R_{exp}(t, \alpha) = 0.82$ ) and  $R_{th}(\alpha, \alpha') = 2.5$  (against  $R_{exp}(\alpha, \alpha') = 3.8$ ) is a direct consequence of the overcompleteness of the basis which is taken care of by the nuclear field theory. While this is a

	$ \alpha\rangle$	$ \beta\rangle$		$ \alpha\rangle$	$ \beta\rangle$		$ \alpha\rangle$	$ \beta\rangle$
$ \alpha\rangle$	-0.010	-0.168	$ \alpha\rangle$	-0.012	-0.434	$ \alpha\rangle$	-0.011	-0.271
$ \beta\rangle$		0.009	$ \beta\rangle$		0.070	$ \beta\rangle$		0.03

Table 1.C.1: Normalization matrices (see Eq. (1.7.74)) associated with the two  $3/2^+$  states of  $^{209}\text{Bi}$ ,  $|I\rangle$  and  $|II\rangle$  (Fig. 1.7.10 (e)) (Bortignon, P. F. et al. (1977), table 4.6).

		Fig. 1.7.10		
$m$	$m'$	(b)	(c)	(b)+(c)
I	II	0.013	-0.181	-0.168
II	II	0.016	-0.450	-0.434
I	II	0.014	-0.285	-0.271

Table 1.C.2: Contributions to the off diagonal elements of the overlap matrix  $M_{ii'}^{mm'}$  associated with the  $3/2$  states in the basis  $|\alpha\rangle, |\beta\rangle$  (Table 1.C.1). See also figure 4.1 of Bortignon, P. F. et al. (1977).

systematic mathematical procedure to deal with the spurious state (in this case due to the overcompleteness of the basis  $\{|\alpha\rangle, |\beta\rangle\}$ ) one can also relate, within the framework of shell model calculations (see Eq. (1.C.1)), the asymmetry between  $R(t, \alpha)$  and  $R(\alpha, \alpha')$  to the finite overlaps between states  $|\alpha\rangle$  and  $|\beta\rangle$ , as discussed in Sect. 1.5.

## Appendix 1.D NFT and reactions

Nuclear Field Theory was systematically developed to describe nuclear structure processes. This fact did not prevent the translation into this graphical language of expressions which embodied the transition amplitude of a variety of reaction processes, in particular second order (in  $v_{np}$ ) transition amplitudes associated with two nucleon transfer reactions<sup>79</sup>.

The new feature to be considered regarding transfer processes and not encountered neither in structure, nor in elastic or anelastic processes, is the graphical representation of recoil effects. That is, a physical phenomenon associated with the change in the coordinate of relative motion reflecting the difference in mass partition between entrance (intermediate, if present) and exit channels. In fact, nuclear structure processes, do not affect the center of mass, with a proviso. In fact, the shell model potential violates the translational of the total nuclear Hamiltonian and, thus, single-particle excitations can be produced by a field proportional to the total center-of-mass coordinate. The translational invariance can be restored by including the effects of the collective field generated by a small displacement  $\alpha$  of the nucleus. Such a displacement, in the  $x$ -direction, gives rise to a coupling which

---

<sup>79</sup>Broglia, R. A. (1979).

can be written as<sup>80</sup>,

$$H_{coul} = \kappa\alpha F, \quad (1.D.1)$$

where

$$F = -\frac{1}{\kappa} \frac{\partial}{\partial x}, \quad (1.D.2)$$

and

$$\kappa = \int \frac{\partial}{\partial x} \frac{\partial \rho_0}{\partial x} d\tau = -A \left( \frac{\partial^2 U}{\partial x^2} \right), \quad (1.D.3)$$

corresponding to a normalization of  $\alpha$  such that  $\langle F \rangle = \alpha$ . It is of notice that both  $\kappa$  and  $A$  are negative for attractive fields (p. 356 of<sup>80</sup>)

The spectrum of normal modes generated by the field coupling (1.D.1), namely by a Galilean transformation of amplitude  $\alpha$ , contains an excitation mode with zero energy for which zero point fluctuations diverge in just the right way to restore translational invariance to leading order in  $\alpha$ . In fact, while

$$\lim_{\omega_\alpha \rightarrow 0} \frac{\hbar^2}{2D_\alpha \hbar \omega_\alpha} \quad (1.D.4)$$

diverges the inertia remains finite and equal to  $D_\alpha = AM$ , as expected.

The additional dipole roots include, in particular, the isoscalar dipole modes associated with  $\hat{D} = \sum_{i=1}^A r_i^3 Y_{1\mu}(\hat{r}_i)$ , which can be viewed as a non-isotropic compression mode<sup>81</sup>.

Naturally, the operators leading to transformations associated with the change in the coordinates of relative motion (recoil effects) are Galilean operators ( $\sim \exp(\mathbf{k}_{\alpha\beta} \cdot (\mathbf{r}_\beta - \mathbf{r}_\alpha))$ ). Their action (on e.g. the entrance channel), as that of (1.D.1) (on the shell model ground state), can be graphically represented in terms of NFT diagrams (or eventual extensions of them). In Figs 1.1.2 and 1.1.3 as well as 1.9.2–1.9.6 they are drawn in terms of jagged lines. How do we calculate such couplings. Let us elaborate on this point.

When one states that the small displacement  $\alpha$  of the nucleus leads to a coupling (1.D.1) one means a coupling between the single-particle and the collective displacement of the system as a whole. When one talks about the spectrum of normal modes associated with such a coupling, one refers to the harmonic approximation (RPA). Thus, to the solutions of the dispersion relation<sup>82</sup>,

$$-\frac{2\kappa}{\hbar} \sum_i \frac{|F_i|^2 \omega_i}{\omega_i^2 - \omega_a^2} = 1, \quad (1.D.5)$$

---

<sup>80</sup>see Bohr, A. and Mottelson (1975).

<sup>81</sup>See e.g. Colò et al. (2000).

<sup>82</sup>Bohr, A. and Mottelson (1975); Eq. (6-244).

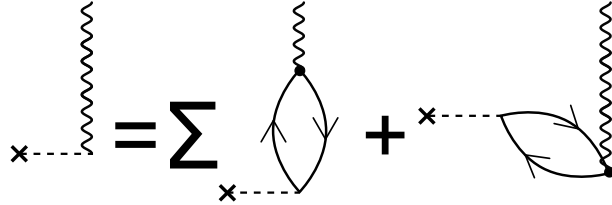


Figure 1.D.1: Self-consistent condition for normal modes

where the sum is over single-particle states. This dispersion relation can be represented graphically through the diagrams shown in Fig. 1.D.1. In particular,  $\alpha$  acting on the vacuum creates the collective mode. This can also be seen by expressing  $\alpha$  in second quantization, namely

$$\alpha = \sqrt{\frac{\hbar\omega_\alpha}{2C_\alpha}}(\Gamma_\alpha^\dagger + \Gamma_\alpha), \quad (1.D.6)$$

where  $\sqrt{\hbar\omega_\alpha/2C_\alpha} = \sqrt{\frac{\hbar^2}{2D_\alpha} \frac{1}{\hbar\omega_\alpha}}$  is the zero-point amplitude of the collective (displacement) mode. Now, none of the above arguments lose their meaning in the case in which there is a root with  $\omega_\alpha = 0$ , also in keeping with the fact the inertia remains finite. In Figs. 1.9.2–1.9.6 we do something similar to what is done in Fig. 1.D.1. The dot, which in this figure represents the particle-vibration coupling, is replaced by a small dashed open square, which we label “particle-recoil coupling vertex” (see labels Fig. 1.9.2). It constitutes a graphical mnemonic to count the degrees of freedom that are at play. In this case the coordinates of relative motion. Also the fact that in connection with the appearance of such vertices one has to calculate matrix elements of precise form factors which involve the recoil phases. As far as the actual calculation of a particle-mode vertex in which  $\omega_\alpha \rightarrow 0$ , an empirical way out is that of a coarse-grained-like symmetry restoration. In this case  $\kappa$  is adjusted in such a way, that the lowest solution of Eq. (1.D.5), although being smaller than the rest of them, remains finite<sup>83</sup>.

### 1.D.1 Potential scattering

The elastic differential cross section expressed in terms of partial waves is

$$\sigma(\theta) = |f(\theta)|^2 = \frac{1}{k^2} \left| \sum_{l=0}^{\infty} (2l+1) e^{i\delta_l} \sin \delta_l P_l(\cos \theta) \right|^2, \quad (1.D.7)$$

---

<sup>83</sup>Within this context we refer to Bohr, A. and Mottelson (1975), p. 446. With no coupling to ZPF  $\alpha_0^{(0)}$  of the nuclear CM are small ( $\sim A^{-1/3}$ ). Thus, it is possible to tune  $\kappa$  so as to make the ZPF associated with the lowest root large as compared to  $\alpha_0^{(0)}$ , but still compatible with the ansatz at the basis of RPA.

where

$$f(\theta) = \frac{1}{2ik} \sum_{l=0}^{\infty} (2l+1) (e^{2i\delta_l} - 1) P_l(\cos \theta), \quad (1.D.8)$$

is the scattering amplitude. The total cross section

$$\sigma = 2\pi \int_0^\infty \sigma(\theta) \sin \theta d\theta = \frac{4\pi}{k^2} \sum_{l=0}^{\infty} (2l+1) \sin^2 \delta_l \quad (1.D.9)$$

expressed in term of  $f$ , namely,

$$\sigma = \frac{4\pi}{k} \Im f(0), \quad (1.D.10)$$

being a particular case of the optical theorem. The quantity  $\delta_l$  is known as the phase shift of the  $l$ th partial wave, namely the difference in phase between the asymptotic form of the actual radial wavefunction describing the scattering process and the radial wavefunction  $j_l(kr)$  in the absence of potential. The phase shifts which completely determine the scattering lead to a change in the scaling between incoming and outgoing waves which results, as expressed in (1.D.10), in the interference between them, so that particle intensity is smaller behind the scattering region ( $\theta \approx 0$ ) than in front of it. It is of notice that  $\delta_l$  cannot be measured directly. In fact, with the exception of the  $l = 0$  phase shift, obtained from low-energy scattering experiments, the values of  $\delta_l$  are inferred as empirical quantities from the parametrization of the potential. Even so, a degree of ambiguity concerning the uniqueness of the findings may remain.

## 1.D.2 Transfer

We now consider a general reaction



in which the nucleus  $a$  impinges on the nucleus  $A$  in the entrance channel  $\alpha(a, A)$  and where the two nuclei in the exit channel  $\beta$ , namely  $b$  and  $B$  may differ from those in  $\alpha$ , by the transfer of one or more nucleons.

In the center-of-mass system, the total Hamiltonian may be written as

$$\begin{aligned} H &= T_{aA} + H_a + H_A + V_{aA}, \\ &= T_{bB} + H_b + H_B + V_{bB}, \end{aligned} \quad (1.D.12)$$

where  $T_{aA}$  is the kinetic energy of the relative motion in channel  $\alpha$

$$T_{aA} = -\frac{\hbar^2}{2m_{aA}} \nabla_{aA}^2, \quad (m_{aA} = \frac{m_a m_A}{m_a + m_A}), \quad (1.D.13)$$

and similarly for  $T_{bB}$ . Assuming the nuclei in (1.D.11) to be heavy ions, we shall solve the time-dependent Schrödinger equation

$$i\hbar \frac{\partial \Psi}{\partial t} = H\Psi \quad (1.D.14)$$

with the initial condition that  $a$  and  $A$  are in their ground states, and that the relative motion is described as a narrow wave-packet of rather well-defined impact parameter and velocity. Because of the quantal nature of the process under consideration, we study the quantal description in the limit of small wavelength of relative motion. One expands  $\Psi$  on the channel wavefunctions

$$\Psi_\beta(t) = \Psi_m^b(\xi_b)\Psi_n^B(\xi_B)e^{i\delta_\beta} \quad (1.D.15)$$

where  $\Psi^b$  and  $\Psi^B$  describe the structure of the two nuclei and satisfy the equations

$$H_b\Psi_m^b(\xi_b) = E_m^b\Psi_m^b(\xi_b) \quad (1.D.16)$$

and

$$H_B\Psi_n^B(\xi_B) = E_n^B\Psi_n^B(\xi_B), \quad (1.D.17)$$

while  $\xi_b$  and  $\xi_B$  denote the intrinsic coordinates. the phase  $\delta_\beta$  is defined by

$$\delta_\beta = \frac{1}{\hbar} \left\{ m_\beta \mathbf{v}_\beta(t)(\mathbf{r}_\beta - \mathbf{R}_\beta(t)) - \int_0^t \left( U_\beta(R_\beta(t')) - \frac{1}{2}m_\beta v_\beta^2(t') \right) dt' \right\}. \quad (1.D.18)$$

The index  $\beta$  labels both the partition of nucleons into  $b$  and  $B$ , as well as the quantal states of the two nuclei. The quantity  $U_\beta$  is the ion-ion potential in this channel. It is equal to the expectation value of  $V_\beta = V_{bB}$  in the channel  $\beta$ . The distance between the centers of mass of the two systems is denoted by

$$\mathbf{r}_\beta = \mathbf{r}_{bB} = \mathbf{r}_b - \mathbf{r}_B. \quad (1.D.19)$$

The quantity  $\mathbf{R}_\beta$  and its derivative  $\mathbf{v}_\beta = \dot{\mathbf{R}}_\beta$  describe the motion of the centers of mass of the wavepackets, and satisfy the corresponding classical equation of motion,

$$m_\beta \dot{\mathbf{v}}_\beta = -\nabla U_\beta(\mathbf{R}_\beta). \quad (1.D.20)$$

The phase factor  $e^{i\delta_\beta}$  in the channel wavefunction, is essentially a Galilean transformation where an additional phase (related with the  $Q$ -value) has been added to eliminate, as far as possible, the diagonal matrix elements of the coupled equations. Using the notation  $E_\beta = E_m^b + E_n^B$  and inserting the ansatz

$$\Psi = \sum_\beta c_\beta((r_\beta - R_\beta), t)\Psi_\beta(t)e^{-iE_\beta t/\hbar} \quad (1.D.21)$$

in eq. (1.D.14) one obtains, assuming narrow wavepackets, product of an amplitude  $a_\beta(t)$  and a shape  $\chi_\beta(\mathbf{r} - \mathbf{R}_\beta(t), t)$ , ( $c_\beta = a_\beta \chi_\beta$ ),

$$\begin{aligned} i\hbar \sum_\beta \dot{a}_\beta(t) \langle \Psi_\xi | \Psi_\beta \rangle_{\mathbf{R}_\xi} e^{-iE_\beta t/\hbar} \\ = \sum_\gamma \langle \Psi_\xi | V_\gamma - U_\gamma(r_\gamma) | \Psi_\gamma \rangle_{\mathbf{R}_\xi} a_\gamma(t) e^{-iE_\gamma t/\hbar}. \end{aligned} \quad (1.D.22)$$

where the sub-index on the matrix elements indicate that the integration over the degree of freedom of the two nuclei, the average center-of-mass coordinate  $\mathbf{r}_{\beta\gamma} = 1/2(\mathbf{r}_\beta + \mathbf{r}_\gamma)$  should be identified with the average classical coordinate, i.e.

$$\mathbf{r}_{\beta\gamma} \rightarrow \mathbf{R}_{\beta\gamma} = \frac{1}{2}(\mathbf{R} + \mathbf{R}_\gamma). \quad (1.D.23)$$

The coupled equations (1.D.22) can be written in a more compact way by an orthogonalization procedure, which makes use of the adjoint channel wavefunctions

$$\omega_\xi = \sum_\gamma g_{\xi\gamma}^{-1} \Psi_\gamma, \quad (1.D.24)$$

where  $g^{-1}$  is the inverse of the overlap matrix

$$g_{\xi\gamma} = \langle \Psi_\xi | \Psi_\gamma \rangle, \quad (1.D.25)$$

that is

$$\sum_\xi g_{\gamma\xi} g_{\xi\beta}^{-1} = \sum_\xi g_{\gamma\xi}^{-1} g_{\xi\beta} = \delta(\gamma, \beta). \quad (1.D.26)$$

With this definition,

$$(\omega_\xi, \Psi_\beta) = \delta(\xi, \beta), \quad (1.D.27)$$

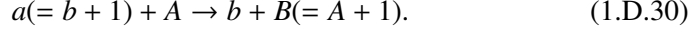
which takes care of non-orthogonality. Making use of the above relations one can rewrite (1.D.22) in the form

$$i\hbar \dot{a}_\beta(t) = \sum_\gamma \langle \omega_\beta | V_\gamma - U_\gamma | \Psi_\gamma \rangle_{\mathbf{R}_\beta} e^{i(E_\beta - E_\gamma)t/\hbar} a_\gamma(t) \quad (1.D.28)$$

By solving these coupled equations with the condition that at  $t = -\infty$  the system is in the ground state of  $a$  and  $A$  (entrance channel  $\alpha$ ), one can calculate the differential cross section

$$\frac{d\sigma_{\alpha \rightarrow \beta}}{d\Omega} = P_{\alpha \rightarrow \beta} \sqrt{\left( \frac{d\sigma_\alpha}{d\Omega} \right)_{el} \left( \frac{d\sigma_\beta}{d\Omega} \right)_{el}}, \quad (1.D.29)$$

where  $P_{\alpha \rightarrow \beta}$  is the absolute value squared of the transition amplitude  $|a_\beta(t = +\infty)|^2$ . It gives the probability that the system at  $t = +\infty$  is in the final channel. The quantities  $(d\sigma/d\Omega)_{el}$  are the (semiclassical) elastic cross sections. Let us now consider the one-particle transfer reaction



in first order perturbation theory

$$(a_\beta(t = +\infty))^{(1)} = \frac{1}{i\hbar} \int_{-\infty}^{\infty} dt' \langle \Psi_\beta | V_\alpha - U_\alpha | \Psi_\alpha \rangle_{\mathbf{R}_{\alpha\beta}} e^{i(E_\beta - E_\alpha)t'/\hbar}, \quad (1.D.31)$$

which is determined from (1.D.28) by inserting the zeroth-order amplitude,

$$a_\gamma(t) = \delta(\gamma, \alpha), \quad (1.D.32)$$

$\alpha$  denoting the entrance channel. Making use of (1.D.15), i.e.

$$\Psi_\alpha = \Psi^a \Psi^A e^{i\delta_\alpha}, \quad (1.D.33)$$

and

$$\Psi_\beta = \Psi^b \Psi^B e^{i\delta_\beta}, \quad (1.D.34)$$

one can write

$$\begin{aligned} \langle \Psi_\beta | V_\alpha - U_\alpha | \Psi_\alpha \rangle_{\mathbf{R}_{\alpha\beta}} &= \langle \Psi^b \Psi^B | (V_\alpha - U_\alpha) e^{i\sigma_{\alpha\beta}} | \Psi^a \Psi^A \rangle_{\mathbf{R}_{\alpha\beta}} e^{i\gamma_{\alpha\beta}} \\ &= \langle \phi^{B(A)}(S^B(n), r_{1A}), U(r_{1b}) e^{i\sigma_{\alpha\beta}} \phi^{a(b)}(S^a(n), r_{1b}) \rangle_{\mathbf{R}_{\alpha\beta}} e^{i\gamma_{\alpha\beta}}. \end{aligned} \quad (1.D.35)$$

To obtain the above relation, we have separated the difference between the phases  $\delta_\alpha$  and  $\delta_\beta$  into a part  $\gamma_{\alpha\beta}$  which only depends on time, and a phase  $\sigma_{\alpha\beta}$  which also depends on the center-of-mass coordinate of the transferred particles. That is

$$\begin{aligned} \gamma_{\alpha\beta}(t) &= \int_0^t \left\{ U_\alpha(R_\alpha(t)) - \frac{1}{2} m_\alpha v_\alpha^2(t') - U_\beta(R_\beta(t')) + \frac{1}{2} m_\beta v_\beta^2(t') \right\} \\ &\quad + \mathbf{k}_{\alpha\beta}(t)(\mathbf{R}_\alpha - \mathbf{R}_\beta), \end{aligned} \quad (1.D.36)$$

where  $\mathbf{k}_{\alpha\beta}$  is the average wave vector

$$\mathbf{k}_{\alpha\beta} = \frac{1}{2\hbar} (m_\alpha \mathbf{v}_\alpha(t) + m_\beta \mathbf{v}_\beta(t)). \quad (1.D.37)$$

Similarly

$$\sigma_{\alpha\beta} = \mathbf{k}_{\alpha\beta}(t) \cdot (\mathbf{r}_\beta - \mathbf{r}_\alpha). \quad (1.D.38)$$

The phase  $\sigma$  is characteristic for transfer processes since the dynamical variables  $\mathbf{r}_\alpha$  and  $\mathbf{r}_\beta$  are identical for inelastic scattering. It arises from the change in the

center-of-mass coordinate taking place when mass is transferred from one system to other. It gives rise to the recoil effect. Within the framework of DWBA it leads to a change of scaling of the DW (see also section elastic transfer). Summing up, the one-particle transfer amplitude reads

$$\begin{aligned} \left(a_\beta(t = +\infty)\right)^{(1)} &= \int_{-\infty}^{\infty} \langle \phi^{B(A)}(S^B(n), \mathbf{r}_{1A}), U_{1b}(r_{1b}) e^{\sigma_{\alpha\beta}} \phi^{a(b)}(S^a(n), \mathbf{r}_{1b}) \rangle_{\mathbf{R}_{\alpha\beta}} \\ &\times \exp\left\{i\left[(E_\beta - E_\alpha)t'/\hbar + \gamma_{\alpha\beta}\right]\right\} \end{aligned} \quad (1.D.39)$$

In a similar way in which the phases  $\delta_l$  determine the elastic scattering cross section, in the present case it is the phase  $\delta_{\alpha\beta}$ . In fact  $\delta_{\alpha\beta}$  determines the shift between incoming and outgoing waves and thus the interference process which is at the basis of the absolute value of the transfer differential cross section. In other words, the reaction part of the elastic and one-nucleon-transfer reaction cross section are embodied in  $\delta_l$  and  $\sigma_{\alpha\beta}$  respectively. The nucleon structure part is contained in the reduced mass  $\mu$  and potential  $U$  in the case of elastic scattering, and in the single-particle wavefunctions, potential  $U_{1b}$  and  $Q$ -value phase in the transfer case. Within the diagrammatic representation of particle-transfer reaction theory, the recoil phase is represented by a jagged line. Similar to  $\delta_l$ ,  $\sigma_{\alpha\beta}$  cannot be measured directly, but can in principle be inferred from the absolute cross section<sup>84</sup>.

---

<sup>84</sup>For more detail see Broglia and Winther (2004).

## Bibliography

- K. Alder and A. Winther. *Electromagnetic Excitations*. North Holland, Amsterdam, 1975.
- K. Alder, A. Bohr, T. Huus, B. Mottelson, and A. Winther. Study of Nuclear Structure by Electromagnetic Excitation with Accelerated Ions. *Rev. Mod. Phys.*, 28:432, 1956.
- N. Austern. *Direct nuclear reaction theories*. Interscience monographs and texts in physics and astronomy. Wiley–Interscience, 1970.
- M. Baranger. Recent progress in the understanding of finite nuclei from the two-nucleon interaction. In M. Jean and R. A. Ricci, editors, *Proceedings of the International school of physics “E. Fermi” XL course Nuclear Structure and Nuclear Reactions*, page 511. Academic Press, New York, 1969.
- Barnes, P., E. Romberg, C. Ellegard, R. Casten, O. Hansen, and J. Mulligan. *Nucl. Phys. A*, 195:1146, 1972.
- F. Barranco, R. A. Broglia, G. Colò, G. Gori, E. Vigezzi, and P. F. Bortignon. Many-body effects in nuclear structure. *European Physical Journal A*, 21:57, 2004.
- F. Barranco, P. F. Bortignon, R. A. Broglia, G. Colò, P. Schuck, E. Vigezzi, and X. Viñas. Pairing matrix elements and pairing gaps with bare, effective, and induced interactions. *Phys. Rev. C*, 72:054314, 2005.
- Barranco, F., P. F. Bortignon, R. A. Broglia, G. Colò, and E. Vigezzi. The halo of the exotic nucleus  $^{11}\text{Li}$ : a single Cooper pair. *Europ. Phys. J. A*, 11:385, 2001.
- B. F. Bayman. Seniority, Quasi-particle and Collective vibrations. *Lecture notes, Palmer Physical Laboratory, Princeton, unpublished*, 1961.
- Bayman, B. F. and C. F. Clement. Sum rules for two-nucleon transfer reactions. *Phys. Rev. Lett.*, 29:1020, 1972.
- S. Beceiro–Novo, T. Ahn, D. Bazin, and W. Mittig. Active targets for the study of nuclei far from stability. *Progress in Particle and Nuclear Physics*, 84:124, 2015.
- Bechara, M. J. and O. Dietzschi. States in  $^{121}\text{Sn}$  from the  $^{120}\text{Sn}(d, p)^{121}\text{Sn}$  reaction at 17 mev. *Phys. Rev. C*, 12:90, 1975.
- S. T. Belyaev. Effect of pairing correlations on nuclear properties. *Kgl. Danske Videnskab. Selskab. Mat.-fys. Medd.*, 31:No11, 1959.

- V. Bernard and N. V. Giai. Single-particle and collective nuclear states and the green's function method. In R. A. Broglia, R. A. Ricci, and C. H. Dasso, editors, *Proc. of the Int. School of Physics "Enrico Fermi", Course LXXVII*, p. 437. North Holland, Amsterdam, 1981.
- G. Bertsch and R. Broglia. *Oscillations in Finite Quantum Systems*. Cambridge University Press, Cambridge, 2005.
- G. F. Bertsch, P. F. Bortignon, and R. A. Broglia. Damping of nuclear excitations. *Rev. Mod. Phys.*, 55:287, 1983.
- D. R. Bès and R. A. Broglia. Effect of the multipole pairing and particle-hole fields in the particle-vibration coupling of  $^{209}\text{Pb}$ . I. *Physical Review C*, 3:2349, 1971a.
- D. R. Bès and R. A. Broglia. Effective operators in the analysis of single-nucleon transfer reactions on closed shell nuclei. *Physical Review C*, 3:2389, 1971b.
- D. R. Bès and R. A. Broglia. Equivalence between Feynman–Goldstone and particle–phonon diagrams for finite many body systems. In G. Alaga, V. Paar, and L. Sips, editors, *Problems of Vibrational Nuclei, in Procs. of the topical Conference on Problems of Vibrational Nuclei*, page 1, Amsterdam, 1975. North Holland.
- D. R. Bès and R. A. Broglia. Nuclear superfluidity and field theory of elementary excitations. In A. Bohr and R. A. Broglia, editors, *International School of Physics "Enrico Fermi" Course LXIX, Elementary Modes of Excitation in Nuclei*, page 55, Amsterdam, 1977. North Holland.
- D. R. Bès and R. A. Sorensen. The pairing–plus–quadrupole model. *Advances in Nuclear Physics*, 2:129, 1969.
- D. R. Bès, R. A. Broglia, and B. Nilsson. Importance of the quadrupole pairing field in the  $J^\pi = 0^+$  vibrations of shape deformed nuclei. *Physics Letters B*, 40:338, 1972.
- D. R. Bès, G. G. Dussel, R. A. Broglia, R. Liotta, and B. R. Mottelson. Nuclear field theory as a method of treating the problem of overcompleteness in descriptions involving elementary modes of both quasi-particles and collective type. *Phys. Lett. B*, 52:253, 1974.
- D. R. Bès, R. A. Broglia, G. G. Dussel, R. J. Liotta, and R. P. J. Perazzo. On the many-body foundation of the Nuclear Field Theory. *Nucl. Phys. A*, 260:77, 1976a.
- D. R. Bès, R. A. Broglia, G. G. Dussel, R. J. Liotta, and H. M. Sofía. The nuclear field treatment of some exactly soluble models. *Nucl. Phys. A*, 260:1, 1976b.

- D. R. Bès, R. A. Broglia, G. G. Dussel, R. J. Liotta, and H. M. Sofía. Application of the nuclear field theory to monopole interactions which include all the vertices of a general force. *Nucl. Phys. A*, 260:27, 1976c.
- Bès, D. R. and R. A. Broglia. Pairing vibrations. *Nucl. Phys.*, 80:289, 1966.
- Bès, D. R. and J. Kurchan. *The treatment of Collective Coordinates in Many-Body Systems*. World Scientific, Singapore, 1990.
- Bès, D. R. and Broglia, R. A. and Dussel, G. G. and Liotta. Simultaneous treatment of surface and pairing nuclear fields. *Phys. Lett. B*, 56:109, 1975.
- D. Bohm and D. Pines. A Collective Description of Electron Interactions. I. Magnetic Interactions. *Phys. Rev.*, 82:625, 1951.
- D. Bohm and D. Pines. A Collective Description of Electron Interactions: III. Coulomb Interactions in a Degenerate Electron Gas. *Phys. Rev.*, 92:609, 1953.
- A. Bohr. *Rotational Motion in Nuclei*, in *Les Prix Nobel en 1975*. Imprimerie Royale Norstedts Tryckeri, Stockholm, 1976. p. 59.
- A. Bohr and B. R. Mottelson. *Nuclear Structure, Vol.I*. Benjamin, New York, 1969.
- A. Bohr and B. R. Mottelson. Features of nuclear deformations produced by the alignment of individual particles or pairs. *Physica Scripta*, 22:468, 1974.
- A. Bohr, B. R. Mottelson, and D. Pines. Possible analogy between the excitation spectra of nuclei and those of the superconducting metallic state. *Physical Review*, 110:936, 1958.
- Bohr, A. and B. R. Mottelson. *Nuclear Structure, Vol.II*. Benjamin, New York, 1975.
- P. F. Bortignon, R. A. Broglia, D. R. Bès, R. Liotta, and V. Paar. Of the role of the pairing modes in the  $(h_{9/2} \otimes 3^-)$  multiplet of  $^{209}\text{Bi}$ . *Phys. Lett. B*, 64:24, 1976.
- Bortignon, P. F., R. A. Broglia, D. R. Bès, and R. Liotta. Nuclear field theory. *Physics Reports*, 30:305, 1977.
- Bortignon, P. F., R. A. Broglia, and D. R. Bès. On the convergence of nuclear field theory perturbation expansion for strongly anharmonic systems. *Phys. Lett. B*, 76:153, 1978.
- Bortignon, P. F., A. Bracco, and R. A. Broglia. *Giant Resonances*. Harwood Academic Publishers, Amsterdam, 1998.
- Brink, D. and R. A. Broglia. *Nuclear Superfluidity*. Cambridge University Press, Cambridge, 2005.

- R. A. Broglia. Microscopic structure of the intrinsic state of a deformed nucleus. In *Interacting Bose–Fermi systems in nuclei*, page 95. Plenum Press, New York, 1981. Iachello, F., Ed.
- R. A. Broglia and A. Winther. *Heavy Ion Reactions*. Westview Press, Boulder, CO., 2004.
- R. A. Broglia, D. R. Bès, and B. S. Nilsson. Strength of the multipole pairing coupling constant. *Physics Letters B*, 50:213, 1974.
- R. A. Broglia, B. R. Mottelson, D. R. Bès, R. Liotta, and H. M. Sofía. Treatment of the spurious state in Nuclear Field Theory. *Physics Letters B*, 64:29, 1976.
- R. A. Broglia, P. F. Bortignon, F. Barranco, E. Vigezzi, A. Idini, and G. Potel. Unified description of structure and reactions: implementing the Nuclear Field Theory program. *Physica Scripta*, in press, 2016.
- Broglia, R. A. Heavy Ion Reactions. *Lecture notes, Brookhaven National Lab. (unpublished)*, 1979.
- Broglia, R. A., J. S. Lilley, R. Perazzo, and W. R. Phillips. *Phys. Rev. C*, 1:1508, 1970.
- Broglia, R. A., V. Paar, and D. Bes. Diagramatic perturbation treatment of the effective interaction between two-photon states in closed shell nuclei: The  $J^\pi = 0^+$  states in  $^{208}\text{Pb}$ . *Physics Letters B*, 37:159, 1971a.
- Broglia, R. A., V. Paar, and D. Bes. Effective interaction between  $J^\pi = 2^+$  two-phonon states in  $^{208}\text{Pb}$ . Evidence of the isovector quadrupole mode. *Physics Letters B*, 37:257, 1971b.
- Broglia, R. A., C. Riedel, and T. Udagawa. Sum rules and two-particle units in the analysis of two-neutron transfer reactions. *Nuclear Physics A*, 184:23, 1972.
- Broglia, R. A. and Zelevinsky, V. . In R. A. Broglia and V. Zelevinsky, editors, *50 Years of Nuclear BCS*. World Scientific, Singapore, 2013.
- Broglia, R.A., O. Hansen, and C. Riedel. Two-neutron transfer reactions and the pairing model. *Advances in Nuclear Physics*, 6:287, 1973. URL [www.mi.infn.it/?vigezzi/BHR/BrogliaHansenRiedel.pdf](http://www.mi.infn.it/?vigezzi/BHR/BrogliaHansenRiedel.pdf).
- A. O. Caldeira and A. J. Leggett. Influence of dissipation on quantum tunneling in macroscopic systems. *Phys. Rev. Lett.*, 46:211, 1981.
- A. O. Caldeira and A. J. Leggett. Quantum tunneling in a dissipative system. *Ann. of Phys.*, 149:374, 1983.
- E. Chabanat, P. Bonche, P. Haensel, J. Meyer, and R. Schaeffer. A Skyrme parametrization from subnuclear to neutron star densities. *Nuclear Physics A*, 627:710, 1997.

- G. Colò, N. V. Giai, P. F. Bortignon, and M. R. Quaglia. On dipole compression modes in nuclei. *Physics Letters B*, 485:362, 2000.
- Dickey, S. A., J. Kraushaar, R. Ristinen, and M. Rumore. The  $^{120}\text{Sn}(p, d)^{119}\text{Sn}$  reaction at 26.3 MeV. *Nuclear Physics A*, 377:137, 1982.
- H. Feshbach. Unified Theory of Nuclear Reactions. *Annals of Physics*, 5:357, 1958.
- R. Feynman. *Theory of fundamental processes*. Benjamin, Reading, Mass., 1975.
- Flynn, E. R., G. J. Igo, and R. A. Broglia. Three-phonon monopole and quadrupole pairing vibrational states in  $^{206}\text{Pb}$ . *Phys. Lett. B*, 41:397, 1972.
- Flynn, E.R. and Igo, G. and Barnes, P.D. and Kovar, D. and Bès, D. R. and Broglia, R.A. Effect of multipole pairing particle-hole fields in the particle-vibration coupling of  $^{208}\text{Pb}$  (II). The  $^{207}\text{Pb}(t, p)^{209}\text{Pb}$  reaction at 20 MeV. *Phys. Rev. C*, 3: 2371, 1971.
- Glendenning, N. K. *Direct nuclear reactions*. World Scientific, Singapore, 2004.
- W. Heisenberg. *The physical principles of quantum theory*. Dover, New York, 1949.
- A. Idini, G. Potel, F. Barranco, E. Vigezzi, and R. A. Broglia. Interweaving of elementary modes of excitation in superfluid nuclei through particle-vibration coupling: Quantitative account of the variety of nuclear structure observables. *Phys. Rev. C*, 92:031304, 2015.
- Idini, A., G. Potel, Barranco, E. Vigezzi, and R. A. Broglia. Dual origin of pairing in nuclei. *arXiv:1404.7365v1 [nucl-th]*, 2014.
- K. Kubo, R. Broglia, and T. Riedel, C. Udagawa. Determination of the  $Y_4$  deformation parameter from  $(p, t)$  reactions. *Phys. Lett. B*, 32:29, 1970.
- L. Landau. *Joun. Phys. USSR*, 5:71, 1941.
- W. A. Lanford. Systematics of two-neutron-transfer cross sections near closed shells: A sum-rule analysis of  $(p, t)$  strengths on the lead isotopes. *Phys. Rev. C*, 16:988, 1977.
- Mahaux, C., P. F. Bortignon, R. A. Broglia, and C. H. Dasso. Dynamics of the shell model. *Physics Reports*, 120:1–274, 1985.
- M. Mayer and J. Jensen. *Elementary Theory of Nuclear Structure*. Wiley, New York, NY, 1955.

- M. H. McFarlane. The reaction matrix in nuclear shell theory. In M. Jean and R. A. Ricci, editors, *Proceedings of the International school of physics “E. Fermi” XL course Nuclear Structure and Nuclear Reactions*, page 457. Academic Press, New York, 1969.
- B. R. Mottelson. Selected topics in the theory of collective phenomena in nuclei. In G. Racah, editor, *International School of Physics “Enrico Fermi” Course XV , Nuclear Spectroscopy*, page 44, New York, 1962. Academic Press.
- B. R. Mottelson. *Elementary Modes of Excitation in Nuclei, Le Prix Nobel en 1975*. Imprimerie Royale Norstedts Tryckeri, Stockholm, 1976a. p. 80.
- B. R. Mottelson. Atomkernens elementære eksitationer. *Naturens Verden*, 6:169, 1976b.
- S. G. Nilsson. Binding states of individual nucleons in strongly deformed nuclei. *Mat. Fys. Medd. Dan. Vid. Selk.*, 29, 1955.
- F. Perey and B. Buck. A non-local potential model for the scattering of neutrons by nuclei . *Nuclear Physics*, 32:353, 1962.
- D. Pines and D. Bohm. A Collective Description of Electron Interactions: II. Collective vs Individual Particle Aspects of the Interactions. *Phys. Rev.*, 85:338, 1952.
- Pines, D. and Nozières. *The theory of quantum liquids*. Benjamin, New York, 1966.
- G. Potel, F. Barranco, E. Vigezzi, and R. A. Broglia. Evidence for phonon mediated pairing interaction in the halo of the nucleus  $^{11}\text{Li}$ . *Phys. Rev. Lett.*, 105:172502, 2010.
- Potel, G., A. Idini, F. Barranco, E. Vigezzi, and R. A. Broglia. Cooper pair transfer in nuclei. *Rep. Prog. Phys.*, 76:106301, 2013.
- I. Ragnarsson and R. A. Broglia. Pairing isomers. *Nuclear Physics A*, 263:315, 1976.
- H. Reinhardt. Foundation of nuclear field-theory. *Nucl. Phys. A*, 241:317, 1975.
- H. Reinhardt. Functional approach to Nuclear Field-theory - schematic model with pairing and particle-hole forces. *Nucl. Phys. A*, 298:60, 1978a.
- H. Reinhardt. Nuclear Field-Theory. *Nucl. Phys. A*, 251:77, 1978b.
- H. Reinhardt. Application of the nuclear-field theory to superfluid nuclei-quasiparticle-phonon multiplet. *Nucl. Phys. A*, 251:176, 1980.
- G. Satchler. *Introduction to Nuclear Reactions*. Mc Millan, New York, 1980.

- G. Satchler. *Direct Nuclear Reactions*. Clarendon Press, Oxford, 1983.
- J. Schwinger. *Quantum Mechanics*. Springer, Heidelberg, 2001.
- I. Tanihata, H. Savajols, and R. Kanungo. Recent experimental progress in nuclear halo structure studies. *Progress in Particle and Nuclear Physics*, 68:215, 2013.
- Tanihata, I., M. Alcorta, D. Bandyopadhyay, R. Bieri, L. Buchmann, B. Davids, N. Galinski, D. Howell, W. Mills, S. Mythili, R. Openshaw, E. Padilla-Rodal, G. Ruprecht, G. Sheffer, A. C. Shotter, M. Trinczek, P. Walden, H. Savajols, T. Roger, M. Caamano, W. Mittig, P. Roussel-Chomaz, R. Kanungo, A. Gallant, M. Notani, G. Savard, and I. J. Thompson. Measurement of the two-halo neutron transfer reaction  ${}^1\text{H}({}^{11}\text{Li}, {}^9\text{Li}){}^3\text{H}$  at 3A MeV. *Phys. Rev. Lett.*, 100:192502, 2008.
- J. Ungrin, R. M. Diamond, P. O. Tjøm, and B. Elbek. Inelastic deuteron scattering in the lead region. *Mat. Fys. Medd. Dan. Vid. Selk.*, 38, 1971.

# Chapter 2

## Pairing with transfer

### 2.1 Nuclear Structure in a nutshell

The low-energy properties of the finite, quantal, many-body nuclear system, in which nucleons interact through the strong force of strength  $v_0(\approx -100 \text{ MeV})$  and range  $a(\approx 1 \text{ fm})$  are controlled, in first approximation, by independent particle motion. This is a consequence of the fact that nucleons display a sizable value of the zero point (kinetic) energy of localization ( $\hbar^2/Ma \approx 40 \text{ MeV}$ ) as compared to the absolute value of the strength of the  $NN$ -potential<sup>1</sup>  $|v_0| = 100 \text{ MeV}$

The corresponding ground state  $|HF\rangle = \prod_i a_i^\dagger |0\rangle$  describes a step function in the probability of the occupied ( $\epsilon_i \leq \epsilon_F$ ) and empty ( $\epsilon_k > \epsilon_F$ ) states. Pushing the system it reacts with an inertia  $AM$ , sum of the nucleon masses. Setting it into rotation, assuming the density  $\rho(r) = \sum_i |\langle \mathbf{r}|i\rangle|^2$  ( $|i\rangle = a_i^\dagger |0\rangle$ ) to be spatially deformed, it responds with the rigid moment of inertia. This is because the single-particle orbitals are solidly anchored to the mean field.

Pairing acting on nucleons moving in time reversal states  $\nu, \bar{\nu}$  ( $\nu \equiv (nlj)$ ), in configurations of the type  $((l)_{L=0}^2, (s)_{S=0}^2)$ , and lying close to the Fermi energy  $\epsilon_F(\approx 36 \text{ MeV})$ , alter this picture in a conspicuous way<sup>2</sup>. Within an energy range of the order of the absolute value of the pair correlation energy<sup>3</sup>  $E_{corr}(\approx -3 \text{ MeV})$

<sup>1</sup>The corresponding ratio  $q = \left(\frac{\hbar^2}{Ma^2}\right) \frac{1}{|v_0|}$  is known as the quantity parameter and was first used in connection with the study of condensed matter (de Boer (1948, 1957); de Boer and Lundbeck (1948); ?). It was introduced in nuclear physics in Mottelson (1998) where its value  $q = 0.4$  testifies to the validity of independent particle motion. It is f notice that questions like the one posed in connection with localization and long mean free path were already discussed by Lindemann (1910) in connection with the study of the stability or less of crystals. The generalization to aperiodic crystals, like e.g. proteins (Schrödinger, E. (1944)) was carried out in Stillinger and Stillinger (1990). Its application to the atomic nucleus is discussed in App. 2.C

<sup>2</sup>Broglia, R. A. and Zelevinsky, V. (2013).

<sup>3</sup>In BCS,  $E_{corr} \approx \frac{N(0)}{2} \Delta^2$ , where  $N(0) = \frac{g}{2}$  is the density of states at the Fermi energy and for one spin orientation,  $g_i = i/16 \text{ MeV}^{-1}$  ( $i = N, Z$ ) being the result of an empirical estimate which takes surface effects into account (Bohr, A. and Mottelson (1975); Bortignon, P. F. et al. (1998)), while  $\Delta$  is the pairing gap. For a typical superfluid, quadrupole deformed nucleus like  $^{170}\text{Yb}$ ,  $N(0) = 5.3 \text{ MeV}^{-1}$ ,  $\Delta \approx 1.1 \text{ MeV}$  and  $E_{corr} = -3.2 \text{ MeV}$  (Shimizu, Y. R. et al. (1989)).

centered around  $\epsilon_F$  ( $|E_{corr}|/\epsilon_F \ll 1$ ), the role of independent particles is taken over by independent pairs of nucleons, correlated distances  $\xi \approx \hbar v_F/(2\Delta) (\approx 30 \text{ fm})$ , which flicker in and out of the corresponding  $L = 0, S = 0$  configuration (Cooper pairs<sup>4,5</sup>).

For intrinsic<sup>6</sup> nuclear excitation energies and rotational frequencies<sup>7</sup> sensibly smaller than  $|E_{corr}/2|$  and  $\hbar\omega_{rot} \approx 0.5 \text{ MeV}$  respectively, the system can be described in terms of independent pair motion. This is a consequence of the fact that the kinetic energy of (Cooper) pair confinement ( $\hbar^2/(2M\xi^2) \approx 10^{-2} \text{ MeV}$ ), is much smaller than the absolute value of the pair binding energy  $|E_{corr}|$ , implying that each pair behaves as an entity<sup>8</sup> of mass  $2M$  and spin  $S = 0$ . Cooper pairs respect Bose–Einstein statistics, the single-particle orbits on which they correlate become dynamically detached from the mean field, leading to a bosonic-like condensate. This has a number of consequences. In particular, the moment of inertia  $\mathcal{J}$  of quadrupole rotational bands of superfluid nuclei with open shells of both protons and neutrons is found to be smaller than the rigid moment of inertia by a factor of 2. The observed values, however, are a factor of 5 larger than the irrotational moment of inertia<sup>9</sup>, testifying to a subtle interplay between pairing and shell effects.

Cooper pairs exist also in situations in which the environmental conditions are above critical. For example, in metals at room temperature, in closed shell nuclei as well as in deformed open shell ones at high values of the angular momentum. However, in such circumstances, they break as soon as they are generated (pairing vibrations). While these pair addition and subtraction fluctuations have little effect in condensed matter systems with the exception that at<sup>10</sup>  $T \approx T_c$ , they play an important role in nuclei. In particular in nuclei around closed shells (Fig. 2.1.1), and specially in the case of light, highly polarizable, exotic halo nuclei<sup>11</sup>. From this vantage point one can posit that it is not so much, or, at least not only, the superfluid

<sup>4</sup>Cooper (1956).

<sup>5</sup>Brink, D. and Broglia (2005).

<sup>6</sup>As opposed to collective excitations, excitations which do not alter the temperature of the system.

<sup>7</sup>Coriolis force acts oppositely on each member of a Cooper pair. When the difference in rotational energy between superfluid and normal rotation becomes about equal to the correlation energy, the nucleon moving opposite to the collective rotation becomes so much retarded in its revolution period with respect to the partner nucleon, that eventually it cannot correlate any more with it and “align” its motion (and spin) with the rotational motion, becoming again a pair of fermions and not participating any more in the condensate. This happens for a (critical) angular momentum  $I_c \approx (120 \times |E_{corr}|)^{1/2} \approx 20\hbar$ , corresponding to a rotational frequency  $\hbar\omega_c \approx 0.5 \text{ MeV}$  (Brink, D. and Broglia (2005)).

<sup>8</sup>The ratio  $q\xi = \frac{\hbar^2}{2M\xi^2} \frac{1}{|E_{corr}|} \approx 0.007$  provides a generalized quantality parameter. It testifies to the stability of nuclear Cooper pairs in superfluid nuclei.

<sup>9</sup>Bohr, A. and Mottelson (1975); Belyaev (1959); Belyaev, S. T. (2013).

<sup>10</sup>Schmid, A. (1966), Schmidt, H. (1968), Schmid, A. (1969) Abrahams, E. and Woo (1968); concerning superfluid  ${}^3\text{He}$  cf. Wölfe, P. (1978).

<sup>11</sup>See Sects. 2.5 and 2.6; Bohr, A. and Mottelson (1975), Bès, D. R. and Broglia (1966), Högaasen-Feldman (1961), Schmidt, H. (1972), Schmidt, H. (1968), Barranco, F. et al. (2001), Potel, G. et al. (2013a), Potel et al. (2014).

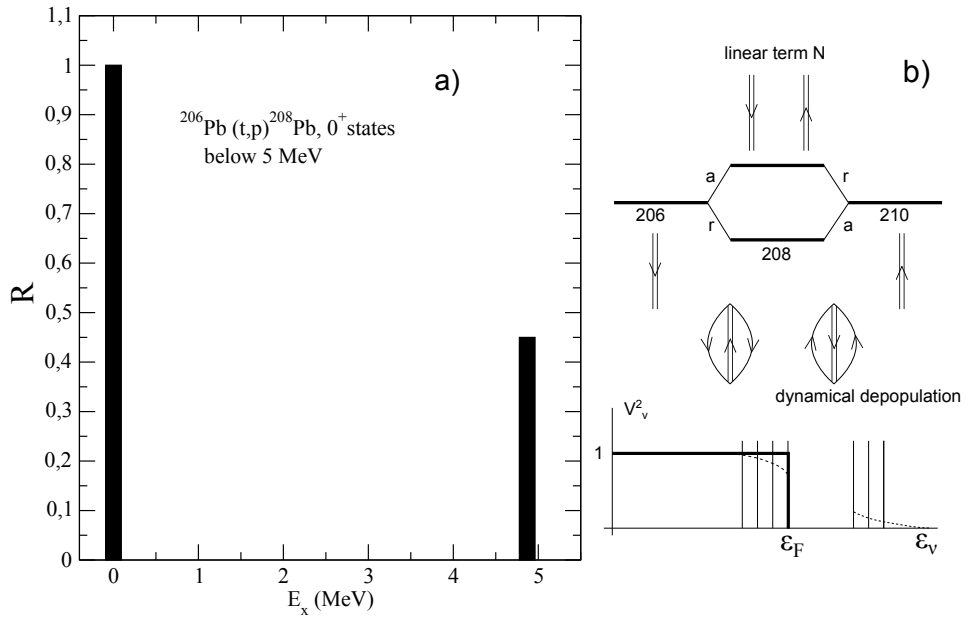


Figure 2.1.1: (a) Ratio of the absolute  $L = 0$  differential cross sections  $d\sigma(E_x, \theta = 59^\circ)/d\sigma(gs, \theta = 59^\circ)$  ( $= (0.05 \text{ mb/sr})/(0.12 \text{ mb/sr})$ ) below 5 MeV for the reaction  $^{206}\text{Pb}(t, p)^{208}\text{Pb}$  at the second minimum ( $\theta = 59^\circ$ ; Bjerregaard, J. H. et al. (1966)). It is of notice the large experimental errors of the corresponding angular distributions associated with the poor statistics of the cross section at the first maximum  $\theta = 5^\circ$ . This is the reason why the maximum at  $59^\circ$  was preferred to report the ratio of the cross sections. (b) Schematic representation of the pairing vibrational spectrum around  $^{208}\text{Pb}$ . Also shown is a cartoon representation of the softening of the sharp mean field Fermi surface due to the ZPF of the pairing vibrational modes. The label  $a$  and  $r$  indicate the pair addition and pair removal modes. It is to be noted that a linear term in  $N$  has been added to the binding energy to make the binding energy values associated with  $^{206}\text{Pb}$  ( $N = 124$ ) and  $^{210}\text{Pb}$  ( $N = 128$ ), equal, in an attempt to emphasize a harmonic picture for the two-phonon state. Concerning the anharmonicities of the modes cf. last paragraph Sect. 2.5.

state which is abnormal in the nuclear case, but the normal state associated with closed shell systems<sup>12</sup>. It is of notice nonetheless, the role pairing vibrations play in the transition between superfluid and normal nuclear phases (cf. Fig. 2.1.2) as a function of the rotational frequency (angular momentum) as emerged from the experimental studies of high spin states carried out by, among others, Garrett and collaborators<sup>13</sup>.

From Fig. 2.1.2 it is seen that while the dynamic pairing gap associated with pairing vibrations leads to a  $\approx 20\%$  increase of the static pairing gap for low rotational frequencies, it becomes the overwhelming contribution above the critical frequency<sup>14</sup>. In any case, the central role played by pairing vibrations within the present circumstances is that to restore particle-number conservation, another example after that provided by the quantality parameter and by its generalization to pair motion, of the fact that potential functionals are, as a rule, best profited by special arrangements of fermions (spontaneous symmetry breaking), while fluctuations restore symmetry<sup>15</sup>.

Within this context, there are a number of methods which allows one to go beyond mean-field approximation (HFB). Generally referred to as number projection methods<sup>16</sup>(NP), they make use of a variety of techniques (Generator Coordinate Method, Pfaffians, etc.) as well as protocols (variation after projection, gradient method, etc.). The advantages of NP methods over the RPA is to lead to smooth functions for both the correlation energy and the pairing gap at the pairing phase transition between normal and superfluid phases. That is, between the pairing vibrational and pairing rotational schemes<sup>17</sup>.

The above results underscore the fact that, at the basis of an operative coarse grained approximation to the nuclear many-body problem (within this context cf. App. 1.D, in particular the discussion following Eq. 1.D.5), one finds a judicious choice of the collective coordinates<sup>18</sup>. In other words, pairing vibrations are elementary modes of excitation containing the right physics to restore gauge invariance through their interweaving with quasiparticle states. Within the framework of the above picture, one can introduce at profit a collective coordinate  $\alpha_0$  (order parameter) which measures the number of Cooper pairs participating in the pairing condensate, and define a wavefunction for each pair  $(U'_v + V'_v a'_v^\dagger a'_{\bar{v}}^\dagger)|0\rangle$  (indepen-

<sup>12</sup>See Potel, G. et al. (2013a) and refs. therein. Also Potel, G. et al. (2013b) in connection with the closed shell system  $^{132}\text{Sn}$ .

<sup>13</sup>cf. Shimizu, Y. R. et al. (1989); cf. also Brink, D. and Broglia (2005), Ch. 6 and references therein.

<sup>14</sup>Shimizu, Y. R. et al. (1989), Shimizu, Y. R. and Broglia (1990), Shimizu, Y. R. (2013), Dönau, F. et al. (1999) Shimizu, Y. R. et al. (2000).

<sup>15</sup>??.

<sup>16</sup>cf. Ring, P. and Schuck (1980), Egido, J. L. (2013), Robledo, R. M. and Bertsch (2013); cf. also Frauendorf, S. (2013), Ring, P. (2013), Heenen, P. H. et al. (2013), and references therein.

<sup>17</sup>Figs. 2.1.1, 2.1.3, 2.1.4, see also Fig. 2.4.1 and Sects. 2.4.2 and 2.5; cf. Bès, D. R. and Broglia (1966), Bohr, A. and Mottelson (1975) and references therein.

<sup>18</sup>In this connection, we quote allegedly from S. Weinberg: “In solving a problem you may choose to use the degrees of freedom you like. But if you choose the wrong ones you will be sorry”.

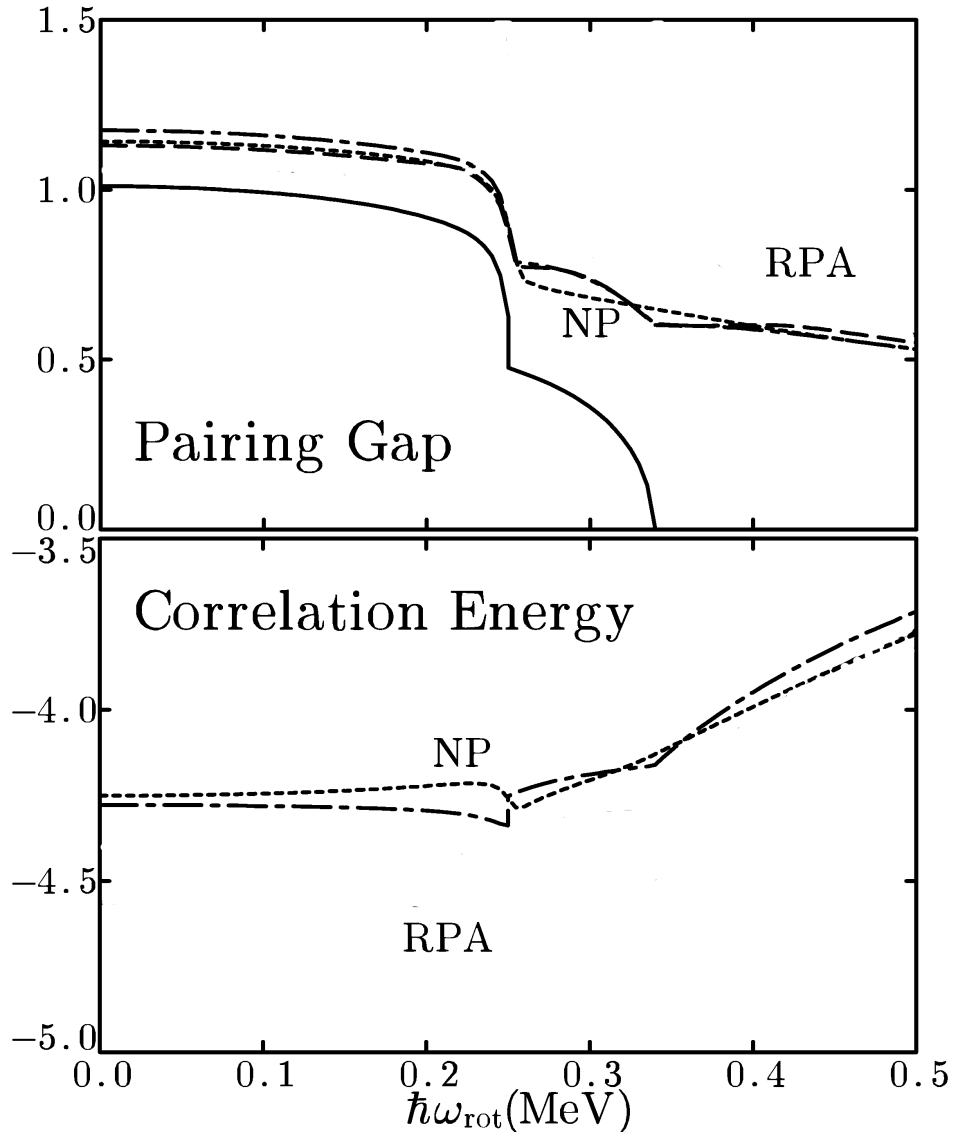


Figure 2.1.2: Pairing gap calculated taking into account the correlation associated with pair vibrations in the RPA approximation ( $\Delta = (\Delta_{BCS}^2 + \frac{1}{2}G^2 S_0(RPA)))^{1/2}$  (upper panel) and RPA correlation energy (lower panel) for neutrons in  $^{164}\text{Er}$  as a function of the rotational frequency. Both quantities are in MeV (dashed-dotted curves). The value of the static (mean-field) pairing gap  $\Delta$ , which vanishes at  $\hbar\omega_{rot} = 0.34$  MeV, is also displayed in the upper panel (continuous curve). The results of the number-projection (NP) calculations are shown as dotted curves.  $S_0(RPA) = \sum_{n \neq AGN} [ \langle n|P|0 \rangle + \langle n|P^\dagger|0 \rangle ]_{RPA}^2$ , where  $\Delta_{BCS} = G \langle BCS|P^\dagger|BCS \rangle$  is the standard, static BCS pairing gap, while  $G$  is the pairing force strength. The non-energy weighted sum rule  $S_0(RPA)$  describes the contribution of pairing fluctuations to the effective (RPA) gap, and is intimately associated with projection in particle number. It is of notice that  $\sum_{n \neq AGN}$  means that the divergent contribution from the zero energy mode (Anderson, Goldstone, Nambu mode, see e.g. Broglia et al. (2000) and references therein), associated with the lowest ( $\hbar\omega_0$ ) solution of the  $H = H'_p + H''_p$  (cf. Sect 6.2.3 and Brink, D. and Broglia (2005) App. J) is to be excluded (after Shimizu, Y. R. and Broglia (1990)).

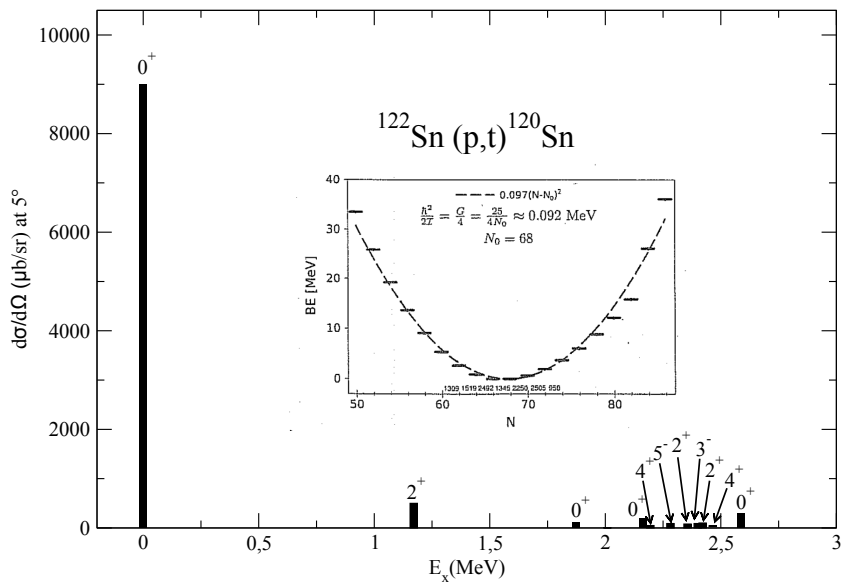


Figure 2.1.3: Excitation function associated with the reaction  $^{122}\text{Sn}(p, t)^{120}\text{Sn}(J^\pi)$ . The absolute experimental values of  $d\sigma(J^\pi)/d\Omega|_{5^\circ}$  are given as a function of the excitation energy  $E_x$  (after Guazzoni, P. et al. (2011)). In the inset the full neutron pairing rotational band between magic numbers  $N = 50$  and  $N = 82$  is also displayed, the absolute  $^{A+2}\text{Sn}(p, t)^A\text{Sn}$  experimental cross sections are reported in the abscissa (Guazzoni, P. et al. (1999), Guazzoni, P. et al. (2004), Guazzoni, P. et al. (2006), Guazzoni, P. et al. (2008), Guazzoni, P. et al. (2011), Guazzoni, P. et al. (2012); see also Potel, G. et al. (2011), Potel, G. et al. (2013b)).

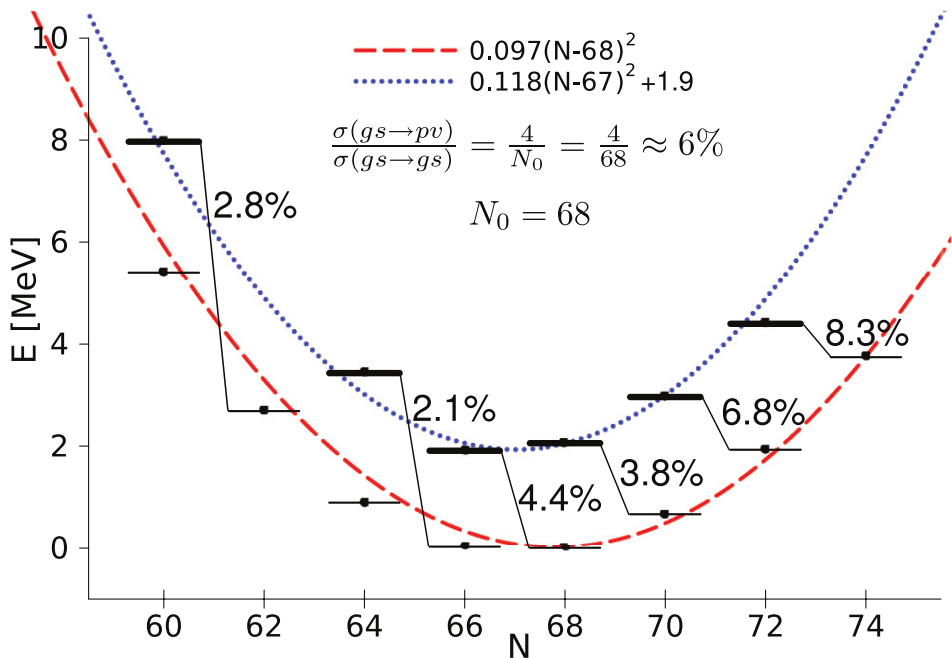


Figure 2.1.4: The weighted average energies ( $E_{exc} = \sum_i E_i \sigma_i / \sum_i \sigma_i$ ) of the excited  $0^+$  states below 3 MeV in the Sn isotopic chain are shown on top of the pairing rotational band, already displayed in Fig. 2.1.3. Also indicated is the percentage of cross section for two-neutron transfer to excited states, normalized to the cross sections populating the ground states (after Potel, G. et al. (2013b)). The estimate of the ratio of cross sections displayed on top of the figure was obtained making use of the single  $j$ -shell model (see, e.g., Brink, D. and Broglia (2005) and references therein).

dent pair motion, BCS approximation, cf. Figs. 2.4.1, 2.4.2 and 2.4.3), adjusting the occupation parameters  $V_\nu$  and  $U_\nu$  (probability amplitudes that the two-fold, Kramer's-degenerate pair state  $(\nu, \bar{\nu})$ , is either occupied or empty), so as to minimize the energy of the system under the condition that the average number of nucleons is equal to  $N_0$  (the Coriolis-like force felt, in the intrinsic system in gauge space by the Cooper pairs, being equal to  $-\lambda N_0$ ). Thus,  $|BCS\rangle = \prod_{\nu>0} (U'_\nu + V'_\nu a'_\nu a'^\dagger_{\bar{\nu}}) |0\rangle$  provides a valid description of the independent pair mean field ground state, and of the associated order parameter  $\alpha'_0 = \langle BCS | P'^\dagger | BCS \rangle = \sum_{\nu>0} U'_\nu V'_\nu$ ,  $P'^\dagger = \sum_{\nu>0} a'^\dagger_\nu a'^\dagger_{\bar{\nu}}$  being the pair creation operator<sup>19</sup>. It is then natural to posit that two-particle transfer reactions are specific to probe pairing correlations in many-body fermionic systems. Examples are provided by the Josephson effect<sup>20</sup> between e.g. metallic superconductors, and  $(t, p)$  and  $(p, t)$  reactions in atomic nuclei<sup>21</sup>

Within this context we now take the basic consequence of pairing condensation in nuclei regarding reaction mechanisms. for this purpose let us consider a *gedanken experiment* in which the superfluid target and the projectile can at best come in such weak contact that only single-nucleon transfer leads to a yield falling within the sensitivity range of the measuring setup. Because  $(\hbar^2/2M\xi^2)/|E_{corr}| \approx 10^{-2}$ , Cooper pairs in superfluid nuclei behave as particles of mass  $2M$  over distances  $\xi$ , even in the case in which the  $NN$ -potential vanishes in the zone between the weakly overlapping densities of the two interacting nuclei. One then expects Cooper pair transfer to be observed. Not only. One also expects that the associated absolute differential cross section contains, for the particular choice of mass number done and within the framework of the theory of quantum measurement, all the information needed to work out a comprehensive description of nuclear superfluidity.

Because  $\alpha_0 \sim N(0)$ , cross sections associated with the transfer of Cooper pairs between members of a pairing rotational band, are proportional to the density of single-particle levels quantity squared. As a consequence, absolute two-nucleon transfer cross sections are expected to be of the same order of magnitude than one-nucleon transfer ones, and to be dominated by successive transfer. These expectations have been confirmed experimentally and by detailed numerical calculations, respectively. The above parlance, being at the basis of the Josephson effect, reflects both one of the most solidly established results in the study of BCS pairing, and explains the workings of a paradigmatic probe of spontaneous symmetry breaking phenomena.

Due to the fact that, away from the Fermi energy pair motion becomes independent particle motion (see Sect. 2.4), one-particle transfer reactions like e.g.  $(d, p)$  and  $(p, d)$  can be used together with  $(t, p)$  and  $(p, t)$  processes, as valid tools

---

<sup>19</sup>cf. Bardeen et al. (1957a), Bardeen et al. (1957b), Schrieffer (1964), Schrieffer, J. R. (1973) and references therein.

<sup>20</sup>Josephson (1962).

<sup>21</sup>cf. e.g. Yoshida (1962), Broglia, R.A. et al. (1973), Bayman (1971), Glendenning, N. K. (1965), Bohr (1964), Hansen (2013) and Potel, G. et al. (2013a) and references therein; cf. also Figs. 2.1.1, 2.1.3 and 2.1.4.

to cross check pair correlation predictions (see Chapter 4). In particular, to shed light on the origin of pairing in nuclei: in a nutshell, the relative importance of the bare  $NN$ -interaction and the induced pairing interaction (within this context see Sect. 2.6).

While the calculation of two-nucleon transfer spectroscopic amplitudes and differential cross sections are, *a priori*, more involved to be worked out than those associated with one-nucleon transfer reactions, the former are, as a rule, more “intrinsically” accurate than the latter ones. This is because, in the case of two nucleon transfer reactions, the quantity (order parameter  $\alpha'_0$ ) which expresses the collectivity of the members of a pairing rotational band, reflects the properties of a coherent state ( $|BCS\rangle$ ). In other words, it results from the sum over many contributions ( $\sqrt{j_\nu + 1/2} U'_\nu V'_\nu$ , cf. Sect. 2.4), all of them having the same phase. Consequently, the relative error decreases as the square root of the number contributions ( $\approx N(0)\Delta \approx 4 \text{ MeV}^{-1} \times 1.4 \text{ MeV} \approx 6$  in the case of the superfluid nucleus  $^{120}\text{Sn}$ ).

There is a further reason which confers  $\alpha'_0 = \sum_j (j + 1/2) U'_j V'_j$  a privileged position with respect to the single contributions  $(j + 1/2) U'_j V'_j$ . It is the fact that  $\alpha'_0 = e^{2i\varphi} \sum_j (j + 1/2) U_j V_j = e^{2i\varphi} \alpha_0$  defines a privileged orientation in gauge space,  $\alpha_0$  being the order parameter referred to the laboratory system which makes an angle  $\varphi$  in gauge space with respect to the intrinsic system to which  $\alpha'_0$  is referred<sup>22</sup>. In other words, the quantities  $\alpha'_0$  which measure the deformation of the superfluid nuclear system in gauge space, and the rotational frequency  $\lambda = \hbar\dot{\varphi}$  in this space, and associated Coriolis force  $-\lambda N_0$  felt by the nucleons referred to the body fixed frame, are the result of solving selfconsistently the BCS number

and gap equations  $N_0 = \sum_j (2j + 1) \left( 1 - \frac{(\epsilon_j - \lambda)/\Delta}{\sqrt{1 + (\frac{\epsilon_j - \lambda}{\Delta})^2}} \right)$  and  $\alpha'_0 = \sum_j (j + 1/2) u'_j v'_j = \sum_j (j + 1/2) \left( 1 - 1/\sqrt{1 + (\frac{\epsilon_j - \lambda}{\Delta})^2} \right)$  making use as inputs  $\epsilon_\nu$ ,  $N_0$  and  $\Delta$ , that is single-particle energies, the average number of particles and the pairing gap.

Similar arguments can be used regarding the excitation of pairing vibrations in terms of Cooper pair transfer from closed shells as compared to one-particle transfer. As seen from Fig. 2.1.5 (b)–(c), the random phase approximation (RPA) amplitudes  $X_\nu^a$  and  $Y_\nu^a$  sum coherently over pairs of time reversal states, to give rise to the spectroscopic amplitudes associated with the direct excitation of the pair addition mode displayed in (d). Because of the (dispersion) relation (b)+(c) $\equiv$ (d), the  $X_\nu$ - and  $Y_\nu$ -amplitudes are correlated, among themselves as well as in phase. As seen from (g) and (h), the situation is quite different in the case of one-particle transfer. The soundness of the above parlance reflects itself in the calculation of the elements resulting from the encounter of structure and reaction, namely one- and two-nucleon modified transfer formfactors. While it is usually considered that these quantities carry all the structure information associated with the calculation

---

<sup>22</sup>See Sect. 2.4.2, see Potel, G. et al. (2013b).

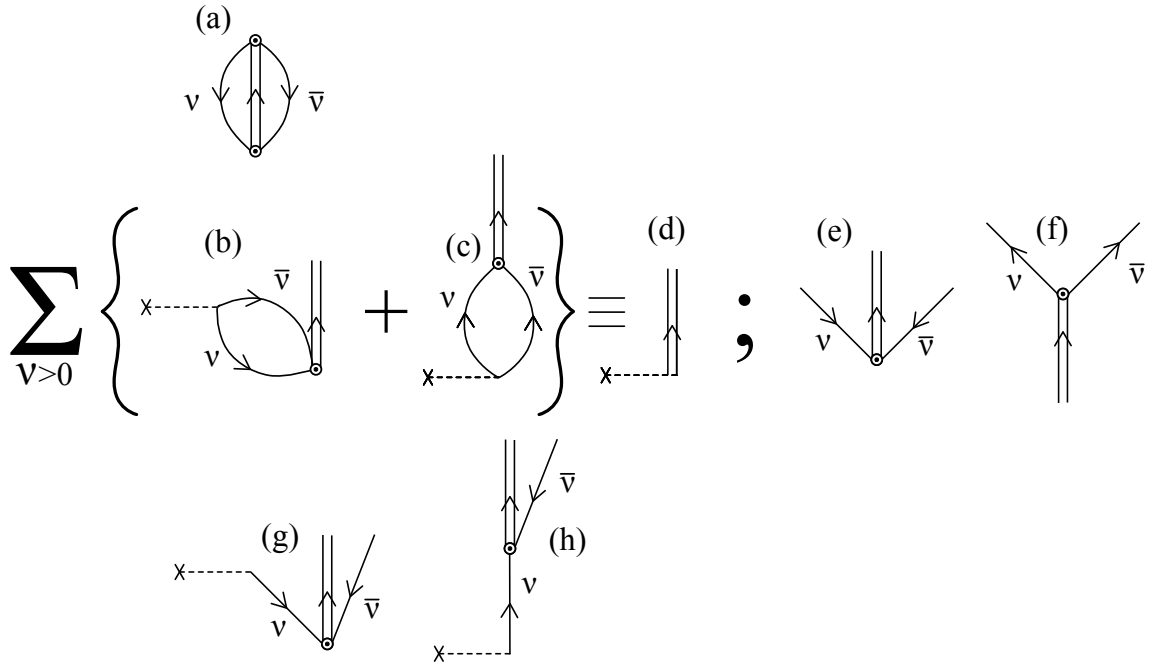


Figure 2.1.5: NFT diagrams associated with one- and two-particle transfer from closed shell. (a) ZPF associated with the virtual excitation of a pair addition mode and two uncorrelated holes. (b) two-particle transfer filling the holes, (c) diagram obtained from the previous one by time ordering. These processes receive contribution from all  $(v, \bar{v})$  pairs (sum over  $v > 0$ ), leading to (d), the direct excitation of the pair addition mode. The relation  $(b)+(c)\equiv(d)$  is the NFT graphical representation of the random phase approximation (RPA) dispersion relation used to calculate the properties of the pair addition mode in the harmonic approximation (Section 2.5). The backwards and forwards going RPA amplitudes are displayed in Figs. (e) and (f) respectively. (g) One-particle stripping proceeding through the filling of a hole associated with the ZPF, (h) processes obtained from the previous by time ordering.

of the corresponding cross sections, a consistent NFT treatment of structure and reaction will posit that equally much is contained in the distorted waves describing the relative motion of the colliding systems. This is because the optical potential ( $U + iW$ ) which determines the scattering waves, emerges from the same elements, eventually including also inelastic transition densities, used in the calculation of the structure properties<sup>23</sup>. In other words, to describe a two-nucleon transfer reaction like  $A + t \rightarrow B (= A + 2) + p$ , one needs to know what the single-particle states and collective modes of the system  $F (= A + 1)$  are, equally well than those

<sup>23</sup>cf. App. 3.5; cf also Broglia, R. A. et al. (1981), Pollaro et al. (1983), Broglia and Winther (2004), Fernández-García, J.P. et al. (2010), Fernández-García, J.P., M. Rodríguez-Gallardo et al. (2010), Dickhoff, W. and Van Neck (2005), Jenning, B. (2011), Montanari et al. (2014).

of nuclei  $A$  and  $B$ . In principle, also the deuteron wavefunction as one knows the triton wavefunction (see Chapter 3, cf. also Chapter 5, Section 5.1). Furthermore one needs to take into account the interweaving of different modes and degrees of freedom resulting in dressed particle states (quasiparticles; fermions) and renormalized normal vibrational modes of excitation (bosons). But these are essentially all the elements needed to calculate the processes leading to the depopulation of e.g. the flux in the incoming channel ( $A + t$  in the case under discussion). In particular, and assuming to work with spherical nuclei, one-particle transfer is, as a rule, the main depopulation process. This is a consequence of the long range tail of the associated formfactors as compared to that of other processes, e.g. inelastic processes (cf. e.g. Fig. 3.5.5).

In keeping with this fact, and because  $U$  and  $W$  are connected by the Kramers–Krönig generalized dispersion relation<sup>24</sup>, it is possible to calculate the nuclear dielectric function (optical potential) associated with the elastic channels under discussion (i.e.  $(A, t)$ ,  $(F, d)$  and  $(B, p)$  in the present case) making use of e.g.  $W$  worked out with the above described elements.

### 2.1.1 Two-nucleon modified formfactors

Concerning the modified formfactor associated with e.g. a  $(t, p)$  process, we shall see in the (Chapter 5, Sect. 5.B) that it can be written as

$$\begin{aligned} u_{LSJ}^{J_f}(R) = & \sum_{\substack{n_1 l_1 j_1 \\ n_2 l_2 j_2, n}} B(n_1 l_1 j_1, n_2 l_2 j_2; JJ_i J_f) \\ & \times \langle SLJ | j_1 j_2 J \rangle \times \langle n0, NL, L | n_1 l_1, n_2 l_2; L \rangle \\ & \times \Omega_n R_{NL}(R), \end{aligned} \quad (2.1.1)$$

where the overlaps

$$\begin{aligned} & B(n_1 l_1 j_1, n_2 l_2 j_2; JJ_i J_f) \\ & = \langle \Psi^{J_f}(\xi_{A+2}) | [\phi^J(n_1 l_1 j_1, n_2 l_2 j_2), \Psi^{J_i}(\xi_A)]^{J_f} \rangle, \end{aligned} \quad (2.1.2)$$

and

$$\Omega_n = \langle \phi_{nlm_l}(\mathbf{r}) | \phi_{000}(\mathbf{r}) \rangle, \quad (2.1.3)$$

encode for the physics of particle–particle (but also, to a large extent, particle–hole) correlations in nuclei,  $\langle SLJ | j_1 j_2 J \rangle$  and  $\langle n0, NL, L | n_1 l_1, n_2 l_2; L \rangle$  being  $LS - jj$  and Moshinsky transformation brackets, keeping track of symmetry and number of degrees of freedom conservation<sup>25</sup>. In fact, the two-nucleon spectroscopic amplitude (B-coefficient) and the overlap  $\Omega_n$  reflect the parentage with which the nucleus  $B$  can be written in terms of the system  $A$  and a Cooper pair,

$$\Psi_{exit} = \Psi_{M_f}^{J_f}(\xi_{A+2}) \times \chi_{M_{S_f}}^{S_f}(\sigma_p), \quad (2.1.4)$$

---

<sup>24</sup>See e.g. Mahaux, C. et al. (1985) and references therein.

<sup>25</sup>Glendenning, N. K. (1965), Broglia, R.A. et al. (1973).

where

$$\begin{aligned} \Psi_{M_f}^{J_f}(\xi_{A+2}) &= \sum_{\substack{n_1 l_1 j_1 \\ n_2 l_2 j_2 \\ J, J'_i}} B(n_1 l_1 j_1, n_2 l_2 j_2; J J'_i J_f) \\ &\times \left[ \phi^J(n_1 l_1 j_1, n_2 l_2 j_2) \Psi_{M_f}^{J_i}(\xi_A) \right]_{M_f}^{J_f}, \end{aligned} \quad (2.1.5)$$

and

$$\Psi_{\text{entrance}} = \Psi_{M_i}^{J_i}(\xi_A) \times \phi_t(\mathbf{r}_{n1}, \mathbf{r}_{n2}, r_p; \sigma_{n1}, \sigma_{n2}, \sigma_p), \quad (2.1.6)$$

with

$$\phi_t = \left[ \chi^S(\sigma_{n1}, \sigma_{n2}) \chi^{S'_f}(\sigma_p) \right]_{M_{S_i}}^{S_i} \times \phi_t^{L=0} \left( \sum_{i>j} |\mathbf{r}_i - \mathbf{r}_j| \right). \quad (2.1.7)$$

Assuming for simplicity a symmetric di-neutron radial wavefunction for the triton (i.e. neglecting the  $d$ -component of the corresponding wavefunction) both for the relative and for the center of mass wavefunctions  $\phi_{nlm}(\mathbf{r})$  and  $\phi_{N\Lambda M}(R)$  ( $n = l = m = 0, N = \Lambda = M = 0$ ), leads to  $\Omega_n$ , a quantity which reflects both the non-orthogonality existing between the di-neutron wavefunctions in the final nucleus (Cooper pair) and in the triton as well as their degree of  $s$ -wave of relative motion. Another way to say the same thing is to state that dineutron correlations in these two systems are different, a fact which underscores the limitations of light ion reactions to probe specifically pairing correlations in nuclei<sup>26</sup>.

One can then conclude that, provided one makes use of a (sensible) complete single-particle basis (eventually including also the continuum), one can capture through  $u_{LSJ}^{J_i J_f}(R)$  most of the coherence of Cooper pair transfer, as a major fraction of the associated di-neutron non-locality is taken care of by the  $n$ -summation appearing in eq. (2.1.1), the different contributions being weighted by the non-orthogonality overlaps  $\Omega_n$ . This is in keeping with the fact that, making use of a more refined triton wavefunction than that employed above, the  $n - p$  (deuteron-like) correlations of this particle can be described with reasonable accuracy and thus, the emergence of successive transfer (see Chapter 3). On the other hand, being the deuteron a bound system, this effective treatment of the associated resonances is not particularly economic. Furthermore, it is of notice that the zero-range approximation ( $V(\rho)\phi_{000}(\rho) = D_0\delta(\vec{\rho})$ ) eliminates the above mentioned possibilities cf. eq. (5.B.19).

Anyhow, the fact that one can still work out a detailed and physically insightful picture of two-nucleon transfer reactions in nuclei in terms of absolute cross sections with the help of a single parameter ( $D_0^2 \approx (31.6 \pm 9.3)10^4 \text{MeV}^2 \text{fm}^2$ ) testifies to the fact that the above picture of Cooper pair transfer<sup>27</sup> is a useful one, as it contains a large fraction of the physics which is at the basis of Cooper pair transfer in nuclei<sup>28</sup>. This is in keeping with the fact that the Cooper pair correlation length

<sup>26</sup>Within this context see von Oertzen and Vitturi (2001), von Oertzen, W. (2013).

<sup>27</sup>Glendenning, N. K. (1965), Bayman and Kallio (1967).

<sup>28</sup>Broglia, R.A. et al. (1973).

is much larger than nuclear dimensions and, consequently, simultaneous and successive transfer feel the same pairing correlations (see Chapter 3). In other words, treating explicitly the intermediate deuteron channel in terms of successive transfer, correcting both this and the simultaneous transfer channels for non-orthogonality contributions, makes the above picture the quantitative probe of Cooper pair correlations in nuclei<sup>29</sup> (Fig. 2.2.1).

Within the above context, we provide below two examples of  $B$ -coefficients associated with coherent states. Namely, one for the case in which  $A$  and  $B (= A+2)$  are members of a pairing rotational band. A second one, in the case in which they are members of a pairing vibrational band. That is,

$$\begin{aligned} \mathbf{1), } B(nlj, nlj; 000) &= \langle BCS(N+2) | \frac{[a_{nlj}^\dagger a_{nlj}^\dagger]_0^0}{\sqrt{2}} | BCS(N) \rangle \\ &= \sqrt{j+1/2} U_{nlj}(N) V_{nlj}(N+2), \end{aligned} \quad (2.1.8)$$

and

$$\begin{aligned} \mathbf{2), } B(nlj, nlj; 000) &= \langle (N_0 + 2)(gs) | \frac{[a_{nlj}^\dagger a_{nlj}^\dagger]_0^0}{\sqrt{2}} | N_0(gs) \rangle \\ &= \left\{ \begin{array}{ll} \sqrt{j_k + 1/2} X^a(n_k l_k j_k) & (\epsilon_{j_k} > \epsilon_F) \\ \sqrt{j_k + 1/2} Y^a(n_i l_i j_i) & (\epsilon_{j_k} \leq \epsilon_F). \end{array} \right. \end{aligned} \quad (2.1.9)$$

Where the  $X$  and  $Y$  coefficients are the forwardgoing and backwardsgoing RPA amplitudes of the pair addition mode. For actual numerical values see Sect. 2.4, Table 2.4.1 and Sect. 2.5 Tables 2.5.2–2.5.5.

We conclude this section by remarking that, in spite of the fact that one is dealing with the connection between structure and direct transfer reactions, no mention has been made of spectroscopic factors in relation with one-particle transfer processes, let alone when discussing two-particle transfer. In fact, one will be using throughout the present monograph, exception made when explicitly mentioned, absolute cross sections as the solely link between spectroscopic amplitudes and experimental observations.

## 2.2 Renormalization and spectroscopic amplitudes

Elementary modes of nuclear excitation, namely single-particle motion, vibrations and rotations, being tailored to economically describe the nuclear response to external probes, contain a large fraction of the many-body correlations. Consequently, their wavefunctions are non-orthogonal to each other, in keeping with the fact that all the degrees of freedom of the nucleus are exhausted by those of the nucleons

---

<sup>29</sup>Bayman and Chen (1982) and Potel, G. et al. (2013a).

(see Chapter 1). The corresponding overlaps give a measure of the strength with which the different modes couple to each other. The resulting particle–vibration coupling Hamiltonian can be diagonalized, making use of Nuclear Field Theory<sup>30</sup>, and of the BRST techniques<sup>31</sup> in the case of particle–rotor coupling.

As a result of the interweaving of single–particle and collective motion, the nucleons acquire a state dependent self energy  $\Delta E_j(\omega)$  which, for levels far away from the Fermi energy can become complex. Consequently, the single–particle potential which was already non–local in space (exchange potential, related to the Pauli principle) becomes also non–local in time (retardation effects; cf. e.g. Fig 2.6.3 (I)). There are a number of techniques to make it local. In particular the Local Density Approximation (LDA) and the effective mass approximation. In this last case one can describe the single–particle motion in terms of a local (complex) potential with a real part given by  $U'(r) = (m/m^*)U(r)$ , where  $m^* = m_k m_\omega / m$  is the effective nucleon mass,  $m_k$  being the so–called  $k$ –mass (non–locality in space in keeping with the fact that  $\Delta x \Delta k_x \geq 1$ ), and  $m_\omega = m(1 + \lambda)$  being the  $\omega$ –mass (non–locality in time, as implied by the relation  $\Delta \omega \Delta t \geq 1$ ),  $\lambda = -\partial \Delta E(\omega) / \partial \hbar \omega$  being the so–called mass enhancement factor. It reflects the ability with which vibrations cloth single–particles. In other words, it measures the probability with which a nucleon moving at  $t = -\infty$  in a “pure” orbital  $j$  can be found at a later time in a  $2p - 1h$  like (doorway state)  $|j'L; j\rangle$ ,  $L$  being the multipolarity of a vibrational state. Within this context, the discontinuity taking place at the Fermi energy in the dressed particle picture ( $Z_\omega = (m/m_\omega)$ ; cf. Apendice D introcucion) is connected with the single–particle occupancy probability.

It is of notice that dressed particles automatically imply an induced pairing interaction (see e.g. Figs. 2.6.3 (I) and (II)) resulting from the exchange of the clothing vibrations between pairs of nucleons moving in time reversal states close to the Fermi energy. In other words, fluctuations in the normal density ( $\delta\rho$ , cf. Fig. 4.A.1 (i)) and the associated particle–vibration coupling vertices lead to abnormal (superfluid) density (deformation in gauge space). Whether this is a dynamic or static effect, depends on whether the parameter (cf. Fig. 2.5.7)

$$x' = G' N'(0), \quad (2.2.1)$$

product of the effective pairing strength,

$$G' = Z_\omega^2 (v_p^{bare} + v_p^{ind}), \quad (2.2.2)$$

and of the renormalized density of levels  $N'(0)$  is considerable smaller (larger) than  $\approx 1/2$ . The quantity  $G'$  is the sum of the bare and induced pairing interaction, renormalized by the degree of single–particle content of the levels where nucleons correlate. The quantity

$$N'(0) = Z_\omega^{-1} N(0) = (1 + \lambda) N(0) \quad (2.2.3)$$

---

<sup>30</sup>NFT, cf. Bortignon, P. F. et al. (1977), Bortignon, P. F. et al. (1978).

<sup>31</sup>cf. Bès, D. R. and Kurchan (1990).

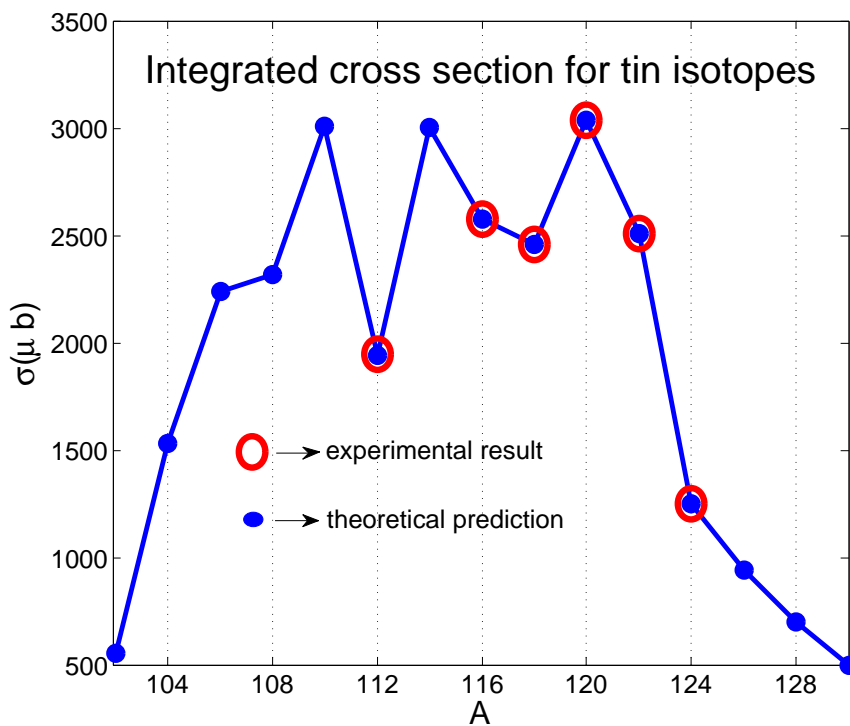


Figure 2.2.1: Absolute value of the two-nucleon transfer cross section  $^{A+2}\text{Sn}(p, t)^A\text{Sn}(\text{gs})$  ( $A = 112, 116, 118, 120, 122, 124$  cf. Potel, G. et al. (2013a) Potel, G. et al. (2013b)) calculated taking into account successive and simultaneous transfer in second order DWBA, properly corrected for non-orthogonality contributions in comparison with the experimental data (Guazzoni, P. et al. (1999), Guazzoni, P. et al. (2004), Guazzoni, P. et al. (2006), Guazzoni, P. et al. (2008), Guazzoni, P. et al. (2011), Guazzoni, P. et al. (2012)).

is the similarly renormalized density of levels at the Fermi energy. From the above relations one obtains

$$x' = Z_\omega(v_p^{bare} + v_p^{ind})N(0). \quad (2.2.4)$$

All of the above many-body,  $\omega$ -dependent effects which imply in many cases a coherent sum of amplitudes, are not simple to capture in a spectroscopic factor in connection with one-particle transfer, let alone two-nucleon transfer processes<sup>32</sup>.

In keeping with the fact that  $m_k \approx 0.6 - 0.7m$  and that  $m^* \approx m$ , as testified by the satisfactory fitting standard Saxon-Woods potentials provides for the valence orbitals of nucleons of mass  $m$  around closed shells, one obtains  $m_\omega \approx 1.4 - 1.7m$ . Thus  $Z_\omega \approx 0.6 - 0.7$ . It is still an open question how much of the observed single-particle depopulation can be due to hard core effects, which shifts the associated strength to high momentum levels<sup>33</sup>. An estimate of such an effect of about 20% will not quantitative change the long wavelength estimate of  $Z_\omega$  given above. Arguably, a much larger depopulation through hard core effects remains an open problem within the overall picture of elementary modes of nuclear excitation and of medium polarization effects.

## 2.3 Quantality Parameter

The quantality parameter<sup>34</sup> is defined as the ratio of the quantal kinetic energy of localization and potential energy, (cf. Fig. 2.3.1 and Table 2.3.1). Fluctuations, quantal or classical, favor symmetry: gases and liquids are homogeneous. Potential energy on the other hand prefers special arrangements: atoms like to be at specific distances and orientations from each other (spontaneous breaking of translational and of rotational symmetry reflecting the homogeneity and isotropy of empty space<sup>35</sup>).

When  $q$  is small, quantal effects are small and the lower state for  $T < T_c$  will have a crystalline structure,  $T_c$  denoting the critical temperature. For sufficiently large values of  $q$  ( $> 0.15$ ) the system will display particle delocalization and, likely, be amenable, within some approximation, to a mean field description (Figs. 2.3.2

<sup>32</sup>See Barranco et al. (2005).

<sup>33</sup>cf. Dickhoff, W. and Van Neck (2005), Jenning, B. (2011), Kramer, G. J. et al. (2001), Barbieri, C. (2009), Schiffer, J. P. et al. (2012), Duguet, T. and Hagen (2012), Furnstahl, R. J. and Schwenk (2010).

<sup>34</sup>Nosanow (1976), de Boer (1957), de Boer (1948), de Boer and Lundbeck (1948), Mottelson (1998).

<sup>35</sup>Within this general context the physics embodied in the quantality parameter is closely related to that which is at the basis of the classical Lindemann criterion (Lindemann (1910)) to measure whether a system is ordered (e.g. a crystal) or disordered (e.g. a melted system) (Bilgram (1987), Löwen, H. (1994), Stillinger (1995)). The above statement is also true for the generalized Lindemann parameter (Stillinger and Stillinger (1990), Zhou et al. (1999)), used to provide similar insight into inhomogeneous finite systems like e.g. proteins (aperiodic crystals Schrödinger, E. (1944), see also Ehrenfest's theorem (Basdevant and Dalibard (2005) pag. 138)).

constituents	$M/M_n$	$a(\text{cm})$	$v_0(\text{eV})$	$q$	phase( $T = 0$ )
${}^3\text{He}$	3	2.9(-8)	8.6(-4)	0.19	liquid <sup>a)</sup>
${}^4\text{He}$	4	2.9(-8)	8.6(-4)	0.14	liquid <sup>a)</sup>
$\text{H}_2$	2	3.3(-8)	32(-4)	0.06	solid <sup>b)</sup>
${}^{20}\text{Ne}$	20	3.1(-8)	31(-4)	0.007	solid <sup>b)</sup>
nucleons	1	9(-14)	100(+6)	0.4	liquid <sup>a),c),d)</sup>

Table 2.3.1: Zero temperature phase for a number of systems. a) delocalized (condensed), b) localized, c) non–Newtonian solid (cf. e.g. Bertsch (1988), de Gennes (1994), p. 25), that is, systems which react elastically to sudden solicitations and plastically under prolonged strain, d) paradigm of quantal, strongly fluctuating, finite many–body systems. While delocalization or less does not seem to depend much on whether one is dealing with fermions or bosons (Mottelson (1998) and refs. therein; cf also Ebran et al. (2014a), Ebran et al. (2014b), Ebran et al. (2013), Ebran et al. (2012)), the detailed properties of the corresponding single–particle motion are strongly dependent on the statistics obeyed by the associated particle (cf. Sect. 2.5).

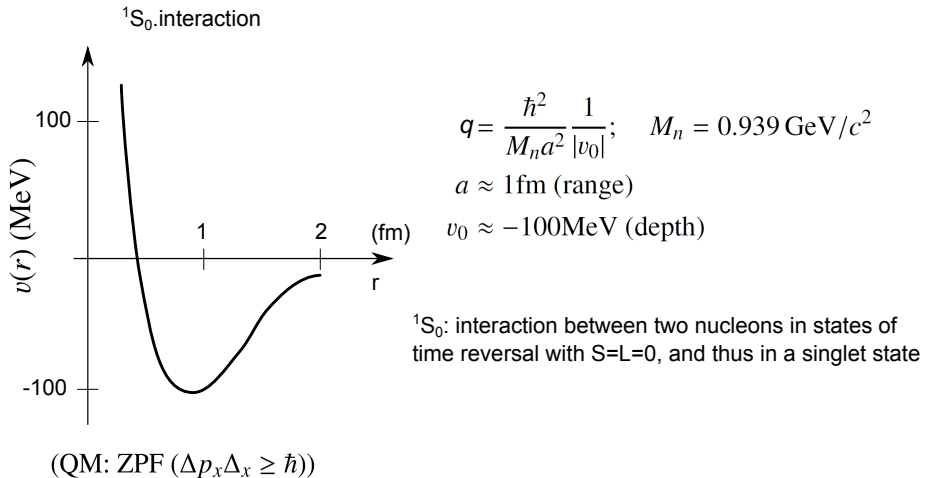


Figure 2.3.1: Schematic representation of the bare  $NN$ –interaction acting among nucleons displayed as a function of the relative coordinate  $r = |\mathbf{r}_1 - \mathbf{r}_2|$ , used to estimate the quantality parameter  $q$ , ratio of the zero point fluctuations (ZPF) of confinement and the potential energy.

and 2.3.3). In fact, the step delocalization → mean field is certainly not automatic, neither guaranteed. In any case, not for all properties neither for all levels of the system. Let us elaborate on these points. Independent particle motion can be viewed as the most collective of all nuclear properties, reflecting the effect of all nucleons on a given one resulting in a macroscopic effect. Namely confinement with long mean free path as compared with nuclear dimensions. Consequently, it should be possible to calculate the mean field in an accurate manner. Arguably, as accurately as one can calculate collective vibrations, e.g. quadrupole vibrations. But this does not mean that one knows how to correctly calculate the energy and associated deformation parameter of each single state of the quadrupole response function. Within this context one may find through mean field approximation a good description for the energy of the valence orbitals of a nucleus but for specific levels (e.g. the  $d_{5/2}$  level of  $^{119-120}\text{Sn}$ , cf. e.g. Fig 4.2.3). It is not said that including particle–vibration coupling corrections, a process which in average makes theory come closer to experiment<sup>36</sup>, single specific quasiparticle energies will agree better with the data<sup>37</sup>. Cases like this one constitute a sobering experience concerning the intricacies of the many–body problem in general, and the nuclear one (finite many–body system, FMBS) in particular. In other words, one is dealing with a self–confined, strongly interacting, finite many–body system generated from collisions originally associated with a variety of astrophysical events and thus with the coupling and interweaving of different scattering channels and resonances, a little bit as e.g. the Hoyle monopole resonance ( $\alpha + \alpha + \alpha \rightarrow ^{12}\text{C}$ ). Within the anthropomorphic (grand design) scenario such phenomena are found in the evolution of the Universe to eventually allow for the presence of organic matter and, arguably, life on earth<sup>38</sup> more likely than to make mean field approximation an “exact” description of nuclear structure and reactions.

## 2.4 Cooper pairs

Let us assume that the motion of nucleons is described by the Hamiltonian,

$$H = \sum_{j_1 j_2} \langle j_1 | T | j_2 \rangle a_{j_1}^\dagger a_{j_2} + \frac{1}{4} \sum_{\substack{j_1 j_2 \\ j_3 j_4}} \langle j_1 j_2 | v | j_3 j_4 \rangle a_{j_2}^\dagger a_{j_1}^\dagger a_{j_3} a_{j_4},$$

written in second quantization<sup>39</sup>. In what follows it will be schematically shown how mean field is extracted from such a Hamiltonian, both in the case of single–particle motion (HF) and of independent pair motion (BCS).

---

<sup>36</sup>cf. e.g. Bohr, A. and Mottelson (1975), Bortignon, P. F. et al. (1977), Mahaux, C. et al. (1985), Bès and Broglia (1971a), Bès and Broglia (1971b), Bès and Broglia (1971c), Bortignon et al. (1976), Bès, D. R. et al. (1988), Barranco et al. (1987), Barranco, F. et al. (2001) and references therein.

<sup>37</sup>cf. also Tarpanov, D. et al. (2014).

<sup>38</sup>cf. e.g. Rees, M. (2000), Meissner, U. G. (2014) and references therein.

<sup>39</sup>cf. e.g. Brink, D. and Broglia (2005), App. A.

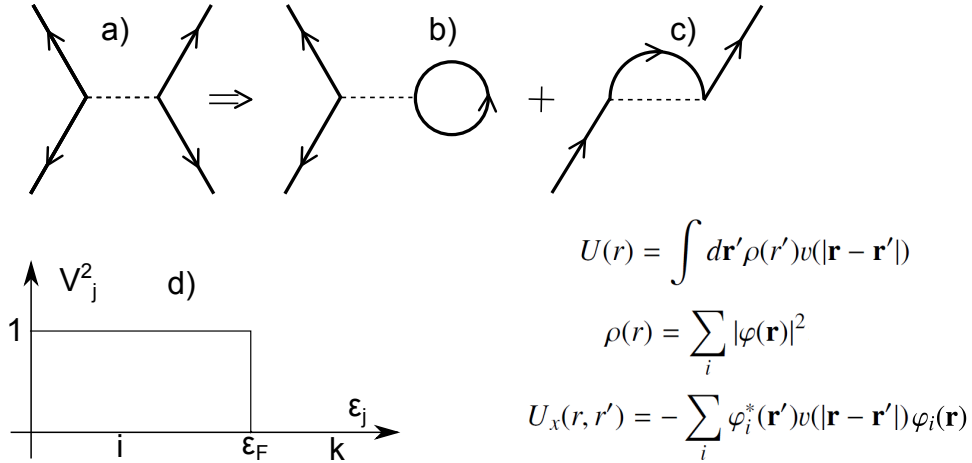


Figure 2.3.2: Schematic representation of (a) nucleon–nucleon scattering through the bare  $NN$ –interaction, (b) the associated contribution to the Hartree potential  $U(r)$  and, (c) to the Fock (exchange) potential  $U_x(r, r')$ ,  $\rho(r)$  being the nucleon density. (d) the Hartree–Fock solution leads to a sharp discontinuity at the Fermi energy  $\epsilon_F$ . That is, single–particle levels with energy  $\epsilon_i \leq \epsilon_F$  are fully occupied. Those with  $\epsilon_k \geq \epsilon_F$  empty.

### 2.4.1 independent-particle motion

In the previous section it was shown that the value of the quantity parameter associated with nuclei ( $q \approx 0.4$ ) leads to particle delocalization and likely makes the system amenable to a mean field description (Fig. 2.3.2; see however the provisos expressed at the end of Sect. 2.3). In such a case, Hartree–Fock approximation is tantamount to a selfconsistent relation between density and potential, weighted by the nucleon–nucleon interaction  $v$ , and leading to a complete separation between occupied ( $|i\rangle$ ) and empty ( $|k\rangle$ ) single–particle states,

$$(U_v^2 + V_v^2) = 1; \quad |\varphi_v\rangle = \bar{a}_v^\dagger |0\rangle = (U_v + V_v a_v^\dagger) |0\rangle; \quad V_v^2 = \begin{cases} 1 & \epsilon_i \leq \epsilon_F, \\ 0 & \epsilon_k > \epsilon_F. \end{cases} \quad (2.4.1)$$

The Hartree–Fock ground state can then be written as,

$$|HF\rangle = |\det(\varphi_v)\rangle = \Pi_\nu \bar{a}_\nu^\dagger |0\rangle = \Pi_i a_i^\dagger |0\rangle = \Pi_{i>0} a_i^\dagger a_{\tilde{i}}^\dagger |0\rangle, \quad (2.4.2)$$

where  $|\tilde{i}\rangle$  is the time reversed state to  $|i\rangle$ .

To be solved, the above self–consistent equations have to be given boundary conditions. In particular, make it explicit whether the system has a spherical or, for example, a quadrupole shape. That is, whether  $\langle HF | Q_2 | HF \rangle$  is zero or has a finite value,  $Q_{2M} = \sum_{j_1 j_2} \langle j_2 | r^2 Y_M^2 | j_1 \rangle [a_{j_1}^\dagger a_{j_2}]_M^2$  being the quadrupole operator which carries particle transfer quantum number  $\beta = 0$ , in keeping with its particle–hole character. In the case in which  $\langle Q_{2M} \rangle = 0$ , the system can display a spectrum of low–lying, large amplitude, collective quadrupole vibrations of frequency

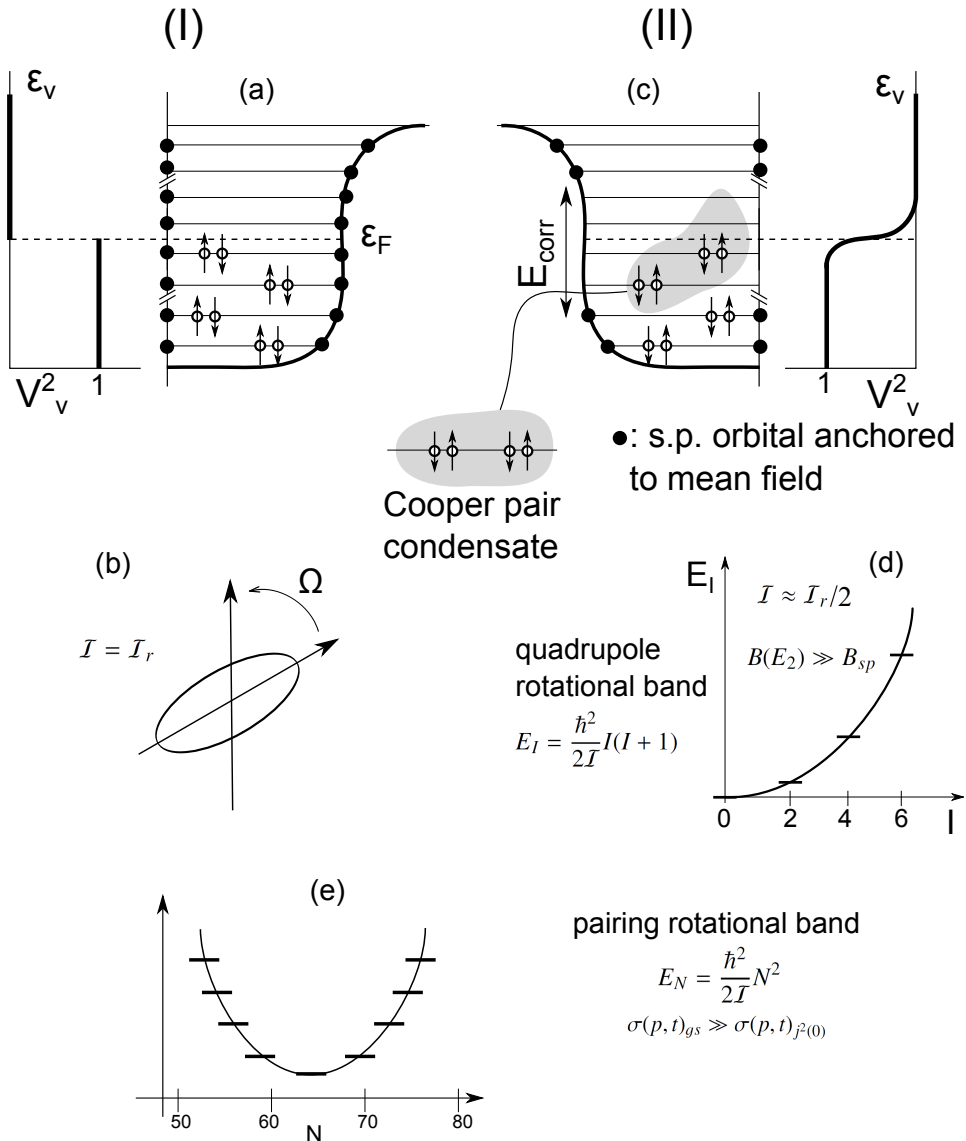


Figure 2.3.3: (I) (a) Schematic representation of “normal” (independent-particle) motion of nucleons in two-fold degenerate (Kramers, time-reversal degeneracy) orbits solidly anchored to the mean field and displaying a sharp, step-function-like, discontinuity in the occupancy at the Fermi energy lead to a deformed (Nilsson (1955)) rotating nucleus with a rigid moment of inertia  $I_r$ , (b). (II) Schematic representation of independent nucleon Cooper pair motion in which few (of the order of 5-8) pairs lead to (c) a sigmoidal occupation transition at the Fermi energy and, having uncoupled themselves from the fermionic mean field being now (quasi) bosons they essentially do not contribute to (d) the moment of inertia of quadrupole rotational bands leading to  $I \approx I_r/2$  (cf. Belyaev, S. T. (2013), Belyaev (1959), Bohr, A. and Mottelson (1975) and references therein), (e) pairing rotational bands in gauge space, an example of which is provided by the ground states of the superfluid Sn-isotopes (see also Figs. 2.1.3 and 2.1.4).

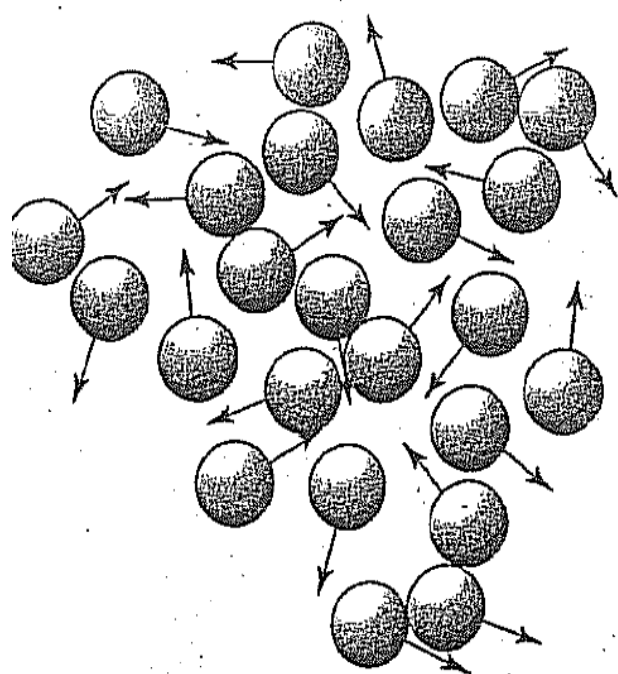


Figure 2.3.4: A system of independent Cooper pairs (Schafroth pairs). This situation corresponds to the incoherent solution of the many Cooper pair problem, the so called Fock state. In cold gases it describes the system after the Feschbach resonance leading to BEC (after Rogovin and Scully (1976)).

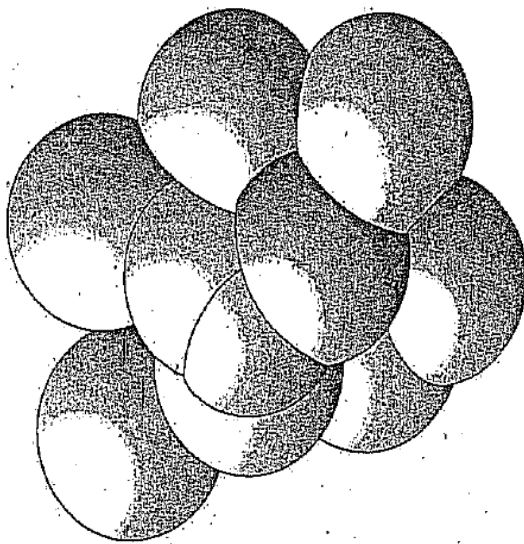


Figure 2.3.5: There are about  $10^{18}$  Cooper pairs per  $\text{cm}^3$  in a superconducting metal. A Cooper pair has a spatial extension of about  $10^{-4}$  cm. Thus a given Cooper pair will overlap with  $10^6$  other Cooper pairs, leading to strong pair–pair correlation, as schematically shown. This solution corresponds to the coherent solution of the many Cooper pair problem (coherent state), also valid in atomic nuclei (cf. Schrieffer (1964), Brink, D. and Broglia (2005), and references therein). (After Rogovin and Scully (1976)).

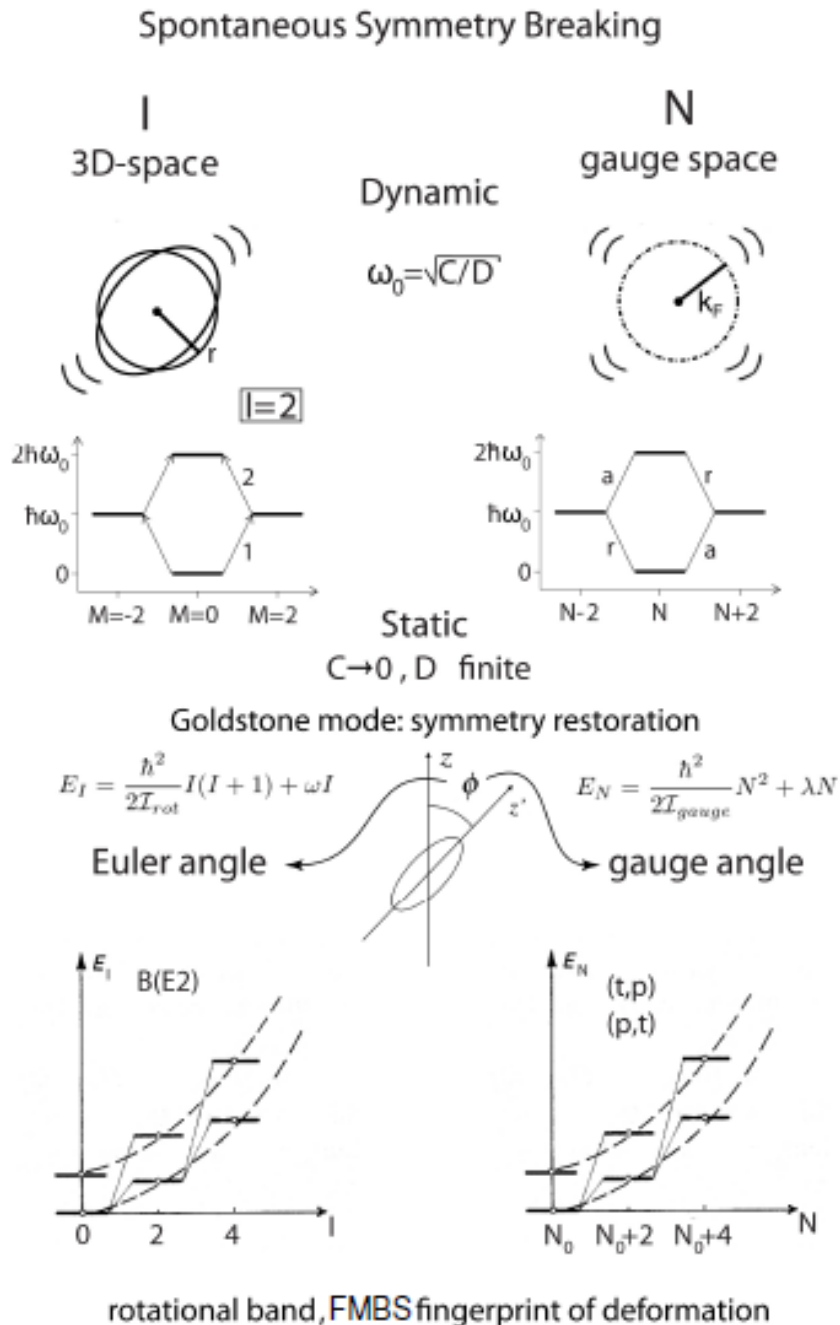


Figure 2.4.1: Parallel between dynamic and static deformations in 3D- and in gauge-space for the nuclear finite many body system (FMBS). In the first case, the angular momentum  $\mathbf{I}$  and the Euler angles are conjugate variables. In the second, particle number  $N$  and gauge angle. While the fingerprint of static (quadrupole and gauge) deformations are quadrupole and pairing rotational bands (see Fig. 2.1.4), vibrational bands are the expression of such phenomena in non deformed systems (after Broglia, R.A. et al. (1973)).

$(C/D)^{1/2}$ , the associated ZPF =  $(\hbar^2/(2D\hbar\omega))^{1/2}$  leading to dynamical violations of rotational invariance. In the case in which  $\langle Q_{2M} \rangle \neq 0$ , the  $|HF\rangle$  state is known as the Nilsson state,  $|\text{Nilsson}\rangle$ , defining a privileged orientation in 3D-space and thus an intrinsic, body-fixed system of reference  $\mathcal{K}'$  which makes an angle  $\Omega$  (Euler angles) with the laboratory frame  $\mathcal{K}$ <sup>40</sup>. Because there is no restoring force associated with the different orientations, fluctuations in  $\Omega$  diverge in just the right way to restore rotational invariance, leading to a rotational band displaying a rigid moment of inertia (cf. Fig. 2.3.3 and 2.4.1), and whose members are the states<sup>41</sup>,

$$|IKM\rangle \sim \int d\Omega \mathcal{D}_{MK}^I(\Omega) |\text{Nilsson}(\Omega)\rangle; E_I = (\hbar^2/2\mathcal{I})I(I+1); \mathcal{I} = \mathcal{I}_{\text{rig.}}$$

One can also view such bands as the limit ( $C \rightarrow 0, D (= \mathcal{I})$  finite) of low energy ( $\omega \rightarrow 0$ ), large-amplitude collective vibration. Similar dynamic and static spontaneous symmetry breaking phenomena take place in connection with particle-particle ( $\beta = +2$  transfer quantum number) and hole-hole ( $\beta = -2$ ) correlations, namely in gauge space (see Fig. 2.4.1; subject discussed also in Sect. 2.5 (dynamic: pairing vibration) and also below (static: pairing rotation); see also Figs. 2.1.1, 2.1.3 and 2.1.4). For a consistent discussion of these subjects<sup>42</sup>.

## 2.4.2 independent-pair motion

Let us make use of the constant pairing matrix element approximation  $\langle j_1 j_2 | v | j_3 j_4 \rangle = G$ , that is,

$$H_P = -G \sum_{\nu, \nu' > 0} a_\nu^\dagger a_{\bar{\nu}}^\dagger a_{\nu'} a_{\bar{\nu}'} \quad (2.4.3)$$

The abnormal density is related to the finite value of the pair operator. The associated independent pair states are written in the BCS approximation as

$$\left( U_\nu^2 + V_\nu^2 \right) = 1; \quad |\varphi_{\nu\bar{\nu}}\rangle = \left( U_j + V_j a_{jm}^\dagger a_{j\tilde{m}}^\dagger \right) |0\rangle, \quad \left. \begin{array}{c} V_\nu \\ U_\nu \end{array} \right\} = \frac{1}{\sqrt{2}} \left( 1 \mp \frac{\epsilon_\nu}{E_\nu} \right)^{1/2}, \quad (2.4.4)$$

where  $E_\nu = \sqrt{\epsilon_\nu^2 + \Delta^2}$  and  $\epsilon_\nu = \varepsilon_\nu - \lambda$ ,  $\lambda = \varepsilon_F$ . The BCS ground state,

$$|BCS\rangle = \Pi_{\nu>0} \left( U_j + V_j a_{jm}^\dagger a_{j\tilde{m}}^\dagger \right) |0\rangle, \quad (2.4.5)$$

describes independent pair motion. Let us introduce the phasing<sup>43</sup>,

$$U_\nu = |U_\nu| = U'_\nu; \quad V_\nu = e^{-2i\phi} V'_\nu; \quad (V'_\nu \equiv |V_\nu|) \quad (\nu \equiv j, m), \quad (2.4.6)$$

---

<sup>40</sup>Nilsson (1955).

<sup>41</sup>Bohr, A. and Mottelson (1975).

<sup>42</sup>See Bès, D. R. and Kurchan (1990).

<sup>43</sup>cf. e.g. Schrieffer, J. R. (1973).

where  $\phi$  is the gauge angle. One can then write the (BCS) wavefunction as,

$$\begin{aligned} |BCS(\phi)\rangle_{\mathcal{K}} &= \prod_{\nu>0} (U'_{\nu} + V'_{\nu} e^{-2i\phi} a_{\nu}^{\dagger} a_{\bar{\nu}}^{\dagger}) |0\rangle = \prod_{\nu>0} (U'_{\nu} + V'_{\nu} a_{\nu}^{\dagger'} a_{\bar{\nu}}^{\dagger'}) |0\rangle \\ &= |BCS(\phi=0)\rangle_{\mathcal{K}'} : \text{lab. system, } \mathcal{K} : \text{intr. system } \mathcal{K}', \end{aligned} \quad (2.4.7)$$

where  $a_{\nu}^{\dagger'} = e^{-i\phi} a_{\nu}^{\dagger}$  is the single-particle creation operator referred to the intrinsic system. The BCS order parameter, two-nucleon spectroscopic amplitudes and number and gap equations are,

$$\langle BCS | \sum_{\nu>0} a_{\nu}^{\dagger} a_{\bar{\nu}}^{\dagger} | BCS \rangle = \alpha'_0 e^{-2i\phi}; \quad \alpha'_0 = \sum_{\nu>0} U'_{\nu} V'_{\nu}; \quad \Delta = G \alpha_0, \quad (2.4.8)$$

$$B_{\nu} = \langle BCS | [a_{\nu}^{\dagger'} a_{\nu}^{\dagger'}]_0 | BCS \rangle = (j_{\nu} + 1/2)^{1/2} U'_{\nu} V'_{\nu}, \quad (2.4.9)$$

and

$$N_0 = 2 \sum_{\nu>0} V_{\nu}^2; \quad \frac{1}{G} = \sum_{\nu>0} \frac{1}{2E_{\nu}}. \quad (2.4.10)$$

Examples of  $B_{\nu}$ -coefficients for the reaction  $^{124}\text{Sn}(p,t)^{122}\text{Sn}$  (gs) are given in Table 2.4.1.

The wavefunction and energies of the members of the pairing rotational band, can be written as

$$\begin{aligned} |N_0\rangle &\sim \int_0^{2\pi} d\phi e^{-iN_0\phi} |BCS(\phi)\rangle_{\mathcal{K}} \sim \left( \sum_{\nu>0} c_{\nu} a_{\nu}^{\dagger} a_{\bar{\nu}}^{\dagger} \right)^{N_0/2} |0\rangle; \\ E_N &= (\hbar^2/2I)N^2; \quad I \approx 2\hbar^2/G, \end{aligned}$$

respectively<sup>44</sup>.

In the case of a quadrupole deformed nucleus, the system acquires not only a privileged orientation in gauge space, but also in 3D-space. Now, as summarized above, in a superfluid system, Cooper pairs and not single-particles are the building blocks of the system (see Figs. 2.4.2 and 2.3.5)<sup>45</sup>. But while the mean square radius of a nucleon at the Fermi energy ( $\langle r^2 \rangle^{1/2} \approx (3/5)^{1/2} R_0$  ( $R_0 = 1.2 A^{1/3} \text{ fm}$ )) is about 4.6 fm ( $A \approx 120$ ), that of a Cooper pair is determined by the correlation length ( $\xi \approx \hbar v_F/m \approx 36 \text{ fm}$ ) between the two nucleons forming the pair (see Figs.

<sup>44</sup>cf. e.g. Brink, D. and Broglia (2005) App. H.

<sup>45</sup>In connection with Fig. 2.4.2, the estimate  $2R = 20/k_F$  was carried out with the help of the Fermi gas model (cf. e.g. Bohr and Mottelson (1969)). The Fermi momentum is written as  $k_F \approx (3\pi^2 A/2V)^{1/3} \approx (\frac{3\pi^2}{2}\rho(0))^{1/3}$ . Making use of  $\rho(0) \approx 0.17 \text{ fm}^{-3}$  one obtains  $k_F \approx 1.36 \text{ fm}^{-1}$ . Now let us rewrite the relation between  $k_F$  and the volume  $V (= (4\pi/3)R^3 = (4\pi/3)r_0^3 A)$ . That is  $k_F \approx (9\pi/8)^{1/3}/r_0 (= 1.52/r_0)$ . Now, to employ  $r_0 = 1.2 \text{ fm}$  and still keep  $1.36 \text{ fm}^{-1}$ , one has to modify the above relation to  $k_F \approx 1.63/r_0$ . Let us now write the diameter of a heavy nucleus of mass  $A \approx 200$  ( $A^{1/3} \approx 5.85$ ). i.e.  $2R = 2r_0 A^{1/3} \approx 20/k_F$ . This is the value used in Fig. 2.4.2.

2.3.3 and 2.3.5). Consequently, orienting the quadrupole deformed potential in different directions (angles  $\Omega$ ), will have less effect on Cooper pairs than on independent particles. Thus the reduction of the moment of inertia from  $\mathcal{I}_r$  to  $\approx \mathcal{I}_r/2$ . Within this context one can mention the fact that low-lying nuclear collective vibrations (and rotations) are essentially not observed at intrinsic excitation energies corresponding to temperatures of  $\approx 1\text{-}2$  MeV. In this case, this is because the surface is strongly fluctuating and thus not well defined, making it non operative its anisotropic orientation in space.

	$^{112}\text{Sn}(p, t)^{110}\text{Sn}(\text{gs})$	$^{124}\text{Sn}(p, t)^{122}\text{Sn}(\text{gs})$		
$nlj^a)$	BCS <sup>b)</sup>	$V_{low-k}^c)$	BCS <sup>d)</sup>	NuShell <sup>e)</sup>
$1g_{7/2}$	0.96	-1.1073	0.44	0.63
$2d_{5/2}$	0.66	-0.7556	0.35	0.60
$2d_{3/2}$	0.54	-0.4825	0.58	0.72
$3s_{1/2}$	0.45	-0.3663	0.36	0.52
$1h_{11/2}$	0.69	-0.6647	1.22	-1.24

Table 2.4.1: Two-nucleon transfer spectroscopic amplitudes associated with the reactions  $^{112}\text{Sn}(p, t)^{110}\text{Sn}(\text{gs})$  and  $^{124}\text{Sn}(p, t)^{122}\text{Sn}(\text{gs})$ . **a)** quantum numbers of the two-particle configurations  $(nlj)_{J=0}^2$  coupled to angular momentum  $J = 0$ . **b,d)**  $\langle BCS | P_\nu | BCS \rangle = \sqrt{2j_\nu + 1} U_\nu(A) V_\nu(A+2)$  ( $A+2 = 112$  and  $124$  respectively), where  $P_\nu = a_\nu a_\nu (\nu \equiv nlj)$  (cf. Potel, G. et al. (2011, 2013a,b)) **c)** two-nucleon transfer spectroscopic amplitudes calculated making use of initial and final state wavefunctions obtained by diagonalizing a  $v_{low-k}$ , that is a renormalized, low-momentum interaction derived from the CD-Bonn nucleon-nucleon potential (see Guazzoni, P. et al. (2006) and references therein). **e)** Two-neutron overlap functions obtained making use of the shell-model wavefunctions for the ground state of  $^{122}\text{Sn}$  and  $^{124}\text{Sn}$  calculated with the code NuShell (Brown, B. A. and Rae, 2007). The wavefunctions were obtained starting with a  $G$ -matrix derived from the CD-Bonn nucleon-nucleon interaction Machleidt, R. et al. (1996). These amplitudes were used in the calculation of  $^{124}\text{Sn}(p, t)^{122}\text{Sn}$  absolute cross sections carried out by I.J. Thompson (Thompson, I.J., 2013).

Because in FMBS quantal fluctuations are very important<sup>46</sup>, deformation in such systems explicit themselves through rotational bands. In particular, superfluid nuclei display well defined pairing rotational bands, an example of such bands being provided by the ground states of the superfluid Sn-isotopes. In this case, the moment of inertia is directly related to the pairing interaction. Pairing rotational bands are specifically excited in two nucleon transfer reactions (cf, Figs. 2.1.3 and 2.1.4). A summary of the physics which is at the basis of independent single-particle and single-pair motion is given in Figs. 2.4.2 and 2.4.3.

---

<sup>46</sup>see Bertsch and Broglia (2005) and references therein.

### Classical localization and quantal ZPF

$$\delta x \delta k \geq 1 \quad \varepsilon = \frac{\hbar^2 k^2}{2M} \quad \delta k = \frac{\delta \varepsilon}{\hbar v_F} \quad (v_F/c \approx 0.3)$$

**[structure]**

Independent motion of

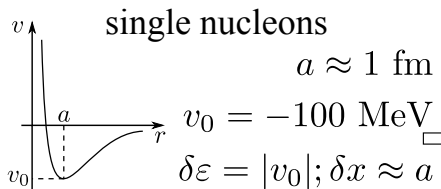
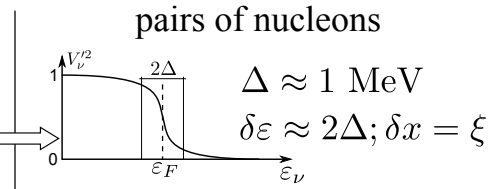
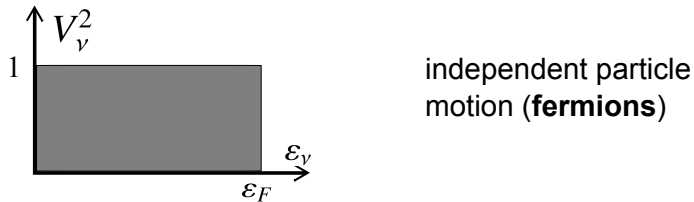
 <p>single nucleons</p> <p><math>a \approx 1 \text{ fm}</math></p> <p><math>v_0 = -100 \text{ MeV}</math></p> <p><math>\delta \varepsilon =  v_0 ; \delta x \approx a</math></p> <p><math>\delta x \delta k = \frac{a v_0 }{\hbar v_F} \geq 1</math></p> <p>quantity parameter</p> <p><math>q = \frac{\hbar v_F}{a v_0 } \approx 0.6 \lesssim 1</math></p> <p>delocalization</p> <p>emergent property: generalized rigidity in 3D-space</p> <p>how does a short range force lead to single-nucleon mean free paths</p> <p><math>2R \approx 20/k_F</math></p> <p>answer: quantal fluctuations</p> <p><b>[reactions]</b></p>	 <p>pairs of nucleons</p> <p><math>\Delta \approx 1 \text{ MeV}</math></p> <p><math>\delta \varepsilon \approx 2\Delta; \delta x = \xi</math></p> <p><math>\delta x \delta k = \frac{\xi 2\Delta}{\hbar v_F} \geq 1</math></p> <p>correlation length</p> <p><math>\xi = \frac{\hbar v_F}{2\Delta} \approx 30 \text{ fm} \gg R</math></p> <p>long range correlation</p> <p>pairing correlations over distances</p> <p>larger than nuclear dimension?</p> <p><math>\frac{\xi}{a} \approx 30</math></p> <p>Successive and simultaneous transfer amplitude contributions to the absolute cross section carry equally efficiently information concerning pair correlations</p>
<p>single particle transfer, e.g. <math>(p,d)</math></p> <p><math>\frac{2R}{a} \approx 15</math></p> <p>absolute cross section reflects the full nucleon probability amplitude distribution, and does not depend of the specific choice of <math>v_{np}</math></p>	<p>Cooper pair transfer, e.g. <math>(p,t)</math></p>

Figure 2.4.2: Classical localization and zero point fluctuations, associated with independent-particle (normal density) and independent-pair motion (abnormal density).

$$\begin{aligned}
 H = T + v &= \underbrace{T + U + V_p}_{\text{mean field}} + (v - U - V_p) \\
 \text{diagonalization} &\quad \text{Kramers degeneracy } v\bar{v} \\
 a_v^\dagger &= U_v a_v^\dagger - V_v a_{\bar{v}}^\dagger; \\
 \text{ground state} & \\
 a_v |\tilde{0}\rangle &= 0 \\
 |\tilde{0}\rangle &= \prod_{v>0} \alpha_v \alpha_{\bar{v}} |0\rangle \sim \prod_{v>0} (U_v + V_v a_v^\dagger a_{\bar{v}}^\dagger) |0\rangle \\
 a_v |0\rangle &= 0
 \end{aligned}$$

Ansatz 1:  $|\tilde{0}\rangle$  sharp step-funct. occ.

$$|HF\rangle = \prod_{i>0} a_i^\dagger a_i^\dagger |0\rangle = \prod_i a_i^\dagger |0\rangle$$



Ansatz 2:  $|\tilde{0}\rangle$  sigmoidal distr. occ.

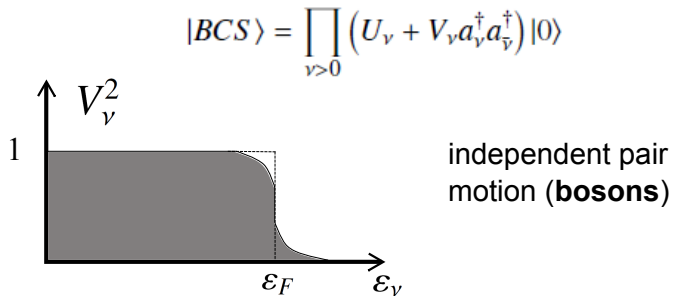


Figure 2.4.3: Schematic representation of the steps to be taken to extract from a two-body interaction independent particle motion ( $U$ , mean field) and independent pair motion ( $V_p = -G\alpha_0(P^\dagger + P)$ , pair potential,  $P^\dagger$  being the pair creation operator), in terms of a generalized quasiparticle transformation, and leading to a sharp step-function occupation distribution and a smooth (sigmoidal) occupation distribution around the Fermi surface respectively.

## 2.5 Two-nucleon spectroscopic amplitudes associated with pairing vibrational modes in closed shell systems: the $^{208}\text{Pb}$ case.

The solution of the pairing Hamiltonian

$$H = H_{sp} + H_p,$$

where

$$H_{sp} = \sum_{\nu} \epsilon_{\nu} a_{\nu}^{\dagger} a_{\nu},$$

and

$$H_p = -GP^{\dagger}P,$$

with

$$P^{\dagger} = \sum_{\nu>0} a_{\nu}^{\dagger} a_{\bar{\nu}}^{\dagger},$$

lead, in the case of closed shell systems and within the harmonic approximation (RPA), to pair addition (*a*) pair removal (*r*) two-particle, two-hole correlated modes, the associated creation and annihilation operator being

$$\Gamma_a^{\dagger}(n) = \sum_k X_n^a(k) \Gamma_k^{\dagger} + \sum_i Y_n^a(i) \Gamma_i,$$

and

$$\Gamma_r^{\dagger}(n) = \sum_i X_n^r(i) \Gamma_i^{\dagger} + \sum_k Y_n^r(k) \Gamma_k,$$

with

$$\sum X^2 - Y^2 = 1,$$

and

$$\Gamma_k^{\dagger} = a_k^{\dagger} a_{\tilde{k}}^{\dagger}, \quad (\epsilon_k > \epsilon_F).$$

Similarly,

$$\Gamma_i^{\dagger} = a_i^{\dagger} a_i, \quad (\epsilon_i \leq \epsilon_F).$$

The relations

$$[H, \Gamma_a^{\dagger}(n)] = \hbar W_n(\beta = +2),$$

and

$$[H, \Gamma_r^{\dagger}(n)] = \hbar W_n(\beta = -2),$$

where  $\beta$  is the transfer quantum number, while  $n$  labels the roots of the corresponding dispersion relations<sup>47</sup>,

$$\frac{1}{G(\pm 2)} = \sum_k \frac{(\Omega_k/2)}{2\epsilon_k \mp W_n(\pm 2)} + \sum_i \frac{(\Omega_i/2)}{2\epsilon_i \pm W_n(\pm 2)},$$

---

<sup>47</sup>cf. Bès, D. R. and Broglia (1966).

orbit	$\epsilon_j$	$\epsilon_{p_{1/2}} - \epsilon_k \equiv  \epsilon_k  -  \epsilon_{p_{1/2}} $
$0h_{9/2}$	-10.62	3.47
$1f_{7/2}$	-9.50	2.35
$0i_{13/2}$	-8.79	1.64
$2p_{3/2}$	-8.05	0.90
$1f_{5/2}$	-7.72	0.57
$2p_{1/2}$	-7.15	0
$\epsilon_F = -5.825$ keV		$\epsilon_k - \epsilon_{g_{9/2}} \equiv  \epsilon_{g_{9/2}}  -  \epsilon_k $
$1g_{9/2}$	-3.74	0.
$0i_{11/2}$	-2.97	0.77
$0j_{15/2}$	-2.33	1.41
$2d_{5/2}$	-2.18	1.56
$3s_{1/2}$	-1.71	2.03
$1g_{7/2}$	-1.27	2.47
$2d_{3/2}$	-1.23	2.51

Table 2.5.1: Valence single-particle levels of  $^{208}\text{Pb}$ . In the upper part the occupied levels ( $\epsilon_i \leq \epsilon_F$ ) are shown while in the lower part the empty levels ( $\epsilon_k \geq \epsilon_F$ ). Of notice that  $\epsilon_{p_{1/2}} - \epsilon_{g_{9/2}} = 3.41$  MeV, is the single-particle gap associated with  $N = 126$  shell closure (from Nuclear Data Center).

$n$  labeling the corresponding solutions in increasing order of energy. In the above equation,  $\Omega_j = j + 1/2$  is the pair degeneracy of the orbital with total angular momentum  $j$ .

For the case of the (neutron) pair addition and pair subtraction modes of  $^{208}\text{Pb}$  the above equations are graphically solved in Fig 2.5.1 (see also Table 2.5.1). The minimum of the dispersion relation defines the Fermi energy of the system under study. This is in keeping with the fact that in the case in which  $W_1(\beta = +2) = W_1(\beta = -2) = 0$ , situation corresponding to the transition between normal and superfluid phases, the energy value at which the dispersion relation touches for the first time the energy axis, coincides with the BCS  $\lambda$  variational parameter. It is of notice that, as a rule, the Fermi energy of closed shell nuclei is empirically defined as half the energy difference between the last occupied and the first empty single particle state<sup>48</sup>. Making use of the values (see Fig. 2.5.1)

$$\begin{cases} E_{corr}(+2) = B(208) + B(210) - 2B(209) = 1.248 \text{ MeV}, \\ E_{corr}(-2) = B(208) + B(206) - 2B(207) = 0.630 \text{ MeV}, \end{cases}$$

one obtains  $W_1(+2) + W_1(-2) = (B(208) - B(206)) - (B(210) - B(208)) = 14.11 - 9.115 = 4.995$  MeV. Notice that in the above calculations all energies differences

<sup>48</sup>cf. e.g. Mahaux, C. et al. (1985).

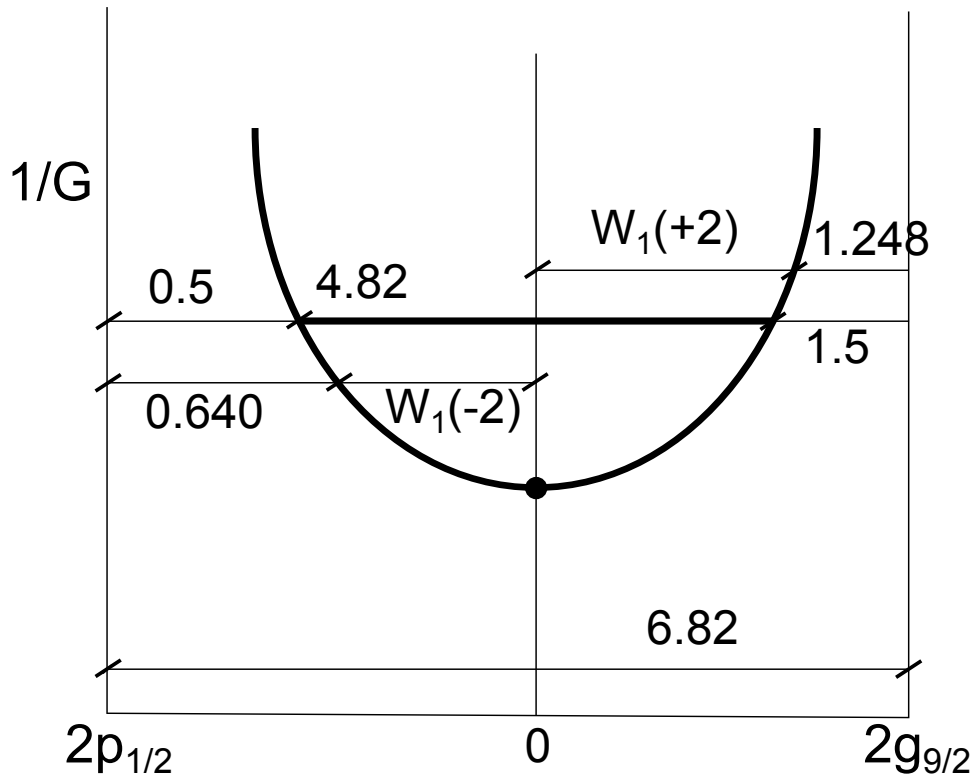


Figure 2.5.1: The right hand side of the RPA pairing vibrational dispersion relation for neutrons in the case of the closed shell system  $^{208}\text{Pb}$  (cf. Bès, D. R. and Broglia (1966)) in the region between the two neighboring shells ( $p_{1/2}$  and  $g_{9/2}$ ). All quantities are in MeV. For each  $G$  there is a straight horizontal line, which is divided by the the curve in three sections. The first one from the left corresponds to the pairing correlation energy of the nucleus  $^{206}\text{Pb}$  (two correlated neutron hole states) while the last segment to the right measures the pairing correlation energy of  $^{210}\text{Pb}$  (two correlated neutrons above closed shell) the intermediate segment measures the energy of the two phonon (correlated  $(2p - 2h)$ ) pairing vibrational state of  $^{208}\text{Pb}$ .

are positive. In particular (see Table 2.5.1)

$$\epsilon_i < \epsilon_F \Rightarrow \epsilon_F - \epsilon_i = -|\epsilon_F| + |\epsilon_i| = |\epsilon_i| - |\epsilon_F| > 0,$$

and

$$\epsilon_k > \epsilon_F \Rightarrow \epsilon_k - \epsilon_F = -|\epsilon_k| + |\epsilon_F| = |\epsilon_F| - |\epsilon_k| > 0.$$

Thus,

$$\begin{cases} 2(\epsilon_F - \epsilon_{p_{1/2}}) = W_1(-2) + E_{corr}(-2) > 0, \\ 2(\epsilon_{g_{9/2}} - \epsilon_F) = W_1(+2) + E_{corr}(+2) > 0. \end{cases}$$

From Fig. 2.5.1 and Table 2.5.1 one can then write,

$$2 \times (-5.825 - (-7.5)) \text{ MeV} = 2.650 \text{ MeV} = W_1(-2) + 0.640 \text{ MeV}$$

and

$$2 \times (-3.74 \text{ MeV} - (-5.825) \text{ MeV}) = 4.17 \text{ MeV} = W_1(+2) + 1.248 \text{ MeV}.$$

Consequently,

$$W_1(-2) = 2.01 \text{ MeV} \quad \text{and} \quad W_1(+2) = 2.92 \text{ MeV},$$

leading to,

$$W_1(+2) + W_1(-2) = 4.93 \text{ MeV}.$$

### 2.5.1 Pair removal mode

In Fig. 2.5.2 the graphical representation of the forwards going RPA amplitude of the pair removal mode is shown. Its expression is

$$X_1^r(i) = \frac{\frac{1}{2}\Omega_i^{1/2}\Lambda(-2)}{2(\epsilon_F - \epsilon_i) - W_1(-2)},$$

where

$$\begin{aligned} 2 \times (\epsilon_F - \epsilon_i) - W_1(-2) &= 2 \times (\epsilon_F - \epsilon_i) - 2 \times (\epsilon_F - \epsilon_{p_{1/2}}) + E_{corr}(-2) \\ &= 2 \times (\epsilon_{p_{1/2}} - \epsilon_i) + E_{corr}(-2) = 2 \times (|\epsilon_i| - |\epsilon_{p_{1/2}}|) + E_{corr}(-2). \end{aligned}$$

Thus,

$$X_1^r(i) = \frac{\frac{1}{2}\Omega_i^{1/2}\Lambda(-2)}{2(|\epsilon_i| - |\epsilon_{p_{1/2}}|) + E_{corr}(-2)}.$$

Making use of the empirical value of  $E_{corr}(-2)$  worked out above one obtains,

$$X_1^r(i) = \frac{\frac{1}{2}\Omega_i^{1/2}\Lambda(-2)}{2(|\epsilon_i| - |\epsilon_{p_{1/2}}|) + 0.640 \text{ MeV}}.$$

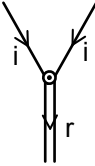


Figure 2.5.2: NFT representation of the forwards going RPA amplitude of the pair removal mode (double downward going arrowed line) describing a two correlated hole state (single downward going arrowed line for each hole with quantum numbers collectively labeled  $i$ ).

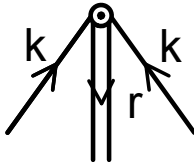


Figure 2.5.3: Same as Fig. 2.5.2 but for the backwards going amplitudes.

In Fig. 2.5.3 we display the graphical process associated with the backwards going RPA amplitude,

$$Y_1^r(k) = \frac{\frac{1}{2}\Omega_k^{1/2}\Lambda(-2)}{2(\epsilon_k - \epsilon_F) + W_1(-2)}.$$

Making use of

$$2 \times (\epsilon_F - \epsilon_{p_{1/2}}) - E_{corr}(-2) = W_1(-2),$$

one can write

$$2 \times (\epsilon_F - \epsilon_{p_{1/2}}) + 2 \times (\epsilon_k - \epsilon_F) - E_{corr}(-2) = 2 \times (\epsilon_k - \epsilon_F) + W_1(-2),$$

leading to

$$2 \times (|\epsilon_{p_{1/2}}| - |\epsilon_k|) - E_{corr}(-2) = 2 \times (|\epsilon_{p_{1/2}}| - |\epsilon_{g_{9/2}}|) + 2 \times (|\epsilon_{g_{9/2}}| - |\epsilon_k|) - E_{corr}(-2).$$

Thus,

$$Y_1^r(k) = \frac{\frac{1}{2}\Omega_k^{1/2}\Lambda(-2)}{2(|\epsilon_{g_{9/2}}| - |\epsilon_k|) + 2(|\epsilon_{p_{1/2}}| - |\epsilon_{g_{9/2}}|) - E_{corr}(-2)}.$$

With the help of  $2 \times (|\epsilon_{p_{1/2}}| - |\epsilon_{g_{9/2}}|) - E_{corr}(-2) = 6.82 \text{ MeV} - 0.640 \text{ MeV} = 6.18 \text{ MeV}$ , one obtains,

$$Y_1^r(k) = \frac{\frac{1}{2}\Omega_k^{1/2}\Lambda(-2)}{2(|\epsilon_{g_{9/2}}| - |\epsilon_k|) + 6.18 \text{ MeV}}.$$

The above expressions of  $X_1^r(i)$  and  $Y_1^r(k)$  contain the experimental values of the 2-hole correlation energies (0.640 MeV). Because (see Fig. 2.5.1) the associated

values of  $G$  does not lead to the observed correlation energy of the pair addition mode (1.248 MeV), we prefer to choose a single intermediate value of  $G$  and use the resulting  $E_{corr}(-2)$  (=0.5 MeV) and  $E_{corr}(+2)$  (=1.5 MeV), correlation energies, to calculate the corresponding  $X, Y$  amplitudes for both the lowest removal and lowest addition pairing modes. Making use of,

$$2 \times (|\epsilon_{p_{1/2}}| - |\epsilon_{g_{9/2}}|) = 6.82 \text{ MeV} \quad \text{and} \quad 2 \times (|\epsilon_{p_{1/2}}| - |\epsilon_{g_{9/2}}|) - E_{corr}(-2) \\ = (6.82 - 0.5) \text{ MeV} = 6.32 \text{ MeV},$$

one can write

$$X_1^r(i) = \frac{\frac{1}{2}\Omega_i^{1/2}\Lambda(-2)}{2(|\epsilon_i| - |\epsilon_{p_{1/2}}|) + 0.5 \text{ MeV}}, \\ Y_1^r(k) = \frac{\frac{1}{2}\Omega_k^{1/2}\Lambda(-2)}{2(|\epsilon_{g_{9/2}}| - |\epsilon_k|) + 6.32 \text{ MeV}}.$$

Tables 2.5.2 and 2.5.3 contain the amplitudes of the pair removal mode of  $^{208}\text{Pb}$  ( $\Gamma_r^\dagger(1) = \sum X_1^r(i)\Gamma_i^\dagger + \sum Y_1^r(k)\Gamma_k$ ), that is of the two neutron correlated hole state describing  $|^{206}\text{Pb}(\text{gs})\rangle = \Gamma_r^\dagger(1)|0\rangle$ .

It is of notice that the coupling strength  $\Lambda(-2)$  with which the pair removal mode couples to the single-particle (-hole) states is calculated by normalizing the amplitudes: 1) (Tamm Dancoff, TD)  $\sum_i A^2(i) = 1.5549 \text{ MeV}^{-2}$  and thus  $\Lambda(-2) = 0.802 \text{ MeV}$ , ( $\sum_i X(i)_{TD}^2 = 1$ ); 2) RPA,  $\Lambda_1^2(-2) \times (\sum_i A^2(i) - \sum_k B^2(k)) = \Lambda_1^2(-2) \times 1.45073 = 1$ . Thus  $\Lambda_1(-2) = 0.830 \text{ MeV}$ . The above results shows that there is a few percentage difference between the two values of  $\Lambda$  (TD and RPA), as well as for the corresponding  $X$  amplitudes. Nonetheless, ground state correlations as expressed by the  $Y$  amplitudes, gives rise to a 52% increase in the  $^{206}\text{Pb}(t, p)^{208}\text{Pb}(\text{gs})$  absolute cross section, from 0.34 mb to 0.52 mb to be compared with experimental data  $\sigma = 0.68 \pm 0.24 \text{ mb}$  (see Fig. 3.4.4).

## 2.5.2 Pair addition mode

In Fig. 2.5.4 the  $X$ -amplitude of the pair addition mode is shown (NFT diagram). The associated expression

$$X_1^a(k) = \frac{\frac{1}{2}\Omega_k^{1/2}\Lambda_1(+2)}{2(\epsilon_k - \epsilon_F) - W_1(+2)},$$

can be written, making use of

$$2 \times (\epsilon_k - \epsilon_F) - W_1(+2) = 2 \times (\epsilon_k - \epsilon_F) - 2 \times (\epsilon_{g_{9/2}} - \epsilon_F) + E_{corr}(+2) \\ = 2 \times (\epsilon_k - \epsilon_{g_{9/2}}) + E_{corr}(+2) = 2 \times (|\epsilon_{g_{9/2}}| - |\epsilon_k|) + E_{corr}(+2),$$

as

$$X_1^a(k) = \frac{\frac{1}{2}\Omega_k^{1/2}\Lambda_1(+2)}{2(|\epsilon_{g_{9/2}}| - |\epsilon_k|) + E_{corr}(+2)}.$$

units		MeV	MeV <sup>-1</sup>	RPA	TD
<i>nlj</i>	$\Omega_i$	$ \epsilon_i  -  \epsilon_{p_{1/2}} $	$A(i) = \frac{\frac{1}{2}\Omega_i^{1/2}}{2( \epsilon_i  -  \epsilon_{p_{1/2}} ) + 0.5 \text{ MeV}}$	$X_1^r(i)$	$X_1^r(i)$
$2p_{1/2}$	1	0	1	0.83	0.80
$1f_{5/2}$	3	0.57	0.528	0.44	0.42
$2p_{3/2}$	2	0.90	0.307	0.25	0.25
$0i_{13/2}$	7	1.64	0.350	0.29	0.28
$1f_{7/2}$	4	2.35	0.192	0.16	0.15
$0h_{9/2}$	5	3.47	0.150	0.12	0.12

Table 2.5.2: Forwards going RPA amplitudes of the pair removal mode of  $^{208}\text{Pb}$  (i.e.  $|^{206}\text{Pb}\rangle$  state), cf. Table XVI Broglia, R.A. et al. (1973).

units		MeV	MeV <sup>-1</sup>	RPA
<i>nlj</i>	$\Omega_k$	$ \epsilon_{g_{9/2}}  -  \epsilon_k $	$B(k) = \frac{\frac{1}{2}\Omega_k^{1/2}}{2( \epsilon_{g_{9/2}}  -  \epsilon_k ) + 6.23 \text{ MeV}}$	$Y_1^r(i)$
$1g_{9/2}$	5	0	0.179	-0.15
$0i_{11/2}$	6	0.77	0.158	-0.13
$0j_{15/2}$	8	1.41	0.156	-0.13
$2d_{5/2}$	3	1.56	0.093	-0.08
$3s_{1/2}$	1	2.03	0.046	-0.04
$1g_{7/2}$	4	2.47	0.090	-0.07
$2d_{3/2}$	2	2.51	0.063	-0.05

Table 2.5.3: Same as Table 2.5.2 but for the backwards amplitude.

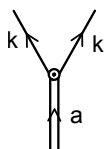


Figure 2.5.4: Same as Fig. 2.5.2 but for the pair addition mode

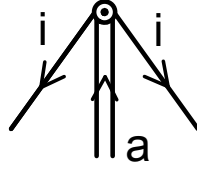


Figure 2.5.5: Same as Fig. 2.5.3 but for the pair addition mode

Similarly (cf. Fig. 2.5.5),

$$Y_1^a(i) = \frac{\frac{1}{2}\Omega_i^{1/2}\Lambda_1(+2)}{2(\epsilon_F - \epsilon_i) + W_1(+2)},$$

can be written, with the help of the relation

$$\begin{aligned} 2 \times (\epsilon_F - \epsilon_i) + W_1(+2) &= 2 \times (\epsilon_F - \epsilon_i) - 2 \times (\epsilon_{g_{9/2}} - \epsilon_F) - E_{corr}(+2) \\ &= 2 \times (\epsilon_{p_{1/2}} - \epsilon_i) + 2 \times (\epsilon_{g_{9/2}} - \epsilon_{p_{1/2}}) - E_{corr}(+2) \\ &= 2 \times (|\epsilon_i| - |\epsilon_{p_{1/2}}|) + 2 \times (|\epsilon_{p_{1/2}}| - |\epsilon_{g_{9/2}}|) - E_{corr}(+2), \end{aligned}$$

as

$$Y_1^a(i) = \frac{\frac{1}{2}\Omega_i^{1/2}\Lambda_1(+2)}{2(|\epsilon_i| - |\epsilon_{p_{1/2}}|) + 2\Delta\epsilon_{sp} - E_{corr}(+2)}.$$

Making use of  $E_{corr}(+2) = 1.5$  MeV (cf. Fig. 2.5.1) and

$$\Delta\epsilon_{sp} = 2 \times (|\epsilon_{p_{1/2}}| - |\epsilon_{g_{9/2}}|) = 6.28 \text{ MeV},$$

one can write  $2\Delta\epsilon_{sp} - E_{corr}(+2) = (6.82 - 1.5)$  MeV = 5.32 MeV, leading to

$$\begin{cases} X_1^a(k) = \frac{\frac{1}{2}\Omega_k^{1/2}\Lambda(-2)}{2(|\epsilon_{g_{9/2}}| - |\epsilon_k|) + 1.5 \text{ MeV}}, \\ Y_1^a(i) = -\frac{\frac{1}{2}\Omega_i^{1/2}\Lambda(+2)}{2(|\epsilon_i| - |\epsilon_{p_{1/2}}|) + 5.32 \text{ MeV}}. \end{cases}$$

The corresponding numerical values are displayed in Tables 2.5.4 and 2.5.5, while in Fig. 2.5.6 we display a schematic summary of the graphical solution of the dispersion relations.

Let us conclude this Appendix by noting that while the harmonic (RPA) description of the pair vibrational mode of  $^{208}\text{Pb}$  provides a fair picture of the two neutron transfer spectroscopic amplitudes, in keeping with the collective character of these (coherent) states, conspicuous anharmonicities in the multi-phonon spectrum have been observed and calculated<sup>49</sup>. Within the framework of Fig. 2.4.1, we schematically emphasize in Fig. 2.5.7 the relative importance of dynamic and static pairing distortions, in comparison with the corresponding quantities in the

---

<sup>49</sup>Cf. for example Flynn, E. R. et al. (1972), Lanford and McGrory (1973), Bortignon, P. F. et al. (1978), Clark, R. M. et al. (2006).

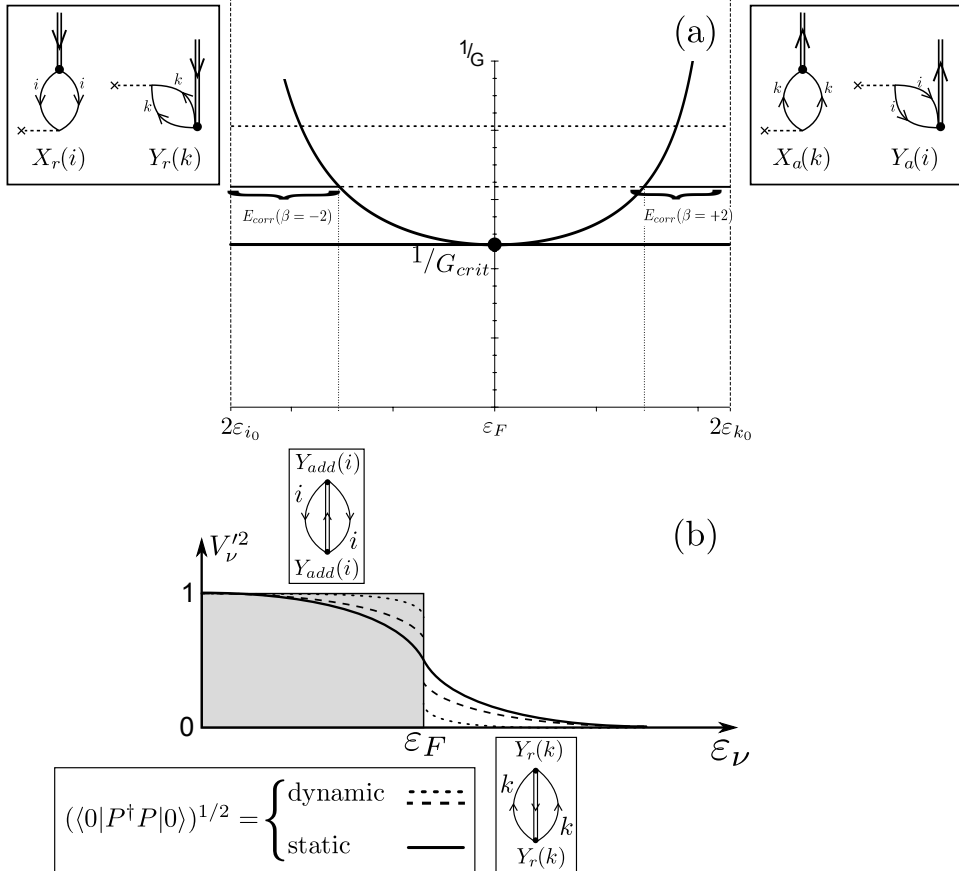


Figure 2.5.6: Schematic representation of the quantal phase transition taking place as a function of the pairing coupling constant in a (model) closed shell nucleus. (a) dispersion relation associated with the RPA diagonalization of the Hamiltonian  $H = H_{sp} + H_p$  for the pair addition and pair removal modes. In the insets are shown the two-particle transfer processes exciting these modes, which testify to the fact that the associated zero point fluctuations (ZPF) which diverge at  $G = G_{crit}$ , blur the distinction between occupied and empty states typical of closed shell nuclei. (b) occupation number associated with the single-particle levels. For  $G < G_{crit}$  there is a dynamical depopulation (population) of levels  $i(k)$  below (above) the Fermi energy. For  $G > G_{crit}$ , the deformation of the Fermi surface becomes static, although with a non-vanishing dynamic component (cf. Fig. 2.1.2).

units		MeV	MeV <sup>-1</sup>	
$nlj$	$\Omega_k$	$ \epsilon_{g_{9/2}}  -  \epsilon_k $	$C(k) = \frac{\frac{1}{2}\Omega_k^{1/2}}{2( \epsilon_{g_{9/2}}  -  \epsilon_k ) + 1.5 \text{ MeV}}^a)$	$X_1^a(k)$
$1g_{9/2}$	5	0	0.745	0.82
$0i_{11/2}$	6	0.77	0.403	0.44
$0j_{15/2}$	8	1.41	0.327	0.36
$2d_{5/2}$	3	1.56	0.187	0.21
$3s_{1/2}$	1	2.03	0.090	0.10
$1g_{7/2}$	4	2.47	0.155	0.17
$2d_{3/2}$	2	2.51	0.108	0.12

Table 2.5.4: Forwards going RPA amplitudes associated with the pair addition mode of  $^{208}\text{Pb}$  (cf. Table XVI Broglia, R.A. et al. (1973)). a)  $\sum_k C^2(k) = 0.903$

units		MeV	MeV <sup>-1</sup>	
$nlj$	$\Omega_i$	$ \epsilon_i  -  \epsilon_{p_{1/2}} $	$D(i) = \frac{\frac{1}{2}\Omega_i^{1/2}}{2( \epsilon_i  -  \epsilon_{p_{1/2}} ) + 5.32 \text{ MeV}}^a)$	$Y_1^a(i)$
$2p_{1/2}$	1	0	-0.094	-0.1
$1f_{5/2}$	3	0.57	-0.134	-0.15
$2p_{3/2}$	2	0.90	-0.099	-0.11
$0i_{13/2}$	7	1.64	-0.154	-0.17
$1f_{7/2}$	4	2.35	-0.100	-0.11
$0h_{9/2}$	5	3.47	-0.091	-0.10

Table 2.5.5: Same as Table 2.5.4 but for the backwards going amplitude. a)  $\sum_i D^2(i) = 0.079$  and  $\Lambda^2(+2)(\sum_k C^2(k) - D^2(i)) = \Lambda^2(+2)(0.903 - 0.079) \text{ MeV}^{-2} = 0.824 \text{ MeV}^{-2}$ ;  $\Lambda(+2) = (0.824)^{-1/2} \text{ MeV}$ , thus  $\Lambda(+2) = 1.102 \text{ MeV}$ .

case of quadrupole surface distortions in 3D space<sup>50</sup> These results underscore the major role pairing vibrations play in nuclei around closed shells, while those collected in Fig. 2.1.2 their importance in gauge invariance restoration in systems far away from closed shells.

## 2.6 Halo pair addition mode and pygmy: a new mechanism to break gauge invariance

Pairing is intimately connected with particle number violation and thus spontaneous breaking of gauge invariance, as testified by the order parameter  $\langle BCS | P^\dagger | BCS \rangle = \alpha_0$ . In the nuclear case and, at variance with condensed matter, dynamical breaking of gauge symmetry is similarly important to that associated with static distortions (e.g. pairing vibrations around closed shell nuclei, cf. Fig. 2.1.1; see also Fig. 2.4.2 and Fig. 2.5.7) The fact that the average single-particle field acts as an external potential (like e.g. a magnetic field in metallic superconductors) is one of the reasons of the existence of a critical value  $G_c$  of the pairing strength  $G$  to bind Cooper pairs in nuclei. Spatial quantization in finite systems at large and in nuclei in particular, is intimately connected with the paramount role the surface plays in these systems<sup>51</sup>. Another consequence of this role is the fact that in nuclei an important fraction (30-50%) of Cooper pair binding is due to the exchange of collective vibrations between the partners of the pair<sup>52</sup>, the rest being associated with the bare  $NN$ -interaction in the  $^1S_0$  channel (cf. Fig. 2.6.1) plus possible  $3N$  corrections<sup>53</sup>. Within this context we note that the results displayed in Fig. 2.1.2 provide one of the clearest quantitative examples of the central and ubiquitous role pairing vibrations play in nuclear pairing correlations.

The study of light exotic nuclei lying along the neutron drip line have revealed a novel aspect of the interplay between shell effects and induced pairing interaction. It has been found that there are situations in which spatial quantization screens, essentially completely, the bare nucleon-nucleon interaction. This happens in the case in which the nuclear valence orbitals are  $s, p$ -states at threshold<sup>54</sup>. An example of situations of this type is provided by  $N = 6$  (parity inversion; cf. Chapter 4 Section 4.2.2) isotones. In particular, by  $^{11}\text{Li}$ , in which case the strongly renormalized  $s_{1/2}$  and  $p_{1/2}$  valence orbitals are a virtual and a resonant state lying at  $\approx 0.2$  and  $0.5$  MeV in the continuum, respectively. Let us elaborate on this point. The binding provided by a contact pairing interaction  $V_\delta(|\mathbf{r} - \mathbf{r}'|)$  ( $\delta$ -force) to a pair of

<sup>50</sup>For details cf. Bès and Broglia (1977), Broglia, R.A. et al. (1968), Bès, D. R. et al. (1988), Shimizu, Y. R. et al. (1989), Shimizu, Y. R. (2013), Vaquero et al. (2013) and references therein.

<sup>51</sup>cf. Broglia, R. A. (2002) and references therein.

<sup>52</sup>Cf. e.g. Barranco et al. (1999), Brink, D. and Broglia (2005), Saperstein and Baldo (2013), Avdeenkov and Kamerdzhiev (2013), Lombardo et al. (2013), and references therein; cf. also Bohr, A. and Mottelson (1975), p. 432.

<sup>53</sup>Cf. e.g. Lesinski et al. (2012), Pankratov et al. (2011), Hergert and Roth (2009).

<sup>54</sup>Pairing anti-halo effect; Bennaceur, K. et al. (2000) , Hamamoto and Mottelson (2003), Hamamoto, I. and Mottelson (2004).

$$\begin{aligned}
P^\dagger &= \sum_{\nu>0} a_\nu^\dagger a_\nu^\dagger \\
x' &= \frac{2G'\Omega'}{D} = GN(0) \\
\begin{array}{c|c}
x > 1 & x < 1 \\
\alpha_0 = \langle P^\dagger \rangle = \frac{\Delta}{G} \approx 7 & \alpha_{dyn} = \frac{\langle PP^\dagger \rangle^{1/2} + \langle P^\dagger P \rangle^{1/2}}{2} \\
& \approx \frac{1}{2} \left( \frac{E_{corr}(A+2)}{G} + \frac{E_{corr}(A-2)}{G} \right) \approx 10 \\
\frac{\alpha_0}{\alpha_{dyn}} & \approx 0.7 \\
\frac{\beta_2}{(\beta_2)_{dyn}} & \approx 3 - 6
\end{array}
\end{aligned}$$

Figure 2.5.7: Relative importance of dynamic and static pairing distortion ( $\alpha_{dyn}$  and  $\alpha_0$  respectively) associated with closed shell and open shell nuclei, calculated in terms of a two level model, as compared with similar quantities for the case of quadrupole surface degrees of freedom ( $\beta_2$ -values). The parameter  $x'$  (product of the effective pairing strength  $G' = Z_\omega^2(v_p^{bare} + v_p^{ind})$  and of the effective density of levels at the Fermi energy  $N'(0) = Z_\omega^{-1}N(0) = Z_\omega^{-1}(2\Omega/D) = 2\Omega'/D = 2\Omega/D'; \Omega' = Z_\omega^{-1}\Omega, D' = Z_\omega D$ ), measures the relative importance of the single-particle gap  $D' = Z_\omega D$  and of the pair correlation  $G'\Omega$  (cf. Brink, D. and Broglia (2005) App. H, Sect. H.4).

fermions moving in time-reversal states<sup>55</sup> is given by the matrix element,

$$M_j = \langle j^2(0) | V_\delta | j^2(0) \rangle = -\frac{(2j+1)}{2} V_0 I(j) \approx \frac{(2j+1)}{2} V_0 \frac{3}{R^3}.$$

Of notice that  $G = V_0 I(j)$  (cf. the expression of  $H_P$  Section 1.D.2). The ratio of the above matrix element for the halo nucleus  $^{11}\text{Li}$  and for an hypothetical normal nucleus of mass  $A = 11$  is

$$r = \frac{(M_j)_{\text{halo}}}{(M_j)_{\text{core}}} = \frac{2}{(2j+1)} \left( \frac{R_0}{R} \right)^3.$$

The quantities  $R_0 = 1.2A^{1/3}\text{fm} = 2.7\text{fm}$  ( $A = 11$ ), and  $R = \sqrt{\frac{5}{3}} \langle r^2 \rangle_{^{11}\text{Li}}^{1/2} = \sqrt{\frac{5}{3}} (3.55 \pm 0.1) \text{ fm} = (4.6 \pm 0.13) \text{ fm}$  are the radius of a stable nucleus of mass  $A = 11$  (systematics), and the measured radius of  $^{11}\text{Li}$ , respectively. The quantity  $j$  is the angular momentum representative for a nucleus of mass  $A = 11$  ( $j \sim k_F R_0 \approx 3 - 4$ ). One thus obtains  $r = 0.048$ . Consequently, the bare  $NN$ -nucleon pairing interaction is expected to become strongly screened, the resulting effective  $G$ -value

$$G' = G \times r = 0.048 \times 25 \text{ MeV}/A \approx 1 \text{ MeV}/A \approx 0.1 \quad (2.6.1)$$

MeV becoming subcritical and thus unable to bind the halo Cooper pair ( $2\epsilon_{s_{1/2}} = 0.4 \text{ MeV}$ ) to the  $^9\text{Li}$  core.

Further insight into this question can be shed making use of the multipole expansion of a general interaction

$$v(|\mathbf{r}_1 - \mathbf{r}_2|) = \sum_{\lambda} V_{\lambda}(r_1, r_2) P_{\lambda}(\cos \theta_{12}).$$

Because the function  $P_{\lambda}$  drops from its maximum at  $\theta_{12} = 0$  in an angular distance  $1/\lambda$ , particles 1 and 2 interact through the component  $\lambda$  of the force, only if  $r_{12} = |\mathbf{r}_1 - \mathbf{r}_2| < R/\lambda$ , where  $R$  is the mean value of the radii  $\mathbf{r}_1$  and  $\mathbf{r}_2$ . Thus, as  $\lambda$  increases, the effective force range decreases. For a force of range much greater than the nuclear size, only the  $\lambda \approx 0$  (long wavelength) term is important. At the other extreme, a  $\delta$ -function force has coefficients  $V_{\lambda}(r_1, r_2) \left( = \frac{(2\lambda+1)}{4\pi r_1^2} \delta(r_1 - r_2) \right)$  that increase with  $\lambda$ . In the case of  $^{11}\text{Li}(\text{gs})$  we are thus forced to accept the need for a long range, low  $\lambda$  pairing interaction, as responsible for the binding of the dineutron, halo Cooper pair to the  $^9\text{Li}$  core. This is equivalent to saying, an induced pairing interaction arising from the exchange of vibrations with low  $\lambda$ -value.

### 2.6.1 Cooper pair binding: a novel embodiment of the Axel–Brink hypothesis.

In what follows we discuss a possible novel test of the Axel–Brink hypothesis<sup>56</sup>. Within the  $s, p$  subspace, the most natural low multipolarity, long wavelength vibration is

<sup>55</sup>cf. e.g. Eq. (2.12) Brink, D. and Broglia (2005).

<sup>56</sup>The color of an object can be determined in two ways: by illuminating it with white light and see which wavelength it absorbs, or by heating it up and see the same wavelength it emits. In both cases

the dipole mode. From systematics, the centroid of these vibrations is  $\hbar\omega_{GDR} \approx 100 \text{ MeV}/R$ ,  $R$  being the nuclear radius<sup>57</sup>. Thus, in the case of  $^{11}\text{Li}$ , one expects the centroid of the Giant Dipole Resonance carrying  $\approx 100\%$  of the energy weighted sum rule (EWSR) at  $\hbar\omega_{GDR} \approx 100 \text{ MeV}/2.7 \approx 37 \text{ MeV}$ . Now, such a high frequency mode can hardly be expected to give rise to anything, but polarization effects (see within this context Eqs. 83.A.12–3.A.15). On the other hand, there exists experimental evidence which testifies to the presence of a rather sharp dipole state with centroid at  $\approx 1 \text{ MeV}$  and carrying  $\approx 8\%$  of the EWSR<sup>58</sup>. The existence of this “pigmy resonance” which can be viewed as a simple consequence of the existence of a low-lying particle-hole state associated with the transition  $s_{1/2} \rightarrow p_{1/2}$  testifies, arguably, to the coexistence<sup>59</sup> of two states with rather different radii in the ground state. One, closely connected with the  $^9\text{Li}$  core, ( $\approx 2.5 \text{ fm}$ ), the second with the diffuse halo ( $\approx 4.6 \text{ fm}$ ), namely displaying a large radial deformation, and thus able to induce a conspicuous inhomogeneous damping to the dipole mode.

Before proceeding, let us estimate the overlap  $\mathcal{O}$  between the two “ground states”. Making use of a schematic expression for the single-particle radial wave-functions

$$\mathcal{R} = \sqrt{3/R_0^3} \Theta(r - R_0), \quad (2.6.2)$$

where

$$\Theta = 1 \quad (r \leq R_0); \quad 0 \quad (r > R_0),$$

leading to,

$$\int_0^\infty dr r^2 \mathcal{R}^2(r) = \frac{3}{R_0^3} \int_0^{R_0} dr r^3 / 3 = 1, \quad (2.6.3)$$

one can work out the overlap  $\mathcal{O}$  between the two halo neutrons an the core nucleons.

---

one is talking about dipole radiation. To describe the de-excitation process of hot nuclei requires the knowledge of the photon interactions with excited states. The common assumption, known as the Axel-Brink hypothesis, has been that each excited state of a nucleus carries a giant dipole resonance (GDR) on top of it, and that the properties of such resonances are unaffected by any excitation of the nucleus (Brink (1955), Lynn (1968) pag. 321, Axel (1962); cf. also Bertsch, G. F. and Broglia (1986) and Bortignon, P. F. et al. (1998))

<sup>57</sup>cf. e.g. Bortignon, P. F. et al. (1998) and Bertsch and Broglia (2005).

<sup>58</sup>Zinsler, M. et al. (1997), T. Nakamura et al. (2006), Shimoura et al. (1995), Ieki et al. (1993), Sackett et al. (1993), ?.

<sup>59</sup>Within this context one can mention similar situations concerning the coexistence of spherical and quadrupole deformed states (cf. e.g. Wimmer, K. et al. (2010), Federman and Talmi (1965), Federman and Talmi (1966), Dönuau et al. (1967) and refs. therein; cf. also Bohr and Mottelson (1963)), typically of nuclei with  $N \approx Z$ . The fact that the associated inhomogeneous damping on the GDR has modest consequences concerning dipole strength at low energies as compared with radial (isotropic) deformations in  $^{11}\text{Li}$  is understood in terms of the (non-Newtonian) plasticity of the atomic nucleus regarding quadrupole deformations (low-lying collective  $2^+$  surface vibrations, fission, exotic decay (cf. Barranco, F. et al. (1988), Barranco et al. (1989), Bertsch et al. (1987))), and of the little compressibility displayed by the same system and connected with saturation properties.

That is,

$$\begin{aligned}\mathcal{O} &= |\langle \mathcal{R}_{\text{halo}} | \mathcal{R}_{\text{core}} \rangle|^2 = \left( \sqrt{\frac{3}{R_0^3}} \sqrt{\frac{3}{R^3}} \int_0^\infty dr r^2 \Theta(r - R) \Theta(r - R_0) \right)^2 \\ &= \left( \sqrt{\frac{3}{R_0^3}} \sqrt{\frac{3}{R^3}} \int_0^{R_0} dr^3 / 3 \right)^2 = (R_0/R)^3 = 0.16,\end{aligned}\quad (2.6.4)$$

where use has been made of  $\Theta(r - R)\Theta(r - R_0) = \Theta(r - R_0)$ ,  $R_0 = 1.2A^{1/3}\text{fm} = 2.5\text{fm}(A = 9)$  and  $R = (4.6 \pm 0.13) \text{ fm}$ . Because of the small value of this overlap, one can posit that a *bona fide* dipole pigmy resonance is a GDR based on an exotic, unusually extended state as compared to systematics ( $A \approx (4.6/1.2)^3 \approx 60$ ), i.e. to a system with an effective  $A$  mass number about 5 times that predicted by systematics.

Of notice that, the small values of  $r$  and of  $\mathcal{O}$  have essentially the same origin. On the other hand, they have apparently, rather different physical consequences. In fact, the first makes the bare interaction strength  $G$  subcritical, while the second one screens the repulsive symmetry potential  $V_1(\approx +25 \text{ MeV}, \text{cf. e.g. Bortignon, P. F. et al. (1998)})$ , that is, the price one has to pay to separate protons from neutrons. This effect allows for a consistent fraction of the dipole Thomas–Reiche–Kuhn sum rule, that is of the  $J^\pi = 1^-$  energy weighted sum rule (EWSR), to come low in energy from the value  $E_{\text{GDR}} \approx (80/A^{1/3}) \text{ MeV}$  and, acting as an intermediate boson between the two halo neutrons, glue them to the  ${}^9\text{Li}$  core. Summing up, the halo anti-pairing effect  $G_{\text{screened}} = r \times G \ll G < G_{\text{crit}}$  triggers ( $OV_1 \ll V_1$ ) the virtual presence of a “gas” of dipole (pigmy) bosons which, exchanged between the two halo neutrons (cf. Fig. 2.6.2), overcompensates the reduction of the bare interaction, leading to the binding of the halo Cooper pair to the core (anti-(halo anti-pairing effect)). It can thus be stated that the halo of  ${}^{11}\text{Li}$  and the pigmy resonance built on top of it constitute a pair of symbiotic states (see also Chapter 6, in particular Fig. 6.1.4).

Let us further elaborate on these issues. Making use of the relation  $\langle r^2 \rangle^{1/2} \approx (3/5)^{1/2}R$  between mean square radius and radius, one may write

$$\langle r^2 \rangle_{{}^{11}\text{Li}} \approx \frac{3}{5} R_{\text{eff}}^2({}^{11}\text{Li}).$$

with

$$R_{\text{eff}}^2({}^{11}\text{Li}) = \left( \frac{9}{11} R_0^2({}^9\text{Li}) + \frac{2}{11} \left( \frac{\xi}{2} \right)^2 \right),$$

where

$$R_0({}^9\text{Li}) = 2.5\text{fm},$$

is the  ${}^9\text{Li}$  radius ( $R_0 = r_0 A^{1/3}$ ,  $r_0 = 1.2\text{fm}$ ), while  $\xi$  is the correlation length of the Cooper pair neutron halo. An estimate of this quantity is provided by the relation

$$\xi = \frac{\hbar v_F}{2E_{\text{corr}}} \approx 20 \text{ fm},$$

in keeping with the fact that in  $^{11}\text{Li}$ ,  $(v_F/c) \approx 0.1$  and  $E_{corr} \approx 0.5$  MeV. Consequently,

$$R_{eff}(^{11}\text{Li}) \approx 4.83 \text{ fm} \quad (2.6.5)$$

and  $\langle r^2 \rangle_{^{11}\text{Li}}^{1/2} \approx 3.74 \text{ fm}$ , in overall agreement with the experimental value  $\langle r^2 \rangle_{^{11}\text{Li}}^{1/2} = 3.55 \pm 0.1 \text{ fm}$ <sup>60</sup>. It is of notice that this value implies the radius  $R(^{11}\text{Li}) = \sqrt{5/3} \langle r^2 \rangle_{^{11}\text{Li}}^{1/2} = 4.58 \pm 0.13 \text{ fm}$ .

We now proceed to the calculation of the centroid of the dipole pigmy resonance of  $^{11}\text{Li}$  in the RPA making use of the separable interaction

$$H_D = -\kappa_1 \vec{D} \cdot \vec{D} \quad (2.6.6)$$

where  $\vec{D} = \vec{r}$  and

$$\kappa_1 = \frac{-5V_1}{AR^2}. \quad (2.6.7)$$

The resulting dispersion relation is<sup>61</sup>

$$W(E) = \sum_{k,i} \frac{2(\epsilon_k - \epsilon_i)|\langle i|F|k\rangle|^2}{(\epsilon_k - \epsilon_i)^2 - E^2}. \quad (2.6.8)$$

Making use of this relation and of the fact that<sup>62</sup>  $\epsilon_{\nu_k} - \epsilon_{\nu_i} = \epsilon_{p_{1/2}} - \epsilon_{s_{1/2}} \approx 0.3 \text{ MeV}$ , and that the EWSR associated with the  $^{11}\text{Li}$  pigmy resonance is  $\approx 8\%$  of the total Thomas–Reiche–Kuhn sum rule

$$\sum_n |\langle 0|F|n\rangle|^2 (E_n - E_0) = \frac{\hbar^2}{2M} \int d\mathbf{r} |\vec{F}|^2 \rho(r), \quad (2.6.9)$$

which, for  $F = r$  has the value  $\hbar^2 A / 2M$  one can write<sup>63</sup>,

$$2 \times 0.08 \times \frac{\hbar^2 A}{2M} = \frac{1}{\kappa_1} [(0.3 \text{ MeV})^2 - (\hbar\omega_{pigmy})^2],$$

and thus

$$(\hbar\omega_{pigmy})^2 = (0.3 \text{ MeV})^2 - 2 \times 0.08 \times \frac{\hbar^2 A}{2M} \kappa_1,$$

where<sup>64</sup>

$$\kappa_1 = -\frac{5V_1}{A(\xi/2)^2} \left( \frac{2}{11} \right) = -\frac{125 \text{ MeV}}{A 100 \text{ fm}^2} \left( \frac{2}{11} \right) \approx \kappa_1^0 \times 0.045 = -\frac{2.5}{A^2} \text{ fm}^{-2} \text{ MeV},$$

---

<sup>60</sup>Kobayashi, T. et al. (1989).

<sup>61</sup>cf. (3.30) p.55 of Bortignon, P. F. et al. (1998).

<sup>62</sup>See Fig. 2.6.3; see also p.264 Brink, D. and Broglia (2005).

<sup>63</sup>cf. Bertsch and Broglia (2005) pag. 53.

<sup>64</sup>see Bortignon, P. F. et al. (1998).

the ratio in parenthesis reflecting the fact that only 2 out of 11 nucleons, slosh back and forth in an extended configuration with little overlap with the other nucleons, while

$$\kappa_1^0 = -\frac{5V_1}{AR_{eff}^2(^{11}\text{Li})} \approx 0.49 \text{ MeV fm}^{-2} \quad (2.6.10)$$

is the standard self consistent dipole strength<sup>65</sup>. One then obtains,

$$-2 \times 0.08 \frac{\hbar^2 A}{2M} \kappa_1 = 2 \times 0.08 \times 20 \text{ MeV fm}^2 \times A \times \frac{2.5}{A^2} \text{ fm}^{-2} \text{ MeV} \approx 0.73 \text{ MeV}^2 \approx (0.85 \text{ MeV})^2.$$

Consequently

$$\hbar\omega_{pigmy} = \sqrt{(0.3)^2 + (0.85)^2} \text{ MeV} \approx 1.0 \text{ MeV},$$

in overall agreement with the experimental findings<sup>66</sup>. It is of notice that the centroid of the pigmy resonance calculated in the RPA with the help of a separable dipole interaction is<sup>67</sup>  $\approx (0.6 \text{ MeV} + 1.6 \text{ MeV})/2 \approx 1.0 \text{ MeV}$ .

Let us now estimate the binding energy which the exchange of the pigmy resonance between two neutron of the Cooper pair halo of <sup>11</sup>Li can provide. The associated particle-vibration coupling<sup>68</sup> is  $\Lambda = (\partial W(E)/\partial E|_{\hbar\omega_{pigmy}})^{-1/2}$  (note the use in what follows of a dimensionless dipole single-particle field  $F' = F/R_{eff}(^{11}\text{Li})$ ). This is in keeping with the fact that one wants to obtain a quantity with energy dimensions ( $[\Lambda] = \text{MeV}$ ), and that  $\kappa_1$  has been introduced through the Hamiltonian  $H_D$  with the self consistent value normalized in terms of  $R_{eff}^2(^{11}\text{Li})$ . One then obtains

$$\begin{aligned} \Lambda^2 &= \left\{ 2\hbar\omega_{pigmy} \frac{2 \times 0.08(\frac{\hbar^2 A}{2M})/R_{eff}^2(^{11}\text{Li})}{[(\epsilon_{p_{1/2}} - \epsilon_{s_{1/2}})^2 - (\hbar\omega_{pigmy})^2]^2} \right\}^{-1}, \\ &= \left\{ 2 \text{ MeV} \frac{0.16(\hbar^2 A/2M)(1/4.83^2 \text{ fm}^2)}{[(0.3)^2 - (1 \text{ MeV})^2]^2 \text{ MeV}^4} \right\}^{-1}, \\ &= \left( \frac{3 \text{ MeV}^2}{(0.91)^2 \text{ MeV}^4} \right)^{-1}, \\ &= \left( \frac{1}{1.7} \right)^2 \text{ MeV}^2 \approx 0.35 \text{ MeV}^2, \end{aligned}$$

leading to  $\Lambda \approx 0.6 \text{ MeV}$ . The value of the induced interaction matrix elements is then given by,

$$M_{ind} = \frac{2\Lambda^2}{DEN} = -\frac{2\Lambda^2}{\hbar\omega_{pigmy}} \approx -0.7 \text{ MeV}, \quad (2.6.11)$$

<sup>65</sup>cf. Bohr, A. and Mottelson (1975).

<sup>66</sup>Zinser, M. et al. (1997).

<sup>67</sup>Barranco, F. et al. (2001); see also Fig. 11.3(a) p.269, Brink, D. and Broglia (2005).

<sup>68</sup>cf. e.g. Brink, D. and Broglia (2005) Eq. (8.42) p.189.

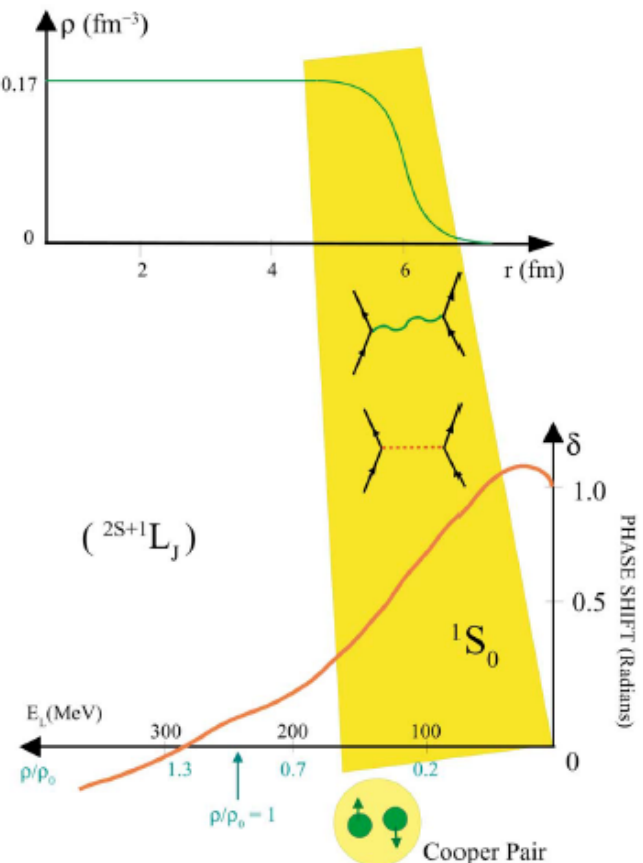


Figure 2.6.1: (top) Nuclear density  $\rho$  in units of  $\text{fm}^{-3}$ , plotted as a function of the distance  $r$  (in units of fm) from the centre of the nucleus (after Bohr and Mottelson (1969)). Saturation density correspond to  $\approx 0.17 \text{ fm}^{-3}$ , equivalent to  $2.8 \times 10^{14} \text{ g/cm}^3$ . Because of the short range of the nuclear force, the strong force, the nuclear density changes from 90% of saturation density to 10% within 0.65 fm, i.e. within the nuclear diffusivity. (bottom) Phase shift parameter associated with the elastic scattering of two nucleons moving in states of time reversal, so called  $^1S_0$  phase shift, in keeping with the fact that the system is in a singlet state of spin zero. The solution of the Schrödinger equation describing the elastic scattering of a nucleon from a scattering centre (in this case another nucleon) is, at large distances from the scattering centre a superposition of the incoming wave and of the outgoing, scattering wave. The interaction of the incoming particle with the target particle changes only the amplitude of the outgoing wave. This amplitude can be written in terms of a real phase shift or scattering phase  $\delta$ . Positive values of  $\delta$  implies an attractive interaction, negative a repulsive one. For low relative velocities (kinetic energies  $E_L$ ), i.e. around the nuclear surface where the density is low, the  $^1S_0$  phase shift arizing from the exchange of mesons (i.g. pions, represented by an horizontal dotted line) between nucleons (represented by upward pointing arrowed lines) is attractive. This mechanism provides about half of the glue to nucleons moving in time reversal states to form Cooper pairs. These pairs behaves like boson and eventually condense in a single quantal state leading to nuclear superfluidity. Cooper pair formation is further assisted by the exchange of collective surface vibrations (wavy curve in the scattering process) between the members of the pair (after Broglia, R. A. (2002)).

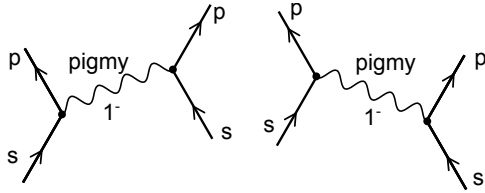


Figure 2.6.2: Diagrammatic representation of the exchange of a collective  $1^-$  pigmy resonance between pairs of nucleons moving in the time-reversal configurations  $s_{1/2}^2(0)$  and  $p_{1/2}^2(0)$ . It is of notice that both these configurations can act as initial states the figure showing only one of the two possibilities. Consequently, the energy denominator to be used in the simple estimate (2.6.11) is the average value  $DEN = (DEN_1 + DEN_2)/2 = -\hbar\omega_{pigmy}$  where  $DEN_1 = \Delta\epsilon - \hbar\omega_{pigmy}$  and  $DEN_2 = -\Delta\epsilon - \hbar\omega_{pigmy}$ , while  $\Delta\epsilon = \epsilon_{s_{1/2}} - \epsilon_{p_{1/2}}$ .

the factor of two resulting from the two time ordering contributions (see Fig. 2.6.2). The resulting correlation energy is thus  $E_{corr} = |2\epsilon_{s_{1/2}} - G' + M_{ind}| = |0.4 - 0.1 - 0.7| \approx 0.4$  MeV, in overall agreement with the experimental<sup>69</sup> findings (0.380 MeV). Of notice that in this estimate the (subcritical) effect of the screened bare pairing interaction has also been used (see Eq. (2.6.1)).

This schematic model has been implemented with microscopic detail<sup>70</sup> within the framework of a field theoretical description of the interweaving of collective vibrations and single-particle motion<sup>71</sup>, and is discussed in more detail within the context of single-particle (Chapter 4) and two-particle (Chapter 6) transfer processes. Here we provide a summary of the theoretical findings.

In Fig. 2.6.3 (I), the single-particle neutron resonances in  $^{10}\text{Li}$  are given. The position of the levels  $s_{1/2}$  and  $p_{1/2}$  determined making use of mean-field theory is shown (hatched area and thin horizontal line, respectively). The coupling of a single-neutron (upward pointing arrowed line) to a vibration (wavy line) calculated making use of NFT Feynman diagrams (schematically depicted also in terms of either solid dots (neutron) or open circles (neutron hole) moving in a single-particle level around or in the  $^9\text{Li}$  core (hatched area)), leads to conspicuous shifts in the energy centroid of the  $s_{1/2}$  and  $p_{1/2}$  resonances (shown by thick horizontal lines) and eventually to an inversion in their sequence. In Fig. 2.6.3 (II) the processes binding the halo neutron system  $^{11}\text{Li}$  are displayed.

Starting with the clothed mean field picture in which two neutrons (solid dots) move in time-reversal states around the core  $^9\text{Li}$  (hatched area) in the  $s_{1/2}$  virtual state leading to an unbound  $s_{1/2}^2(0)$  state where the two neutrons are coupled to angular momentum zero. The associated spatial structure of the uncorrelated pair is shown in a). The exchange of vibrations between the two neutrons displayed in the upper part of the figure leads to a density-dependent interaction which, added to

<sup>69</sup>C. Bachelet et al. (2008), M. Smith et al. (2008).

<sup>70</sup>cf. Barranco, F. et al. (2001).

<sup>71</sup>Nuclear Field Theory (NFT); cf. Bortignon, P. F. et al. (1977) and references therein.

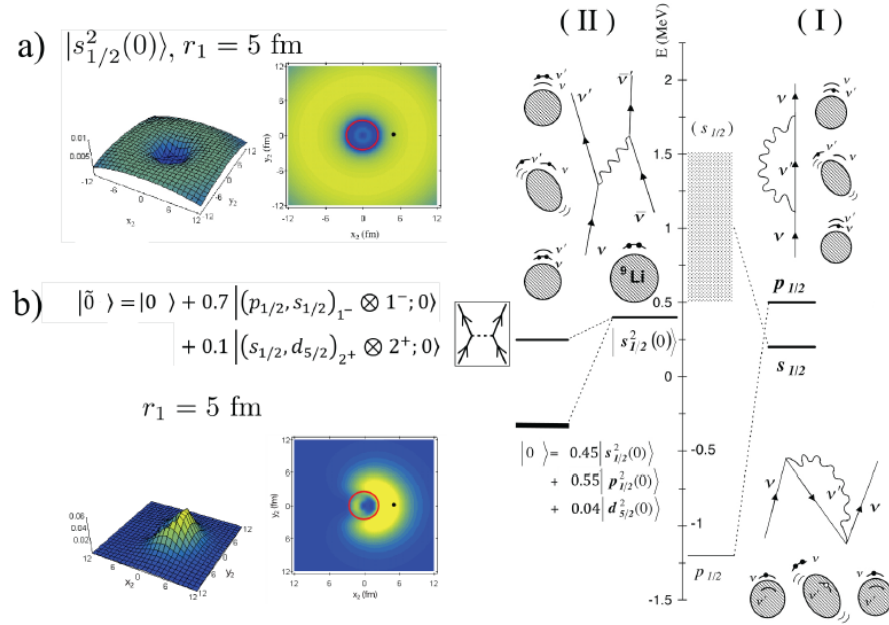


Figure 2.6.3: In (I) and (II) the NFT processes renormalizing the single-particle motion ( $^{10}\text{Li}$ ) and leading to the effective interaction, sum of the bare (horizontal dotted lines) and induced (wavy curves) interactions which bind the two-neutron halo to the core of  $^{9}\text{Li}$  thus leading to the  $^{11}\text{Li}\rangle$  state are displayed. In b) the corresponding wavefunction is shown. In a) and b) are also displayed the spatial structure of the pure  $|s_{1/2}^2(0)\rangle$  configuration and that of the two-neutron halo  $|\tilde{0}\rangle$ . Cooper pair. The modulus squared wave function  $|\Psi_0(\mathbf{r}_1, \mathbf{r}_2)|^2 = |\langle \mathbf{r}_1, \mathbf{r}_1 | 0^+ \rangle|^2$  describing the motion of the two halo neutrons around the  $^{9}\text{Li}$  core is shown as a function of the cartesian coordinates of particle 2, for fixed values of the position of particle 1 ( $r_1 = 5$  fm) represented by a solid dot, while the core  $^{9}\text{Li}$  is shown as a circle. The numbers appearing on the  $z$ -axis of the three-dimensional plots displayed on the left side of the figure are in units of fm $^{-2}$ . After Barranco, F. et al. (2001).

the nucleon–nucleon bare interaction (see boxed inset) which, as can be seen from the figure, is subcritical, correlates the two-neutron system leading to a bound state  $|\tilde{0}\rangle$  whose wavefunction is displayed in **b**), together with the spatial structure of the Cooper pair. It is of notice that a large fraction of the induced interaction arises from the exchange of the pigmy resonance (see Fig. 2.6.2) between the two halo neutrons. Within this scenario one can posit that the  $^{11}\text{Li}$  dipole pigmy resonance can hardly be viewed but in symbiosis with the  $^9\text{Li}$  halo neutron pair addition mode and vice versa. For details see Chapter 6 as well as<sup>72</sup>.

Let us conclude this Section by stating that the detailed consequences of the diagonalization of self-energy processes and of the bare and induced interactions tantamount to the diagonalization of the many-body Hamiltonian, provides in the case of  $^{10}\text{Li}$  an example of minimal mean field description (cf. apendice D de la introducción and App. 4.A) and in the case of  $^{11}\text{Li}$  an example of the fact that pairs of dressed single-particle states lead to abnormal density (induced pairing interaction), also in the case of closed shell systems, due to the strong ZPF associated with pairing vibrations (Fig. 2.6.3; cf. also discussion around eq. (2.2.2)). In keeping with the fact that  $^9\text{Li}$  is a normal, bound nucleus, while  $^{10}\text{Li}$  is not bound testifies to the fact that the binding of two neutrons to the  $^9\text{Li}$  core leading to  $^{11}\text{Li}$  ground state ( $S_{2n} \approx 380$  keV), is a pairing phenomenon.

## Appendix 2.A Nuclear van der Waals Cooper pair

The atomic van der Waals (dispersive; retarded) interaction which, like gravitation, acts between all atoms and molecules, also non-polar, can be written for two systems placed at a distance  $R$  as (see App. 2.D),

$$\Delta E = -\frac{6 \times e^2 \times a_0^5}{R^6} = -\frac{6 \times e^2}{(R/a_0)^6} \frac{1}{a_0}, \quad (2.A.1)$$

where  $a_0$  is the Bohr radius. A possible nuclear parallel can be established making the following correspondences,

$$e^2 \rightarrow \Lambda R_0(^{11}\text{Li}) = 0.6 \text{ MeV} \times 2.7 \text{ fm}; \quad a_0 \rightarrow d = 4 \text{ fm}; \quad R \rightarrow R_{eff}(^{11}\text{Li}) = 4.83 \text{ fm}.$$

That is,

$$\begin{aligned} \Delta E &= -\frac{6 \times \Lambda \times R_0}{R^6} = -\frac{6 \times e^2}{(R_{eff}(^{11}\text{Li})/d)^6} \frac{1}{d} = \frac{6 \times 0.6 \text{ MeV} \times 2.7 \text{ fm}}{(4.83/4)^6} \frac{1}{4 \text{ fm}} \\ &= -\frac{9.72 \text{ MeV}}{12.4} \approx -0.8 \text{ MeV} \rightarrow M_{ind}. \end{aligned}$$

Thus,

$$E_{corr} = |2E_{s_{1/2}} - G' + \Delta E| = |0.4 \text{ MeV} - 0.1 \text{ MeV} - 0.8 \text{ MeV}| \approx 0.5$$

---

<sup>72</sup>Barranco, F. et al. (2001).

to be compared to

$$(S_{2n})_{exp} \approx 0.380 \text{ MeV.}$$

## Appendix 2.B Renormalized coupling constants $^{11}\text{Li}$ : résumé

Let us make use of the experimental (empirical),

$$\begin{aligned}\epsilon_{s_{1/2}} &= 0.2 \text{ MeV}, \\ \epsilon_{p_{1/2}} &= 0.5 \text{ MeV}, \\ V_1 &= 25 \text{ MeV},\end{aligned}$$

and theoretical

$$\begin{aligned}R_0(^{11}\text{Li}) &= 1.2(11)^{1/3} \text{ fm} = 2.7 \text{ fm}, \\ \xi &= 20 \text{ fm}, \\ R_{eff}(^{11}\text{Li}) &= 4.83 \text{ MeV}, \\ G &= \frac{25}{A} \text{ MeV} = 2.3 \text{ fm}, \\ \kappa_1^0 &= -\frac{5V_1}{AR_{eff}(^{11}\text{Li})} \approx -0.49 \text{ MeV fm}^{-2}, \\ \kappa_1 &= -\frac{5V_1}{A(\xi/2)^2} = -0.022 \text{ MeV fm}^{-2},\end{aligned}$$

inputs.

One can then calculate the ratio

$$r = \frac{2}{(2j+1)} \frac{R_0}{R_{eff}}^3 \approx 0.042,$$

where use was made of  $(2j+1) \approx (2k_F R_0 + 1) \approx 8.34$ . Thus, the screened bare pairing interaction is,

$$(G)_{scr} = rG = 0.042 \times \frac{25}{A} \text{ MeV} = \frac{1 \text{ MeV}}{A} \approx 0.1 \text{ MeV.}$$

Similarly

$$\kappa_1 = s\kappa_1^0,$$

where the screening factor is

$$s = \frac{R_{eff}^2}{(\xi/2)^2} \frac{2}{11} \approx 0.042.$$

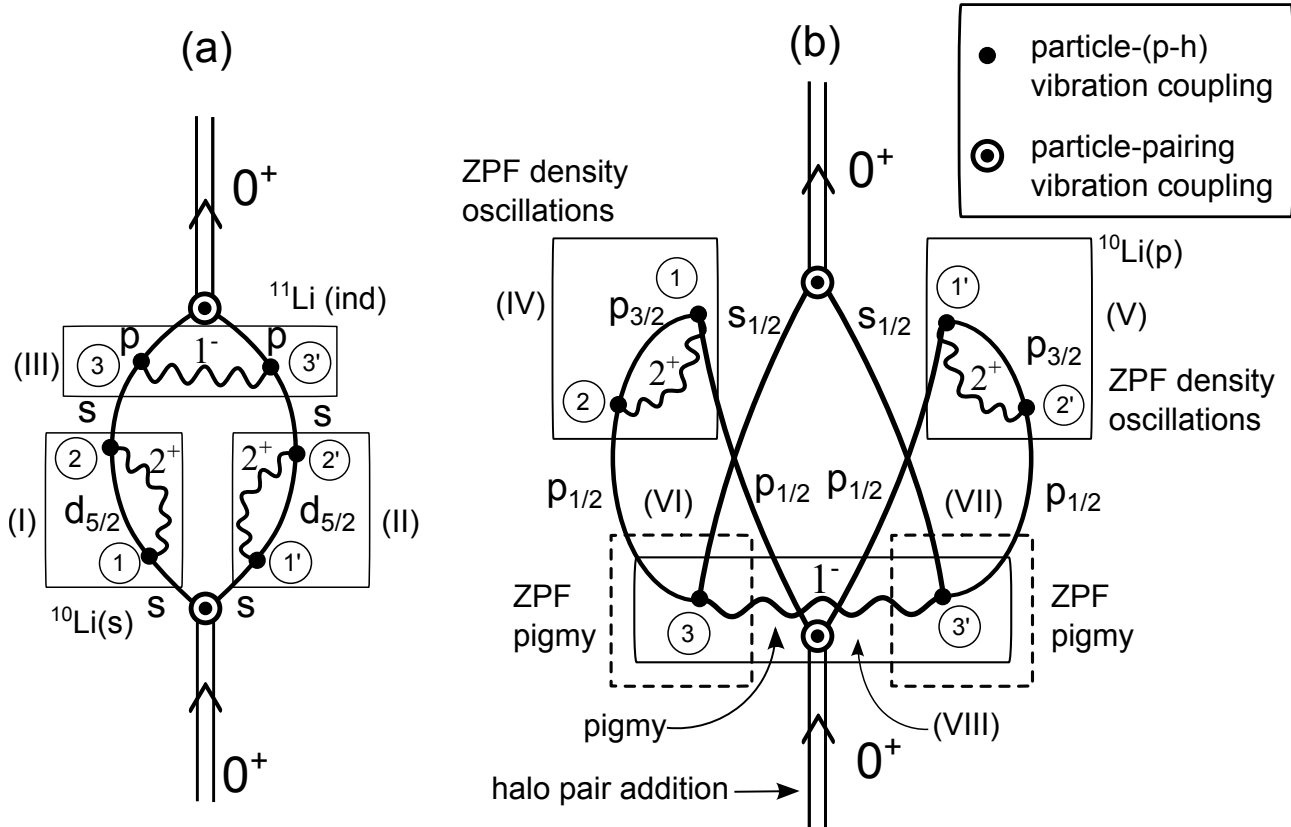


Figure 2.A.1: NFT Feynman diagrams describing the binding of the halo Cooper pair through pigmy. That is, producing the symbiotic mode involving the pair addition mode and the GDPR. The single-particle states  $s_{1/2}$  and  $p_{1/2}$  are labeled in (a)  $s$  and  $p$  for simplicity. The different particle-vibration coupling vertices (either with the quadrupole ( $2^+$ ) or with the pigmy ( $1^-$ ) modes drawn as solid wavy lines) are denoted by a solid dot, and numbered in increasing sequence so as to show that diagram (b) emerges from (a) through time ordering. The motion of the neutrons are drawn in terms of continuous solid curves. In keeping with the fact that the occupation of the single-particle states is neither 1 nor 0 (cf. Eqs. (6.1.1)–(6.1.3)), these states are treated as quasiparticle states. Thus no arrow is drawn on them. Diagram (a) emphasizes the self-energy renormalization of the state  $s_{1/2}$  lying in the continuum and which through its clothing with the quadrupole mode is brought down becoming a virtual ( $\epsilon_{s_{1/2}} = 0.2$  MeV) state (see (I) and (II)), while (III) contributes to the induced pairing interaction through pigmy (see also Fig. 2.6.2). Diagram (b) contains (cf. (IV) and (V)) Pauli corrections which push the bound state  $p_{1/2}$  into a resonant state in the continuum ( $\epsilon_{p_{1/2}} = 0.5$  MeV). In other words, processes (I), (II), (III), (IV) and (V) are at the basis of parity inversion, and of the appearance of the new magic number  $N = 6$ . Processes (VI) and (VII) are associated with the pigmy ZPF, while (VIII) contributes to the induced pairing interaction through pigmy (van der Waals-like process).

Thus, the screened symmetry potential is,

$$(V_1)_{scr} = sV_1 = 0.042 \times 25 \text{ MeV} = 1 \text{ MeV}.$$

The fact that  $r$  and  $s$  coincide within numerical approximations is in keeping with the fact that both quantities are closely related to the overlap

$$\mathcal{O} = \left( \frac{R_0}{R_{eff}} \right)^3 = \left( \frac{2.7 \text{ fm}}{4.83 \text{ fm}} \right)^3 = 0.17,$$

quantity which has a double hit effect concerning the mechanism which is at the basis of much of the nuclear structure of exotic nuclei at threshold: 1) it makes subcritical the screened bare  $NN$ -pairing interaction  $(G)_{scr} = rG < G_c$  ( $(G)_{scr} = 1 \text{ MeV}/A$ ); 2) it screens the symmetry potential drastically, reducing the price one has to pay to separate protons from delocalized neutrons, permitting a consistent chunk ( $\approx 8\%$ ) of the TRK sum rule to become essentially degenerate with the ground state ( $(V_1)_{scr} = 1 \text{ MeV}$ ), thus allowing for the first nuclear example of a van der Waals Cooper pair and a novel mechanism to break dynamically gauge invariance: dipole-dipole fluctuating fields associated with the exchange of the pigmy resonance between the halo neutrons of  $^{11}\text{Li}$ . As a result, a new, (composite) elementary mode of nuclear excitation joins the ranks of the previously known: the halo pair addition mode carrying on top of it, a low-lying collective pigmy resonance. This symbiotic mode can be studies through two-particle transfer reactions, eventually in coincidence with  $\gamma$ -decay. In particular, making use of the reactions,

$${}^9\text{Li}(t, p){}^{11}\text{Li}(f), \\ |f\rangle; \text{ground state } (L = 0), \text{pygmy } (L = 1),$$

and

$${}^{10}\text{Be}(t, p){}^{12}\text{Be}(f), \\ |f\rangle; \text{first excited } 0^+ \text{ state } (E_x = 2.24 \text{ MeV}) (L = 0), \\ \text{pygmy on top of it } (L = 1, \text{arguably the state at } E_x = 2.70 \text{ MeV is part of it}).$$

## Appendix 2.C Lindemann criterion and connection with quantity parameter

## Appendix 2.D The van der Waals interaction

## Bibliography

- Abrahams, E. and J. W. F. Woo. *Phys. Lett. A*, 27:117, 1968.
- A. Avdeenkov and S. Kamerdzhev. Phonon Coupling and the Single-Particle Characteristics of Sn Isotopes. In R. A. Broglia and V. Zelevinsky, editors, *50 Years of Nuclear BCS*, page 274. World Scientific, Singapore, 2013.
- P. Axel. Electric Dipole Ground-State Transition Width Strength Function and 7-Mev Photon Interactions. *Phys. Rev.*, 126:671, 1962.
- Barbieri, C. Role of Long-Range Correlations in the quenching of spectroscopic factors. *Phys. Rev. Lett.*, 103:202502, 2009.
- J. Bardeen, L. N. Cooper, and J. R. Schrieffer. Microscopic theory of superconductivity. *Physical Review*, 106:162, 1957a.
- J. Bardeen, L. N. Cooper, and J. R. Schrieffer. Theory of superconductivity. *Physical Review*, 108:1175, 1957b.
- F. Barranco, M. Gallardo, and R. A. Broglia. Nuclear field theory of spin dealignment in strongly rotating nuclei and the vacuum polarization induced by pairing vibrations. *Phys. Lett. B*, 198:19, 1987.
- F. Barranco, E. Vigezzi, , and R. A. Broglia. Calculation of the absolute lifetimes of the variety of decay modes of  $^{234}\text{U}$ . *Phys. Rev. C*, 39:210, 1989.
- F. Barranco, R. A. Broglia, G. Gori, E. Vigezzi, P. F. Bortignon, and J. Terasaki. Surface vibrations and the pairing interaction in nuclei. *Phys. Rev. Lett.*, 83: 2147, 1999.
- F. Barranco, P. F. Bortignon, R. A. Broglia, G. Colò, P. Schuck, E. Vigezzi, and X. Viñas. Pairing matrix elements and pairing gaps with bare, effective, and induced interactions. *Phys. Rev. C*, 72:054314, 2005.
- Barranco, F., R. A. Broglia, and G. F. Bertsch. Exotic radioactivity as a superfluid tunneling phenomenon. *Phys. Rev. Lett.*, 60:507, 1988.
- Barranco, F., P. F. Bortignon, R. A. Broglia, G. Colò, and E. Vigezzi. The halo of the exotic nucleus  $^{11}\text{Li}$ : a single Cooper pair. *Europ. Phys. J. A*, 11:385, 2001.
- J. L. Basdevant and J. Dalibard. *Quantum Mechanics*. Springer, Berlin, 2005.
- B. F. Bayman. Finite-range calculation of the two-neutron transfer reaction. *Nuclear Physics A*, 168:1, 1971.
- B. F. Bayman and J. Chen. One-step and two-step contributions to two-nucleon transfer reactions. *Phys. Rev. C*, 26:1509, 1982.

- B. F. Bayman and A. Kallio. Relative-angular-momentum-zero part of two-nucleon wave functions. *Phys. Rev.*, 156:1121, 1967.
- S. T. Belyaev. Effect of pairing correlations on nuclear properties. *Kgl. Danske Videnskab. Selskab, Mat.-fys. Medd.*, 31:No11, 1959.
- Belyaev, S. T. Pair correlations in nuclei: Copenhagen 1958. In R. A. Broglia and V. Zelevinski, editors, *50 Years of Nuclear BCS*, page 3. World Scientific, Singapore, 2013.
- Bennaceur, K., J. Dobaczewski, and M. Ploszajczak. Pairing anti-halo effect. *Physics Letters B*, 496:154, 2000.
- G. Bertsch. In R. Broglia and J. R. Schrieffer, editors, *International School of Physics “Enrico Fermi” Collective motion in Fermi droplets*, page 41, Amsterdam, 1988. North Holland.
- G. Bertsch and R. Broglia. *Oscillations in Finite Quantum Systems*. Cambridge University Press, Cambridge, 2005.
- G. Bertsch, F. Barranco, and B. R.A. How nuclei change shape. In T. Kuo and I. Speth, editors, *Windsurfing the Fermi sea*, page 33. Elsevier, 1987.
- Bertsch, G. F. and R. A. Broglia. Giant resonances in hot nuclei. *Physics Today*, 39 (8):44, 1986.
- D. R. Bès and R. A. Broglia. Effect of the multipole pairing and particle-hole fields in the particle-vibration coupling of  $^{209}\text{Pb}$ . I. *Physical Review C*, 3:2349, 1971a.
- D. R. Bès and R. A. Broglia. Effect of the multipole pairing and particle-hole fields in the particle-vibration coupling of  $^{209}\text{Pb}$ . II. *Physical Review C*, 3:2371, 1971b.
- D. R. Bès and R. A. Broglia. Effect of the multipole pairing and particle-hole fields in the particle-vibration coupling of  $^{209}\text{Pb}$ . III. *Physical Review C*, 3:2389, 1971c.
- D. R. Bès and R. A. Broglia. Nuclear superfluidity and field theory of elementary excitations. In A. Bohr and R. A. Broglia, editors, *International School of Physics “Enrico Fermi” Course LXIX, Elementary Modes of Excitation in Nuclei*, page 55, Amsterdam, 1977. North Holland.
- Bès, D. R. and R. A. Broglia. Pairing vibrations. *Nucl. Phys.*, 80:289, 1966.
- Bès, D. R. and J. Kurchan. *The treatment of Collective Coordinates in Many-Body Systems*. World Scientific, Singapore, 1990.
- Bès, D. R., R. A. Broglia, J. Dudek, W. Nazarewicz, and Z. Szymański. Fluctuation effects in the pairing field of rapidly rotating nuclei. *Annals of Physics*, 182:237, 1988.

- J. H. Bilgram. Dynamics at the solid-liquid transition: Experiments at the freezing point. *Physics Reports*, 153:1, 1987.
- Bjerregaard, J. H., O. Hansen, Nathan, and S. Hinds. States of  $^{208}\text{Pb}$  from double triton stripping. *Nucl. Phys.*, 89:337, 1966.
- A. Bohr. Elementary modes of excitation and their coupling. In *Comptes Rendus du Congrès International de Physique Nucléaire*, volume 1, page 487. Centre National de la Recherche Scientifique, 1964.
- A. Bohr and B. R. Mottelson. Submission letter to H. Lipkin Febr. 13th, 1963 for non publication in his jocular but quite influential journal of non-pUBLISHABLE results in nuclear physics concerning the remarkable (coexistence) properties of low-lying  $0^+$  excited states in  $^{16}\text{O}$ ,  $^{40}\text{Ca}$ ,  $^{42}\text{Ca}$ ,  $^{70}\text{Ge}$ , and  $^{24}\text{Mg}$ (5.465 MeV)  $l = 0$  strength. . February 1963.
- A. Bohr and B. R. Mottelson. *Nuclear Structure, Vol.I.* Benjamin, New York, 1969.
- Bohr, A. and B. R. Mottelson. *Nuclear Structure, Vol.II.* Benjamin, New York, 1975.
- P. F. Bortignon, R. A. Broglia, D. R. Bès, R. Liotta, and V. Paar. Of the role of the pairing modes in the  $(h_{9/2} \otimes 3^-)$  multiplet of  $^{209}\text{Bi}$ . *Phys. Lett. B*, 64:24, 1976.
- Bortignon, P. F., R. A. Broglia, D. R. Bès, and R. Liotta. Nuclear field theory. *Physics Reports*, 30:305, 1977.
- Bortignon, P. F., R. A. Broglia, and D. R. Bès. On the convergence of nuclear field theory perturbation expansion for strongly anharmonic systems. *Phys. Lett. B*, 76:153, 1978.
- Bortignon, P. F., A. Bracco, and R. A. Broglia. *Giant Resonances*. Harwood Academic Publishers, Amsterdam, 1998.
- D. M. Brink. *PhD Thesis*. Oxford University, 1955.
- Brink, D. and R. A. Broglia. *Nuclear Superfluidity*. Cambridge University Press, Cambridge, 2005.
- R. A. Broglia and A. Winther. *Heavy Ion Reactions*. Westview Press, Boulder, CO., 2004.
- R. A. Broglia, J. Terasaki, and N. Giovanardi. The Anderson–Goldstone–Nambu mode in finite and in infinite systems. *Physics Reports*, 335:1, 2000.
- Broglia, R. A. The surfaces of compact systems: from nuclei to stars. *Surface Science*, 500:759, 2002.
- Broglia, R. A., G. Pollarolo, and A. Winther. On the absorptive potential in heavy ion scattering. *Nuclear Physics A*, 361:307, 1981.

- Broglia, R. A. and Zelevinsky, V. . In R. A. Broglia and V. Zelevinsky, editors, *50 Years of Nuclear BCS*. World Scientific, Singapore, 2013.
- Broglia, R.A., C. Riedel, and B. Sørensen. Two-nucleon transfer and pairing phase transition. *Nuclear Physics A*, 107:1, 1968.
- Broglia, R.A., O. Hansen, and C. Riedel. Two-neutron transfer reactions and the pairing model. *Advances in Nuclear Physics*, 6:287, 1973. URL [www.mi.infn.it/~vigezzi/BHR/BrogliaHansenRiedel.pdf](http://www.mi.infn.it/~vigezzi/BHR/BrogliaHansenRiedel.pdf).
- Brown, B. A. and W. D. M. Rae. In *NuShell @ MSU*. MSU–NSCL report, 2007.
- C. Bachelet et al. New Binding Energy for the Two-Neutron Halo of  $^{11}\text{Li}$ . *Phys. Rev. Lett.*, 100:182501, 2008.
- Clark, R. M., A. O. Macchiavelli, L. Fortunato, and R. Krücken. Critical-point description of the transition from vibrational to rotational regimes in the pairing phase. *Phys. Rev. Lett.*, 96:032501, 2006.
- L. N. Cooper. Bound electron pairs in a degenerate fermi gas. *Phys. Rev.*, 104: 1189, 1956.
- J. de Boer. Quantum theory of condensed permanent gases in the law of corresponding states. *Physica*, 14:139, 1948.
- J. de Boer. Chapter i quantum effects and exchange effects on the thermodynamic properties of liquid helium. volume 2 of *Progress in Low Temperature Physics*, page 1. 1957.
- J. de Boer and R. J. Lundbeck. Quantum theory of condensed permanent gases III. The equation of state of liquids. *Physica*, 14:520, 1948.
- P. G. de Gennes. *Les objets fragiles*. Plon, Paris, 1994.
- Dickhoff, W. and D. Van Neck. *Many–Body Theory Exposed: Propagator description of quantum mechanics in many–body systems*. World Scientific, Singapore, 2005.
- F. Dönau, K. Hehl, C. Riedel, R. A. Broglia, and P. Federman. Two-nucleon transfer reaction on oxygen and the nuclear coexistence model. *Nucl. Phys. A*, 101: 495, 1967.
- Dönau, F., D. Almehed, and R. G. Nazmitdinov. Integral representation of the random–phase approximation correlation energy. *Phys. Rev. Lett.*, 83:280, 1999.
- Duguet, T. and G. Hagen. *Ab initio* approach to effective single-particle energies in doubly closed shell nuclei. *Phys. Rev. C*, 85:034330, 2012.
- J. Ebran, E. Khan, T. Niksic, and D. Vretenar. Density Functional Theory studies of cluster states in nuclei. 2014a.

- J.-P. Ebran, E. Khan, T. Nikšić, and D. Vretenar. How atomic nuclei cluster. *Nature*, 487:341, 2012.
- J.-P. Ebran, E. Khan, T. Nikšić, and D. Vretenar. Localization and clustering in the nuclear fermi liquid. *Phys. Rev. C*, 87:044307, 2013.
- J.-P. Ebran, E. Khan, T. Nikšić, and D. Vretenar. Cluster-liquid transition in finite, saturated fermionic systems. *Phys. Rev. C*, 89:031303, 2014b.
- Egido, J. L. Projection methods, variational diagonalization of the pairing hamiltonian and restoration of rotational and gauge invariance. In R. A. Broglia and V. Zelevinski, editors, *50 Years of Nuclear BCS*, page 553. World Scientific, Singapore, 2013.
- P. Federman and I. Talmi. Coexistence of shell model and deformed states in oxygen isotopes. *Physics Letters*, 19:490, 1965.
- P. Federman and I. Talmi. Nuclear energy levels of Calcium isotopes. *Physics Letters*, 22:469, 1966.
- Fernández-García, J.P., M. Alvarez, A. Moro, and M. Rodriguez-Gallardo. Simultaneous analysis of elastic scattering and transfer/breakup channels for the  $^6\text{He} + ^{208}\text{Pb}$  reaction at energies near the Coulomb barrier. *Phys.Lett.*, B693:310, 2010.
- Fernández-García, J.P., M. Rodríguez-Gallardo, M. Alvarez, and A. Moro. Long range effects on the optical model of  $^6\text{He}$  around the Coulomb barrier. *Nuclear Physics A*, 840:19, 2010.
- Flynn, E. R., G. J. Igo, and R. A. Broglia. Three–phonon monopole and quadrupole pairing vibrational states in  $^{206}\text{Pb}$ . *Phys. Lett. B*, 41:397, 1972.
- Frauendorf, S. Pairing at high spin. In R. A. Broglia and V. Zelevinski, editors, *50 Years of Nuclear BCS*, page 536. World Scientific, Singapore, 2013.
- Furnstahl, R. J. and A. Schwenk. How should one formulate, extract and interpret ‘non-observables’ for nuclei? *Journal of Physics G*, 37:064005, 2010.
- Glendenning, N. K. Nuclear Spectroscopy with Two–Nucleon Transfer Reactions. *Phys. Rev.*, 137:B102, 1965.
- Guazzoni, P., M. Jaskola, L. Zetta, A. Covello, A. Gargano, Y. Eisermann, G. Graw, R. Hertenberger, A. Metz, F. Nuoffer, and G. Staudt. Level structure of  $^{120}\text{Sn}$ : High resolution ( $p, t$ ) reaction and shell model description. *Phys. Rev. C*, 60: 054603, 1999.
- Guazzoni, P., L. Zetta, A. Covello, A. Gargano, G. Graw, R. Hertenberger, H.-F. Wirth, and M. Jaskola. High-resolution study of the  $^{116}\text{Sn}$  ( $p, t$ ) reaction and shell model structure of  $^{114}\text{Sn}$ . *Phys. Rev. C*, 69:024619, 2004.

- Guazzoni, P., L. Zetta, A. Covello, A. Gargano, B. F. Bayman, G. Graw, R. Hertenberger, H.-F. Wirth, and M. Jaskola. Spectroscopy of  $^{110}\text{Sn}$  via the high-resolution  $^{112}\text{Sn}(p, t) ^{110}\text{Sn}$  reaction. *Phys. Rev. C*, 74:054605, 2006.
- Guazzoni, P., L. Zetta, A. Covello, A. Gargano, B. F. Bayman, T. Faestermann, G. Graw, R. Hertenberger, H.-F. Wirth, and M. Jaskola.  $^{118}\text{Sn}$  levels studied by the  $^{120}\text{Sn}(p, t)$  reaction: High-resolution measurements, shell model, and distorted-wave Born approximation calculations. *Phys. Rev. C*, 78:064608, 2008.
- Guazzoni, P., L. Zetta, A. Covello, A. Gargano, B. F. Bayman, T. Faestermann, G. Graw, R. Hertenberger, H.-F. Wirth, and M. Jaskola. High-resolution measurement of the  $^{118,124}\text{Sn}(p,t) ^{116,122}$  reactions: Shell-model and microscopic distorted-wave Born approximation calculations. *Phys. Rev. C*, 83:044614, 2011.
- Guazzoni, P., L. Zetta, A. Covello, A. Gargano, B. F. Bayman, G. Graw, R. Hertenberger, H. F. Wirth, T. Faestermann, and M. Jaskola. High resolution spectroscopy of  $^{112}\text{Sn}$  through the  $^{114}\text{Sn}(p, t) ^{112}\text{Sn}$  reaction. *Phys. Rev. C*, 85:054609, 2012.
- I. Hamamoto and B. R. Mottelson. Pair correlation in neutron drip line nuclei. *Phys. Rev. C*, 68:034312, 2003.
- Hamamoto, I. and B. R. Mottelson. Weakly bound  $s_{1/2}$  neutrons in the many-body pair correlation of neutron drip line nuclei. *Phys. Rev. C*, 69:064302, 2004.
- O. Hansen. Experimental establishment of the nuclear pairing phases. In R. A. Broglia and V. Zelevinsky, editors, *50 Years of Nuclear BCS*, page 449. World Scientific, Singapore, 2013.
- Heenen, P. H., V. Hellemans, and R. V. F. Janssens. Pairing correlations at superdeformation. In R. A. Broglia and V. Zelevinski, editors, *50 Years of Nuclear BCS*, page 579. World Scientific, Singapore, 2013.
- H. Hergert and R. Roth. Pairing in the framework of the unitary correlation operator method (UCOM): Hartree-Fock-Bogoliubov calculations. *Phys. Rev. C*, 80: 024312, 2009.
- J. Högaasen-Feldman. A study of some approximations of the pairing force. *Nuclear Physics*, 28:258, 1961.
- K. Ieki, D. Sackett, A. Galonsky, C. A. Bertulani, J. J. Kruse, W. G. Lynch, D. J. Morrissey, N. A. Orr, H. Schulz, B. M. Sherrill, A. Sustich, J. A. Winger, F. Deák, A. Horváth, A. Kiss, Z. Seres, J. J. Kolata, R. E. Warner, and D. L. Humphrey. Coulomb dissociation of  $^{11}\text{Li}$ . *Phys. Rev. Lett.*, 70:730, 1993.

- Jenning, B. Non observability of spectroscopic factors. *arXiv: 1102.3721v1 [nucl-th]*, 2011.
- B. D. Josephson. Possible new effects in superconductive tunnelling. *Phys. Lett.*, 1:251, 1962.
- Kobayashi, T., S. Shimoura, I. Tanihata, K. Katori, K. Matsuta, T. Minamisono, K. Sugimoto, W. Mller, D. L. Olson, T. J. M. Symons, and H. Wieman. Electromagnetic dissociation and soft giant dipole resonance of the neutron-dripline nucleus  $^{11}\text{Li}$ . *Physics Letters B*, 232:51, 1989.
- Kramer, G. J., H. P. Blok, and L. Lapikás. A consistence analisys of  $(e, e' p)$  and  $(d, ^3\text{He})$  experiments. *Nucl. Phys. A*, 679:267, 2001.
- W. A. Lanford and J. B. McGrory. Two-neutron pickup strengths on the even lead isotopes: the transition from single-particle to “collective”. *Physics Letters B*, 45:238, 1973.
- T. Lesinski, K. Hebeler, T. Duguet, and A. Schwenk. Chiral three-nucleon forces and pairing in nuclei. *Journal of Physics G: Nuclear and Particle Physics*, 39: 015108, 2012.
- F. A. Lindemann. The calculation of molecular vibration frequencies. *Physik. Z.*, 11:609, 1910.
- U. Lombardo, H. J. Schulze, and W. Zuo. Induced Pairing Interaction in Neutron Star Matter. In R. A. Broglia and V. Zelevinsky, editors, *50 Years of Nuclear BCS*, page 338. World Scientific, Singapore, 2013.
- Löwen, H. Melting, freezing and colloidal suspensions. *Phys. Rep.*, 237:249, 1994.
- J. E. Lynn. *Theory of neutron resonance reactions*. Oxford University Press, Oxford, 1968.
- M. Smith et al. First penning-trap mass measurement of the exotic halo nucleus  $^{11}\text{Li}$ . *Phys. Rev. Lett.*, 101:202501, 2008.
- Machleidt, R., F. Sammarruca, and Y. Song. Nonlocal nature of the nuclear force and its impact on nuclear structure. *Phys. Rev. C*, 53:R1483, 1996.
- Mahaux, C., P. F. Bortignon, R. A. Broglia, and C. H. Dasso. Dynamics of the shell model. *Physics Reports*, 120:1–274, 1985.
- Meissner, U. G. Anthropic considerations in nuclear physics. *arXiv:1409.2959v1[hep-th]*, 2014.
- D. Montanari, L. Corradi, S. Szilner, G. Pollarolo, E. Fioretto, G. Montagnoli, F. Scarlassara, A. M. Stefanini, S. Courtin, A. Goasduff, F. Haas, D. Jelavić Malenica, C. Michelagnoli, T. Mijatović, N. Soić, C. A. Ur, and M. Varga Pajtler.

- Neutron Pair Transfer in  $^{60}\text{Ni} + ^{116}\text{Sn}$  Far below the Coulomb Barrier. *Phys. Rev. Lett.*, 113:052501, 2014.
- B. Mottelson. Elementary features of nuclear structure. In Niefnecker, Blaizot, Bertsch, Weise, and David, editors, *Trends in Nuclear Physics, 100 years later, Les Houches, Session LXVI*, page 25, Amsterdam, 1998. Elsevier.
- S. G. Nilsson. Binding states of individual nucleons in strongly deformed nuclei. *Mat. Fys. Medd. Dan. Vid. Selsk.*, 29, 1955.
- L. Nosanow. On the possible superfluidity of  $^6\text{He}$ ?Its phase diagram and those of  $^6\text{He}-^4\text{He}$  and  $^6\text{He}-^3\text{He}$  mixtures. *Journal of Low Temperature Physics*, 23:605, 1976.
- S. S. Pankratov, M. V. Zverev, M. Baldo, U. Lombardo, and E. E. Saperstein. Semi-microscopic model of pairing in nuclei. *Phys. Rev. C*, 84:014321, 2011.
- G. Pollarolo, R. Broglia, and A. Winther. Calculation of the imaginary part of the heavy ion potential. *Nuclear Physics A*, 406:369, 1983.
- G. Potel, A. Idini, F. Barranco, E. Vigezzi, and R. A. Broglia. Nuclear Field Theory predictions for  $^{11}\text{Li}$  and  $^{12}\text{Be}$ : shedding light on the origin of pairing in nuclei. *Phys. At. Nucl.*, 7:941, 2014.
- Potel, G., F. Barranco, F. Marini, A. Idini, E. Vigezzi, and R. A. Broglia. Calculation of the Transition from Pairing Vibrational to Pairing Rotational Regimes between Magic Nuclei  $^{100}\text{Sn}$  and  $^{132}\text{Sn}$  via Two-Nucleon Transfer Reactions. *Physical Review Letters*, 107:092501, 2011.
- Potel, G., A. Idini, F. Barranco, E. Vigezzi, and R. A. Broglia. Cooper pair transfer in nuclei. *Rep. Prog. Phys.*, 76:106301, 2013a.
- Potel, G., A. Idini, F. Barranco, E. Vigezzi, and R. A. Broglia. Quantitative study of coherent pairing modes with two-neutron transfer: Sn isotopes. *Phys. Rev. C*, 87:054321, 2013b.
- Rees, M. *Just six numbers*. Basic Books, New York, 2000.
- Ring, P. Berry phase and backbending. In R. A. Broglia and V. Zelevinski, editors, *50 Years of Nuclear BCS*, page 522. World Scientific, Singapore, 2013.
- Ring, P. and P. Schuck. *The Nuclear Many-Body Problem*. Springer, Berlin, 1980.
- Robledo, R. M. and G. F. Bertsch. Pairing in Finite Systems: Beyond the HFB Theory. In R. A. Broglia and V. Zelevinski, editors, *50 Years of Nuclear BCS*, page 89. World Scientific, Singapore, 2013.
- D. Rogovin and M. Scully. Superconductivity and macroscopic quantum phenomena. *Physics Reports*, 25:175, 1976.

- D. Sackett, K. Ieki, A. Galonsky, C. A. Bertulani, H. Esbensen, J. J. Kruse, W. G. Lynch, D. J. Morrissey, N. A. Orr, B. M. Sherrill, H. Schulz, A. Sustich, J. A. Winger, F. Deák, A. Horváth, A. Kiss, Z. Seres, J. J. Kolata, R. E. Warner, and D. L. Humphrey. Electromagnetic excitation of  $^{11}Li$ . *Phys. Rev. C*, 48:118, 1993.
- E. E. Saperstein and M. Baldo. Microscopic Origin of Pairing. In R. A. Broglia and V. Zelevinsky, editors, *50 Years of Nuclear BCS*, page 263. World Scientific, Singapore, 2013.
- Schiffer, J. P., C. R. Hoffman, B. P. Kay, J. A. Clark, C. M. Deibel, S. J. Freeman, A. M. Howard, A. J. Mitchell, P. D. Parker, D. K. Sharp, and J. S. Thomas. Test of sum rules in nucleon transfer reactions. *Phys. Rev. Lett.*, 108:022501, 2012.
- Schmid, A. A time dependent Ginzburg–Landau equation and its application to the problem of resistivity in the mixed state. *Phys. d. Kond. Materie*, 5:302, 1966.
- Schmid, A. Diamagnetic susceptibility at the transition to the superconducting state. *Phys. Rev.*, 180:527, 1969.
- Schmidt, H. The onset of superconductivity in the time dependent ginzburg-landau theory. *Zeits. Phys.*, 216:336, 1968.
- Schmidt, H. Pairing vibrations in nuclei and solids. In Morinaga H., editor, *Proceedings of the International School of Physics “Enrico Fermi” Course LIII*, page 144, NY, 1972. Academic Press.
- J. Schrieffer. *Superconductivity*. Benjamin, New York, 1964.
- Schrieffer, J. R. Macroscopic quantum phenomena from pairing in superconductors. *Physics Today*, 26 (7):23, 1973.
- Schrödinger, E. *What is life? The physical aspect of the living cell*. Cambridge University Press, 1944.
- Shimizu, Y. R. Pairing fluctuations and gauge symmetry restoration in rotating superfluid nuclei. In R. A. Broglia and V. Zelevinsky, editors, *50 Years of Nuclear BCS*, page 567. World Scientific, Singapore, 2013.
- Shimizu, Y. R. and R. A. Broglia. A comparison of the RPA and number projection approach for calculations of pairing fluctuations in fast rotating nuclei. *Nucl. Phys. A*, 515:38, 1990.
- Shimizu, Y. R., J. D. Garrett, R. A. Broglia, M. Gallardo, and E. Vigezzi. Pairing fluctuations in rapidly rotating nuclei. *Reviews of Modern Physics*, 61:131, 1989.
- Shimizu, Y. R., P. Donati, and R. A. Broglia. Response function technique for calculating the random–phase approximation correlation energy. *Phys. Rev. Lett.*, 85:2260, 2000.

- S. Shimoura, T. Nakamura, M. Ishihara, N. Inabe, T. Kobayashi, T. Kubo, R. Siemssen, I. Tanihata, and Y. Watanabe. Coulomb dissociation reaction and correlations of two halo neutrons in  $^{11}\text{Li}$ . *Physics Letters B*, 348:29, 1995.
- F. H. Stillinger. A topographic view of supercooled liquids and glass formation. *Science*, 237:1935, 1995.
- F. H. Stillinger and D. K. Stillinger. Computational study of transition dynamics in 55-atom clusters. *J. Chem. Phys.*, 93:6013, 1990.
- T. Nakamura et al. Observation of Strong Low-Lying E1 Strength in the Two-Neutron Halo Nucleus  $^{11}\text{Li}$ . *Phys. Rev. Lett.*, 96:252502, 2006.
- Tarpanov, D., J. Dobaczewski, J. Toivanen, and B. G. Carlsson. Spectroscopic properties of nuclear Skyrme energy density functionals. *arXiv:1405.4823v1 [nucl-th]*, 2014.
- Thompson, I.J. Reaction mechanism of pair transfer. In R. A. Broglia and V. Zelevinsky, editors, *50 Years of Nuclear BCS*, page 455. World Scientific, Singapore, 2013.
- N. L. Vaquero, J. L. Egido, and T. R. Rodríguez. Large amplitude pairing fluctuations in atomic nuclei. *arXiv:1311.7573[nucl-th]*, 2013.
- W. von Oertzen and A. Vitturi. Pairing correlations of nucleons and multi-nucleon transfer between heavy nuclei. *Reports on Progress in Physics*, 64:1247, 2001.
- von Oertzen, W. Enhanced two-nucleon transfer due to pairing correlations. In R. A. Broglia and V. Zelevinsky, editors, *50 Years of Nuclear BCS*, page 405. World Scientific, Singapore, 2013.
- Wimmer, K., T. Kröll, R. Krücken, V. Bildstein, R. Gernhäuser, B. Bastin, N. Bree, J. Diriken, P. Van Duppen, M. Huyse, N. Patronis, P. Vermaelen, D. Voulot, J. Van de Walle, F. Wenander, L. M. Fraile, R. Chapman, B. Hadinia, R. Orlandi, J. F. Smith, R. Lutter, P. G. Thirolf, M. Labiche, A. Blazhev, M. Kalkühler, P. Reiter, M. Seidlitz, N. Warr, A. O. Macchiavelli, H. B. Jeppesen, E. Fiori, G. Georgiev, G. Schrieder, S. Das Gupta, G. Lo Bianco, S. Nardelli, J. Butterworth, J. Johansen, and K. Riisager. Discovery of the Shape Coexisting  $0^+$  State in  $^{32}\text{Mg}$  by a Two Neutron Transfer Reaction. *Phys. Rev. Lett.*, 105:252501, 2010.
- Wölfe, P. Sound propagation and kinetic coefficients in superfluid  $^3\text{He}$ . *Progr. Low Temp. Phys.*, 7:191, 1978.
- S. Yoshida. Note on the two-nucleon stripping reaction. *Nuclear Physics*, 33:685, 1962.

Y. Zhou, D. Vitkup, and M. Karplus. Native proteins are surface-molten solids: applications of the Lindemann Criterion for the solid versus liquid state. *J. Mol. Biol.*, 285:1371, 1999.

Zinser, M., F. Humbert, T. Nilsson, W. Schwab, H. Simon, T. Aumann, M. J. G. Borge, L. V. Chulkov, J. Cub, T. W. Elze, H. Emling, H. Geissel, D. Guillemaud-Mueller, P. G. Hansen, R. Holzmann, H. Irnich, B. Jonson, J. V. Kratz, R. Kulessa, Y. Leifels, H. Lenske, A. Magel, A. C. Mueller, G. Mnzenberg, F. Nickel, G. Nyman, A. Richter, K. Riisager, C. Scheidenberger, G. Schrieder, K. Stelzer, J. Stroth, A. Surowiec, O. Tengblad, E. Wajda, and E. Zude. Invariant-mass spectroscopy of  $^{10}\text{Li}$  and  $^{11}\text{Li}$ . *Nuclear Physics A*, 619:151, 1997.



# Chapter 3

## Pair transfer in a nutshell

### 3.1 Simultaneous versus successive Cooper pair transfer in nuclei

Cooper pair transfer is commonly thought to be tantamount to simultaneous transfer. In this process a nucleon goes over through the  $NN$ -interaction  $v$ , the second one does it making use of the correlations with its partner (cf. Figs. 3.1.1 and 5.C.1 (I)). Consequently, in the independent particle limit, simultaneous transfer should not be possible (see Sect. 5.C.1). Nonetheless, it remains operative. This is because, in this limit, the particle transferred through  $v$  does it together with a second one which profits from the non-orthogonality of the wavefunctions describing the single-particle motion in target and projectile (Figs. 3.1.2 and 5.C.1 (II)). This is the reason why this (non-orthogonality) transfer amplitude has to be treated on equal footing with the previous one representing, within the overcomplete basis employed, a natural contribution to simultaneous transfer (cf. also the discussion carried out in Ch.2 in connection with the overlap  $\Omega_n$  Eq. (2.1.3)). In other words,  $T^{(1)}$  gives the wrong cross section, even at the level of simultaneous transfer, as it violates two-nucleon transfer sum rules<sup>1</sup>. In fact  $(T^{(1)} - T_{NO}^{(1)})$  is the correct, sum rule conserving two-nucleon transfer amplitude to lowest order (first) in  $v$  (Fig. 3.1.2). The resulting cancellation is quite conspicuous in actual nuclei, in keeping with the fact that Cooper pairs are weakly correlated systems (see e.g. Figs. 3.4.2 (b) and 3.4.3, see also Fig. 3.4.4). This is the reason why the successive transfer process in which  $v$  acts twice (implying the mean field  $U$  in the post-post representation<sup>2</sup>), is the dominant mechanism in pair transfer reactions (within this context see Sect. 3.3). While this mechanism seems antithetical to the transfer of correlated fermions pairs (bosons), it probes, in the nuclear case, the same pairing correlations as simultaneous transfer does (Sect. 3.4). This is because nuclear Cooper pairs (quasi-bosons) are quite extended objects, the two nucleons being

---

<sup>1</sup>Broglia, R. A. et al. (1972), Bayman, B. F. and Clement (1972); cf. also Chapter 1

<sup>2</sup>Potel, G. et al. (2013a), Eq. (A7).

(virtually) correlated over distances much larger than typical nuclear dimensions<sup>3</sup> (cf. Fig. 3.1.3; cf. also Sect. 2.6.1). In a two–nucleon transfer process this virtual property becomes real, in the sense that the present of (normal) density over regions larger than that of the dimensions of each of the interacting nuclei allows for incipient  $\xi$  nuclear Cooper pair manifestation, the difference between the character of simultaneity and of succession becoming strongly blurred.

Within this context, let us refer to the Josephson effect, associated with the Cooper pair tunneling across a thin barrier separating two metallic superconductors. Because the probability of one–electron–tunneling is of the order of  $10^{-10}$ , (conventional) simultaneous tunneling associated with a probability of  $(10^{-10})^2$  would hardly be observed (cf. Sect 3.3). Nonetheless, Josephson currents are standard measures in low temperature laboratories<sup>4</sup>.

The same arguments related to the large value of the correlation length is operative in explaining the fact that Coulomb repulsion is rather weak between partners of Cooper pairs which are, in average, at a distance  $\xi (\approx 10^4 \text{ \AA})$  much larger than the Wigner–Seitz radius  $r_s$  typical of metallic elements ( $\approx 1 – 2 \text{ \AA}$ ). Consequently, it can be overwhelmed by the long range electron phonon pairing. Similarly, in widely extended light halo nuclei, the short range bare pairing interaction plays little role, becoming subcritical (cf. Sect. 2.6). The fact that such systems are nonetheless bound, although weakly, testifies to the dominant role the exchange of collective vibrations between halo nucleons have in binding the associated halo Cooper pair (e.g.  $^{11}\text{Li(gs)}$ , and, arguably, also<sup>5</sup> of  $^{12}\text{Be}$  ( $0^{++}$ ; 2.251 MeV) to the core ( $^9\text{Li(gs)}$  and  $^{10}\text{Be}$  respectively) (cf. Section 6.1.2 and Fig. 6.1.4).

The above arguments are at the basis of the fact that second order DWBA theory which add both successive and non–orthogonality contributions to the simultaneous transfer amplitudes, provides a quantitative account of the experimental findings (see e.g. Figs. 2.2.1, 3.4.2 (a), 3.4.3 (a) and Chapter 6).

## 3.2 Two–nucleon transfer probabilities, enhancement factor

As discussed in Chapter 1 the enhancement factor in a two–nucleon transfer reaction can be defined in terms of two–particle units<sup>6</sup>, similar to what is done in the case of electromagnetic decay (Weisskopf units)<sup>7</sup>. Let us, for simplicity, write such

---

<sup>3</sup>Within this context one can put the following question. Is anybody worried that a photon can, in a two slit experiment, be broken in two? No. Why should then one worry that successive transfer can break a Cooper pair?

<sup>4</sup>cf. e.g. Rogalla and Kes (2012) and references therein.

<sup>5</sup>See e.g. Johansen et al. (2013).

<sup>6</sup>cf. e.g. Broglia, R. A. et al. (1972); Broglia, R.A. et al. (1973) and references therein.

<sup>7</sup>See e.g. Bohr and Mottelson (1969).

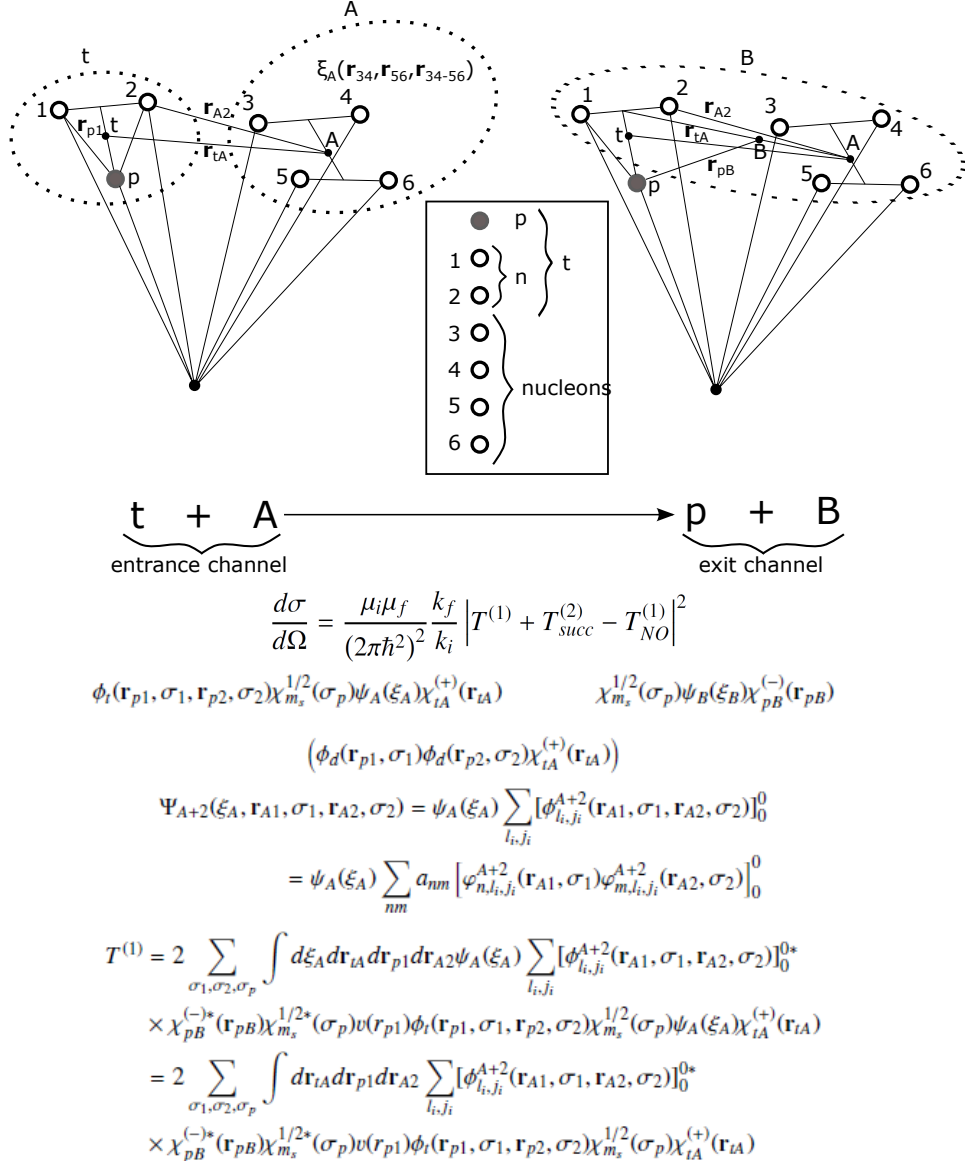


Figure 3.1.1: Contribution of simultaneous transfer, in first order DWBA, to the reaction  $A(t, p)B(\equiv A+2)$ . The nucleus  $A$  is schematically assumed to contain four nucleons, the triton being composed of two neutrons and one proton. The set of coordinates used to describe the entrance and exit channels are shown in the upper part, while in the lower part the simultaneous two-nucleon transfer amplitude is written in detail (cf. Potel, G. et al. (2013b)). Of notice that the expression of  $T^{(1)}$  violates, in the independent particle basis used, the two-nucleon transfer sum rule by exactly  $T_{NO}^{(1)}$ , amplitude operative also in lowest order of  $v$  (Fig. 3.1.2; see also text). It is of notice that of all the relative motion coordinates, only those describing the relative motion of  $(t, A)$  and of  $(p, B)$  have asymptotic values.

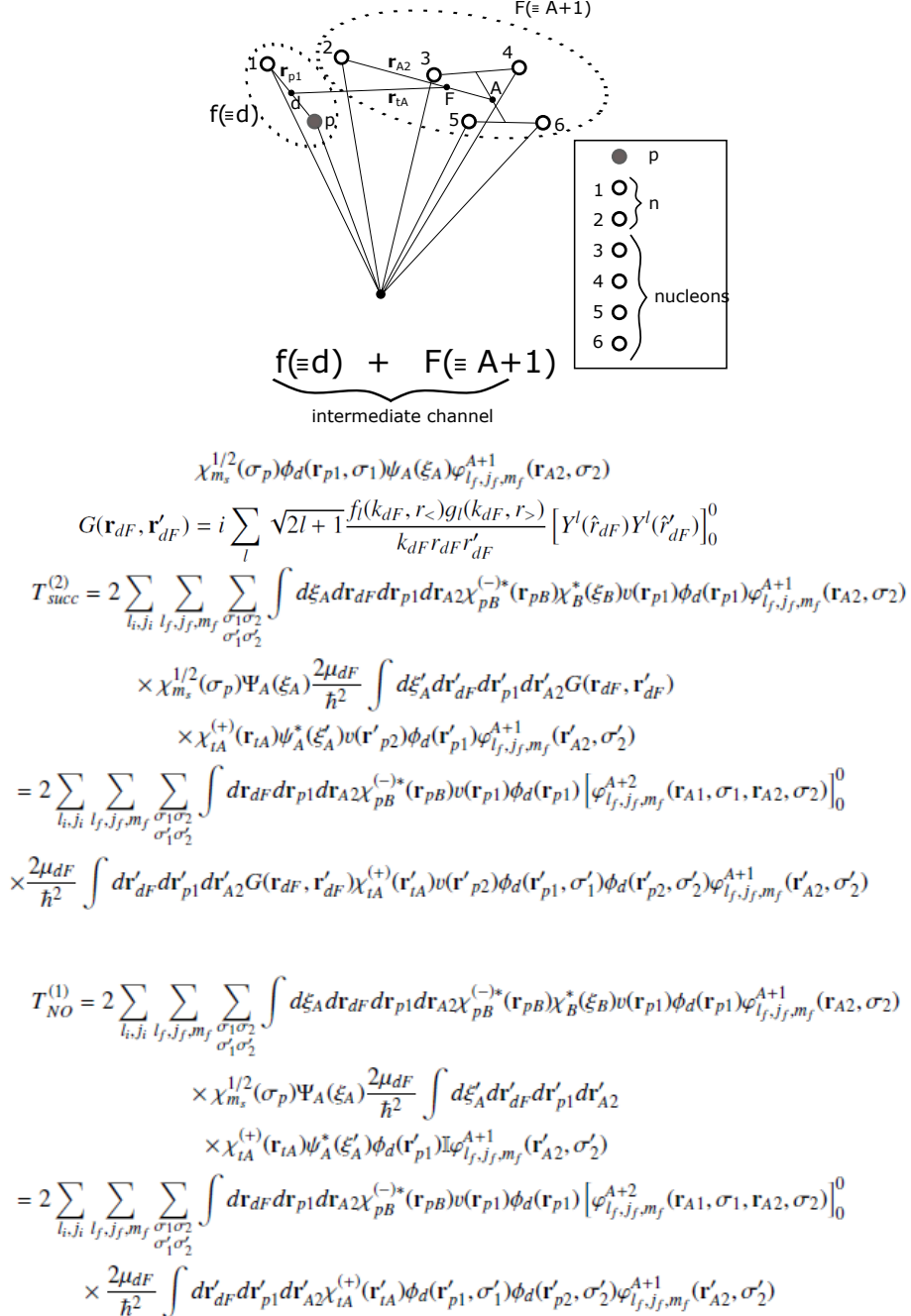


Figure 3.1.2: Successive and non-orthogonality contributions to the amplitude describing two-nucleon transfer in second order DWBA, entering in the expression of the absolute differential cross section  $d\sigma/d\Omega = \frac{\mu_i \mu_f}{(4\pi\hbar^2)^2} \frac{k_f}{k_i} |T^{(1)} + T_{succ}^{(2)} - T_{NO}^{(1)}|^2$ . Concerning  $T^{(1)}$  we refer to Fig. 3.1.1. In the upper part of the figure the coordinates used to describe the intermediate channel  $d + F(\equiv A + 1)$  are given, while in the lower part the corresponding expressions are displayed (Potel, G. et al., 2013b) in the case of a  $(t, p)$  process. Schematically, the three contributions  $T^{(1)}$ ,  $T_{succ}^{(2)}$  and  $T_{NO}^{(1)}$  to the transfer amplitude can be written as  $\langle pB|v|tA \rangle$ ,  $\sum \langle pB|v|dF \rangle \langle dF|v|tA \rangle$  and  $\sum \langle pB|v|dF \rangle \langle dF|\mathbf{1}|tA \rangle$  respectively, where  $v$  is the proton-neutron interaction and  $\mathbf{1}$  the unit operator. Within this context, while  $T_{NO}^{(1)}$  receives contributions from the intermediate (virtual) closed  $(d + F)$  channel as  $T_{succ}^{(2)}$  does, it is first order in  $v$  as  $T^{(1)}$ .

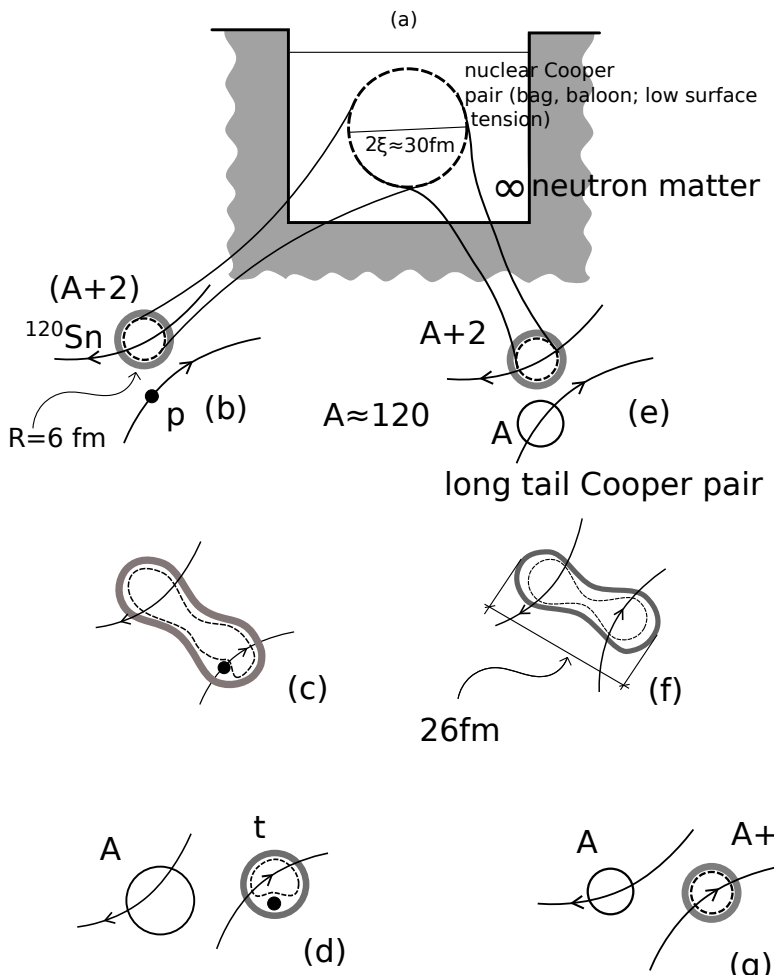


Figure 3.1.3: The correlation length associated with a nuclear Cooper pair is of the order of  $\xi \approx \hbar v_F / \Delta \approx 30 \text{ fm}$  (see App. 3.4). (a) in neutron matter at typical densities of the order of 0.5–0.8 saturation density, the  $NN^{-1}S_0$  short range force, eventually renormalized by medium polarization effects, makes pairs of nucleons moving in time reversal states to correlate over distances of the order of 5–6 times typical nuclear radii. How can one get evidence for such an extended object? Certainly not when the Cooper bag (balloon) is introduced in (b) the mean field of a superfluid nucleus which, acting as an external field, constrains the Cooper pair to be within the nuclear radius with some spill out (long tail of Cooper pair, grey, shaded area extending outside the nuclear surface defined by  $R_0 = 1.2A^{1/3} \text{ fm}$ ). But yes in (c), (d) that is in the case of two-nucleon transfer process (e.g.  $(p, t)$  reaction) in which the absolute cross section can change by orders of magnitude in going from pure two-particle (uncorrelated configurations) to long tail Cooper pair spill outs. This effect is expected to become stronger by allowing , pair transfer between similar superfluid nuclei, in which case one profits of the same type of correlations (superfluidity) as resulting from very similar pair mean fields (e), (f), (g) (cf. e.g. von Oertzen, W. (2013) and references therein; see also Eqs. (2.1.2) and (2.1.3). For the case under discussion  $\Omega_n = 1$ ). Within this context, it is apparent that pairs of nucleons will feel equally well pairing correlations whether they are transferred simultaneously or one after the other (cf. (c) and (f)).

a relation as

$$\left(\frac{d\sigma}{d\Omega}\right)_{2n} = \left|\langle f|P^\dagger|i\rangle\right|^2 \left(\frac{d\sigma}{d\Omega}\right)_{2n}^{(0)}, \quad (3.2.1)$$

where  $\left(\frac{d\sigma}{d\Omega}\right)_{2n}^{(0)}$  is the absolute differential cross section associated with a typical pure single-pair configuration  $|j^2(0)\rangle$  (or the average value over pairs based on the valence orbitals). In the case of a superfluid nucleus like e.g.  $^{120}\text{Sn}$  and for  $i = \text{gs(A)}$  and  $f = \text{gs(A+2)}$  as well as  $f = 2qp(\text{A+2})$  one can write

$$\left|\langle f|P^\dagger|i\rangle\right|^2 = \begin{cases} \alpha_0'^2 = (\sum_{\nu>0} U_\nu' V_\nu')^2 = \left(\frac{\Delta}{G}\right)^2 = \left(\frac{12A}{\sqrt{A}25}\right)^2 \approx \frac{A}{4} \approx 30 \ (f = \text{gs}), \\ U_\nu^4 \approx 1 \ (f = 2qp). \end{cases} \quad (3.2.2)$$

Thus, the expected enhancement factor<sup>8</sup> is given by the ratio,

$$R = \frac{\left(\frac{d\sigma}{d\Omega}(\text{gs} \rightarrow \text{gs})\right)_{2n}}{\left(\frac{d\sigma}{d\Omega}(\text{gs} \rightarrow 2qp)\right)_{2n}} \approx 30. \quad (3.2.3)$$

In other words, in superfluid nuclei one expects the  $0^+$  pairing vibrational states to carry a (summed) cross section of the order of 3% that of the  $\text{gs} \rightarrow \text{gs}$  transition (cf. Fig. 2.1.4). Now, in defining the quantity  $R$  used was made of (3.2.1). Because both numerator and denominator are linear in  $\left(\frac{d\sigma}{d\Omega}\right)_{2n}^{(0)}$ , one could as well posit that one has used (3.2.2) in defining  $R$ .

The situation is quite different when one intends to define the probability associated with a transfer process. One could be tempted again to use (3.2.1) for the case of  $2n$ -transfer and eventually

$$\left(\frac{d\sigma}{d\Omega}\right)_{1n} = S \left(\frac{d\sigma}{d\Omega}\right)_{1n}^{(0)}, \quad (3.2.4)$$

in the case of  $1n$ -transfer,  $S$  being known in the literature as the spectroscopic factor, and used here for illustration purposes only. However, in trying to define an enhancement factor in terms of  $P_{2n}/P_{1n}^2$ , the approximate relations (3.2.1) and (3.2.4) will now condition the physics one is trying to extract from the experimental (empirical) information. In fact, in this case the actual values of  $\left(\frac{d\sigma}{d\Omega}\right)_{1n}^{(0)}$  and of  $\left(\frac{d\sigma}{d\Omega}\right)_{2n}^{(0)}$  will play an important role, and this could hardly be correct. In fact, the proper definition of the transfer probabilities is to be made in terms of the total reaction cross section.

For this purpose let us remind some useful relations. In particular that of the differential reaction cross section

$$\frac{d\sigma}{d\Omega} = |f(\theta)|^2, \quad (3.2.5)$$

---

<sup>8</sup>See e.g. Brink, D. and Broglia (2005) p. 324

where

$$f(\theta) = \frac{1}{k} \sum_l (2l+1) e^{i\delta_l} \sin \delta_l P_l(\cos \theta), \quad (3.2.6)$$

$\delta_l$  being the partial wave  $l$  phase shift. Let us now use for simplicity the results associated with hard sphere scattering<sup>9</sup> in the low and high energy limit. Making use of the fact that in the case under discussion the phase shifts  $\delta_l$  are related to the regular and irregular spherical Bessel functions,

$$\tan \delta_l = \frac{j_l(kR)}{n_l(kR)}, \quad (3.2.7)$$

and that  $\sin^2 \delta_l = \tan^2 \delta_l / (1 + \tan^2 \delta_l)$ , one can write in the case in which  $kR \ll 1$ , i.e. in the low-energy, long wavelength, regime

$$\tan \delta_l \approx \frac{-(kR)^{2l+1}}{(2l+1)[(2l-1)!!]^2}, \quad (3.2.8)$$

implying that one can ignore all  $\delta_l$  with  $l \neq 0$ . Because  $\delta_0 = -kR$  (cf. (3.2.7)) regardless the value of  $k$ , one obtains,

$$\frac{d\sigma}{d\Omega} = \frac{\sin^2 \delta_0}{k^2} = R^2, \quad (3.2.9)$$

and thus

$$\sigma_{tot} = \int \frac{d\sigma}{d\Omega} d\Omega = 4\pi R^2 \quad (kR \ll 1), \quad (3.2.10)$$

a cross section which is four times the geometric cross section  $\pi R^2$ , namely the area of the disc of radius  $R$  that blocks the propagation of the incoming (plane) wave, and has the same value as that of a hard sphere. Because  $kR \ll 1$  implies long wavelength scattering, it is not surprising that quantal effects are important, so as to overwhelm the classical picture. Let us now consider the high energy limit  $kR \gg 1$ . The total cross section is in this case, given by

$$\begin{aligned} \sigma_{tot} &= \int |f_l(\theta)|^2 d\Omega = \frac{1}{k^2} \int_0^{2\pi} d\phi \int_{-1}^1 d(\cos \theta) \sum_{l=1}^{kR} \sum_{l'=1}^{kR} (2l+1)(2l'+1) \\ &\times e^{i\delta_l} \sin \delta_l e^{-i\delta_{l'}} \sin \delta_{l'} P_l P_{l'} = \frac{4\pi}{k^2} \sum_{l=1}^{kR} (2l+1) \sin^2 \delta_l = \frac{4\pi}{k^2} \sum_{l=1}^{kR} (2l+1) p_l. \end{aligned} \quad (3.2.11)$$

Making use of the relation

$$\sin^2 \delta_l = \frac{\tan^2 \delta_l}{1 + \tan^2 \delta_l} = \frac{[j_l(kR)]^2}{[j_l(kR)]^2 + [n_l(kR)]^2} \approx \sin^2 \left( kR - \frac{\pi l}{2} \right), \quad (3.2.12)$$

---

<sup>9</sup>cf. e.g. Sakurai (1994)

and the fact that so many  $l$ -values contribute to (3.2.11), one can replace  $\sin^2 \delta_l$  by its average value 1/2. Because the number of terms of the sum is roughly  $kR$ , the same being true for the average value of  $(2l + 1)$ . Thus one can write

$$\sigma_{tot} = \frac{4\pi}{k^2}(kR)^2 \frac{1}{2} = 2\pi R^2, \quad (kR \gg 1) \quad (3.2.13)$$

which, in this short wavelength limit, is not the geometric cross section either. In fact, (3.2.13) can be split into two contributions each of value  $\pi R^2$ . One due to reflection in which it can be shown that there is no interference amongst contributions from different  $l$ -values. A second one (coherent contribution in the forward direction) called shadow because for hard-sphere scattering at high energies, waves with impact parameter less than  $R$  must be deflected. Consequently, behind the scatterer there must be zero probability for finding the scattered particle and a shadow must be generated.

In terms of wave mechanics, this shadow is due to the destructive interference between the original wave (which would be there even if the scatterer was absent), and the newly scattered wave. Thus, one needs scattering in order to create a shadow. This contribution is intimately related to the optical theorem<sup>10</sup>

$$\sigma_{tot} = \frac{4\pi}{k} \Im[f(\theta = 0, k)] = \frac{4\pi}{k} [f_{shad}(\theta = 0, k)] = \frac{4\pi}{k^2} \sum_l (2l + 1) \sin^2 \delta_l, \quad (3.2.14)$$

to which it provides its physical interpretation. In fact, there are two independent ways of measuring  $\sigma_{tot}$ , namely: i) by integrating the differential cross section  $d\sigma/d\Omega = |f(\theta)|^2$  moving around the detector, ii) measuring the attenuation of the incoming beam. Both procedures should give the same result. One then identifies  $(4\pi/k)f(\theta = 0, k)$  with the attenuation arising from the interference of the elastic wave with the incoming wave. Of notice that in (3.2.11) the factor  $(\pi/k^2)(2l + 1) = \pi\lambda(2l + 1)$  is the area of a ring with radius  $b = (l + 1/2)\lambda$  and width  $\lambda$  due to quantal uncertainties. Thus

$$\sigma_{tot} = 2\pi(R + \lambda/2)^2 \quad (kR \gg 1). \quad (3.2.15)$$

The quantity

$$\lambda = \frac{\lambda}{2\pi} = \frac{h}{2\pi p} = \frac{\hbar}{p} = \frac{1}{k} = \frac{\hbar}{\sqrt{2mE}}, \quad (3.2.16)$$

is the reduced de Broglie wavelength for a massive particle ( $E = p^2/2m$ ). For a proton of energy  $E_p \approx 20$  MeV, typical of beams used in  $^{120}\text{Sn}(p, t)^{118}\text{Sn}(\text{gs})$  and  $^{120}\text{Sn}(p, d)^{119}\text{Sn}(\text{j})$  reactions (cf. Figs. 4.2.1, 4.2.3 and 6.2.1)<sup>11</sup>  $\lambda \approx 1$  fm, to be

---

<sup>10</sup>Sakurai (1994) pp. 420–421

<sup>11</sup>Of notice that the reduced wavelength of a photon ( $p = E/c$ ) of the same energy ( $E = 20$  MeV) is  $\lambda (= \lambda/2\pi = \hbar/p = \hbar c/E) \approx 10$  fm (cf. Table 2.1 p. 22 Satchler (1980)).

compared with the value  $R \approx 6$  fm of the radius of  $^{120}\text{Sn}$ . Consequently, we are in a situation of type (3.2.15), that is,

$$\sigma_{tot} = 2\pi(6 + 0.5)^2 \text{ fm}^2 \approx 2.7 \text{ b.} \quad (3.2.17)$$

Because typical values of the absolute one-particle cross section associated with the  $(p, d)$  reaction mentioned above are few mb (cf. Fig. 4.2.3 right panel) one can use, for order of estimate purposes,

$$P_1 \approx \frac{5.35 \text{ mb}}{2.7 \text{ b}} \approx 10^{-3}, \quad (3.2.18)$$

as the typical probability for such processes. Consequently, one may argue that the probability for a pair of nucleons to simultaneously tunnel in e.g. the  $(p, t)$  process mentioned above is  $(P_1)^2 \approx 10^{-6}$ , as near impossible as no matter. Within this context we note that the integrated  $\text{gs} \rightarrow \text{gs}$  absolute cross section  $\sigma(^{120}\text{Sn}(p, t)^{118}\text{Sn(gs)}) \approx 2.5 \pm 0.2$  mb (cf. Figs. 2.2.1 and 6.2.1). This fact implies that the empirical two-nucleon transfer probability is of the order of  $P_2 \approx 10^{-3}$ . Consequently,  $P_2/(P_1)^2 \approx 10^3$ , a ratio which can hardly be explained in terms of a physical enhancement factor.

The above contradictions<sup>12</sup> are, to a large extent, connected with the fact that one is addressing the subject of pairing correlations in nuclei as probed by two-nucleon transfer reactions, treating separately the associated questions of structure and reactions, while they are but complementary aspects of the same physics. Let us elaborate on this point.

When one turns on, in an open shell atomic nucleus like e.g.  $^{50}_{50}\text{Sn}_{70}$ , a pairing interaction of strength larger than critical, the system moves into an independent pair regime<sup>13</sup> (cf. e.g. Sects. 2.4.1 and 2.4.2 as well as Fig. 2.4.3; see Fig. 3.2.1). This fact has essentially no consequence concerning the one-particle transfer mechanism, exception made regarding the size of the mismatch between the relative motion–incoming ( $p+^{120}\text{Sn(gs)}$ ) and –outgoing ( $d+^{119}\text{Sn(gs)}$ ) trajectories ( $Q$ -value and recoil effect), in keeping with the fact that one has to break a Cooper pair to populate a single quasiparticle state. From a structure point of view the depletion of the occupation probability measured in a  $(p, d)$  process is correlated with the corresponding increase in occupation observed in  $(d, p)$  ( $U^2, V^2$  factors). Aside from the quantitative values, this is also observed in dressed single-particle

---

<sup>12</sup>Within this context it is of notice that similar questions were raised by Bardeen (1962, 1961); Pippard (2012); Cohen et al. (1962); McDonald (2001) in connection with the prediction of Josephson (Josephson (1962)) that there should be a contribution to the current through an insulating barrier between two superconductors which would behave like direct tunneling of condensed pairs. This is in keeping with the fact that a single electron has a probability of  $\approx 10^{-10}$  of getting through, the “classical” estimate of simultaneous pair tunneling being  $\approx 10^{-20}$ , an impossible observation as stated above (cf. App. 3.8).

<sup>13</sup>Regime which is conditioned by the “external” mean field. In other words, regime which express itself provided there is nucleon density available (see Sect. 3.2). It is of notice that pairing in turn may help extend the range over which nucleon density is available, as in the case of the neutron halo nucleus  $^{11}\text{Li}$ .

states, the single-particle sum rule implying both the (A-1) and (A+1) system (see App. 4.I). Concerning the phase coherence of the pair correlated wavefunction it has no consequence for one-particle transfer process, in keeping with the fact that  $|e^{i\phi} \sqrt{P_1}|^2 = P_1$ .

The situation is very different concerning (Cooper) pair transfer. From a reaction point of view, and in keeping with the non-orthogonality existing between the wavefunctions in target and projectile, the associated contributions to the transfer process have to be eliminated. This is in keeping with the fact that simultaneous two-nucleon transfer can take place also in first order in the proton-neutron interaction  $v_{np}$ . When this is a consequence of the correlation between the partners of the Cooper pair (cf. Fig. 5.C.1 (I)) it constitutes a *bona fide* contribution. Not when it is a consequence of non-orthogonality (see Fig. 5.C.1 (II)). Continuing within the realm of reaction theory, second order processes in  $v_{np}$  are to be included (Fig. 5.C.2) and as a rule neglect higher orders in keeping with the small value of  $P_2$  ( $\approx 10^{-3}$ , cf. also Table 6.B.1). Let us now bring structure into the discussion. The fact that the wave function of the nucleons in the pair are phase-coherent ( $(U_\nu + V_\nu e^{-2i\phi} a_\nu^\dagger a_{\bar{\nu}}^\dagger) |0\rangle$ ) implies that one has to add the amplitudes before one takes modulus squared (cf. also Sect. 3.6 and Sect. 3.7), that is,

$$\begin{aligned} P_2 &= \lim_{\epsilon \rightarrow 0} \left| \frac{1}{\sqrt{2}} (e^{i\phi'} \sqrt{P_1} + e^{i\phi} \sqrt{P_1}) \right|^2 \\ &= P_1 \lim_{\epsilon \rightarrow 0} (1 + \cos \epsilon) = 2P_1 \quad (\epsilon = \phi - \phi'), \end{aligned} \quad (3.2.19)$$

again, an unexpected quantum mechanical result as e.g. (3.2.13). Because the range of  $v_{np}$  ( $a \approx 1$  fm) is much smaller than the correlation length ( $\xi \approx 20$ –30 fm), in the successive process (3.2.19), the Cooper pair tunnels between target and projectile equally formed and “unharmed” as in the simultaneous process. Think again that in the nuclear pairing correlated system only Cooper pairs exist (in which the partners nucleons are correlated over 20–30 fm from each other) and not single nucleons (normal system) at  $\approx 4$  fm (2 fm being the radius of the Wigner-Seitz nucleus cell) from each other (cf. Fig. 3.2.1). To the extent that the mean field acting as an “external” field allows particle density to be present, the properties of independent Cooper pair motion will explicit themselves. And thus is a physical condition which is assumed fulfilled each time one will make use of Fig. 3.2.1 (b). In other words, inside  $^{120}\text{Sn}$  all Cooper pairs will be found within a volume of radius  $R_0 \approx 6$  fm, in the same way in which a Cooper pair will be distributed over two similar volumes during the contact time in e.g. a Sn+Sn heavy ion reaction<sup>14</sup>

---

<sup>14</sup>The interest of the picture shown in Fig. 3.2.1 (b) can also be exemplified by referring to a single stable nucleus lying along the stability valley, with the fact that the moment of inertia of heavy deformed nuclei is considerably smaller than the rigid moment of inertia, but still larger than the irrotational one ( $5\mathcal{J}_{irrot} \lesssim \mathcal{J} \lesssim \mathcal{J}_r/2$ ). Even confined within the mean field of the nucleus, the small but finite number of pairs of correlated nucleons having the “intrinsic”, infinite-matter-like tendency displayed if Fig. 3.2.1 (b), will, to some extent, average out the different orientations of the rotating system and react to it in terms of an effective deformation smaller than the one related to the B(E2)

(see also Sect. 3.2). This explains the importance of long-range induced pairing interaction (exchange of phonons) in general, let alone in very extended light halo nuclei like  $^{11}\text{Li}$ .

Within this context we note that the (approximate) form of the (local) pair wavefunction can be written as (cf. Leggett (2006) p. 185; for the non local nuclear version cf. e.g. Broglia and Winther (1983))

$$F(r) \approx \Delta N(0) \frac{\sin k_F r}{k_F} \exp\left(\frac{\sqrt{2}r}{\xi}\right), \quad (3.2.20)$$

where  $N(0)$  is the density of levels at the Fermi energy for one spin orientation. For  $r \leq \xi$  the pair wavefunction is approximately proportional to that of two particles at the Fermi energy moving freely in a relative  $s$ -wave state. In a typical metallic superconductor  $\xi$  is of the order of  $10^4$  Å, much larger than the inter electron spacing ( $\approx 1$  Å). Note that relative to the Fermi energy, the correlation energy ( $E_{corr} = (-1/2)N(0)\Delta^2$ ) associated with Cooper pairing is very small,  $\approx 10^{-7} - 10^{-8}$ . Arguably, the most important consequence of this fact, is the exponentially large radius and thus very small value of the relative momentum associated with Cooper pairs. In other words, the typical scenario for a very small value of the localization kinetic energy and thus of the generalized quantality parameter (cf. App. 6.H), implying that the two partners, are rigidly anchored to each other (Cooper pair). This phenomenon is at the basis of the emergence of new elementary modes of excitation (pairing vibrations for single Cooper pairs, pairing rotations for few ones, supercurrents and Josephson currents for macroscopic amounts of them).

The situation sounds, in principle, very different from atomic nuclei, in keeping with the fact that nuclear Cooper pairs are, as a rule, subject to an overwhelming external (mean) fields ( $|E_{corr}| \approx 1$  MeV  $\ll |U(r \approx R_0)| \approx |V_0/2| \approx 25$  MeV). But even in this case, one can posit that the transition from independent particle to independent pair motion implies that Cooper pair partners recede from each other. Let us clarify this point for the case of a single pair, e.g.  $^{208}\text{Pb(gs)}$ . It is true that allowing the pair of neutrons to correlate in the valence orbitals leads to a pair wavefunction which is angle correlated ( $\Omega_{12} \approx 0$ ), as compared to the pure  $j^2(0)(j = g_{9/2})$  configuration<sup>15</sup>. On the other hand, the correlated pair addition mode (Tables 2.5.4 and 2.5.5) will display a sizeable spill out as compared to the pure two particle state, and thus a lower density and larger related average distance between Cooper pair partners. This is also the reason why close to  $\approx 40\%$  of the pairing matrix elements is contributed by the induced pairing interaction resulting from the exchange of long wavelength, low-lying, collective modes, the other  $\approx 60\%$  resulting from the bare nucleon-nucleon  $^1S_0$  pairing interaction (cf. Fig. 2.6.1). In carrying out the above arguments the values of  $(E_{corr}/\epsilon_F)^2 \approx \left(\frac{1\text{ MeV}}{37\text{ MeV}}\right)^2 \approx$

---

collective (rotational) values. However, constrained as they are they cannot fully profit of pairing superfluidity.

<sup>15</sup>Bertsch, G. F. et al. (1967), Ferreira, L. et al. (1984); Matsuo, M. (2013).

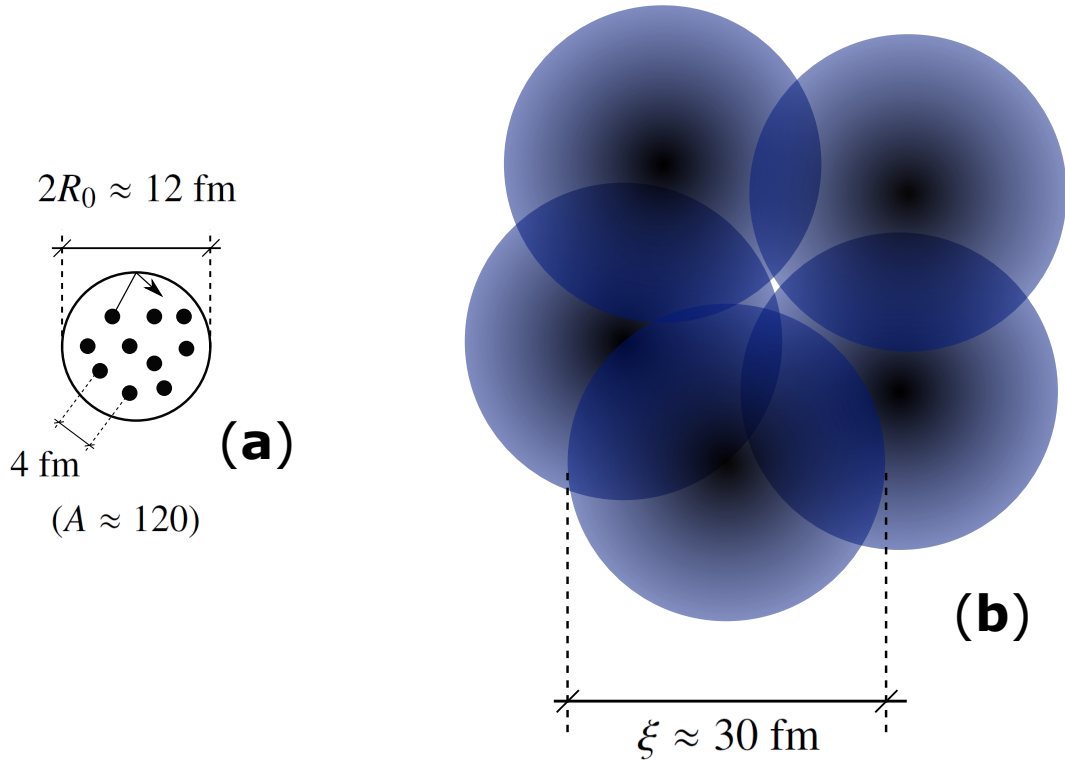


Figure 3.2.1: (a) Schematic representation of independent-particle motion and (b) independent-pair motion. In the first case nucleons (fermions) move independently of each other reflecting elastically from the wall of the mean field created by all the other nucleons, each of which is associated with a Wigner–Seitz cell of radius  $d = ((4\pi/3)R_0^3/A)^{1/3}$  implying a relative distance of  $2d$  (the actual numbers correspond to e.g.  $^{120}\text{Sn}$ ). Switching on the pairing interaction (bare plus induced) leads to Cooper pair formation in which the correlation length is  $\xi$ . Thus, pair of nucleons moving in time reversal states close to the Fermi energy will tend to recede from each other lowering their relative momentum ( $2d \rightarrow \xi$ ) thus boosting the stability of the system, provided that the external mean field allows it. Or better, if there is nucleon density available to do so, something controlled to a large extent by the single-particle potential. From this point on, and at least for the levels lying close to the Fermi surface, one cannot talk about particles but about Cooper pairs (unless one does not intervene the system with an external field, e.g.  $(p, d)$  and provides the energy, angular and linear momentum needed to break a pair). Of course that the system to the right under the influence of an external field (like e.g. the HF of  $^{120}\text{Sn}$ ) Cooper pairs will be constrained within its boundaries. But this will be true with two nuclei of  $^{120}\text{Sn}$  at a relative (CM) distance much larger than  $2R_0$  ( $\approx 12 \text{ fm}$ ). The pair field associated with a Cooper pair will extend from one to the other partner of the heavy ion reaction through the weakly overlapping interaction region, allowing two nucleons to correlate over  $\xi$  and, eventually, in a reaction like e.g.  $\text{Sn} + \text{Sn} \rightarrow \text{Sn(gs)} + \text{Sn(gs)}$  allow for the transfer of two nucleons correlated over tens of fm.

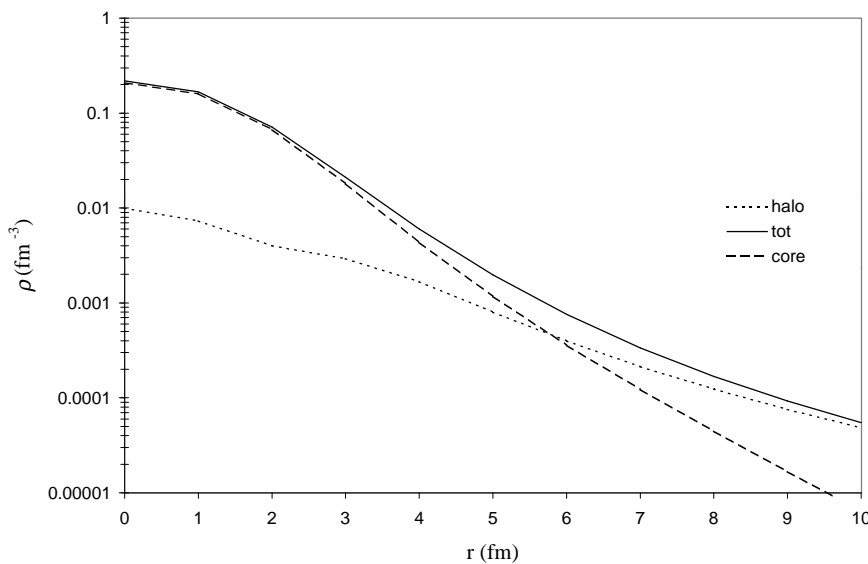


Figure 3.2.2: The nuclear density associated with  $^{11}\text{Li}$ , as resulting from the microscopic NFT calculations which are at the basis of the results displayed in Figs. 2.6.3 and 6.1.3 (Barranco, F. et al. (2001)). The contribution arising from the core ( $^9\text{Li}$ ) is displayed with a dashed curve, while that associated with the two halo neutrons (cf. Eqs. (6.1.1)–(6.1.3)) is shown in term of a dotted curve. The sum of these two contributions labeled tot (total) is drawn with a continuous curve.

$10^{-3}$  and  $\xi = \frac{\hbar v_F}{2E_{corr}} \approx 30 \text{ fm}$  ( $(\frac{v_F}{c}) \approx 0.3$ ), valid for nuclei along the stability valley, were used.

The situation described above becomes clearer, even if extreme, in the case of  $^{11}\text{Li}$ . In this case, the Fermi momentum is  $k_F \approx 0.8 \text{ fm}^{-1}$ , the radius  $R \approx 4.58 \text{ fm}$ , much larger than  $R_0 = 2.7 \text{ fm}$  expected from systematics. Furthermore essentially all of the correlation energy ( $E_{corr} \approx 0.5 \text{ MeV}$ ,  $(E_{corr}/\epsilon_F)^2 \approx (0.5/14)^2 \approx 10^{-3}$ ,  $\xi \approx 20 \text{ fm}$  ( $v_F/c \approx 0.1$ )) is associated with the exchange of the dipole pigmy resonance between the halo neutrons. It is of notice that in this case, renormalization effects due to the clothing of single-particle states by vibrations, in particular the lowest lying quadrupole vibration of the core  $^9\text{Li}$ , are as strong as mean field effects, as testified by parity inversion and the appearance of a new magic number, namely  $N = 6$  (cf. Fig. 2.6.3 (I)). Again in this case  $s_{1/2}^2(0)$  and  $p_{1/2}^2(0)$  are not correlated in  $\Omega_{12}$ , while the Cooper state probability density displays a clear angular correlation (see Fig. 2.6.3 (II) (a) and (b)). Nonetheless, the average distance between the partners of the neutron halo Cooper pair, is considerably larger than that associated with the  $^9\text{Li}$  core nucleons, as testified by the following figures (cf. also Fig. 3.2.2):

$$\text{a)} \quad R(^{11}\text{Li}) = 4.58 \pm 0.13 \text{ fm} \quad (V = (4\pi/3)R^3 = 402.4 \text{ fm}^3) \quad (3.2.21)$$

$$\text{b)} \quad R_0(^{11}\text{Li}) = 2.7 \text{ fm} \quad (V = 82.4 \text{ fm}^3) \quad (3.2.22)$$

$$\text{c)} \quad R_0(^9\text{Li}) = 2.5 \text{ fm} \quad (V = 65.4 \text{ fm}^3), \quad (3.2.23)$$

and associated mean distance between nucleons,

$$\text{a)} \quad \left( \frac{402.4 \text{ fm}^3}{2} \right)^{1/3} \approx 5.9 \text{ fm}, \quad (3.2.24)$$

$$\text{b)} \quad \left( \frac{82.4 \text{ fm}^3}{11} \right)^{1/3} \approx 1.96 \text{ fm}, \quad (3.2.25)$$

$$\text{c)} \quad \left( \frac{65.4 \text{ fm}^3}{9} \right)^{1/3} \approx 1.94 \text{ fm}. \quad (3.2.26)$$

The above quantities are to be compared with the standard definition,

$$d = \left( \frac{\frac{4\pi}{3}R^3}{A} \right)^{1/3} = \left( \frac{4\pi}{3} \right)^{1/3} r_0 \approx 1.93 \text{ fm}, \quad (3.2.27)$$

consistent with the standard parametrization  $R_0 = r_0 A^{1/3}$  of the nuclear radius written in terms of the Wigner–Seitz-like radius  $r_0$  (=1.2 fm) of the sphere associated with each nucleon, derived from systematics of stable nuclei lying along the stability valley.

### 3.2.1 Interplay between mean field and correlation length

In Fig. 3.2.1 one displays a schematic representation of two *gedanken experiments*: **(a)** (*independent particle motion*) non-interacting nucleons confined in a mean field potential, e.g. a Saxon–Woods potential with standard parametrization (Bohr and Mottelson (1969)); **(b)** *independent pair motion*, nucleons interacting through an effective pairing interaction, sum of a short ( $v_p^{bare}$ ) and long range ( $v_p^{ind}$ )  $NN$ -pairing potential, confined by a mean field whose parameters are freely adjusted so as to profit at best the pair coupling scheme.

In other words, one moves from a situation in which one assumes: (a)  $H = T + v \approx T + U$  (ansatz  $\langle v - U \rangle \approx 0$ ) to another in which (b)  $H = T + v \approx T + U' + v_p^{eff}$  (ansatz  $\langle v - U' - v_p^{eff} \rangle \approx 0$  and  $|U'| < |U|$ ,  $|v_p^{eff}| \ll |U'|$ ). Switching from the first to the second situation pairs of nucleons moving in time reversal states will tend to recede from each other. Now, to the extent that one is interested in describing real nuclei lying along the stability valley like e.g.  $^{120}\text{Sn}$ , one will rightly posit that the ansatz (a) is more realistic than (b), in keeping with the fact that  $(U' + v_p^{eff})$  represent a much smaller fraction of  $v$  than  $U$  does. Consequently, the right view seems to be that of (a) plus pairing, in which case Cooper pair partners approach each other, if nothing else, because of angular correlation<sup>16</sup>. The “correctness” of picture (b) reemerges, as already stated, e.g. in connection with transfer reactions, also in keeping with the fact that one- and two-particle transfer absolute cross sections have the same order of magnitude. And it is likely that picture (b) becomes quite useful in discussing the structure of light halo nuclei.

Within this context we note that the fact that  $^9\text{Li}_6$  is well bound ( $N = 6$  isotope parity-inverted closed shell),  $^{10}\text{Li}_7$  is not while  $^{11}\text{Li}_8$  is again bound, indicates that we are confronted with a pairing phenomenon. Allowing the two neutrons moving outside  $N = 6$  closed shell to correlate in the configurations  $j^2(0)(s_{1/2}^2, p_{1/2}^2, d_{5/2}^2 \dots)$  through a short range bare pairing interaction, e.g. the  $v_{14}$  Argonne  $NN$ -potential, does not lead to a bound state. The system lowers the relative momentum of the pair exchanging at the same time the low-lying dipole vibration of the associated diffuse system becoming, eventually, bound, ever so weakly ( $S_{2n} = 380$  MeV). The radius of the resulting system ( $R(^{11}\text{Li}) = 4.58 \pm 0.13$  fm) corresponds, in the parametrization  $R_0 = 1.2A^{1/3}$  fm, to an effective mass  $A \approx 60$ . So undoubtedly the system has swelled in moving from  $A = 9$  to  $A = 11$  in a manner that goes beyond the  $1.2A^{1/3}$  (fm) expected dependence. Although the correlation length of the neutron Cooper is restricted to  $2 \times R(^{11}\text{Li}) \approx 9$  fm, half of the estimated value  $\xi \approx 20$  fm, it is double as large as  $2 \times R_0(^{11}\text{Li}) \approx 5.4$  fm. Consequently, the function ( $|\Psi_0(\mathbf{r}_1, \mathbf{r}_2)|^2$ ) displayed in Fig. 2.6.3 (II) b) should be read with care. It is also noted that the associated mean field potential can be parametrized in terms of a standard Woods–Saxon potential (see Bohr and Mottelson (1969), Eq. (2–182) p. 239) of depth  $U' \approx -36$  MeV, much weaker than the typical value of  $U \approx -50$  MeV.

---

<sup>16</sup>Bertsch, G. F. et al. (1967); Ferreira, L. et al. (1984); Matsuo, M. (2013) and refs. therein.

It will be surprising if this bootstrap-like mechanism to profit from very low, (unstable) nuclear densities to generate transient medium polarization effects which acting between Cooper pair partners (separated by distances of the order of  $\xi$ ) to eventually stabilize a halo system, was a unique property of  $^{11}\text{Li}$ . In fact, one can expect particular situations of  $s$  and  $p$  states at threshold eventually leading to a symbiotic halo Cooper pair with such a small value of  $S_{2n}$ , which eventually gives rise to a value of  $2R \approx \xi$ . A problem in the quest of such exotic, but standard Cooper pair picture in condensed matter superconductors, may be related in the nuclear case to the very short lifetime of the resulting system (within this context one is reminded of the fact that  $\tau_{1/2}(^{11}\text{Li})=8.75\text{ ms}$ ).

In the above discussion, mention has been made to a bootstrap generation of infinite, condensed-matter-like situation (also in connection with Fig. 3.7.1, in which one was referring to finite density overlap across barriers between superfluid nuclei). Let us remind us that such a methodologic approach is no new to nuclear physics. For this purpose we can use as example the definition of a nuclear temperature and of the associated energy reservoir which can be shared statistically. How does one make a heat reservoir in the nucleus? While it is not a thermal bath in the classical sense, when the system emits a neutron or a  $\gamma$ -ray in the cooling process, it exchanges energy statistically with the freed particle. This is in keeping with the fact that the energy distribution of the emitted nucleon or  $\gamma$ -ray is determined by the density of levels of the daughter states (Bortignon, P. F. et al. (1998)). Concerning the  $\gamma$ -decay of the compound nucleus, it proceeds through  $E1$ -transitions, essentially profiting of the Axel-Brink ansatz introduced in nuclear physics to deal with this types of cooling processes. Within the bootstrap ansatz of symbiotic Cooper pair binding, we introduce a straightforward generalization of the Axel-Brink hypothesis based on well established experimental results. Namely the fact that the line shape and thus also the percentage of EWSR per energy interval as well as the decay properties of the GDR will reflect the static (splitting) and dynamic (motional narrowing) deformation properties of the state on which the GDR is built upon<sup>17</sup>

In the case of halo nuclei this generalization is not only quantitative but also qualitative. A sensible fraction of the TRK sum rule is found almost degenerate with the ground state. From the elastic antenna-like response typical of the high energy ( $\hbar\omega_{GDR} \approx 80\text{MeV}/A^{1/3}$ ) GDR one is now confronted with a very low energy ( $<1\text{ MeV}$ ) plastic dipole response (GDPR). Regarding the consequences this phenomenon has for the  $L = 1$  induced interaction between nucleons, one moves from dipole-dipole (static moment interactions) to dispersive (retarded) contributions, emerging essentially from quantum mechanical ZPF. In other words, and making use of an analogy with atomic physics, one moves from an interaction between polar molecules, to a “purely” quantal interaction arising from the mutual polarization of one molecule in the rapidly changing field of the other (due to

---

<sup>17</sup>Le Tourneau (1965); Bohr, A. and Mottelson (1975); Bortignon, P. F. et al. (1998) and refs. therein.

the instantaneous configuration of electrons and nuclei associated with ZPF) and viceversa, only one operative in the case of non-polar molecules. It is this second one which dominates the van der Waals interaction (App. 2.D) and, similarly, it is one which can lead to an almost resonant gluing of Cooper pair halos, a mechanism found also at the basis of superconductivity in metals. In other words, the extension of the Axel–Brink hypothesis within the present context allegedly implies to move from a possibility to a must. If one sees a halo one expects a GDPR.

The challenges faced to learn about the physical basis of pairing in nuclei are comparable to those encountered to extract a collective vibration from a background much larger than the signal, as it was the case in the case in the discovery of the GDR in hot nuclei<sup>18</sup>. In trying to observe the full range of pairing effects in nuclei, one has the advantage to start with the system at zero temperature for free. On the other hand one needs to subtract the very large, state dependent effects of the “external” mean field, a challenge not second to that faced by condensed matter practitioners to study low-temperature superconductivity in general, and the Josephson effect in particular.

### 3.3 Correlations between nucleons in Cooper pair tunneling

Let us call  $x_1$  and  $x_2$  the coordinates of the Cooper pair partners. Let us furthermore assume they can only take two values: 0 when they are bound to the target nucleus, 1 when they have tunneled and become part of the outgoing particle (see Fig. 3.3.1).

The correlation between the two nucleons is measured by the value<sup>19</sup>

$$\langle x_1 x_2 \rangle - \langle x_1 \rangle \langle x_2 \rangle = \int d\gamma P_2 \times 1 \times 1 - \int d\gamma P_1 \times 1 \int d\gamma' P'_1 \times 1 = P_2 - P_1 P'_1, \quad (3.3.1)$$

$d\gamma$  being the differential volume in phase space, normalized with respect to the corresponding standard deviations, that is, with respect to

$$\sigma_{x_1} \sigma_{x_2} = \left[ (\langle x_1^2 \rangle - \langle x_1 \rangle^2) (\langle x_2^2 \rangle - \langle x_2 \rangle^2) \right]^{1/2}. \quad (3.3.2)$$

Making use of the fact that

$$\langle x_1^2 \rangle = \int d\gamma P_1 \times 1^2 = P_1, \quad (3.3.3)$$

and

$$\langle x_1 \rangle = \int d\gamma P_1 \times 1 = P_1, \quad (3.3.4)$$

---

<sup>18</sup>See e.g. Bortignon, P. F. et al. (1998) Figs. 1.4 and 6.8, and refs. therein.

<sup>19</sup>Basdevant and Dalibard (2005).

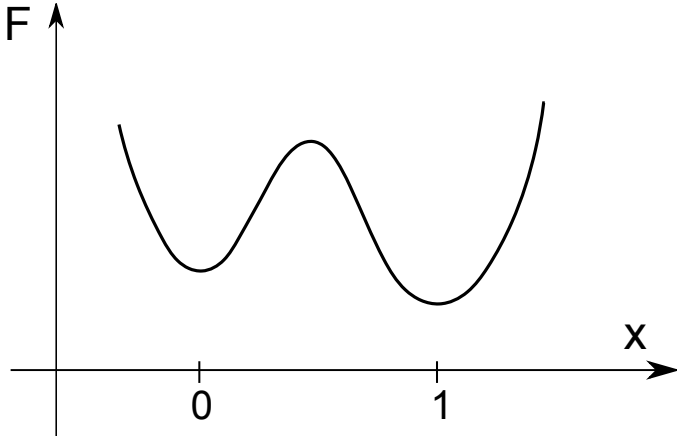


Figure 3.3.1: A schematic representation of nucleon tunneling between target and projectile. The free energy  $F = U - TS$  which for the zero temperature situation under consideration (e.g.  $^{120}\text{Sn}(p, d)^{119}\text{Sn}$ ,  $^{120}\text{Sn}(p, d)^{118}\text{Sn}$ ) coincides with the potential energy as a function of the nucleon coordinate  $x$ . For  $x = 0$  the nucleon is assumed to be bound to the target system. For  $x = 1$  the nucleon has undergone tunneling becoming bound to the outgoing particle. In other words  $x_1$  jumps from the value 0 to the value 1 in the tunneling process ( $x_1, 0 \rightarrow 1$ ), the same for the coordinate of the second nucleon.

One obtains the function which measures the correlations between nucleons 1 and 2, namely,

$$C = \frac{\langle x_1 x_2 \rangle - \langle x_1 \rangle \langle x_2 \rangle}{\sqrt{(\langle x_1^2 \rangle - \langle x_1 \rangle^2)(\langle x_2^2 \rangle - \langle x_2 \rangle^2)}} = \frac{P_2 - P_1 P'_1}{\sqrt{(P_1 - P_1^2)(P'_1 - P'_1^2)}}. \quad (3.3.5)$$

Because both nucleons are identical and thus interchangeable,  $P_1 = P'_1$ . Thus

$$C = \frac{P_2 - P_1^2}{P_1 - P_1^2}. \quad (3.3.6)$$

Making use of the empirical values

$$P_1 \approx P_2 \approx 10^{-3} \quad (3.3.7)$$

leads to,

$$C = \frac{10^{-3} - 10^{-6}}{10^{-3} - 10^{-6}} \approx 1. \quad (3.3.8)$$

In other words, within the independent pair motion regime, nucleon partners are solidly anchored to each other: if one nucleon goes over, the other does it also. This is so in spite of the very liable and fragile structure of the nuclear Cooper pairs

$l$	$p_l$
0	$1.02 \times 10^{-3}$
1	$2.40 \times 10^{-3}$
2	$1.26 \times 10^{-2}$
3	$1.84 \times 10^{-2}$
4	$6.13 \times 10^{-3}$
5	$1.39 \times 10^{-3}$
6	$2.89 \times 10^{-4}$
7	$5.04 \times 10^{-5}$
8	$6.51 \times 10^{-6}$
9	$5.87 \times 10^{-7}$

Table 3.3.1: Probabilities  $p_l$  (see Eq. (3.2.14) and App. 6.B) associated with the reaction  ${}^1\text{H}({}^{11}\text{Li}, {}^{10}\text{Li(gs)}){}^2\text{H}$  calculated with the same bombarding conditions as those associated with  ${}^1\text{H}({}^{11}\text{Li}, {}^9\text{Li(gs)}){}^3\text{H}$  cf. Table 6.B.1. It was assumed that the amplitude with which the single particle orbital  $s_{1/2}$  enters in the  $|{}^{10}\text{Li}(1/2^+)\rangle$  (gs) is  $\sqrt{0.5}$  (cf. Eqs. (6.1.1)–(6.1.3)).

$(\Delta/\epsilon_F \ll 1)$ , a clear example of which is being provided by  ${}^{11}\text{Li}$ . In fact, if one picks-up a neutron from  ${}^{11}\text{Li}$  ( ${}^{11}\text{Li}(p, d){}^{10}\text{Li}$ ), the other one breaks up essentially instantaneously,  ${}^{10}\text{Li}$  being unbound. In spite of this fact, the probability associated with the reaction  ${}^{11}\text{Li}({}^{11}\text{Li}, {}^9\text{Li(gs)}){}^1\text{H}$  is (see Table II Potel et al. (2010) and eq. (2.6.5) as well as Sect. 2.B) is given by,

$$P_2 = \frac{5.7 \pm 0.9 \text{ mb}}{2\pi(4.83 \text{ fm})^2} \approx 4 \times 10^{-3}, \quad (3.3.9)$$

a value which is much larger than the value of  $4.81 \times 10^{-6}$  associated with the breakup process mentioned above (see  $l = 0$  columns 1 and 3 of Table 6.B.1), let alone  $P_1^2 (1.02 \times 10^{-3})^2 \approx 10^{-6}$  as given in Table 3.3.1. One may be surprised of this result, in keeping with the fact that most of the two-nucleon transfer reaction cross section ( $\approx 80\%$ ) is associated with successive transfer (see Fig. 6.B.3). The answer is in any case contained in the relation (3.2.19), applicable both for static and dynamic pair modes, in keeping with the fact that in nuclei, dynamic spontaneous breaking of gauge invariance is of similar importance as the static one<sup>20</sup>. It is of notice that in successive transfer processes the one-particle channels are virtual, that is with no outgoing running waves and thus with a very different coupling to the continuum states than in the case of real asymptotic waves. This coupling influences in an important way the structure aspects of the problem, less the reaction ones. But again, the simple answer is that the halo Cooper pair in its tunneling between  ${}^{11}\text{Li}$  and  ${}^1\text{H}$  does not see neither  ${}^{10}\text{Li}$  nor  ${}^2\text{H}$ , behaving as an entity. Surprisingly, the regime of independent pair motion extends also to the single pair situation. Two-particle tunneling can specifically probe such a regime.

<sup>20</sup>cf. Fig. 2.5.7, cf. also Sect. 3.8 and Fig. 4 Potel, G. et al. (2013b); cf. Fig. 3.3.2

$$\text{Order parameter} \quad \left( \langle \tilde{0} | P P^\dagger | \tilde{0} \rangle \right)^{1/2} = \begin{cases} \alpha_0 = \sum_{\nu>0} U'_\nu V'_\nu \\ \alpha_{dyn} = \sum_{\nu>0} U_\nu^{eff} V_\nu^{eff} \end{cases}$$

**pairing vibrations**

$$(U_\nu^{eff})^2 = 2Y_a^2(j_\nu)/\Omega_\nu; \quad (U_\nu^{eff})^2 = 1 - (U_\nu^{eff})^2$$

$$\begin{aligned} X_n(j_\nu) \\ Y_n(j_\nu) \end{aligned} \Bigg\} = \frac{\left(\sqrt{\Omega_j}/2\right)\Gamma_n}{2|E_j| \mp W_n}$$

**pairing rotations**

$$\begin{aligned} U'_\nu \\ V'_\nu \end{aligned} \Bigg\} = \frac{1}{\sqrt{2}} \left( 1 \pm \frac{\epsilon_\nu}{\sqrt{\epsilon_\nu^2 + \Delta^2}} \right)^{1/2}$$

Figure 3.3.2: Order parameter associated with static and dynamic pair correlations (see Potel, G. et al. (2013b)).

*A direct consequence of the above parlance is the fact that the Cooper pair rigidity emerges from phase coherence (in gauge space), and leads to the generalized rigidity of pairing rotational (static) and vibrational (dynamic) bands which can be instantaneously set into rotation (vibration) with just the push imparted in gauge space by the transferred pair, without this fact violating any limiting velocity, neither of medium propagating signals nor of light.*

### 3.4 Pair transfer

The semiclassical two–nucleon transfer amplitudes fulfill, in the **independent particle limit**, the relations<sup>21</sup>,

$$a_{sim}^{(1)} = a_{NO}^{(1)}, \quad (3.4.1)$$

and

$$a_{succ}^{(2)} = a_{one-part}^{(1)} \times a_{one-part}^{(1)}, \quad (3.4.2)$$

with

$$a + A \rightarrow f + F \rightarrow b + B, \quad (3.4.3)$$

---

<sup>21</sup>see App. 5.C, also Potel, G. et al. (2013a).

corresponding to the product of two single nucleon transfer processes. On the other hand, in the **strong correlation limit** one can write, making use of the post–prior representation

$$\tilde{a}_{succ}^{(2)} = a_{succ}^{(2)} - a_{NO}^{(1)}. \quad (3.4.4)$$

Thus

$$\lim_{E_{corr} \rightarrow \infty} \tilde{a}_{succ}^{(2)} = 0, \quad (3.4.5)$$

and all transfer is, in this case, due to simultaneous transfer. Actual nuclei are close to the independent particle limit ( $E_{corr}$  (1–2 MeV)  $\ll \epsilon_F \approx 37$  MeV). Then successive transfer is the major contribution to pair transfer processes. But successive transfer seems to break the pair *right? Wrong. Why?* let us see below.

### 3.4.1 Cooper pair dimensions

Typical correlation energies of Cooper pairs are 1–2 MeV. Now, such a system (dineutron or diproton) is not bound and needs of an external field to be confined. This is the role played by the single-particle field (cf. Fig. 3.1.3). Let us now calculate the dimensions of a Cooper pair (correlation length). We start with the relation

$$\delta x \delta p \geq \hbar \quad \delta \epsilon \approx 2E_{corr}, \quad (3.4.6)$$

where

$$\epsilon = \frac{p^2}{2m}; \quad \delta \epsilon = \frac{2p\delta p}{m} \approx v_F \delta p, \quad (3.4.7)$$

and thus

$$\delta \epsilon \approx 2E_{corr} \approx v_F \delta p, \quad (3.4.8)$$

leading to

$$\xi = \delta x = \frac{\hbar}{\delta p} \approx \frac{\hbar v_F}{2E_{corr}} \quad (\text{correlation length}). \quad (3.4.9)$$

Making use of the fact that in nuclei,

$$\frac{v_F}{c} \approx 0.3, \quad (3.4.10)$$

one obtains

$$\xi \approx \frac{200 \text{ MeV fm} \times 0.3}{2 \text{ MeV}} \approx 30 \text{ fm}. \quad (3.4.11)$$

Consequently, successive and simultaneous transfer feel equally well the pairing correlations giving rise to long range order. This virtual property can become<sup>22</sup> real in e.g. a pair transfer between two superfluid tin isotopes (Fig. 3.4.1).

### Objection

What about  $v_{pairing}$  (=  $G$ ) becoming zero, e.g. between the two nuclei?

---

<sup>22</sup>See von Oertzen, W. (2013)

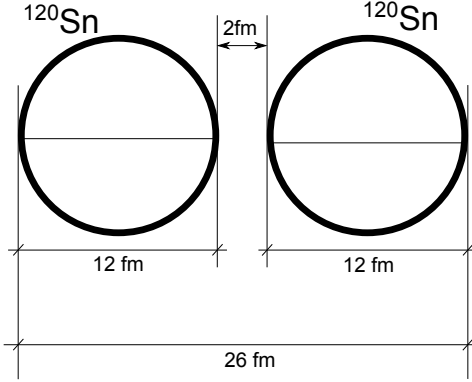


Figure 3.4.1: Schematic representation of two Sn-isotopes (radius  $R_0 \approx 6$  fm) at the distance of closest approach in a heavy ion collision.

### Answer

$$\frac{d\sigma(a = b + 2) + A \rightarrow b + B(A + 2))}{d\Omega} \sim |\alpha_0|^2, \quad (3.4.12)$$

$$\alpha_0 = \langle BCS(A + 2)|P^\dagger|BCS(A)\rangle = \sum_{\nu>0} U_\nu(A)V_\nu(A + 2). \quad (3.4.13)$$

(cf. also App. 3.8).

### Objection

Relation (3.4.13) is only valid for simultaneous transfer, *right? Wrong.*

### Answer

The order parameter can also be written as,

$$\begin{aligned} \alpha_0 &= \sum_{\nu,\nu'>0} \langle BCS|a_\nu^\dagger|int(\nu')\rangle\langle int(\nu')|a_{\bar{\nu}}^\dagger|BCS\rangle \\ &\approx \sum_{\nu,\nu'>0} \langle BCS(A + 2)|a_\nu^\dagger a_{\nu'}^\dagger|BCS(A + 1)\rangle\langle BCS(A + 1)|a_{\nu'} a_{\bar{\nu}}^\dagger|BCS(A)\rangle \\ &= \sum_{\nu,\nu'>0} \langle BCS(A + 2)|V_\nu(A + 2)a_{\bar{\nu}} a_{\nu'}^\dagger|BCS(A + 1)\rangle \\ &\times \langle BCS(A + 1)|\alpha_{\nu'} U_\nu(A)a_{\bar{\nu}}^\dagger|BCS(A)\rangle = \sum_{\nu>0} V_\nu(A + 2)U_\nu(A), \end{aligned} \quad (3.4.14)$$

where the (inverse) quasiparticle transformation relation  $a_\nu^\dagger = U_\nu a_\nu^\dagger + V_\nu a_{\bar{\nu}}^\dagger$  was used. Examples of two-nucleon spectroscopic amplitudes involving superfluid targets, namely those associated with the reactions  $^{112}\text{Sn}(p,t)^{110}\text{Sn(gs)}$  and  $^{124}\text{Sn}(p,t)^{122}\text{Sn(gs)}$  are given in Table 2.4.1. Making use of these amplitudes (first

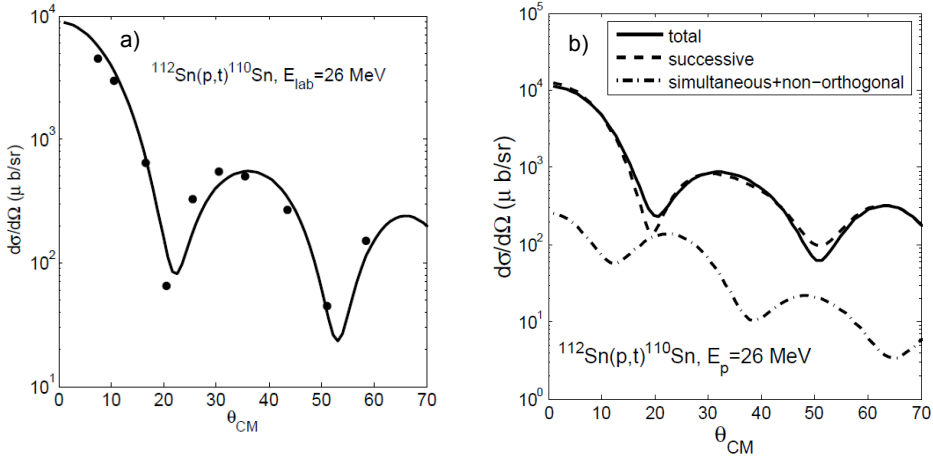


Figure 3.4.2: a) Absolute differential cross section associated with the reaction  $^{112}\text{Sn}(p,t)^{110}\text{Sn}(\text{gs})$  calculated with the software COOPER (mentionar apendice software) in comparison with the experimental data (Guazzoni, P. et al. (2006)). b) Details of the different contributions to the total absolute  $(p,t)$  differential cross section (for details see Potel, G. et al. (2013a), Potel, G. et al. (2013b)).

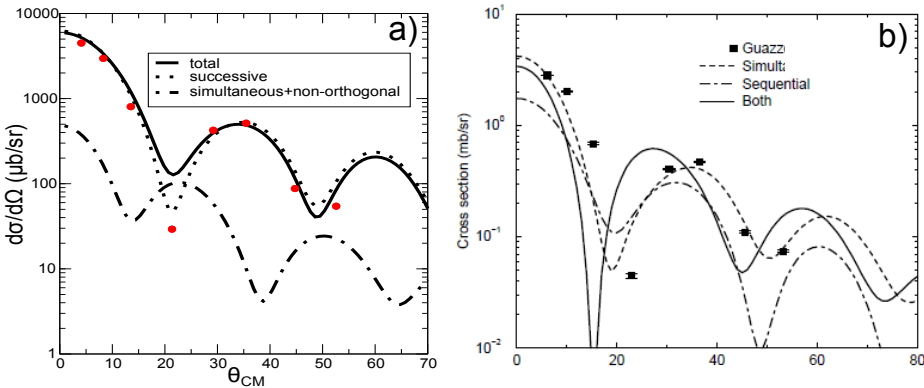


Figure 3.4.3: Absolute differential cross section associated with the reaction  $^{124}\text{Sn}(p,t)^{122}\text{Sn}(\text{gs})$  calculated making use of: a) second order DWBA taking into account non-orthogonality corrections and the two-nucleon spectroscopic amplitudes resulting from BCS (see Table 2.4.1, third column; for details see Potel, G. et al. (2013a), Potel, G. et al. (2013b)) in comparison with experimental data (Guazzoni, P. et al. (2011)). b) As above, but making use of FRESCO (reaction) and of shell model two-nucleon overlaps (structure); cf. Table 2.4.1 fourth column (for details cf. Thompson, I.J. (2013)).

column) and of global optical parameters, the two-nucleon transfer absolute differential cross section of the reaction  $^{112}\text{Sn}(p, t)^{110}\text{Sn}(\text{gs})$  at center of mass bombarding energy of  $E_p = 26$  MeV, was calculated making use of the software COOPER based on second order DWBA and taking into account successive and simultaneous transfer properly corrected for non-orthogonality (cf. Chapter 5 and App. 6.D). It is compared with experimental data in Fig. 3.4.2 (a). The corresponding absolute integrated cross sections are  $1310 \mu\text{b}$  and  $1309 \pm 200 \mu\text{b}$  respectively. The largest contribution to the cross section arises from successive transfer, the cancellation between simultaneous and non-orthogonality amplitudes being important (Fig. 3.4.2 (b)). The above is a typical example of results of a systematic study of two-nucleon transfer reactions in terms of absolute cross sections<sup>23</sup>.

Making use of two-nucleon spectroscopic amplitudes worked out within the framework of an extended shell model calculation (Table 2.4.1, second column) one obtains very similar results to those displayed in Fig. 3.4.2 (a). In Fig. 3.4.3 (a) we report results similar to those displayed in Fig. 3.4.2, but for the case of the reaction  $^{124}\text{Sn}(p, t)^{122}\text{Sn}(\text{gs})$  calculated within second order DWBA making use of the BCS spectroscopic amplitudes (Table 2.4.1 third column). We display in Fig. 3.4.3 (b) the absolute differential cross section calculated with NuShell spectroscopic amplitudes and the coupled channel software FRESKO<sup>24</sup>.

Let us now provide an example of two-nucleon transfer around a closed shell nucleus displaying well defined collective pairing vibrational modes. We refer, in particular, to the pair removal mode of  $^{206}\text{Pb}$ , that is, to the reaction,  $^{206}\text{Pb}(t, p)^{208}\text{Pb}(\text{gs})$ . Making use of the spectroscopic amplitudes displayed in Tables 2.5.2 and 2.5.3 and of global optical parameters, the associated absolute differential cross sections was calculated again with the software COOPER. It is displayed in Fig. 3.4.4 in comparison with experimental findings. In the same figure, the total differential cross section is compared with that associated with the TD (Tamm–Dankoff) description of  $^{206}\text{Pb}(\text{gs})$ , that is, setting the pairing ground state correlations to zero ( $\sum_i X_r^2(i) = 1$ ,  $Y_r(k) \equiv 0$ , see Table 2.5.2). In this case, theory underpredicts observation by about a factor of 2, let alone the fact that the TD solution does not conserve the two-nucleon transfer sum rule. Also given in Fig. 3.4.4 is the predicted cross section associated with the pure configuration  $|p_{1/2}^{-2}(0)\rangle$ . These results underscore the role pairing correlations play in the properties of  $^{208}\text{Pb}$  pair removal mode  $|r\rangle \equiv |^{206}\text{Pb}(\text{gs})\rangle$ . Not only they make the two holes correlate both in angle and, radially on the surface. It lowers the momentum by increasing the volume over which the two fermions are allowed to move (spill out) and thus correlate, as required by the calculated correlation length  $\xi$ <sup>25</sup>.

It is of notice, that within the effective reaction mechanism described in Sect. 2.1 pairing correlations increase the value of  $\Omega_0 (\approx 0.97)$ . As a consequence the  $l = n = 0$  two-neutron system gives a much larger contribution to the two-nucleon

---

<sup>23</sup>Potel, G. et al. (2013a), Potel, G. et al. (2013b) see also Ch. 6, in particular Fig. 6.2.1.

<sup>24</sup>Thompson, I.J. (2013).

<sup>25</sup>Bertsch, G. F. et al. (1967), Ferreira, L. et al. (1984); Matsuo, M. (2013) see also Figs. 2.6.3 a and b) i.e. left part.

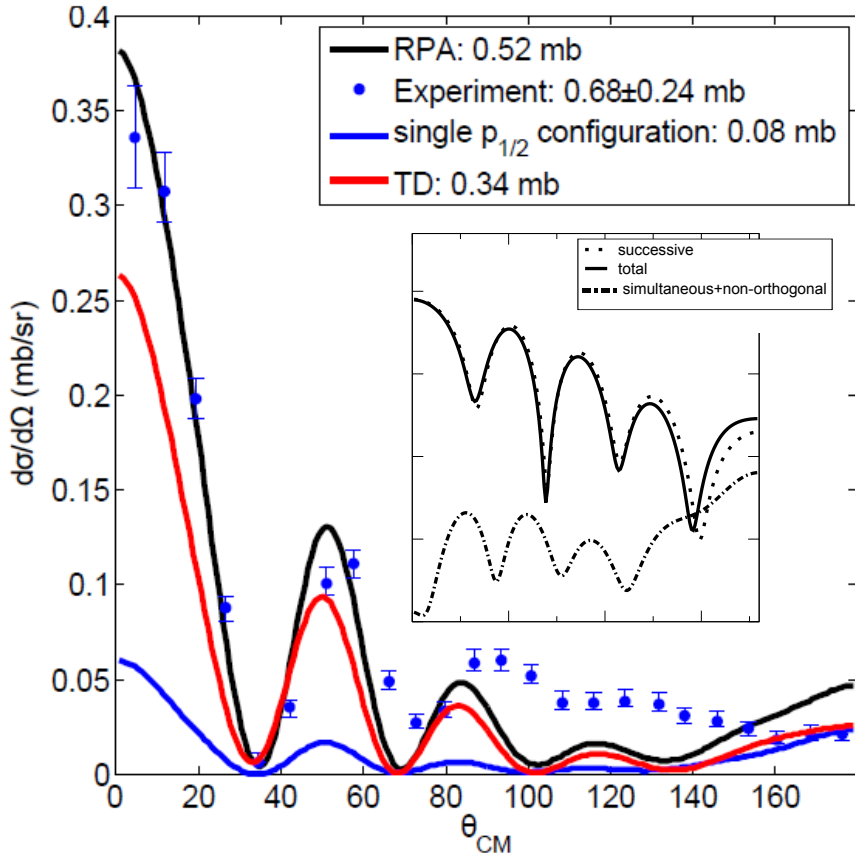


Figure 3.4.4: Absolute two-nucleon transfer differential cross section associated with the  $^{206}\text{Pb}(t, p)^{208}\text{Pb}(\text{gs})$  transfer reaction, that is, the annihilation of the pair removal mode of  $^{208}\text{Pb}$  in comparison with the data (Bjerregaard, J. H. et al. (1966)). The theoretical cross sections were calculated making use of the spectroscopic amplitudes given in Tables 2.5.2 and 2.5.3 and of global optical parameters as reported in the reference above. Both RPA and TD amplitudes were used as well as a pure configuration  $p_{1/2}^2(0)$ .

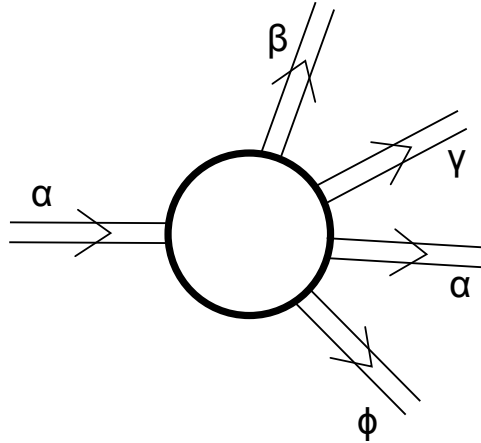


Figure 3.5.1: Schematic representation of entrance ( $\alpha$ ) and exit channels ( $\beta, \gamma, \alpha, \phi$ ) of a nuclear reaction and of the interaction region.

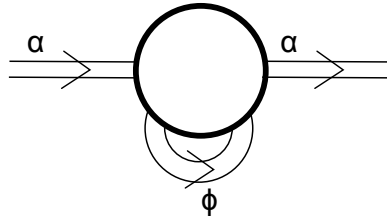


Figure 3.5.2: Schematic representation of the change in role of the one–nucleon transfer channel  $\phi$  from being an open channel, (Fig. 3.5.1) to one which acts as a virtual channel contributing to the optical potential.

transfer process than those associated with  $n = 1$  and  $2$ , that is those proportional to  $\Omega_1$  and  $\Omega_2$  whose values are  $0.25$  and  $0.06$  respectively (cf. Eq. (2.1.3)). All these features boost the effective absolute two–nucleon pure configuration transfer cross section to the observed experimental value. While the results displayed in Fig. 3.4.4 were calculated making use of the full formalism of second order DWBA (cf. Figs. 3.1.1 and 3.1.2) the simplified expressions given in Eqs. (2.1.1–2.1.7) are useful to gain physical insight into the two–nucleon transfer process.

### 3.5 Comments on the optical potential

As a rule, the depopulation of the entrance, elastic channel  $\alpha(a, A)$  (see Fig. 3.5.1) is mainly due to one–particle transfer channels  $\phi(f(= a - 1), F(= A + 1))$ . Other channels, like e.g. inelastic ones  $\beta(a^*, A)$ ,  $\gamma(a, A^*)$  being operative in particular situations, for example, when deformed nuclei are involved in the reaction process. Let us assume that this is not the case. Thus, quite likely, the one–particle transfer channel  $\phi$  is expected to be the main depopulating channel of the entrance channel

$\alpha$  (cf. Fig. 3.5.2). This is also in keeping with the fact that the tail of the corresponding form factors, reaches further away than that of any other channel (cf. Fig. 3.5.5). In this case, the calculation of the optical potential<sup>26</sup>, is quite reminiscent to the calculation of two-particle transfer (2nd order process), and can be carried out with essentially the same tools. In fact,

$$\begin{aligned} T_{succ}^{(2)} &\sim \langle fin|v|int\rangle\langle int|v|in\rangle \\ T_{NO}^{(2)} &\sim \langle fin|v|int\rangle\langle int|\mathbf{1}|in\rangle, \end{aligned} \quad (3.5.1)$$

where  $|in\rangle = |a, A\rangle$ ,  $|int\rangle = |f, F\rangle$  and  $|fin\rangle = |b, B\rangle$  are the initial, intermediate, and final channels in a two-nucleon transfer reactions, which become

$$\begin{aligned} \langle in|v|int\rangle\langle int|v|in\rangle \\ \langle in|v|int\rangle\langle int|\mathbf{1}|in\rangle, \end{aligned} \quad (3.5.2)$$

as contributions to the optical potential (Fig. 3.5.2).

Let us elaborate on the above arguments within the context, for concreteness, of  $^{11}\text{Li}$  and of the reaction  $^{11}\text{Li}(p, t)^9\text{Li}$ . In keeping with the fact that structure and reactions are just but two aspects of the same physics and that in the study of light halo nuclei, continuum states are to be treated on, essentially, equal footing in the calculation of the wavefunctions describing bound states (structure) as well as of the asymptotic distorted waves entering in the calculation of the absolute two-particle transfer differential cross sections (reaction; see Figs. 3.5.3 (a) and (b)), the calculation of the optical potentials is essentially within reach (reaction, see Figs. 3.5.3 (c) and 3.5.4). Because the real and imaginary parts of complex functions are related by simple dispersion relations<sup>27</sup> it is sufficient to calculate only one of the two (real or imaginary) components of the self-energy function to obtain the full scattering, complex, nuclear dielectric function (optical potentials). Now, absorption is controlled by on-the-energy-shell contributions. Within this scenario it is likely that the simplest way to proceed is that of calculating the absorptive

---

<sup>26</sup>It is of notice that the optical potential can be viewed as the complex “dielectric” function of direct nuclear reactions. In other words, the function describing the properties of the medium in which incoming and outgoing distorted waves propagate, properties which are, as a rule determined through the analysis of elastic scattering processes, under the assumption that the coupling between the relative motion(reaction) and intrinsic (structure) coordinates, occur only through a Galilean transformation (recoil effect) which smoothly matches the incoming with te outgoing waves (trajectories). Now, within the present context, namely that of the microscopic calculation of  $U + iW$ , non-locality and  $\omega$ -dependence can be microscopically treated on equal footing through the calculation of structure properties. In particular, within the framework of NFT, taking into account the variety of correlations and couplings between single-particle and collective motion, elementary modes of nuclear excitation. Such an approach to structure and reaction provides the elements and rules for an *ab initio* calculations of the texture of the corresponding vacuum states, and thus of the bound and continuum properties of the nuclear quantal system by itself and in interaction. It is of notice that such a scenario includes also limiting situations like sub-barrier fusion processes (cf. e.g. Sargsyan, V. V. et al. (2013) and refs. therein) and also exotic decay (cf. e.g. Barranco, F. et al. (1988, 1990); Montanari et al. (2014), cf. also Brink, D. and Broglia (2005)).

<sup>27</sup>See, e.g., Mahaux, C. et al. (1985) and references therein.

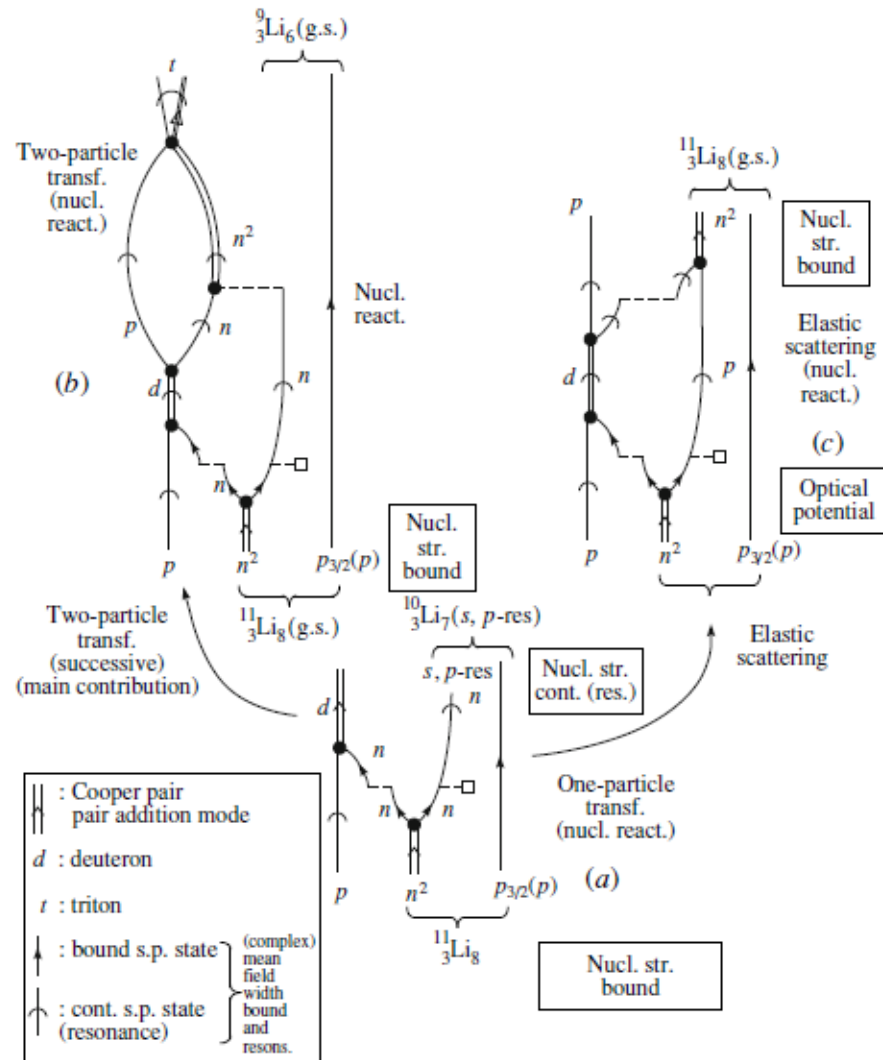


Figure 3.5.3: NFT diagrams summarizing the physics which is at the basis of the structure of  $^{11}\text{Li}$  (Barranco, F. et al. (2001)) and of the analysis of the  $^{11}\text{Li}(p,t)^{9}\text{Li}(\text{g.s.})$  reaction (Potel et al. (2010)). In the figure emphasis is set on intermediate (like, e.g.,  $^{10}\text{Li} + d$ , see (a) and (b)) and elastic (see (c), see also Fig. 3.5.4) channels.

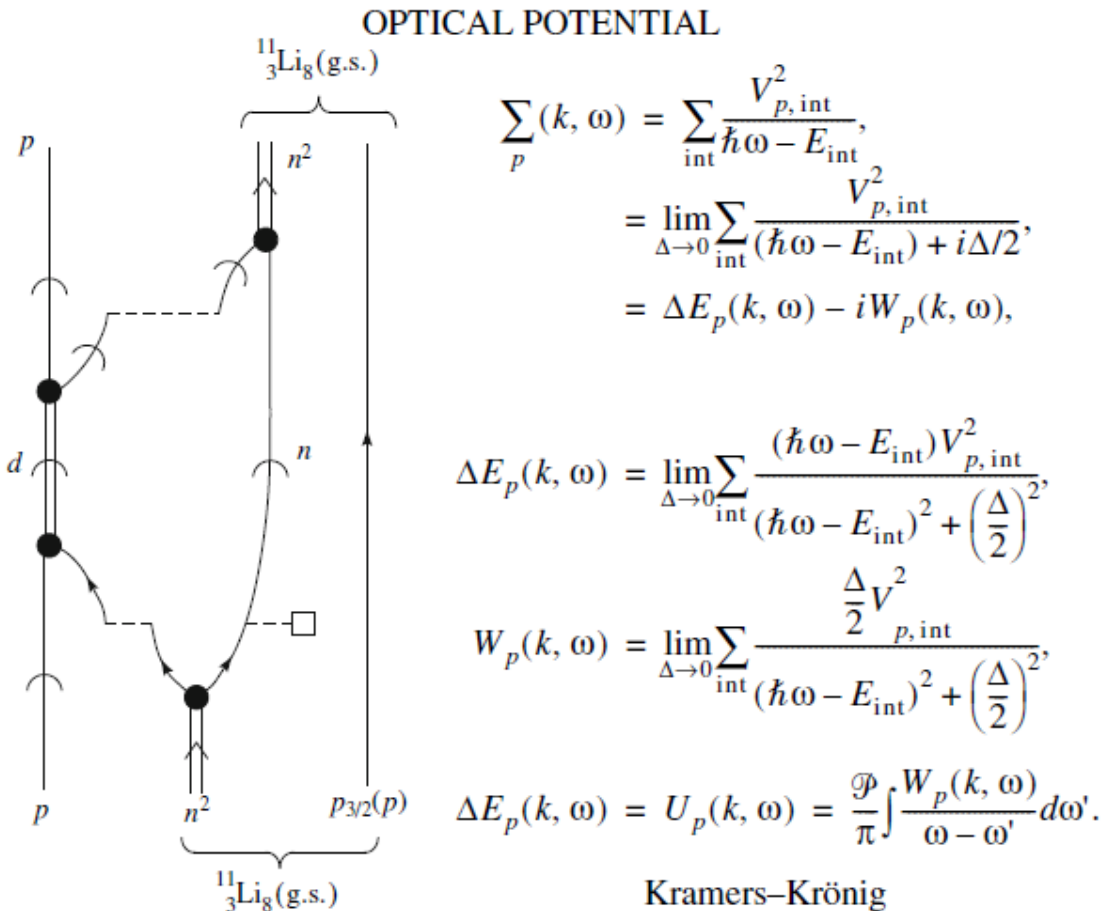


Figure 3.5.4: NFT diagrams and summary of the expression (see, e.g., Mahaux, C. et al. (1985) and references therein) entering the calculation of one of the contributions (that associated with one-particle transfer and, arguably, the dominant one) to the  $^{11}\text{Li} + p$  elastic channel optical potential. The self-energy function is denoted  $\Sigma_p$ , while the real and imaginary parts are denoted  $\Delta E_p (= U_p)$  and  $W_p$ , respectively, the subindex  $p$  indicating the incoming proton. These quantities are, in principle, functions of frequency and momentum.

potential and then obtain the real part by dispersion. Of notice that in heavy-ion reactions, one is dealing with leptodermous systems. Thus, the real part of the optical potential can, in principle, be obtained by convolution of the nuclear densities and of the surface tension<sup>28</sup>. Within the present context, one can mention the ambiguities encountered in trying to properly define a parentage coefficient relating the system of  $(A + 1)$  nucleons to the system of  $A$  nucleons, and thus a spectroscopic amplitude. In other words, a prefactor which allows to express the absolute one-particle transfer differential cross section in terms of the elastic cross section. Making use of NFT diagrams like the one shown in Fig. 3.5.4 , it is possible to calculate, one at a time, the variety of contributions leading to one- and two- particle transfer processes as well as of the associated optical potential. Summing up the different contributions, taking also proper care of those arising from four-point vertex, tadpole processes, etc., a consistent description of the different channels can be worked out, in which the predicted quantities to be directly compared with observables are absolute differential cross sections, or, more generally, absolute values of strength functions for different scattering angles.

### 3.6 Weak link between superconductors

Two-nucleon transfer reactions involving superfluid nuclei display some similarities with Cooper pair tunneling between weakly coupled superconductors, in particular when discussing heavy ion reactions, but not only<sup>29</sup>. Within this context it is useful to remind the basic elements of the pair tunneling which is at the basis of the Josephson effect. In this section we essentially reproduce the description of the tunneling of Cooper pairs between two weakly coupled superconductors to be found in<sup>30</sup>, arguably, the best physical presentation of the Josephson effect<sup>31</sup>.

One starts with the many-body Hamiltonian of<sup>32</sup>

$$H = H_1 + H_2 + \sum_{kq} T_{kq} (a_{k\uparrow}^\dagger a_{k\uparrow} + a_{-q\downarrow}^\dagger a_{-q\downarrow}) + HC \quad (3.6.1)$$

where  $H_1$  and  $H_2$  are the separate Hamiltonian of the two superconductors on each side of the barrier,  $T_{kq}$  being the (exponentially) small tunneling matrix element from state  $k$  on one side to  $q$  on the other.

One can arrive to (3.6.1) by first finding sets of single-particle wavefunctions for each side separately, in the absence of the potential of the other system. Then one eliminates the non-orthogonality effects by perturbation theory (cf. the similarity with the arguments used in Sect. 3.2 as well as Sect. 5.C; for details see Sect. 5.1). It is of notice that a nuclear embodiment of such strategy but for the

---

<sup>28</sup>Cf. e.g. Broglia and Winther (2005) and references therein.

<sup>29</sup>von Oertzen and Vitturi (2001); von Oertzen, W. (2013); Broglia and Winther (2004).

<sup>30</sup>Anderson (1964)

<sup>31</sup>Josephson (1962).

<sup>32</sup>Cohen et al. (1962)

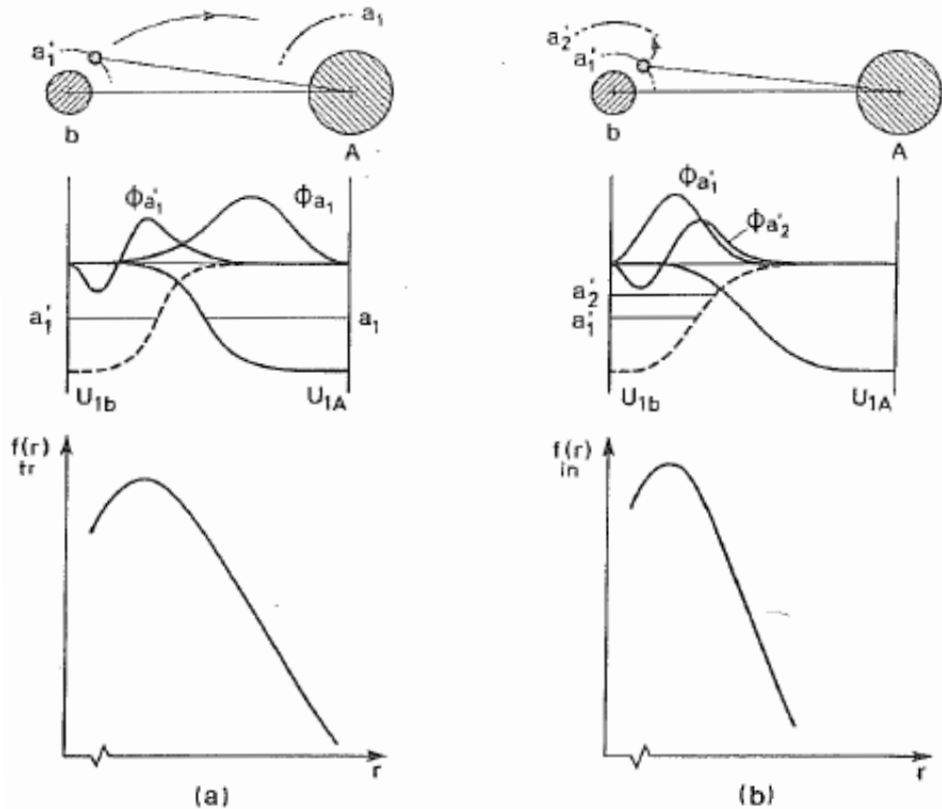


Figure 3.5.5: Schematic representation of the radial dependence of the one-particle transfer and inelastic form factors. In (a) a nucleon moving in the orbital with quantum numbers  $a'_1$  in the projectile  $a$  is transferred under the action of the shell model potential  $U_{1A}$  to the target nucleus  $A$  into an orbital  $a_1$ . The dependence of the form factor on the distance between the two nuclei is determined by the overlap of the product of the single-particle wavefunctions  $\phi_{a'_1}$  and  $\phi_{a_1}$  with the potential  $U_{1A}$ . A schematic representation of this dependence is given at the bottom of figure (a). In (b) a nucleon in the projectile  $a$  is excited under the influence of the target field  $U_{1A}$  from the single-particle orbital with quantum numbers  $a'_1$  to the orbital with quantum numbers  $a'_2$ . The dependence of the form factor on the distance between the cores is here determined by the overlap of the product of the functions  $\phi_{a'_1}$  and  $\phi_{a'_2}$  with the potential  $U_{1A}$ . A representation of this dependence is shown at the bottom of (b) (after Broglia and Winther (2005)).

case superfluid–normal<sup>33</sup> tunneling is worked out in Ch. 5 and implemented in COOPER<sup>34</sup>.

Let us now calculate the second order expression of (3.6.1) in the case in which the gaps of the two weakly linked superconductors are different. Making use of relations presented in Sect. 2.4.2 one can write, for  $T = 0$ ,

$$\Delta E_2 = -2 \sum_{kq} |T_{kq}|^2 \frac{|V_k U_q + V_q U_k|^2}{E_k + E_q}. \quad (3.6.2)$$

With the help of

$$2U_k V_k^* = \frac{\Delta_k}{E_k}, \quad 2U_q V_q^* = \frac{\Delta_q}{E_q}, \quad (3.6.3)$$

and

$$|U_k|^2 - |V_k|^2 = \frac{\epsilon_k}{E_k}, \quad |U_q|^2 - |V_q|^2 = \frac{\epsilon_q}{E_q}, \quad (3.6.4)$$

where

$$E = \sqrt{\epsilon^2 + \Delta^2} \quad (3.6.5)$$

and

$$\Delta_k = \Delta_1 e^{i\phi_1}, \quad \Delta_q = \Delta_2 e^{i\phi_2} \quad (3.6.6)$$

one can write for the numerator of Eq. (3.6.2),

$$\begin{aligned} NUM &= (V_k U_q + V_q U_k)(V_k^* U_q^* + V_q^* U_k^*) \\ &= \left[ V_k^2 U_q^2 + V_q^2 U_k^2 \right] + \left[ (U_k^* V_k)(U_q V_q^*) + (U_q^* V_q)(U_k V_k^*) \right]. \end{aligned} \quad (3.6.7)$$

It is of notice that, for simplicity, throughout this Appendix

$$V^2 \equiv |V|^2. \quad (3.6.8)$$

---

<sup>33</sup>It is of notice that pairing vibrations in nuclei are quite collective, leading to effective  $U$  and  $V$  occupation factor (cf. Fig. 3.3.2) (see also Potel, G. et al. (2013b)), the nuclear and the condensed matter expressions are very similar. Of course no supercurrent is expected between nuclei. However, the systems <sup>120</sup>Sn(gs), <sup>119</sup>Sn(j), <sup>118</sup>Sn(gs) form an ensemble of weakly coupled Fermi superfluids, with different (average) number of particles ( $N, N - 1, N - 2$ ), to which essentially all the BCS techniques, including those of the present Appendix can be applied (cf. Fig. 3.7.1). Of notice the parallel of this scenario with that associated with nuclei excited at rather high energies for which one defines a temperature. This is possible, because the excited (thermalized) nucleus is in equilibrium with the particles, namely neutrons and gamma-rays it emits, particles which act as a thermal bath, let alone the very high density of levels, of the compound nucleus (cf. Bertsch and Broglia (2005) p 171).

<sup>34</sup>Cf. App. 6.D; cf. also Broglia and Winther (2005).

With the help of (3.6.3) the expression in the squared bracket in (3.6.7) can be written as

$$[ ] = \frac{1}{4E_k E_q} (\Delta_k^* \Delta_q + (\Delta_k^* \Delta_q)^*) = \frac{1}{4E_k E_q} 2\Re(\Delta_k^* \Delta_q). \quad (3.6.9)$$

Making use of the relations

$$\begin{aligned} (U_k^2 - V_k^2)(U_q^2 - V_q^2) &= U_k^2 U_q^2 - U_k^2 V_q^2 - V_k^2 U_q^2 + V_k^2 V_q^2 \\ &= -(U_k^2 V_q^2 + V_k^2 U_q^2) + (U_k^2 U_q^2 + V_k^2 V_q^2), \end{aligned} \quad (3.6.10)$$

and

$$\begin{aligned} 1 &= (U_k^2 + V_k^2)(U_q^2 + V_q^2) = U_k^2 U_q^2 + U_k^2 V_q^2 + V_k^2 U_q^2 + V_k^2 V_q^2 \\ &= (U_k^2 V_q^2 + V_k^2 U_q^2) + (U_k^2 U_q^2 + V_k^2 V_q^2), \end{aligned} \quad (3.6.11)$$

one obtains,

$$1 - (U_k^2 - V_k^2)(U_q^2 - V_q^2) = 2(U_k^2 V_q^2 + V_k^2 U_q^2), \quad (3.6.12)$$

that is, twice the expression written in curly brackets in (3.6.7). Consequently

$$\{ \} = \frac{1}{2} (1 - (U_k^2 - V_k^2)(U_q^2 - V_q^2)) = \frac{1}{2} \left( 1 - \frac{\epsilon_k \epsilon_q}{E_k E_q} \right). \quad (3.6.13)$$

Thus, the sum of (3.6.9) and (3.6.13) leads to,

$$NUM = \frac{1}{2} \left( 1 - \frac{\epsilon_k \epsilon_q}{E_k E_q} + \frac{\Re(\Delta_k^* \Delta_q)}{E_k E_q} \right) \quad (3.6.14)$$

and

$$\Delta E_2 = - \sum_{kq} \frac{|T_{kq}|^2}{E_k + E_q} \left( 1 - \frac{\epsilon_k \epsilon_q}{E_k E_q} + \frac{\Re(\Delta_k^* \Delta_q)}{E_k E_q} \right). \quad (3.6.15)$$

With the help of (3.6.6) one can write

$$\Delta_k \Delta_q^* = \Delta_1 \Delta_2 e^{i(\phi_1 - \phi_2)} = \Delta_1 \Delta_2 (\cos(\phi_1 - \phi_2) + i \sin(\phi_1 - \phi_2)). \quad (3.6.16)$$

Thus

$$\Re(\Delta_k \Delta_q^*) = \Delta_1 \Delta_2 \cos(\phi_1 - \phi_2), \quad (3.6.17)$$

where  $\Re$  stands for real part. Making use of

$$\sum_k \rightarrow N_1 \int d\epsilon_1, \quad \sum_q \rightarrow N_2 \int d\epsilon_2 \quad (3.6.18)$$

where  $N_1$  and  $N_2$  are the density of levels of one spin at the Fermi energy one finally obtains

$$\begin{aligned}\Delta E_2 &\approx -N_1 N_2 \Delta_1 \Delta_2 \langle |T_{kq}|^2 \rangle \cos(\phi_1 - \phi_2) \int_{-\infty}^{\infty} \int_{-\infty}^{\infty} \frac{d\epsilon_1 d\epsilon_2}{E_1 E_2 (E_1 + E_2)} \\ &\approx -N_1 N_2 \langle |T_{kq}|^2 \rangle \cos(\phi_1 - \phi_2) 2\pi^2 \frac{\Delta_1 \Delta_2}{\Delta_1 + \Delta_2}\end{aligned}\quad (3.6.19)$$

Consequently, the maximum possible supercurrent is the same as the normal current at a voltage  $V_{equiv}$  equal to  $\pi \Delta_1 \Delta_2 / (\Delta_1 + \Delta_2)$ .

### 3.7 Phase coherence

The phase of a wavefunction and the number of nucleons (electrons in condensed matter) are conjugate variables: gauge invariance, i.e. invariance under phase changes, implies number conservation in the same way that rotational invariance implies angular momentum conservation.

Example:

$$\Psi = a_1^\dagger a_2^\dagger \cdots a_N^\dagger \Psi_{vac}.$$

Multiplying the creation operators by a phase factor,

$$a'^\dagger = e^{-i\phi} a^\dagger,$$

one can rewrite

$$\begin{aligned}\Psi &= (e^{i\phi} a'_1^\dagger)(e^{i\phi} a'_2^\dagger) \cdots (e^{i\phi} a'_N^\dagger) \Psi_{vac} \\ &= e^{iN\phi} \Psi'.\end{aligned}$$

Thus

$$-i \frac{\partial}{\partial \phi} \Phi = N e^{iN\phi} \Psi' = \Psi,$$

where

$$N = -i \frac{\partial}{\partial \phi}; \quad \phi = i \frac{\partial}{\partial N}$$

and

$$[\phi, N] = 1; \quad \Delta\phi \Delta N = 1.$$

In this case  $\Psi$  (wavefunction referred to the laboratory system) and  $\Psi'$  (wavefunction referred to the intrinsic system) represent the same state. A phase change for a gauge invariant function is just a trivial operation. Like to rotate a rotational invariant function. Quantum mechanically nothing happens rotating a spherical system (in 3D-, gauge, etc.) space.

The situation is very different in the case of the wavefunction

$$\begin{aligned} |BCS(\phi)\rangle_{\mathcal{K}} &= \prod_{\nu>0} (U_\nu + V_\nu a_\nu^\dagger a_{\bar{\nu}}^\dagger) |0\rangle, \\ &= \prod_{\nu>0} (U_\nu + e^{2i\phi} V_\nu a_\nu'^\dagger a_{\bar{\nu}}'^\dagger) |0\rangle, \\ &= \prod_{\nu>0} (U'_\nu + V'_\nu a_\nu'^\dagger a_{\bar{\nu}}'^\dagger) |0\rangle, \\ &= |BCS(\phi = 0)\rangle_{\mathcal{K}'}, \end{aligned}$$

where

$$U_\nu = |U_\nu| = U'_\nu; \quad V_\nu = e^{2i\phi} V'_\nu (V'_\nu = |V_\nu|),$$

and

$$|BCS(\phi)\rangle_{\mathcal{K}} = \left( \prod_{\nu>0} U_\nu \right) \sum_{n=0,1,2}^{N_0/2} e^{i2n\phi} \left( \sum_{\nu>0}^{N/2} \frac{c_\nu}{\sqrt{n}} P_\nu'^\dagger \right)^n |0\rangle,$$

with

$$c_\nu = \frac{V_\nu}{U_\nu}; \quad n : \# \text{ of pairs}; \quad P_\nu'^\dagger = a_\nu'^\dagger a_{\bar{\nu}}'^\dagger,$$

is a wavepacket in particle number,

$$\begin{aligned} |BCS(\phi)\rangle_{\mathcal{K}} &= \left( \prod_{\nu>0} U_\nu \right) \sum_n e^{i2n\phi} |2n\rangle, \\ &= \left( \prod_{\nu>0} U_\nu \right) \sum_n e^{i2n\phi} |N\rangle. \end{aligned} \tag{3.7.1}$$

Let us now apply the gauge angle operator

$$\begin{aligned} \hat{\phi}|BCS(\phi)\rangle_{\mathcal{K}} &= i \frac{\partial}{\partial N} |BCS(\phi)\rangle_{\mathcal{K}} \\ &= -\phi \left( \prod_{\nu>0} U_\nu \right) \sum_n e^{i2n\phi} |N\rangle = -\phi |BCS(\phi)\rangle_{\mathcal{K}}. \end{aligned}$$

Thus the state  $|BCS(\phi = 0)\rangle_{\mathcal{K}'}$  is rigidly aligned in gauge space in which it defines a privileged orientation ( $z'$ ).

An isolated nucleus will not remain long in this product type state. Due to the term  $(G/4) \left( \sum_{\nu>0} (U_\nu^2 + V_\nu^2) (\Gamma_\nu^\dagger - \Gamma_\nu) \right)^2$  in the residual quasiparticle Hamiltonian it will fluctuate, (QM, ZPF Goldstone mode) it will decay into a state

$$|N\rangle \sim \int d\phi e^{iN\phi} |BCS(\phi)\rangle_{\mathcal{K}}, \tag{3.7.2}$$

member of a pairing rotational band around neutron mass number  $N$ : for example the ground states of the Sn-isotopes around  $N_0 = 68$  (see Fig. 2.1.3). Because  $E_R = (\hbar^2/2I)(N - N_0)^2 = (G/4)(N - N_0)^2 = G/4(\frac{1}{\delta\phi})^2$  is the kinetic energy of rotation in (nuclear) gauge space, and  $G/4 \approx 25/(4N_0) \approx 0.0092$  MeV, the wavepacket (3.7.1) will decay<sup>35</sup> in the state (3.7.2) in a time of the order of  $\hbar/E_R \approx \hbar/(4 \times 0.0092 \text{ MeV}) (N = N_0 \pm 2) \approx 10^{-19} \text{ sec}$ . In other words, superfluid nuclei cannot be prepared, in isolation, in states with coherent superposition of different  $N$ -values. The common assumption that  $N$  is fixed,  $\phi$  meaningless is correct. This is also the case for real superconductors. In fact, the corresponding state (3.7.1) even if prepared in isolation would dissipate because there is actually a term in the energy of the superconductor depending on  $N$ , namely the electrostatic energy  $e(N - N_0)^2/2C = e^2/2C(\partial/\partial\phi)^2$ , where  $C$  is the electrostatic capacity. The system will dissipate, no matter how small  $\delta\phi$  is. In fact, let us assume  $\delta\phi = 1$  degree ( $= \pi/180 = 0.017$ ). The kinetic energy of rotation in gauge space is  $\sim (e^2/2C)(1/\delta)^2(\delta N\delta\phi/2\pi \sim 1)$ , and

$$\Delta E = \frac{1.44 \text{ fm MeV}}{1 \text{ cm } (1^\circ)^2} \sim 1.44 \times 10^{-13} \text{ MeV}, \quad (3.7.3)$$

which corresponds to an interval of time

$$\Delta t \approx \frac{\hbar}{1 \text{ MeV}} \frac{10^{13}}{1.44} \approx \frac{0.667 \times 10^{-21} \text{ sec}}{1.44} \times 10^{13} \approx 10^{-9} \text{ sec}. \quad (3.7.4)$$

The opposite situation is that of the case in which one considers different parts of the same superconductor. In this case one can define relative variables  $n = N_1 - N_2$  and  $\phi = \phi_1 - \phi_2$  and again  $n = -i\partial/\partial\phi$  and  $\phi = i\partial/\partial n$ . Thus, locally there is a superposition of different  $n$  states:  $\phi$  is fixed so  $n$  is uncertain. It is clear that there must be a dividing line between these two behaviors, perfect phase coherence and negligible coherence, namely the Josephson effect.

In the nuclear case, one can view the systems  $|BCS(A+2)\rangle$  and  $|BCS(A)\rangle$  as parts of a fermion superfluid (superconductor) which, in presence of a proton ( $p + (A+2)$ ) are in weak contact to each other, the  $d + |BCS(A+1)\rangle$  system (without scattering, running waves, but as a closed, virtual, channel) acting as the dioxide layer of a Josephson junction.

Clearly, again, the total phase of the assembly is not physical. However, the relative phases can be given a meaning when one observes, as one does in e.g.

---

<sup>35</sup>Within this context note that setting in phase at  $t = 0$  all the states in which a GDR breaks down through the hierarchy of doorway-states-coupling, they would dissipate like a wavepacket of free particles after  $10^{-22}$  sec (assuming  $\Gamma_{GDR} \approx 3 - 4$  MeV). It is of notice that the GDR will eventually branch into the ground state, although  $\Gamma_\gamma \ll \Gamma_{GDR}$ , in keeping with the fact that the  $t = 0$  phase coherent states are individually stationary. What is not stationary is its phase coherence. Pushing the analogy a step further, one can say that in quantum mechanics, while the outcome of an experiment is probabilistic the associated probability evolve in a deterministic way (Born (1926)). This is the reason why a large gamma ray detector will reveal a well defined peak of the resonant dipole state long after its lifetime deadline ( $\hbar/\Gamma$ ). Also, while one can obtain a completely (classical) picture of a face making use of single photons, provided one waits long enough.

metallic superconductors, that electrons can pass back and forth through the barrier, leading to the possibility of coherence between states in which the total number of electrons is not fixed *locally*. Under such conditions there is, for instance, a coherence between the state with  $N/2$  electrons in one half of the block and  $N/2$  in the other, and that with  $(N/2) + 2$  on one side and  $(N/2) - 2$  on the other.

Under favorable conditions, in particular of  $Q$ -value for the different channels involved and, similarly to the so called backwards rise effect, one may, arguably, observe signals of the coherence between systems  $(A + 2)$  and  $A$  in the elastic scattering process  $^{A+2}X + p \rightarrow ^{A+2}X + p$ ,  $^{A+2}X$  denoting a member of a pairing rotational band (cf. Fig. 3.7.1, see also Fig 2.1.3). It is of notice that the process  $^{A+2}X + p \rightarrow ^{A+1}X + d \rightarrow ^{A+2}X + p$  is likely to be the dominant one concerning the optical potential describing the  $^{A+2}X + p$  scattering process. Because  $P_2 \approx P_1$ , a likely better estimate of  $U + iW$  can be obtained taking into account also the transfer back and forth of two nucleons. In keeping with the fact that the sum of the simultaneous and non-orthogonality contributions are much smaller than the successive transfer, only this last process is shown in the NFT reaction-structure diagram displayed in Fig. 3.7.1.

Whether an effect which may parallel that shown in (c) (backwards rise) can be seen or not depends on a number of factors, but very likely it is expected to be a weak effect. This was also true in the case of the Josephson effect in its varied versions (AC, DC, etc.). In fact, its observation required to take into account the effect of the earth magnetic field, let alone quantal and thermal fluctuations.

## 3.8 Hindsight

The formulation of superconductivity (BCS theory) described by Gor'kov<sup>36</sup> allows, among other things for a simple visualization of spatial dependences. In this formulation  $F(\mathbf{x}, \mathbf{x}')$  is the amplitude for two Fermions (electrons) at  $\mathbf{x}, \mathbf{x}'$ , to belong to the Cooper pair (within the framework of nuclear physics cf. e.g. Fig. 2.6.3  $\Psi_0(\mathbf{r}_1, \mathbf{r}_2)$ ). The phase of  $F$  is closely related to the angular orientation of the spin variable in Anderson's quasiparticle formulation of BCS theory<sup>37</sup>. The gap function  $\Delta(x)$  is given by  $V(\mathbf{x})F(\mathbf{x}, \mathbf{x})$  where  $V(\mathbf{x})$  is the local two-body interaction at the point  $\mathbf{x}$ . In the insulating barrier between the two superconductors of a Josephson junction,  $V(\mathbf{x})$  is zero and thus  $\Delta(x)$  is also zero.

The crucial point is that vanishing  $\Delta(x)$  does not imply vanishing  $F$ , provided, of course, that one has within the insulating barrier, a non-zero particle (electron) density, resulting from the overlap of densities from right (R) and left (L) superconductors. Now, these barriers are such that they allow for one-electron-tunneling with a probability of the order of  $10^{-10}$  and, consequently, the above requirement is

---

<sup>36</sup>Gor'kov, L.P. (1959).

<sup>37</sup>Anderson (1958); within the framework of nuclear physics cf. e.g. Bohr and Ulfbeck (1988), Potel, G. et al. (2013b) and references therein.

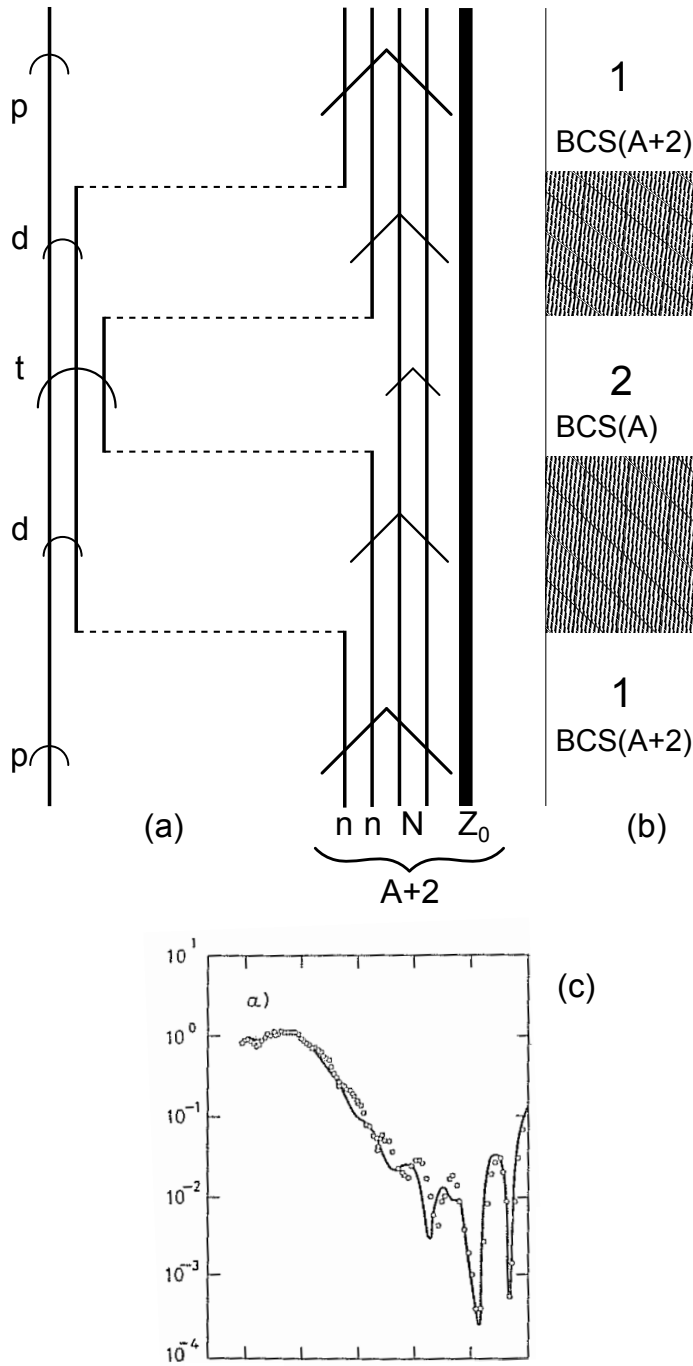


Figure 3.7.1: Gedanken experiment concerning the possibility of observing weak coupling coherence phenomena between states  $|BCS(A + 2)\rangle$  and  $|BCS(A)\rangle$  in an elastic reaction involving superfluid nuclei (a), e.g.  $p + {}^{120}\text{Sn} \rightarrow p + {}^{120}\text{Sn}$ , the system  ${}^{119}\text{Sn} + d$  acting as a dynamical barrier (hatched areas arguably play role of that of dioxide layers in Josephson junctions) between the two even  $N$  superfluid systems arising from the successive transfer of two nucleons (b) and eventually allowing for a time dependent gauge phase difference between the  $(A + 2)$  and  $A$  superfluid systems, thus leading, in the case in which  $Q$ -value effects are appropriate, to an oscillating enhancement of the elastic cross section at large angles as observed, for quite different reasons, in the case of the elastic angular distribution of the reaction  ${}^{16}\text{O} + {}^{28}\text{Si}$  (c) (cf. Pollarolo and Broglia (1984)).

fulfilled<sup>38</sup>. Nonetheless, conventional (normal) simultaneous pair transfer, with a probability of  $(10^{-10})^2$  will not be observed. But because one electron at a time can tunnel profiting of the small, but finite electron density within the layer,  $F(\mathbf{x}, \mathbf{x}')$  can have large amplitude for electrons, on each side of the barrier (i.e. L and R), separated by distances  $|\mathbf{x} - \mathbf{x}'|$  up to the coherence length. Hence, for barriers thick to only allow for essentially the tunneling of one electron at a time, but thin compared with the coherence length, two electrons on opposite sides of the barrier can still be correlated and the pair current can consistent. An evaluation of its value shows that, at zero temperature, the pair current is equal to the single particle current at an equivalent voltage<sup>39</sup>  $\pi\Delta/2e$ .

The translation of the above parlance to the language of nuclear physics has to come to terms with the basic fact that nuclei are self-bound, finite many-body systems in which the surface, as well as space quantization, play a very important role both as a static element of confinement, as well as a dynamic source for renormalization effects<sup>40,41</sup>. Under the influence of the average potential which can be viewed as very strong external field ( $|V_0| \approx 50$  MeV), Cooper pairs ( $|E_{corr}| \approx 1.5$  MeV; see Fig. 2.5.1) will become constrained within its boundaries with some amount of spill out. In the case of the single open shell superfluid nucleus  $^{120}\text{Sn}$ , the boundary can be characterized by the radius  $R_0 \approx 6$  fm ( $\ll \xi \approx 30$  fm), the spill out being connected with the diffusivity  $a \approx 0.65$  fm.

Let us now consider a two nucleon transfer reaction in the collision  $\text{Sn}+\text{Sn}$  assuming a distance of closest approach of  $\approx 14$  fm, in which the two nuclear surfaces are separated by  $\approx 2$  fm (Fig 3.4.1). In keeping with the fact that this distance is about  $3 \times a$ , the heavy ion system will display a few percent (of saturation) density overlap in the interacting region. Ever so small this overlap of the nuclear surfaces, and so narrow the hole between the two leptodermic systems resulting from it, Cooper pairs can now extend over the two volumes, in a similar way as electron Cooper pairs could be partially found in the R and L superconductors in a Josephson junction. If this is the case, Cooper pair partners can be at distance as large as 26 fm, of the same order of magnitude of the correlation length. In other words, in the reaction  $\text{Sn}+\text{Sn} \rightarrow \text{Sn(gs)}+\text{Sn(gs)}$  one expects (mainly successive) Cooper pair transfer of two neutrons which are away from each other by tens of

<sup>38</sup>Pippard (2012) see also McDonald (2001).

<sup>39</sup>In the case of Pb at low temperatures ( $< 7.19$  K (0.62 meV)) this voltage is  $\approx 1$  meV/e = 1 mV (Ambegaokar and Baratoff (1963); McDonald (2001); Tinkham (1996)).

<sup>40</sup>Within this context it is of notice that the liquid drop model is a very successful nuclear model, able to accurately describe not only large amplitude motion (fission, exotic decay, low-lying collective density and surface vibrations, cf. e.g. Bohr and Wheeler (1939), Barranco, F. et al. (1990), Bertsch (1988), see also Brink, D. and Broglia (2005) and references therein), but also the masses of nuclides (cf. e.g. Moller and Nix), provided the superfluid inertia and shell corrections respectively, are properly considered. Thus, it is an open question whether in the quest of developing more predictive theoretical tools of the global nuclear properties one should develop ever more “accurate” zero range (Skyrme-like) forces, or deal with the long wavelength, renormalization effects and induced interaction.

<sup>41</sup>Broglia, R. A. (2002).

fm.

An example of the fact that Cooper pairs will “expand” if the external mean field is weakened, is provided by  $^{11}\text{Li}$  in which case, profiting of the weak binding ( $\approx 380$  keV), the extension of the constrained Cooper pair ( $\approx 4.58$  fm  $\pm 0.13$  fm) is similar to that expected in a nucleus of mass number  $A \approx 60$ , assuming a standard radial behavior, i.e.  $r_0 A^{1/3}$  fm. In keeping with this scenario, it could be expected that moving from one neutron pair addition  $0^+$  mode of the  $N = 6$  isotones to another one ( $|^{11}\text{Li}(\text{gs})\rangle$ ,  $|^{12}\text{Be}(\text{gs})\rangle$  and  $|^{12}\text{Be}(0^{++}; 2.24 \text{ MeV})\rangle$ ) one would see the system expanding, contracting and expanding again, respectively, in keeping with the fact that the external (mean) field is weak, strong, weak respectively, as testified by  $S_{2n}$  (380 keV, 3672 keV, 1432 keV). Within this context, the dipole resonance built on top of them is expected to vary in energy from very low ( $< 1$  MeV) to high (2.71 MeV) to low (0.460 MeV), that is from a symbiotic, to an independent, and, likely, to a (quasi) symbiotic role again. Within this context, in Fig. 3.8.1 an overall view of the pairing vibrational modes associated with  $N = 6$  parity inverted closed shell isotones, together with low-energy  $E1$ -strength modes is given. The possible candidates to the role of neutron halo pair addition modes and symbiotic state are explicitly indicated (boxed levels). In Fig. 3.8.2 the  $^{11}\text{Li}(\text{gs})$ ,  $^{12}\text{Be}(\text{gs})$  and  $\text{Be}(0^{++}; 2.25 \text{ MeV})$  wavefunctions and  $|\Psi_0(\mathbf{r}_1, \mathbf{r}_2)|^2$  probability distribution of one Cooper pair partner with respect to the other located at a fixed distance from the CM of the nucleus under study are shown (see also Fig. 2.6.3 (II)). While the results associated with the two ground states have been tested in connection with the experimental findings (Barranco, F. et al. (2001); Potel et al. (2010, 2014); Gori et al. (2004)), much less is known regarding the accuracy of the predictions associated with  $^{12}\text{Be}(0^{++})$ .

## Appendix 3.A Medium polarization effects and pairing

### 3.A.1 Nuclei

#### Polarization contributions to the bare nucleon–nucleon pairing interaction through elementary modes of excitation

Elementary modes of excitation constitute a basis of states in which correlations, as found in observables, play an important role. As a consequence, it allows for an economic solution of the nuclear many–body problem of structure and reaction. A first step in this quest is to eliminate the non–orthogonality associated with single–particle motion in different nuclei (target and projectile (*reaction*)). Also between single–particle degrees of freedom and collective modes (vibrations and rotations (*structure*)) typical of an overcomplete, Pauli principle violating, basis. This can be done by diagonalizing, making use of the rules of nuclear field theory (NFT), the particle–vibration coupling (PVC), and the  $v_{np}$  ( $v$  : four point vertex, bare  $NN$ –) interaction. In this way one obtains quantities (energies, transition probabilities, absolute value of reaction cross sections) which can be directly compared

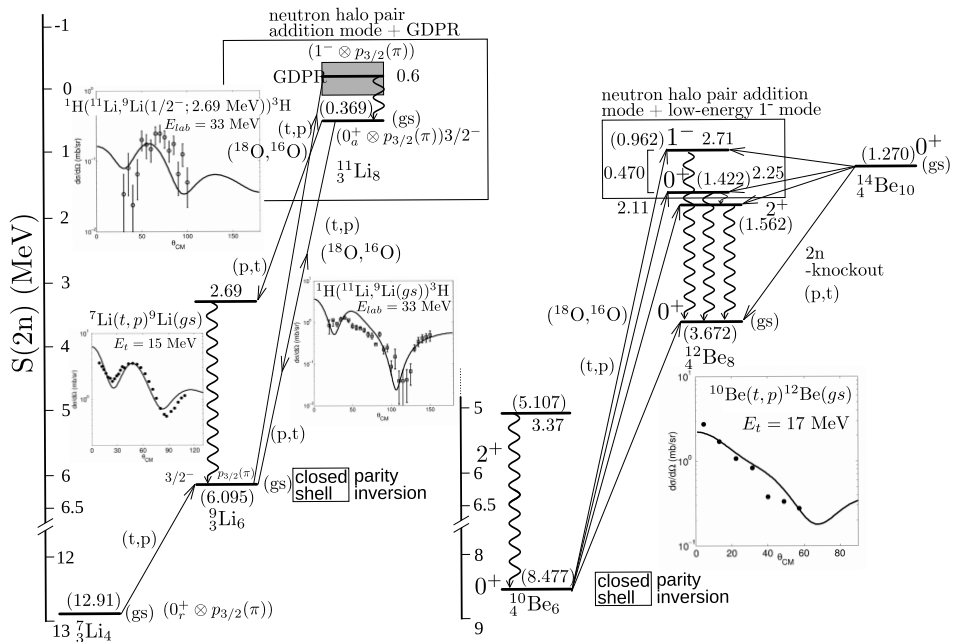
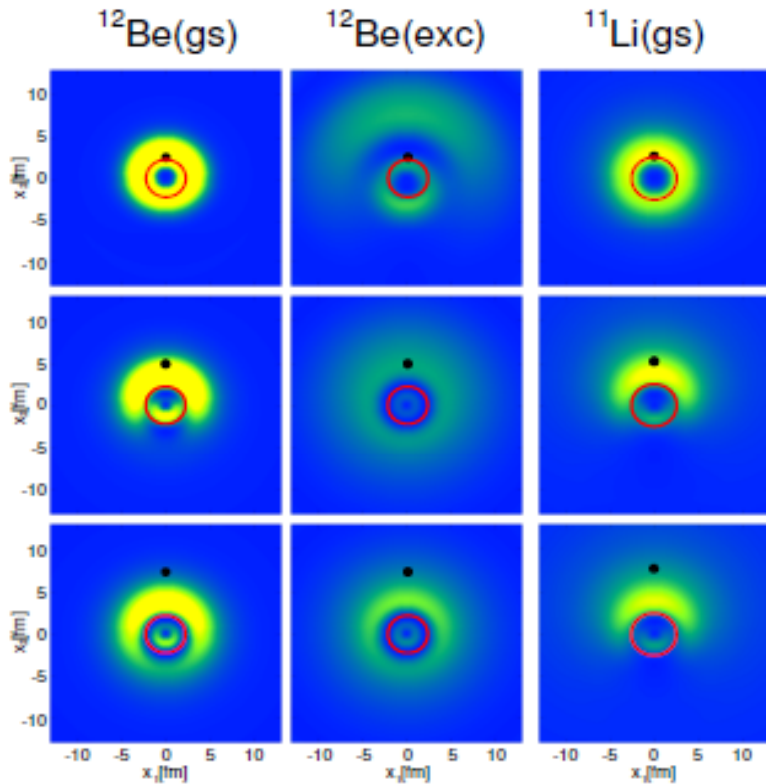


Figure 3.8.1: Monopole pairing vibrational modes associated with  $N = 6$  parity inverted closed shell isotones, together with low-energy E1-strength modes. The levels are displayed as a function of the two-neutron separation energies  $S(2n)$ . These quantities are shown in parenthesis on each level, the excitation energies with respect to the ground state are quoted in MeV. Absolute differential cross sections from selected (t,p) and (p,t) reactions calculated as described in the text (cf. Potel et al. (2010, 2014)), in comparison with the experimental data (Young and Stokes (1971); Fortune et al. (1994)).



$$|0\rangle_\nu = |0\rangle + \alpha|(p,s)_{1-} \otimes 1^-; 0\rangle + \beta|(s,d)_{2+} \otimes 2^+; 0\rangle + \gamma|(p,d)_{3-} \otimes 3^-; 0\rangle$$

$$|0\rangle_\nu = a|s^2(0)\rangle + b|p^2(0)\rangle + c|d^2(0)\rangle$$

	<sup>11</sup> Li(gs)	<sup>12</sup> Be(gs)	<sup>12</sup> Be(exc)
$\alpha$	0.7	0.10	0.08
$\beta$	0.1	0.30	-0.39
$\gamma$	-	0.37	-0.1
$a$	0.45	0.37	0.89
$b$	0.55	0.50	0.17
$c$	0.04	0.60	0.19

Figure 3.8.2

with the experimental findings. Such a protocol can be carried out, in most cases, within the framework of perturbation theory. For example, second order perturbation theory, in both reaction and structure, as exemplified in Fig. 1.9.3 displaying a NFT (r+s) graphical representation of contributions to the  $^{11}\text{Li}(p,t)^9\text{Li}(\text{gs})$  and  $^{11}\text{Li}(p,t)^9\text{Li}(1/2^-; 2.69 \text{ MeV})$  processes (see also Fig. 6.1.3). As a result, single-particle states move in a gas of vibrational quanta and become clothed by coupling to them. The quanta couple, in turn, to doorway states which renormalize their properties through self energy and vertex corrections. Similar couplings renormalize the bare  $NN$ -interaction in the different channels. In particular in the  $^1S_0$  (pairing) channel.

Also as a result of their interweaving, the variety of elementary modes of excitation may break in a number of states, eventually acquiring a lifetime and, within a coarse grain approximation, a damping width (imaginary component of the self energy). Moving into the continuum, as for example in the case of direct reactions, one such component is the imaginary part of the optical potential operating in the particular channel selected. It can be calculated microscopically using similar techniques and elements as e.g. those used in the calculation of the damping width of giant resonances. With the help of dispersion relations, the real part of the optical potential can be obtained from the knowledge of the energy dependence of the absorptive potential. In this way, the consistency circle structure–reaction based on elementary modes and codified by NFT could be closed. The rich variety of emergent properties found along the way eventually acquiring a conspicuous level of physical validation. In the case of halo exotic nuclei, in particular in the case of  $^{11}\text{Li}$  (bootstrap, Van der Waals Cooper binding, halo pair addition mode (symbiosis of pairing vibration and pigmy) being few of the associated emergent properties) one is rather close to his goal. At that time it would be possible, arguably if there is one, to posit that the *ultima ratio* of structure and reactions, in any case that associated with pairing and Cooper pair transfer in nuclei, have been unveiled<sup>42</sup>

### Effective moments

At the basis of the coupling between elementary modes of excitation, for example of single-particle motion and of collective vibrations, is the fact that, in describing the nuclear structure it is necessary to make reference to both (all) of them simultaneously and in an unified way.

Within the harmonic approximation the above statement is economically embodied in e.g. the relation existing between the collective ( $\hat{\alpha}$ ) and the single-

---

<sup>42</sup>In the above paragraph we allow ourselves to paraphrase Jacques Monod writing in connection with biology and life: *L'ultima ratio de toutes les structures et performances téléonomiques des êtres vivants est donc enfermée dans les séquences des radicaux des fibres polypeptidiques "embryons" de ces démons de Maxwell biologiques que sont les protéines globulaires. En un sens, très réel, c'est à ce niveau d'organisation chimique qui git, s'il y en a un, le secret de la vie. Et saurait-on non seulement décrire les séquences, mais énoncer la loi d'assemblage à laquelle obéissent, on pourrait dire que le secret est percé, l'ultima ratio découverte (J. Monod, *Le hasard et la nécessité*, Editions du Seuil, Paris, 1970).*

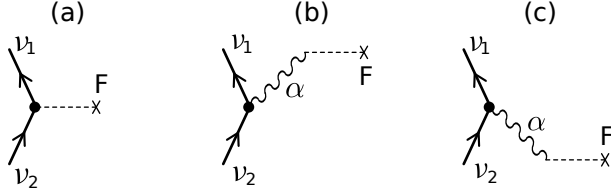


Figure 3.A.1: (a)  $F$ -moment of single-particle and (b,c) renormalization effects induced by the collective vibration  $\alpha$ .

particle ( $\hat{F}$ ) representation of the operator creating a particle-hole excitation. That is<sup>43</sup>,

$$\begin{aligned}
 \hat{F} &= \left\{ \langle k|F|\tilde{i}\rangle \Gamma_{ki}^\dagger + \langle \tilde{i}|F|k\rangle \Gamma_{ki} \right\} \\
 &= \sum_{k,i,\alpha'} X_{ki}^{\alpha'} \Gamma_{\alpha'}^\dagger - Y_{ki}^{\alpha'} \Gamma_{\alpha'} \\
 &= \sum_{\alpha'} \Lambda_{\alpha'} \sum_{ki} \frac{|\langle \tilde{i}|F|k\rangle|^2}{(\epsilon_k - \epsilon_i)^2 - (\hbar\omega_{\alpha'})^2} (\Gamma_{\alpha'}^\dagger + \Gamma_{\alpha'}) \\
 &= \sum_{\alpha'} \frac{\Lambda_{\alpha'}}{\kappa} (\Gamma_{\alpha'}^\dagger + \Gamma_{\alpha'}) = \sum_{\alpha'} \sqrt{\frac{\hbar\omega_{\alpha'}}{2C'_\alpha}} (\Gamma_{\alpha'}^\dagger + \Gamma_{\alpha'}) = \hat{\alpha}. \tag{3.A.1}
 \end{aligned}$$

This is a consequence of the self consistent relation

$$\delta U(r) = \int d\mathbf{r}' \delta\rho(r) v(|\mathbf{r}-\mathbf{r}'|), \tag{3.A.2}$$

existing between density (collective) and potential (single-particle) distortion, typical of normal modes of many-body systems.

Relation (3.A.1) implies that at the basis of these normal modes one finds the (attractive  $\kappa < 0$ ) separable interaction

$$H = \frac{\kappa}{2} \hat{F} \hat{F}, \tag{3.A.3}$$

but where now (Fig. 3.A.1 (a))

$$\hat{F} = \sum_{\nu_1, \nu_2} \langle \nu_1 | F | \nu_2 \rangle a_{\nu_1}^\dagger a_{\nu_2}, \tag{3.A.4}$$

is a general single-particle operator, while  $\hat{F}$  in Eq. (3.A.1) is its harmonic representation acting in the particle ( $k$ )-hole ( $i$ ) space,  $\Gamma_{ki}^\dagger$  and  $\Gamma_{ki}$  being (quasi) bosons, i.e. respecting the commutation relation

$$[\Gamma_{ki}, \Gamma_{k'i'}^\dagger] = \delta(k, k') \delta(i, i'). \tag{3.A.5}$$

---

<sup>43</sup>cf. Bohr, A. and Mottelson (1975), cf. also Brink, D. and Broglia (2005) App. C.

In other words, the representation (3.A.1), which is at the basis of the RPA (as well as QRPA), does not allow for scattering vertices, processes which become operative by rewriting (3.A.3) in terms of the particle–vibration coupling Hamiltonian

$$H_c = \kappa \hat{\alpha} \hat{F} \quad (3.A.6)$$

It is of notice that  $\kappa$  is negative for an attractive field. Let us now calculate the effective single-particle moments (cf. Fig. 3.A.1 (b)),

$$\begin{aligned} \langle v_2 | \hat{F} | v_1 \rangle_{(b)} &= \frac{\langle v_2 | \hat{F} | v_2, n_\alpha = 1 \rangle \langle v_2, n_\alpha = 1 | H_c | v_1 \rangle}{(\epsilon_{v_1} - \epsilon_{v_2}) - \hbar\omega_\alpha}, \\ &= \frac{\langle 0 | \alpha | n_\alpha = 1 \rangle \kappa \alpha \langle v_2 | F | v_1 \rangle}{(\epsilon_{v_1} - \epsilon_{v_2}) - \hbar\omega_\alpha}, \\ &= \kappa \alpha^2 \frac{\langle v_2 | F | v_1 \rangle}{(\epsilon_{v_1} - \epsilon_{v_2}) - \hbar\omega_\alpha}, \end{aligned} \quad (3.A.7)$$

and (Fig. 3.A.1 (c))

$$\begin{aligned} \langle v_2 | \hat{F} | v_1 \rangle_{(c)} &= \frac{\langle v_2 | H_c | v_1, n_\alpha = 1 \rangle \langle v_1, n_\alpha = 1 | F | v_1 \rangle}{\epsilon_{v_2} - (\epsilon_{v_1} + \hbar\omega_\alpha)}, \\ &= \kappa \alpha^2 \left( -\frac{\langle v_2 | F | v_1 \rangle}{(\epsilon_{v_1} - \epsilon_{v_2}) + \hbar\omega_\alpha} \right), \end{aligned} \quad (3.A.8)$$

leading to

$$\begin{aligned} \langle v_2 | \hat{F} | v_1 \rangle_{(b)} + \langle v_2 | \hat{F} | v_1 \rangle_{(c)} &= \kappa \alpha^2 \frac{2\hbar\omega_\alpha \langle v_2 | F | v_1 \rangle}{(\epsilon_{v_1} - \epsilon_{v_2})^2 - (\hbar\omega_\alpha)^2}, \\ &= \frac{\kappa}{C_\alpha} \frac{(\hbar\omega_\alpha)^2 \langle v_2 | F | v_1 \rangle}{(\epsilon_{v_1} - \epsilon_{v_2})^2 - (\hbar\omega_\alpha)^2}. \end{aligned} \quad (3.A.9)$$

This is in keeping with the fact that the ZPF of the  $\alpha$ -vibrational mode is,

$$\alpha = \sqrt{\frac{\hbar\omega_\alpha}{2C_\alpha}}, \quad (3.A.10)$$

the particle–vibration coupling strength being

$$\Lambda_\alpha = \kappa \alpha. \quad (3.A.11)$$

Together with  $\langle v_2 | \hat{F} | v_1 \rangle_{(a)} = \langle v_2 | F | v_1 \rangle$  (see Fig. 3.A.1 (a)) one obtains

$$\langle v_2 | \hat{F} | v_1 \rangle = (1 + \chi(\omega)) \langle v_2 | F | v_1 \rangle, \quad (3.A.12)$$

where

$$\chi(\omega) = \frac{\kappa}{C_\alpha} \frac{\omega_\alpha^2}{\omega^2 - \omega_\alpha^2} \quad (3.A.13)$$

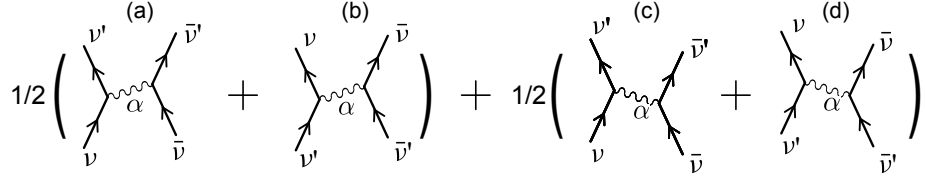


Figure 3.A.2: Diagrams associated with nuclear pairing induced interaction.

is the polarizability coefficient while

$$\omega = |\epsilon_{\nu_1} - \epsilon_{\nu_2}|/\hbar. \quad (3.A.14)$$

In the static limit, e.g. in the case in which  $\alpha$  is a giant resonance and  $\omega_\alpha \gg \omega$  one obtains

$$\chi(0) = -\frac{\kappa}{C}. \quad (3.A.15)$$

The sign of  $\chi(0)$  is opposite to that of  $\kappa$ , since the static polarization effect produced by an attractive coupling ( $\kappa < 0$ ) is in phase with the single-particle moment, while a repulsive coupling ( $\kappa > 0$ ) implies opposite phases for the polarization effect and the one-particle moment<sup>44</sup>.

Let us now calculate the two-body pairing induced interaction (Fig. 3.A.2) arising from the exchange of collective vibrations<sup>45</sup> (summing over the two time orderings and symmetrizing between initial and final states)<sup>46</sup>

$$\begin{aligned} v_{\nu\nu'}^{ind}(a) + v_{\nu\nu'}^{ind}(b) &= \kappa^2 \alpha^2 |\langle \nu' | F | \nu \rangle|^2 \left( \frac{1}{\epsilon_\nu - \epsilon_{\nu'} - \hbar\omega_\alpha} + \frac{1}{\epsilon_{\nu'} - \epsilon_\nu - \hbar\omega_\alpha} \right), \\ &= \kappa^2 \alpha^2 |\langle \nu' | F | \nu \rangle|^2 \left( \frac{1}{(\epsilon_\nu - \epsilon_{\nu'}) - \hbar\omega_\alpha} - \frac{1}{(\epsilon_\nu - \epsilon_{\nu'}) - \hbar\omega_\alpha} \right), \\ &= \Lambda_\alpha^2 |\langle \nu' | F | \nu \rangle|^2 \left( \frac{2\hbar\omega_\alpha}{(\epsilon_\nu - \epsilon_{\nu'})^2 - (\hbar\omega_\alpha)^2} \right), \\ &= v_{\nu\nu'}^{ind}(c) + v_{\nu\nu'}^{ind}(d). \end{aligned} \quad (3.A.16)$$

Thus

$$\begin{aligned} v_{\nu\nu'}^{ind} &= \frac{1}{2} (v_{\nu\nu'}^{ind}(a) + v_{\nu\nu'}^{ind}(b)) + \frac{1}{2} (v_{\nu\nu'}^{ind}(c) + v_{\nu\nu'}^{ind}(d)) \\ &= \Lambda_\alpha^2 |\langle \nu' | F | \nu \rangle|^2 \left( \frac{2\hbar\omega_\alpha}{(\epsilon_\nu - \epsilon_{\nu'})^2 - (\hbar\omega_\alpha)^2} \right). \end{aligned} \quad (3.A.17)$$

The diagonal matrix element,

$$v_{\nu\nu}^{ind} \equiv -\frac{2\Lambda_\alpha^2 |\langle \nu | F | \nu \rangle|^2}{\hbar\omega_\alpha},$$

<sup>44</sup>Bohr, A. and Mottelson (1975); Mottelson (1962).

<sup>45</sup>In the present discussion we do not consider spin modes. For details see e.g. Idini et al. (2015). See also Bortignon et al. (1983).

<sup>46</sup>Cf. Brink, D. and Broglia (2005) p. 217.

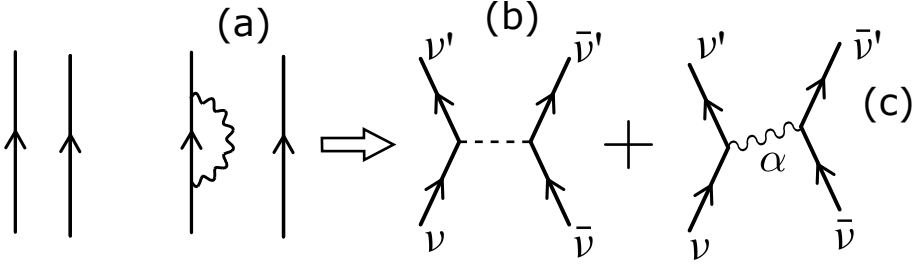


Figure 3.A.3: Starting with two bare nucleons moving around a closed shell system  $N_0$  in Hartree–Fock orbitals (arrowed lines far left), a graphical (NFT) representation of (a) self energy processes and of (b) bare and (c) induced pairing interactions are displayed.

testifies to the fact, for values of  $\omega_\alpha \gtrsim \omega$ , with

$$\omega = |\epsilon_\nu - \epsilon_{\nu'}|/\hbar, \quad (3.A.18)$$

namely the frequencies of the single-particle excitation energy, the induced pairing interaction is attractive. Summing to (3.A.17) the matrix element of the bare interaction (3.A.3), (Fig. 3.A.3)

$$v_{\nu\nu'}^{bare} = \kappa |\langle \nu' | F | \nu \rangle|^2 \quad (3.A.19)$$

and making use of (3.A.13) one obtains for the total pairing matrix element<sup>47</sup>

$$v_{\nu\nu'} = v_{\nu\nu'}^{bare} (1 + \chi(\omega)) = v_{\nu\nu'}^{bare} \left( 1 + v_{\nu\nu'}^{bare} \Pi_{\nu\nu'}(\omega, \omega_\alpha) \right), \quad (3.A.20)$$

where

$$\Pi_{\nu,\nu'} = \begin{cases} \left( C_\alpha |\langle \nu' | F | \nu \rangle|^2 \right)^{-1} \frac{\omega_\alpha^2}{\omega^2 - \omega_\alpha^2}, \\ \left( D_\alpha |\langle \nu' | F | \nu \rangle|^2 \right)^{-1} \frac{1}{\omega^2 - \omega_\alpha^2}. \end{cases} \quad (3.A.21)$$

Concerning  $\omega$  see the definition (3.A.14). It is of notice that in the second expression of  $\Pi_{\nu,\nu'}$  the inertia of the phonon appears in the denominator, similar to the factor  $(Z/AM)$  in (3.A.68) below.

Let us now rewrite (3.A.20) as

$$v_{\nu\nu'} = v_{\nu\nu'}^{bare} \left( 1 + |\chi(0)| \frac{\omega_\alpha^2}{\omega_\alpha^2 - \omega^2} \right), \quad (3.A.22)$$

<sup>47</sup>Within the framework of (3.A.3) and of its role in (3.A.20) one finds, in the case of superconductivity in metals to be discussed below, that the bare unscreened Coulomb interaction can be written as

$$U_c(r) = \frac{1}{2} \sum_{i,j} \frac{q_i q_j}{|\mathbf{r}_i - \mathbf{r}_j|},$$

$i, j$  running over all particles (nuclei and electrons) and  $q_i = -e$  for electrons and  $Ze$  for nuclei.

to discuss two ( $i = 1, 2$ ) particular situations of interest:

$$1) \quad \omega = \omega_\alpha - \delta\omega/2, \quad (\delta\omega \ll \omega_\alpha), \quad (3.A.23)$$

$$2) \quad \omega_\alpha \gg \omega. \quad (3.A.24)$$

That is

$$\lim_{\omega \rightarrow i} \frac{\omega_\alpha^2}{\omega_\alpha^2 - \omega^2} = \begin{cases} \frac{\omega_\alpha}{\delta\omega} \gg 1 & (i = 1) \text{ plastic-}\alpha \text{ modes} \\ 1 & (i = 2) \text{ elastic-}\alpha \text{ modes} \end{cases} \quad (3.A.25)$$

The first situation is typical of low-lying collective surface vibrations. The second of high lying giant resonances. While in this last case one can parametrize the effect in terms of constant effective moments<sup>48</sup>, the explicit treatment of the state- ( $\omega$ -dependence) of the first one is unavoidable.

Let us conclude this section by making a simple estimate of the contribution of the induced pairing interaction to the (empirical) nuclear pairing gap. For this purpose we introduce the quantity

$$\lambda = N(0)v_{vv'}^{ind} \quad (3.A.26)$$

where  $N(0)$  is the density of levels of a single spin orientation at the Fermi energy. The above quantity is known as the nuclear mass enhancement factor. This is because of the role it plays in the nucleon  $\omega$ -mass

$$m_\omega = (1 + \lambda)m. \quad (3.A.27)$$

Systematic studies of this quantity, and of the related discontinuity occurring by the single-particle occupation number at the Fermi energy, namely  $Z_\omega = (m/m_\omega)$  testifies to the fact that  $\lambda \approx 0.4$ .

The BCS expressions of the pairing gap in terms of  $\lambda$  are

$$\Delta = \begin{cases} 2\hbar\omega_D e^{-1/\lambda}, & (\text{weak coupling } \lambda \ll 1) \\ \hbar\omega_D \lambda, & (\text{strong coupling } \lambda \geq 1) \end{cases} \quad (3.A.28)$$

where  $\omega_D$  is the limiting frequency of the low-lying collective modes of nuclear excitation, typically of quadrupole and octupole vibrations. While for weak coupling one can use  $\hbar\omega_D \approx 10$  MeV, for the strong coupling situation it seems more proper  $\hbar\omega_D \approx 2$  MeV.

Making use of  $\lambda = 0.4$ , intermediate between weak and strong coupling situation one obtains

$$\Delta \approx 1.6 \text{ MeV} \quad (3.A.29)$$

and

$$\Delta \approx 0.8 \text{ MeV}, \quad (3.A.30)$$

---

<sup>48</sup>See e.g. Bohr, A. and Mottelson (1975) pp. 421 and 432.

to be compared with the empirical value

$$\Delta \approx 1.4 \text{ MeV} \quad (3.A.31)$$

of superfluid medium heavy mass nuclei like  $^{120}\text{Sn}$ .

While the relations (3.A.28) can hardly be relied to provide a quantitative number, they testify to the fact that induced pairing is expected to play an important role in nuclei. These expectations have been confirmed by detailed confrontation of theory and experiment<sup>49</sup>.

### Hindsight

Static polarization effects can be important in clothing single-particle states. For example, effective charges and induced interactions associated with moments induced by giant resonances<sup>50</sup>. However, retarded  $\omega$ -dependent self-energy effects and induced interactions are essential in describing structure and reactions of many-body systems. Examples are provided by the bootstrap binding of the halo neutrons (pair addition mode) to  $^9\text{Li}$ , leading to the fragile  $|^{11}\text{Li}(gs)\rangle$ , displaying a  $S_{2n} \approx 0.380$  MeV as compared to typical values of  $S_{2n} \approx 18$  MeV as far as structure goes, and by the  $^1\text{H}(^{11}\text{Li}, ^9\text{Li}(1/2^-; 2.69 \text{ MeV}))^3\text{H}$  population of the lowest member of the  $(2^+ \times p_{3/2}(\pi))_{J^-}$  multiplet of  $^9\text{Li}$ , as far as reaction goes. If there was need for support coming from other fields of research, one can mention just two: van der Waals force and superconductivity.

It was recognized early in the study of dipole-dipole interaction in atomic systems that, of the variety of contributions to the van der Waals interaction, the retarded, fully quantal contribution, arising from (dipole) zero point fluctuations (ZPF) of the two interacting atoms or molecules, and the only active also in the case of non-polar molecules<sup>51</sup>, play an overwhelming role, static-induced interactions being less important (App. 2.D). A consequence of this result is the fact that the limiting size of globular proteins ( $\approx 50$  Å) is controlled by the strong damping undergone by the retarded contribution to the amino acid interaction, when the frequency associated with the back and forth propagation of the force matches the molecules electronic frequencies<sup>52</sup>.

---

<sup>49</sup>See e.g. Idini et al. (2015).

<sup>50</sup>See e.g. Bohr, A. and Mottelson (1975), Eqs. (6-217) and (6-228).

<sup>51</sup>Within this context van der Waals and gravitation are two forces which are universally operative, acting among all bodies.

<sup>52</sup>It is of notice that similar arguments (cf. Sect. 2.6) are at the basis of the estimate (2.6.5) concerning the size of the halo nucleus  $^{11}\text{Li}$ , a quantity which is influenced to a large extent by the maximum distance (correlation length) over which partners of a Cooper pair are virtually (it materializes only if particle, normal, density allows for) but solidly anchored to each other (localized), and have to be seen as an (extended) bosonic entity and not as two fermions. The fact that Cooper pair transfer proceeds mainly in terms of successive transfer controlled by the single-particle mean field, reinforces the above physical picture of nuclear pairing. Even under the effect of extremely large, as compared to the pair correlation energy, external single-particle fields, namely that of target and projectile, the Cooper pair field extends over the two nuclei, permeating the whole summed nuclear volume also through a tiny density overlap.

Concerning superconductivity, the overscreening effect which binds weakly Cooper pairs stems from a delicate  $\omega$ -dependent phenomenon leading, eventually, to one of the first macroscopic manifestations of quantum mechanics, as e.g. “permanent” magnetic fields associated with supercurrents.

The statement “*Life at the edge of chaos*” coined in connection with the study of emergent properties in biological molecules (e.g. protein evolution, folding and stability) reflects the idea, as expressed by de Gennes<sup>53</sup>, that truly important new properties and results can emerge in systems lying at the border between rigid order and randomness, as testified by the marginal stability and conspicuous fluctuations characterizing, for example, nuclear Cooper pairs at the dripline and in metals, and that of proteins of e.g. viral particles like the HIV-1 and HCV-proteases<sup>54</sup>.

Let us conclude this short comment, quoting again de Gennes but doing so with the hindsight of twenty years of nuclear research which have elapsed since “Les objets fragiles” was first published. The chapter entitled “Savoir s’arrêter, savoir changer” starting at p. 180 opens with the statement ‘En ce moment, la physique nucléaire (la science des noyaux atomiques) est une science qui, à mon avis, se trouve en fin de parcours... C’est une physique qui demande des moyens coûteux, et qui s’est constituée par ailleurs en un puissant lobby. Mais elle me semble naturellement exténuée... je suis tenté de dire: “Arrêtons”... mais ce serait aussi absurde que de vouloir arrêter un train à grande vitesse. Le mieux serait d’aiguiller ce train sur une autre voie, plus nouvelle et plus utile à la collectivité.’

In a way, and even without knowing de Gennes remark, part of the nuclear physics community have followed it, capitalizing on the novel embodiment that concepts like elementary modes of excitation, spontaneous symmetry breaking and phase transitions have had in this paradigm of finite many-body (FMB) system the nucleus represents, where fluctuations, as a rule, dominate over potential energy effects. The use of these concepts tainted by FMB system effects as applied to proteins, in particular to the understanding of protein folding may, arguably shed light on the possibility of designing leads to drugs which are less prone to create resistance<sup>55</sup>.

### 3.A.2 Metals

#### Plasmons and phonons (jellium model)

The expression of the electron plasmon frequency of the antenna-like oscillations of the free, conduction electrons of mass  $m_e$  and charge  $-e$ , against the positive charged background (jellium model) is

$$\omega_{ep}^2 = \frac{4\pi n_e e^2}{m_e} = \frac{3e^2}{m_e r_s^2}, \quad (3.A.32)$$

---

<sup>53</sup>de Gennes (1994).

<sup>54</sup>See e.g. Broglia, R. A. (2013).

<sup>55</sup>See e.g. Broglia, R. A. (2013) and refs. therein.

where

$$n_e = \frac{3}{4\pi} \frac{1}{r_s^3}, \quad (3.A.33)$$

are the number of electrons per unit volume,  $r_s$  being the radius of a sphere whose volume is equal to the volume per conduction electron,

$$r_s = \left( \frac{3}{4\pi n_e} \right)^{1/3}, \quad (3.A.34)$$

that is, the radius of the Wigner–Seitz cell.

For metallic Li<sup>56</sup>

$$n_e = 4.70 \frac{10^{22}}{\text{cm}^3} = \frac{4 \times 10^{-2}}{\text{\AA}^3}, \quad (3.A.35)$$

while

$$r_s = \left( \frac{3\text{\AA}^3}{4\pi \times 4.7 \times 10^{-2}} \right)^{1/3} = 1.72\text{\AA}, \quad (3.A.36)$$

implying a value  $(r_s/a_0) = 3.25$  in units of Bohr radius ( $a_0 = 0.529\text{\AA}$ ).

Making use of

$$\alpha = 7.2973 = \frac{e^2}{\hbar c} \quad (3.A.37)$$

and

$$e^2 = 14.4 \text{ eV \AA}, \quad (3.A.38)$$

one obtains

$$\hbar c = \frac{14.4 \text{ eV \AA}}{7.2973} = 1973.3 \text{ eV \AA}. \quad (3.A.39)$$

Making use of the above values and of

$$m_e c^2 = 0.511 \text{ MeV}, \quad (3.A.40)$$

one can write

$$\hbar^2 \omega_{ep}^2 = \frac{(\hbar c)^2}{m_e c^2} \frac{3e^2}{r_s^3} = \frac{(1973.3 \text{ eV \AA})}{0.511 \times 10^6 \text{ eV}} \frac{3 \times 14.4 \text{ eV \AA}}{(1.72 \text{\AA})^3} = 64.69 \text{ eV}^2 \quad (3.A.41)$$

leading to<sup>57</sup>

$$\hbar \omega_{ep} = 8.04 \text{ eV} \approx 1.94 \times 10^9 \text{ MHz} \quad (3.A.42)$$

For the case of metal clusters of Li, the Mie resonance frequency is

$$\hbar \omega_M = \frac{\hbar \omega_{ep}}{\sqrt{3}} = 4.6 \text{ eV}. \quad (3.A.43)$$

---

<sup>56</sup>cf. page 5, table 1.1 of Ashcroft and Mermin (1987).

<sup>57</sup>Kittel (1996) Table 2, p. 278.

### 3.A.3 Elementary theory of phonon dispersion relation

Again, within the framework of the jellium model, one can estimate the long wavelength ionic plasma frequency introducing, in (3.A.32) the substitution  $e \rightarrow Ze$ ,  $m_e \rightarrow AM$  ( $A = N + Z$ , mass number,  $M$  nucleon mass),  $n_e \rightarrow n_i = n_e/Z$ ,

$$\omega_{ip}^2 = \frac{4\pi n_i (Ze)^2}{AM} = \frac{Zm_e}{AM} \omega_{ep}^2, \quad (3.A.44)$$

$AM(Ze)$  being the mass (charge) of the ions<sup>58</sup>. For metallic Li, one obtains

$$\begin{aligned} \hbar\omega_{ip} &= \left( \frac{Zm_e}{AM} \right)^{1/2} \hbar\omega_{ep} = \left( \frac{3 \times 0.5}{9 \times 10^3} \right)^{1/2} \times 1.94 \times 10^{15} \text{ sec}^{-1} \\ &\approx 2.5 \times 10^{-2} \times 10^{15} \text{ sec}^{-1} \approx 10^{13} \text{ sec}^{-1} \approx 1.04 \times 10^2 \text{ meV}. \end{aligned} \quad (3.A.45)$$

Now, both the relations (3.A.32) and (3.A.44), although being quite useful, are wrong from a many-body point of view:  $\omega_{ep}$  because electrons appear as bare electrons not dressed by the phonons, neither by the plasmons;  $\omega_{ip}$  because the static negative background does not allow for an exchange of electron plasmons between ions, exchange eventually leading to a screened, short-range ionic Coulomb repulsive field. Namely ions interact, in the approximation used above, in terms of the “bare” ion–ion Coulomb interaction. Being it infinite range it does not allow for a dispersion relation linear in  $k$  at long wavelengths (sound waves) but forces a finite “mass” also to the lattice phonons. Allowing for electron screening of the “bare” ion–ion Coulomb interaction, as embodied in the electron gas dielectric function  $\epsilon(0, q) = q^2/(k_s^2 + q^2)$ , one obtains the dressed phonon frequency

$$\omega_q^2 = \frac{\omega_{ip}^2}{\epsilon(q)} = \frac{Zm_e}{AM} \frac{\omega_{ep}^2}{q^2 + k_s^2} q^2 = \frac{\omega_{ip}^2}{q^2 + k_s^2} q^2. \quad (3.A.46)$$

The quantity  $k_s$  is the Thomas–Fermi screening wave vector, a quantity which is of the order of the Fermi momentum, the associated screening length being then of the order of the Wigner–Seitz radius. Thus,

$$\lim_{q \rightarrow 0} \omega_q = c_s q \quad (3.A.47)$$

where

$$c_s^2 = \frac{Zm_e}{AM} \frac{\omega_{ep}^2}{k_s^2}, \quad (3.A.48)$$

is the sound velocity. Making use of<sup>59</sup>

$$k_s = \left( \frac{6\pi n_e e^2}{\epsilon_F} \right)^{1/2} = \left( \frac{6\pi Z n_i e^2}{\epsilon_F} \right)^{1/2} = \left( \frac{4k_F}{\pi a_0} \right)^{1/2} \approx 1.6 \text{ \AA}^{-1}, \quad (3.A.49)$$

<sup>58</sup>Ketterson and Song (1999), p. 230.

<sup>59</sup>cf. Ashcroft and Mermin (1987) Eq. (17.55), Kittel Ch. 8 Eq. (23). It is of notice that the corresponding expression in Ketterson and Song (1999) carries a factor  $\pi^2$  instead of the correct factor  $\pi$ .

and of (3.A.32), one can write

$$c_s^2 = \frac{Zm_e}{AM} \frac{4\pi n_e e^2}{m_e} \frac{\epsilon_F}{6\pi n_e e^2} = \frac{2Z}{3AM} \epsilon_F = \frac{Zm_e}{3AM} v_F^2, \quad (3.A.50)$$

where use has been made of

$$n_e = \frac{3}{4\pi} \frac{1}{r_s^3} = 4.7 \times 10^{-2} \text{ \AA}^{-3} \quad (r_s = 1.72 \text{ \AA}, \text{Li}), \quad (3.A.51)$$

and

$$\epsilon_F = \frac{50.1}{(r_s/a_0)} \approx 15.42 \text{ eV} \quad (r_s/a_0 = 3.25, \text{Li}), \quad (3.A.52)$$

With the help of

$$k_F = \frac{1.92}{r_s}, \quad (3.A.53)$$

and of the velocity of light,

$$c = 3 \times 10^{10} \text{ cm/sec}, \quad (3.A.54)$$

one obtains,

$$\begin{aligned} v_F &= \left( \frac{\hbar}{m_e} \right) k_F = \left( \frac{\hbar c}{m_e c^2} \right) \times 3 \times 10^{10} \frac{\text{cm}}{\text{sec}} \frac{1.92}{r_s} \\ &= \left( \frac{2 \times 10^3 \text{ \AA eV}}{0.5 \times 10^6 \text{ eV}} \right) \times 3 \times 10^{10} \frac{\text{cm}}{\text{sec}} \frac{1.92}{r_s} \approx 1.29 \times 10^8 \frac{\text{cm}}{\text{sec}} \end{aligned} \quad (3.A.55)$$

Thus, for Li (<sup>9</sup>Li)

$$c_s^2 = \frac{1}{3} \frac{3m_e}{9M} v_F^2 \approx 6.1 \times 10^{-5} v_F^2, \quad (3.A.56)$$

and

$$c_s \approx 7.8 \times 10^{-3} v_F \approx 1.0 \times 10^5 \frac{\text{cm}}{\text{sec}}. \quad (3.A.57)$$

That is, about a hundredth of the Fermi velocity, or of the order of 10<sup>5</sup> cm/sec, in overall with experimental findings<sup>60</sup>.

Let us now discuss the effective electron-electron interaction. Within the jellium model used above one can write it as

$$V(\mathbf{q}, \omega) = \frac{U_c(q)}{\epsilon(\mathbf{q}, \omega)}, \quad (3.A.58)$$

where the dielectric function

$$\epsilon(\mathbf{q}, \omega) = \frac{\omega^2(q^2 + k_s^2) - \omega_{ip}^2 q^2}{\omega^2 q^2} \quad (3.A.59)$$

---

<sup>60</sup>Ashcroft and Mermin (1987), p. 51, Ketterson and Song (1999) p. 234.

contains the effects due to both the ions and the background electrons, while

$$U_c(q) = \frac{4\pi e^2}{q^2} \quad (3.A.60)$$

is the Fourier transform of the bare Coulomb interaction

$$U_c(r) = \frac{e^2}{r}. \quad (3.A.61)$$

For  $\omega \gg \omega_{ip}$  one obtains the so called screened Coulomb field,

$$V(\mathbf{q}, \omega) = \frac{4\pi e^2 n_e}{q^2 + k_s^2} = U_c^{scr}(q), \quad (3.A.62)$$

its  $\mathbf{r}$  space Fourier transform being

$$U_c^{scr}(r) = \frac{e^2}{r} e^{-k_s r}. \quad (3.A.63)$$

A quantity that for large values of  $r$  falls off exponentially. Thus, in the high frequency limit, the electron-electron interaction, although strongly renormalized by the exchange of plasmons, as testified by the fact that (e.g. for Li),

$$U_c^{scr}(r = 5 \text{ \AA}) \approx U_c(r = 5 \text{ \AA}) e^{-1.6 \times 5} \approx 1 \text{ meV}, \quad (3.A.64)$$

as compared to  $U_c(r = 5 \text{ \AA}) \approx 2.9 \text{ eV}$ , is still repulsive.

Let us now consider frequencies  $\omega \ll \omega_{ip}$  but for values of  $q$  of the order of  $a^{-1}$ , where  $a$  is the lattice constant ( $a \approx 3 - 5 \text{ \AA}$ ,  $a^{-1} \approx 0.25 \text{ \AA}^{-1}$ ) to be compared to  $k_s \approx 1.6 \text{ \AA}^{-1}$  and  $k_F \approx 1.12 \text{ \AA}^{-1}$  (metallic Li). In the case in which  $\omega_{ip}^2/\omega^2 > (q^2 + k_s^2)/q^2$ ,  $V$  is attractive. This behavior explicitly involves the ions through  $\omega_{ip}$  (electron-phonon coupling).

The dispersion relation of the associated frequency collective modes follows from

$$\epsilon(\mathbf{q}, \omega) = 0. \quad (3.A.65)$$

Making use of Eq. (3.A.59) one obtains the relation (3.A.46), as expected. One can now rewrite the reciprocal of the dielectric functions in terms of  $\omega_q$ , that is,

$$\frac{1}{\epsilon(\mathbf{q}, \omega)} = \frac{\omega^2 q^2}{(q^2 + k_s^2)(\omega^2 - \omega_q^2)} = \frac{q^2}{q^2 + k_s^2} \left[ 1 + \frac{\omega_q^2}{\omega^2 - \omega_q^2} \right]. \quad (3.A.66)$$

For  $\omega \gg \omega_q$  one recovers the Thomas-Fermi dielectric function. For  $\omega$  near, but smaller than  $\omega_q$  the interaction is attractive<sup>61</sup>. The effective electron-electron interaction can be then written as

$$\begin{aligned} V(q, \omega) &= \frac{4\pi e^2}{q^2 + k_s^2} + \frac{4\pi e^2}{q^2 + k_s^2} \frac{\omega_q^2}{\omega^2 - \omega_q^2} \\ &= U_c^{scr}(q) + U_c^{scr}(q) \frac{\omega_q^2}{\omega^2 - \omega_q^2} = U_c^{scr}(q) (1 + U_c^{scr}(q) \Pi(q, \omega)) \end{aligned} \quad (3.A.67)$$

---

<sup>61</sup>Schrieffer (1964), Fig. 6-11, p. 152.

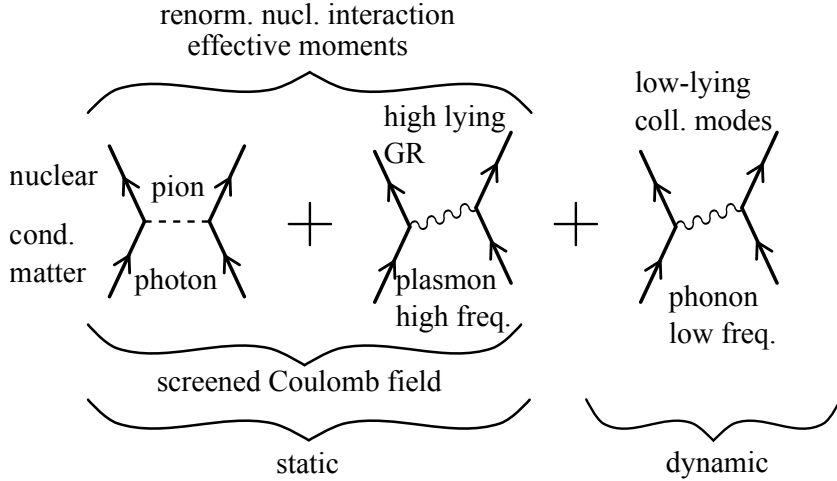


Figure 3.A.4: Schematic representation of the variety of contributions to the effective interaction in nuclei and in metals.

The quantity

$$\Pi(q, \omega) = \left( \frac{Z}{AM} \right) \frac{q^2}{\omega^2 - \omega_q^2} \quad (3.A.68)$$

is intimately connected with Lindhard's function<sup>62</sup>. See also the close relation with the expression (3.A.20) of the nuclear renormalized pairing interaction. The first term of  $V(q, \omega)$  contains the screened Coulomb field arising from the exchange of plasmons between electrons (cf. Fig. 3.A.4). The second term with the exchange of collective low frequency phonons calculated making use of the same screened interaction as emerges from (3.A.67).

Let us now introduce the dimensionless quantity

$$\lambda = \langle F|V|I \rangle = N(0)U_c^{scr} (1 + U_c^{scr}\Pi). \quad (3.A.69)$$

In the weak coupling limit ( $\lambda^2 \ll \lambda$ )

$$\Delta = 2\omega_D e^{-1/\lambda}, \quad (3.A.70)$$

where  $\omega_D$  is the Debye energy. Now, provided that we are in a situation in which  $\omega$  is consistently different from  $\omega_q$ ,

$$\frac{1}{\lambda} = \frac{1}{N(0)U_c^{scr}(1 + U_c^{scr}\Pi)} \approx \frac{1}{N(0)U_c^{scr}} (1 - U_c^{scr}\Pi), \quad (3.A.71)$$

Thus

$$\frac{1}{\lambda} = \frac{1}{N(0)U_c^{scr}} - \frac{\Pi}{N(0)}, \quad (3.A.72)$$

---

<sup>62</sup>Lindhard (1953).

System	$\Delta_0$		$N_0$		$W_{con}$		$E_c$	$BE/A$	$\frac{W_{con}}{E_c}$	$\frac{W_{con}}{BE}$
	meV	MeV	$\frac{\text{mev}^{-1}}{\text{atom}}$	$\text{MeV}^{-1}$	$\frac{\text{mev}}{\text{atom}}$	MeV	$\frac{\text{mev}}{\text{atom}}$	$\frac{\text{MeV}}{A}$	$10^{-7}$	$10^{-3}$
Pb	$^{120}\text{Sn}$	1.4	1.5	276	4	$3 \times 10^{-4}$	4.3	2030	8.5	

Table 3.A.1: Summary of the quantities entering the calculation of the condensation energy superconducting lead, and of the single open shell superfluid nucleus  $^{120}\text{Sn}$ .

and

$$\Delta = \left( 2\omega_D e^{\frac{\Pi}{N(0)}} \right) e^{-\frac{1}{N(0)U_c^{scr}}} . \quad (3.A.73)$$

Consequently, the renormalization effects of the pairing gap associated with phonon exchange are independent of the approximation used to calculate  $U_c^{scr}$  (Thomas-Fermi in the above discussion), provided one has used the same “bare” (screened) Coulomb interaction to calculate  $\omega_q^2$ . Otherwise, the error introduced through a resonant renormalization process entering the expression of e.g. the pairing gap may be quite large.

### 3.A.4 Pairing condensation (correlation) energy beyond level density

The condensation energy, namely the energy difference  $W_N - W_S$  between the normal  $N$ - and superfluid  $S$ -state is defined as (Eq. (2-35) of ref<sup>63</sup>)

$$W_{con} = W_N - W_S = \frac{1}{2} N(0) \Delta_0^2, \quad (3.A.74)$$

where  $N(0)$  is the density of single-electron states of one-spin orientation evaluated at the Fermi surface (p. 31 of ref.<sup>64</sup>), and  $\Delta_0$  is the pairing gap at  $T = 0$ .

The correlation energy  $E_{corr}$  introduced in equation (6-618) of<sup>64</sup>

$$E_{corr} = -\frac{1}{2d} \Delta^2 \quad (3.A.75)$$

to represent  $W_S - W_N$  in the nuclear case, was calculated making use of a (single particle) spectrum of two-fold degenerate (Kramer degeneracy) equally spaced (spacing  $d$ ) single-particle levels. Consequently,  $2/d$  corresponds to the total level density, and  $1/d = N(0)$ . In keeping with the fact that a nucleus in the ground state (or in any single quantal state), is at zero temperature, (3.A.74) coincides with (3.A.75), taking into account the difference in sign in the definitions.

### Nuclei

The empirical value of the level density parameter for both states ( $\nu, \bar{\nu}$ ) (Kramers degeneracy, both spin orientations) is  $a = A/8 \text{ MeV}^{-1}$ ,  $A = N + Z$  being the mass

<sup>63</sup>Schrieffer (1964)

<sup>64</sup>Bohr, A. and Mottelson (1975)

number. Thus, for neutrons one can write  $a_N = N/8$  and  $N_N(0) = N/16 \text{ MeV}^{-1}$ . For  $^{120}_{50}\text{Sn}$ ,  $N_N(0) \approx 4 \text{ MeV}^{-1}$ . Because  $\Delta = 1.46 \text{ MeV}$ , (Table 3.A.1)

$$W_{con} = \frac{1}{2} \times 4 \text{ MeV}^{-1} \times (1.46)^2 \text{ MeV}^2 \approx 4.3 \text{ MeV}. \quad (3.A.76)$$

The binding energy per nucleon is  $BE/A = 8.504 \text{ MeV}$ . Thus  $BE = 120 \times 8.504 \text{ MeV} = 1.02 \times 10^3 \text{ MeV}$ , and

$$\frac{W_{con}}{BE} \approx 4.2 \times 10^{-3}. \quad (3.A.77)$$

### Superconducting lead

Making use of the value<sup>65</sup>

$$N(0) = \frac{0.276 \text{ eV}^{-1}}{\text{atom}}, \quad (3.A.78)$$

and of  $\Delta_0 = 1.4 \text{ meV}$ , one obtains

$$W_{con} = 0.27 \times 10^{-6} \text{ eV/atom}. \quad (3.A.79)$$

In keeping with the fact that the cohesive energy of lead, namely the energy required to break all the bonds associated with one of its atoms is

$$E_c = 2.03 \frac{\text{eV}}{\text{atom}}, \quad (3.A.80)$$

one obtains

$$\frac{W_{con}}{E_c} \approx 1.3 \times 10^{-7}. \quad (3.A.81)$$

The different quantities are summarized in Table 3.A.1.

### 3.A.5 Hindsight

The function  $\Pi(q + \omega)$  essentially at resonance ( $\omega \lesssim \omega_q$ ) and its nuclear analogue being  $|\chi(0)| \frac{\omega_a^2}{\omega_a^2 - \omega^2}$  again close to resonance ( $\omega \lesssim \omega_a$ ), are the sources of new physics eventually leading to observable emergent properties, provided one finds the proper embodiments. In the case of metals at low temperature there are permanent magnetic fields in a superconducting ring, the Josephson effect, etc. In the case of halo neutron drip line nuclei one finds (see Sect. 3.C in particular paragraph before Eq. (3.C.6)) symbiotic pair addition modes, essentially equality of the absolute one- and two-particle transfer cross section, etc.

In Fig. 3.A.5 we present a schematic parallel between the physical mechanisms at the basis of the origin of pairing in metals and in nuclei, and of some of the consequences associated with spontaneous breaking of gauge symmetry in these systems, in particular Cooper pair tunneling.

---

<sup>65</sup>Beck and Claus (1970).

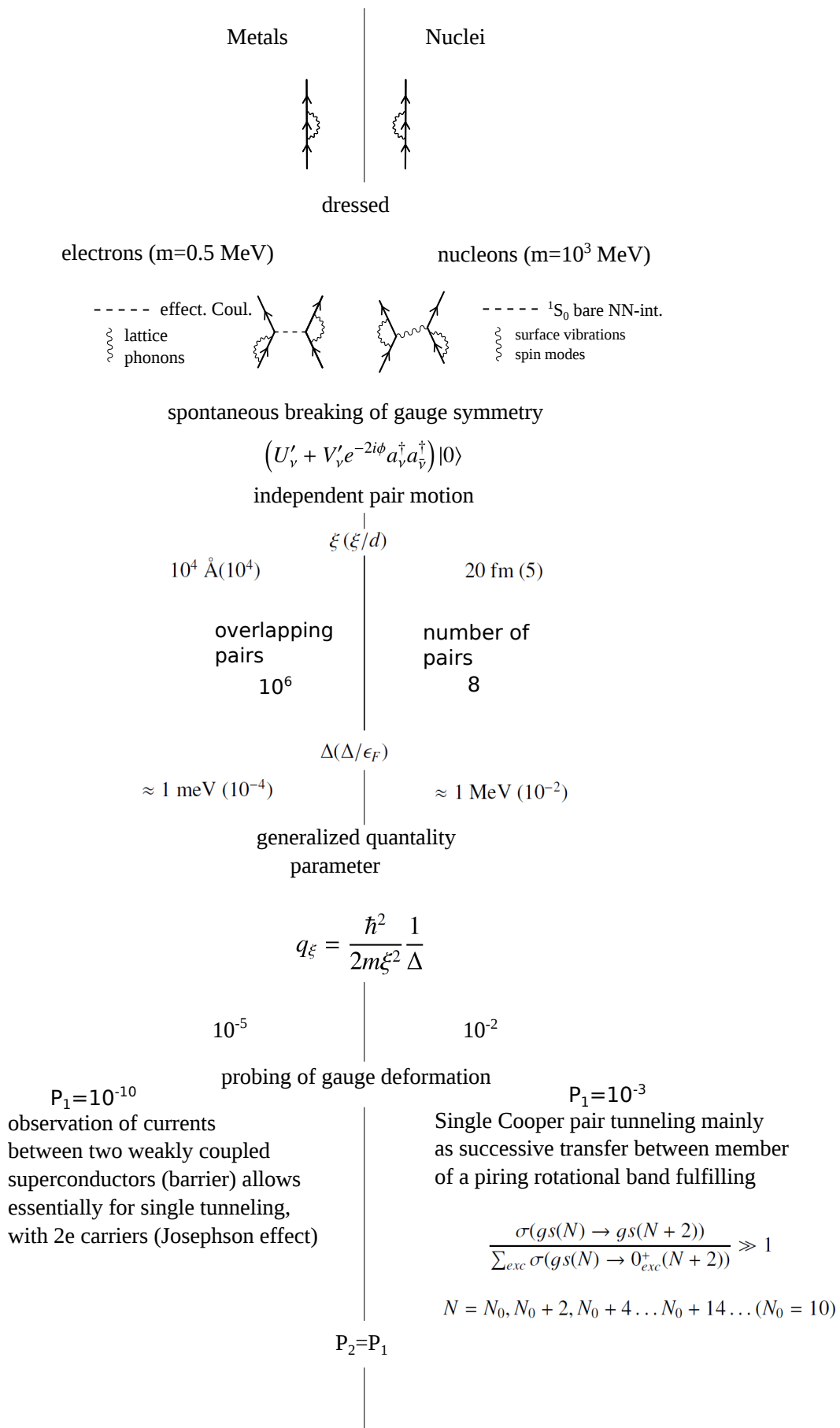


Figure 3.A.5

## Appendix 3.B Cooper pair: radial dependence

The fact that one is still trying to understand (BCS-like) pairing (abnormal density phenomena) in nuclei is, to a non negligible extent, due to the fact that, as a rule, pairing in these systems is constrained to manifest itself subject to a very strong “external” (mean, normal density) field<sup>66</sup>. Also, to same extent, due to the fact that the analysis of two-nucleon transfer data was made in terms of relative cross sections and not absolute cross sections as done now<sup>67</sup>. Within this context, Cooper pair transfer was viewed as simultaneous transfer, successive implying a breakup or, at least an anti-pairing disturbance of the pair. There exist a number of evidences which testify to the fact that the picture in which nucleon Cooper pairs are viewed as independent correlated entities over distances of the order of tens of fm (Fig. 3.2.1), contains a number of correct elements (see e.g. Fig. 3.B.1). In this Appendix an attempt at summarizing these evidences, already mentioned or partially discussed before is attempted<sup>68</sup>.

The problem that Cooper solved was that of a pair of electrons which interact above a quiescent Fermi sphere with an interaction of the kind that might be expected due to the phonon and screened Coulomb field<sup>69</sup>. What he showed approximating this retarded interaction by a non-local one, active on a thin energy shell near (above) the Fermi surface<sup>70</sup>, was that the resulting spectrum has an eigenvalue  $E = 2\epsilon_F - 2\Delta$ , regardless how weak the interaction is (and as a consequence the binding energy  $2\Delta$  of the pair), so long as the interaction is attractive. This result is a consequence of the Fermi statistic and of the existence of a Fermi sea background –the two electrons interact with each other but not with those in the sea, except via the Pauli principle– since it is well known that binding does not ordinarily occur in the two-body problem in three dimensions, until the strength of the attraction exceeds a finite threshold value.

The wavefunction of the two electrons can be written as

$$\Psi(\mathbf{r}_1, \mathbf{r}_2) = \phi_q(\mathbf{r})e^{i\mathbf{q}\cdot\mathbf{R}}\chi(\sigma_1, \sigma_2) \quad (3.B.1)$$

where  $\mathbf{R} = (\mathbf{r}_1 + \mathbf{r}_2)/2$ ,  $\mathbf{r} = \mathbf{r}_1 - \mathbf{r}_2$ , and  $\sigma_1$  and  $\sigma_2$  denote the spins<sup>71</sup>.

Let us consider the state with zero center of mass ( $q = 0$ ) and relative momentum, so that the two electrons carry equal and opposite momenta, aside of

<sup>66</sup>c.f. e.g. Matsuo, M. (2013).

<sup>67</sup>See Potel, G. et al. (2013a) and references therein.

<sup>68</sup>Of course such manifestation will be latent, expressing themselves indirectly. In other words, abnormal density can only be present when normal density, at ever so low values already is present. The pairing field does not have within this context an existence by itself uncoupled from the normal density. On the other hand this, in most cases latent (more than virtual), and in only few cases factual existence, has important consequences on nuclear properties. Within this context one can mention that the neutron halo normal density in  $^{11}\text{Li}$  is not there before the associated abnormal density is operative. In fact one density requires the other to exist in this neutron dripline nucleus.

<sup>69</sup>Cooper (1956).

<sup>70</sup>States below the Fermi surface are frozen because of Pauli principle.

<sup>71</sup>In the limit  $q \rightarrow 0$  the relative coordinate problem is spherically symmetric so that  $\phi_0(\mathbf{r})$  (Schrieffer (1964)).

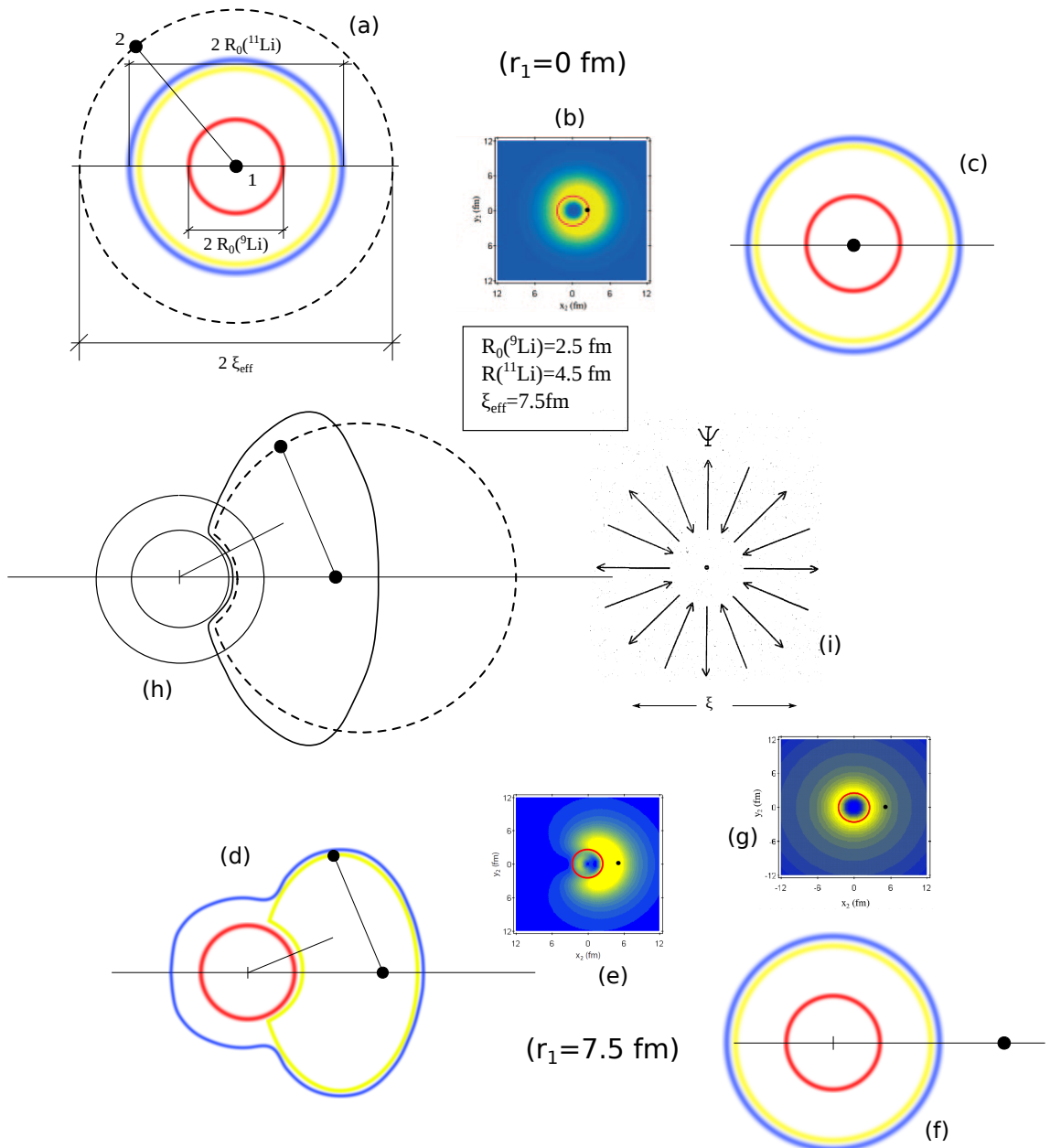


Figure 3.B.1

being in the singlet spin state state, with

$$\chi = \frac{1}{\sqrt{2}} \left[ \begin{pmatrix} 1 \\ 0 \end{pmatrix} \begin{pmatrix} 0 \\ 1 \end{pmatrix} - \begin{pmatrix} 0 \\ 1 \end{pmatrix} \begin{pmatrix} 1 \\ 0 \end{pmatrix} \right] \quad (3.B.2)$$

We have thus a pair of electrons moving in time reversal states and can write<sup>72</sup>,

$$\phi_0(\mathbf{r}) = \sum_{k>k_F} g(\mathbf{k}) e^{i\mathbf{k}\cdot\mathbf{r}}. \quad (3.B.3)$$

In the above wavefunction Pauli principle ( $k > k_F$ ) and translational invariance (dependence on the relative coordinate  $\mathbf{r}$ ) are apparent. The pair wavefunction is likely a superposition of one-electron levels with energies of the order of  $2\Delta$  close to  $\epsilon_F$ , since tunneling experiments indicate that for higher energies the one-electron density is little altered from the form it has in normal metals. The spread in momenta of the single-electron levels entering (3.B.3) is thus fixed by the condition

$$2\Delta \approx \delta E \approx \delta \left( \frac{p^2}{2m} \right)_{\epsilon_F} \approx v_F \delta p. \quad (3.B.4)$$

Consequently

$$\frac{\delta p}{p_F} = \frac{2\Delta}{mv_F^2} = \frac{\Delta}{\epsilon_F} \ll 1. \quad (3.B.5)$$

Thus,  $\phi_0(\mathbf{r})$  consists mainly of waves of wavenumber  $k_F$ . Now, because the wavefunction of a Cooper pair represents a bound  $s$ -state, the motion it describes is a periodic back and forth movement of the two electrons in directions which are uniformly distributed, covering a relative distance ( $\delta x \delta p = \hbar$ )

$$\xi = \delta x = \frac{\hbar}{\delta p} = \frac{\hbar v_F}{2\Delta} \quad (3.B.6)$$

as schematically shown in Fig. 3.B.1 (i). It is analogous to the motion of the two nucleon in a deuteron or the main ( $L = 0$ ) component of the two neutrons in the triton. The hydrogen atom in  $s$ -state is also an example; in that case it is the electron that does most of the back and forth moving, whereas the proton only recoils slightly.

In keeping with the above arguments and with (3.B.6),  $\phi_0(\mathbf{r})$  will look like  $e^{i\mathbf{k}_F \cdot \mathbf{r}}$  for  $r \ll \xi$ , while for  $r \gg \xi$  the waves  $e^{i\mathbf{k} \cdot \mathbf{r}}$  weighted by  $g(k)$  will destroy themselves by interference Fig. 3.B.2. From the above physical arguments,  $\phi_0(\mathbf{r})$  will look like  $e^{i\mathbf{k}_F \cdot \mathbf{r}}$  for  $r \ll \xi$  while for  $r \gtrsim \xi$  one can approximate the weighing function as,

$$g(k) \sim \delta(\mathbf{k}, \mathbf{k}_F + i\hat{\mathbf{k}}_F/\xi), \quad (3.B.7)$$

---

<sup>72</sup>In other words, one expands the  $l = 0$  wavefunction  $\phi_0$  in terms of  $s$ -states of relative momentum  $k$  and total momentum zero.

resulting in

$$\phi_0(\mathbf{r}) \sim e^{-r/\xi} e^{ik_F r}. \quad (3.B.8)$$

Because we are dealing with a singlet state, and the total wavefunction has to be antisymmetric,

$$\phi_0(\mathbf{r}) \sim e^{-r/\xi} \cos k_F r, \quad (3.B.9)$$

A more proper solution of the Cooper pair problem leads to<sup>73</sup>

$$\phi_0(\mathbf{r}) \sim K_0(r/\pi\xi) \cos k_F r, \quad (3.B.10)$$

where  $K_0$  is the zeroth-order modified Bessel function. For  $x \gg 0$ ,  $K_0(x) \sim (\pi/2x)^{1/2} \exp(-x)$ , where  $x = r/\pi\xi$ .

A wavefunction which extends over distances much larger than the binding potential is a well-known phenomenon when the binding energy is small. For example, in the case of the deuteron. In any case, it is of notice that here we are discussing a rather subtle phenomenon, pairing or better Cooper pairing, which has to express itself in the presence of a very strong “external” field. Unless one does not relate the  $NN$  interaction binding the deuteron to proton–neutron pairing.

Be as it may, the large size of the Cooper pair wavefunction also explains why the electrostatic repulsion between electron pair does not appreciably influence the binding. The repulsion acts only over distances of the order of the correlation length.

### Caption Fig 3.B.1

Synthesis of the spatial structure of  $^{11}\text{Li}$  neutron halo Cooper pair calculated in NFT (Barranco, F. et al. (2001)). To make more direct the comparison between the simple estimates and the results of the above reference, it is assumed that  $\xi = 7.5$  fm (dashed circle) instead of 10–11 fm as obtained from  $\xi = \hbar v_F / (\pi |E_{corr}|)$  ( $v_F/c \approx 0.08$ ,  $E_{corr} \approx 0.4$  MeV). Diagrams (a) and (d) are the schematic representations of the modulus square  $|\Psi_0(\mathbf{r}_1, \mathbf{r}_2)|^2 = |\langle \mathbf{r}_1, \mathbf{r}_2 | 0 \rangle|^2$  describing the motion of the two halo neutrons of  $^{11}\text{Li}$ , moving around the  $^{11}\text{Li}$  core. Diagrams (b), (e) and (g) are the results of NFT (see also Fig. 2.6.3 (II) a and b)). **(a)** The circles drawn with continuous lines correspond to the relative distance  $r$  at the radius of the  $^9\text{Li}$  core and of  $^{11}\text{Li}$ . The Cooper pair “intrinsic coordinate”  $r_{12}$  is also shown. Particle 1 of the Cooper pair is assumed to occupy the center of the nucleus ( $r = 0$ ). **(b)** Result of NFT for a situation similar to the above. **(c)** Schematic representation of an uncorrelated pair in a potential weakly binding the pure configuration  $p_{1/2}^2(0)(r = 0)$ . **(d)** Same as (a) but for  $r = 7.5$  fm. **(e)** Result of the NFT calculation for this configuration. **(f)** Schematic representation of a pure configuration  $p_{1/2}^2(0)(r = 7$  fm), **(g)** The result of the microscopic calculation for a weakly bound

---

<sup>73</sup>Kadin (2007).

$p_{1/2}^2(0)$  configuration ( $r = 7.5$  fm). **(h)** The variety of situations in (a) and (d) in comparison to each other in a single cartoon. **(i)** Schematic picture of the dynamics in the quantum state of the Cooper pair. It is a linear combination of motions away and towards one another. The electrons stay within a distance of the order  $\xi$ , root mean square radius of the Cooper pair (After Weisskopf (1981), see also Kadin (2007) and van Witsen (2014)).

Within the nuclear scenario, to interact at profit through long wavelength medium polarization pairing, pairs of nucleons have to have low momentum. To do so they have to reduce the effect of the strong external (mean) field by moving away from it, possible mechanisms being among other: halo (3.B.1), transfer processes (see e.g. 3.4.1), exotic decay<sup>74</sup> (see Fig. 3.B.3.)

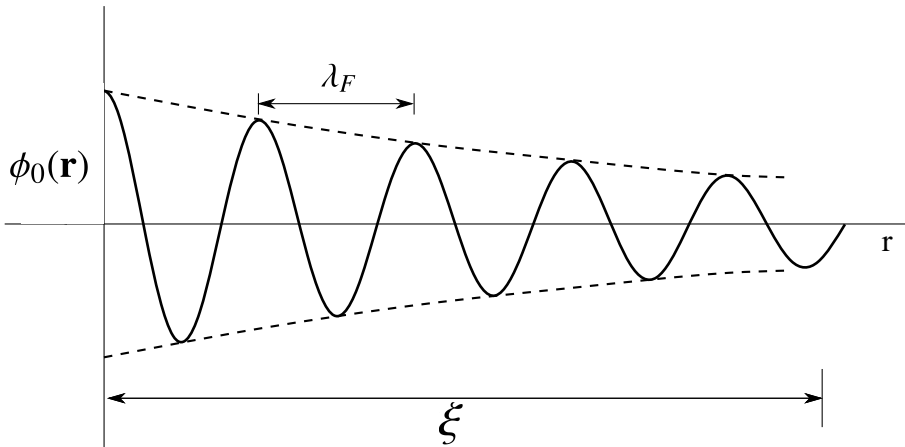


Figure 3.B.2: Schematic representation of the Cooper pair wavefunction. Indicated are the coherence length  $\xi$  and the Fermi wavelength  $\lambda_F = h/p_F = 2\pi/k_F$ . In the nuclear case  $\lambda_F \approx 4.6$  fm and  $\xi \approx \hbar v_F / 2\Delta \approx 30$  fm ( $v_F/c \approx 0.3$ ,  $\Delta \approx 1$  MeV). Thus  $\xi/\lambda_F \approx 7$  (after Weisskopf (1981)).

### 3.B.1 Number of overlapping pairs

The coherence length for low-temperature superconductors is of the order of  $10^4$  Å. In fact, in the case of e.g. Pb, for which<sup>75</sup>  $\Delta_0 = 0.62$  meV and  $v_F = 1.83 \times 10^8$  cm/s one obtains  $\xi \approx 10^{-4}$  cm, where use of  $c = 3 \times 10^{10}$  cm/s and  $\hbar c \approx 2 \times 10^3$  Å×eV has been made.

<sup>74</sup>In Fig. 3.B.3, a parallel is made between correlation lengths between pairing particle-particle modes and particle-hole vibrations, modes which also display a consistent spatial correlation (see e.g. Broglia et al. (1971)).

<sup>75</sup>The standard quoted value is  $\Delta_0 = \Delta(T = 0) = 7.19$  K. Making use of the conversion factor 1K →  $8.6217 \times 10^{-5}$  eV one obtains 0.62 meV.

Since electrons in metals typically occupy a volume of the order of  $(2\text{\AA})^3$  (Wigner–Seitz cell), there would be of the order of<sup>76</sup>  $\xi^3/(2\text{\AA})^3 \approx 10^{11}$  other electrons within a “coherence volume”. Eliminating the electrons deep within the Fermi sea as they behave essentially as the metal was in the normal phase, one gets<sup>77</sup>  $10^6$ . In other words, about a million of other Cooper pairs have their center of mass falling inside the coherence volume of a pair. Thus, the isolated pair picture is not correct.

In the nuclear case, the number of Cooper pairs participating in the condensate is

$$\alpha_0 = \langle BCS | P'^\dagger | BCS \rangle = \sum_j \frac{2j+1}{2} U'_j V'_j. \quad (3.B.11)$$

A simple estimate of this number can be made with the help of the single  $j$ -shell model, in which case  $V_j = (N/2\Omega)^{1/2}$  and  $U_j = (1 - N/2\Omega)^{1/2}$ , where  $\Omega = (2j + 1)/2$ . For a half-filled shell ( $N = \Omega$ ) one obtains<sup>78</sup>  $\alpha'_0 = \Omega/2$ . In the case of  $^{120}\text{Sn}$ ,  $\alpha'_0 = 6 - 8$ .

In keeping with the fact that  $\xi > R_0$ , in the nuclear case one has a complete overlap between all Cooper pairs participating in the condensate. This, together with the fact that the nuclear Cooper pairs press against the nuclear surface in an attempt to expand and are forced to bounce elastically off from it, receive strong circumstantial evidence from the following experimental results: **1)** while the moment of inertia of rotational bands is  $\mathcal{J}_r/2$  it is  $5\mathcal{J}_{irrot}$ . In other words, while pairing in nuclei is important its role is only partially exhausted, and certainly strongly distorted (Bohr, A. and Mottelson (1975)); **2)** One- and two-nucleon transfer reactions in pairing correlated nuclei have the same order of magnitude. For example  $\sigma(^{120}\text{Sn}(p, d)^{119}\text{Sn}(5/2^+; 1.09 \text{ MeV})) = 5.35 \text{ mb}$  ( $2^\circ < \theta_{cm} < 55^\circ$ ), while  $\sigma(^{120}\text{Sn}(p, t)^{118}\text{Sn}(gs)) = 2.25 \text{ mb}$  ( $7.6^\circ < \theta_{cm} < 59.7^\circ$ ). In this last reaction Cooper pair partners can be as far as 12–13 fm. In the case of a heavy ion reaction this distance becomes almost double (Fig. 3.4.1); **3)** The decay constant of the exotic decay  $^{223}_{88}\text{Ra}_{135} \rightarrow ^{14}_6\text{C}_8 + ^{209}_{82}\text{Pb}_{127}$  has been measured to be  $\lambda_{exp} = 4.3 \times 10^{-16} \text{ sec}^{-1}$ . For theoretical purposes it can be written as  $\lambda = PfT$ , product of the formation probability  $P$  of  $^{14}\text{C}$  in  $^{223}\text{Ra}$  (saddle configuration, see bottom Fig. 3.B.3), the knocking rate  $f$  and the tunneling probability  $T$ . These two last quantities hardly depend on pairing. On the other hand  $P$  changes from  $\approx 2 \times 10^{-76}$  to  $2.3 \times 10^{-10}$ , and consequently the associated lifetimes from  $10^{75} \text{ y}$  to the observed value of  $10^8 \text{ y}$  by allowing Cooper pairs to be correlated over distances which can be as large as 20 fm.

Within the above context, and as discussed in App. 3.C, exotic halo nuclei open new possibilities to understand the physics at the basis of pairing in nuclei.

---

<sup>76</sup>Ketterson and Song (1999) p. 198.

<sup>77</sup>Schrieffer (1964) p. 43.

<sup>78</sup>Making use of the harmonic oscillator, one can write  $\Omega = \frac{1}{2}(N + 1)(N + 2) \sim A^{2/3}$ , where the proportionality constant has a value between 1/2 and 2/3.

### 3.B.2 Coherence length and quantality parameter for (*ph*) vibrations

Vibrations: correlated (*ph*) ( $\alpha = 0$ ) (*pp*) ( $\alpha = +2$ ) and (*hh*) ( $\alpha = -2$ ) modes, with energy  $E_{corr} (< 0)$  and fulfilling the dispersion relation in nuclear matter,

$$\begin{aligned}|E_{corr}| &= \frac{\hbar^2 k^2}{2m}. \\ \lambda &= \frac{1}{k} \approx \frac{\hbar^2 k_F}{2m} \frac{1}{|E_{corr}|} \\ &= \frac{\hbar v_F}{2|E_{corr}|}\end{aligned}\quad (3.B.12)$$

To be compared with

$$\xi = \frac{\hbar v_F}{2\Delta} \quad (3.B.13)$$

for superfluid nuclei. Thus, one can assume that both  $\lambda$  and  $\xi$  describe the same physical phenomenon: correlation length of two fermions in normal ((*ph*), (*pp*), (*hh*)) or in superfluid ((*pp*) + (*hh*)) nuclei (see Fig. 3.B.3).

#### Caption Fig 3.B.3

Vibrations can be classified by the transfer quantum number  $\alpha$ . Collective modes with  $\alpha = 0$  correspond to correlated particle-hole (*ph*) excitation. For example low-lying quadrupole or octupole (surface and/or density) vibrations. Modes with  $\alpha = \pm 2$  are known as correlated (*pp*) or (*hh*) modes, that is, pair addition and pair subtraction modes. Thinking of these modes propagating in uniform nuclear matter, the reduced wavelength  $\lambda = \lambda/2\pi = 1/k$  is estimated in terms of the correlation energy  $E_{corr}$ . The (generalized) quantality parameter, ratio of the quantal kinetic energy of localization and the correlation energy, gives a measure of the tendency to independent particle ( $q_\xi \approx 1$ ) or pair ( $q_\xi \ll 1$ ) motion, in keeping with the fact that potential energy is best profited by special arrangements between nucleons and thus lower symmetry than the original Hamiltonian, while fluctuations favor symmetry. Going from the infinite to the finite nuclear system, these modes change somewhat character, e.g. density turns into surface modes, becoming distorted by the mean field which acts as a strong external field (see also Fig. 3.B.1). A concrete example which testifies to the fact that (*ph*) excitations (large amplitude surface distortion) and independent (*pp*) motion (superfluidity) are correlated over dimensions larger than typical nuclear dimensions, is provided by e.g. fission and exotic decay, in particular  $^{223}\text{Ra} \rightarrow ^{14}\text{C} + ^{209}\text{Pb}$ . In keeping with the uncertainties affecting the above simple estimates (factor 2 or  $\pi$  in the denominator of  $\xi, \langle r^2 \rangle_{Cooper}^{1/2}$  or  $\sqrt{\frac{3}{5}} \langle r^2 \rangle_{Cooper}^{1/2}$ , etc.), it seems fair to conclude that  $10 \lesssim \xi \lesssim 20$ . Thus, one is likely faced with an intermediate situation in which  $1.3 \lesssim \xi/R \lesssim 2.6$ .

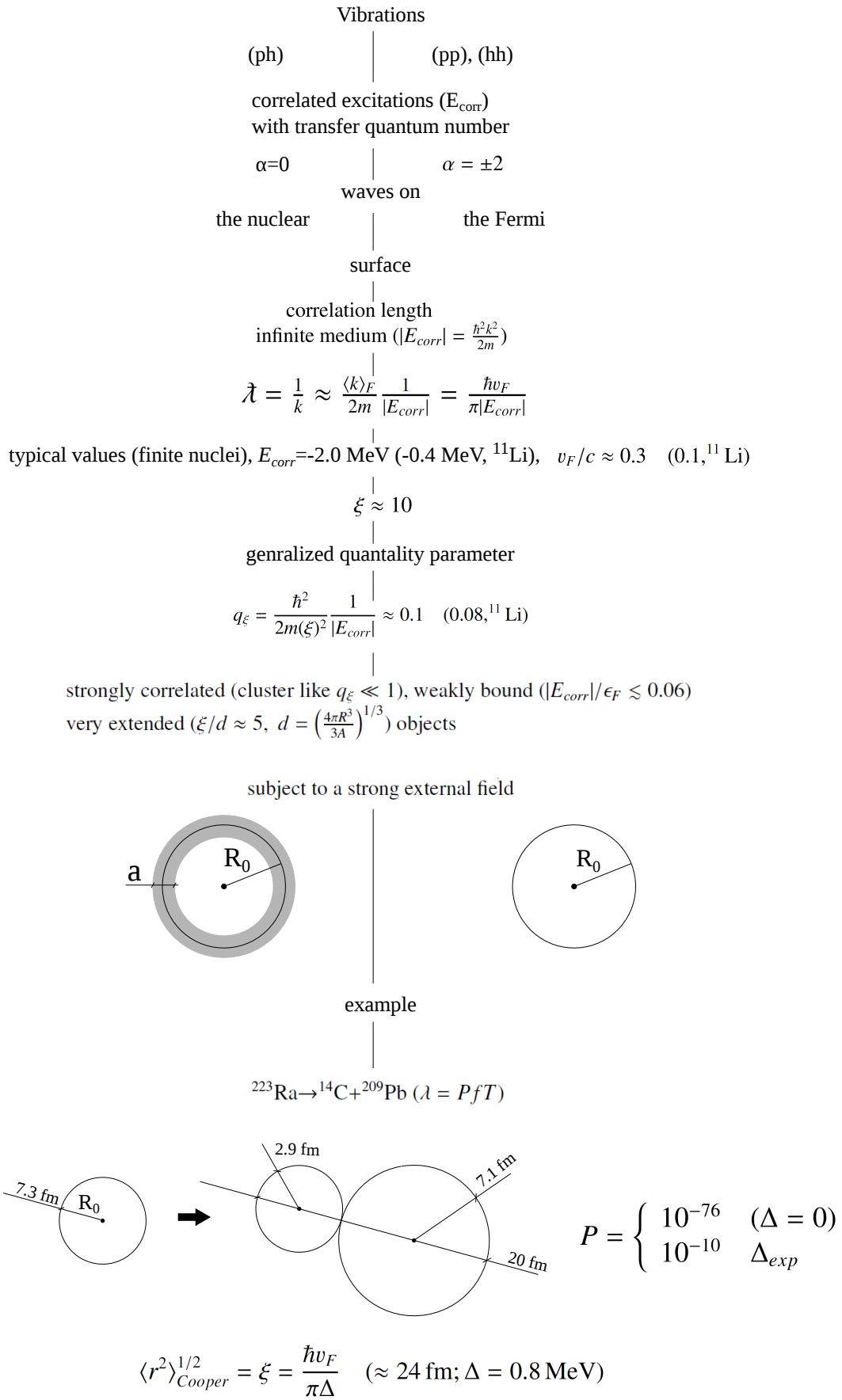


Figure 3.B.3

$f$		$\sigma(gs \rightarrow f)/\sigma(gs \rightarrow gs)$	Table A
$J^\pi$	$E_x$		
$0^+(gs)$	0	100	pair removal ( $hh$ )
$3^-$	2.62	21	( $ph$ ) collective mode
$5^-$	3.20	45	( $ph$ ) collective mode
$0^+$	4.87	45	pair addition

Table 3.B.1: Relative two-nucleon transfer cross sections  $\sigma(^{206}\text{Pb} (t, p)^{208}\text{Pb}(f))/\sigma(^{206}\text{Pb} (t, p)^{208}\text{Pb}(gs))$  integrated in the range  $5^\circ - 175^\circ$  of cm angles. (After Broglia, R.A. et al. (1973), Table A. VIII b)

$J^\pi$	$\sigma(gs \rightarrow f)$ (mb)	$\sigma(gs \rightarrow f)/\sigma(gs \rightarrow gs)$
$0^+(gs)$	$2250 \pm 338$	100
$2^+$	$613 \pm 92$	27

Table 3.B.2: Absolute cross section associated with the reaction  $^{120}\text{Sn} (p, t)^{118}\text{Sn}$  to the ground state and first excited state integrated in the range  $7.6^\circ < \theta_{cm} < 69.7^\circ$ . After Guazzoni, P. et al. (2008).

Typical order of magnitude:  $E_{corr} \approx -1.2$  MeV and  $\Delta \approx 1.2$  MeV for medium heavy nuclei lying along the stability valley. Thus

$$\xi = \frac{\hbar v_F}{2|E_{corr}|} \approx \frac{\hbar c(V_F/c)}{2.4 \text{ MeV}} \approx \frac{200 \text{ MeV fm} \times 0.3}{2.4} \approx 25 \text{ fm} \quad (3.B.14)$$

In the case of  $^{11}\text{Li}$ ,  $E_{corr} \approx -400$  keV and  $v_F/c \approx 0.1$ . Thus

$$\xi = \frac{200 \text{ MeV fm} \times 0.1}{0.8} \approx 25 \text{ fm}. \quad (3.B.15)$$

Generalized quantality parameter

$$q_\xi = \frac{\hbar^2}{2m\xi^2} \frac{1}{|E_{corr}|} = \begin{cases} \frac{20 \text{ MeV fm}}{25^2 1.2 \text{ MeV}} \approx 0.03 \\ \frac{20 \text{ MeV fm}}{25^2 0.4 \text{ MeV}} \approx 0.08 \quad ^{11}\text{Li} \end{cases} \quad (3.B.16)$$

The parallel which can be traced between Cooper pairs and correlated particle-hole excitations is further testified by the fact that two-nucleon transfer reaction do excite quite strongly also these modes (see Tables 3.B.1 and 3.B.2).

### 3.B.3 tunneling probabilities

In general, the coefficients  $U_\nu, V_\nu$  entering the BCS wavefunction  $\prod_{\nu>0} (U_\nu + V_\nu a_\nu^\dagger a_\nu^\dagger) |0\rangle$  are complex. Let us employ the standard phasing  $U_\nu = U'_\nu e^{i\phi}, V_\nu = V'_\nu e^{-i\phi}$ , where

$U'_\nu$  and  $V'_\nu$  are real, and define the state,

$$\begin{aligned} |BCS(\phi)\rangle_{\mathcal{K}} &= \mathcal{G}(\phi) \prod_{\nu>0} (U_\nu + V_\nu a_\nu^\dagger a_{\bar{\nu}}^\dagger) |0\rangle = e^{\frac{iN}{2}\phi} \prod_{\nu>0} (U'_\nu + V'_\nu e^{-2i\phi} a_\nu^\dagger a_{\bar{\nu}}^\dagger) |0\rangle \\ &= e^{\frac{iN}{2}\phi} \prod_{\nu>0} (U'_\nu + V'_\nu a'^\dagger a'^\dagger) |0\rangle = |BCS(\phi)\rangle_{\mathcal{K}'} \end{aligned} \quad (3.B.17)$$

where use has been made of the gauge transformation  $a'^\dagger = \mathcal{G}(\phi) a_\nu^\dagger \mathcal{G}^{-1}(\phi)$ ,  $\mathcal{G}(\phi) = e^{-iN\phi}$  inducing a rotation in gauge space. The labels  $\mathcal{K}$  and  $\mathcal{K}'$  indicate the laboratory and body-fixed reference frames respectively.

The state (3.B.17) displays off-diagonal-long-range-order (ODLRO) because each pair is in a state  $(U'_\nu + V'_\nu e^{-2i\phi} a_\nu^\dagger a_{\bar{\nu}}^\dagger) |0\rangle$  with the same phase as all the others. In fact, the wavefunction (3.B.17) leads to a two-particle density matrix with the property  $\lim_{\mathbf{r}_1, \mathbf{r}_2, \mathbf{r}_3, \mathbf{r}_4 \rightarrow \infty} \phi(\mathbf{r}_1, \mathbf{r}_2; \mathbf{r}_3, \mathbf{r}_4) \neq 0$  under the assumption that  $r_{12}, r_{34} < \xi$ , ( $\mathbf{r}_1, \mathbf{r}_2$ ) and ( $\mathbf{r}_3, \mathbf{r}_4$ ) being the coordinates of a Cooper pair,  $r_{ij}$  the relative modulus of it and  $\xi$  the coherence length<sup>79</sup>.

Let us bring this structure result into reaction. The fact that the wavefunction of the nucleons in the pair are phase-coherent ( $(U'_\nu + V'_\nu e^{-2i\phi} a_\nu^\dagger a_{\bar{\nu}}^\dagger) |0\rangle$ ) implies that to calculate the probability of two-nucleon transfer, one has to add the amplitudes of one-nucleon transfer before taking modulus squared, that is,

$$\begin{aligned} P_2 &= \lim_{\epsilon \rightarrow 0} \left| \frac{1}{\sqrt{2}} (e^{i\phi'} \sqrt{P_1} + e^{i\phi} \sqrt{P_1}) \right|^2 \quad (\epsilon = \phi - \phi') \\ &= P_1 \lim_{\epsilon \rightarrow 0} (1 + \cos \epsilon) = P_1. \end{aligned} \quad (3.B.18)$$

In keeping with the parallel made with superconductors (see Fig. 3.A.5) one can mention that Josephson showed that at very low temperatures, the pair current is equal to the single-particle current at an equivalent voltage<sup>80</sup>  $\pi\Delta/2e$ . How conclusive this result is concerning the mechanism at the basis of Cooper pair transfer is connected with the fact that the probability of one-electron-tunneling across a typical dioxide layer giving rise to a weak  $S - S$  coupling is  $10^{-10}$ . Consequently, simultaneous pair transfer between two superconductors ( $S$ ), with a probability  $(10^{-10})^2$  cannot be observed<sup>81</sup>.

One could argue that in the reaction  $^{120}\text{Sn}(p, t)^{118}\text{Sn(gs)}$  one can hardly consider the triton as a pairing condensate. While this is correct one can hardly claim either that six-eight Cooper pairs ( $^{120}\text{Sn}$ ) make a *bona fide* one. In any case, when one experimentally observes such unexpected behaviour ( $\sigma_{2n} \approx \sigma_{1n}$ ) one is likely somewhat authorized at using similar concepts<sup>82</sup>.

<sup>79</sup>See e.g. Ambegaokar (1969) and refs. therein.

<sup>80</sup>In the case of Pb  $\Delta = 0.62$  meV (see footnote <sup>75</sup>) this voltage is  $(\pi \times 0.62/2) \times 10^{-3} \times \text{eV/e} \approx 1\text{mV}$  (see e.g. McDonald (2001)).

<sup>81</sup>See e.g. McDonald (2001).

<sup>82</sup>Anderson (1972).

### 3.B.4 Nuclear correlation (condensation) energy

The BCS mean field can be written as<sup>83</sup>

$$H_{MF} = U + H_{11} \quad (3.B.19)$$

where

$$U = 2 \sum_{\nu>0} (\epsilon_\nu - \epsilon_F) V_\nu^2 - G \alpha_0^2 \quad (3.B.20)$$

while

$$H_{11} = \sum_{\nu>0} E_\nu (\alpha_\nu^\dagger \alpha_\nu + \alpha_{\bar{\nu}}^\dagger \alpha_{\bar{\nu}}), \quad (3.B.21)$$

$E_\nu$  being the quasiparticle energy, and  $\alpha_\nu^\dagger$  the quasiparticle creation operator. The pair-correlation energy is the difference between the energy with and without pairing, the energy including pair correlations is

$$E_p = 2 \sum_{\nu>0} |V_\nu|^2 \epsilon_\nu - G |\alpha_0|^2 \quad (3.B.22)$$

while the energy without correlation is

$$E_0 = \sum_{\nu>0} |V_\nu^0|^2 \epsilon_\nu. \quad (3.B.23)$$

The occupation probabilities  $|V_\nu^0|$  are unity below the Fermi energy level and zero above. In both Eqs. (3.B.22) and (3.B.23) the Fermi energy has to be chosen to give the correct number of particles. The pairing correlation energy is

$$E_{corr} = E_p - E_0 - G |\alpha_0|^2, \quad (3.B.24)$$

where

$$E_p = \sum_{\nu>0} 2(|V_\nu|^2 - |V_\nu^0|^2) \epsilon_\nu. \quad (3.B.25)$$

The total pairing energy  $-G|\alpha_0|^2$  is partially canceled by the first term describing the fact that, in the BCS ground state, particles moving in levels close to the Fermi energy are partially excited across the Fermi surface, in keeping with the fact that  $V_\nu^2$  changes smoothly from 1 to 0 around  $\epsilon_F$ , being 1/2 at the Fermi energy.

In other words, the energy gain resulting from the potential energy term, where  $G$  is the pairing coupling constant while  $|\alpha_0|$  measures the number of Cooper pairs is partially compensated by a quantal, zero point fluctuation like term. It can, in principle, be related to the Cooper pair kinetic energy of confinement  $T_\xi =$

---

<sup>83</sup>Brink, D. and Broglia (2005), Appendix G.

$\frac{\hbar^2}{2m} \frac{1}{\xi^2}$  already discussed in connection with the generalized quantality parameter, through the relation  $2|\alpha_0|T_\xi$  (for one type of nucleons), in keeping with the fact that (3.B.25) is expressed in term of single nucleon energies. Let us make a simple estimate which can help at providing a qualitative example of the above argument, and consider for the purpose the nucleus  $^{223}\text{Ra}$  and  $G \approx (22/A)$  MeV,  $|\alpha_0| \approx 6$  and  $\xi \approx 10$  fm:  $T_\xi \approx 0.2$  MeV,  $2 \times (2 \times |\alpha_0| \times T_\xi) = 4.8$  MeV,  $2 \times (-G|\alpha_0|^2) = -7.2$  MeV<sup>84</sup> (factors of 2, both protons and neutrons). The resulting pairing correlation energy thus being  $E_{corr} = -2.6$  MeV. This number can be compared with a “realistic” estimate provided by the relation<sup>85</sup>

$$E_{corr} = -\frac{g\Delta^2}{4}, \quad (3.B.26)$$

where  $g_n = N/16$  MeV $^{-1}$  and  $g_p = Z/16$  MeV $^{-1}$ . Taking into account both types of particles  $g = g_n + g_p = A/16$  MeV $^{-1}$  and making use of  $\Delta = 12/\sqrt{A}$  MeV, one obtains  $E_{corr} = -\frac{144}{64}$  MeV = -2.25 MeV. With the help of  $E_{corr}$  and  $T_\xi$ , one can estimate the generalized quantality parameter,  $q_\xi = T_\xi/|E_{corr}| = 0.2/2 \approx 0.08$ , as well as make a consistency check on the value of  $\xi$  used, namely  $\hbar v_F/(2|E_{corr}|) \approx 11.5$  fm.

### 3.B.5 Possible (dream?) experiment<sup>86</sup>

The nuclear Cooper pair not only is forced to exist in a very strong external field, the HF mean field, of very reduced dimensions as compared to the correlation length. Because of spatial quantization, it is also forced to exist on selected orbitals of varied angular momentum and parity<sup>87</sup>.

Correlations, in particular pairing correlations within such constraints will have opposite and apparently contradictory effects. As an example let's consider two neutrons moving around  $^9\text{Li}$  in the  $s_{1/2}^2(0)$  or in the  $p_{1/2}^2(0)$  (pure) uncorrelated configurations. In such a situation, fixing one of the neutrons of the pair at a radius  $r_1$ , the other one will display equal possibility to be close or in the opposite side of the nucleus ( $\theta_{12} = 0^\circ$  or  $\theta_{12} = 180^\circ$ ), the average distance between neutrons

<sup>84</sup>This quantity, but divided by 2, i.e. -3.6 MeV can be compared with the effective pairing matrix element  $v = \left(\frac{\Delta_n^2 + \Delta_p^2}{4}\right) \approx -2.9$  MeV, operative at level crossing in the calculation of the inertia of the exotic decay  $^{223}\text{Ra} \rightarrow ^{14}\text{Ca} + ^{209}\text{Pb}$ , cf. Brink, D. and Broglia (2005) p.159 and refs. therein.

<sup>85</sup>Brink, D. and Broglia (2005).

<sup>86</sup>The breaking of a prejudice: pairing plus long range force, i.e. pairing short range, many (high) relative angular momenta contributing ( Kisslinger, L. S. and Sorensen, R. A. (1963); Soloviev (1965); Mottelson (1962, 1998).

<sup>87</sup>Some of them allowing for pure  $j^2(0)$  configurations, with large (little) probability of  $L = 0$  relative motion, which behaves as hot (cold) orbitals, their contribution to pairing correlations and to two-nucleon transfer reactions being very inhomogeneous, at variance of the situation found in solid state (see e.g. Broglia (2005)). This is also the reason why the second-order-like phase transition normal-superfluid taking place in nuclei as e.g. the number of pairs of nucleons moving outside closed shells, affected by strong pairing fluctuations, are conspicuously blurred as compared to the  $N \rightarrow \infty$  case.

being of the order of  $d = \left(\frac{\frac{4\pi}{3}R^3}{A}\right)^{1/3} \approx 2$  fm (3.3 fm using  $R(^{11}\text{Li})=4.6$  fm instead of  $R = 1.2A^{1/3}$  fm).

By exchanging the GDPR between the two outer neutrons, the halo Cooper pair becomes stabilized, becoming weakly bound ( $S_{2n} = 380$  keV). Assuming that the odd neutron  $p_{3/2}(\pi)$  plays only a spectator role, the ground state of  $^{11}\text{Li}$  can be written as  $|^{11}\text{Li}(gs)\rangle = |\tilde{0}\rangle \otimes |p_{3/2}(\pi)\rangle$ , the neutron halo Cooper pair state being

$$\begin{aligned} |\tilde{0}\rangle \approx & 0.45|s_{1/2}^2(0)\rangle + 0.55|p_{1/2}^2(0)\rangle + 0.04|d_{5/2}^2(0)\rangle \\ & + 0.71|(p_{1/2}, s_{1/2})_{1^-} \otimes 1^-; 0\rangle + 0.1|(s_{1/2}, d_{5/2})_{2^+} \otimes 2^+; 0\rangle. \end{aligned} \quad (3.B.27)$$

Studying this state microscopically one observes two contrasting effects taking place:

1) The two neutrons will switch from a regime of single-particle motion to that of independent pair motion and adopt the configuration proper to a Cooper pair (radial motion against each other, Weisskopf) and expand radially consistent with the fact that its mean surface radius ( $\xi = \langle r^2 \rangle \approx \frac{\hbar v_F}{\pi E_{corr}} \approx \hbar c(v_F/c)/\pi E_{corr} \approx \frac{200 \text{ MeV fm} \times 0.15}{\pi 0.4 \text{ MeV}} = 24$  fm,  $\epsilon_F(^{11}\text{Li}) \approx 24$  MeV  $\rightarrow v_F/c \approx 0.15$ ). This can be appreciated by the fact that the radius of  $^{11}\text{Li}$  is much larger than that expected from systematic ( $R(^{11}\text{Li}) = 4.6$  fm, corresponding to an effective mass number  $A_{eff} \approx 60$ ). Such long range correlations are likely at the basis of the large cross section observed in the reaction  $^1\text{H}(^{11}\text{Li}, ^9\text{Li})^3\text{H}$ , in keeping with the fact that a large interval of relative motion coordinate will contribute to the transfer amplitude, consistent with the fact that the process is dominated by successive transfer. In other words, large two-nucleon transfer cross sections are not a consequence of the fact that the two halo neutrons are close to each other like in the triton, as simultaneous transfer (a process resulting from the single action of the mean field, the second nucleon coming along because of correlation) contributes little to the transfer amplitude, which is dominated by successive transfer. The associated  $(p, d)$  and subsequent  $(d, t)$  processes are both mediated by the mean field over a range of relative distances between target and projectile determined by the tail of the Cooper pair partners wave function, each decaying with a  $\kappa \approx \left(\frac{2mS_n}{\hbar}\right)^{1/2}$  ( $S_n \approx 380$  keV). They extend over distances not incompatible with a consistent fraction of the correlation length (i.e.  $r \approx 1/\kappa \approx 7$  fm). *Within this scenario, one can expect, that the cross section associated with the reaction  $^{10}\text{Be}(^{11}\text{Li}, ^9\text{Li})^{12}\text{Be}(0^{++}; 2.24 \text{ MeV})$  can be larger than that populating the ground state (eventually correcting for Q-value effects), in keeping with the expected halo character of the excited  $0^{++}$  state. The eventual population, in the same reaction, of the 2.70 MeV dipole state can provide important information concerning the alleged symbiotic character of neutron halo pair addition modes.*

Further insight in the role played by the GDPR in gluing Cooper pairs made out of halo neutrons, in particular in the case of  $^{11}\text{Li}$ , can be obtained by studying the reaction  $^9\text{Li}(t, p)^{11}\text{Li(gs)}$  as a function of the bombarding energy  $E_{CM}$ . For values of  $E_{CM}/A$  much larger than  $\hbar\omega_{GDPR} (\lesssim 1 \text{ MeV})$  this mode will have hardly time to

act, and the main component of halo pairing to become established, the associated cross section being expected to decrease. Similar effects are expected in connection with the cross section associated with the process  ${}^9\text{Li}(t, p){}^{11}\text{Li}(1^-; \text{GDPR})$ , and the eventual observation of its  $\gamma$  decay. (see Fig. 3.C.1 below).

**2)** Interference between positive ( $(-1)^l = +1$ ) and negative ( $(-1)^l = -1$ ) single-particle based  $|(l, j)_0^2\rangle$  configurations, constructive at  $\theta = 0^\circ$  and destructive at  $\theta = 180^\circ$ ,  $\theta = r_1 \hat{r}_2$  been the relative angle between the coordinates  $\mathbf{r}_1$  and  $\mathbf{r}_2$  of the Cooper pair partners. In other words the two nucleons will tend to be close to each other, in particular on the nuclear surface. As can be seen from (1), this effect is extreme in the case of the ground state of  ${}^{11}\text{Li}$ . Now, such an effect has not much to do with pairing, BCS pairing at it and thus superconductivity<sup>88</sup>, but with the properties of the nuclear mean field, result of spatial quantization which not only distorts the Cooper pair through isotropic confinement, but through admixtures of odd and even parity states controlled also by the very strong spin orbit term.

Summing up, the difficulties of understanding pairing in nuclei as compared with condensed matter is (at least threefold): **a**) the bare interaction is attractive, a fact which lead to the prejudice that pairing force is short range and delayed the discovery of the other half of pairing, namely the retarded, medium polarization interaction, for a long time; **b**) particle number is small, thus pairing vibrations are important, and renormalize in a conspicuous way the variety of nuclear phenomena, in particular single-particle motion. The fact that such effects are still not being really considered is testified by the fact that a serious treatment of multipole pairing vibrations is still missing; **c**) spatial quantization leading to phenomena which by themselves can be very interesting<sup>89</sup>, but which again has conditioned nuclear structure research, let alone reaction mechanism studies and the physics emerging from their interweaving.

### Appendix 3.C Absolute Cooper pair tunneling cross section: quantitative novel physics at the edge between stability and chaos

In the study of many-body systems, in particular of finite many-body systems (FMBS) like the atomic nucleus, much can be learned from symmetries (group theory) as well as from the general phenomena of spontaneous symmetry breaking.

---

<sup>88</sup>Within this context it is of notice that in condensed matter literature Cooper pairs are viewed as fragile, extended di-electron entities, overlapping with a conspicuous number of other pairs, and displaying a delicate “rigid” quantal correlation between partners (generalized quantity parameter) and among Cooper pairs (off diagonal long range order). In fact, Weisskof’s representation of the radial (opposite) motion of electrons provides a useful picture of Cooper pair internal dynamics, In other words, approaching to or recessing from each other does not favour a particular anisotropic configuration , the two electrons being at the mean square radius of the Cooper pair, i.e. the coherence length  $\xi$ .

<sup>89</sup>Bertsch, G. F. et al. (1967); Ferreira, L. et al. (1984); Lotti et al. (1989); Matsuo (2006); Matsuo, M. (2013)

However, it is the texture of the associated emergent properties, concrete embodiment of symmetry breaking (potential energy) and of its restoration (fluctuations, collective modes), which provides insight into the eventual new physics. In fact, when one understands the many-body system under study, in terms of the detailed motion of single-particles (nucleons) and collective motion, taking properly into account their couplings and associated zero point fluctuations, is that one can hope to have reached a solid, quantitative, understanding of the problem and of its solutions. Even more, that these solutions are likely transferable, at profit, to the study of other FMBS like e.g. metal clusters, fullerenes<sup>90</sup>, quantum dots<sup>91</sup>, and eventually proteins, let alone the fact that one can make predictions. Predictions which, in connection with the study of halo nuclei, in particular of pairing<sup>92</sup> in such exotic, highly extended systems lying at the nucleon drip line, involve true novel physics<sup>93</sup>. Within this context one can quote from Leon Cooper's contribution to the volume<sup>94</sup> BCS: 50 years: "It has become fashionable... to assert... that once gauge symmetry is broken the properties of superconductors follow... with no need to inquire into the mechanism by which the symmetry is broken<sup>95</sup>. This is not... true, since broken gauge symmetry might lead to molecule-like and a Bose-Einstein rather than BCS condensation... in 1957... the major problem was to show... how... an order parameter or condensation in momentum space could come about... to show how... gauge-invariant symmetry of the Lagrangian could be spontaneously broken due to interactions which were themselves gauge invariant".

Nuclear physics has brought this quest a step further. This time in connection with the "extension" of the study of BCS condensation to its origin, a single Cooper pair in the rarified atmosphere resulting from the strong radial (isotropic) deformation observed in light halo, exotic nuclei in general, and in  $^{11}\text{Li}$  in particular. During the last few years, the probing of this system in terms of absolute two-nucleon transfer (pick-up) reactions, has made this field a quantitative one, errors below the %10 limit being the rule. This achievement which has its basis

<sup>90</sup>Cf. e.g. Gunnarsson (2004), Broglia et al. (2004) and refs. therein.

<sup>91</sup>Lipparini (2003).

<sup>92</sup>Cf. e.g. Broglia, R. A. and Zelevinsky, V. (2013).

<sup>93</sup>Cf. e.g. Barranco, F. et al. (2001); Tanihata, I. et al. (2008); Potel et al. (2010) and references therein.

<sup>94</sup>Cooper (2011).

<sup>95</sup>Detailed quoting (Weinberg (2011)): "...In consequence of this spontaneous symmetry breaking, products of any even number of electron fields have non-vanishing expectation values in a superconductor, though a single electron field does not. All of the dramatic exact properties of superconductors –zero electric resistance, the expelling of the magnetic fields from superconductors known as the Meissner effect, the quantization of magnetic flux through a thick superconducting ring, and the Josephson formula for the frequency of the ac current at a junction between two superconductors with different voltages– follow from the assumption that electromagnetic gauge invariance is broken in this way, with no need to inquire into the mechanism by which the symmetry is broken." The above quotation is similar to saying that once the idea of a double DNA helix was thought, all about inheritance was solved and known, and that one could forget the X-ray plates of Rosalind Franklin, Maurice Wilkins and collaborators, let alone how DNA and proteins interact with each other (cf. e.g. G.S. Stent (1980) and references therein).

on the remarkable experiments of Tanihata, I. et al. (2008), is also the result of the combined effort made in treating the structure and reaction aspects of the subject, two sides of the same physics, on equal footing. In particular regarding the description of the continuum and of the fluctuations leading to both single-particle and collective modes clothing, as well as present as ZPF of the ground state. New physics has been seen to emerge from situations in which these fluctuations diverge (like was also known to occur in the case of e.g. pairing rotational bands) or are on (quasi) resonance, as in the case of the halo pair addition mode of  ${}^9\text{Li}$  (i.e.  ${}^{11}\text{Li}(\text{gs})$ ) and likely of  ${}^{10}\text{Be}$  (i.e.  $\text{Be}(0^{+*}; 2.24 \text{ MeV})$ ).

### 3.C.1 Saturation density, spill out and halo

In the incipit to the Chapter on bulk properties of nuclei of Bohr and Mottelson (1969) p. 139 one reads: “The almost constant density of nuclear matter is associated with the finite range of nuclear forces; the range of the forces is  $r_0$  (where  $r_0$  enters the nuclear radius in the expression  $R = r_0 A^{1/3}$ ) thus small compared to nuclear size. This “saturation” of nuclear matter is also reflected in the fact that the total binding energy of the nucleus is roughly proportional to  $A$ . In a minor way, these features are modified by surface effects and long-range Coulomb forces acting between the protons”.

Electron scattering experiments (see the figure 2-1, 159 of the above reference) yield

$$\rho(0) = 0.17 \text{ fm}^{-3}. \quad (3.C.1)$$

Thus, one can posit that

$$\frac{4\pi}{3} R_0^3 \rho(0) = A, \quad (3.C.2)$$

leading to

$$r_0 = \left( \frac{3}{4\pi} \frac{1}{\rho(0)} \right)^{1/3} \approx 1.12 \text{ fm}. \quad (3.C.3)$$

Because the above relations imply a step function distribution, we have to add to (3.C.3) the nucleon spill out<sup>96</sup>  $(a_0/R_0) \ln 2 \approx 0.07$  ( $\approx (a_0/R_0) \ln 2 \approx (0.5/6) \times 0.69 (A = 120)$ ) associated with the fact that a more realistic distribution is provided by a Fermi function of diffusivity  $a_0 \approx 0.5 \text{ fm}$ . Thus  $r_0 = (1.12 + 0.07) \text{ fm} \approx 1.2 \text{ fm}$ . In the case of the nucleus  ${}^{11}\text{Li}$ , observations indicate a mean square (gyration radius<sup>97</sup>) radius  $\langle r^2 \rangle^{1/2} = 3.55 \pm 0.1 \text{ fm}$ <sup>98</sup>. Thus

$$R({}^{11}\text{Li}) = \sqrt{\frac{5}{3}} \langle r^2 \rangle^{1/2} \approx 4.58 \pm 0.13 \text{ fm}. \quad (3.C.4)$$

---

<sup>96</sup>Bertsch and Broglia (2005).

<sup>97</sup>The radius of gyration  $R_g$  is a measure of an object of arbitrary shape,  $R_g^2$  being the second moment in 3D space. In the case of a sphere of radius  $R$ ,  $R_g^2 = 3R^2/5$ .

<sup>98</sup>Kobayashi, T. et al. (1989).

Making use of the relation  $R(= R_0) \approx 1.2A^{1/3}$  fm, the quantity (3.C.4) leads to  $(4.58/1.2)^3 \approx 56$ , an effective mass number larger five times the actual value  $A = 11$ . To be noted that the actual mass number predicts a “systematic” value of the nuclear radius  $R_0(^{11}\text{Li}) \approx 2.7$  fm.

The above results testifies to a very large “**isotropic radial deformation**”, or halo region (skin), in keeping with the fact that<sup>99</sup>  $R(^{11}\text{Li}) - R_0(^9\text{Li}) = R_0(^9\text{Li}) \left( \frac{R(^{11}\text{Li})}{R_0(^9\text{Li})} - 1 \right) = 0.83R_0(^9\text{Li})$ . In other words, <sup>11</sup>Li can be viewed as a normal <sup>9</sup>Li core and of a skin made out of two neutrons extending over a shell radius of the order of that of the core. But even more important, the above mentioned “deformation” affects matter which is little compliant to undergo either compressions or, for that sake, “depressions”, without resulting in nuclear instability. In one case, through a mini supernova. In the second, by obliterating the effect of the short range strong force acting in the <sup>1</sup>S<sub>0</sub> channel (pairing interaction).

In fact, in the case of the halo Cooper pair of <sup>11</sup>Li, that is of the last two weakly bound neutrons, one is dealing with a rarefied nuclear atmosphere of density

$$\rho \approx \frac{2}{\frac{4\pi}{3}(R^3(^{11}\text{Li}) - R_0^3(^9\text{Li}))} \approx 0.6 \times 10^{-2} \text{ fm}^{-3} \quad (3.C.5)$$

where the value  $R_0(^9\text{Li}) \approx 2.5$  fm was used. That is, we are dealing with pairing in a nuclear system at a density which is only 4% of saturation density.

The quest for the long range pairing mechanism which is at the basis of the binding of the halo Cooper pair of <sup>11</sup>Li to the <sup>9</sup>Li core ( $S_{2n} \approx 0.380$  keV, to be compared to typical systematic values of  $S_{2n} \approx 16$  MeV), has lead to the discovery of a novel nuclear mode of elementary excitation. The symbiotic halo pair addition mode, which has to carry its own source of binding (glue) like the hermit crab who carries a gastropod shell to protect his body. A novel embodiment of the Axel–Brink scenario in which not only the line shape, but the main structure of the resonance depends on the state on which it is built, and to which it is deeply interweaved as to guarantee its stability<sup>100</sup>. It also provides a novel realization of the Bardeen–Frölich–Pines microscopic mechanism to break gauge invariance: through the exchange of quite large ZPF which ensures Galilean invariance to a nucleus displaying essentially a permanent dipole moment, as a consequence of the almost degeneracy of the giant dipole pigmy resonance (**centroid**  $\lesssim 1$  MeV) with the ground state. To our knowledge, this is the first example of a van der Waals Cooper pair, atomic or nuclear (App. 2.A).

The NFT diagram shown in Fig. 2.A.1 describing this binding seems quite involved and high order. Thus unlikely to be at the basis of a new elementary mode of nuclear excitation, if nothing else because of the apparent lack of “elementarity”. This is not the case and, in fact, the physics at the basis of the process depicted

---

<sup>99</sup>One can parametrize the radius of <sup>11</sup>Li as (see Bohr, A. and Mottelson (1975)),  $R = R_0(1 + \alpha_{00}Y_{00}) = R_0(1 + \beta_0 \frac{1}{\sqrt{4\pi}})$ . Thus  $\beta_0 = \sqrt{4\pi}(\frac{R}{R_0} - 1) \approx 2.5$  which testifies to the extreme “exoticity” of the phenomenon.

<sup>100</sup>Axel (1962); Brink (1955).

by the oyster-like and eagle-like networks displayed in (a) and (b) is quite simple and present throughout nuclear structure and reactions, let alone many-body theories and QED. In fact, it encompasses (see Fig. 2.A.1): (I,II) the changes in energy of single-particle levels as a function of quadrupole deformations (Nilsson model) (III) the interaction between particles through the exchange of (bosons) vibrations, (IV,V) Pauli principle, (VI,VII) the softening of collective modes due to ground state correlations ((ZPF)-components, QRPA) and eventually the permanent distortion of the system (phase transition), (VIII) the interaction between two non-polar systems through ZPF generated dipoles. Referring to general many-degree of freedom systems, (I,II) and (III) are at the basis of the fact that, in QED, the coupling between one and two photons is zero (Furry's theorem). It is also at the basis, through cancellation, of the small width displayed by giant resonances as compared with single-particle widths at similar energies as well as quadrupole inhomogeneous damping in NMR of molecules and in GDR of atomic nuclei. Concerning (VIII), one can mention resonant interactions between fluctuating systems like e.g. two coupled harmonic oscillators. It is like to find a new particle. Either one is at the right energy (on resonance) or one would not see it.

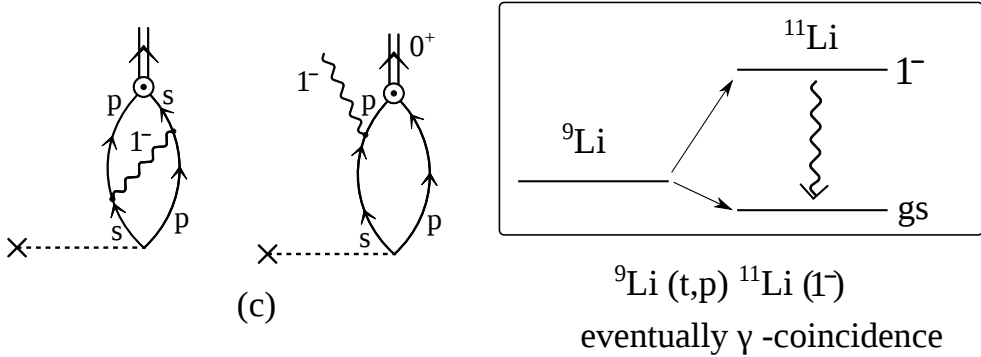
In the case of halo Cooper pair binding by GDPR in  $^{11}\text{Li}$ , the system is essentially on resonance, in keeping with the fact  $\epsilon_{p_{1/2}} - \epsilon_{s_{1/2}} \approx 0.3$  MeV, and that independent particle motion emerges from the same properties of the force from which collective modes emerge. In other words the  $^{10}\text{Li}$  inverted parity system is poised to acquire a permanent dipole moment or, almost equivalent, to display a large amplitude, dipole mode at very low energy as well as a collective  $B(E1)$  to the halo ground state, of the order of a single-particle unit  $B_{sp}$ . This is the GDPR (see Fig. 3.C.1, see also Fig. 1.9.1) with centroid about 0.6–0.8 MeV, 8% of the EWSR and so screened from the GDR through the poor overlap between core and single-particle wavefunctions so as to be able to retain essentially all of its  $B_{sp}$ ,  $E1$ -strength which can rightly be considered a new mode of excitation (see discussion after Eq. (3.C.9)). In other words we are faced, already at the level of single-particle spectrum, with the possibility of a plastic dipole mode, as it materializes in  $^{11}\text{Li}$ . In this case, and making use of the relation

$$\frac{dn}{d\beta_L} = \frac{1}{4} \sqrt{\frac{2L+1}{3\pi}} A \quad (3.C.6)$$

defining the number of crossings  $n$  in terms of deformation (cf. Bertsch and Broglia (2005)), one obtains for  $L = 0$  and  $\beta_0 = 2.5$ ,  $n \approx 2$ .

It is of notice that all of these processes takes place inside the halo neutron pair addition vibrational mode of the closed shell system  $^9\text{Li}_6(\text{gs})$ , and thus in terms of virtual states. On the other hand intervening the processes depicted in Fig. 2.A.1 with external fields, e.g. those associated with one-and two-particle transfer processes, provides much of the physics which is at the basis of the exotic properties of  $^{10}\text{Li}$  and  $^{11}\text{Li}$  (see e.g. Fig. 2.6.3 (I), 1.9.4 and 1.9.5. See also 6.1.3).

But let us now proceed one step at a time. A very attractive, simple and eco-



$$|0\rangle_\nu = |0\rangle + 0.7|(p_{1/2}, s_{1/2})_1 \otimes 1^-; 0\rangle + 0.1|(s_{1/2}, d_{5/2})_2 \otimes 2^+; 0\rangle$$

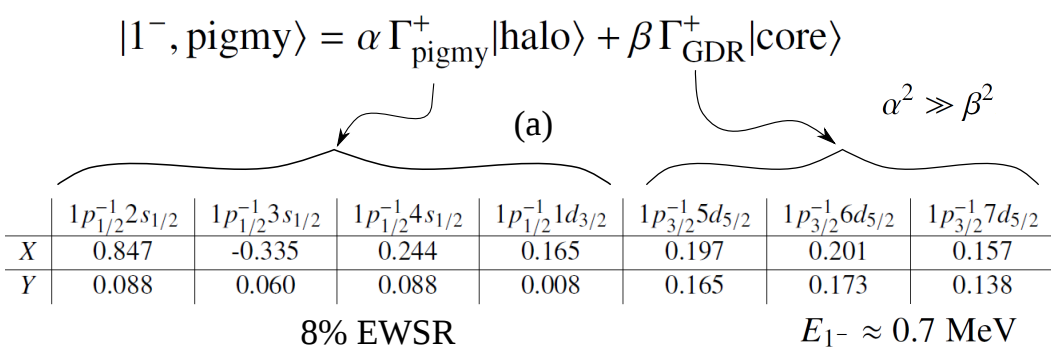
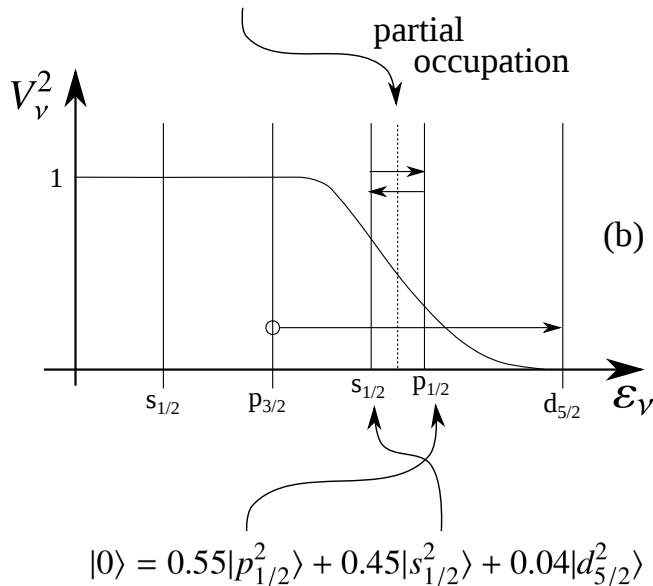


Figure 3.C.1: Schematic representation of (a) the QRPA calculation of the GDPR of  ${}^{11}\text{Li}$  and associated results: namely  $X$  and  $Y$  amplitudes divided, for didactical purposes, into low-lying (pigmy) and high lying (GDPR)  $p - h$  excitations. It is of notice that throughout the odd  $p_{3/2}$  proton state is not shown being treated as a spectator, although the corresponding couplings are properly taken into account in the actual calculations (Barranco, F. et al. (2001)). (b) Schematic representation of the connection between occupation numbers and NFT wavefunction describing the two halo neutrons. (c) Gedanken eksperiment ( ${}^9\text{Li}(t, p){}^{11}\text{Li}(\text{GDPR})$ ) to probe the GDPR wavefunction.

nomic picture of the giant dipole pygmy resonance was proposed in<sup>101</sup>. To explain parity inversion use is made of the fact that, for large prolate quadrupole deformations ( $\beta_2 \approx 0.6 - 0.7$ ), the  $m = 1/2$  member of the  $1d_{5/2}$  and  $1p_{1/2}$  orbitals, i.e. [220 1/2] and [101 1/2] in the Nilsson labeling of levels ( $[Nn_3\Lambda\Omega]$ ), cross. This is in keeping with the fact that quadrupole distortion changes the energy of single-particle states; those having orbits lying in a plane containing the poles become, in the case of prolate deformations, lower in energy, while those lying preferentially in a plane perpendicular to the symmetry axis, increase their energy. Now, this parity inversion is already observed between the resonant  $1/2^-$  ( $\approx 0.5$  MeV) and the virtual  $1/2^+$  ( $\approx 0.2$  MeV) states of  $^{10}\text{Li}$  ( $p_{1/2}$  and  $2_{1/2}$  states). Thus, the energy difference of 0.3 MeV is not very different from the value of 0.6-0.7 MeV of the GDR centroid. In any case, adjusting  $\beta_2$  to the appropriate value this centroid energy is within reach. On the other hand, because the radius is affected by deformation, one can posit that the above model predicts  $R = R_0(1 + \frac{\beta_2}{\sqrt{5}} \sqrt{\frac{5}{4\pi}}) = 2.7 \text{ fm} \times 1.2 \text{ fm} \approx 3.2 \text{ fm}$  ( $\beta_2 \approx 0.7$ ), in disagreement with the experimental finding.

Nonetheless, the fact furthermore that the observed  $\approx 8\%$  of the EWSR below  $\approx 5$  MeV for the GDR corresponds to about  $1B_{sp}(E1)$  for a single particle transition, provides another confirmation of the attractiveness of the model. Now, static models (including also the group theoretical models like that provided by  $SU_3$ ) imply that single-particle states are either occupied or empty. Experimentally, this does not seem the case in the reaction  $^9\text{Li}(d, p)^{10}\text{Li}$ , although one can argue that the situation is different in the case of the single-particle states in  $^{11}\text{Li}$ .

Second, the  $1/2^+ \longleftrightarrow 1/2^-$  single-particle transitions are also part of the GDR transition, resonance which will essentially absorb most of the  $E1$  strength into the high energy mode. In fact, typical  $E1$ -low energy single particle transition display  $\approx 10^{-4}B_{sp}(E1)$ . Inhomogeneous damping brings the dipole oscillations along the symmetry axis to an energy of

$$(\hbar\omega_D) \approx \frac{100 \text{ MeV}}{3.2} \approx 30 \text{ MeV} \quad (3.C.7)$$

far away from the less than 1 MeV energy corresponding to the GDR centroid.

In order to calculate the giant dipole pygmy resonance based on the ground state of  $^{11}\text{Li}$  one needs to know the occupation factors of the  $s_{1/2}$  and  $p_{1/2}$  states. This has been done microscopically making use of the diagonalization of the NFT diagrams taking into account self-energy and induced interaction (vertex renormalization processes) leading to

$$|\tilde{0}\rangle = |0\rangle + 0.71|(p_{1/2}, s_{1/2})_{1^-} \otimes 1^-; 0\rangle + 0.1|(s_{1/2}, d_{5/2})_{2^+} \otimes 2^+; 0\rangle, \quad (3.C.8)$$

and

$$|0\rangle = 0.45|s_{1/2}^2\rangle + 0.55|p_{1/2}^2\rangle + 0.04|d_{5/2}^2\rangle. \quad (3.C.9)$$

---

<sup>101</sup>Hamamoto and Shimoura (2007).

In Eq. (3.C.8), the state  $|1^-\rangle$  and  $|2^+\rangle$  stand for the giant dipole pygmy resonance, and for the low-lying collective quadrupole vibration of  ${}^9\text{Li}$ , respectively. As it emerges from (3.C.8) and (3.C.9), to calculate the microscopic structure of the state  $|1^-\rangle$  (both wavefunction and transition density and consequently the particle-vibration coupling vertex) one needs to calculate  $|0\rangle$ . But to do so one needs to know the same  $|1^-\rangle$  state, the vibrational mode which exchanged between the two neutrons of the halo provides most of its glue to the  ${}^9\text{Li}$  core. From here, the symbiotic character of the  $0^+$  and  $1^-$  (GDPR) entering the  $|{}^{11}\text{Li}(0_v^+ \otimes p_{3/2}(\pi))_{3/2^-}; gs\rangle$  and  $|{}^{11}\text{Li}(1_v^- \otimes p_{3/2}(\pi))_{1/2,3/2,5/2^+}; \approx 0.8 \text{ MeV}\rangle$  states.

Similar calculations have been carried out for  ${}^{12}\text{Be}(gs)$  and  ${}^{12}\text{Be}(0^{+*}; 2.24 \text{ MeV})$ . In the first case no pygmy is found, while in the second case a well developed GDPR is predicted displaying a number of peaks below 2 MeV and carrying a summed EWSR in the interval 0-5 of  $\approx 6\%$ . This result testifies to the fact that the symbiotic halo pair addition mode is a *bona fide* elementary mode of excitation. Its symbiotic GDPR allows to probe the state on which it is based, making the Axel-Brink mechanism a tool to study the structure of halo states. Within this context see Fig. 3.8.1.

## Bibliography

- Kisslinger,L. S. and Sorensen, R. A. Spherical nuclei with simple residual forces. *Review of Modern Physics*, 35:853, 1963.
- V. Ambegaokar. *The Green's function method in superconductivity, Vol I*, page 259. Marcel Dekker, New York, 1969.
- V. Ambegaokar and A. Baratoff. Tunneling between superconductors. *Phys. Rev. Lett.*, 10:486, 1963.
- P. W. Anderson. New method in the theory of superconductivity. *Phys. Rev.*, 110: 985, 1958.
- P. W. Anderson. Special effects in superconductivity. In E. R. Caianello, editor, *The Many-Body Problem, Vol.2*, page 113. Academic Press, New York, 1964.
- P. W. Anderson. More is different. *Science*, 177:393, 1972.
- N. W. Ashcroft and N. D. Mermin. *Solid state physics*. Holt, Reinhardt and Winston, Hong Kong, 1987.
- P. Axel. Electric Dipole Ground-State Transition Width Strength Function and 7-Mev Photon Interactions. *Phys. Rev.*, 126:671, 1962.
- J. Bardeen. Tunnelling from a many-particle point of view. *Phys. Rev. Lett.*, 6:57, 1961.
- J. Bardeen. Tunneling into superconductors. *Physical Review Letters*, 9:147, 1962.
- Barranco, F., R. A. Broglia, and G. F. Bertsch. Exotic radioactivity as a superfluid tunneling phenomenon. *Phys. Rev. Lett.*, 60:507, 1988.
- Barranco, F., G. Bertsch, R. Broglia, and E. Vigezzi. Large-amplitude motion in superfluid fermi droplets. *Nuclear Physics A*, 512:253, 1990.
- Barranco, F., P. F. Bortignon, R. A. Broglia, G. Colò, and E. Vigezzi. The halo of the exotic nucleus  $^{11}\text{Li}$ : a single Cooper pair. *Europ. Phys. J. A*, 11:385, 2001.
- J. L. Basdevant and J. Dalibard. *Quantum Mechanics*. Springer, Berlin, 2005.
- Bayman, B. F. and C. F. Clement. Sum rules for two-nucleon transfer reactions. *Phys. Rev. Lett.*, 29:1020, 1972.
- P. A. Beck and H. Claus. Density of States Information from Low Temperature Specific Heat Measurements. *Journal of research of the National Bureau of Standards A. Physics and Chemistry*, 74A:449, 1970.

- G. Bertsch. In R. Broglia and J. R. Schrieffer, editors, *International School of Physics “Enrico Fermi” Collective motion in Fermi droplets*, page 41, Amsterdam, 1988. North Holland.
- G. Bertsch and R. Broglia. *Oscillations in Finite Quantum Systems*. Cambridge University Press, Cambridge, 2005.
- Bertsch, G. F., R. A. Broglia, and C. Riedel. Qualitative description of nuclear collectivity. *Nucl. Phys. A*, 91:123, 1967.
- Bjerregaard, J. H., O. Hansen, Nathan, and S. Hinds. States of  $^{208}\text{Pb}$  from double triton stripping. *Nucl. Phys.*, 89:337, 1966.
- A. Bohr and B. R. Mottelson. *Nuclear Structure, Vol.I*. Benjamin, New York, 1969.
- A. Bohr and O. Ulfbeck. Quantal structure of superconductivity gauge angle. In *First Topsøe summer School on Superconductivity and Workshop on Superconductors*, Roskilde, Denmark Riso/M/2756, 1988.
- N. Bohr and J. A. Wheeler. The mechanism of nuclear fission. *Phys. Rev.*, 56:426, 1939.
- Bohr, A. and B. R. Mottelson. *Nuclear Structure, Vol.II*. Benjamin, New York, 1975.
- M. Born. Zur Quantenmechanik der Stoßvorgänge. *Zeitschr.f. Phys.*, 37:863, 1926.
- P. F. Bortignon, R. A. Broglia, and C. H. Dasso. Quenching of the mass operator associated with collective states in many-body systems. *Nuclear Physics A*, 398: 221, 1983.
- Bortignon, P. F., A. Bracco, and R. A. Broglia. *Giant Resonances*. Harwood Academic Publishers, Amsterdam, 1998.
- D. M. Brink. *PhD Thesis*. Oxford University, 1955.
- Brink, D. and R. A. Broglia. *Nuclear Superfluidity*. Cambridge University Press, Cambridge, 2005.
- R. Broglia and A. Winther. *Heavy Ion Reactions, 2nd ed.* Westview Press, Perseus Books, Boulder, 2005.
- R. Broglia, G. Coló, G. Onida, and H. Roman. *Solid State Physics of Finite Systems: metal clusters, fullerenes, atomic wires*. Springer Verlag, Berlin, Heidelberg, 2004.
- R. A. Broglia. From phase transitions in finite systems to protein folding and non-conventional drug design. *La Rivista del Nuovo Cimento*, 28(1):1, 2005.

- R. A. Broglia and A. Winther. On the pairing field in nuclei. *Physics Letters B*, 124:11, 1983.
- R. A. Broglia and A. Winther. *Heavy Ion Reactions*. Westview Press, Boulder, CO., 2004.
- R. A. Broglia, C. Riedel, and T. Udagawa. Coherence properties of two-neutron transfer reactions and their relation to inelastic scattering. *Nuclear Physics A*, 169:225, 1971.
- Broglia, R. A. The surfaces of compact systems: from nuclei to stars. *Surface Science*, 500:759, 2002.
- Broglia, R. A. More is different: 50 Years of Nuclear BCS. In R. A. Broglia and V. Zelevinsky, editors, *50 Years of Nuclear BCS*, page 642. World Scientific, Singapore, 2013.
- Broglia, R. A., C. Riedel, and T. Udagawa. Sum rules and two-particle units in the analysis of two-neutron transfer reactions. *Nuclear Physics A*, 184:23, 1972.
- Broglia, R. A. and Zelevinsky, V. . In R. A. Broglia and V. Zelevinsky, editors, *50 Years of Nuclear BCS*. World Scientific, Singapore, 2013.
- Broglia, R.A., O. Hansen, and C. Riedel. Two-neutron transfer reactions and the pairing model. *Advances in Nuclear Physics*, 6:287, 1973. URL [www.mi.infn.it/?vigezzi/BHR/BrogliaHansenRiedel.pdf](http://www.mi.infn.it/?vigezzi/BHR/BrogliaHansenRiedel.pdf).
- M. H. Cohen, L. M. Falicov, and J. C. Phillips. Superconductive tunneling. *Phys. Rev. Lett.*, 8:316, 1962.
- L. Cooper. In L. Cooper and D. Feldman, editors, *BCS: 50 years*. World Scientific, Singapore, 2011.
- L. N. Cooper. Bound electron pairs in a degenerate fermi gas. *Phys. Rev.*, 104: 1189, 1956.
- P. G. de Gennes. *Les objets fragiles*. Plon, Paris, 1994.
- Ferreira, L., R. Liotta, C. Dasso, R. A. Broglia, and A. Winther. Spatial correlations of pairing collective states. *Nuclear Physics A*, 426:276, 1984.
- H. T. Fortune, G.-B. Liu, and D. E. Alburger. ( $sd$ )<sup>2</sup> states in  $^{12}\text{Be}$ . *Phys. Rev. C*, 50:1355, 1994.
- G. Gori, F. Barranco, E. Vigezzi, and R. A. Broglia. Parity inversion and breakdown of shell closure in Be isotopes. *Phys. Rev. C*, 69:041302, 2004.
- Gor'kov, L.P. Microscopic derivation of the Ginzburg–Landau equations in the theory of superconductivity. *Soviet Phys. JETP*, 9:1364, 1959.

- G.S. Stent. . In G. Stent, editor, *The double helix*. Norton and Co., New York, 1980.
- Guazzoni, P., L. Zetta, A. Covello, A. Gargano, B. F. Bayman, G. Graw, R. Hertenberger, H.-F. Wirth, and M. Jaskola. Spectroscopy of  $^{110}\text{Sn}$  via the high-resolution  $^{112}\text{Sn}(p, t)$   $^{110}\text{Sn}$  reaction. *Phys. Rev. C*, 74:054605, 2006.
- Guazzoni, P., L. Zetta, A. Covello, A. Gargano, B. F. Bayman, T. Faestermann, G. Graw, R. Hertenberger, H.-F. Wirth, and M. Jaskola.  $^{118}\text{Sn}$  levels studied by the  $^{120}\text{Sn}(p, t)$  reaction: High-resolution measurements, shell model, and distorted-wave Born approximation calculations. *Phys. Rev. C*, 78:064608, 2008.
- Guazzoni, P., L. Zetta, A. Covello, A. Gargano, B. F. Bayman, T. Faestermann, G. Graw, R. Hertenberger, H.-F. Wirth, and M. Jaskola. High-resolution measurement of the  $^{118,124}\text{Sn}(p,t)$   $^{116,122}$  reactions: Shell-model and microscopic distorted-wave Born approximation calculations. *Phys. Rev. C*, 83:044614, 2011.
- O. Gunnarsson. *Alkali-doped Fullerides: Narrow-band Solids with Unusual Properties*. World Scientific, Singapore, 2004.
- I. Hamamoto and S. Shimoura. Properties of  $^{12}\text{Be}$  and  $^{11}\text{Be}$  in terms of single-particle motion in deformed potential. *Journal of Physics G: Nuclear and Particle Physics*, 34:2715, 2007.
- A. Idini, G. Potel, F. Barranco, E. Vigezzi, and R. A. Broglia. Interweaving of elementary modes of excitation in superfluid nuclei through particle-vibration coupling: Quantitative account of the variety of nuclear structure observables. *Phys. Rev. C*, 92:031304, 2015.
- J. G. Johansen, V. Bildstein, M. J. G. Borge, M. Cubero, J. Diriken, J. Elseviers, L. M. Fraile, H. O. U. Fynbo, L. P. Gaffney, R. Gernhäuser, B. Jonson, G. T. Koldste, J. Konki, T. Kröll, R. Krücken, D. Mücher, T. Nilsson, K. Nowak, J. Pakarinen, V. Pesudo, R. Raabe, K. Riisager, M. Seidlitz, O. Tengblad, H. Törnqvist, D. Voulot, N. Warr, F. Wenander, K. Wimmer, and H. De Witte. Experimental study of bound states in  $^{12}\text{Be}$  through low-energy  $^{11}\text{Be}(d, p)$ -transfer reactions. *Phys. Rev. C*, 88:044619, 2013.
- B. D. Josephson. Possible new effects in superconductive tunnelling. *Phys. Lett.*, 1:251, 1962.
- A. M. Kadin. Spatial structure of the cooper pair. *Journal of Superconductivity and Novel Magnetism*, 20:285, 2007.
- J. B. Ketterson and S. N. Song. *Superconductivity*. Cambridge University Press, Cambridge, 1999.

- C. Kittel. *Introduction to solid state physics*. Wiley, NJ, 1996.
- Kobayashi, T., S. Shimoura, I. Tanihata, K. Katori, K. Matsuta, T. Minamisono, K. Sugimoto, W. Mller, D. L. Olson, T. J. M. Symons, and H. Wieman. Electromagnetic dissociation and soft giant dipole resonance of the neutron-dripline nucleus  $^{11}\text{Li}$ . *Physics Letters B*, 232:51, 1989.
- Le Tourneau. *Mat. Fys. Medd. Dan. Vid. Selsk.*, 34, 1965.
- A. Leggett. *Quantum Liquids*. Oxford University Press, Oxford, 2006.
- J. Lindhard. *Kgl. Danske Videnshab. Selskab, Mat. Fys. Medd.*, 28, 1953.
- E. Lipparini. *Modern Many-Particle Physics: Atomic gases, Quantum Dots and Quantum Fluids*,. World Scientific, Singapore, 2003.
- P. Lotti, F. Cazzola, P. F. Bortignon, R. A. Broglia, and A. Vitturi. Spatial correlation of pairing modes in nuclei at finite temperature. *Phys. Rev. C*, 40:1791, 1989.
- Mahaux, C., P. F. Bortignon, R. A. Broglia, and C. H. Dasso. Dynamics of the shell model. *Physics Reports*, 120:1–274, 1985.
- M. Matsuo. Spatial structure of neutron cooper pair in low density uniform matter. *Phys. Rev. C*, 73:044309, 2006.
- Matsuo, M. Spatial Structure of Cooper Pairs in Nuclei. In R. A. Broglia and V. Zelevinsky, editors, *50 Years of Nuclear BCS*, page 66. World Scientific, Singapore, 2013.
- D. G. McDonald. The nobel laureate versus the graduate student. *Physics Today*, page 46, July 2001.
- D. Montanari, L. Corradi, S. Szilner, G. Pollarolo, E. Fioretto, G. Montagnoli, F. Scarlassara, A. M. Stefanini, S. Courtin, A. Goasduff, F. Haas, D. Jelavić Malenica, C. Michelagnoli, T. Mijatović, N. Soić, C. A. Ur, and M. Varga Pajtler. Neutron Pair Transfer in  $^{60}\text{Ni} + ^{116}\text{Sn}$  Far below the Coulomb Barrier. *Phys. Rev. Lett.*, 113:052501, 2014.
- B. Mottelson. Elementary features of nuclear structure. In Niefnecker, Blaizot, Bertsch, Weise, and David, editors, *Trends in Nuclear Physics, 100 years later, Les Houches, Session LXVI*, page 25, Amsterdam, 1998. Elsevier.
- B. R. Mottelson. Selected topics in the theory of collective phenomena in nuclei. In G. Racah, editor, *International School of Physics “Enrico Fermi” Course XV , Nuclear Spectroscopy*, page 44, New York, 1962. Academic Press.
- A. B. Pippard. The historical context of Josephson discovery. In H. Rogalla and P. H. Kes, editors, *100 years of superconductivity*, page 30. CRC Press, Taylor and Francis, FL, 2012.

- G. Pollarolo and R. A. Broglia. Microscopic Description of the Backward Rise of the Elastic Angular Distribution  $^{16}\text{O} + ^{28}\text{Si}$ . *Nuovo Cimento*, 81:278, 1984.
- G. Potel, F. Barranco, E. Vigezzi, and R. A. Broglia. Evidence for phonon mediated pairing interaction in the halo of the nucleus  $^{11}\text{Li}$ . *Phys. Rev. Lett.*, 105:172502, 2010.
- G. Potel, A. Idini, F. Barranco, E. Vigezzi, and R. A. Broglia. Nuclear Field Theory predictions for  $^{11}\text{Li}$  and  $^{12}\text{Be}$ : shedding light on the origin of pairing in nuclei. *Phys. At. Nucl.*, 7:941, 2014.
- Potel, G., A. Idini, F. Barranco, E. Vigezzi, and R. A. Broglia. Cooper pair transfer in nuclei. *Rep. Prog. Phys.*, 76:106301, 2013a.
- Potel, G., A. Idini, F. Barranco, E. Vigezzi, and R. A. Broglia. Quantitative study of coherent pairing modes with two-neutron transfer: Sn isotopes. *Phys. Rev. C*, 87:054321, 2013b.
- H. Rogalla and P. H. Kes. . In H. Rogalla and P. H. Kes, editors, *100 years of superconductivity*. CRC Press, Taylor and Francis, FL, 2012.
- J. J. Sakurai. *Modern Quantum Mechanics*. Addison-Wesley, Cambridge, MA, 1994.
- Sargsyan, V. V., G. Scamps, G. G. Adamian, N. V. Antonenko, and D. Lacroix. Neutron pair transfer in sub-barrier capture processes. *arXiv:1311.4353v1*, 2013.
- G. Satchler. *Introduction to Nuclear Reactions*. Mc Millan, New York, 1980.
- J. Schrieffer. *Superconductivity*. Benjamin, New York, 1964.
- V. G. Soloviev. Quasi-particle and collective structure of the states of even, strongly-deformed nuclei. *Nuclear Physics*, 69(1):1, 1965.
- Tanihata, I., M. Alcorta, D. Bandyopadhyay, R. Bieri, L. Buchmann, B. Davids, N. Galinski, D. Howell, W. Mills, S. Mythili, R. Openshaw, E. Padilla-Rodal, G. Ruprecht, G. Sheffer, A. C. Shotter, M. Trinczek, P. Walden, H. Savajols, T. Roger, M. Caamano, W. Mittig, P. Roussel-Chomaz, R. Kanungo, A. Gallant, M. Notani, G. Savard, and I. J. Thompson. Measurement of the two-halo neutron transfer reaction  $^1\text{H}(^{11}\text{Li}, ^9\text{Li})^3\text{H}$  at 3A MeV. *Phys. Rev. Lett.*, 100:192502, 2008.
- Thompson, I.J. Reaction mechanism of pair transfer. In R. A. Broglia and V. Zelevinsky, editors, *50 Years of Nuclear BCS*, page 455. World Scientific, Singapore, 2013.
- M. Tinkham. *Introduction to Superconductivity*. Mc Graw-Hill, New York, 1996.

- M. van Witsen. *Superconductivity in real space*. University of Twente (unpublished), 2014.
- W. von Oertzen and A. Vitturi. Pairing correlations of nucleons and multi-nucleon transfer between heavy nuclei. *Reports on Progress in Physics*, 64:1247, 2001.
- von Oertzen, W. Enhanced two-nucleon transfer due to pairing correlations. In R. A. Broglia and V. Zelevinsky, editors, *50 Years of Nuclear BCS*, page 405. World Scientific, Singapore, 2013.
- L. Weinberg. Bcs: 50 years. In L. Cooper and D. Feldman, editors, *BCS: 50 years*. World Scientific, Singapore, 2011.
- V. F. Weisskopf. The formation of superconducting pairs and the nature of superconducting currents. *Contemporary Physics*, 22:375, 1981.
- P. G. Young and R. H. Stokes. New States in  ${}^9\text{Li}$  from the Reaction  ${}^7\text{Li}(t, p){}^9\text{Li}$ . *Phys. Rev. C*, 4:1597, 1971.

## Chapter 4

# One-particle transfer

In what follows we present a derivation of the one-particle transfer differential cross section within the framework of the distorted wave Born approximation (DWBA) (cf. Tobocman (1961), Austern (1963), Satchler (1980); Broglia and Winther (2004), Satchler (1983), Austern (1970), Glendenning, N. K. (2004) and refs. therein).

The structure input in the calculations are mean field potentials and single-particle states dressed, within the formalism of Nuclear Field Theory, (Bohr, A. and Mottelson, 1975; Bès et al., 1974; Bès and Broglia, 1975; Bès et al., 1976a,b,c; Mottelson, 1976; Broglia et al., 1976; Bès and Broglia, 1977; Bortignon, P. F. et al., 1977; Bès, D. R. and Kurchan, 1990) through the coupling with the variety of collective, (quasi-) bosonic vibrations, leading to modified formfactors<sup>1</sup>. With the help of these modified formfactors (cf. also Vaagen et al. (1979); Bang et al. (1980); Hamamoto (1970) and refs. therein), and of global optical potentials, one can calculate the absolute differential cross sections, quantities which can be directly compared with the experimental findings.

In this way one avoids to introduce, let alone use spectroscopic factors, quantities which are rather elusive to calculate consistently (cf. Duguet, T. and Hagen (2012); Jenning, B. (2011); Dickhoff and Barbieri (2004); Dickhoff, W. and Van Neck (2005), and refs. therein). This is in keeping with the fact that as a nucleon moves through the nucleus it feels the presence of the other nucleons whose configurations change as time proceeds. It takes time for this information to be feed back on the nucleon. This renders the average potential nonlocal in time (cf. Mahaux, C. et al. (1985) and references therein, cf. also App. 4.I). A time-dependent operator can always be transformed into an energy-dependent operator, implying an  $\omega$ -dependence of the properties which are usually adscribed to particles like (effective) mass, charge, etc (see App. 4.B). Furthermore, due to

---

<sup>1</sup>It is of notice that single-particle modified formfactors have their counterpart in the renormalised transition densities (Apéndice introducción (inelastic scattering)) and in the modified two-nucleon transfer formfactors (Chapter 5, Eqs. (5.2.48; simultaneous), (5.2.135–5.2.136; successive) and (5.2.155–5.2.156; non-orthogonality) associated with inelastic and with pair transfer reactions (cf. Broglia, R.A. et al. (1973); Potel, G. et al. (2013) and refs. therein), respectively (cf. App. 4.H).

Pauli principle, the average potential is also non local in space (cf. App. 4.A). Consequently, one is forced to deal with nucleons which carry around a cloud of (quasi) bosons, aside from exchanging its position with that of the other nucleons, properties which eventually result in a dynamical shell model. It is of notice that the above mentioned phenomena are not only found in nuclear physics, but are universal within the framework of many-body systems as well as of field theories like quantum electrodynamics (QED). In fact, a basic result of such theories is that nothing is really free (Feynman, 1975). A textbook example of this fact is provided by the Lamb shift, resulting from the dressing of the hydrogen's atom electron, as a result of the exchange of this electron with those participating in the spontaneous, virtual excitation (zero point fluctuations (ZPF)) of the QED vacuum (cf. Apps 4.C, 4.D and 4.E). Within this context, in Section 4.2.1 we provide examples of one-particle transfer processes between nuclei lying along the stability valley, populating strongly renormalized quasiparticle states. In Section 4.2.2 (Poner aqui el apendice W) we again take up the subject, but in this case for the exotic, halo nucleus  $^{11}\text{Li}$ , in particular in connection with the phenomenon of parity inversion in connection with  $N=6$  magic number.

## 4.1 General derivation

We now proceed to derive the transition amplitude for the reaction (cf. Fig. 4.1.1).

$$A + a (= b + 1) \longrightarrow B (= A + 1) + b. \quad (4.1.1)$$

For a simplified version we refer to App 4.F, while for an alternative derivation within the framework of one-particle knock-out reactions we refer to App 4.G. Let us assume that the nucleon bound initially to the core  $b$  is in a single-particle state with orbital and total angular momentum  $l_i$  and  $j_i$  respectively, and that the nucleon in the final state (bound to core  $A$ ) is in the  $l_f, j_f$  state. The total spin and magnetic quantum numbers of nuclei  $A, a, B, b$  are  $\{J_A, M_A\}, \{J_a, M_a\}, \{J_B, M_B\}, \{J_b, M_b\}$  respectively. Denoting  $\xi_A$  and  $\xi_b$  the intrinsic coordinates of the wavefunctions describing the structure of nuclei  $A$  and  $b$  respectively, and  $\mathbf{r}_{An}$  and  $\mathbf{r}_{bn}$  the relative coordinates of the transferred nucleon with respect to the CM of nuclei  $A$  and  $b$  respectively, one can write the “intrinsic” wavefunctions of the colliding nuclei  $A, a$  as

$$\begin{aligned} & \phi_{M_A}^{J_A}(\xi_A), \\ & \Psi(\xi_b, \mathbf{r}_{b1}) = \sum_{m_i} \langle J_b \ j_i \ M_b \ m_i | J_a \ M_a \rangle \phi_{M_b}^{J_b}(\xi_b) \psi_{m_i}^{j_i}(\mathbf{r}_{bn}, \sigma), \end{aligned} \quad (4.1.2)$$

while the “intrinsic” wavefunctions describing the structure of nuclei  $B$  and  $b$  are

$$\begin{aligned} & \phi_{M_b}^{J_b}(\xi_b), \\ & \Psi(\xi_A, \mathbf{r}_{A1}) = \sum_{m_f} \langle J_A \ j_f \ M_A \ m_f | J_B \ M_B \rangle \phi_{M_A}^{J_A}(\xi_A) \psi_{m_f}^{j_f}(\mathbf{r}_{An}, \sigma). \end{aligned} \quad (4.1.3)$$

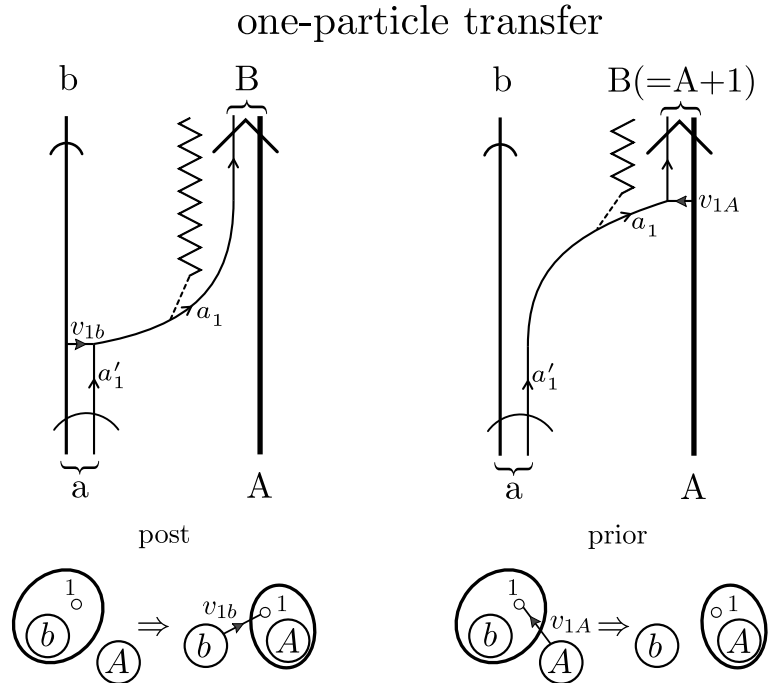


Figure 4.1.1: NFT graphical representation of the one-particle transfer reaction  $a (= b + 1) + A \rightarrow b + B (= A + 1)$  (for details in the notation we refer to Figs. 5.C.1 and 5.C.2 and to the last paragraph before Sect. 5.C.1 of App. 5.C). The time arrow is assumed to point upwards. The quantum numbers characterizing the states in which the transferred nucleon moves in projectile and target are denoted  $a'_1$  and  $a_1$  respectively. The interaction inducing the nucleon to be transferred can act either in the entrance channel  $((a, A); v_{1A}$ , prior representation) or in the exit channel  $((b, B); v_{1b}$ , post representation), in keeping with energy conservation. In the transfer process, the nucleon changes orbital at the same time that a change in the mass partition takes place. The corresponding relative motion mismatch is known as the recoil process, and is represented by a jagged curve (this is the recoil elementary mode, mode which couples to the particle degrees of freedom through a Galilean transformation operator). The recoil mode provides information on the evolution of  $r_{1A}$  ( $r_{1b}$ ). In other words, on the coupling between structure and reaction (relative motion) degrees of freedom.

For an unpolarized incident beam (sum over  $M_A, M_a$  and divide by  $(2J_A + 1), (2J_a + 1)$ ), and assuming that one does not detect the final polarization (sum over  $M_B, M_b$ ), the differential cross section in the DWBA can be written as

$$\frac{d\sigma}{d\Omega} = \frac{k_f}{k_i} \frac{\mu_i \mu_f}{4\pi^2 \hbar^4} \frac{1}{(2J_A + 1)(2J_a + 1)} \times \sum_{\substack{M_A, M_a \\ M_B, M_b}} \left| \sum_{m_i, m_f} \langle J_b j_i M_b m_i | J_a M_a \rangle \langle J_A j_f M_A m_f | J_B M_B \rangle T_{m_i, m_f} \right|^2, \quad (4.1.4)$$

where  $k_i$  and  $k_f$  are the relative motion linear momentum in both initial and final channels (flux), while  $\mu_i$  and  $\mu_f$  are the corresponding relative masses. The two quantities within  $\langle \rangle$  brackets are Clebsch–Gordan coefficients taking care of angular momentum conservation (cf. Brink and Satchler (1968) and Edmonds (1960), also Bohr and Mottelson (1969)).

The transition amplitude  $T_{m_i, m_f}$  is

$$T_{m_i, m_f} = \sum_{\sigma} \int d\mathbf{r}_f d\mathbf{r}_{bn} \chi^{(-)*}(\mathbf{r}_f) \psi_{m_f}^{j_f*}(\mathbf{r}_{An}, \sigma) V(r_{bn}) \psi_{m_i}^{j_i}(\mathbf{r}_{bn}, \sigma) \chi^{(+)}(\mathbf{r}_i), \quad (4.1.5)$$

where

$$\psi_{m_i}^{j_i}(\mathbf{r}_{An}, \sigma) = u_{j_i}(r_{bn}) \left[ Y^{l_i}(\hat{r}_i) \chi(\sigma) \right]_{j_i, m_i}, \quad (4.1.6)$$

is the single-particle wavefunction describing the motion of the nucleon to be transferred, when in the initial state,  $u$ ,  $Y$  and  $\chi$  being the radial, angular (spherical harmonics) and spin components. Similarly for  $\psi_{m_f}^{j_f}$ . The distorted waves describing the relative motion of the incoming projectile and of the target nucleus and of the outgoing system and the residual nucleus are,

$$\chi^{(+)}(\mathbf{k}_i, \mathbf{r}_i) = \frac{4\pi}{k_i r_i} \sum_{l'} i^{l'} e^{i\sigma_i l'} g_{l'}(\hat{r}_i) \left[ Y^{l'}(\hat{r}_i) Y^{l'}(\hat{k}_i) \right]_0^0, \quad (4.1.7)$$

and

$$\chi^{(-)*}(\mathbf{k}_f, \mathbf{r}_f) = \frac{4\pi}{k_f r_f} \sum_l i^{-l} e^{i\sigma_f l} f_l(\hat{r}_f) \left[ Y^l(\hat{r}_f) Y^l(\hat{k}_f) \right]_0^0, \quad (4.1.8)$$

respectively. In the above relations  $f$  and  $g$  are, respectively, the solutions of the radial Schrödinger equation describing the relative motion associated with the corresponding optical potential (“elastic” scattering) in entrance and exit channel. Let us now discuss the angular components involved in the reaction process, starting with the relation

$$\begin{aligned} \left[ Y^l(\hat{r}_f) Y^l(\hat{k}_f) \right]_0^0 \left[ Y^{l'}(\hat{r}_i) Y^{l'}(\hat{k}_i) \right]_0^0 &= \sum_K ((ll)_0 (l'l')_0 | (ll')_K (ll')_K)_0 \\ &\times \left\{ \left[ Y^l(\hat{r}_f) Y^{l'}(\hat{r}_i) \right]^K \left[ Y^l(\hat{k}_f) Y^{l'}(\hat{k}_i) \right]^K \right\}_0^0. \end{aligned} \quad (4.1.9)$$

The 9j-symbol can be explicitly evaluated to give,

$$((ll)_0(l'l')_0|(ll')_K(l'l')_K)_0 = \sqrt{\frac{2K+1}{(2l+1)(2l'+1)}}, \quad (4.1.10)$$

while the coupled expression can be written as

$$\begin{aligned} & \left\{ \left[ Y^l(\hat{r}_f)Y^{l'}(\hat{r}_i) \right]^K \left[ Y^l(\hat{k}_f)Y^{l'}(\hat{k}_i) \right]^K \right\}_0^0 = \sum_M \langle K \ K \ M \ -M | 0 \ 0 \rangle \left[ Y^l(\hat{r}_f)Y^{l'}(\hat{r}_i) \right]_M^K \\ & \times \left[ Y^l(\hat{k}_f)Y^{l'}(\hat{k}_i) \right]_{-M}^K = \sum_M \frac{(-1)^{K+M}}{\sqrt{2K+1}} \left[ Y^l(\hat{r}_f)Y^{l'}(\hat{r}_i) \right]_M^K \left[ Y^l(\hat{k}_f)Y^{l'}(\hat{k}_i) \right]_{-M}^K. \end{aligned} \quad (4.1.11)$$

Thus,

$$\begin{aligned} & \left[ Y^l(\hat{r}_f)Y^l(\hat{k}_f) \right]_0^0 \left[ Y^{l'}(\hat{r}_i)Y^{l'}(\hat{k}_i) \right]_0^0 \\ & = \sum_{K,M} \frac{(-1)^{K+M}}{\sqrt{(2l+1)(2l'+1)}} \left[ Y^l(\hat{r}_f)Y^{l'}(\hat{r}_i) \right]_M^K \left[ Y^l(\hat{k}_f)Y^{l'}(\hat{k}_i) \right]_{-M}^K. \end{aligned} \quad (4.1.12)$$

For the angular integral to be different from zero, the integrand must be coupled to zero angular momentum (scalar). Noting that the only variables over which one integrates in the above expression are  $\hat{r}_i, \hat{r}_f$ , we have to couple the remaining functions of the angular variables, namely the wavefunctions  $\psi_{m_f}^{j_f*}(\mathbf{r}_{An}, \sigma) = (-1)^{j_f-m_f} \psi_{-m_f}^{j_f}(\mathbf{r}_{An}, -\sigma)$  and  $\psi_{m_i}^{j_i}(\mathbf{r}_{bn}, \sigma)$  to angular momentum  $K$ , as well as to fulfill  $M = m_f - m_i$ . Let us then consider

$$\begin{aligned} & (-1)^{j_f-m_f} \psi_{-m_f}^{j_f}(\mathbf{r}_{An}, -\sigma) \psi_{m_i}^{j_i}(\mathbf{r}_{bn}, \sigma) = (-1)^{j_f-m_f} u_{j_f}(r_{An}) u_{j_i}(r_{bn}) \\ & \times \sum_P \langle j_f \ j_i \ -m_f \ m_i | P \ m_i - m_f \rangle \left\{ \left[ Y^{l_f}(\hat{r}_{An}) \chi^{1/2}(-\sigma) \right]^{j_f} \left[ Y^{l_i}(\hat{r}_{bn}) \chi^{1/2}(\sigma) \right]^{j_i} \right\}_{m_i-m_f}^P. \end{aligned} \quad (4.1.13)$$

Recoupling the spherical harmonics to angular momentum  $K$  and the spinors to  $S = 0$ , only one term survives the angular integral in (4.1.5), namely

$$\begin{aligned} & (-1)^{j_f-m_f} u_{j_f}(r_{An}) u_{j_i}(r_{bn}) ((l_f \frac{1}{2})_{j_f} (l_i \frac{1}{2})_{j_i} | (l_f l_i)_K (\frac{1}{2} \frac{1}{2})_0)_K \\ & \times \langle j_f \ j_i \ -m_f \ m_i | K \ m_i - m_f \rangle \left[ Y^{l_f}(\hat{r}_{An}) Y^{l_i}(\hat{r}_{bn}) \right]_{m_i-m_f}^K [\chi(-\sigma) \chi(\sigma)]_0^0. \end{aligned} \quad (4.1.14)$$

Making use of the fact that the sum over spins yields a factor  $-\sqrt{2}$ , and in

keeping with the fact that  $M = m_f - m_i$ , one obtains,

$$\begin{aligned} T_{m_i, m_f} &= (-1)^{j_f - m_f} \frac{-16\sqrt{2}\pi^2}{k_f k_i} \sum_{ll'} i^{l'-l} e^{\sigma'_f + \sigma'_i} \sum_K ((l_f \frac{1}{2})_{j_f} (l_i \frac{1}{2})_{j_i} | (l_f l_i)_K (\frac{1}{2} \frac{1}{2})_0)_K \\ &\times \langle j_f \ j_i \ -m_f \ m_i | K \ m_i - m_f \rangle \left[ Y^l(\hat{k}_f) Y^{l'}(\hat{k}_i) \right]_{m_i - m_f}^K \int d\mathbf{r}_f d\mathbf{r}_{bn} \frac{f_l(r_f) g_{l'}(r_i)}{r_f r_i} \\ &\times u_{j_f}(r_{An}) u_{j_i}(r_{bn}) V(r_{bn}) (-1)^{K+m_f-m_i} \left[ Y^l(\hat{r}_f) Y^{l'}(\hat{r}_i) \right]_{m_f - m_i}^K \left[ Y^{l_f}(\hat{r}_{An}) Y^{l_i}(\hat{r}_{bn}) \right]_{m_i - m_f}^K. \end{aligned} \quad (4.1.15)$$

Again, the only term of the expression

$$\begin{aligned} &(-1)^{K+m_f-m_i} \left[ Y^l(\hat{r}_f) Y^{l'}(\hat{r}_i) \right]_{m_f - m_i}^K \left[ Y^{l_f}(\hat{r}_{An}) Y^{l_i}(\hat{r}_{bn}) \right]_{m_i - m_f}^K = \\ &(-1)^{K+m_f-m_i} \sum_P \langle K \ K \ m_f - m_i \ m_i - m_f | P \ 0 \rangle \left\{ \left[ Y^l(\hat{r}_f) Y^{l'}(\hat{r}_i) \right]^K \left[ Y^{l_f}(\hat{r}_{An}) Y^{l_i}(\hat{r}_{bn}) \right]^K \right\}_0^P \end{aligned}$$

which survives after angular integration is the one with  $P = 0$ , that is,

$$\begin{aligned} &\frac{1}{\sqrt{(2K+1)}} \left\{ \left[ Y^l(\hat{r}_f) Y^{l'}(\hat{r}_i) \right]^K \left[ Y^{l_f}(\hat{r}_{An}) Y^{l_i}(\hat{r}_{bn}) \right]^K \right\}_0^0 \\ &= \frac{1}{\sqrt{(2K+1)}} \sum_{M_K} \langle K \ K \ M_K \ -M_K | 0 \ 0 \rangle \left[ Y^l(\hat{r}_f) Y^{l'}(\hat{r}_i) \right]_{M_K}^K \\ &\times \left[ Y^{l_f}(\hat{r}_{An}) Y^{l_i}(\hat{r}_{bn}) \right]_{-M_K}^K = \frac{1}{\sqrt{(2K+1)}} \sum_{M_K} \frac{(-1)^{K+M_K}}{\sqrt{(2K+1)}} \left[ Y^l(\hat{r}_f) Y^{l'}(\hat{r}_i) \right]_{M_K}^K \\ &\times \left[ Y^{l_f}(\hat{r}_{An}) Y^{l_i}(\hat{r}_{bn}) \right]_{-M_K}^K \\ &= \frac{1}{2K+1} \sum_{M_K} (-1)^{K+M_K} \left[ Y^l(\hat{r}_f) Y^{l'}(\hat{r}_i) \right]_{M_K}^K \left[ Y^{l_f}(\hat{r}_{An}) Y^{l_i}(\hat{r}_{bn}) \right]_{-M_K}^K, \end{aligned}$$

an expression which is spherically symmetric. One can evaluate it for a particular configuration, for example setting  $\hat{r}_f = \hat{z}$  and the center of mass  $A, b, n$  in the  $x - z$  plane (see Fig. 4.1.2). Once the orientation in space of this “standard” configuration is specified (through, for example, a rotation  $0 \leq \alpha \leq 2\pi$  around  $\hat{z}$ , a rotation  $0 \leq \beta \leq \pi$  around the new  $x$  axis and a rotation  $0 \leq \gamma \leq 2\pi$  around  $\hat{r}_{bB}$ ), the only remaining angular coordinate is  $\theta$ , while the integral over the other three angles yields  $8\pi^2$ . Setting  $\hat{r}_f = \hat{z}$  one obtains

$$\left[ Y^l(\hat{r}_f) Y^{l'}(\hat{r}_i) \right]_{M_K}^K = \langle l \ l' \ 0 \ M_K | K \ M_K \rangle \sqrt{\frac{2l+1}{4\pi}} Y_{M_K}^{l'}(\hat{r}_i). \quad (4.1.16)$$

Because of  $M = m_i - m_f$ , and  $m = m_f$ ,  $T_{m_i, m_f} \equiv T_{m, M}$  where

$$\begin{aligned} T_{m, M} &= (-1)^{j_f - m} \frac{-64\sqrt{2}\pi^{7/2}}{k_f k_i} \sum_{ll'} i'^l - l e^{\sigma_f^l + \sigma_i'^l} \sqrt{2l+1} \sum_K \frac{(-1)^K}{2K+1} ((l_f \frac{1}{2})_{j_f} (l_i \frac{1}{2})_{j_i} | (l_f l_i)_K (\frac{1}{2} \frac{1}{2})_0)_K \\ &\quad \times \langle j_f j_i - m | M + m | K M \rangle [Y^l(\hat{k}_f) Y^{l'}(\hat{k}_i)]_M^K \int d\mathbf{r}_f d\mathbf{r}_{bn} \frac{f_l(r_f) g_{l'}(r_i)}{r_f r_i} \\ &\quad \times u_{j_f}(r_{An}) u_{j_i}(r_{bn}) V(r_{bn}) \sum_{M_K} (-1)^{M_K} \langle l l' 0 | M_K | K M_K \rangle [Y^{l_f}(\hat{r}_{An}) Y^{l_i}(\hat{r}_{bn})]_{-M_K}^K Y^{l'}_{M_K}(\hat{r}_i). \end{aligned} \quad (4.1.17)$$

We now turn our attention to the sum

$$\sum_{\substack{M_A, M_a \\ M_B, M_b}} \left| \sum_{m, M} \langle J_b j_i M_b m | J_a M_a \rangle \langle J_A j_f M_A M | J_B M_B \rangle T_{m, M} \right|^2, \quad (4.1.18)$$

appearing in the expression for the differential cross section (4.1.4). For any given value  $m', M'$  of  $m, M$ , the sum will be

$$\begin{aligned} &\sum_{M_a, M_b} |\langle J_b j_i M_b m' | J_a M_a \rangle|^2 \sum_{M_A, M_B} |\langle J_A j_f M_A M' | J_B M_B \rangle|^2 |T_{m', M'}|^2 \\ &= \frac{(2J_a + 1)(2J_B + 1)}{(2j_i + 1)(2j_f + 1)} \sum_{M_a, M_b} |\langle J_b J_a M_b - M_a | j_i m' \rangle|^2 \\ &\quad \times \sum_{M_A, M_B} |\langle J_A J_B M_A - M_B | j_f M' \rangle|^2 |T_{m', M'}|^2, \end{aligned} \quad (4.1.19)$$

by virtue of the symmetry property of Clebsch–Gordan coefficients

$$\langle J_b j_i M_b m | J_a M_a \rangle = (-1)^{J_b - M_b} \sqrt{\frac{(2J_a + 1)}{(2j_i + 1)}} \langle J_b J_a M_b - M_a | j_i m \rangle. \quad (4.1.20)$$

The sum over the Clebsch–Gordan coefficients in (4.1.19) is equal to 1, so (4.1.18) becomes

$$\frac{(2J_a + 1)(2J_B + 1)}{(2j_i + 1)(2j_f + 1)} \sum_{m, M} |T_{m, M}|^2, \quad (4.1.21)$$

and the differential cross section can be written as,

$$\frac{d\sigma}{d\Omega} = \frac{k_f}{k_i} \frac{\mu_i \mu_f}{4\pi^2 \hbar^4} \frac{(2J_B + 1)}{(2j_i + 1)(2j_f + 1)(2J_A + 1)} \sum_{m, M} |T_{m, M}|^2. \quad (4.1.22)$$

where

$$T_{m, M} = \sum_{Kll'} (-1)^{-m} \langle j_f j_i - m | M + m | K M \rangle [Y^l(\hat{k}_f) Y^{l'}(\hat{k}_i)]_M^K t_{ll'}^K. \quad (4.1.23)$$

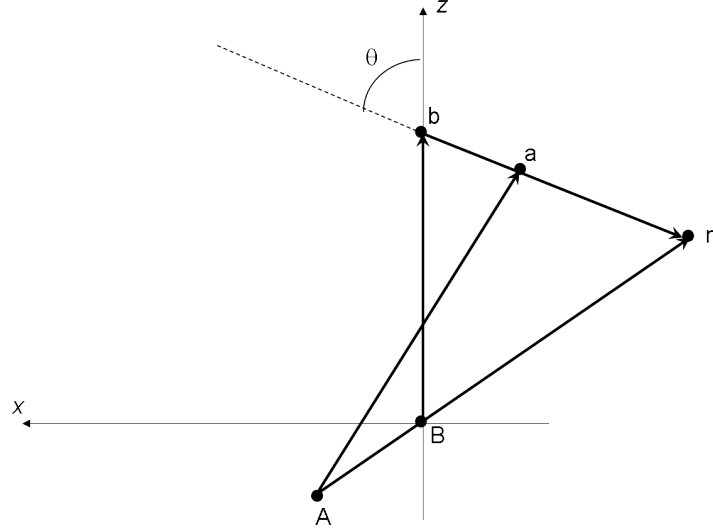


Figure 4.1.2: Coordinate system in the “standard” configuration. Note that  $\mathbf{r}_f \equiv \mathbf{r}_{Bb}$ , and  $\mathbf{r}_i \equiv \mathbf{r}_{Aa}$ .

Orienting  $\hat{k}_i$  along the incident  $z$ -direction leads to,

$$\left[ Y^l(\hat{k}_f) Y^{l'}(\hat{k}_i) \right]_M^K = \langle l l' M 0 | K M \rangle \sqrt{\frac{2l'+1}{4\pi}} Y_M^l(\hat{k}_f) t_{ll'}^K, \quad (4.1.24)$$

and

$$T_{m,M} = \sum_{Kll'} (-1)^{-m} \langle l l' M 0 | K M \rangle \langle j_f j_i - m | M + m | K M \rangle Y_M^l(\hat{k}_f) t_{ll'}^K, \quad (4.1.25)$$

with

$$\begin{aligned} t_{ll'}^K &= (-1)^{K+j_f} \frac{-32\sqrt{2}\pi^3}{k_f k_i} i^{l'-l} e^{\sigma_f^l + \sigma_i^{l'}} \frac{\sqrt{(2l+1)(2l'+1)}}{2K+1} ((l_f \frac{1}{2})_{j_f} (l_i \frac{1}{2})_{j_i} | (l_f l_i)_K (\frac{1}{2} \frac{1}{2})_0)_K \\ &\times \int dr_f dr_{bn} d\theta r_{bn}^2 \sin \theta r_f \frac{f_l(r_f) g_{l'}(r_i)}{r_i} u_{j_f}(r_{An}) u_{j_i}(r_{bn}) V(r_{bn}) \\ &\times \sum_{M_K} (-1)^{M_K} \langle l l' 0 M_K | K M_K \rangle \left[ Y^{l_f}(\hat{r}_{An}) Y^{l_i}(\hat{r}_{bn}) \right]_{-M_K}^K Y_{M_K}^{l'}(\hat{r}_i). \end{aligned} \quad (4.1.26)$$

### 4.1.1 Coordinates

To perform the integral in (4.1.26), one needs the expression of  $r_i, r_{An}, \hat{r}_{An}, \hat{r}_{bn}, \hat{r}_i$  in term of the integration variables  $r_f, r_{bn}, \theta$ . Because one is interested in evaluating

these quantities in the particular configuration depicted in Fig. 4.1.2, one has

$$\mathbf{r}_f = r_f \hat{z}, \quad (4.1.27)$$

$$\mathbf{r}_{bn} = -r_{bn}(\sin \theta \hat{x} + \cos \theta \hat{z}), \quad (4.1.28)$$

$$\mathbf{r}_{Bn} = \mathbf{r}_f + \mathbf{r}_{bn} = -r_{bn} \sin \theta \hat{x} + (r_f - r_{bn} \cos \theta) \hat{z}. \quad (4.1.29)$$

One can then write

$$\mathbf{r}_{An} = \frac{A+1}{A} \mathbf{r}_{Bn} = -\frac{A+1}{A} r_{bn} \sin \theta \hat{x} + \frac{A+1}{A} (r_f - r_{bn} \cos \theta) \hat{z}, \quad (4.1.30)$$

$$\mathbf{r}_{an} = \frac{b}{b+1} \mathbf{r}_{bn} = -\frac{b}{b+1} r_{bn} (\sin \theta \hat{x} + \cos \theta \hat{z}), \quad (4.1.31)$$

and

$$\mathbf{r}_i = \mathbf{r}_{An} - \mathbf{r}_{an} = -\frac{2A+1}{(A+1)A} r_{bn} \sin \theta \hat{x} + \left( \frac{A+1}{A} r_f - \frac{2A+1}{(A+1)A} r_{bn} \cos \theta \right) \hat{z}, \quad (4.1.32)$$

where  $A, b$  are the number of nucleons of nuclei  $A$  and  $b$  respectively.

### 4.1.2 Zero-range approximation

In the zero range approximation,

$$\int dr_{bn} r_{bn}^2 u_{j_i}(r_{bn}) V(r_{bn}) = D_0; \quad u_{j_i}(r_{bn}) V(r_{bn}) = \delta(r_{bn}) / r_{bn}^2. \quad (4.1.33)$$

It can be shown (see Fig. 4.1.2) that for  $r_{bn} = 0$

$$\mathbf{r}_{An} = \frac{m_A + 1}{m_A} \mathbf{r}_f, \quad \mathbf{r}_i = \frac{m_A + 1}{m_A} \mathbf{r}_f. \quad (4.1.34)$$

One then obtains

$$\begin{aligned} t_{ll'}^K &= \frac{-16 \sqrt{2} \pi^2}{k_f k_i} (-1)^K \frac{D_0}{\alpha} l'^{-l} e^{\sigma_f^l + \sigma_i^{l'}} \frac{\sqrt{(2l+1)(2l'+1)(2l_i+1)(2l_f+1)}}{2K+1} ((l_f \frac{1}{2})_{j_f} (l_i \frac{1}{2})_{j_i} | (l_f l_i)_K (\frac{1}{2} \frac{1}{2})_0)_K \\ &\times \langle l' l' 0 0 | K 0 \rangle \langle l_f l_i 0 0 | K 0 \rangle \int dr_f f_l(r_f) g_{l'}(ar_f) u_{j_f}(ar_f), \end{aligned} \quad (4.1.35)$$

with

$$\alpha = \frac{A+1}{A}. \quad (4.1.36)$$

## 4.2 Examples and Applications

In this section we discuss some examples which illustrate the workings of single-particle transfer processes.

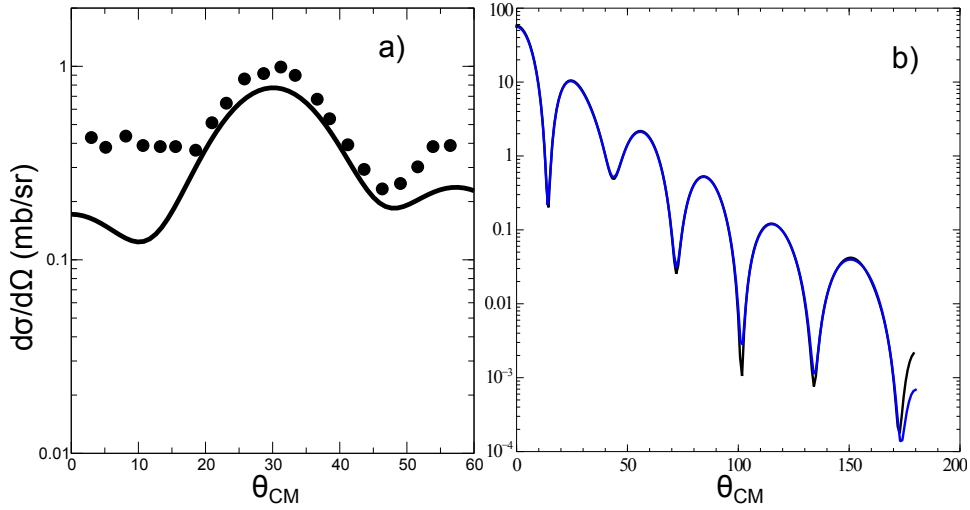


Figure 4.2.1: The absolute differential cross section  $^{120}\text{Sn}(p, d)^{119}\text{Sn}(j^\pi)$  associated with the state  $j^\pi = 7/2^+$ . a) the theoretical prediction discussed in the text are displayed in comparison with the experimental data (Dickey, S. A. et al. (1982)). The corresponding integrated cross sections are 5.0 and  $5.2 \pm 0.6$  mb respectively. b) Comparison of the results of ONE and of the software FRESCO for the same reaction as in (a) but populating the  $s_{1/2}$  state.

#### 4.2.1 $^{120}\text{Sn}(p, d)^{119}\text{Sn}$ and $^{120}\text{Sn}(d, p)^{121}\text{Sn}$ reactions.

In the calculation of absolute reaction cross section two elements melt together: reaction and structure. In the case of weakly coupled probes like, as a rule, direct one-particle transfer processes are, the first element can be further divided into two essentially separated components: elastic scattering (optical potentials), and transfer amplitudes connecting entrance and exit channels. In other words, the habitat of DWBA.

In Fig. 4.2.1 (a) a concrete embodiment of the formalism presented in the first part of this Chapter, worked out with the help of the software ONE (Potel, G. (2012)), of global optical parameters (Dickey, S. A. et al. (1982)) and of NFT spectroscopic amplitudes (cf. Table 4.2.1), is given. In it, the absolute differential cross section associated with the population of the low-lying state  $|^{119}\text{Sn}(11/2^-; 88\text{keV})\rangle$  in the one-particle pick-up process  $^{120}\text{Sn}(p, d)^{119}\text{Sn}$  is compared with the experimental data. In Fig. 4.2.1 (b) the theoretical predictions were obtained with the help of ONE.

Similar calculations (ONE, NFT spectroscopic amplitudes and global optical parameters), have been carried for the reaction  $^{120}\text{Sn}(d, p)^{121}\text{Sn}(j^\pi; E_x)$  in connection with the population of the  $|3/2^+; \text{gs}\rangle$  and  $|11/2^-; E_x \approx 0 \text{ MeV}\rangle$  states. In the stripping experiment (Bechara, M. J. and Dietzsch (1975)) the ground state and the  $11/2^-$  state were not resolved in energy. This is the reason why theory and experiment are only compared to the data for the summed  $l = 2 + 5$  differential cross

section (cf. Fig. 4.2.2 (a)), the separate theoretical predictions been displayed in Figs. 4.2.2 (b) and (c).

Let us now turn to the most fragmented low-lying quasiparticle state around  $^{120}\text{Sn}$ , namely that associated with the  $d_{5/2}$  orbital (cf. Idini, A. (2013), Idini, A. et al. (2012)) As shown in Fig. 4.2.3 five low-lying  $5/2^+$  states have been populated in the reaction  $^{120}\text{Sn}(p, d)^{119}\text{Sn}$  with a summed cross section  $\sum_{i=1}^5 \sigma(2^\circ - 25^\circ) \approx 8 \text{ mb} \pm 2 \text{ mb}$  (Dickey, S. A. et al. (1982)) while four are theoretically predicted with  $\sum_{i=1}^4 \sigma(2^\circ - 25^\circ) = 6.2 \text{ mb}$  (cf. also Idini, A. et al. (2014)). Within the present context, namely that of probing the single-particle content of an elementary excitation, the study of the  $5/2^+$  quasiparticle strength is a rather trying situation. Arguably, it provides a measure of the limitations encountered in such studies.

Analysis of the type presented above allows one to posit that structure and reactions are but just two aspects of the same physics. If one adds to this picture the fact that the optical potential –that is, the energy and momentum dependent nuclear dielectric function describing the medium where direct nuclear chemistry takes place– can be calculated microscopically (cf. Mahaux, C. et al. (1985), Fernández-García, J.P. et al. (2010), Fernández-García, J.P., M. Rodríguez-Gallardo et al. (2010), Broglia, R. A. et al. (1981), Pollarolo et al. (1983), Broglia and Winther (2004), Dickhoff, W. and Van Neck (2005), Jenning, B. (2011), Montanari et al. (2014)) in terms of the same elements entering structure calculations (i.e. spectroscopic amplitudes, single-particle wavefunctions, transition densities and eventually effective formfactors), the structure reaction loop closes itself.

Allowing halo nuclei to be part of the daily nuclear structure paradigm, the equivalence between structure and reactions becomes even stronger, in keeping with the central role the continuum plays in the structure of these nuclei.

Searching for further contact points between structure and reactions, one can posit that the above parlance, although being essentially correct, does not emphasize enough the central role virtual, correlated particle-hole excitations play in the single-particle transfer process. In fact, as a result of the interweaving of single-particle (quasiparticle) motion and e.g. collective surface vibrations, particles become dressed, being able to contribute less (differently) to the direct transfer process but, eventually, opening new doorway channels (states) (cf. Feshbach (1958), Rawitscher, G. H. (1987), Bortignon and Broglia (1981), Bertsch et al. (1983)) to depopulate the entrance channel (cf. figura 1D4 de la introducción), similar to those responsible for the breaking of the single-particle strength ( $Z_\omega (= m/m_\omega)$ ) and of the damping of giant resonances and of the renormalization of low-lying collective states (cf. Figs. 4.C.2, 4.C.3, 4.E.1, 4.E.2, cf. also App. 4.I).

It seems then fair to state that the importance of the coupled channels approach to reactions (cf. e.g. Thompson (1988), Thompson, I.J. (2013), Tamura, T. et al. (1970), Ascuitto and Glendenning (1969), Ascuitto, R. J. and Glendenning (1970), Ascuitto R. J. et al. (1971), Ascuitto R.J. and Sørensen (1972); cf. also Fernández-García, J.P. et al. (2010), Fernández-García, J.P., M. Rodríguez-Gallardo et al. (2010)) is not so much, or at least not only, that it is able to handle situations like for example one-particle transfer to members of a rotational band, alas at the

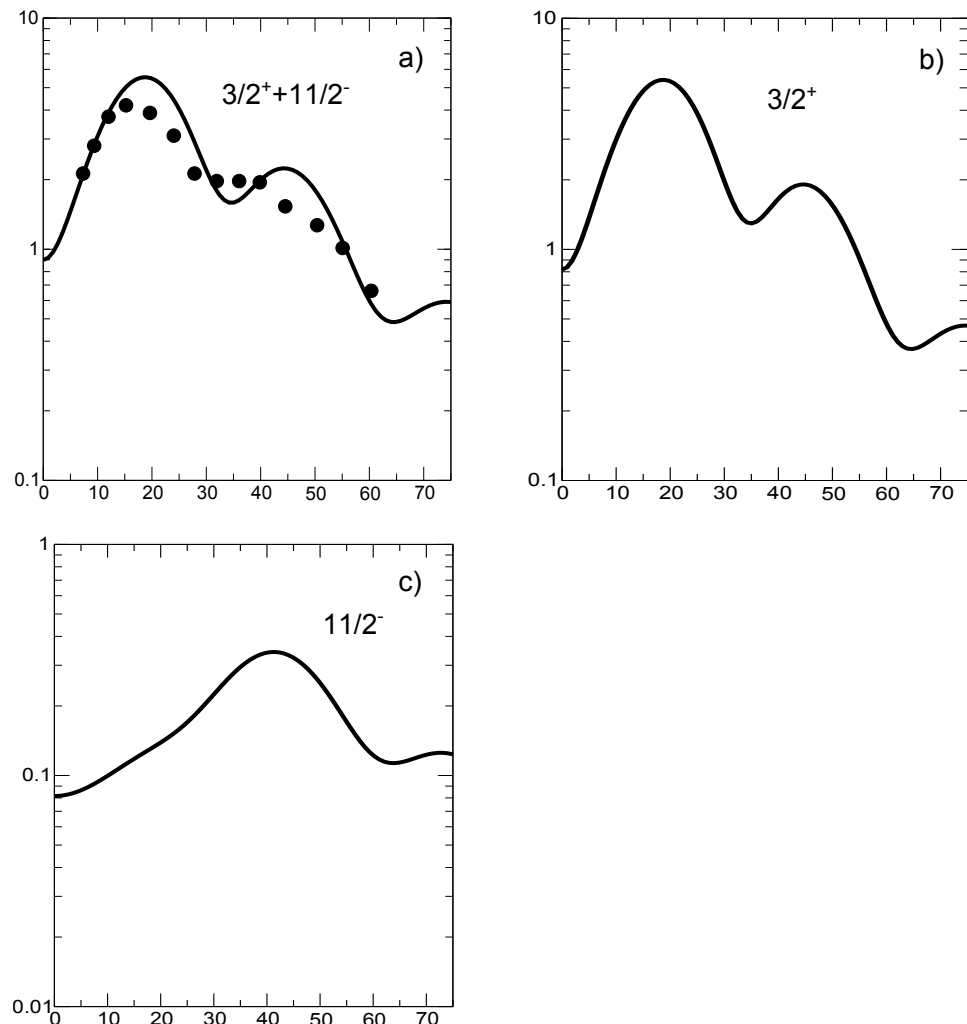


Figure 4.2.2: The theoretical absolute differential cross section (continuous curve) associated with the reaction  $^{120}\text{Sn}(d, p)^{121}\text{Sn}$  and populating the low-lying states  $3/2^+$  and  $11/2^-$  are shown in b) and c), while the summed differential cross section is displayed in a) in comparison with the data (Bechara, M. J. and Dietzsch (1975)).

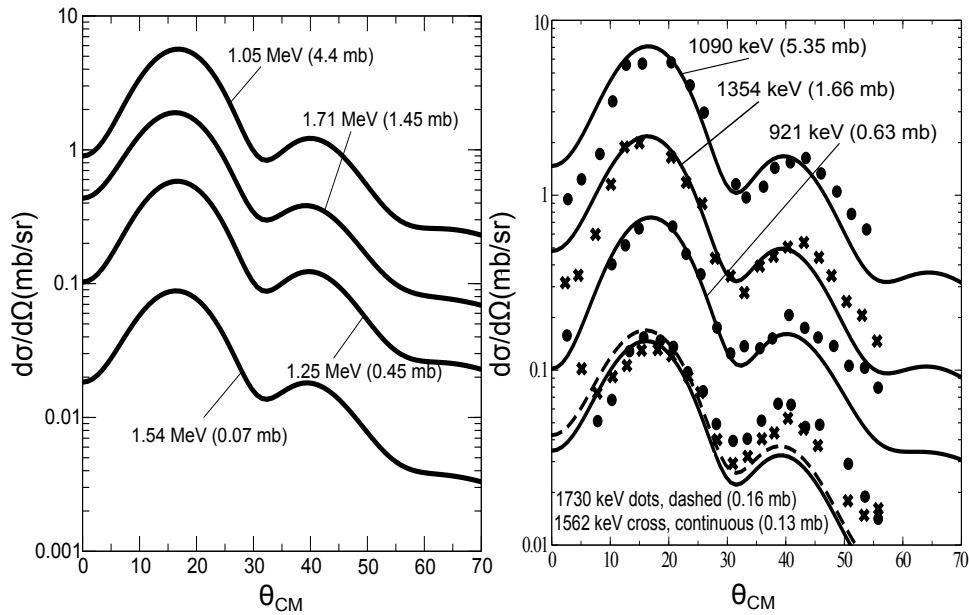


Figure 4.2.3:  $^{120}\text{Sn}(p, d)^{119}\text{Sn}(5/2^+)$  absolute experimental cross sections (dots, Dickey, S. A. et al. (1982)), together with the DWBA fit carried out in the analysis of the data (right panel) in comparison with the finite range, full recoil DWBA calculations carried out with global optical potentials making use of NFT structure inputs as explained in the text (after Idini, A. et al. (2014)) and of the software ONE (Potel, G. (2012)); see also App. 6.D.

		$^{120}\text{Sn}(p, d)^{119}\text{Sn}(j)$	$^{120}\text{Sn}(d, p)^{121}\text{Sn}(j)$
$j$	$E_j$ (MeV)	$\bar{V}_j^2$	$\bar{U}_j^2$
$h_{11/2}$	1.54	(1.34) 0.25 (0.28)	(1.25) 0.55 (0.49)
$d_{3/2}$	1.27	(1.27) 0.35 (0.41)	(1.25) 0.41 (0.44)

Table 4.2.1: The properties of the main peaks of the  $h_{11/2}$  and  $d_{3/2}$  strength functions of  $^{120}\text{Sn}$  calculated taking into account the interweaving of fermionic and bosonic elementary modes of excitation within NFT and of their consequences in both the normal and abnormal densities (cf. Idini, A. et al. (2012); Idini, A. (2013) see also Idini, A. et al. (2014) where the spin degrees of freedom, solely repulsive pairing channel ( ${}^1S_0$ ) in finite nuclei, has also been included). In parenthesis, experimental (energies) and empirical (single-particle strength) data are given (Bechara, M. J. and Dietzsch (1975), Dickey, S. A. et al. (1982)).

expenses of eventually adjusting the optical potential, but that it reminds us how intimately connected probed and probe are in nuclei.

On the other hand, for most of the situations dealt in the present monograph, it is transparent the power, also to reflect the physics, of the approach based in perturbative DWBA (e.g. 1st order for one-nucleon transfer and 2nd for Cooper pair tunneling), coupled with NFT elementary modes of nuclear excitation.

To which extent a FRESCO like software built on a NFT basis will ever be attempted is an open question. Note in any case the serious attempts made at incorporating so called core excitations within the FRESCO framework (Fernández-García, J.P. et al. (2010), Fernández-García, J.P., M. Rodríguez-Gallardo et al. (2010)).

We conclude this section by recalling the fact that the dressing of single particles with pairing vibrations plays also a central role in the structure properties of nuclei (cf. e.g. Barranco et al. (1987), Bès, D. R. et al. (1988), Baroni, S. et al. (2004) and refs. therein).

#### 4.2.2 Dressing of single-particle states: parity inversion in $^{11}\text{Li}$ .

The  $N = 6$  isotope of  ${}^9\text{Li}$  displays quite ordinary structural properties and can, at first glance, be thought of a two-neutron hole system in the  $N = 8$  closed shell. That this is not the case emerges clearly from the fact that  ${}^{10}\text{Li}$  is not bound. In addition, the observation that the two lowest unoccupied states are the virtual ( $1/2^+$ ) and the resonant ( $1/2^-$ ) states, testify to the fact that, in the present case,  $N = 6$  is a far better magic neutron number than  $N = 8$ . In addition, the observation that the unbound  $s_{1/2}$  state lies lower than the unbound  $p_{1/2}$  state, a phenomenon known in the literature as parity inversion (see Fig. 4.2.4), is in plain contradiction with static mean field theory. Dressing the (standard) mean field (e.g. Saxon-Woods potential, cf. Bohr and Mottelson (1969) Eqs. (2–181)–(2–182)) single-particle states with vibrations of the  ${}^9\text{Li}$  core in terms of polarization (effective mass-like) and correlation (vacuum zero point fluctuations (ZPF)) diagrams, similar to those

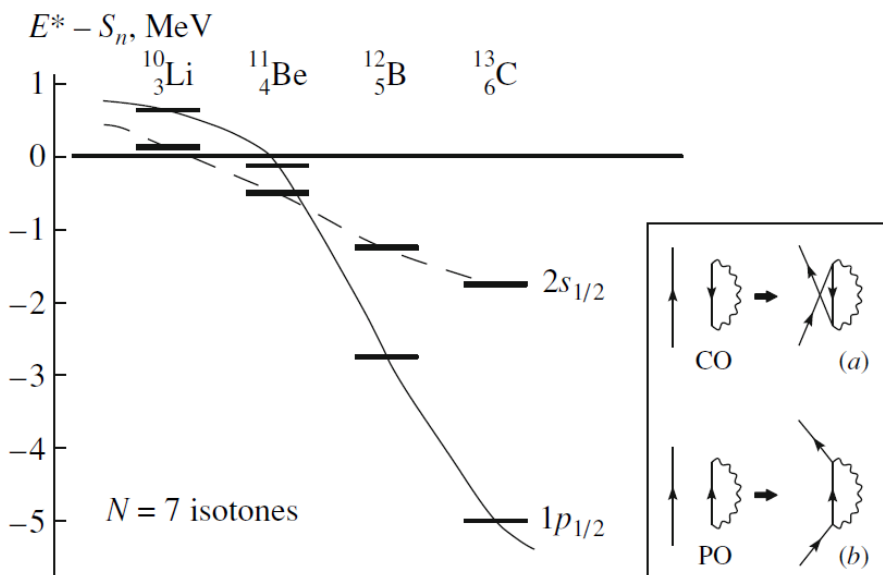


Figure 4.2.4: Single-particle states for  $N = 7$  isotones around  $^{11}\text{Be}$  associated with parity inversion. The thin horizontal lines represent the  $1p_{1/2}$  single-particle state, while the thick ones the  $2s_{1/2}$  orbital. In the case of  $^{10}\text{Li}$  one reports the centroid of the virtual and of the resonant states.  $E^*$  stands for excitation energy and  $S_n$  is the neutron separation energy. In the case of  $^{10}\text{Li}$  e.g.  $S_n = 0$ , while  $E_{s_{1/2}}^* = 0.2 \text{ MeV}$  and  $E_{p_{1/2}}^* = 0.5 \text{ MeV}$ . In the inset the correlation (CO) and polarization (PO) (virtual) contribution to the single-particle self-energy are shown. An arrowed line pointing upwards represents a particle moving in a level with energy  $\epsilon_k > \epsilon_F$ , a downwards pointing line represents a hole state  $\epsilon_i < \epsilon_F$ , while a wavy line stands for a ph-like vibrational state. Their contribution to the real (single-particle “legs” propagating to  $\pm\infty$  times) processes dressing the  $1p_{1/2}$  and  $2s_{1/2}$  neutron states of  $^{10}\text{Li}$  and  $^{11}\text{Be}$  are (a) and (b), respectively. In the first case the phonon corresponds essentially only to the  $2^+$  vibration of the corresponding core ( $^9\text{Li}$  and  $^{10}\text{Be}$ , respectively) and pushes the orbital upwards (Pauli principle, Lamb-shift-like process) making the dressed  $p_{1/2}$  orbital more strongly unbound than what it was originally in the SaxonWoods potential. In the case of the  $2s_{1/2}$  orbital, it is mainly the process (b) which dresses the state making it almost bound (virtual state) as compared with the SaxonWoods state. Within this context, it is of notice that in the binding of the two halo neutrons of  $^{11}\text{Li}$  to the  $^9\text{Li}$  core, it is essentially the pigmy resonance of  $^{11}\text{Li}$  which provides the largest contribution, the coupling to the  $2^+$  vibration of the core  $^9\text{Li}$  giving a small shift in energy (nonetheless, it is this weak component of the self energy which is responsible for the excitation, in the  $^{11}\text{Li}(p, t)^{10}\text{Li}$  reaction, of the  $1/2, 2.69 \text{ MeV}$  state). In the case of  $^{11}\text{Be}$  the (ph) vibrations are the  $2^+, 1$ , and  $3$  of the core  $^{10}\text{Be}$ , in keeping also with the fact that  $^{12}\text{Be}$  does not display a pigmy  $1$  resonance, not at least based on the ground state. It is of notice that graphs (a) and (b) give rise to an effective mass known as the  $\omega$ -mass. Associated with it are the  $Z(\omega) = (m_\omega/m) - 1$  occupation factors (discontinuity at the Fermi energy).

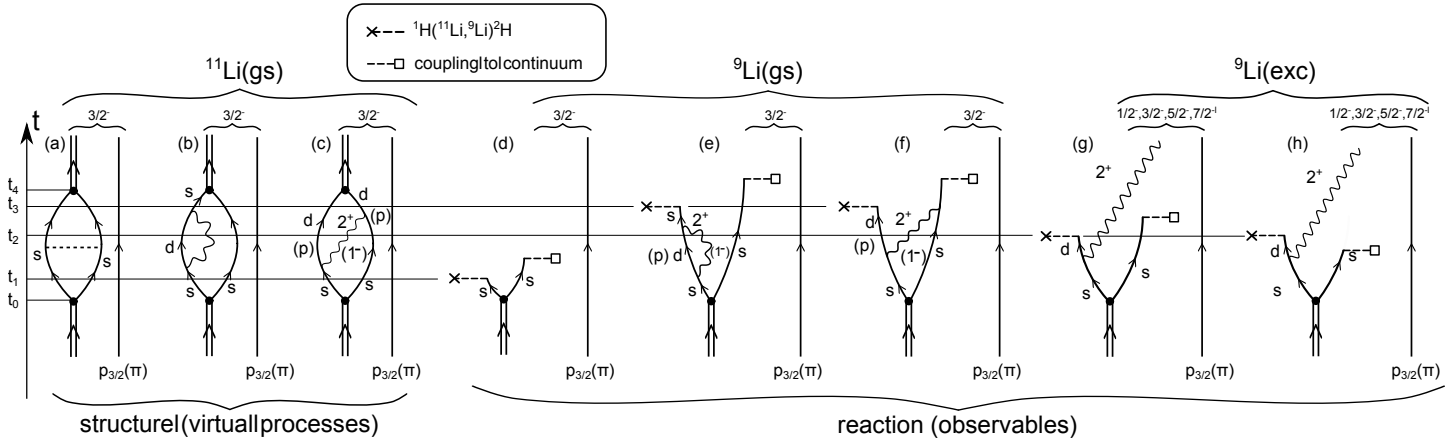


Figure 4.2.5: Nuclear Field Theory diagrams describing the basic, lowest order processes, by which the di-neutron halo binds to the  ${}^9\text{Li}_6$  core to give rise to  ${}^{11}\text{Li}$  ground state (**structure**), and those associated with a one-neutron pick-up process, e.g.  ${}^1\text{H}({}^{11}\text{Li}, {}^{10}\text{Li}){}^2\text{H}$  (**reaction**). The vibrational states of the core  ${}^9\text{Li}$  are here represented by the quadrupole mode  $2^+$ , although in the calculations particle-hole modes with  $\lambda^\pi = 3^-, 4^+$  and  $5^-$  were also considered. The state  $(1^-)$  associated with the  $s \rightarrow (p)$  single-particle states shown in (c) corresponds to the giant dipole resonance of  ${}^{11}\text{Li}$  (see  $\alpha$  component in Eq. (6.1.1)). The contribution of this mode to the binding of the Cooper pair is overwhelming (cf. e.g. App. 2.6).

associated with the (lowest order) Lamb shift Feynman diagrams, (cf. App 4.D), shifts the  $s_{1/2}$  and  $p_{1/2}$  mean field levels around. In particular the  $p_{1/2}$  from a bound state ( $\approx -1.2\text{ MeV}$ ) to a resonant state lying at  $\approx 0.5\text{ MeV}$  (Pauli principle, vacuum ZPF process), the  $s_{1/2}$  being lowered and becoming a virtual state ( $\approx 0.2\text{ MeV}$ ) (cf. Fig. 2.6.3 1F3; cf. also Barranco, F. et al. (2001)). While  ${}^{10}\text{Li}$  is not bound, adding a second dressed neutron and allowing them to exchange density vibrations of the core, as well as the pigmy giant resonance resulting from the sloshing back and forth of the outer neutrons as well as those of  ${}^9\text{Li}$  against the protons (cf. Appendix 1F y App. 6.A) binds the Cooper pair to  ${}^9\text{Li}$ . In fact  ${}^{11}\text{Li}_8$  displays a two-neutron separation energy  $S_{2n} \approx 400\text{ keV}$  (for further details we refer to Ch. 6, Sect. 6.1).

The two dimensional landscapes (surfaces) displayed in Figs. 2.6.3 figura 1F3 (II) a) and b) attempt at describing the becoming of the neutron halo Cooper pair of  ${}^{11}\text{Li}$ , from an uncorrelated  $s_{1/2}^2(0)$  configuration to a correlated, (weakly) bound two-neutron state. It is of notice that the bare interaction (boxed inset in (II)), lowers the  $s_{1/2}^2(0)$  (as well as the  $p_{1/2}^2(0)$ ) pure configurations by only 100 keV, and thus it is not able, by itself, to bind the pair, nor to give rise to any significant mixing between these two configurations. The surfaces display the modulus square of the two-neutron wavefunction as a function of the coordinates of the two nucleons (left) and the probability distribution of one neutron with respect to the second one held fixed on the x-axis (at a radius of 5fm, solid dot). The red circle schematically

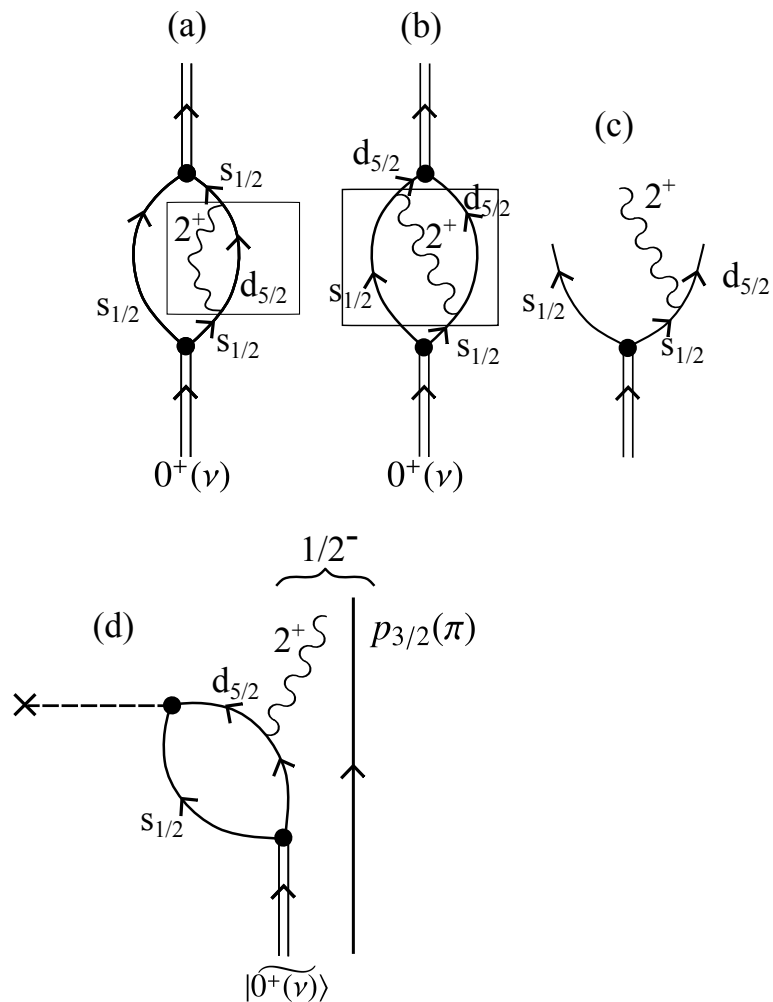


Figure 4.2.6: (a) Self-energy (see boxed process) and (b) vertex (pairing induced interaction) renormalization process, both diagrams associated with (c) a (two-particle)-(quadrupole vibration) intermediate (virtual state) which can be forced to become real in a  $(p, t)$  reaction like e.g.  ${}^1\text{H}({}^{11}\text{Li}, {}^9\text{Li}){}^3\text{H}$  exciting the first excited state  $|2.69\text{MeV}; 1/2^-\rangle$  of  ${}^9\text{Li}$  (see Ch.6).

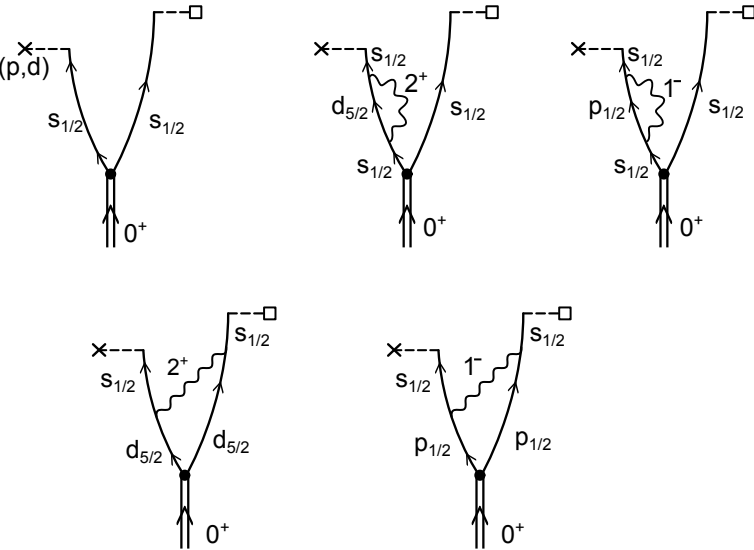


Figure 4.2.7: Lowest order, NFT contributions, to the population of the  $s_{1/2}$  lowest resonant  ${}^{10}\text{Li}(1/2^+)$  through the pick-up reaction  ${}^1\text{H}({}^{11}\text{Li}, {}^{10}\text{Li}(1/2^+)){}^2\text{H}$ . Concerning the notation cf. Caption to Fig. 4.2.5.

represents the core.

How can one check that CO and PO like processes as the ones shown in Fig. 2.6.3 (I) (cf. also Fig. 4.B.1) are the basic processes dressing the odd neutron of  ${}^{10}\text{Li}$ , and thus the mechanism at the basis of parity inversion? The answer is, forcing these virtual processes to become real. In other words, act on the system with an external field so that certain off-the-energy shell states become on-the-energy shell. In fact, a reaction like  ${}^1\text{H}({}^{11}\text{Li}, {}^{10}\text{Li}){}^2\text{H}$  can populate single-particle states in  ${}^{10}\text{Li}$  (see Fig. 4.2.5), in particular the two lowest states of  ${}^{10}\text{Li}$ , namely the virtual and the resonant  $|s_{1/2}\rangle$  and  $|p_{1/2}\rangle$  states respectively. The same can be of course done through the reaction  ${}^2\text{H}({}^9\text{Li}, {}^{10}\text{Li}){}^1\text{H}$  (see Orrigo, S. E. A. and Lenske (2009) and Jepesen, H. B. et al. (2004)). Being these states embedded in the continuum the system will eventually decay into both the ground and excited states of  ${}^9\text{Li}$  (cf. Fig. 4.2.5) (referir al apendice W).

Now, indirect information on this questions can also be obtained with the help of two-particle transfer processes, namely that associated with inverse kinematics ( $p, t$ ) reaction  ${}^1\text{H}({}^{11}\text{Li}, {}^9\text{Li}(2.69\text{MeV}; 1/2^-)){}^3\text{H}$  (Tanihata, I. et al., 2008) populating the first excited state of  ${}^9\text{Li}$ , thought to be the lowest member of the multiplet  $2^+ \otimes p_{3/2}(\pi)$  (cf. Figs. 6.1.1–6.1.3 and 4.2.6). A price to pay for not using the specific probe for single-particle modes (one-particle transfer), is that of adding to the self-energy contributions in question those corresponding to vertex corrections (for details cf. App 4.E, Figs 4.E.1 and 4.E.2 and Ch. 6).

Within the present context, it is difficult if not impossible to talk about single-particle motion without also referring to collective vibrational states (cf. e.g. Fig.

2.6.3 (II)), or to talk about pair addition and pair subtraction modes, without at the same time talking about correlated particle–hole (e.g. density) vibrations and dressed quasiparticle motion (see e.g. Fig. 4.2.6 (a) and (b) ), again concerning both structure and reactions. Within the framework of the present monograph, the above facts imply that Chapters 1, in particular App. ?? 1E, Chapters 4 (one-particle transfer), 5, and 6 (two-particle transfer and applications), form a higher unity. This unity extends also to the content of App 4.G (knock-out reactions), as well as to the question of inelastic channels and of final state interactions, and thus of the possibility that the population of the excited state  $1/2^-$  receives contributions other, and more involved, than those associated with the direct two-nucleon pick-up process depicted in Figs. 4.2.5 (g) and (h) and 4.2.6 (d) (for details cf. Ch. 6, in particular App. 6.B, Table 6.B.1; cf. also (Potel et al., 2010)).

Let us now return to the discussion of the one-particle transfer process  $^1\text{H}(^{11}\text{Li}, ^{10}\text{Li})^2\text{H}$ , that is the pickup of a neutron from the pair addition halo state  $|^{11}\text{Li(gs)}\rangle$  (cf. Fig. 4.2.5). In keeping with the fact that  $^{10}\text{Li}$  is not bound, such a reaction populates only transiently the virtual and resonant states of  $^{10}\text{Li}$  and eventually, after the second neutron of the pair spoliated of its dynamical glue leaves the system by decaying into the continuum, a state in  $^9\text{Li}$  is populated (cf. Figs. 4.2.5 (d)–(f) and (g) and (h)). In drawing the different NFT diagrams time  $t$  is assumed to run upwards. External fields and the bare  $NN$ -interaction are assumed to act instantaneously, while the couplings to the phonon modes (wavy lines) lead to retarded ( $\omega$ -dependent) effects. For simplicity, only the quadrupole vibrational mode of the  $^8\text{He}$  core is considered, as well as only the virtual  $s$ - and continuum  $d$ - single-particle states are taken into account. The halo Cooper pair (pair addition mode of the  $N = 6$  closed shell system) carries angular momentum  $0^+$  and is represented by a double arrowed line, the odd proton ( $\pi$ ) which occupies a  $p_{3/2}$  state, is represented by a single arrowed line and is here treated as a spectator. The di-neutron system binds to the core through (a) the bare interaction (horizontal dashed line) acting between the two-neutron, each represented by a single arrowed line, and through the renormalizing processes associated with the coupling of the neutrons with vibrations; (b) effective mass processes associated with the quadrupole vibration of  $^9\text{Li}$  (wavy line) renormalizing the energy of the  $s_{1/2}$  continuum state and leading to an almost bound (virtual) state ( $\approx 0.2$  MeV) as well as of the  $p$ -state and giving rise to a resonant state ( $\approx 0.5$  MeV). (c) Vertex correction (induced pairing interaction) associated with the quadrupole vibration of  $^9\text{Li}$  and with the giant dipole pigmy resonance of  $^{11}\text{Li}$ . While the quadrupole vibration is essential for parity inversion (single-particle renormalization effect) it plays little role regarding vertex corrections (induced pairing interaction), the pigmy resonance of  $^{11}\text{Li}$  plays a central role in binding the Cooper pair, as testified by components  $\beta (= 0.1)$  and  $\alpha (= 0.7)$  of  $|^{11}\text{Li(gs)}\rangle$  (cf. eq. (6.1.1)). Of course, the pigmy resonance plays no role in parity inversion in  $^{10}\text{Li}$ , being an excitation of  $^{11}\text{Li}$ , nucleus in which it plays little role in the virtual effective mass process of the  $s_{1/2}$  and  $p_{1/2}$  states of  $|0_\nu\rangle$ . Picking up a neutron from the halo pair addition mode of  $^9\text{Li}$  (that is  $|^{11}\text{Li(gs)}\rangle$ ), it obliterates its symbiotic pigmy resonant state. This is a peculiar

example of the fact that not all virtual states can be forced to become real even with the proper external field. On the other hand, the absolute cross section associated with the reaction  ${}^1\text{H}({}^{11}\text{Li}, {}^{10}\text{Li}(1/2^+)) {}^2\text{H}$  will depend on the variety of renormalization processes displayed in Fig. 4.2.7 (d) Intervening the process (a) at any time after  $\mathbf{t}_0$  and before  $\mathbf{t}_4$  with an external single-neutron pick-up field (cross followed by an horizontal dashed line), and processes (b) and (c) at  $\mathbf{t}_0 < \mathbf{t} < \mathbf{t}_1$ , leads to the ground state of  ${}^9\text{Li}$ , in keeping with the fact that the second neutron will leave the system almost immediately,  ${}^{10}\text{Li}$  not being stable. (e) Same as above but in connection with process (b) and now after the nucleon has reabsorbed the quadrupole phonon and before  $\mathbf{t}_4$ , i.e. acting at  $\mathbf{t}_3 < \mathbf{t} < \mathbf{t}_4$  leads again to the population of the  ${}^9\text{Li}$  ground state. (f) same as (e) but in this case the external field acts on the process (c). Let us now consider the one-nucleon pickup processes populating the  $(2 \otimes p_{3/2}(\pi))_{J^\pi}, (J^\pi = 1/2^-, 3/2^-, 5/2^- \text{ and } 7/2^-)$  multiplet of  ${}^9\text{Li}$ , in particular the lowest  $|1/2^-; 2.69 \text{ MeV}\rangle$  state. In this case the external field has to act at a time  $\mathbf{t}_2$  on (b) and on (c) leading to identical final states displayed in (g) and on (h). While the single contribution associated with mass renormalization process ((b)→(g)) and vertex corrections ((c)→(h)) cannot be distinguished experimentally, one can estimate the relative contribution to the corresponding absolute cross section making use of, microscopic wavefunctions (cf. e.g. Barranco, F. et al. (2001)).

Before concluding the present section, and in connection with Figs. 4.2.5 (g,h) and 4.2.6 (d), it may be useful to remind us what, within the framework of quantum mechanics, one can learn from a reaction experiment. It is not “what is the state after the collision” but “how probable is a given effect of the collision”. Within this context: “The motion of particles follows probability laws, but the probability itself propagates according to the laws of causality” (Born, 1926)<sup>2</sup>.

---

<sup>2</sup>If there is a lesson to be learned from the above discussion is the fact that, in dealing with a specific feature of a quantal many-body system, e.g. single-particle motion in nuclei (structure) and one-particle transfer process (reaction), one can hardly avoid to talk about other elementary modes of excitation and reaction channels, respectively. Within the scenario of the chosen example, this is because a nucleon which, in first approximation is in a mean field stationary state, can actually be viewed as a fermion moving through a gas of ephemeral  $2p - 2h$  composite virtual excitations, that is  $(p-h) +$  density and/or  $2h(2p) +$  pair addition (subtraction) modes, arising from vacuum (ground state) ZPF and giving rise to the nuclear vacuum  $\omega$ -dependent dielectric function. Because of Pauli principle (Pauli, 1947) the nucleon in question is forced to exchange role with the virtual, off-the-energy-shell nucleons, thus leading to CO processes (cf. Fig. 4.B.1 (b)) and eventually, through time ordering, to PO ones (cf. Fig. 4.B.1 (a)). Such processes, eventually carried on to higher orders of perturbation in the nucleon-vibration coupling, diagonalize the nuclear Hamiltonian, taking care of the overcompleteness (non-orthogonality) and of Pauli violations of the basis made out of elementary modes of nuclear excitation, thus leading to dressed (observable) modes, single-particle states in the present case, whose properties, e.g. absolute single-particle transfer cross sections, can be compared with the data without further ado.

## Appendix 4.A Minimal requirements for a consistent mean field theory

In what follows the question of why, rigorously speaking, one cannot talk about single-particle motion, let alone spectroscopic factors, not even within the framework of Hartree–Fock theory, is briefly touched upon (see also App. 4.I).

As can be seen from Fig. 4.A.1 the minimum requirements of selfconsistency to be imposed upon single-particle motion requires both non-locality in space (HF) and in time (TDHF)

$$i\hbar \frac{\partial \varphi_v}{\partial t} = -\frac{\hbar^2}{2m} \nabla^2 \varphi_v(x, t) + \int dx' dt' U(x - x', t - t') \varphi_v(x', t'), \quad (4.A.1)$$

and consequently also of collective vibrations and, consequently, from their interweaving to dressed single-particles (quasiparticles), let alone renormalized collective modes (cf. Fig. 4.C.3). Assuming for simplicity infinite nuclear matter (confined by a constant potential of depth  $V_0$ ), and thus plane wave solutions, the above time-dependent Schrödinger equation leads to the quasiparticle dispersion relation

$$\hbar\omega = \frac{\hbar^2 k^2}{2m^*} + \frac{m}{m^*} V_0, \quad (4.A.2)$$

where the effective mass

$$m^* = \frac{m_k m_\omega}{m}, \quad (4.A.3)$$

in the product of the  $k$ -mass

$$m_k = m \left( 1 + \frac{m}{\hbar^2 k} \frac{\partial U}{\partial k} \right)^{-1}, \quad (4.A.4)$$

closely connected with the Pauli principle  $\left( \frac{\partial U}{\partial k} \approx \frac{\partial U_x}{\partial k} \right)$ , while the  $\omega$ -mass

$$m_\omega = m \left( 1 - \frac{\partial U}{\partial \hbar\omega} \right), \quad (4.A.5)$$

results from the dressing of the nucleon through the coupling with the (quasi) bosons. Because typically  $m_k \approx 0.7m$  and  $m_\omega \approx 1.4m$   $m^* \approx m$ , one could be tempted to conclude that the results embodied in the dispersion relation (4.A.2) reflects the fact that the distribution of levels around the Fermi energy can be described in terms of the solutions of a Schrödinger equation in which nucleons of mass equal to the bare nucleon mass  $m$  move in a Saxon–Woods potential of depth  $V_0$ .

Now, it can be shown that the occupancy of levels around  $\varepsilon_F$  is related to  $Z_\omega$ , a quantity which measures the discontinuity at the Fermi energy (cf. Fig. 4.A.1 (h)) and which is equal to  $m/m_\omega = 1/(1+\lambda_{p-v}) \approx 0.7$ ,  $\lambda_{p-v}$  being the mass enhancement factor ( $\lambda_{p-v} = N(0)g_{p-v}$ ), product of the density of levels at the Fermi energy and

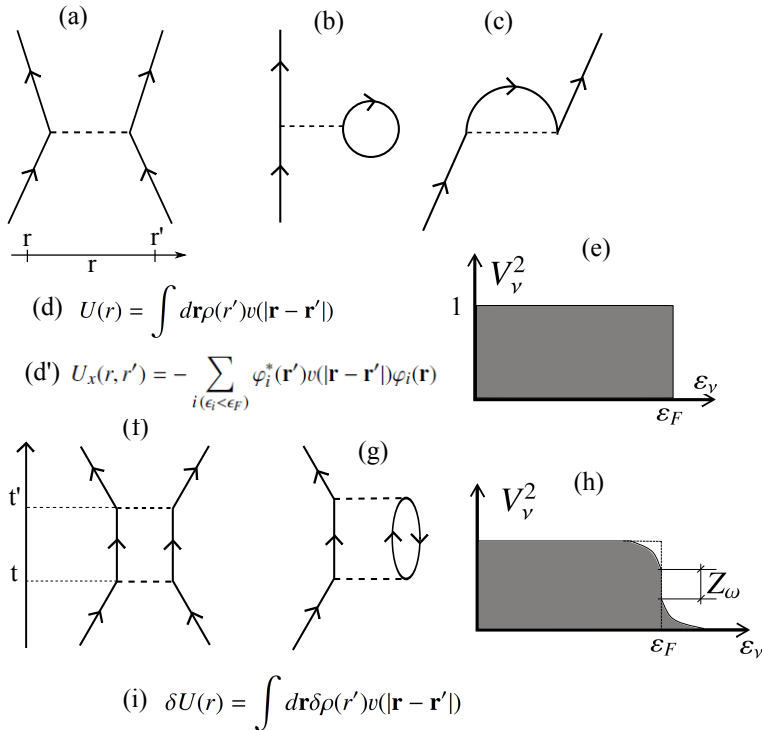


Figure 4.A.1: (a) Scattering of two nucleons through the bare  $NN$  interaction  $v|\mathbf{r} - \mathbf{r}'|$ , (b) contribution to the direct ( $U$ , Hartree) and (c) to the exchange ( $U_x$ , Fock) potential, resulting in (d) the (static) self-consistent relation between potential and density (non-local (d')), which (e) uncouples occupied ( $\varepsilon_v \leq \varepsilon_F$ ) from empty states ( $\varepsilon_v > \varepsilon_F$ ), (f) multiple scattering of two nucleons lead, through processes like the one depicted in (g), eventually propagated to all orders, to: (h) softening of the discontinuity of the occupancy of levels at  $\varepsilon_F$ , as well as to: (i) generalization of the static selfconsistency into a dynamic relation encompassing also collective vibrations (Time-Dependent HF solutions of the nuclear Hamiltonian, conserving energy weighted sum rules (EWSR)).

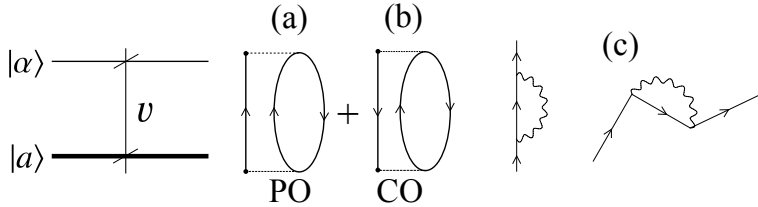


Figure 4.B.1: Two state schematic model describing the breaking of the strength of the pure single-particle state  $|a\rangle$ , through the coupling to collective vibrations (wavy line) associated with polarization (PO) and correlation (CO) processes.

the particle–vibration coupling parameter (cf. e.g. Bohr, A. and Mottelson (1975); Brink, D. and Broglia (2005) and refs. therein). This is in keeping with the fact that the time the nucleon is coupled to the vibrations it cannot behave as a single-particle and can thus not contribute to e.g. the single-particle pickup cross section.

It is of notice that the selfconsistence requirements for the iterative solution of Eq. (4.A.1) (see Fig. 4.A.1 (d) and (d')) remind very much those associated with the solution of the Kohn–Sham equations in finite systems,

$$H^{KS} \varphi_\gamma(\mathbf{r}) = \lambda_\gamma \varphi_\gamma(\mathbf{r}), \quad (4.A.6)$$

where

$$H^{KS} = -\frac{\hbar^2}{2m_e} \nabla^2 + U_H(\mathbf{r}) + V_{ext}(\mathbf{r}) + U_{xc}(\mathbf{r}), \quad (4.A.7)$$

$H^{KS}$  being known as the Kohn–Sham Hamiltonian,  $V_{ext}(\mathbf{r})$  being the field created by the ions and acting on the electrons. Both the Hartree and the exchange–correlation potentials  $U_H(\mathbf{r})$  and  $U_{xc}(\mathbf{r})$  depend on the (local) density, hence on the whole set of wavefunctions  $\varphi_\gamma(\mathbf{r})$ . Thus, the set of  $KS$ –equations must be solved selfconsistently (cf. e.g. (Broglia et al., 2004) and refs. therein).

## Appendix 4.B Model for single–particle strength function: Dyson equation

In the previous Appendix we schematically introduced arguments regarding the “impossibility” of defining a “bona fide” single–particle spectroscopic factor. It was done with the help of Feynman (NFT) diagrams. In what follows we essentially repeat the arguments, but this time in terms of Dyson’s (Schwinger) language. For simplicity, we consider a two–level model where the pure single–particle state  $|a\rangle$  couples to a more complicated (doorway) state  $|\alpha\rangle$ , made out of a fermion (particle or hole), coupled to a particle–hole excitation which, if iterated to all orders can give rise to a collective state (cf. Fig.4.B.1). The Hamiltonian describing the system is (Bohr and Mottelson, 1969)

$$H = H_0 + v, \quad (4.B.1)$$

where

$$H_0|a\rangle = E_a|a\rangle, \quad (4.B.2)$$

and

$$H_0|\alpha\rangle = E_\alpha|\alpha\rangle. \quad (4.B.3)$$

Let us call  $\langle a|v|\alpha\rangle = v_{a\alpha}$  and assume  $\langle a|v|a\rangle = \langle \alpha|v|\alpha\rangle = 0$ .

From the secular equation

$$\begin{pmatrix} E_\alpha & v_{a\alpha} \\ v_{a\alpha} & E_a - E_i \end{pmatrix} \begin{pmatrix} C_\alpha(i) \\ C_a(i) \end{pmatrix} = 0, \quad (4.B.4)$$

and associated normalization condition

$$C_a^2(i) + C_\alpha^2(i) = 0, \quad (4.B.5)$$

one obtains

$$C_a^2(i) = \left( 1 + \frac{v_{a\alpha}^2}{(E_\alpha - E_i)^2} \right)^{-1}, \quad (4.B.6)$$

and

$$\Delta E_a(E) = E_a - E = \frac{v_{a\alpha}^2}{E_a - E}. \quad (4.B.7)$$

The energy of the correlated state

$$|\tilde{a}\rangle = C_a(i)|a\rangle + C_\alpha(i)|\alpha\rangle, \quad (4.B.8)$$

is obtained by the (iterative) solution of the Dyson equation (4.B.7), which propagate the bubble diagrams shown in Figs 4.B.1 (a) and (b) to infinite order leading to collective vibrations (see Fig. 4.B.1 (c))

With the help of the definition given in eq (4.A.5), and making use of the fact that in the present case, the quantity  $U$  appearing in this equation coincides, within the present context with  $\Delta E_a(E)$ , one obtains that the discontinuity of the single-particle levels at the Fermi energy is given by

$$Z_\omega = C_a^2(i) = \left( \frac{m_\omega}{m} \right)^{-1}. \quad (4.B.9)$$

Making use of the solution of the Dyson equation (4.B.7), and of the relations (4.B.5) and (4.B.6), one can calculate the renormalized state  $|\tilde{a}\rangle$  (Eq. 4.B.8) to be employed in working out the associated, modified, single-particle transfer form factor needed in the calculation of the absolute value of one-particle transfer cross sections (cf. e.g. Sect. 4.2.1, where the above concepts and techniques are applied to the study of one-neutron transfer reactions in open shell, superfluid ( $^{120}\text{Sn}$ )).

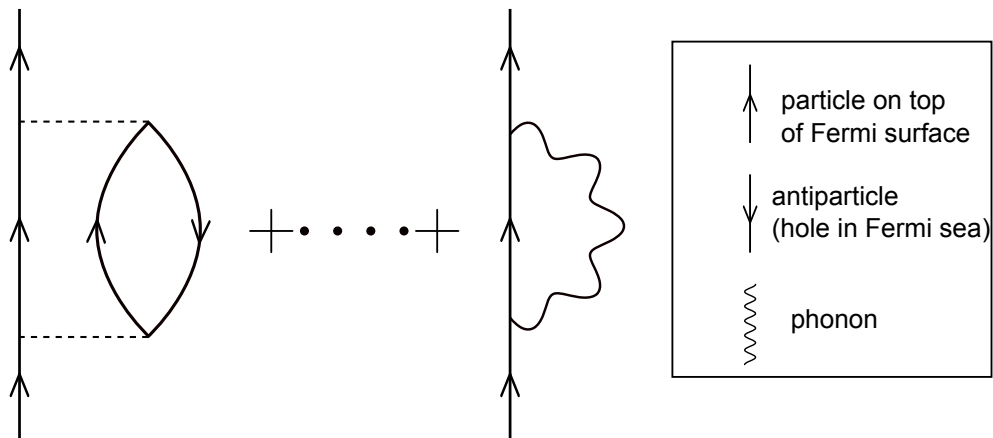


Figure 4.C.1: Feynman diagrams renormalizing the properties of a fermion.

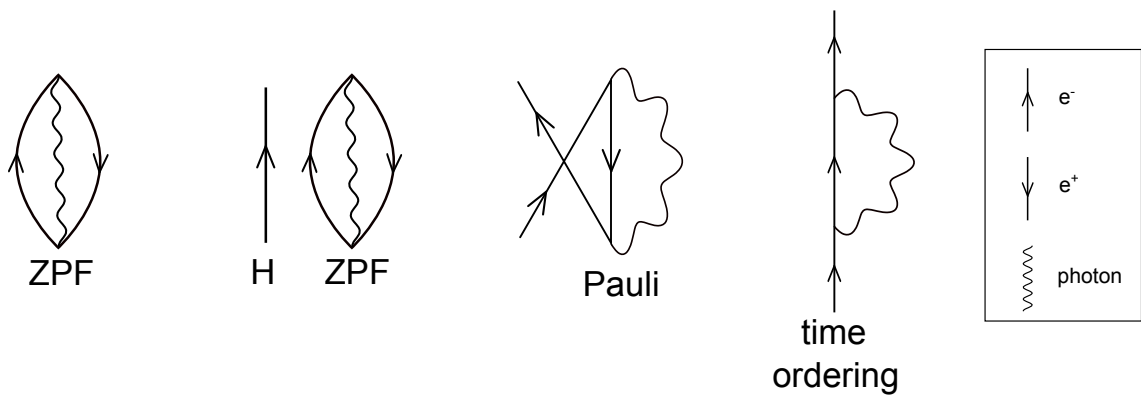


Figure 4.C.2: QED vacuum fluctuation (ZPF). In presence of e.g. an hydrogen atom (H), its electron is forced by Pauli principle to exchange with that of the ZPF, leading to a CO (correlation) like process. Time ordering leads to PO (polarization) processes.

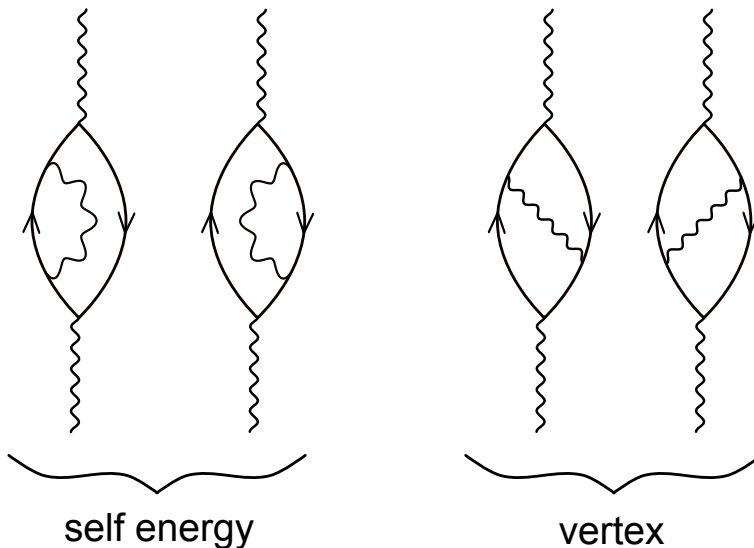


Figure 4.C.3: Lowest order diagrams which dress collective nuclear vibrations and GR.

### Appendix 4.C Antiparticles: proof of concept of the quantal vacuum and of medium polarization effects

Let us consider a massive quantal particle, e.g., an electron, which moves at a velocity close of that of light. Because of Heisenberg relations, there exists a finite possibility to observe the particle moving at a velocity larger than its average velocity, and thus faster than light, a possibility ruled out by special relativity. The only way to avoid this, is by introducing antiparticles, that is a hole in the “vacuum” filled to the rim (Fermi energy) with particles, thus providing the physics to the negative energy solutions of Dirac equation.

In other words, when an electron approaches the maximum speed with which information propagates in a medium, like e.g. in the case of an electron in the QED vacuum, processes like the one depicted in Fig. 4.C.1 become operative. In other words, one can take care of the position indeterminacy of a quantal particle (electron) accepting the possibility to observe it through specific measurements which unavoidably create different particles, each of them identical to the original one, but with different positions, to keep track of conserved quantum numbers, these particles are to be accompanied by an equal number of antiparticles (positrons).

Similar results can be obtained by considering vacuum fluctuations (ZPF), and forcing them to become real through e.g. the Pauli principle (Pauli, 1947), as observed in the Lamb shift (Fig. 4.C.2, cf. also Fig. 4.D.1).

In the nuclear case the medium can, due to spatial quantization typical of Finite Many-Body Systems (FMBS), propagate information with varied frequency. Typ-

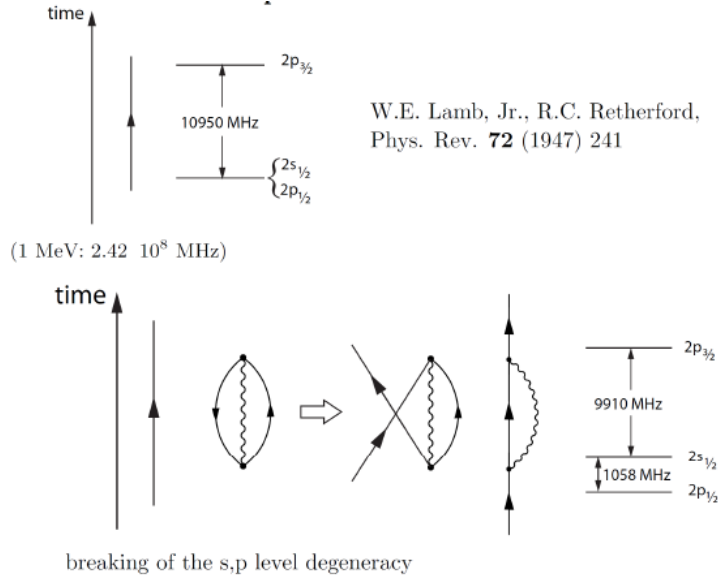


Figure 4.D.1: Schematic representation of the processes associated with the Lamb shift.

ically, few MeV (low-lying collective vibrations of which one has to add dipole pigmy resonances ( $\hbar\omega_{pigmy} \leq 1$  MeV) as for example that involved in the glue of the halo neutrons of  $^{11}\text{Li}(\text{gs})$  (cf. App. 2.6)) and tens of MeV (giant resonances), leading to a rich number of CO and PO processes. This is in keeping with the fact that the intermediate boson (photon QED, vibrations of nuclear medium) propagates in a medium which is not isotropic, thus undergoing fragmentation of the associated strength (inhomogeneous damping). To make even richer the nuclear scenario, collisional damping plays also a role in the strength function of GR. Nonetheless, the associated widths (lifetimes) are controlled by the coupling to doorway states (cf. figura1d6 apendice D introducción), even at nuclear temperatures of 1–2 MeV, let alone when the GR is based on the ground state (Fig. 4.C.3; cf. Bortignon, P.F. et al. (1998) and refs. therein, cf. also Broglia, R. A. et al. (1987)). The strong cancellation found between self-energy and vertex correction diagrams, testify to the collectivity of nuclear vibrations (generalized Ward identities), and reminds of Furry's theorem (no coupling between one- and two-photon states). Summing up, nothing is really free in the quantal world (cf. also App. 4.E). Selected measurements carried out with specific probes, can make virtual processes become real, and shed light on the variety of these processes leading to renormalized elementary modes of nuclear excitation (dressed fermions and bosons).

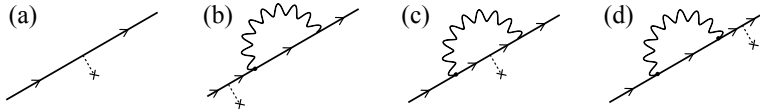


Figure 4.E.1: Self energy (effective-mass-like) processes. The result of the probing with an external field (dotted line started with a cross, observer) of the properties (mass, single-particle energy, etc) of a fermion (e.g. an electron or a nucleon, arrowed line) dressed through the coupling of (quasi) bosons (photons or collective vibrations, wavy line), corresponds to the modulus squared of the sum of the amplitudes associated with each of the four diagrams (a)–(d) (cf. (Feynman, 1975)). A concrete embodiment of the above parlance is provided by the process  $^1\text{H}(^{11}\text{Li}, ^{10}\text{Li})^2\text{H}$  (cf. Figs. 4.2.5 and 4.2.6).

## Appendix 4.D The Lamb Shift

In Fig. 4.D.1 we display a schematic summary of the electron–photon processes, associated with Pauli principle corrections, leading to the splitting of the lowest  $s, p$  states of the hydrogen atom known as the Lamb shift.

In the upper part of the figure the predicted position of the electronic single-particle levels of the hydrogen atom as resulting from the solution of the Schrödinger equation (Coulomb field). In the lowest part of the figure one displays the electron of an hydrogen atom (upwards going arrowed line) in presence of vacuum ZPF (electron–positron pair plus photon, oyster-like diagram) (within this scenario we refer to App. 4.C concerning to the central role ZPF of the vacuum and the concept of antiparticle (hole) has in the description of physical, dressed observable states of quantal many-body systems). Because the associate electron virtually occupies states already occupied by the hydrogen’s electron, thus violating Pauli principle, one has to antisymmetrize the corresponding two-electron state. Such process gives rise to the exchange of the corresponding fermionic lines and thus to CO-like diagrams as well as, through time ordering, to PO-like diagrams. The results provide a quantitative account of the experimental findings.

## Appendix 4.E Self-energy and vertex corrections

In Fig. 4.E.1 an example of the fact that in field theories (e.g. QED or NFT), nothing is really free and that e.g., the bare mass of a fermion (electron or nucleon), is the parameter one adjusts ( $m_k$ ) so that the result of a measurement gives the observed mass (single particle energy). In Fig. 4.E.2, lowest order diagrams associated with the renormalization of the fermion–boson interaction (vertex corrections) are given. The sum of contributions (a) and (b) can, in principle, be represented by a renormalized vertex (cf. diagram (c)). It is of notice, however, that there is, as a rule, conspicuous interference (e.g. cancellation) in the nuclear case between

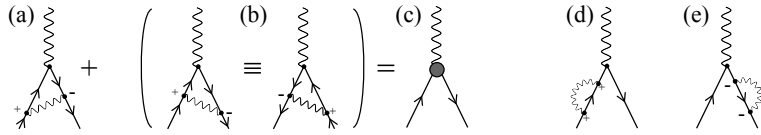


Figure 4.E.2: Vertex corrections. These are triple-interaction diagrams (phonon, particle and hole lines) in which none of the incoming lines can be detached from either of the other two by cutting one line. In connection with condensed matter Migdal's theorem (Migdal (1958)) states that for phonons, (Bardeen and Pines (1955), Fröhlich, H. (1952)) vertex corrections can be neglected (cf. also Anderson (1984)). Vertex corrections are, as a rule, important in the nuclear case where they lead to conspicuous cancellations of the self-energy contributions (cf. e.g. Bortignon et al. (1983), cf. also Anderson (1984)). The solid grey circle in (c) represents the effective, renormalized vertex.

vertex and self-energy contributions (cf. diagrams (a) and (d)+(e) of Fig. 4.E.2, a phenomenon closely related with conservation laws (generalized Ward identities; cf. e.g. Schrieffer (1964)); cf. also Fig. 4.C.3 and refs. Bortignon and Broglia (1981); Bertsch et al. (1983) and Bortignon, P.F. et al. (1998) pp. 82–86). In particular, cancellation in the case in which the bosonic modes are isoscalar (Bortignon et al., 1983). Consequently, one has to sum explicitly the different amplitudes with the corresponding phases and eventually take the modulus squared of the result to eventually obtain the quantities to be compared with the data, a fact that precludes the use of an effective,  $\omega$ -independent (renormalized) vertex.

Within the framework of QED the above mentioned cancellations are exact implying that the interaction between one- and two-photon states vanishes (Furry theorem). The physics at the basis of the cancellation found in the nuclear case can be exemplified by looking at a spherical nucleus displaying a low-lying collective quadrupole vibration. The associated zero point fluctuations (ZPF) lead to time dependent shapes with varied instantaneous values of the quadrupole moment, and of its orientation (dynamical spontaneous breaking of rotational invariance, ver apendice 1B correlations and fluctuations). In other words, a component of the ground state wavefunction ( $| (j_p \otimes j_h^{-1})_{2^+} \otimes 2^+; 0^+ \rangle$ ), which can be viewed as a gas of quadrupole (quasi) bosons promoting a nucleon across the Fermi energy (particle-hole excitation) will lead to fermionic states which behave as having a positive (particle) and a negative (hole) effective quadrupole moment, in keeping with the fact that the closed shell system is spherical, thus carrying zero quadrupole moment.

## Appendix 4.F Single-nucleon transfer for pedestrians

In this Appendix we discuss some aspects of the relations existing between nuclear structure and one-particle transfer cross sections. To do so, we repeat some of the steps carried out in the text but this time in a simpler and straightforward way, ignoring the complications associated with the spin carried out by the particles, the spin-orbit dependence of the optical model potential, the recoil effect, etc.

We consider the case of  $A(d, p)A + 1$  reaction, namely that of neutron stripping. The intrinsic wave functions  $\psi_\alpha$  and  $\psi_\beta$ , where  $\alpha = (A, d)$  and  $\beta = ((A + 1), p)$ ,

$$\psi_\alpha = \psi_{M_A}^{I_A}(\xi_A)\phi_d(\vec{r}_{np}), \quad (4.F.1a)$$

$$\begin{aligned} \psi_\beta &= \psi_{M_{A+1}}^{I_{A+1}}(\xi_{A+1}) \\ &= \sum_{l, I'_A} (I'_A; l | I_{A+1}) [\psi_{M_A}^{I_A}(\xi_A)\phi_d^l(\vec{r}_n)]_{M_{A+1}-M_A}^{I_{A+1}}, \end{aligned} \quad (4.F.1b)$$

where  $(I'_A; l | I_{A+1})$  is a generalized fractional parentage coefficient. It is of notice that this fractional parentage expansion is not well defined. In fact, as a rule,  $(I'_A; l | I_{A+1})\phi_d^l(\vec{r}_n)_{M_{A+1}-M_A}$  is an involved, dressed quasiparticle state containing only a fraction of the “pure” single particle strength (cf. Apps 4.A and 4.B). For simplicity we assume the expansion to be operative. To further simplify the derivation we assume we are dealing with spinless particles. This is the reason why no “intrinsic” proton wavefunction appears in (4.F.1b). The variable  $\vec{r}_{np}$  is the relative coordinate of the proton and the neutron (see Fig. 4.F.1).

The transition matrix element can now be written as

$$\begin{aligned} T_{d,p} &= \langle \psi_{M_{A+1}}^{I_{A+1}}(\xi_{A+1})\chi_p^{(-)}(k_p, \vec{r}_p), V'_\beta \psi_{M_A}^{I_A}(\xi_A)\chi_d^{(+)}(k_d, \vec{r}_d) \rangle \\ &= \sum_{\substack{l, I'_A \\ M'_A}} (I'_A; l | I_{A+1})(I'_A M'_A l M_{A+1} - M' A | I_{A+1} M_{A+1}) \\ &\quad \times \int d\vec{r}_n d\vec{r}_p \chi_p^{*(-)}(k_p, \vec{r}_p) \phi_{M_{A+1}-M'_A}^{*l}(\vec{r}_n) (\psi_{M_A}^{I_A}(\xi_A), V'_\beta \psi_{M'_A}^{I'_A}(\xi_A)) \\ &\quad \times \phi_d(\vec{r}_{np}) \chi_d^{(+)}(k_d, \vec{r}_d) \delta_{I'_A, I_A} \delta_{M'_A, M_A}. \end{aligned} \quad (4.F.2)$$

In the stripping approximation

$$\begin{aligned} V'_\beta &= V_\beta(\xi, \vec{r}_\beta) - \bar{U}_\beta(r_\beta) \\ &= V_\beta(\xi_A, \vec{r}_{pA}) + V_\beta(\vec{r}_{pn}) - \bar{U}_\beta(r_{pA}). \end{aligned} \quad (4.F.3)$$

Then

$$\begin{aligned} (\psi_{M_A}^{I_A}(\xi_A), V'_\beta \psi_{M_A}^{I_A}(\xi_A)) &= (\psi_{M_A}^{I_A}(\xi_A), V_\beta(\xi_A, \vec{r}_{pA}) \psi_{M_A}^{I_A}(\xi_A)) \\ &\quad + (\psi_{M_A}^{I_A}(\xi_A), V_\beta(\vec{r}_{pn}) \psi_{M_A}^{I_A}(\xi_A)) - \bar{U}_\beta(r_{pA}). \end{aligned} \quad (4.F.4)$$

We assume

$$U_\beta(r_{pA}) = (\psi_{M_A}^{I_A}(\xi_A), V_\beta(\xi_A, \vec{r}_{pA}) \psi_{M_A}^{I_A}(\xi_A)). \quad (4.F.5)$$

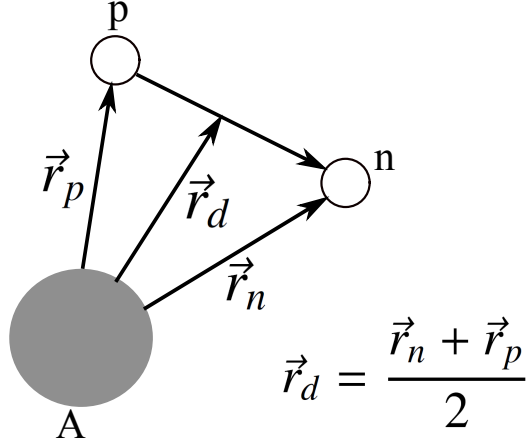


Figure 4.F.1: Coordinates used in the description of the  $A(d, p)(A + 1)$  stripping process.

Then

$$(\psi_{M_A}^{I_A}(\xi_A), V'_\beta \psi_{M_A}^{I_A}(\xi_A)) = V_{np}(\vec{r}_{pn}). \quad (4.F.6)$$

Inserting eq. (4.F.6) into eq. (4.F.2) we obtain

$$\begin{aligned} T_{d,p} &= \sum_l (I_A; l| I_{A+1}) (I_A M_A l M_{A+1} - M_A | I_{A+1} M_{A+1}) \\ &\times \int d\vec{r}_n d\vec{r}_p \chi_p^{*(-)}(k_p, \vec{r}_p) \phi_{M_{A+1}-M_A}^{*l}(\vec{r}_n) V(\vec{r}_{pn}) \phi_d(\vec{r}_{np}) \chi_d^{(+)}(k_d, \vec{r}_d) \end{aligned} \quad (4.F.7)$$

The differential cross section is then equal to

$$\frac{d\sigma}{d\Omega} = \frac{2}{3} \frac{\mu_p \mu_d}{(2\pi\hbar^2)^2} \frac{(2I_{A+1} + 1)}{(2I_A + 1)} \frac{k_p}{k_d} \sum_{l,m_l} \frac{(I_A; l| I_{A+1})^2}{2l + 1} |B_{m_l}^l|^2, \quad (4.F.8)$$

where

$$B_{m_l}^l(\theta) = \int d\vec{r}_n d\vec{r}_p \chi_p^{*(-)}(k_p, \vec{r}_p) Y_m^l(\hat{r}_n) u_{nl}(r_n) V(\vec{r}_{pn}) \phi_d(\vec{r}_{np}) \chi_d^{(+)}(k_d, \vec{r}_d) \quad (4.F.9)$$

and

$$\phi_m^l(\vec{r}_n) = u_{nl}(r_n) Y_m^l(\hat{r}_n), \quad (4.F.10)$$

is the single-particle wave function of a neutron bound to the core A. For simplicity, the radial wave function  $u_{nl}(r_n)$  can be assumed to be a solution of a Saxon-Woods potential of parameters  $V_0 \approx 50$  MeV,  $a = 0.65$  fm and  $r_0 = 1.25$  fm.

The relation (4.F.8) gives the cross section for the stripping from the projectile of a neutron that would correspond to the  $n^{\text{th}}$  valence neutron in the nucleus  $(A + 1)$ . If we now want the cross section for stripping any of the valence neutrons of the final

nucleus from the projectile, we must multiply eq. (4.F.8) by  $n$ . A more careful treatment of the antisymmetry with respect to the neutrons shows this to be the correct answer.

Finally we get

$$\frac{d\sigma}{d\Omega} = \frac{(2I_{A+1} + 1)}{(2I_A + 1)} \sum_l S_l \sigma_l(\theta), \quad (4.F.11)$$

where

$$S_l = n(I_A; l|I_{A+1})^2, \quad (4.F.12)$$

and

$$\sigma_l(\theta) = \frac{2}{3} \frac{\mu_p \mu_d}{(2\pi\hbar^2)^2} \frac{k_p}{k_d} \frac{1}{2l+1} \sum_m |B_m^l|^2 \quad (4.F.13)$$

The distorted wave softwares evaluate numerically the quantity  $B_m^l(\theta)$ , using for the wave functions  $\chi^{(-)}$  and  $\chi^{(+)}$  the solution of the optical potentials that fit the elastic scattering, i.e.

$$(-\nabla^2 + \bar{U} - k^2)\chi = 0, \quad (4.F.14)$$

Note that if the target nucleus is even–even,  $I_A = 0$ ,  $l = I_{A+1}$ . That is, only one  $l$  value contributes in Eq. (4.F.8), and the angular distribution is uniquely given by  $\sum_m |B_m^l|^2$ . The  $l$ -dependence of the angular distributions helps to identify  $l = I_{A+1}$ . The factor  $S_l$  needed to normalize the calculated function to the data yields (assuming a good fit to the angular distribution), is known in the literature as the spectroscopic factor. It was assumed in the early stages of studies of nuclear structure with one–particle transfer reactions not only that it could be defined, but also that it contained all the nuclear structure information (aside from that associated with the angular distribution) which could be extracted from single–particle transfer. In other words, that it was the bridge directly connecting theory with experiment. Because nucleons are never bare, but are dressed by the coupling to collective modes as previously discussed in this chapter, the spectroscopic factor approximation is at best a helpful tool to get order of magnitude information from one–particle transfer data.

There is a fundamental problem which makes the handling of integrals like that of (4.F.9) difficult to handle, if not numerically at least conceptually. This difficulty is connected with the so called recoil effect <sup>3</sup>, namely the fact that the center of mass of the two interacting particles in entrance ( $\mathbf{r}_\alpha : \alpha = a + A$ ) and exit ( $\mathbf{r}_\beta : \beta = b + B$ ) channels is different. This is at variance with what one is accustomed to deal with in nuclear structure calculations, in which the Hartree potential depends on a single coordinate, as well as in the case of elastic and inelastic reactions, situations in which  $\mathbf{r}_\alpha = \mathbf{r}_\beta$ . When  $\mathbf{r}_\alpha \neq \mathbf{r}_\beta$  we enter a rather more complex many–body problem, in particular if continuum states are to be considered, than nuclear structure practitioners were accustomed to.

---

<sup>3</sup>While this effect could be treated in a cavalier fashion in the case of light ion reactions ( $m_a/m_A \ll 1$ ), this was not possible in the case of heavy ion reactions, as the change in momenta involved was always sizeable (cf. Broglia and Winther (2004) and refs. therein).

Of notice that similar difficulties have been faced in connection with the non-local Fock (exchange) potential. As a rule, the corresponding (HF) mean field equations are rendered local making use of the  $k$ -mass approximation or within the framework of Local Density Functional Theory (DFT), in particular with the help of the Kohn–Sham equations (see e.g. Mahaux, C. et al. (1985), Broglia et al. (2004) and refs. therein; cf. also App. 4.A). Although much of the work in this field is connected with the correlation potential (interweaving of single-particle and collective motion), an important fraction is connected with the exchange potential.

In any case, and returning to the subject of the present appendix, it is always useful to be able to introduce approximations which can help the physics which is at the basis of the phenomenon under discussion (single-particle motion) emerge in a natural way, if not to compare in detail with the experimental data. Within this context, to reduce the integral (4.F.9) one can assume that the proton-neutron interaction  $V_{np}$  has zero-range, i.e.

$$V_{np}(\vec{r}_{np})\phi_d(\vec{r}_{np}) = D_0\delta(\vec{r}_{np}) \quad (4.F.15)$$

so that  $B_m^l$  becomes equal to

$$B_{m_l}^l(\theta) = D_0 \int d\vec{r} \chi_p^{*(-)}(k_p, \vec{r}) Y_{m_l}^{*l}(\hat{r}) u_l(r) \chi_d^{(+)}(k_d, \vec{r}), \quad (4.F.16)$$

which is a three dimensional integral, but in fact essentially a one-dimensional integral, as the integration over the angles can be worked out analytically.

#### 4.F.1 Plane-wave limit

If in Eq. (4.F.14) one sets  $\bar{U} = 0$ , the distorted waves become plane waves i.e.

$$\chi_d^{(+)}(k_d, \vec{r}) = e^{i\vec{k}_d \cdot \vec{r}}, \quad (4.F.17a)$$

$$\chi_d^{*(-)}(k_p, \vec{r}) = e^{-i\vec{k}_p \cdot \vec{r}}. \quad (4.F.17b)$$

Equation (4.F.16) can now be written as

$$B_m^l = D_0 \int d\vec{r} e^{i(\vec{k}_d - \vec{k}_p) \cdot \vec{r}} Y_m^{*l}(\hat{r}) u_l(r). \quad (4.F.18)$$

The linear momentum transferred to the nucleus is  $\vec{k}_d - \vec{k}_p = \vec{q}$ . Let us expand  $e^{i\vec{q} \cdot \vec{r}}$  in spherical harmonics, i.e.

$$\begin{aligned} e^{i\vec{q} \cdot \vec{r}} &= \sum_l l! j_l(qr) (2l+1) P_l(\hat{q} \cdot \hat{r}) \\ &= 4\pi \sum_l l! j_l(qr) \sum_m Y_m^{*l}(\hat{q}) Y_m^l(\hat{r}), \end{aligned} \quad (4.F.19)$$

so

$$\int d\hat{r} e^{i\hat{q}\cdot\hat{r}} Y_m^l(\hat{r}) = 4\pi i^l j_l(qr) Y_m^{*l}(\hat{q}). \quad (4.F.20)$$

Then

$$\begin{aligned} \sum_m |B_m^l|^2 &= \sum_m |Y_m^l(\hat{q})|^2 D_0^2 16\pi^2 \times \\ &\quad \left| \int r^2 dr j_l(qr) u_l(r) \right|^2 = \\ &\quad \frac{2l+1}{4\pi} D_0^2 16\pi^2 \left| \int r^2 dr j_l(qr) u_l(r) \right|^2. \end{aligned} \quad (4.F.21)$$

Thus, the angular distribution is given by the integral  $\left| \int r^2 dr j_l(qr) u_l(r) \right|^2$ . If one assumes that the process takes place mostly on the surface, the angular distribution will be given by  $|j_l(qR_0)|^2$ , where  $R_0$  is the nuclear radius.

We then have

$$\begin{aligned} q^2 &= k_d^2 + k_p^2 - 2k_d k_p \cos(\theta) \\ &= (k_d^2 + k_p^2 - 2k_d k_p) + 2k_d k_p (1 - \cos(\theta)) \\ &= (k_d - k_p)^2 + 4k_d k_p (\sin(\theta/2))^2 \\ &\approx 4k_d k_p (\sin(\theta/2))^2, \end{aligned} \quad (4.F.22)$$

since  $k_d \approx k_p$  for stripping reactions at typical energies. Thus the angular distribution has a diffraction-like structure given by

$$|j_l(qR_0)|^2 = j_l^2(2R_0 \sqrt{k_d k_p} \sin(\theta/2)). \quad (4.F.23)$$

The function  $j_l(x)$  has its first maximum at  $x = l$ , i.e. where

$$\sin(\theta/2) = \frac{l}{2R_0 k}, \quad (k_p \approx k_d = k), \quad (4.F.24)$$

Examples of the above relation are provided in Fig. 4.F.2.

## Appendix 4.G One-particle knockout within DWBA

### 4.G.1 Spinless particles

We are going to consider the reaction  $A + a \rightarrow a + b + c$ , in which the cluster  $b$  is knocked out from the nucleus  $A (= c + b)$ . Cluster  $b$  is thus initially bound, while the final states of  $a, b$  and the initial state of  $a$  are all in the continuum, and can be described with distorted waves defined as scattering solutions of an optical potential. A schematic depiction of the situation is shown in Fig. 4.G.1. While the derivation presented below is quite general, special emphasis is set to one-particle knock-out processes.

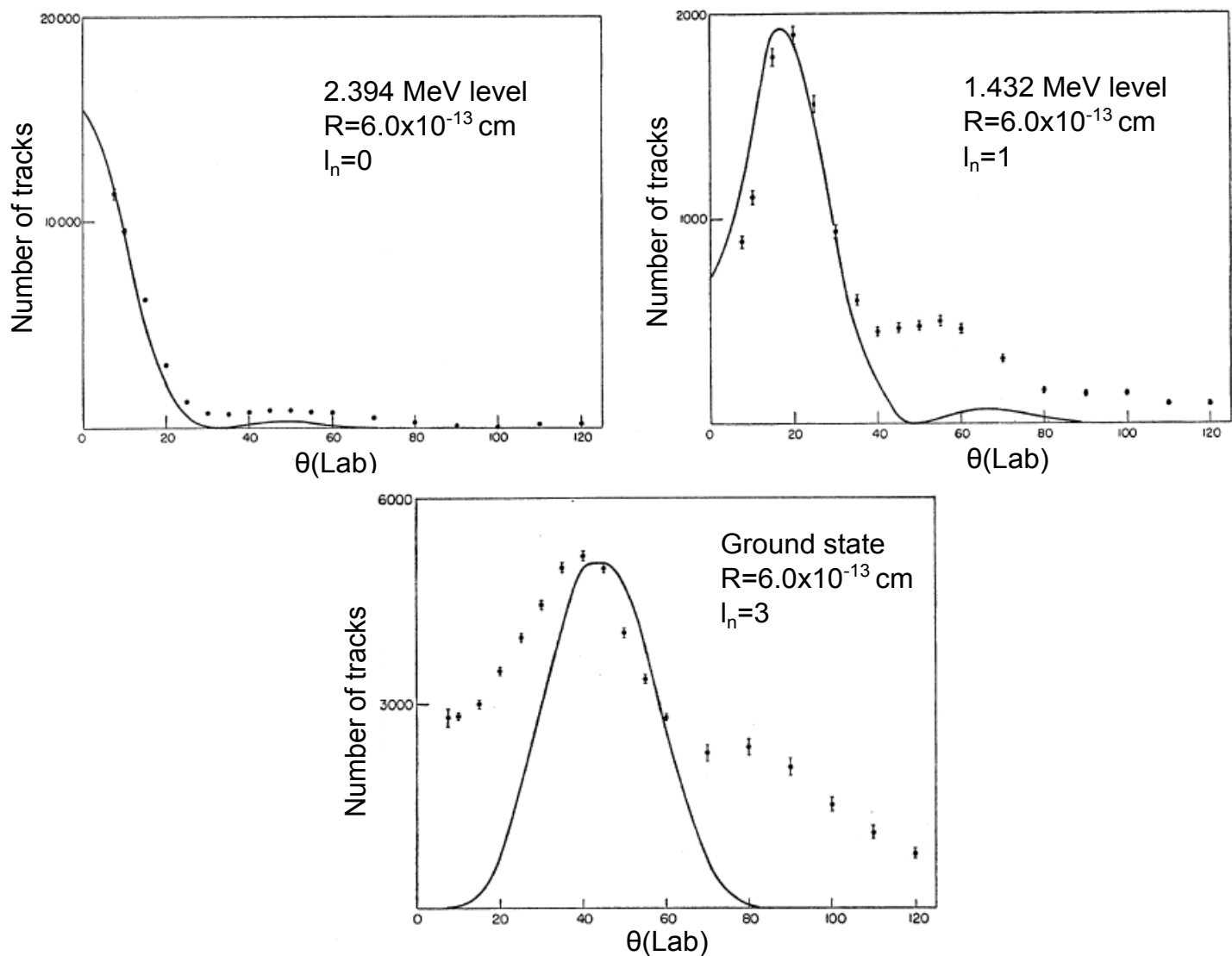


Figure 4.F.2: Plane wave approximation analysis of three  $^{44}\text{Ca}(\text{d},\text{p})^{45}\text{Ca}$  differential cross sections leading to the ground state ( $l_n = 3$ ) and to the 1.9 MeV state ( $l_n = 1$ ) and 2.4 MeV ( $l_n = 0$ ) excited states, i.e.  $f_{9/2}$ ,  $p_{1/2}$  and  $s_{1/2}$  states (Cobb and Guthe, 1957).

### Transition amplitude

A first derivation will be given in which, for simplicity, all the “particles” (nuclei) involved in the reaction process are spinless and inert. Use is made of central, complex optical potentials ( $U(r_{aA})$ ,  $U(r_{cb})$ ,  $U(r_{ac})$ ) potentials without a spin-orbit term. In addition, the interaction  $v(r_{ab})$  between  $a$  and  $b$  is taken to be a function of the distance  $r_{ab}$ . Within this scenario, the transition amplitude which is at the basis of the evaluation of the multi-differential cross section is the 6-dimensional integral

$$T_{mb} = \int d\mathbf{r}_{aA} d\mathbf{r}_{bc} \chi^{(-)*}(\mathbf{r}_{ac}) \chi^{(-)*}(\mathbf{r}_{bc}) v(r_{ab}) \chi^{(+)}(\mathbf{r}_{aA}) u_{lb}(r_{bc}) Y_m^l(\hat{\mathbf{r}}_{bc}). \quad (4.G.1)$$

### Coordinates

The vectors  $\mathbf{r}_{ab}$ ,  $\mathbf{r}_{ac}$  can easily be written in function of the integration variables  $\mathbf{r}_{aA}$ ,  $\mathbf{r}_{bc}$  (see Fig. 4.G.1), namely

$$\begin{aligned} \mathbf{r}_{ac} &= \mathbf{r}_{aA} + \frac{b}{A} \mathbf{r}_{bc}, \\ \mathbf{r}_{ab} &= \mathbf{r}_{aA} - \frac{c}{A} \mathbf{r}_{bc}, \end{aligned} \quad (4.G.2)$$

where  $b, c, A$  stand for the number of nucleons of the species  $b, c$  and  $A$  respectively.

### Distorted waves in the continuum

A standard way to reduce the dimensionality of the integral (4.G.1) consists in expanding the continuum wave functions  $\chi^{(+)}(\mathbf{r}_{aA})$ ,  $\chi^{(-)*}(\mathbf{r}_{ac})$ ,  $\chi^{(-)*}(\mathbf{r}_{bc})$  in a basis of eigenstates of the angular momentum operator (partial waves). Then one can exploit the transformation properties of these eigenstates under rotations to conveniently carry out the angular integrations. Making use of time-reversed phasing, that is

$$Y_m^l(\theta, \phi) = i^l \sqrt{\frac{2l+1}{4\pi} \frac{(l-m)!}{(l+m)!}} P_l^m(\cos \theta) e^{im\phi}, \quad (4.G.3)$$

the general form of these expansions is

$$\chi^{(+)}(\mathbf{k}, \mathbf{r}) = \sum_l \frac{4\pi}{kr} i^l \sqrt{2l+1} e^{i\sigma_l} F_l(r) [Y^l(\hat{\mathbf{r}}) Y^l(\hat{\mathbf{k}})]_0^0, \quad (4.G.4)$$

and

$$\chi^{(-)*}(\mathbf{k}, \mathbf{r}) = \sum_l \frac{4\pi}{kr} i^{-l} \sqrt{2l+1} e^{i\sigma_l} F_l(r) [Y^l(\hat{\mathbf{r}}) Y^l(\hat{\mathbf{k}})]_0^0, \quad (4.G.5)$$

$\sigma_l$  being the Coulomb phase shift. The radial functions  $F_l(r)$  are regular (finite at  $r = 0$ ) solutions of the one-dimensional Schrödinger equation with an effective

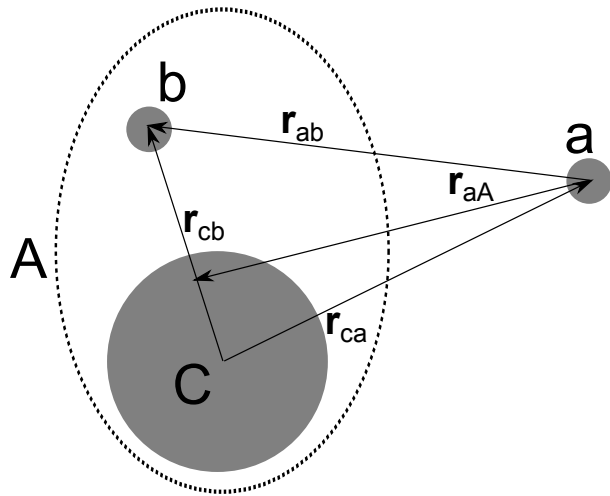


Figure 4.G.1: System of coordinates used to describe the reaction  $A + a \rightarrow a + b + c$ . The nucleus  $A$  is viewed as an inert cluster  $b$  bounded to an inert core  $c$ .

potential  $U(r) + \frac{\hbar^2 l(l+1)}{2\mu r^2}$  and suitable asymptotic behaviour at  $r \rightarrow \infty$  as boundary conditions. Thus, the distorted waves appearing in (4.G.1) are,

$$\chi^{(+)}(\mathbf{k}_a, \mathbf{r}_{aA}) = \sum_{l_a} \frac{4\pi}{k_a r_{aA}} i^{l_a} \sqrt{2l_a + 1} e^{i\sigma^{l_a}} F_{l_a}(r_{aA}) [Y^{l_a}(\hat{\mathbf{r}}_{aA}) Y^{l_a}(\hat{\mathbf{k}}_a)]_0^0, \quad (4.G.6)$$

describing the relative motion of  $A$  and  $a$  in the entrance channel as determined by the complex optical potential  $U(r_{aA})$ ,

$$\chi^{(-)*}(\mathbf{k}'_a, \mathbf{r}_{ac}) = \sum_{l'_a} \frac{4\pi}{k'_a r_{ac}} i^{-l'_a} \sqrt{2l'_a + 1} e^{i\sigma^{l'_a}} F_{l'_a}(r_{ac}) [Y^{l'_a}(\hat{\mathbf{r}}_{ac}) Y^{l'_a}(\hat{\mathbf{k}}'_a)]_0^0, \quad (4.G.7)$$

which describes the relative motion of  $c$  and  $a$ , in the final channel controlled by the complex optical potential  $U(r_{ac})$ , and finally

$$\chi^{(-)*}(\mathbf{k}'_b, \mathbf{r}_{bc}) = \sum_{l'_b} \frac{4\pi}{k'_b r_{bc}} i^{-l'_b} \sqrt{2l'_b + 1} e^{i\sigma^{l'_b}} F_{l'_b}(r_{bc}) [Y^{l'_b}(\hat{\mathbf{r}}_{bc}) Y^{l'_b}(\hat{\mathbf{k}}'_b)]_0^0, \quad (4.G.8)$$

final channel wavefunction describing the relative motion of  $b$  and  $c$ , as defined by the complex optical potential  $U(r_{bc})$ .

### Recoupling of angular momenta

One now proceeds to the evaluation of the 6-dimensional integral

$$\begin{aligned} & \frac{64\pi^3}{k_a k'_a k'_b} \int d\mathbf{r}_{aA} d\mathbf{r}_{bc} u_{l_b}(r_{cb}) v(r_{ab}) \sum_{l_a, l'_a, l'_b} \sqrt{(2l_a + 1)(2l'_a + 1)(2l'_b + 1)} \\ & \times e^{i(\sigma^{l_a} + \sigma^{l'_a} + \sigma^{l'_b})} \frac{F_{l_a}(r_{aA}) F_{l'_a}(r_{ac}) F_{l'_b}(r_{bc})}{r_{ac} r_{aA} r_{bc}} \\ & \times [Y^{l_a}(\hat{\mathbf{r}}_{aA}) Y^{l_a}(\hat{\mathbf{k}}_a)]_0^0 [Y^{l'_a}(\hat{\mathbf{r}}_{ac}) Y^{l'_a}(\hat{\mathbf{k}}'_a)]_0^0 [Y^{l'_b}(\hat{\mathbf{r}}_{bc}) Y^{l'_b}(\hat{\mathbf{k}}'_b)]_0^0 Y_{m_b}^{l_b}(\hat{\mathbf{r}}_{bc}), \end{aligned} \quad (4.G.9)$$

an expression which explicitly depends on the asymptotic kinetic energies and scattering angles  $(\hat{\mathbf{k}}_a, \hat{\mathbf{k}}'_a, \hat{\mathbf{k}}'_b)$  of  $a, b$  as determined by  $k_a, k'_a, k'_b$  and  $\hat{\mathbf{k}}_a, \hat{\mathbf{k}}'_a, \hat{\mathbf{k}}'_b$  respectively. In what follows we will take advantage of the partial wave expansion to reduce the dimensionality of the integral from 6 to 3. A possible strategy to follow is that of recoupling together all the terms that depend on the integration variables to a global angular momentum and retain only the term coupled to 0 as the only one surviving the integration. Let us start to separately couple the terms corresponding to particles  $a$  and  $b$ . For particle  $a$  we write

$$\begin{aligned} & [Y^{l_a}(\hat{\mathbf{r}}_{aA}) Y^{l_a}(\hat{\mathbf{k}}_a)]_0^0 [Y^{l'_a}(\hat{\mathbf{r}}_{ac}) Y^{l'_a}(\hat{\mathbf{k}}'_a)]_0^0 = \sum_K ((l_a l_a)_0 (l'_a l'_a)_0 | (l_a l'_a)_K (l_a l'_a)_K)_0 \\ & \times \left\{ [Y^{l_a}(\hat{\mathbf{r}}_{aA}) Y^{l'_a}(\hat{\mathbf{r}}_{ac})]_M^K [Y^{l_a}(\hat{\mathbf{k}}_a) Y^{l'_a}(\hat{\mathbf{k}}'_a)]_{-M}^K \right\}_0^0. \end{aligned} \quad (4.G.10)$$

We can now evaluate the 9- $j$ -symbol,

$$((l_a l_a)_0 (l'_a l'_a)_0 | (l_a l'_a)_K (l_a l'_a)_K)_0 = \sqrt{\frac{2K+1}{(2l'_a+1)(2l_a+1)}}, \quad (4.G.11)$$

and expand the coupling,

$$\begin{aligned} & \left\{ [Y^{l_a}(\hat{\mathbf{r}}_{aA}) Y^{l'_a}(\hat{\mathbf{r}}_{ac})]_M^K [Y^{l_a}(\hat{\mathbf{k}}_a) Y^{l'_a}(\hat{\mathbf{k}}'_a)]_{-M}^K \right\}_0^0 = \sum_M \langle K \ K \ M \ -M | 0 \ 0 \rangle \\ & \times [Y^{l_a}(\hat{\mathbf{r}}_{aA}) Y^{l'_a}(\hat{\mathbf{r}}_{ac})]_M^K [Y^{l_a}(\hat{\mathbf{k}}_a) Y^{l'_a}(\hat{\mathbf{k}}'_a)]_{-M}^K = \sum_M \frac{(-1)^{K+M}}{\sqrt{2K+1}} \\ & \times [Y^{l_a}(\hat{\mathbf{r}}_{aA}) Y^{l'_a}(\hat{\mathbf{r}}_{ac})]_M^K [Y^{l_a}(\hat{\mathbf{k}}_a) Y^{l'_a}(\hat{\mathbf{k}}'_a)]_{-M}^K. \end{aligned} \quad (4.G.12)$$

Thus,

$$\begin{aligned} & [Y^{l_a}(\hat{\mathbf{r}}_{aA}) Y^{l_a}(\hat{\mathbf{k}}_a)]_0^0 [Y^{l'_a}(\hat{\mathbf{r}}_{ac}) Y^{l'_a}(\hat{\mathbf{k}}'_a)]_0^0 = \sqrt{\frac{1}{(2l'_a+1)(2l_a+1)}} \\ & \times \sum_{KM} (-1)^{K+M} [Y^{l_a}(\hat{\mathbf{r}}_{aA}) Y^{l'_a}(\hat{\mathbf{r}}_{ac})]_M^K [Y^{l_a}(\hat{\mathbf{k}}_a) Y^{l'_a}(\hat{\mathbf{k}}'_a)]_{-M}^K. \end{aligned} \quad (4.G.13)$$

One can further simplify the above expression by choosing the direction of the initial momentum to be parallel to the  $z$  axis, so that  $Y_m^{l_a}(\hat{\mathbf{k}}_a) = Y_m^{l_a}(\hat{\mathbf{z}}) = \sqrt{\frac{2l_a+1}{4\pi}}\delta_{m,0}$ . Then,

$$\begin{aligned} \left[ Y^{l_a}(\hat{\mathbf{r}}_{aA}) Y^{l_a}(\hat{\mathbf{k}}_a) \right]_0^0 \left[ Y^{l'_a}(\hat{\mathbf{r}}_{ac}) Y^{l'_a}(\hat{\mathbf{k}}'_a) \right]_0^0 &= \sqrt{\frac{1}{4\pi(2l'_a + 1)}} \sum_{KM} (-1)^{K+M} \\ &\times \langle l_a 0 | l'_a - M | K - M \rangle \left[ Y^{l_a}(\hat{\mathbf{r}}_{aA}) Y^{l'_a}(\hat{\mathbf{r}}_{ac}) \right]_M^K Y_{-M}^{l'_a}(\hat{\mathbf{k}}'_a). \end{aligned} \quad (4.G.14)$$

For particle  $b$  we have

$$Y_{m_b}^{l_b}(\hat{\mathbf{r}}_{bc}) \left[ Y^{l'_b}(\hat{\mathbf{r}}_{bc}) Y^{l'_b}(\hat{\mathbf{k}}'_b) \right]_0^0 = Y_{m_b}^{l_b}(\hat{\mathbf{r}}_{cb}) \sum_m \frac{(-1)^{l'_b+m}}{\sqrt{2l'_b + 1}} Y_m^{l'_b}(\hat{\mathbf{r}}_{bc}) Y_{-m}^{l'_b}(\hat{\mathbf{k}}'_b), \quad (4.G.15)$$

and can write

$$Y_{m_b}^{l_b}(\hat{\mathbf{r}}_{bc}) Y_m^{l'_b}(\hat{\mathbf{r}}_{bc}) = \sum_{K'} \langle l_b m_b l'_b m | K' m_b + m \rangle \left[ Y^{l_b}(\hat{\mathbf{r}}_{bc}) Y^{l'_b}(\hat{\mathbf{r}}_{bc}) \right]_{m_b+m}^{K'}. \quad (4.G.16)$$

In order to couple to 0 angular momentum with (4.G.14) we must only keep the term with  $K' = K$ ,  $m = -M - m_b$  so

$$\begin{aligned} Y_{m_b}^{l_b}(\hat{\mathbf{r}}_{bc}) \left[ Y^{l'_b}(\hat{\mathbf{r}}_{bc}) Y^{l'_b}(\hat{\mathbf{k}}'_b) \right]_0^0 &= \frac{(-1)^{l'_b-M-m_b}}{\sqrt{2l'_b + 1}} \langle l_b m_b l'_b - M - m_b | K - M \rangle \\ &\times \left[ Y^{l_b}(\hat{\mathbf{r}}_{bc}) Y^{l'_b}(\hat{\mathbf{r}}_{bc}) \right]_{-M}^{K'} Y_{-M-m_b}^{l'_b}(\hat{\mathbf{k}}'_b), \end{aligned} \quad (4.G.17)$$

and (4.G.9) becomes

$$\begin{aligned} \frac{32\pi^2}{k_a k'_a k'_b} \sum_{KM} (-1)^{K+l'_b-m_b} \langle l_a 0 | l'_a - M | K - M \rangle \langle l_b m_b l'_b - M - m_b | K - M \rangle \\ \times \sum_{l_a, l'_a, l'_b} \sqrt{(2l_a + 1)} e^{i(\sigma^{l_a} + \sigma^{l'_a} + \sigma^{l'_b})} Y_{-M-m_b}^{l'_b}(\hat{\mathbf{k}}'_b) Y_{-M}^{l'_a}(\hat{\mathbf{k}}'_a) \int d\mathbf{r}_{aA} d\mathbf{r}_{bc} u_{l_b}(r_{bc}) v(r_{ab}) \\ \times \frac{F_{l_a}(r_{aA}) F_{l'_a}(r_{ac}) F_{l'_b}(r_{bc})}{r_{ac} r_{aA} r_{bc}} \left[ Y^{l_a}(\hat{\mathbf{r}}_{aA}) Y^{l'_a}(\hat{\mathbf{r}}_{ac}) \right]_M^K \left[ Y^{l_b}(\hat{\mathbf{r}}_{bc}) Y^{l'_b}(\hat{\mathbf{r}}_{bc}) \right]_{-M}^{K'}. \end{aligned} \quad (4.G.18)$$

Note that

$$\begin{aligned} \left[ Y^{l_a}(\hat{\mathbf{r}}_{aA}) Y^{l'_a}(\hat{\mathbf{r}}_{ac}) \right]_M^K \left[ Y^{l_b}(\hat{\mathbf{r}}_{bc}) Y^{l'_b}(\hat{\mathbf{r}}_{bc}) \right]_{-M}^{K'} &= \sum_P \langle K M K - M | P 0 \rangle \\ &\times \left\{ \left[ Y^{l_a}(\hat{\mathbf{r}}_{aA}) Y^{l'_a}(\hat{\mathbf{r}}_{ac}) \right]_M^K \left[ Y^{l_b}(\hat{\mathbf{r}}_{bc}) Y^{l'_b}(\hat{\mathbf{r}}_{bc}) \right]_{-M}^{K'} \right\}_0^P, \end{aligned} \quad (4.G.19)$$

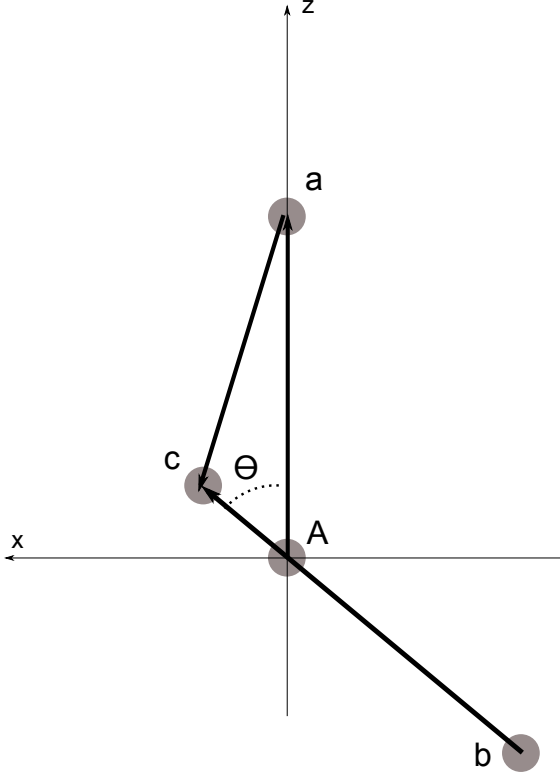


Figure 4.G.2: Coordinates in the “standard” configuration.

and that to survive the integration the rotational tensors must be coupled to  $P = 0$ . Keeping only this term in the sum over  $P$ , we get

$$\begin{aligned} & \left[ Y^{l_a}(\hat{\mathbf{r}}_{aA}) Y'^{l_a}(\hat{\mathbf{r}}_{ac}) \right]_M^K \left[ Y^{l_b}(\hat{\mathbf{r}}_{bc}) Y'^{l_b}(\hat{\mathbf{r}}_{bc}) \right]_{-M}^K = \\ & \frac{(-1)^{K+M}}{\sqrt{2K+1}} \left\{ \left[ Y^{l_a}(\hat{\mathbf{r}}_{aA}) Y'^{l_a}(\hat{\mathbf{r}}_{ac}) \right]^K \left[ Y^{l_b}(\hat{\mathbf{r}}_{bc}) Y'^{l_b}(\hat{\mathbf{r}}_{bc}) \right]^K \right\}_0^0. \end{aligned} \quad (4.G.20)$$

The coordinate-dependent part of the latter expression is a rotationally invariant scalar, so it can be evaluated in any conventional “standard” configuration such as the one depicted in Fig. 4.G.2. It must then be multiplied by a factor resulting of the integration of the remaining angular variables, which accounts for the rigid rotations needed to connect any arbitrary configuration to one of this type. This factor turns out to be  $8\pi^2$  (a  $4\pi$  factor for all possible orientations of, say,  $\mathbf{r}_{aA}$  and a

$2\pi$  factor for a complete rotation around its direction). According to Fig. 4.G.2,

$$\begin{aligned}\mathbf{r}_{bc} &= r_{bc} (\sin \theta \hat{x} + \cos \theta \hat{z}), \\ \mathbf{r}_{aA} &= -r_{aA} \hat{z}, \\ \mathbf{r}_{ac} &= \frac{b}{A} r_{bc} \sin \theta \hat{x} + \left( \frac{b}{A} r_{bc} \cos \theta - r_{aA} \right) \hat{z}.\end{aligned}\quad (4.G.21)$$

As  $\mathbf{r}_{aA}$  lies parallel to the  $z$  axis,  $Y_{M_K}^{l_a}(\hat{\mathbf{r}}_{aA}) = \sqrt{\frac{2l_a+1}{4\pi}} \delta_{M_K,0}$  and

$$\begin{aligned}\left[ Y^{l_a}(\hat{\mathbf{r}}_{aA}) \ Y^{l'_a}(\hat{\mathbf{r}}_{ac}) \right]_{M_K}^K &= \sum_m \langle l_a \ m \ l'_a \ M_K - m | K \ M_K \rangle Y_m^{l_a}(\hat{\mathbf{r}}_{aA}) Y_{M_K-m}^{l'_a}(\hat{\mathbf{r}}_{ac}) = \\ &\sqrt{\frac{2l_a+1}{4\pi}} \langle l_a \ 0 \ l'_a \ M_K | K \ M_K \rangle Y_{M_K}^{l'_a}(\hat{\mathbf{r}}_{ac}).\end{aligned}\quad (4.G.22)$$

Then

$$\begin{aligned}\left\{ \left[ Y^{l_a}(\hat{\mathbf{r}}_{aA}) Y^{l'_a}(\hat{\mathbf{r}}_{ac}) \right]_{M_K}^K \left[ Y^{l_b}(\hat{\mathbf{r}}_{bc}) Y^{l'_b}(\hat{\mathbf{r}}_{bc}) \right]_{-M_K}^K \right\}_0^0 &= \\ \sum_{M_K} \langle K \ M_K \ K - M_K | 0 \ 0 \rangle \left[ Y^{l_a}(\hat{\mathbf{r}}_{aA}) Y^{l'_a}(\hat{\mathbf{r}}_{ac}) \right]_{M_K}^K \left[ Y^{l_b}(\hat{\mathbf{r}}_{bc}) Y^{l'_b}(\hat{\mathbf{r}}_{bc}) \right]_{-M_K}^K &= \\ \sqrt{\frac{2l_a+1}{4\pi}} \sum_{M_K} \frac{(-1)^{K+M_K}}{\sqrt{2K+1}} \langle l_a \ 0 \ l'_a \ M_K | K \ M_K \rangle \\ \times \left[ Y^{l_b}(\hat{\mathbf{r}}_{bc}) Y^{l'_b}(\hat{\mathbf{r}}_{bc}) \right]_{-M_K}^K Y_{M_K}^{l'_a}(\hat{\mathbf{r}}_{ac}).\end{aligned}\quad (4.G.23)$$

Remembering the  $8\pi^2$  factor, the term arising from (4.G.20) to be considered in the integral is

$$\begin{aligned}4\pi^{3/2} \frac{\sqrt{2l_a+1}}{2K+1} (-1)^K \sum_{M_K} (-1)^{M_K} \langle l_a \ 0 \ l'_a \ M_K | K \ M_K \rangle \\ \times \left[ Y^{l_b}(\cos \theta, 0) Y^{l'_b}(\cos \theta, 0) \right]_{-M_K}^K Y_{M_K}^{l'_a}(\cos \theta_{ac}, 0),\end{aligned}\quad (4.G.24)$$

with

$$\cos \theta_{ac} = \frac{\frac{b}{A} r_{bc} \cos \theta - r_{aA}}{\sqrt{\left( \frac{b}{A} r_{bc} \sin \theta \right)^2 + \left( \frac{b}{A} r_{bc} \cos \theta - r_{aA} \right)^2}},\quad (4.G.25)$$

(see (4.G.21)). The final expression of the transition amplitude is

$$\begin{aligned}T_{mb}(\mathbf{k}'_a, \mathbf{k}'_b) &= \frac{128\pi^{7/2}}{k_a k'_a k'_b} \sum_{KM} \frac{(-1)^{l'_b+m_b}}{2K+1} \langle l_a \ 0 \ l'_a - M | K - M \rangle \langle l_b \ m_b \ l'_b - M - m_b | K - M \rangle \\ &\times \sum_{l_a, l'_a, l'_b} (2l_a + 1) e^{i(\sigma^{l_a} + \sigma^{l'_a} + \sigma^{l'_b})} Y_{-M-m_b}^{l'_b}(\hat{\mathbf{k}}'_b) Y_{-M}^{l'_a}(\hat{\mathbf{k}}'_a) I(l_a, l'_a, l'_b, K),\end{aligned}\quad (4.G.26)$$

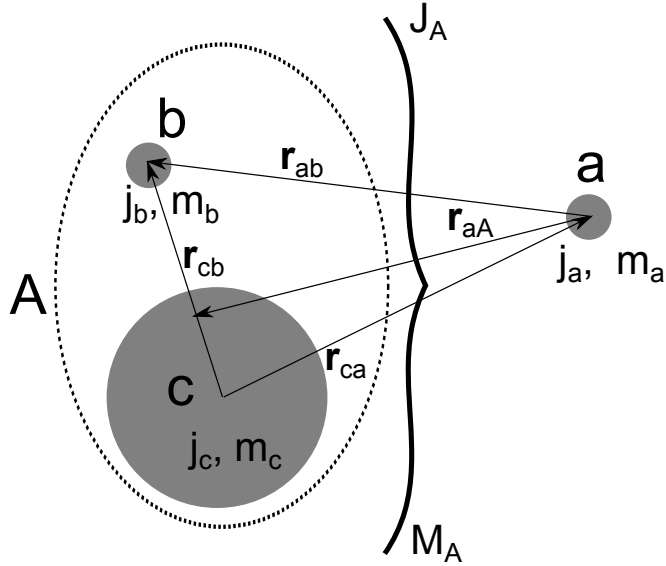


Figure 4.G.3: In the present case all three clusters  $a, b, c$  have definite spins and projections. The nucleus  $A$  is coupled to total spin  $J_A, M_A$ .

where

$$\begin{aligned} \mathcal{I}(l_a, l'_a, l'_b, K) = & \int dr_{aA} dr_{bc} d\theta r_{aA} r_{bc} \frac{\sin \theta}{r_{ac}} u_{l_b}(r_{bc}) v(r_{ab}) F_{l_a}(r_{aA}) F_{l'_a}(r_{ac}) F_{l'_b}(r_{bc}) \\ & \times \sum_{M_K} (-1)^{M_K} \langle l_a \ 0 \ l'_a \ M_K | K \ M_K \rangle \left[ Y^{l_b}(\cos \theta, 0) Y^{l'_b}(\cos \theta, 0) \right]_{-M_K}^K Y_{M_K}^{l'_a}(\cos \theta_{ac}, 0) \end{aligned} \quad (4.G.27)$$

is a 3-dimensional integral that can be numerically evaluated with the help of, e.g., Gaussian integration.

#### 4.G.2 Particles with spin

We now treat the case in which the clusters have a definite spin (see Fig. 4.G.3), and the complex optical potentials  $U(r_{aA}), U(r_{cb}), U(r_{ac})$  contain now a spin-orbit term proportional to the product  $\mathbf{l} \cdot \mathbf{s} = 1/2(j(j+1) - l(l+1) - 3/4)$  for particles with spin  $1/2$ . In addition, the interaction  $V(r_{ab}, \sigma_a, \sigma_b)$  between  $a$  and  $b$  is taken to be a separable function of the distance  $r_{ab}$  and of the spin orientations,  $V(r_{ab}, \sigma_a, \sigma_b) = v(r_{ab})v_\sigma(\sigma_a, \sigma_b)$ . Note that this ansatz rules out spin-orbit as well

as tensor terms in the  $NN$ -interaction. For the time being we will assume that the spin-dependent interaction is rotationally invariant (scalar with respect to rotations), such as, e.g.,  $v_\sigma(\sigma_a, \sigma_b) \propto \sigma_a \cdot \sigma_b$ . Again, this assumption excludes tensor terms in the interaction. The transition amplitude is then,

$$\begin{aligned} T_{m_a, m_b}^{m'_a, m'_b} = & \sum_{\sigma_a, \sigma_b} \int d\mathbf{r}_{aA} d\mathbf{r}_{bc} \chi_{m'_a}^{(-)*}(\mathbf{r}_{ac}, \sigma_a) \chi_{m'_b}^{(-)*}(\mathbf{r}_{bc}, \sigma_b) \\ & \times v(r_{ab}) v_\sigma(\sigma_a, \sigma_b) \chi_{m_a}^{(+)}(\mathbf{r}_{aA}, \sigma_a) \psi_{m_b}^{l_b, j_b}(\mathbf{r}_{bc}, \sigma_b). \end{aligned} \quad (4.G.28)$$

### Distorted waves

The distorted waves in (4.G.28)  $\chi_m(\mathbf{r}, \sigma) = \chi(\mathbf{r}) \phi_m^{1/2}(\sigma)$  have a spin dependence contained in the spinor  $\phi_m^{1/2}(\sigma)$ , where  $\sigma$  is the spin degree of freedom and  $m$  the projection of the spin along the quantization axis. The superscript  $1/2$  reminds us that we are considering spin  $1/2$  particles, which have important consequences when dealing with the spin-orbit term of the optical potentials. As for the spin-dependent term  $v_\sigma(\sigma_a, \sigma_b)$ , the actual value of the spin of particles involved in the reaction process do not make much difference, *as long as this term is rotationally invariant*. Following (4.G.4),

$$\chi^{(+)}(\mathbf{k}, \mathbf{r}) \phi_m(\sigma) = \sum_{l,j} \frac{4\pi}{kr} i^l \sqrt{2l+1} e^{i\sigma l} F_{l,j}(r) [Y^l(\hat{\mathbf{r}}) Y^l(\hat{\mathbf{k}})]_0^0 \phi_m^{1/2}(\sigma). \quad (4.G.29)$$

Note that now one also sums over the total angular momentum  $j$ , as the radial functions  $F_{l,j}(r)$  depend both on  $j$  as well as on  $l$ , in keeping with the fact that they are solutions of an optical potential containing a spin-orbit term proportional to  $1/2(j(j+1) - l(l+1) - 3/4)$ . One must then couple the radial and spin functions to total angular momentum  $j$ , noting that

$$\begin{aligned} [Y^l(\hat{\mathbf{r}}) Y^l(\hat{\mathbf{k}})]_0^0 \phi_m^{1/2}(\sigma) &= \sum_{m_l} \langle l \ m_l \ l - m_l | 0 \ 0 \rangle Y_{m_l}^l(\hat{\mathbf{r}}) Y_{-m_l}^l(\hat{\mathbf{k}}) \phi_m^{1/2}(\sigma) = \\ &\sum_{m_l} \frac{(-1)^{l-m_l}}{\sqrt{2l+1}} Y_{m_l}^l(\hat{\mathbf{r}}) Y_{-m_l}^l(\hat{\mathbf{k}}) \phi_m^{1/2}(\sigma), \end{aligned} \quad (4.G.30)$$

and

$$Y_{m_l}^l(\hat{\mathbf{r}}) \phi_m^{1/2}(\sigma) = \sum_j \langle l \ m_l \ 1/2 \ m | j \ m_l + m \rangle [Y^l(\hat{\mathbf{r}}) \phi^{1/2}(\sigma)]_{m_l+m}^j, \quad (4.G.31)$$

we can write

$$\begin{aligned} [Y^l(\hat{\mathbf{r}}) Y^l(\hat{\mathbf{k}})]_0^0 \phi_m^{1/2}(\sigma) &= \sum_{m_l, j} \frac{(-1)^{l+m_l}}{\sqrt{2l+1}} \langle l \ m_l \ 1/2 \ m | j \ m_l + m \rangle \\ &\times [Y^l(\hat{\mathbf{r}}) \phi^{1/2}(\sigma)]_{m_l+m}^j Y_{-m_l}^l(\hat{\mathbf{k}}), \end{aligned} \quad (4.G.32)$$

and the distorted waves in (4.G.28) are

$$\begin{aligned} \chi_{m_a}^{(+)}(\mathbf{r}_{aA}, \mathbf{k}_a, \sigma_a) &= \sum_{l_a, m_{l_a}, j_a} \frac{4\pi}{k_a r_{aA}} i^{l_a} (-1)^{l_a + m_{l_a}} e^{i\sigma^{l_a}} F_{l_a, j_a}(r_{aA}) \\ &\times \langle l_a \ m_{l_a} \ 1/2 \ m_a | j_a \ m_{l_a} + m_a \rangle \left[ Y^{l_a}(\hat{\mathbf{r}}_{aA}) \phi^{1/2}(\sigma_a) \right]_{m_{l_a} + m_a}^{j_a} Y_{-m_{l_a}}^{l_a}(\hat{\mathbf{k}}_a), \end{aligned} \quad (4.G.33)$$

$$\begin{aligned} \chi_{m'_b}^{(-)*}(\mathbf{r}_{bc}, \mathbf{k}'_b, \sigma_b) &= \sum_{l'_b, m'_{l'_b}, j'_b} \frac{4\pi}{k'_b r_{bc}} i^{-l'_b} (-1)^{l'_b + m'_{l'_b}} e^{i\sigma^{l'_b}} F_{l'_b, j'_b}(r_{bc}) \\ &\times \langle l'_b \ m_{l'_b} \ 1/2 \ m'_b | j'_b \ m_{l'_b} + m'_b \rangle \left[ Y^{l'_b}(\hat{\mathbf{r}}_{bc}) \phi^{1/2}(\sigma_b) \right]_{m'_{l'_b} + m'_b}^{j'_b} Y_{-m'_{l'_b}}^{l'_b}(\hat{\mathbf{k}}'_b), \end{aligned} \quad (4.G.34)$$

$$\begin{aligned} \chi_{m'_a}^{(-)*}(\mathbf{r}_{ac}, \mathbf{k}'_a, \sigma_a) &= \sum_{l'_a, m'_{l'_a}, j'_a} \frac{4\pi}{k'_a r_{ac}} i^{-l'_a} (-1)^{l'_a + m'_{l'_a}} e^{i\sigma^{l'_a}} F_{l'_a, j'_a}(r_{ac}) \\ &\times \langle l'_a \ m_{l'_a} \ 1/2 \ m'_a | j'_a \ m_{l'_a} + m'_a \rangle \left[ Y^{l'_a}(\hat{\mathbf{r}}_{ac}) \phi^{1/2}(\sigma_a) \right]_{m'_{l'_a} + m'_a}^{j'_a} Y_{-m'_{l'_a}}^{l'_a}(\hat{\mathbf{k}}'_a). \end{aligned} \quad (4.G.35)$$

The initial bound particle  $b$  wavefunction is

$$\psi_{m_b}^{l_b, j_b}(\mathbf{r}_{bc}, \sigma_b) = u_{l_b, j_b}(r_{bc}) \left[ Y^{l_b}(\hat{\mathbf{r}}_{bc}) \phi^{1/2}(\sigma_b) \right]_{m_b}^{j_b}, \quad (4.G.36)$$

Substituting in (4.G.28), one obtains,

$$\begin{aligned} T_{m_a, m_b}^{m'_a, m'_b}(\mathbf{k}'_a, \mathbf{k}'_b) &= \frac{64\pi^3}{k_a k'_a k'_b} \sum_{\sigma_a, \sigma_b} \sum_{l_a, m_{l_a}, j_a} \sum_{l'_a, m'_{l'_a}, j'_a} \sum_{l'_b, m'_{l'_b}, j'_b} e^{i(\sigma^{l_a} + \sigma^{l'_a} + \sigma^{l'_b})} i^{l_a - l'_a - l'_b} (-1)^{l_a - m_{l_a} + l'_a - j'_a + l'_b - j'_b} \\ &\times \langle l'_a \ m_{l'_a} \ 1/2 \ m'_a | j'_a \ m_{l'_a} + m'_a \rangle \langle l_a \ m_{l_a} \ 1/2 \ m_a | j_a \ m_{l_a} + m_a \rangle \langle l'_b \ m'_{l'_b} \ 1/2 \ m'_b | j'_b \ m'_{l'_b} + m'_b \rangle \\ &\times Y_{-m_{l_a}}^{l_a}(\hat{\mathbf{k}}_a) Y_{-m'_{l'_a}}^{l'_a}(\hat{\mathbf{k}}'_a) Y_{-m'_{l'_b}}^{l'_b}(\hat{\mathbf{k}}'_b) \int d\mathbf{r}_{aA} d\mathbf{r}_{bc} \left[ Y^{l'_a}(\hat{\mathbf{r}}_{ac}) \phi^{1/2}(\sigma_a) \right]_{-m'_{l'_a} - m'_a}^{j'_a} \left[ Y^{l'_b}(\hat{\mathbf{r}}_{bc}) \phi^{1/2}(\sigma_b) \right]_{-m'_{l'_b} - m'_b}^{j'_b} \\ &\times \frac{F_{l_a, j_a}(r_{aA}) F_{l'_a, j'_a}(r_{ac}) F_{l'_b, j'_b}(r_{bc})}{r_{ac} r_{aA} r_{bc}} u_{l_b, j_b}(r_{bc}) v(r_{ab}) v_\sigma(\sigma_a, \sigma_b) \\ &\times \left[ Y^{l_a}(\hat{\mathbf{r}}_{aA}) \phi^{1/2}(\sigma_a) \right]_{m_{l_a} + m_a}^{j_a} \left[ Y^{l_b}(\hat{\mathbf{r}}_{bc}) \phi^{1/2}(\sigma_b) \right]_{m_b}^{j_b}, \end{aligned} \quad (4.G.37)$$

where use was made of the relation

$$\left[ Y^l(\hat{\mathbf{r}}) \phi^{1/2}(\sigma) \right]_m^{j*} = (-1)^{j-m} \left[ Y^l(\hat{\mathbf{r}}) \phi^{1/2}(\sigma) \right]_{-m}^j. \quad (4.G.38)$$

### Recoupling of angular momenta

Let us now separate spatial and spin coordinates, noting that the spin functions must be coupled to  $S = 0$ , a consequence of the fact that the interaction  $v_\sigma(\sigma_a, \sigma_b)$  is rotationally invariant. Starting with particle  $a$ ,

$$\begin{aligned} & \left[ Y^{l'_a}(\hat{\mathbf{r}}_{ac}) \phi^{1/2*}(\sigma_a) \right]_{-m_{l'_a}-m'_a}^{j'_a} \left[ Y^{l_a}(\hat{\mathbf{r}}_{aA}) \phi^{1/2}(\sigma_a) \right]_{m_{l_a}+m_a}^{j_a} = \\ & \sum_K ((l'_a \frac{1}{2})_{j'_a} (l_a \frac{1}{2})_{j_a} | (l_a l'_a)_K (\frac{1}{2} \frac{1}{2} 0)_K \\ & \times \left[ Y^{l'_a}(\hat{\mathbf{r}}_{ac}) Y^{l_a}(\hat{\mathbf{r}}_{aA}) \right]_{-m_{l'_a}-m'_a+m_{l_a}+m_a}^K \left[ \phi^{1/2*}(\sigma_a) \phi^{1/2}(\sigma_a) \right]_0^0. \quad (4.G.39) \end{aligned}$$

For particle  $b$ ,

$$\begin{aligned} & \left[ Y^{l'_b}(\hat{\mathbf{r}}_{bc}) \phi^{1/2*}(\sigma_b) \right]_{-m_{l'_b}-m'_b}^{j'_b} \left[ Y^{l_b}(\hat{\mathbf{r}}_{bc}) \phi^{1/2}(\sigma_b) \right]_{m_b}^{j_b} = \\ & \sum_{K'} ((l'_b \frac{1}{2})_{j'_b} (l_b \frac{1}{2})_{j_b} | (l_b l'_b)_{K'} (\frac{1}{2} \frac{1}{2} 0)_{K'} \\ & \times \left[ Y^{l'_b}(\hat{\mathbf{r}}_{bc}) Y^{l_b}(\hat{\mathbf{r}}_{bc}) \right]_{-m_{l'_b}-m'_b+m_b}^{K'} \left[ \phi^{1/2*}(\sigma_b) \phi^{1/2}(\sigma_b) \right]_0^0. \quad (4.G.40) \end{aligned}$$

The spin summation yields a constant factor,

$$\sum_{\sigma_a, \sigma_b} \left[ \phi^{1/2*}(\sigma_a) \phi^{1/2}(\sigma_a) \right]_0^0 \left[ \phi^{1/2*}(\sigma_b) \phi^{1/2}(\sigma_b) \right]_0^0 v_\sigma(\sigma_a, \sigma_b) \equiv T_\sigma, \quad (4.G.41)$$

and what we have yet to do is very similar to what we have done in the case of spinless particles. First of all note that the constrain of coupling all angular momenta to 0, imposes  $K' = K$  and  $m_{l_a} + m_a - m_{l'_a} - m'_a = m_{l'_b} + m'_b - m_b$  (see (4.G.39) and (4.G.40)). If we set  $M = m_{l_a} + m_a - m_{l'_a} - m'_a$  and take, as before,  $\hat{\mathbf{k}}_a \equiv \hat{z}$

$$\begin{aligned} & T_{m_a, m_b}^{m'_a, m'_b}(\mathbf{k}'_a, \mathbf{k}'_b) = \frac{32\pi^{5/2}}{k_a k'_a k'_b} T_\sigma \sum_{l_a, j_a} \sum_{l'_a, j'_a} \sum_{l'_b, j'_b} \sum_{K, M} e^{i(\sigma^{l_a} + \sigma^{l'_a} + \sigma^{l'_b})} i^{l_a - l'_a - l'_b} (-1)^{l_a + l'_a + l'_b - j'_a - j'_b} \\ & \times \sqrt{2l_a + 1} ((l'_a \frac{1}{2})_{j'_a} (l_a \frac{1}{2})_{j_a} | (l_a l'_a)_K (\frac{1}{2} \frac{1}{2} 0)_K) ((l'_b \frac{1}{2})_{j'_b} (l_b \frac{1}{2})_{j_b} | (l_b l'_b)_K (\frac{1}{2} \frac{1}{2} 0)_K) \\ & \times \langle l'_a m_a - m'_a - M \mid 1/2 \mid m'_a | j'_a m_a - M \rangle \langle l_a 0 \mid 1/2 \mid m_a | j_a m_a \rangle \langle l'_b m_b - m'_b + M \mid 1/2 \mid m'_b | j'_b M + m_b \rangle \\ & \times Y_{m'_b - m_b - M}^{l'_b}(\hat{\mathbf{k}}'_b) Y_{m'_a - m_a + M}^{l'_a}(\hat{\mathbf{k}}'_a) \int d\mathbf{r}_{aA} d\mathbf{r}_{bc} \frac{F_{l_a, j_a}(r_{aA}) F_{l'_a, j'_a}(r_{ac}) F_{l'_b, j'_b}(r_{bc})}{r_{ac} r_{aA} r_{bc}} \\ & \times u_{l_b, j_b}(r_{bc}) v(r_{ab}) \left[ Y^{l_a}(\hat{\mathbf{r}}_{aA}) Y^{l'_a}(\hat{\mathbf{r}}_{ac}) \right]_M^K \left[ Y^{l_b}(\hat{\mathbf{r}}_{bc}) Y^{l'_b}(\hat{\mathbf{r}}_{bc}) \right]_{-M}^K. \quad (4.G.42) \end{aligned}$$

The integral of the above expression is similar to the one in (4.G.18), so we obtain

$$\begin{aligned}
 T_{m_a, m_b}^{m'_a, m'_b}(\mathbf{k}'_a, \mathbf{k}'_b) &= \frac{128\pi^4}{k_a k'_a k'_b} T_\sigma \sum_{l_a, j_a} \sum_{l'_a, j'_a} \sum_{l'_b, j'_b} \sum_{K, M} e^{i(\sigma l_a + \sigma l'_a + \sigma l'_b)} i^{l_a - l'_a - l'_b} (-1)^{l_a + l'_a + l'_b - j'_a - j'_b} \\
 &\times \frac{2l_a + 1}{2K + 1} ((l'_a \frac{1}{2})_{j'_a} (l_a \frac{1}{2})_{j_a} | (l_a l'_a)_K (\frac{1}{2} \frac{1}{2})_0)_K ((l'_b \frac{1}{2})_{j'_b} (l_b \frac{1}{2})_{j_b} | (l_b l'_b)_K (\frac{1}{2} \frac{1}{2})_0)_K \\
 &\times \langle l'_a m_a - M 1/2 m'_a | j'_a m_a - M \rangle \langle l'_b m_b - m'_b + M 1/2 m'_b | j'_b M + m_b \rangle \\
 &\times \langle l_a 0 1/2 m_a | j_a m_a \rangle Y_{m'_b - m_b - M}^{l'_b}(\hat{\mathbf{k}}'_b) Y_{m_a - m'_a + M}^{l'_a}(\hat{\mathbf{k}}'_a) \mathcal{I}(l_a, l'_a, l'_b, j_a, j'_a, j'_b, K),
 \end{aligned} \tag{4.G.43}$$

with

$$\begin{aligned}
 \mathcal{I}(l_a, l'_a, l'_b, j_a, j'_a, j'_b, K) &= \int dr_{aA} dr_{bc} d\theta r_{aA} r_{bc} \frac{\sin \theta}{r_{ac}} u_{l_b}(r_{bc}) v(r_{ab}) \\
 &\times F_{l_a, j_a}(r_{aA}) F_{l'_a, j'_a}(r_{ac}) F_{l'_b, j'_b}(r_{bc}) \\
 &\times \sum_{M_K} \langle l_a 0 l'_a M_K | K M_K \rangle \left[ Y^{l_b}(\cos \theta, 0) Y^{l'_b}(\cos \theta, 0) \right]_{-M_K}^K Y_{M_K}^{l'_a}(\cos \theta_{ac}, 0). \tag{4.G.44}
 \end{aligned}$$

Again, this is a 3-dimensional integral that can be evaluated with the method of Gaussian quadratures. The transition amplitude  $T_{m_a, m_b}^{m'_a, m'_b}(\mathbf{k}'_a, \mathbf{k}'_b)$  depends explicitly on the initial  $(m_a, m'_a)$  and final  $(m'_a, m'_b)$  polarizations of  $a, b$ . If the particle  $b$  is initially coupled to core  $c$  to total angular momentum  $J_A, M_A$ , the amplitude to be considered is rather

$$T_{m_a}^{m'_a, m'_b}(\mathbf{k}'_a, \mathbf{k}'_b) = \sum_{m_p} \langle j_b m_b j_c M_A - m_b | J_A M_A \rangle T_{m_a, m_b}^{m'_a, m'_b}(\mathbf{k}'_a, \mathbf{k}'_b), \tag{4.G.45}$$

and the multi-differential cross section for detecting particle  $c$  (or  $a$ ) is

$$\frac{d\sigma}{d\mathbf{k}'_a d\mathbf{k}'_b} \Big|_{m_a}^{m'_a, m'_b} = \frac{k'_a}{k_a} \frac{\mu_{aA} \mu_{ac}}{4\pi^2 \hbar^4} \left| \sum_{m_b} \langle j_b m_b j_c M_A - m_b | J_A M_A \rangle T_{m_a, m_b}^{m'_a, m'_b}(\mathbf{k}'_a, \mathbf{k}'_b) \right|^2. \tag{4.G.46}$$

All spin-polarization observables (analysing powers, etc.,) can be derived from this expression. But let us now work out the expression of the cross section for an unpolarized beam (sum over initial spin orientations divided by the number of such orientations) and when we do not detect the final polarizations (sum over final spin orientations),

$$\begin{aligned}
 \frac{d\sigma}{d\mathbf{k}'_a d\mathbf{k}'_b} &= \frac{k'_a}{k_a} \frac{\mu_{aA} \mu_{ac}}{4\pi^2 \hbar^4} \frac{1}{(2J_A + 1)(2j_a + 1)} \\
 &\times \sum_{\substack{m_a, m'_a \\ M_A, m'_b}} \left| \sum_{m_b} \langle j_b m_b j_c M_A - m_b | J_A M_A \rangle T_{m_a, m_b}^{m'_a, m'_b}(\mathbf{k}'_a, \mathbf{k}'_b) \right|^2. \tag{4.G.47}
 \end{aligned}$$

The sum above can be simplified a bit. Let us consider a single particular value of  $m_b$  in the sum over  $m_b$ ,

$$\begin{aligned} \sum_{m_a, m'_a, m'_b} & \left| T_{m_a, m_b}^{m'_a, m'_b}(\mathbf{k}'_a, \mathbf{k}'_b) \right|^2 \sum_{M_A} \left| \langle j_b \ m_b \ j_c \ M_A - m_b | J_A \ M_A \rangle \right|^2 = \\ & \frac{2J_A + 1}{2j_b + 1} \sum_{m_a, m_a, m'_b} \left| T_{m_a, m_b}^{m'_a, m'_b}(\mathbf{k}'_a, \mathbf{k}'_b) \right|^2 \\ & \times \sum_{M_A} \left| \langle J_A - M_A \ j_c \ M_A - m_b | j_b \ m_b \rangle \right|^2, \end{aligned} \quad (4.G.48)$$

where we have used

$$\langle j_b \ m_b \ j_c \ M_A - m_b | J_A \ M_A \rangle = (-1)^{j_c - M_A + m_b} \sqrt{\frac{2J_A + 1}{2j_b + 1}} \langle J_A - M_A \ j_c \ M_A - m_b | j_b \ m_b \rangle. \quad (4.G.49)$$

As

$$\sum_{M_A} \left| \langle J_A - M_A \ j_c \ M_A - m_b | j_b \ m_b \rangle \right|^2 = 1, \quad (4.G.50)$$

we finally have

$$\frac{d\sigma}{d\mathbf{k}'_a d\mathbf{k}'_b} = \frac{k'_a \mu_{aA} \mu_{ac}}{k_a 4\pi^2 \hbar^4} \frac{1}{(2j_b + 1)(2j_a + 1)} \sum_{m_a, m'_a, m'_b} \left| \sum_{m_b} T_{m_a, m_b}^{m'_a, m'_b}(\mathbf{k}'_a, \mathbf{k}'_b) \right|^2. \quad (4.G.51)$$

### Zero range approximation.

The zero range approximation consists in taking  $v(r_{ab}) = D_0 \delta(r_{ab})$ . Then, (see (4.G.21))

$$\begin{aligned} \mathbf{r}_{aA} &= \frac{c}{A} \mathbf{r}_{bc}, \\ \mathbf{r}_{ac} &= \mathbf{r}_{bc}. \end{aligned} \quad (4.G.52)$$

The angular dependence of the integral can be readily evaluated. From (5.D.20), noting that  $\hat{\mathbf{r}}_{aA} = \hat{\mathbf{r}}_{ac} = \hat{\mathbf{r}}_{bc} \equiv \hat{\mathbf{r}}$ ,

$$\begin{aligned} & \left[ Y^{l_a}(\hat{\mathbf{r}}) Y^{l'_a}(\hat{\mathbf{r}}) \right]_M^K \left[ Y^{l_b}(\hat{\mathbf{r}}) Y^{l'_b}(\hat{\mathbf{r}}) \right]_{-M}^K = \\ & \frac{(-1)^{K-M}}{\sqrt{2K+1}} \left\{ \left[ Y^{l_a}(\hat{\mathbf{r}}) Y^{l'_a}(\hat{\mathbf{r}}) \right]^K \left[ Y^{l_b}(\hat{\mathbf{r}}) Y^{l'_b}(\hat{\mathbf{r}}) \right]^K \right\}_0^0. \end{aligned} \quad (4.G.53)$$

We can as before evaluate this expression in the configuration shown in Fig. 4.G.2 ( $\hat{\mathbf{r}} = \hat{z}$ ), but now the multiplicative factor is  $4\pi$ . The corresponding contribution to the integral is

$$\frac{(-1)^K}{4\pi(2K+1)} \langle l_a \ 0 \ l'_a \ 0 | K \ 0 \rangle \sqrt{(2l_a + 1)(2l'_a + 1)(2l_b + 1)(2l'_b + 1)}, \quad (4.G.54)$$

and

$$\begin{aligned}
T_{m_a, m_b}^{m'_a, m'_b}(\mathbf{k}'_a, \mathbf{k}'_b) = & \frac{16\pi^2}{k_a k'_a k'_b A} D_0 T_\sigma \sum_{l_a, j_a} \sum_{l'_a, j'_a} \sum_{l'_b, j'_b} \sum_{K, M} e^{i(\sigma^{l_a} + \sigma^{l'_a} + \sigma^{l'_b})} i^{l_a - l'_a - l'_b} (-1)^{l_a + l'_a + l'_b - j'_a - j'_b} \\
& \times \sqrt{(2l_a + 1)(2l'_a + 1)(2l_b + 1)(2l'_b + 1)} \langle l_a 0 l'_a 0 | K 0 \rangle \\
& \times \frac{2l_a + 1}{2K + 1} ((l'_a \frac{1}{2})_{j_a} (l_a \frac{1}{2})_{j_a} | (l_a l'_a)_K (\frac{1}{2} \frac{1}{2})_0)_K ((l'_b \frac{1}{2})_{j'_b} (l_b \frac{1}{2})_{j_b} | (l_b l'_b)_K (\frac{1}{2} \frac{1}{2})_0)_K \\
& \times \langle l'_a m_a - M 1/2 m'_a | j'_a m_a - M \rangle \langle l'_b m_b - m'_b + M 1/2 m'_b | j'_b M + m_b \rangle \\
& \times \langle l 0 1/2 m_a | j m_a \rangle Y_{M+m_b+m'_b}^{l'_b}(\hat{\mathbf{k}}'_b) Y_{m_a+m'_a-M}^{l'_a}(\hat{\mathbf{k}}'_a) \mathcal{I}_{ZR}(l_a, l'_a, l'_b, j_a, j'_a, j'_b), \quad (4.G.55)
\end{aligned}$$

where now the 1-dimensional integral to solve is

$$\mathcal{I}_{ZR}(l_a, l'_a, l'_b, j_a, j'_a, j'_b) = \int dr u_{l_b}(r) F_{l_a, j_a}(\frac{c}{A} r) F_{l'_a, j'_a}(r) F_{l'_b, j'_b}(r)/r. \quad (4.G.56)$$

### 4.G.3 One-particle transfer

It may be interesting to state the expression for the one particle transfer reaction within the same context and using the same elements, in order to better compare these two type of experiments. In particle transfer, the final state of  $b$  is a bound state of the  $B (= a + b)$  nucleus (cf. Fig. 4.G.4), and we can carry on in a similar way as done previously just by substituting the distorted wave (continuum) wave function (4.G.34) with

$$\psi_{m'_b}^{l'_b, j'_b*}(\mathbf{r}_{ab}, \sigma_b) = u_{l'_b, j'_b}^*(r_{ab}) \left[ Y^{l'_b}(\hat{\mathbf{r}}_{ab}) \phi^{1/2}(\sigma_b) \right]_{m'_b}^{j'_b*}, \quad (4.G.57)$$

so the transition amplitude is now

$$\begin{aligned}
T_{m_a, m_b}^{m'_a, m'_b}(\mathbf{k}'_a) = & \frac{8\pi^{3/2}}{k_a k'_a} \sum_{\sigma_a, \sigma_b} \sum_{l_a, j_a} \sum_{l'_a, m'_a, j'_a} e^{i(\sigma^{l_a} + \sigma^{l'_a})} i^{l_a - l'_a} (-1)^{l_a + l'_a - j'_a - j'_b} \\
& \times \sqrt{2l_a + 1} \langle l'_a m_{l'_a} 1/2 m'_a | j'_a m_{l'_a} + m'_a \rangle \langle l_a 0 1/2 m_a | j_a m_a \rangle \\
& \times Y_{-m'_{l'_a}}^{l'_a}(\hat{\mathbf{k}}'_a) \int d\mathbf{r}_{aA} d\mathbf{r}_{bc} \left[ Y^{l'_a}(\hat{\mathbf{r}}_{bc}) \phi^{1/2}(\sigma_a) \right]_{-m'_{l'_a} - m'_a}^{j'_a} \left[ Y^{l'_b}(\hat{\mathbf{r}}_{ab}) \phi^{1/2}(\sigma_b) \right]_{-m'_b}^{j'_b} \\
& \times \frac{F_{l_a, j_a}(r_{aA}) F_{l'_a, j'_a}(r_{bc})}{r_{bc} r_{aA}} u_{l'_b, j'_b}^*(r_{ab}) u_{l_b, j_b}(r_{bc}) v(r_{ab}) v_\sigma(\sigma_a, \sigma_b) \\
& \times \left[ Y^{l_a}(\hat{\mathbf{r}}_{aA}) \phi^{1/2}(\sigma_a) \right]_{m_a}^{j_a} \left[ Y^{l_b}(\hat{\mathbf{r}}_{bc}) \phi^{1/2}(\sigma_b) \right]_{m_b}^{j_b}. \quad (4.G.58)
\end{aligned}$$

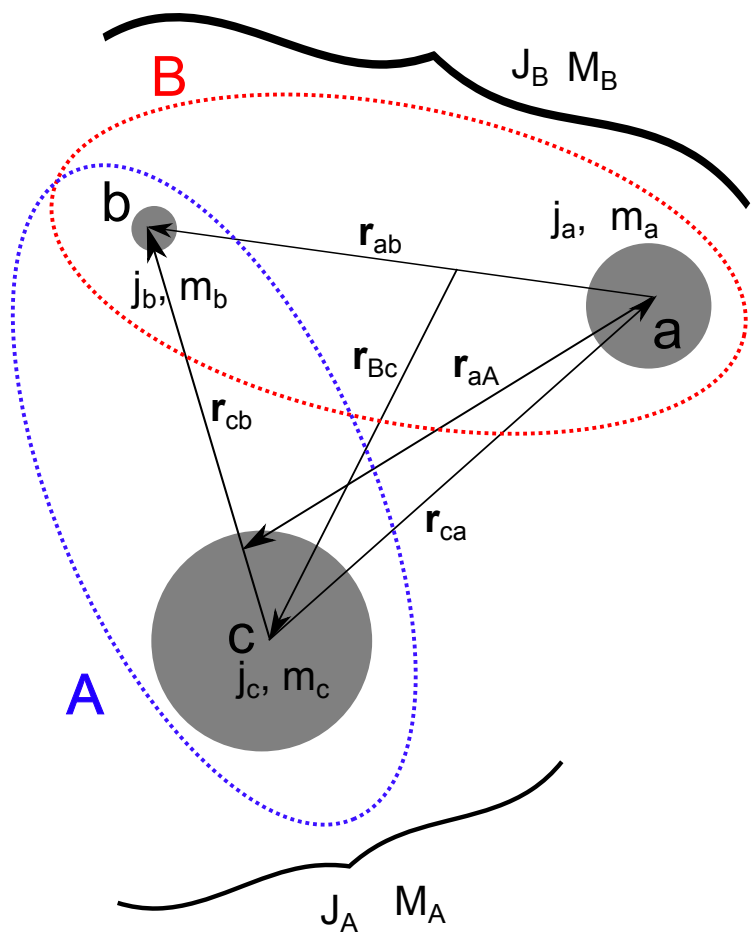


Figure 4.G.4: One particle transfer reaction  $A(= c + b) + a \rightarrow B(= a + b) + c$ .

Using (4.G.39), (4.G.40), (5.F.4), and setting  $M = m_a - m'_a - m_{l'_a}$

$$\begin{aligned} T_{m_a, m_b}^{m'_a, m'_b}(\mathbf{k}'_a) &= \frac{8\pi^{3/2}}{k_a k'_a} T_\sigma \sum_{l_a, j_a} \sum_{l'_a, j'_a} \sum_{K, M} e^{i(\sigma^{l_a} + \sigma^{l'_a}) l'_a - l'_a} (-1)^{l_a + l'_a - j'_a - j'_b} \\ &\quad \times ((l'_a \frac{1}{2})_{j'_a} (l_a \frac{1}{2})_{j_a} | (l_a l'_a)_K (\frac{1}{2} \frac{1}{2})_0)_K ((l'_b \frac{1}{2})_{j'_b} (l_b \frac{1}{2})_{j_b} | (l_b l'_b)_K (\frac{1}{2} \frac{1}{2})_0)_K \\ &\quad \times \sqrt{2l_a + 1} \langle l'_a m_a - m'_a - M 1/2 m'_a | j'_a m_a - M \rangle \langle l_a 0 1/2 m_a | j_a m_a \rangle \\ &\quad \times Y_{m_a - m'_a - M}^{l'_a}(\hat{\mathbf{k}}'_a) \int d\mathbf{r}_{aA} d\mathbf{r}_{bc} \frac{F_{l_a, j_a}(r_{aA}) F_{l'_a, j'_a}(r_{Bc})}{r_{Bc} r_{aA}} u_{l'_b, j'_b}^*(r_{ab}) u_{l_b, j_b}(r_{bc}) v(r_{ab}) \\ &\quad \times [Y^{l_a}(\hat{\mathbf{r}}_{aA}) Y^{l'_a}(\hat{\mathbf{r}}_{Bc})]_M^K [Y^{l_b}(\hat{\mathbf{r}}_{bc}) Y^{l'_b}(\hat{\mathbf{r}}_{ab})]_{-M}^K. \quad (4.G.59) \end{aligned}$$

Aside from (4.G.21), we also need

$$\mathbf{r}_{Bc} = \frac{a+B}{B} \mathbf{r}_{aA} + \frac{b}{A} \mathbf{r}_{bc}. \quad (4.G.60)$$

From (4.G.20–4.G.25), one gets

$$\begin{aligned} T_{m_a, m_b}^{m'_a, m'_b}(\mathbf{k}'_a) &= \frac{32\pi^3}{k_a k'_a} T_\sigma \sum_{l_a, j_a} \sum_{l'_a, j'_a} \sum_{K, M} e^{i(\sigma^{l_a} + \sigma^{l'_a}) l'_a - l'_a} (-1)^{l_a + l'_a - j'_a - j'_b} \\ &\quad \times ((l'_a \frac{1}{2})_{j'_a} (l_a \frac{1}{2})_{j_a} | (l_a l'_a)_K (\frac{1}{2} \frac{1}{2})_0)_K ((l'_b \frac{1}{2})_{j'_b} (l_b \frac{1}{2})_{j_b} | (l_b l'_b)_K (\frac{1}{2} \frac{1}{2})_0)_K \\ &\quad \times \frac{2l_a + 1}{2K + 1} \langle l'_a m_a - m'_a - M 1/2 m'_a | j'_a m_a - M \rangle \\ &\quad \times \langle l_a 0 1/2 m_a | j_a m_a \rangle Y_{m_a - m'_a - M}^{l'_a}(\hat{\mathbf{k}}'_a) \mathcal{I}(l_a, l'_a, j_a, j'_a, j'_b, K), \quad (4.G.61) \end{aligned}$$

with

$$\begin{aligned} \mathcal{I}(l_a, l'_a, j_a, j'_a, K) &= \int dr_{aA} dr_{bc} d\theta r_{aA} r_{bc}^2 \frac{\sin \theta}{r_{Bc}} \\ &\quad \times F_{l_a, j_a}(r_{aA}) F_{l'_a, j'_a}(r_{ac}) u_{l'_b, j'_b}^*(r_{ab}) u_{l_b, j_b}(r_{bc}) v(r_{ab}) \\ &\quad \times \sum_{M_K} \langle l_a 0 l'_a M_K | K M_K \rangle [Y^{l_b}(\cos \theta, 0) Y^{l'_b}(\cos \theta_{ab}, 0)]_{-M_K}^K Y_{M_K}^{l'_a}(\cos \theta_{Bc}, 0), \quad (4.G.62) \end{aligned}$$

where (see (4.G.21), (4.G.60) and Fig. 4.G.2)

$$\cos \theta_{ab} = \frac{-r_{aA} - \frac{c}{A} r_{bc} \cos \theta}{\sqrt{\left(\frac{c}{A} r_{bc} \sin \theta\right)^2 + \left(r_{aA} + \frac{c}{A} r_{bc} \cos \theta\right)^2}}, \quad (4.G.63)$$

$$\cos \theta_{Bc} = \frac{\frac{a+B}{B} r_{aA} + \frac{b}{A} r_{bc} \cos \theta}{\sqrt{\left(\frac{b}{A} r_{bc} \sin \theta\right)^2 + \left(\frac{a+B}{B} r_{aA} + \frac{b}{A} r_{bc} \cos \theta\right)^2}}, \quad (4.G.64)$$

and

$$r_{Bc} = \sqrt{\left(\frac{b}{A}r_{bc}\sin\theta\right)^2 + \left(\frac{a+B}{B}r_{AA} + \frac{b}{A}r_{bc}\cos\theta\right)^2}. \quad (4.G.65)$$

By the way, (4.G.61) can also be used when particle  $b$  populates a resonant state in the continuum of nucleus  $B$ .

## Appendix 4.H Modified formfactors

### 4.H.1 Two-particle transfer

### 4.H.2 One-particle transfer

### 4.H.3 Inelastic scattering

### 4.H.4 Elastic scattering

## Appendix 4.I Dynamical shell model in a nutshell

In the extreme shell model the nucleons move independently, feeling the presences of the other nucleons when bouncing elastically off the nuclear surface of the average potential. The properly normalized probability for removing nucleon from such orbitals is one for  $\omega$  equal to the (unperturbed) energy of the orbital  $k$  and zero otherwise. (cf. Fig 4.I.1)

In the dynamical shell model (cf. Mahaux, C. et al. (1985) and references therein) the nucleons can bounce inelastically off the nuclear surface setting the nucleus in a vibrational state and changing the state of motion (Fig. 4.I.1). In this case the strength of the levels becomes in general distributed over a range of energies both below and above the Fermi energy. That is, the state  $k$  is found both in the system  $(A - 1)$  produced in a pick-up process and in the system  $(A + 1)$  populated through a stripping reaction as indicated in Fig 4.I.1.

It is still an open question whether this distribution is concentrated in discrete states or displays a continuous behavior. Both situations can in principle be found depending of whether the original single-particle state is close or far away from the Fermi energy. The sum of the spectroscopic factors associated with all the states excited in the pick-up process of a nucleon with quantum numbers  $k$  gives the occupation number associated with the orbital, i.e.  $\int_{-\infty}^{\epsilon_F} S_h(k; \omega) d\omega = n_k$ , where  $S_h$  is the (hole) strength function. The full single-particle strength is found adding to this quantity the spectroscopic factors associated with the excitation of states in the  $(A + 1)$  system where a particle with quantum numbers  $k$  is deposited in the target.

It is noted that the fact that in the dynamical shell model the single-particle strength is distributed not only over an energy range in the  $(A - 1)$  system but also in the  $(A + 1)$  system is intimately connected with the ground state correlations associated with the vibrational modes which produce particle-hole excitations in

the ground state (also pair addition and subtraction modes). In this way single-particle states which originally were filled become partially empty, and vice versa.

The transfer process shown in (b) for both stripping and pick-up reactions are closely associated with the polarization and correlation contributions to the mass operator  $\mathcal{M}(k; \omega) = \mathcal{V}(k; \omega) + i\mathcal{W}(k; \omega)$ . The associated total strength distribution

$$\begin{aligned} S(k; \omega) &= S_h(k; \omega) + S_p(k; \omega), \\ &= \frac{1}{2\pi} \frac{\mathcal{W}(k; \omega) + \Delta}{(E_k + \mathcal{V}(k; \omega) - E)^2 + \frac{1}{4}(\mathcal{W}(k; \omega) + \Delta)^2}, \end{aligned}$$

can display a variety of shapes, as  $\mathcal{V}(k; \omega)$  and  $\mathcal{W}(k; \omega)$  are energy dependent.

The intermediate states of the polarization and correlation diagrams which in the present discussion are the doorway states to the renormalization of the single-particle motion must be mixed with more complicated configurations. The mechanism for these couplings and their consequences are quite involved and, to some extent, open problems. Thus, the extension in the complex plane of the associated expressions in terms of an imaginary parameter  $\Delta$  is made to take these effects into account in some average way. In any case, most of the results are not dependent on the detailed value this quantity has.

The picture shown in Fig. 4.I.1 (b) although accurate and controlled by only few parameters is much too rich as compared to the originally extreme shell model picture.

A major simplification can be achieved recognizing that the essential difference between the situation depicted in Figs 4.I.1 (a) and (b) is the value of the mean free path. In the first case it is infinite while in the second it is finite. That is, due to the coupling to the surface modes (and eventually pair modes) single-particle motion acquires a lifetime. In this sense the detailed shape of the strength distribution which reflects the specificity of the different couplings and which is of central importance for a detailed analysis of the data becomes of secondary importance within the present context.

Making the ansatz that the single-particle motion decays exponentially a Breit-Wigner shape can be fitted to the different strength concentration resulting from the detailed calculation (cf. Fig. 4.I.1 (b)) The centroid of the corresponding peaks defines an energy which can be viewed as the energy of the dressed single-particle state. On the other hand, caution should be exercised in interpreting the area under the fitted curve as a spectroscopic factor, if only because this quantity can become larger than one. It is only for the levels not too far away from the Fermi energy that such interpretation can be reasonably accurate.

Another quantity which can be used to characterize the dressed single-particle states is the rate of change of the energy shift as a function of the energy, i.e. the effective mass. Again, for the orbitals close to the Fermi energy this quantity is inversely proportional to the area under the Breit-Wigner shapes. The energy range over which the effective mass deviates from one determine the region where the dynamical couplings change the density of single-particle levels.

The trend of the effective masses shown in Fig. 4.I.1 (d) can be quantitatively understood as follows. For single-particle states close to the Fermi energy the intermediate states have all energies larger than the unperturbed single-particle energy, and the resulting shape is  $\delta$ -like with a tail extending away from the Fermi energy. For single-particle orbital 5–7 MeV away from  $\epsilon_F$  there are a number of intermediate states which have the same energy of the initial state leading to zero energy denominators and thus to a marked structure in the strength function. Finally, for single-particle states far away from  $\epsilon_F$ , the density of intermediate states is so large that the matrix elements of these couplings average out to a constant with a value much larger than typical distances between successive intermediate states. These are the conditions which lead to a Breit–Wigner shape.

It is then to be expected that the single-particle levels in the intermediate region will be associated with strength functions which deviate much from a smooth function and for which comparatively large errors can be made through a Breit–Wigner fitting. This is also seen from Fig. 4.I.1 (d) where the effective mass becomes smaller than one, indicating that the area of the fitted shapes are larger than that of the original strength function  $S(k; \omega)$ . This result emphasizes the difficulties found in trying to translate effective masses into spectroscopic factors in a general situation.

Starting from the extreme picture shown in Fig. 4.I.1 (a) where the relation  $\omega = \hbar^2 k^2 / 2m$  holds one arrives at the picture (c) where the relation  $d\omega = \hbar^2 k \delta k / m^*$  again accounts for the main properties of the single-particle motion and where the effect of the couplings are contained in  $m^*$  (see Eq. (4.A.3)). The numerical implementation of the single-particle self-energies scenario have been carried out for different regions of the mass table. In particular, for the valence levels of  $^{208}\text{Pb}$ . In this case the mass operator associated with each orbital was calculated as a function of the energy. The numerical derivative of the real part of the mass operator was then calculated and the  $\omega$ -dependent effective mass obtained as a function of the energy.

The question then arises of how to define an average quantity which depends only on the energy of the orbital and is state independent. Rather different prescriptions have been used to deal with the question. In any case the main result obtained was that the  $\omega$ -dependent effective mass shows a well defined peak at the Fermi surface, its maximum value being considerably larger than one ( $\approx 1.4$ ). The associated full width at half maximum is of the order of 10 MeV. This quantity is much smaller than the Fermi energy ( $\sim 36$  MeV) and is essentially determined by the energy of the low-lying collective modes and of the single-article gap around  $^{208}\text{Pb}$ .

## Bibliography

P. W. Anderson. *Basic notions of condensed matter physics*. Benjamin, Menlo Park, California, 1984.

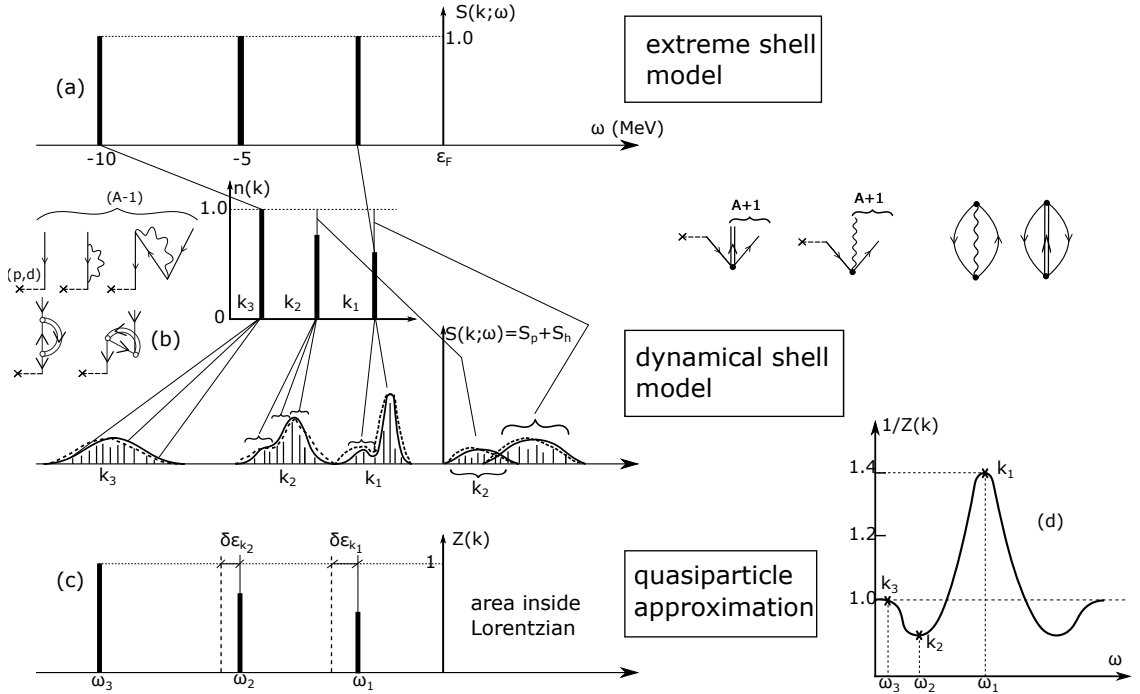


Figure 4.I.1: Schematic representation of the main quantities characterizing the single-particle motion in the nuclear shell model taking into account the residual interaction among the particles at different levels of approximation. In (a) the interaction is treated in the Hartree–Fock approximation and the particles feel the presence of the other particles through their own confinement in the average field. The strength function shows sharp peaks, each of them carrying the full strength of the states. In fact, the occupation number associated with each state  $k$  contains only one contribution. In (b) the particles still couple only with the average field. However in this case they can set the surface into vibrations by changing its state of motion. The strength associated with each orbital is distributed over a finite energy range. The corresponding occupation numbers arise from the sum of many contributions. Fitting a Lorentzian shape to each peak one can regain the simplicity of the extreme shell model by defining new levels with energy equal to that of the centroid and strength equal to that of the area covered by the Lorentzian shape (cf. (c)). In (d) the energy variation of the shift of the centroids is contained into an effective  $\omega$ -mass according to the standard relation  $\frac{m_\omega}{m} = \left(1 - \frac{\partial \Delta E}{\partial \hbar \omega}\right)$  (see Eq. (4.A.5)). The resulting curve resembles the shape obtained by calculating the inverse of the area below the different Lorentzians (quasiparticle approximation).

- R. J. Ascuitto and N. K. Glendenning. Inelastic processes in particle transfer reactions. *Physical Review*, 181:1396, 1969.
- Ascuitto, R. J. and N. K. Glendenning. Assessment of two-step processes in  $(p, t)$  reactions. *Phys. Rev. C*, 2:1260, 1970.
- Ascuitto R. J., N. K. Glendenning, and B. Sørensen. Confirmation of strong second order processes in  $(p, t)$  reactions on deformed nuclei. *Physics Letters B*, 34:17, 1971.
- Ascuitto R.J. and B. Sørensen. Coupling effects in  $^{208}\text{Pb}$ . *Nuclear Physics A*, 186: 641, 1972.
- N. Austern. Direct reactions. In F. Janouch, editor, *Select Topics in Nuclear Theory*, Vienna, 1963. IAEA.
- N. Austern. *Direct nuclear reaction theories*. Interscience monographs and texts in physics and astronomy. Wiley–Interscience, 1970.
- J. Bang, S. Ershov, F. Gareev, and G. Kazacha. Discrete expansions of continuum wave functions. *Nuclear Physics A*, 339:89, 1980.
- J. Bardeen and D. Pines. Electron-phonon interaction in metals. *Phys. Rev.*, 99: 1140, 1955.
- Baroni, S., M. Armati, F. Barranco, R. A. Broglia, G. Colò, G. Gori, and E. Vigezzi. Correlation energy contribution to nuclear masses. *Journal of Physics G: Nuclear and Particle Physics*, 30:1353, 2004.
- F. Barranco, M. Gallardo, and R. A. Broglia. Nuclear field theory of spin dealignment in strongly rotating nuclei and the vacuum polarization induced by pairing vibrations. *Phys. Lett. B*, 198:19, 1987.
- Barranco, F., P. F. Bortignon, R. A. Broglia, G. Colò, and E. Vigezzi. The halo of the exotic nucleus  $^{11}\text{Li}$ : a single Cooper pair. *Europ. Phys. J. A*, 11:385, 2001.
- Bechara, M. J. and O. Dietzsch. States in  $^{121}\text{Sn}$  from the  $^{120}\text{Sn}(d, p)^{121}\text{Sn}$  reaction at 17 mev. *Phys. Rev. C*, 12:90, 1975.
- G. F. Bertsch, P. F. Bortignon, and R. A. Broglia. Damping of nuclear excitations. *Rev. Mod. Phys.*, 55:287, 1983.
- D. R. Bès and R. A. Broglia. Equivalence between Feynman–Goldstone and particle–phonon diagrams for finite many body systems. In G. Alaga, V. Paar, and L. Sips, editors, *Problems of Vibrational Nuclei, in Procs. of the topical Conference on Problems of Vibrational Nuclei*, page 1, Amsterdam, 1975. North Holland.

- D. R. Bès and R. A. Broglia. In A. Bohr and R. Broglia, editors, *International School of Physics “Enrico Fermi” Course LXIX, Elementary Modes of Excitation in Nuclei*, page 55, Amsterdam, 1977. North Holland.
- D. R. Bès, G. G. Dussel, R. Broglia, R. Liotta, and B. R. Mottelson. Nuclear field theory as a method of treating the problem of overcompleteness in descriptions involving elementary modes of both quasi-particles and collective type. *Phys. Lett. B*, 52:253, 1974.
- D. R. Bès, R. A. Broglia, G. G. Dussel, R. J. Liotta, and R. P. J. Perazzo. On the many-body foundation of the Nuclear Field Theory. *Nucl. Phys. A*, 260:77, 1976a.
- D. R. Bès, R. A. Broglia, G. G. Dussel, R. J. Liotta, and H. M. Sofía. The nuclear field treatment of some exactly soluble models. *Nucl. Phys. A*, 260:1, 1976b.
- D. R. Bès, R. A. Broglia, G. G. Dussel, R. J. Liotta, and H. M. Sofía. Application of the nuclear field theory to monopole interactions which include all the vertices of a general force. *Nucl. Phys. A*, 260:27, 1976c.
- Bès, D. R. and J. Kurchan. *The treatment of Collective Coordinates in Many-Body Systems*. World Scientific, Singapore, 1990.
- Bès, D. R., R. A. Broglia, J. Dudek, W. Nazarewicz, and Z. Szymański. Fluctuation effects in the pairing field of rapidly rotating nuclei. *Annals of Physics*, 182:237, 1988.
- A. Bohr and B. R. Mottelson. *Nuclear Structure, Vol.I*. Benjamin, New York, 1969.
- Bohr, A. and B. R. Mottelson. *Nuclear Structure, Vol.II*. Benjamin, New York, 1975.
- M. Born. Zur Quantenmechanik der Stoßvorgänge. *Zeitschr.f. Phys.*, 37:863, 1926.
- P. F. Bortignon and R. A. Broglia. Role of the nuclear surface in a unified description of the damping of single-particle states and giant resonances. *Nucl. Phys. A*, 371:405, 1981.
- P. F. Bortignon, R. A. Broglia, and C. H. Dasso. Quenching of the mass operator associated with collective states in many-body systems. *Nuclear Physics A*, 398: 221, 1983.
- Bortignon, P. F., R. A. Broglia, D. R. Bès, and R. Liotta. Nuclear field theory. *Physics Reports*, 30:305, 1977.
- Bortignon, P.F., A. Bracco, and R. Broglia. *Giant Resonances*. Harwood Academic Publishers, Amsterdam, 1998.
- D. Brink and G. R. Satchler. *Angular Momentum*. Clarendon Press, 1968.

- Brink, D. and R. A. Broglia. *Nuclear Superfluidity*. Cambridge University Press, Cambridge, 2005.
- R. Broglia and A. Winther. *Heavy Ion Reactions*. Westview Press, Boulder, CO., 2004.
- R. Broglia, G. Coló, G. Onida, and H. Roman. *Solid State Physics of Finite Systems: metal clusters, fullerenes, atomic wires*. Springer Verlag, Berlin, Heidelberg, 2004.
- R. A. Broglia, B. R. Mottelson, D. R. Bès, R. Liotta, and H. M. Sofía. Treatment of the spurious state in Nuclear Field Theory. *Physics Letters B*, 64:29, 1976.
- Broglia, R. A., G. Pollarolo, and A. Winther. On the absorptive potential in heavy ion scattering. *Nuclear Physics A*, 361:307, 1981.
- Broglia, R. A., T. Døssing, B. Lauritzen, and B. R. Mottelson. Nuclear rotational damping: Finite-system analogue to motional narrowing in nuclear magnetic resonances. *Phys. Rev. Lett.*, 58:326, 1987.
- Broglia, R.A., O. Hansen, and C. Riedel. Two-neutron transfer reactions and the pairing model. *Advances in Nuclear Physics*, 6:287, 1973. URL [www.mi.infn.it/~vigezzi/BHR/BrogliaHansenRiedel.pdf](http://www.mi.infn.it/~vigezzi/BHR/BrogliaHansenRiedel.pdf).
- W. R. Cobb and D. B. Guthe. Angular distribution of protons from the  $^{44}\text{Ca}(d, p)^{45}\text{Ca}$  reaction. *Phys. Rev.*, 107:181, 1957.
- Dickey, S. A., J. Kraushaar, R. Ristinen, and M. Rumore. The  $^{120}\text{Sn}(p, d)^{119}\text{Sn}$  reaction at 26.3 MeV. *Nuclear Physics A*, 377:137, 1982.
- W. H. Dickhoff and C. Barbieri. Self-consistent Green's function method for nuclei and nuclear matter. *Progress in Particle and Nuclear Physics*, 52:377, 2004.
- Dickhoff, W. and D. Van Neck. *Many-Body Theory Exposed: Propagator description of quantum mechanics in many-body systems*. World Scientific, Singapore, 2005.
- Duguet, T. and G. Hagen. *Ab initio* approach to effective single-particle energies in doubly closed shell nuclei. *Phys. Rev. C*, 85:034330, 2012.
- A. R. Edmonds. *Angular momentum in quantum mechanics*. Princeton University Press, 1960.
- Fernández-García, J.P., M. Alvarez, A. Moro, and M. Rodriguez-Gallardo. Simultaneous analysis of elastic scattering and transfer/breakup channels for the  $^6\text{He} + ^{208}\text{Pb}$  reaction at energies near the Coulomb barrier. *Phys. Lett.*, B693:310, 2010.

- Fernández-García, J.P., M. Rodríguez-Gallardo, M. Alvarez, and A. Moro. Long range effects on the optical model of  $^6\text{He}$  around the Coulomb barrier. *Nuclear Physics A*, 840:19, 2010.
- H. Feshbach. Unified Theory of Nuclear Reactions. *Annals of Physics*, 5:357, 1958.
- R. Feynman. *Theory of fundamental processes*. Benjamin, Reading, Mass., 1975.
- Fröhlich, H. Interaction of electrons with lattice vibrations. *Procs. Royal Soc.*, 215:291, 1952.
- Glendenning, N. K. *Direct nuclear reactions*. World Scientific, Singapore, 2004.
- I. Hamamoto. Single-particle components of particle-vibrational states in the nuclei  $^{209}\text{Pb}$ ,  $^{209}\text{Bi}$ ,  $^{207}\text{Pb}$  and  $^{207}\text{Tl}$ . *Nuclear Physics A*, 141:1, 1970.
- Idini, A. Renormalization effects in nuclei. *Ph.D. thesis, University of Milan*, 2013.
- Idini, A., F. Barranco, and E. Vigezzi. Quasiparticle renormalization and pairing correlations in spherical superfluid nuclei. *Phys. Rev. C*, 85:014331, 2012.
- Idini, A., G. Potel, Barranco, E. Vigezzi, and R. A. Broglia. Dual origin of pairing in nuclei. *arXiv:1404.7365v1 [nucl-th]*, 2014.
- Jenning, B. Non observability of spectroscopic factors. *arXiv: 1102.3721v1 [nucl-th]*, 2011.
- Jeppesen, H. B. et al. Experimental investigation of the  $^9\text{Li}+\text{d}$  reaction at REX-ISOLDE. *Nucl. Phys. A*, 738:511, 2004.
- Mahaux, C., P. F. Bortignon, R. A. Broglia, and C. H. Dasso. Dynamics of the shell model. *Physics Reports*, 120:1–274, 1985.
- A. Migdal. Interaction between electrons and lattice vibrations in a normal metal. *Soviet Physics JETP*, 7:996, 1958.
- D. Montanari, L. Corradi, S. Szwilner, G. Pollaro, E. Fioretto, G. Montagnoli, F. Scarlassara, A. M. Stefanini, S. Courtin, A. Goasduff, F. Haas, D. Jelavić Malenica, C. Michelagnoli, T. Mijatović, N. Soić, C. A. Ur, and M. Varga Pajtler. Neutron Pair Transfer in  $^{60}\text{Ni} + ^{116}\text{Sn}$  Far below the Coulomb Barrier. *Phys. Rev. Lett.*, 113:052501, 2014.
- B. R. Mottelson. *Elementary Modes of Excitation in Nuclei, Le Prix Nobel en 1975*. Imprimerie Royale Norstedts Tryckeri, Stockholm, 1976. p. 80.
- Orrigo, S. E. A. and H. Lenske. Pairing resonances and the continuum spectroscopy of  $^{10}\text{Li}$ . *Phys. Lett. B*, 677:214, 2009.

- W. Pauli. *Exclusion principle and quantum mechanics, Nobel Lecture 1945*. Editions du Griffon, Neuchâtel, Switzerland, 1947.
- G. Pollarolo, R. Broglia, and A. Winther. Calculation of the imaginary part of the heavy ion potential. *Nuclear Physics A*, 406:369, 1983.
- G. Potel, F. Barranco, E. Vigezzi, and R. A. Broglia. Evidence for phonon mediated pairing interaction in the halo of the nucleus  $^{11}\text{Li}$ . *Phys. Rev. Lett.*, 105:172502, 2010.
- Potel, G. ONE: single-particle transfer DWBA software for both light and heavy ions. *Private communication*, 2012.
- Potel, G., A. Idini, F. Barranco, E. Vigezzi, and R. A. Broglia. Cooper pair transfer in nuclei. *Rep. Prog. Phys.*, 76:106301, 2013.
- Rawitscher, G. H. The microscopic Feshbach optical potential for a schematic coupled channel example. *Nuclear Physics A*, 475:519, 1987.
- G. Satchler. *Introduction to Nuclear Reactions*. Mc Millan, New York, 1980.
- G. Satchler. *Direct Nuclear Reactions*. Clarendon Press, Oxford, 1983.
- J. Schrieffer. *Superconductivity*. Benjamin, New York, 1964.
- Tamura, T., D. R. Bès, R. A. Broglia, and S. Landowne. Coupled-channel born-approximation calculation of two-nucleon transfer reactions in deformed nuclei. *Physical Review Letters*, 25:1507, 1970.
- Tanikawa, I., M. Alcorta, D. Bandyopadhyay, R. Bieri, L. Buchmann, B. Davids, N. Galinski, D. Howell, W. Mills, S. Mythili, R. Openshaw, E. Padilla-Rodal, G. Ruprecht, G. Sheffer, A. C. Shotter, M. Trinczek, P. Walden, H. Savajols, T. Roger, M. Caamano, W. Mittig, P. Roussel-Chomaz, R. Kanungo, A. Gallant, M. Notani, G. Savard, and I. J. Thompson. Measurement of the two-halo neutron transfer reaction  $^1\text{H}(^{11}\text{Li}, ^9\text{Li})^3\text{H}$  at 3A MeV. *Phys. Rev. Lett.*, 100:192502, 2008.
- I. J. Thompson. Coupled reaction channels calculations in nuclear physics. *Computer Physics Reports*, 7(4):167, 1988.
- Thompson, I.J. Reaction mechanism of pair transfer. In R. A. Broglia and V. Zelevinsky, editors, *50 Years of Nuclear BCS*, page 455. World Scientific, Singapore, 2013.
- W. Tobocman. *Theory of direct eactions*. Oxford University Press, Oxford, 1961.
- J. Vaagen, B. Nilsson, J. Bang, and R. Ibarra. One- and two-nucleon overlaps generated by a Sturmian method. *Nuclear Physics A*, 319:143, 1979.



# Chapter 5

## Two-particle transfer

Cooper pairs are the building blocks of pairing correlations in many-body fermionic systems. In particular in atomic nuclei. As a consequence, nuclear superfluidity can be specifically probed through Cooper pair tunneling. In the simultaneous transfer of two nucleons, one nucleon goes over from target to projectile, or viceversa, under the influence of the nuclear interaction responsible of the existence of a mean field potential, while the other follows suit by profiting of: 1) pairing correlations (simultaneous transfer); 2) the fact that the single-particle wavefunctions describing the motion of Cooper pair partners in both target and projectile are solutions of different single-particle potentials (non-orthogonality term). In the limit of independent particle motion, in which all of the nucleon-nucleon interaction is used up in generating a mean field, both contributions to the transfer process (simultaneous and non-orthogonality) cancel out exactly (cf. App. 5.C)

In keeping with the fact that nuclear Cooper pairs are weakly bound ( $E_{corr} \ll \epsilon_F$ ), this cancellation is, in actual nuclei, quite strong. Consequently, successive transfer, a process in which the nuclear interaction acts twice is, as a rule, the main mechanism at the basis of Cooper pair transfer. Because of the same reason (weak binding), the correlation length of Cooper pairs is larger than nuclear dimensions ( $\xi = \hbar v_F / (2E_{corr}) \gg R$ ), a fact which allows the two members of a Cooper pair to move between target and projectile, essentially as a whole, also in the case of successive transfer. In other words, because of its (intrinsic, virtual extension) Cooper pair transfer display equivalent pairing correlations both in simultaneous as in successive transfer.<sup>1</sup>

---

<sup>1</sup>In order for a nucleon to display independent particle motion, all other nucleons must act coherently so as to leave the way free making feel their pullings and pushings only when the nucleon in question tries to leave the self-bound system, thus acting as a reflecting surface which inverts the momentum of the particle. It is then natural to consider the nuclear mean field the most striking and fundamental collective feature in all nuclear phenomena (Mottelson (1962)). A close second is provided by the BCS mean field, resulting from the condensation of a number of strongly overlapping Cooper pairs ( $\approx \langle BCS | \sum_{\nu>0} a_\nu^\dagger a_\nu^\dagger | BCS \rangle = \alpha_0 \neq 0$ ) and leading to independent pair motion. It is a rather unfortunate perversity of popular terminology that regards these collective fields (HF and HFB) as well as successive transfer, as in some sense an antithesis to the nuclear collective modes and to simultaneous transfer respectively. Within this context it is of notice that the differential cross

The present Chapter is structured in the following way. In section 5.1 we present a summary of two-nucleon transfer reaction theory. It provides, together with Section 3.1 the elements needed to calculate the absolute two-nucleon transfer differential cross sections in second order DWBA, and thus to compare theory with experiment. Within this context one can, after reading this section, move directly to Chapter 6 containing examples of applications of this formalism. For the practitioner in search of details and clarification we present in section 5.2 a derivation of the equations presented in section 5.1. These equations are implemented and made operative in the software COOPER used in the applications (cf. App. 6.D).

A number of Appendices are provided. Appendix 5.A briefly reminds the quantum basis for the dressing of elementary modes of excitation and of pairing interaction. In App. 5.B the derivation of first order DWBA simultaneous transfer is worked out within a formalism tailored to focus the attention on the nuclear structure correlations aspects of the process leading to effective two-nucleon transfer form factors. In App. 5.C the variety of contributions to two-nucleon transfer amplitudes (successive, simultaneous and non-orthogonality) are discussed in detail within the framework of the semi-classical approximation which provides a rather intuitive vision of the different processes. Appendices 5.D–5.G contain relations used in Sect. 5.2 as well as in the derivation of two-nucleon transfer spectroscopic amplitudes. Finally Appendix 5.H provides a glimpse of original material due to Ben Bayman (Bayman and Kallio (1967), Bayman (1970), Bayman (1971), Bayman and Chen (1982)) which was instrumental to render quantitative, studies of two-nucleon transfer, studies which can now be carried out in terms of absolute cross sections and not relative ones as done previously.

## 5.1 Summary of second order DWBA

Let us illustrate the theory of second order DWBA two-nucleon transfer reactions with the  $A + t \rightarrow B(\equiv A + 2) + p$  reaction, in which  $A + 2$  and  $A$  are even nuclei in their  $0^+$  ground state. The extension of the expressions to the transfer of pairs coupled to arbitrary angular momentum is discussed in subsection 5.2.10.

The wavefunction of the nucleus  $A + 2$  can be written as

$$\Psi_{A+2}(\xi_A, \mathbf{r}_{A1}, \sigma_1, \mathbf{r}_{A2}, \sigma_2) = \psi_A(\xi_A) \sum_{l_i, j_i} [\phi_{l_i, j_i}^{A+2}(\mathbf{r}_{A1}, \sigma_1, \mathbf{r}_{A2}, \sigma_2)]_0^0, \quad (5.1.1)$$

where

$$[\phi_{l_i, j_i}^{A+2}(\mathbf{r}_{A1}, \sigma_1, \mathbf{r}_{A2}, \sigma_2)]_0^0 = \sum_{nm} a_{nm} [\varphi_{n, l_i, j_i}^{A+2}(\mathbf{r}_{A1}, \sigma_1) \varphi_{m, l_i, j_i}^{A+2}(\mathbf{r}_{A2}, \sigma_2)]_0^0, \quad (5.1.2)$$

---

section associated with the two-nucleon transfer transitions between the ground state of superfluid nuclei is proportional to  $\alpha_0^2$  and not to  $\Delta^2$ . In fact, Cooper pairs partners remain correlated even over regions in which  $G = 0$ .

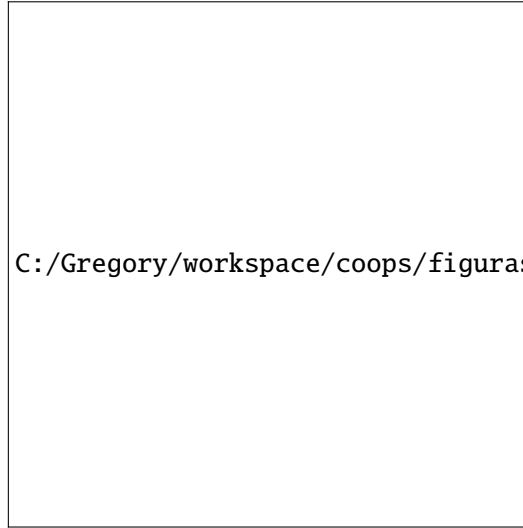


Figure 5.1.1: Radial function  $\rho(r)$  (hard core 0.45 fm) entering the tritium wavefunction (cf. Tang and Herndon (1965)).

while the wavefunctions  $\varphi_{n,l_i,j_i}^{A+2}(\mathbf{r})$  are eigenfunctions of a Saxon–Woods potential

$$U(r) = -\frac{V_0}{1 + \exp\left[\frac{r-R_0}{a}\right]}, \quad R_0 = r_0 A^{1/3}, \quad (5.1.3)$$

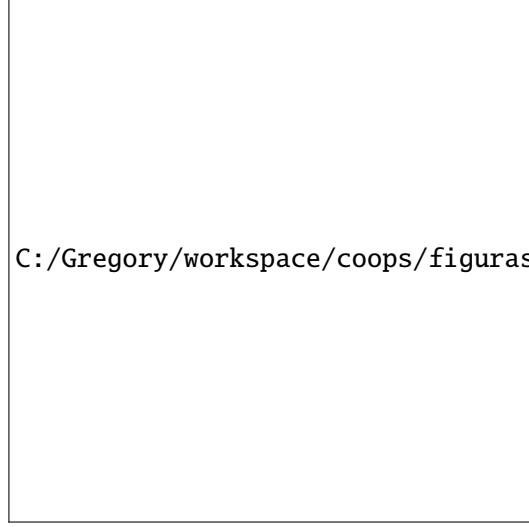
of depth  $V_0$  adjusted to reproduce the experimental single-particles energies, together with a standard spin-orbit potential. The radial dependence of the wavefunction of the two neutrons in the triton is written as  $\phi_t(\mathbf{r}_{p1}, \mathbf{r}_{p2}) = \rho(r_{p1})\rho(r_{p2})\rho(r_{12})$ , where  $r_{p1}, r_{p2}, r_{12}$  are the distances between neutron 1 and the proton, neutron 2 and the proton and between neutrons 1 and 2 respectively, while  $\rho(r)$  is the hard core ( $r_{core} = 0.45$  fm) potential wavefunction depicted in Fig 5.1.1.

The two-nucleon transfer differential cross section is written as

$$\frac{d\sigma}{d\Omega} = \frac{\mu_i \mu_f}{(4\pi\hbar^2)^2} \frac{k_f}{k_i} \left| T^{(1)}(\theta) + T_{succ}^{(2)}(\theta) - T_{NO}^{(2)}(\theta) \right|^2, \quad (5.1.4)$$

where (see e.g. Bayman and Chen (1982) and App. 5.H),

$$\begin{aligned} T^{(1)}(\theta) = 2 \sum_{l_i, j_i} \sum_{\sigma_1 \sigma_2} \int d\mathbf{r}_{tA} d\mathbf{r}_{p1} d\mathbf{r}_{A2} [\phi_{l_i, j_i}^{A+2}(\mathbf{r}_{A1}, \sigma_1, \mathbf{r}_{A2}, \sigma_2)]_0^{0*} \chi_{pB}^{(-)*}(\mathbf{r}_{pB}) \\ \times v(\mathbf{r}_{p1}) \phi_t(\mathbf{r}_{p1}, \mathbf{r}_{p2}) \chi_{tA}^{(+)}(\mathbf{r}_{tA}), \quad (5.1.5a) \end{aligned}$$



C:/Gregory/workspace/coops/figuras/deuteron.pdf

Figure 5.1.2: Radial wavefunction  $\rho_d(r)$  (hard core 0.45 fm) entering the deuteron wavefunction (cf. Tang and Herndon (1965)).

$$\begin{aligned}
 T_{succ}^{(2)}(\theta) = & 2 \sum_{l_i, j_i} \sum_{l_f, j_f, m_f} \sum_{\substack{\sigma_1 \sigma_2 \\ \sigma'_1 \sigma'_2}} \int d\mathbf{r}_{dF} d\mathbf{r}_{p1} d\mathbf{r}_{A2} [\phi_{l_i, j_i}^{A+2}(\mathbf{r}_{A1}, \sigma_1, \mathbf{r}_{A2}, \sigma_2)]_0^{0*} \chi_{pB}^{(-)*}(\mathbf{r}_{pB}) v(\mathbf{r}_{p1}) \\
 & \times \phi_d(\mathbf{r}_{p1}) \varphi_{l_f, j_f, m_f}^{A+1}(\mathbf{r}_{A2}) \int d\mathbf{r}'_{dF} d\mathbf{r}'_{p1} d\mathbf{r}'_{A2} G(\mathbf{r}_{dF}, \mathbf{r}'_{dF}) \\
 & \times \phi_d(\mathbf{r}'_{p1})^* \varphi_{l_f, j_f, m_f}^{A+1*}(\mathbf{r}'_{A2}) \frac{2\mu_{dF}}{\hbar^2} v(\mathbf{r}'_{p2}) \phi_d(\mathbf{r}'_{p1}) \phi_d(\mathbf{r}'_{p2}) \chi_{tA}^{(+)}(\mathbf{r}'_{tA}), \quad (5.1.5b)
 \end{aligned}$$

$$\begin{aligned}
 T_{NO}^{(2)}(\theta) = & 2 \sum_{l_i, j_i} \sum_{l_f, j_f, m_f} \sum_{\substack{\sigma_1 \sigma_2 \\ \sigma'_1 \sigma'_2}} \int d\mathbf{r}_{dF} d\mathbf{r}_{p1} d\mathbf{r}_{A2} [\phi_{l_i, j_i}^{A+2}(\mathbf{r}_{A1}, \sigma_1, \mathbf{r}_{A2}, \sigma_2)]_0^{0*} \chi_{pB}^{(-)*}(\mathbf{r}_{pB}) v(\mathbf{r}_{p1}) \\
 & \times \phi_d(\mathbf{r}_{p1}) \varphi_{l_f, j_f, m_f}^{A+1}(\mathbf{r}_{A2}) \int d\mathbf{r}'_{p1} d\mathbf{r}'_{A2} d\mathbf{r}'_{dF} \\
 & \times \phi_d(\mathbf{r}'_{p1})^* \varphi_{l_f, j_f, m_f}^{A+1*}(\mathbf{r}'_{A2}) \phi_d(\mathbf{r}'_{p1}) \phi_d(\mathbf{r}'_{p2}) \chi_{tA}^{(+)}(\mathbf{r}'_{tA}). \quad (5.1.5c)
 \end{aligned}$$

The quantities  $\mu_i, \mu_f(k_i, k_f)$  are the reduced masses (relative linear momenta) in both entrance (initial,  $i$ ) and exit (final,  $f$ ) channels, respectively. In the above expressions,  $\varphi_{l_f, j_f, m_f}^{A+1}(\mathbf{r}_{A1})$  are the wavefunctions describing the intermediate states of the nucleus  $F (\equiv (A + 1))$ , generated as solutions of a Woods–Saxon potential,  $\phi_d(\mathbf{r}_{p2})$  being the deuteron bound wavefunction (see Fig. 5.1.2). Note that some or all of the single-particle states described by the wavefunctions  $\varphi_{l_f, j_f, m_f}^{A+1}(\mathbf{r}_{A1})$  may lie in the continuum (case in which the nucleus  $F$  is loosely bound or unbound). Although there are a number of ways to exactly treat such states, discretization processes may be sufficiently accurate. They can be implemented by, for example,

embedding the Woods–Saxon potential in a spherical box of sufficiently large radius. In actual calculations involving the halo nucleus  $^{11}\text{Li}$ , and where  $|F\rangle = |^{10}\text{Li}\rangle$ , one achieved convergence making use of approximately 20 continuum states and a box of 30 fm of radius. Concerning the components of the triton wavefunction describing the relative motion of the dineutron, it was generated with the  $p - n$  interaction (Tang and Herndon, 1965)

$$v(r) = -v_0 \exp(-k(r - r_c)) \quad r > r_c \quad (5.1.6)$$

$$v(r) = \infty \quad r < r_c, \quad (5.1.7)$$

where  $k = 2.5 \text{ fm}^{-1}$  and  $r_c = 0.45 \text{ fm}$ , the depth  $v_0$  being adjusted to reproduce the experimental separation energies. The positive-energy wavefunctions  $\chi_{tA}^{(+)}(\mathbf{r}_{tA})$  and  $\chi_{pB}^{(-)}(\mathbf{r}_{pB})$  are the ingoing distorted wave in the initial channel and the outgoing distorted wave in the final channel respectively. They are continuum solutions of the Schrödinger equation associated with the corresponding optical potentials.

The transition potential responsible for the transfer of the pair is, in the *post* representation (cf. Fig. 5.C.1),

$$V_\beta = v_{pB} - U_\beta, \quad (5.1.8)$$

where  $v_{pB}$  is the interaction between the proton and nucleus  $B$ , and  $U_\beta$  is the optical potential in the final channel. We make the assumption that  $v_{pB}$  can be decomposed into a term containing the interaction between  $A$  and  $p$  and the potential describing the interaction between the proton and each of the transferred nucleons, namely

$$v_{pB} = v_{pA} + v_{p1} + v_{p2}, \quad (5.1.9)$$

where  $v_{p1}$  and  $v_{p2}$  is the hard–core potential (5.1.6). The transition potential is

$$V_\beta = v_{pA} + v_{p1} + v_{p2} - U_\beta. \quad (5.1.10)$$

Assuming that  $\langle\beta|v_{pA}|\alpha\rangle \approx \langle\beta|U_\beta|\alpha\rangle$  (i.e., assuming that the matrix element of the core–core interaction between the initial and final states is very similar to the matrix element of the real part of the optical potential), one obtains the final expression of the transfer potential in the *post* representation, namely,

$$V_\beta \simeq v_{p1} + v_{p2} = v(\mathbf{r}_{p1}) + v(\mathbf{r}_{p2}). \quad (5.1.11)$$

We make the further approximation of using the same interaction potential in all the (i.e. initial, intermediate and final) channels.

The extension to a heavy–ion reaction  $A + a(\equiv b + 2) \longrightarrow B(\equiv A + 2) + b$  imply no essential modifications in the formalism. The deuteron and triton wavefunctions appearing in Eqs. (5.1.5a), (5.1.5b) and (5.1.5c) are to be substituted with the corresponding wavefunctions  $\Psi_{b+2}(\xi_b, \mathbf{r}_{b1}, \sigma_1, \mathbf{r}_{b2}, \sigma_2)$ , constructed in a similar way as those appearing in (5.1.1 and 5.1.2). The interaction potential used in Eqs. (5.1.5a), (5.1.5b) and (5.1.5c) will now be the Saxon–Woods used to define the

initial (final) state in the post (prior) representation, instead of the proton–neutron interaction (5.1.6).

The Green’s function  $G(\mathbf{r}_{dF}, \mathbf{r}'_{dF})$  appearing in (5.1.5b) propagates the intermediate channel  $d, F$ . It can be expanded in partial waves as,

$$G(\mathbf{r}_{dF}, \mathbf{r}'_{dF}) = i \sum_l \sqrt{2l+1} \frac{f_l(k_{dF}, r_<) g_l(k_{dF}, r_>)}{k_{dF} r_{dF} r'_{dF}} [Y^l(\hat{r}_{dF}) Y^l(\hat{r}'_{dF})]_0^0. \quad (5.1.12)$$

The  $f_l(k_{dF}, r)$  and  $g_l(k_{dF}, r)$  are the regular and the irregular solutions of a Schrödinger equation for a suitable optical potential and an energy equal to the kinetic energy of the intermediate state. In most cases of interest, the result is hardly altered if we use the same energy of relative motion for all the intermediate states. This representative energy is calculated when both intermediate nuclei are in their corresponding ground states. It is of notice that the validity of this approximation can break down in some particular cases. If, for example, some relevant intermediate state become off shell, its contribution is significantly quenched. An interesting situation can arise when this happens to all possible intermediate states, so they can only be virtually populated.

## 5.2 Detailed derivation of second order DWBA

### 5.2.1 Simultaneous transfer: distorted waves

For a  $(t, p)$  reaction, the triton is represented by an incoming distorted wave. We make the assumption that the two neutrons are in an  $S = L = 0$  state, and that the relative motion of the proton with respect to the dineutron is also  $l = 0$ . Consequently, the total spin of the triton is entirely due to the spin of the proton. We will explicitly treat it, as we will consider a spin-orbit term in the optical potential acting between the triton and the target. In what follows we will use the notation of Bayman (1971) (cf. also App. 5.H).

Following (5.E.1), we can write the triton distorted wave as

$$\psi_{m_t}^{(+)}(\mathbf{R}, \mathbf{k}_i, \sigma_p) = \sum_{l_t} \exp(i\sigma_{l_t}^t) g_{l_t j_t} Y_0^{l_t}(\hat{\mathbf{R}}) \frac{\sqrt{4\pi(2l_t + 1)}}{k_i R} \chi_{m_t}(\sigma_p), \quad (5.2.1)$$

where use was made of  $Y_0^{l_t}(\hat{\mathbf{k}}_i) = i^{l_t} \sqrt{\frac{2l_t + 1}{4\pi}} \delta_{m_t, 0}$ , in keeping with the fact that  $\mathbf{k}_i$  is oriented along the  $z$ -axis. Note the phase difference with eq. (7) of Bayman (1971), due to the use of time-reversal rather than Condon–Shortley phase convention. Making use of the relation

$$Y_0^{l_t}(\hat{\mathbf{R}}) \chi_{m_t}(\sigma_p) = \sum_{j_t} \langle l_t 0 1/2 m_t | j_t m_t \rangle [Y^{l_t}(\hat{\mathbf{R}}) \chi(\sigma_p)]_{m_t}^{j_t}, \quad (5.2.2)$$

we have

$$\begin{aligned} \psi_{m_t}^{(+)}(\mathbf{R}, \mathbf{k}_t, \sigma_p) &= \sum_{l_t, j_t} \exp(i\sigma_{l_t}^t) \frac{\sqrt{4\pi(2l_t + 1)}}{k_t R} g_{l_t j_t}(R) \\ &\times \langle l_t 0 1/2 m_t | j_t m_t \rangle \left[ Y^{l_t}(\hat{\mathbf{R}}) \chi(\sigma_p) \right]_{m_t}^{j_t}. \end{aligned} \quad (5.2.3)$$

We now turn our attention to the outgoing proton distorted wave, which, following (5.E.3) can be written as

$$\psi_{m_p}^{(-)}(\zeta, \mathbf{k}_f, \sigma_p) = \sum_{l_p j_p} \frac{4\pi}{k_f \zeta} i^{l_p} \exp(-i\sigma_{l_p}^p) f_{l_p j_p}^*(\zeta) \sum_m Y_m^{l_p}(\hat{\zeta}) Y_m^{l_p*}(\hat{\mathbf{k}}_f) \chi_{m_p}(\sigma_p). \quad (5.2.4)$$

Making use of the relation

$$\begin{aligned} \sum_m Y_m^{l_p}(\hat{\zeta}) Y_m^{l_p*}(\hat{\mathbf{k}}_f) \chi_{m_p}(\sigma_p) &= \sum_{m, j_p} Y_m^{l_p*}(\hat{\mathbf{k}}_f) \langle l_p m 1/2 m_p | j_p m + m_p \rangle \\ &\times \left[ Y^{l_p}(\hat{\zeta}) \chi_{m_p}(\sigma_p) \right]_{m+m_p}^{j_p} \\ &= \sum_{m, j_p} Y_{m-m_p}^{l_p*}(\hat{\mathbf{k}}_f) \langle l_p m - m_p 1/2 m_p | j_p m \rangle \left[ Y^{l_p}(\hat{\zeta}) \chi_{m_p}(\sigma_p) \right]_m^{j_p}, \end{aligned} \quad (5.2.5)$$

one obtains

$$\begin{aligned} \psi_{m_p}^{(-)}(\zeta, \mathbf{k}_f, \sigma_p) &= \frac{4\pi}{k_f \zeta} \sum_{l_p j_p, m} i^{l_p} \exp(-i\sigma_{l_p}^p) f_{l_p j_p}^*(\zeta) Y_{m-m_p}^{l_p*}(\hat{\mathbf{k}}_f) \\ &\times \langle l_p m - m_p 1/2 m_p | j_p m \rangle \left[ Y^{l_p}(\hat{\zeta}) \chi(\sigma_p) \right]_m^{j_p}. \end{aligned} \quad (5.2.6)$$

### 5.2.2 matrix element for the transition amplitude

We now turn our attention to the evaluation of

$$\begin{aligned} \langle \Psi_f^{(-)}(\mathbf{k}_f) | V(r_{1p}) | \Psi_i^{(+)}(k_i, \hat{\mathbf{z}}) \rangle &= \frac{(4\pi)^{3/2}}{k_i k_f} \sum_{l_p l_t j_p j_t m} ((\lambda_2^1)_k (\lambda_2^1)_k | (\lambda \lambda)_0 (\frac{1}{2} \frac{1}{2})_0)_0 \sqrt{2l_t + 1} \\ &\times \langle l_p m - m_p 1/2 m_p | j_p m \rangle \langle l_t 0 1/2 m_t | j_t m_t \rangle i^{-l_p} \exp[i(\sigma_{l_p}^p + \sigma_{l_t}^t)] \\ &\times 2Y_{m-m_p}^{l_p}(\hat{\mathbf{k}}_f) \sum_{\sigma_1 \sigma_2 \sigma_p} \int \frac{d\zeta dr d\eta}{\zeta R} u_{\lambda k}(r_1) u_{\lambda k}(r_2) \left[ Y^\lambda(\hat{\mathbf{r}}_1) Y^\lambda(\hat{\mathbf{r}}_2) \right]_0^{0*} \\ &\times f_{l_p j_p}(\zeta) g_{l_t j_t}(R) \left[ \chi(\sigma_1) \chi(\sigma_2) \right]_0^{0*} \left[ Y^{l_p}(\hat{\zeta}) \chi(\sigma_p) \right]_m^{j_p*} V(r_{1p}) \\ &\times \theta_0^0(\mathbf{r}, \mathbf{s}) \left[ \chi(\sigma_1) \chi(\sigma_2) \right]_0^0 \left[ Y^{l_t}(\hat{\mathbf{R}}) \chi(\sigma_p) \right]_{m_t}^{j_t}, \end{aligned} \quad (5.2.7)$$

where

$$\begin{aligned}\mathbf{r} &= \mathbf{r}_2 - \mathbf{r}_1, \\ \mathbf{s} &= \frac{1}{2}(\mathbf{r}_1 + \mathbf{r}_2) - \mathbf{r}_p, \\ \boldsymbol{\eta} &= \frac{1}{2}(\mathbf{r}_1 + \mathbf{r}_2), \\ \boldsymbol{\zeta} &= \mathbf{r}_p - \frac{\mathbf{r}_1 + \mathbf{r}_2}{A+2}.\end{aligned}\tag{5.2.8}$$

The sum over  $\sigma_1, \sigma_2$  in (5.2.7) is found to be equal to 1. We will now simplify the term  $[Y^{l_p}(\hat{\zeta})\chi(\sigma_p)]_m^{j_p*} [Y^{l_t}(\hat{\mathbf{R}})\chi(\sigma_p)]_{m_t}^{j_t}$ , noting that, (5.D.13)

$$[Y^{l_p}(\hat{\zeta})\chi(\sigma_p)]_m^{j_p*} = (-1)^{1/2-\sigma_p+j_p-m} [Y^{l_p}(\hat{\zeta})\chi(-\sigma_p)]_{-m}^{j_p}.\tag{5.2.9}$$

and that

$$\begin{aligned}[Y^{l_p}(\hat{\zeta})\chi(-\sigma_p)]_{-m}^{j_p} [Y^{l_t}(\hat{\mathbf{R}})\chi(\sigma_p)]_{m_t}^{j_t} &= \sum_{JM} \langle j_p - m | j_t | m_t | J M \rangle \\ &\times \left\{ [Y^{l_p}(\hat{\zeta})\chi(-\sigma_p)]_{-m}^{j_p} [Y^{l_t}(\hat{\mathbf{R}})\chi(\sigma_p)]_{m_t}^{j_t} \right\}_M^J\end{aligned}\tag{5.2.10}$$

The only term which does not vanish after the integration is performed is the one in which the angular and spin functions are coupled to  $L = 0, S = 0, J = 0$ . Thus,

$$\begin{aligned}\langle j_p - m | j_t | m_t | 0 0 \rangle &\left\{ [Y^{l_p}(\hat{\zeta})\chi(-\sigma_p)]_{-m}^{j_p} [Y^{l_t}(\hat{\mathbf{R}})\chi(\sigma_p)]_{m_t}^{j_t} \right\}_0^0 \delta_{l_p l_t} \delta_{j_p j_t} \delta_{m m_t} \\ &= \frac{(-1)^{j_p+m_t}}{\sqrt{2j_p+1}} \left\{ [Y^{l_p}(\hat{\zeta})\chi(-\sigma_p)]_{-m}^{j_p} [Y^{l_t}(\hat{\mathbf{R}})\chi(\sigma_p)]_{m_t}^{j_t} \right\}_0^0 \delta_{l_p l_t} \delta_{j_p j_t} \delta_{m m_t}.\end{aligned}\tag{5.2.11}$$

Coupling separately the spin and angular functions, one obtains

$$\begin{aligned}\left\{ [Y^l(\hat{\zeta})\chi(-\sigma_p)]^j [Y^l(\hat{\mathbf{R}})\chi(\sigma_p)]^j \right\}_0^0 &= ((l\frac{1}{2})_j (l\frac{1}{2})_j) ((ll)_0 (\frac{1}{2}\frac{1}{2})_0)_0 [\chi(-\sigma_p)\chi(\sigma_p)]_0^0 [Y^l(\hat{\zeta})Y^l(\hat{\mathbf{R}})]_0^0.\end{aligned}\tag{5.2.12}$$

We substitute (5.2.9), (5.2.30),(5.2.31) in (5.2.7) to obtain

$$\begin{aligned}
 \langle \Psi_f^{(-)}(\mathbf{k}_f) | V(r_{1p}) | \Psi_i^{(+)}(k_i, \hat{\mathbf{z}}) \rangle &= -\frac{(4\pi)^{3/2}}{k_i k_f} \sum_{lj} ((\lambda \frac{1}{2})_k (\lambda \frac{1}{2})_k | (\lambda \lambda)_0 (\frac{1}{2} \frac{1}{2})_0)_0 \sqrt{\frac{2l+1}{2j+1}} \\
 &\times \langle l m_t - m_p 1/2 m_p | j m_t \rangle \langle l 0 1/2 m_t | j m_t \rangle i^{-l} \exp[i(\sigma_l^p + \sigma_l^t)] \\
 &\times 2Y_{m_t - m_p}^l(\hat{\mathbf{k}}_f) \int \frac{d\zeta d\mathbf{r} d\boldsymbol{\eta}}{\zeta R} u_{\lambda k}(r_1) u_{\lambda k}(r_2) [Y^\lambda(\hat{\mathbf{r}}_1) Y^\lambda(\hat{\mathbf{r}}_2)]_0^{0*} \\
 &\times f_{lj}(\zeta) g_{lj}(R) [Y^l(\hat{\zeta}) Y^l(\hat{\mathbf{R}})]_0^0 V(r_{1p}) \theta_0^0(\mathbf{r}, \mathbf{s}) \\
 &\times ((l \frac{1}{2})_j (l \frac{1}{2})_j | (ll)_0 (\frac{1}{2} \frac{1}{2})_0)_0 \sum_{\sigma_p} (-1)^{1/2-\sigma_p} [\chi(-\sigma_p) \chi(\sigma_p)]_0^0.
 \end{aligned} \tag{5.2.13}$$

The last sum over  $\sigma_p$  leads to

$$\begin{aligned}
 \sum_{\sigma_p} (-1)^{1/2-\sigma_p} [\chi(-\sigma_p) \chi(\sigma_p)]_0^0 &= \sum_{\sigma_p m} (-1)^{1/2-\sigma_p} \langle 1/2 m 1/2 - m | 0 0 \rangle \\
 &\times \chi_m(-\sigma_p) \chi_{-m}(\sigma_p) \\
 &= \frac{1}{\sqrt{2}} \sum_{\sigma_p m} (-1)^{1/2-\sigma_p} (-1)^{1/2-m} \delta_{m, -\sigma_p} \delta_{-m, \sigma_p} = -\sqrt{2}.
 \end{aligned} \tag{5.2.14}$$

The 9j-symbols can be evaluated to find

$$\begin{aligned}
 ((\lambda \frac{1}{2})_k (\lambda \frac{1}{2})_k | (\lambda \lambda)_0 (\frac{1}{2} \frac{1}{2})_0)_0 &= \sqrt{\frac{2k+1}{2(2\lambda+1)}} \\
 ((l \frac{1}{2})_j (l \frac{1}{2})_j | (ll)_0 (\frac{1}{2} \frac{1}{2})_0)_0 &= \sqrt{\frac{2j+1}{2(2l+1)}},
 \end{aligned} \tag{5.2.15}$$

and consequently,

$$\begin{aligned}
 \langle \Psi_f^{(-)}(\mathbf{k}_f) | V(r_{1p}) | \Psi_i^{(+)}(k_i, \hat{\mathbf{z}}) \rangle &= \frac{(4\pi)^{3/2}}{k_i k_f} \sum_{lj} \sqrt{\frac{2k+1}{2\lambda+1}} \\
 &\times \langle l m_t - m_p 1/2 m_p | j m_t \rangle \langle l 0 1/2 m_t | j m_t \rangle i^{-l} \exp[i(\sigma_l^p + \sigma_l^t)] \\
 &\times \sqrt{2} Y_{m_t - m_p}^l(\hat{\mathbf{k}}_f) \int \frac{d\zeta d\mathbf{r} d\boldsymbol{\eta}}{\zeta R} u_{\lambda k}(r_1) u_{\lambda k}(r_2) [Y^\lambda(\hat{\mathbf{r}}_1) Y^\lambda(\hat{\mathbf{r}}_2)]_0^{0*} \\
 &\times f_{lj}(\zeta) g_{lj}(R) [Y^l(\hat{\zeta}) Y^l(\hat{\mathbf{R}})]_0^0 V(r_{1p}) \theta_0^0(\mathbf{r}, \mathbf{s}).
 \end{aligned} \tag{5.2.16}$$

The values of the Clebsh–Gordan coefficients are, for  $j = l - 1/2$ ,

$$\begin{aligned}
 \langle l m_t - m_p 1/2 m_p | l - 1/2 m_t \rangle \langle l 0 1/2 m_t | l - 1/2 m_t \rangle \\
 = \begin{cases} \frac{l}{2l+1} & \text{if } m_t = m_p \\ -\frac{\sqrt{l(l+1)}}{2l+1} & \text{if } m_t = -m_p \end{cases}
 \end{aligned} \tag{5.2.17}$$

and, for  $j = l + 1/2$ :

$$\begin{aligned} \langle l m_t - m_p 1/2 m_p | l + 1/2 m_t \rangle \langle l 0 1/2 m_t | l + 1/2 m_t \rangle \\ = \begin{cases} \frac{l+1}{2l+1} & \text{if } m_t = m_p \\ \frac{\sqrt{l(l+1)}}{2l+1} & \text{if } m_t = -m_p \end{cases} \quad (5.2.18) \end{aligned}$$

One thus can write,

$$\begin{aligned} \langle \Psi_f^{(-)}(\mathbf{k}_f) | V(r_{1p}) | \Psi_i^{(+)}(k_i, \hat{\mathbf{z}}) \rangle &= \frac{(4\pi)^{3/2}}{k_i k_f} \sum_l \frac{1}{(2l+1)} \sqrt{\frac{(2k+1)}{(2\lambda+1)}} \exp[i(\sigma_l^p + \sigma_l^t)] i^{-l} \\ &\times \sqrt{2} Y_{m_t - m_p}^l(\hat{\mathbf{k}}_f) \int \frac{d\zeta d\mathbf{r} d\mathbf{n}}{\zeta R} u_{\lambda k}(r_1) u_{\lambda k}(r_2) [Y^\lambda(\hat{\mathbf{r}}_1) Y^\lambda(\hat{\mathbf{r}}_2)]_0^{0*} \\ &\times V(r_{1p}) \theta_0^0(\mathbf{r}, \mathbf{s}) [Y^l(\hat{\zeta}) Y^l(\hat{\mathbf{R}})]_0^0 \\ &\times \left[ (f_{ll+1/2}(\zeta) g_{ll+1/2}(R)(l+1) + f_{ll-1/2}(\zeta) g_{ll-1/2}(R)l) \delta_{m_p, m_t} \right. \\ &\left. + (f_{ll+1/2}(\zeta) g_{ll+1/2}(R) \sqrt{l(l+1)} - f_{ll-1/2}(\zeta) g_{ll-1/2}(R) \sqrt{l(l+1)}) \delta_{m_p, -m_t} \right]. \quad (5.2.19) \end{aligned}$$

We can further simplify this expression using

$$\begin{aligned} [Y^\lambda(\hat{\mathbf{r}}_1) Y^\lambda(\hat{\mathbf{r}}_2)]_0^{0*} &= [Y^\lambda(\hat{\mathbf{r}}_1) Y^\lambda(\hat{\mathbf{r}}_2)]_0^0 = \sum_m \langle \lambda m \lambda - m | 0 0 \rangle Y_m^\lambda(\hat{\mathbf{r}}_1) Y_{-m}^\lambda(\hat{\mathbf{r}}_2) \\ &= \sum_m (-1)^{\lambda-m} \langle \lambda m \lambda - m | 0 0 \rangle Y_m^\lambda(\hat{\mathbf{r}}_1) Y_m^{\lambda*}(\hat{\mathbf{r}}_2) \\ &= \frac{1}{\sqrt{2\lambda+1}} \sum_m Y_m^\lambda(\hat{\mathbf{r}}_1) Y_m^{\lambda*}(\hat{\mathbf{r}}_2) \\ &= \frac{\sqrt{(2\lambda+1)}}{4\pi} P_\lambda(\cos \theta_{12}). \quad (5.2.20) \end{aligned}$$

Note that when using Condon–Shortley phases this last expression is to be multiplied by  $(-1)^\lambda$ , and that

$$\begin{aligned} [Y^l(\hat{\zeta}) Y^l(\hat{\mathbf{R}})]_0^0 &= \sum_m \langle l m l - m | 0 0 \rangle Y_m^l(\hat{\zeta}) Y_{-m}^l(\hat{\mathbf{R}}) \\ &= \frac{1}{\sqrt{(2l+1)}} \sum_m (-1)^{l+m} Y_m^l(\hat{\zeta}) Y_{-m}^l(\hat{\mathbf{R}}). \quad (5.2.21) \end{aligned}$$

Because the integral of the above expression is independent of  $m$ , one can eliminate the  $m$ -sum and multiply by  $2l+1$  the  $m=0$  term, leading to

$$\begin{aligned} [Y^l(\hat{\zeta}) Y^l(\hat{\mathbf{R}})]_0^0 &\Rightarrow (-1)^l \sqrt{(2l+1)} Y_0^l(\hat{\zeta})_0 Y^l(\hat{\mathbf{R}}) \\ &= \sqrt{(2l+1)} Y_0^l(\hat{\zeta}) Y_0^{l*}(\hat{\mathbf{R}}). \quad (5.2.22) \end{aligned}$$

We now change the integration variables from  $(\zeta, \mathbf{r}, \boldsymbol{\eta})$  to  $(\mathbf{R}, \alpha, \beta, \gamma, r_{12}, r_{1p}, r_{2p})$ , the quantity

$$\left| \frac{\partial(\mathbf{r}, \boldsymbol{\eta}, \zeta)}{\partial(\mathbf{R}, \alpha, \beta, \gamma, r_{12}, r_{1p}, r_{2p})} \right| = r_{12} r_{1p} r_{2p} \sin \beta, \quad (5.2.23)$$

being the Jacobian of the transformation. Finally,

$$\begin{aligned} \langle \Psi_f^{(-)}(\mathbf{k}_f) | V(r_{1p}) | \Psi_i^{(+)}(k_i, \hat{\mathbf{z}}) \rangle &= \frac{\sqrt{8\pi}}{k_i k_f} \sum_l \sqrt{\frac{2k+1}{2l+1}} \exp[i(\sigma_l^p + \sigma_l^t)] i^{-l} \\ &\times Y_{m_t - m_p}^l(\hat{\mathbf{k}}_f) \int d\mathbf{R} Y_0^{l*}(\hat{\mathbf{R}}) \int \frac{d\alpha d\beta d\gamma dr_{12} dr_{1p} dr_{2p} \sin \beta}{\zeta R} Y_0^l(\hat{\zeta}) \\ &\times u_{\lambda k}(r_1) u_{\lambda k}(r_2) V(r_{1p}) \theta_0^0(\mathbf{r}, \mathbf{s}) P_\lambda(\cos \theta_{12}) r_{12} r_{1p} r_{2p} \\ &\times \left[ (f_{ll+1/2}(\zeta) g_{ll+1/2}(R)(l+1) + f_{ll-1/2}(\zeta) g_{ll-1/2}(R)l) \delta_{m_p, m_t} \right. \\ &\quad \left. + (f_{ll+1/2}(\zeta) g_{ll+1/2}(R) \sqrt{l(l+1)} - f_{ll-1/2}(\zeta) g_{ll-1/2}(R) \sqrt{l(l+1)}) \delta_{m_p, -m_t} \right]. \end{aligned} \quad (5.2.24)$$

It is noted that the second integral is a function of solely  $\mathbf{R}$  transforming under rotations as  $Y_0^l(\hat{\mathbf{R}})$ , in keeping with the fact that the full dependence on the orientation of  $\mathbf{R}$  is contained in the spherical harmonic  $Y_0^l(\hat{\zeta})$ . The second integral can thus be cast into the form

$$\begin{aligned} A(R) Y_0^l(\hat{\mathbf{R}}) &= \int d\alpha d\beta d\gamma dr_{12} dr_{1p} dr_{2p} \sin \beta \\ &\times F(\alpha, \beta, \gamma, r_{12}, r_{1p}, r_{2p}, R_x, R_y, R_z). \end{aligned} \quad (5.2.25)$$

To evaluate  $A(R)$ , we set  $\mathbf{R}$  along the  $z$ -axis

$$\begin{aligned} A(R) &= 2\pi i^{-l} \sqrt{\frac{4\pi}{2l+1}} \int d\beta d\gamma dr_{12} dr_{1p} dr_{2p} \sin \beta \\ &\times F(\alpha, \beta, \gamma, r_{12}, r_{1p}, r_{2p}, 0, 0, R), \end{aligned} \quad (5.2.26)$$

where a factor  $2\pi$  results from the integration over  $\alpha$ , the integrand not depending on  $\alpha$ . Substituting (5.2.25) and (5.2.26) in (5.2.24) and, after integration over the angular variables of  $\mathbf{R}$ , we obtain

$$\begin{aligned} \langle \Psi_f^{(-)}(\mathbf{k}_f) | V(r_{1p}) | \Psi_i^{(+)}(k_i, \hat{\mathbf{z}}) \rangle &= 2 \frac{(2\pi)^{3/2}}{k_i k_f} \sum_l \sqrt{\frac{2k+1}{2l+1}} \exp[i(\sigma_l^p + \sigma_l^t)] i^{-l} \\ &\times Y_{m_t - m_p}^l(\hat{\mathbf{k}}_f) \int dR d\beta d\gamma dr_{12} dr_{1p} dr_{2p} R \sin \beta r_{12} r_{1p} r_{2p} \\ &\times u_{\lambda k}(r_1) u_{\lambda k}(r_2) V(r_{1p}) \theta_0^0(\mathbf{r}, \mathbf{s}) P_\lambda(\cos \theta_{12}) P_l(\cos \theta_\zeta) \\ &\times \left[ (f_{ll+1/2}(\zeta) g_{ll+1/2}(R)(l+1) + f_{ll-1/2}(\zeta) g_{ll-1/2}(R)l) \delta_{m_p, m_t} \right. \\ &\quad \left. + (f_{ll+1/2}(\zeta) g_{ll+1/2}(R) \sqrt{l(l+1)} - f_{ll-1/2}(\zeta) g_{ll-1/2}(R) \sqrt{l(l+1)}) \delta_{m_p, -m_t} \right] / \zeta, \end{aligned} \quad (5.2.27)$$

where use was made of the relation

$$Y_0^l(\hat{\zeta}) = i^l \sqrt{\frac{2l+1}{4\pi}} P_l(\cos \theta_\zeta). \quad (5.2.28)$$

The final expression of the differential cross section involves a sum over the spin orientations:

$$\frac{d\sigma}{d\Omega}(\hat{\mathbf{k}}_f) = \frac{k_f}{k_i} \frac{\mu_i \mu_f}{(2\pi\hbar^2)^2} \frac{1}{2} \sum_{m_t m_p} |\langle \Psi_f^{(-)}(\mathbf{k}_f) | V(r_{1p}) | \Psi_i^{(+)}(k_i, \hat{\mathbf{z}}) \rangle|^2. \quad (5.2.29)$$

When  $m_p = 1/2, m_t = 1/2$  or  $m_p = -1/2, m_t = -1/2$ , the terms proportional to  $\delta_{m_p, m_t}$  including the factor

$$|Y_{m_t - m_p}^l(\hat{\mathbf{k}}_f) \delta_{m_p, m_t}| = |Y_0^l(\hat{\mathbf{k}}_f)| = \left| i^l \sqrt{\frac{2l+1}{4\pi}} P_l^0(\cos \theta) \right|, \quad (5.2.30)$$

in the case in which  $m_p = -1/2, m_t = 1/2$

$$|Y_{m_t - m_p}^l(\hat{\mathbf{k}}_f) \delta_{m_p, -m_t}| = |Y_1^l(\hat{\mathbf{k}}_f)| = \left| i^l \sqrt{\frac{2l+1}{4\pi}} \frac{1}{l(l+1)} P_l^1(\cos \theta) \right|, \quad (5.2.31)$$

and

$$|Y_{m_t - m_p}^l(\hat{\mathbf{k}}_f) \delta_{m_p, -m_t}| = |Y_{-1}^l(\hat{\mathbf{k}}_f)| = |Y_1^l(\hat{\mathbf{k}}_f)| = \left| i^l \sqrt{\frac{2l+1}{4\pi}} \frac{1}{l(l+1)} P_l^1(\cos \theta) \right|, \quad (5.2.32)$$

when  $m_p = 1/2, m_t = -1/2$ . Taking the squared modulus of (5.2.27), the sum over  $m_t$  and  $m_p$  yields a factor 2 multiplying each one of the 2 different terms of the sum ( $m_t = m_p$  and  $m_t = -m_p$ ). This is equivalent to multiply each amplitude by  $\sqrt{2}$ , so the final constant that multiply the amplitudes is

$$\frac{8\pi^{3/2}}{k_i k_f}. \quad (5.2.33)$$

Now, for the triton wavefunction we use

$$\theta_0^0(\mathbf{r}, \mathbf{s}) = \rho(r_{1p}) \rho(r_{2p}) \rho(r_{12}), \quad (5.2.34)$$

$\rho(r)$  being a Tang–Herndon (1965) wave function also used by Bayman (1971). We obtain

$$\frac{d\sigma}{d\Omega}(\hat{\mathbf{k}}_f) = \frac{1}{2E_i^{3/2} E_f^{1/2}} \sqrt{\frac{\mu_f}{\mu_i}} \left( |I_{\lambda k}^{(0)}(\theta)|^2 + |I_{\lambda k}^{(1)}(\theta)|^2 \right), \quad (5.2.35)$$

where

$$\begin{aligned} I_{\lambda k}^{(0)}(\theta) &= \sum_l P_l^0(\cos \theta) \sqrt{2k+1} \exp[i(\sigma_l^p + \sigma_l^t)] \\ &\times \int dR d\beta d\gamma dr_{12} dr_{1p} dr_{2p} R \sin \beta \rho(r_{1p}) \rho(r_{2p}) \rho(r_{12}) \\ &\times u_{\lambda k}(r_1) u_{\lambda k}(r_2) V(r_{1p}) P_\lambda(\cos \theta_{12}) P_l(\cos \theta_\zeta) r_{12} r_{1p} r_{2p} \\ &\times (f_{ll+1/2}(\zeta) g_{ll+1/2}(R)(l+1) + f_{ll-1/2}(\zeta) g_{ll-1/2}(R) l)/\zeta, \end{aligned} \quad (5.2.36)$$

and

$$\begin{aligned} I_{\lambda k}^{(1)}(\theta) &= \sum_l P_l^1(\cos \theta) \sqrt{2k+1} \exp[i(\sigma_l^p + \sigma_l^t)] \\ &\times \int dR d\beta d\gamma dr_{12} dr_{1p} dr_{2p} R \sin \beta \rho(r_{1p}) \rho(r_{2p}) \rho(r_{12}) \\ &\times u_{\lambda k}(r_1) u_{\lambda k}(r_2) V(r_{1p}) P_\lambda(\cos \theta_{12}) P_l(\cos \theta_\zeta) r_{12} r_{1p} r_{2p} \\ &\times (f_{ll+1/2}(\zeta) g_{ll+1/2}(R) - f_{ll-1/2}(\zeta) g_{ll-1/2}(R))/\zeta. \end{aligned} \quad (5.2.37)$$

Note that the absence of the  $(-1)^l$  factor with respect to what is found in Bayman (1971), is due to the use of time-reversed phases instead of Condon–Shortley phasing. This is compensated in the total result by a similar difference in the expression of the spectroscopic amplitudes. This ensures that, in either case, the contribution of all the single particle transitions tend to have the same phase for superfluid nuclei, adding coherently to enhance the transfer cross section.

### Heavy-ion Reactions

In dealing with a heavy ion reaction,  $\theta_0^0(\mathbf{r}, \mathbf{s})$  are be the spatial part of the wave-function

$$\begin{aligned} \Psi(\mathbf{r}_{b1}, \mathbf{r}_{b2}, \sigma_1, \sigma_2) &= [\psi^{j_i}(\mathbf{r}_{b1}, \sigma_1) \psi^{j_i}(\mathbf{r}_{b2}, \sigma_2)]_0^0 \\ &= \theta_0^0(\mathbf{r}, \mathbf{s}) [\chi(\sigma_1) \chi(\sigma_2)]_0^0, \end{aligned} \quad (5.2.38)$$

where  $\mathbf{r}_{b1}, \mathbf{r}_{b2}$  are the positions of the two neutrons with respect to the  $b$  core. It can be shown to be

$$\theta_0^0(\mathbf{r}, \mathbf{s}) = \frac{u_{l_i j_i}(r_{b1}) u_{l_i j_i}(r_{b2})}{4\pi} \sqrt{\frac{2j_i+1}{2}} P_{l_i}(\cos \theta_i), \quad (5.2.39)$$

where  $\theta_i$  is the angle between  $\mathbf{r}_{b1}$  and  $\mathbf{r}_{b2}$ . Neglecting the spin-orbit term in the optical potential, as is usually done for heavy ion reactions, one obtains

$$\frac{d\sigma}{d\Omega}(\hat{\mathbf{k}}_f) = \frac{\mu_f \mu_i}{16\pi^2 \hbar^4 k_i^3 k_f} |T^{(1)}(\theta)|^2, \quad (5.2.40)$$

where

$$\begin{aligned}
 T^{(1)}(\theta) = & \sum_l (2l+1) P_l(\cos \theta) \sqrt{(2j_i+1)(2j_f+1)} \exp[i(\sigma_l^p + \sigma_l^t)] \\
 & \times \int dR d\beta d\gamma dr_{12} dr_{b1} dr_{b2} R \sin \beta u_{l_i j_i}(r_{b1}) u_{l_i j_i}(r_{b2}) \\
 & \times u_{l_f j_f}(r_{A1}) u_{l_f j_f}(r_{A2}) V(r_{b1}) P_\lambda(\cos \theta_{12}) P_l(\cos \theta_\zeta) \\
 & \times r_{12} r_{b1} r_{b2} P_{l_i}(\cos \theta_i) \frac{f_l(\zeta) g_l(R)}{\zeta},
 \end{aligned} \tag{5.2.41}$$

obtained by using Eq. (5.2.39) in Eq. (5.2.7) instead of (5.2.34),  $\mathbf{r}_{A1}, \mathbf{r}_{A2}$  being the coordinates of the two transferred neutrons with respect to the  $A$  core.

For control, in what follows we work out the same transition amplitude but starting from the distorted waves for a reaction taking place between spinless nuclei, namely

$$\psi^{(+)}(\mathbf{r}_{Aa}, \mathbf{k}_{Aa}) = \sum_l \exp(i\sigma_l^i) g_l Y_0^l(\hat{\mathbf{r}}_{aA}) \frac{\sqrt{4\pi(2l+1)}}{k_{aA} r_{aA}}, \tag{5.2.42}$$

and

$$\psi^{(-)}(\mathbf{r}_{bB}, \mathbf{k}_{bB}) = \frac{4\pi}{k_{bB} r_{bB}} \sum_{\tilde{l}} i^{\tilde{l}} \exp(-i\sigma_{\tilde{l}}^f) f_{\tilde{l}}^*(r_{bB}) \sum_m Y_m^{\tilde{l}*}(\hat{\mathbf{k}}_{bB}) Y_m^{\tilde{l}}(\hat{\mathbf{r}}_{bB}). \tag{5.2.43}$$

One can then write,

$$\begin{aligned}
 T_{2N}^{1step} = & \langle \Psi_f^{(-)}(\mathbf{k}_{bB}) | V(r_{1p}) | \Psi_i^{(+)}(k_{aA}, \hat{\mathbf{z}}) \rangle = \frac{(4\pi)^{3/2}}{k_{aA} k_{bB}} \sum_{\tilde{l} l m} ((l_f \frac{1}{2})_{j_f} (l_f \frac{1}{2})_{j_f} | (l_f l_f)_0 (\frac{1}{2} \frac{1}{2})_0)_0 \\
 & \times ((l_i \frac{1}{2})_{j_i} (l_i \frac{1}{2})_{j_i} | (l_i l_i)_0 (\frac{1}{2} \frac{1}{2})_0)_0 \sqrt{2l+1} i^{-l_p} \exp[i(\sigma_{\tilde{l}}^f + \sigma_l^i)] \\
 & \times 2Y_m^{\tilde{l}}(\hat{\mathbf{k}}_{bB}) \sum_{\sigma_1 \sigma_2} \int \frac{d\mathbf{r}_{bB} d\mathbf{r} d\boldsymbol{\eta}}{r_{bB} r_{aA}} u_{l_f j_f}(r_{A1}) u_{l_f j_f}(r_{A2}) u_{l_i j_i}(r_{b1}) u_{l_i j_i}(r_{b2}) \\
 & \times \left[ Y^{l_f}(\hat{\mathbf{r}}_{A1}) Y^{l_f}(\hat{\mathbf{r}}_{A2}) \right]_0^{0*} \left[ Y^{l_i}(\hat{\mathbf{r}}_{b1}) Y^{l_i}(\hat{\mathbf{r}}_{b2}) \right]_0^0 \\
 & \times f_{\tilde{l}}(r_{bB}) g_l(r_{aA}) \left[ \chi(\sigma_1) \chi(\sigma_2) \right]_0^{0*} Y_m^{\tilde{l}*}(\hat{\mathbf{k}}_{bB}) V(r_{1p}) \\
 & \times \left[ \chi(\sigma_1) \chi(\sigma_2) \right]_0^0 Y_0^l(\hat{\mathbf{r}}_{aA}),
 \end{aligned} \tag{5.2.44}$$

which, after a number of simplifications becomes

$$\begin{aligned} \langle \Psi_f^{(-)}(\mathbf{k}_{bB}) | V(r_{1p}) | \Psi_i^{(+)}(k_{aA}, \hat{\mathbf{z}}) \rangle &= \frac{(4\pi)^{3/2}}{k_{aA} k_{bB}} \sum_{\tilde{l}lm} \sqrt{\frac{(2j_f + 1)(2j_i + 1)}{(2l_f + 1)(2l_i + 1)}} \\ &\times \sqrt{2l + 1} i^{-\tilde{l}} \exp[i(\sigma_l^f + \sigma_l^i)] \\ &\times Y_m^{\tilde{l}}(\hat{\mathbf{k}}_{bB}) \int \frac{d\mathbf{r}_{bB} d\mathbf{r} d\boldsymbol{\eta}}{r_{bB} r_{aA}} u_{l_f j_f}(r_{A1}) u_{l_f j_f}(r_{A2}) u_{l_i j_i}(r_{b1}) u_{l_i j_i}(r_{b2}) \\ &\times \left[ Y^{l_f}(\hat{\mathbf{r}}_{A1}) Y^{l_f}(\hat{\mathbf{r}}_{A2}) \right]_0^{0*} \left[ Y^{l_i}(\hat{\mathbf{r}}_{b1}) Y^{l_i}(\hat{\mathbf{r}}_{b2}) \right]_0^0 \\ &\times f_{\tilde{l}}(r_{bB}) g_l(r_{aA}) Y_m^{l*}(\hat{\mathbf{r}}_{bB}) V(r_{1p}) Y_0^l(\hat{\mathbf{r}}_{aA}), \end{aligned} \quad (5.2.45)$$

where  $l = \tilde{l}$  and  $m = 0$ . Making use of Legendre polynomials leads to,

$$\begin{aligned} \langle \Psi_f^{(-)}(\mathbf{k}_{bB}) | V(r_{1p}) | \Psi_i^{(+)}(k_{aA}, \hat{\mathbf{z}}) \rangle &= \frac{(4\pi)^{-1/2}}{k_{aA} k_{bB}} \sum_l \sqrt{(2j_f + 1)(2j_i + 1)} \\ &\times \sqrt{2l + 1} i^{-l} \exp[i(\sigma_l^f + \sigma_l^i)] Y_0^l(\hat{\mathbf{k}}_{bB}) \\ &\times \int \frac{d\mathbf{r}_{bB} d\mathbf{r} d\boldsymbol{\eta}}{r_{bB} r_{aA}} u_{l_f j_f}(r_{A1}) u_{l_f j_f}(r_{A2}) u_{l_i j_i}(r_{b1}) u_{l_i j_i}(r_{b2}) \\ &\times P_{l_f}(\cos \theta_A) P_{l_i}(\cos \theta_b) \\ &\times f_l(r_{bB}) g_l(r_{aA}) Y_0^{l*}(\hat{\mathbf{r}}_{bB}) V(r_{1p}) Y_0^l(\hat{\mathbf{r}}_{aA}). \end{aligned} \quad (5.2.46)$$

Changing the integration variables and proceeding as in last section, (implying the multiplicative factor  $2\pi \sqrt{\frac{4\pi}{2l+1}}$ ), the above expression becomes

$$\begin{aligned} \langle \Psi_f^{(-)}(\mathbf{k}_{bB}) | V(r_{1p}) | \Psi_i^{(+)}(k_{aA}, \hat{\mathbf{z}}) \rangle &= \frac{2\pi}{k_{aA} k_{bB}} \sum_l \sqrt{(2j_f + 1)(2j_i + 1)} \\ &\times i^{-l} \exp[i(\sigma_l^f + \sigma_l^i)] Y_0^l(\hat{\mathbf{k}}_{bB}) \\ &\times \int dr_{aA} d\beta d\gamma dr_{12} dr_{b1} dr_{b2} r_{aA} \sin \beta r_{12} r_{b1} r_{b2} \\ &\times P_{l_f}(\cos \theta_A) P_{l_i}(\cos \theta_b) u_{l_f j_f}(r_{A1}) u_{l_f j_f}(r_{A2}) u_{l_i j_i}(r_{b1}) u_{l_i j_i}(r_{b2}) \\ &\times f_l(r_{bB}) g_l(r_{aA}) Y_0^{l*}(\hat{\mathbf{r}}_{bB}) V(r_{1p}) / r_{bB}, \end{aligned} \quad (5.2.47)$$

which eventually can be recasted, through the use of Legendre polynomials, in the expression,

$$\begin{aligned} T_{2N}^{1step} &= \langle \Psi_f^{(-)}(\mathbf{k}_{bB}) | V(r_{1p}) | \Psi_i^{(+)}(k_{aA}, \hat{\mathbf{z}}) \rangle = \frac{1}{2k_{aA} k_{bB}} \sum_l \sqrt{(2j_f + 1)(2j_i + 1)} \\ &\times i^{-l} \exp[i(\sigma_l^f + \sigma_l^i)] P_l(\cos \theta) (2l + 1) \\ &\times \int dr_{aA} d\beta d\gamma dr_{12} dr_{b1} dr_{b2} r_{aA} \sin \beta r_{12} r_{b1} r_{b2} \\ &\times P_{l_f}(\cos \theta_A) P_{l_i}(\cos \theta_b) u_{l_f j_f}(r_{A1}) u_{l_f j_f}(r_{A2}) V(r_{1p}) \\ &\times u_{l_i j_i}(r_{b1}) u_{l_i j_i}(r_{b2}) f_l(r_{bB}) g_l(r_{aA}) P_l(\cos \theta_{if}) / r_{bB}, \end{aligned} \quad (5.2.48)$$

expression which gives the same results as (5.2.41)

### 5.2.3 Coordinates for the calculation of simultaneous transfer

In what follows we explicit the coordinates used in the calculation of the above equations. Making use of the notation of Bayman (1971), we find the expression of the variables appearing in the integral as functions of the integration variables  $r_{1p}, r_{2p}, r_{12}, R, \beta, \gamma$  (remember that  $\mathbf{R} = R \hat{\mathbf{z}}$ , see last section).  $\mathbf{R}$  being the center of mass coordinate. Thus, one can write

$$\mathbf{R} = \frac{1}{3} (\mathbf{r}_1 + \mathbf{r}_2 + \mathbf{r}_p) = \frac{1}{3} (\mathbf{R} + \mathbf{d}_1 + \mathbf{R} + \mathbf{d}_2 + \mathbf{R} + \mathbf{d}_p), \quad (5.2.49)$$

so

$$\mathbf{d}_1 + \mathbf{d}_2 + \mathbf{d}_p = 0. \quad (5.2.50)$$

Together with

$$\mathbf{d}_1 + \mathbf{r}_{12} = \mathbf{d}_2 \quad \mathbf{d}_2 + \mathbf{r}_{2p} = \mathbf{d}_p, \quad (5.2.51)$$

we find

$$\mathbf{d}_1 = \frac{1}{3} (2\mathbf{r}_{12} + \mathbf{r}_{2p}), \quad (5.2.52)$$

and

$$d_1^2 = \frac{1}{9} (4r_{12}^2 + r_{2p}^2 + 4\mathbf{r}_{12}\mathbf{r}_{2p}). \quad (5.2.53)$$

Making use of

$$\begin{aligned} \mathbf{r}_{12} + \mathbf{r}_{2p} &= \mathbf{r}_{1p} \\ r_{1p}^2 &= r_{12}^2 + r_{2p}^2 + 2\mathbf{r}_{12}\mathbf{r}_{2p} \\ 2\mathbf{r}_{12}\mathbf{r}_{2p} &= r_{1p}^2 - r_{12}^2 - r_{2p}^2. \end{aligned} \quad (5.2.54)$$

one obtains

$$d_1 = \frac{1}{3} \sqrt{2r_{12}^2 + 2r_{1p}^2 - r_{2p}^2}. \quad (5.2.55)$$

Similarly,

$$d_2 = \frac{1}{3} \sqrt{2r_{12}^2 + 2r_{2p}^2 - r_{1p}^2} \quad d_p = \frac{1}{3} \sqrt{2r_{2p}^2 + 2r_{1p}^2 - r_{12}^2}. \quad (5.2.56)$$

We now express the angle  $\alpha$  between  $\mathbf{d}_1$  and  $\mathbf{r}_{12}$ . We have

$$-\mathbf{d}_1 \mathbf{r}_{12} = r_{12} d_1 \cos(\alpha), \quad (5.2.57)$$

and

$$\begin{aligned} \mathbf{d}_1 + \mathbf{r}_{12} &= \mathbf{d}_2 \\ d_1^2 + r_{12}^2 + 2\mathbf{d}_1 \mathbf{r}_{12} &= d_2^2. \end{aligned} \quad (5.2.58)$$

Consequently,

$$\cos(\alpha) = \frac{d_1^2 + r_{12}^2 - d_2^2}{2r_{12}d_1}. \quad (5.2.59)$$

The complete determination of  $\mathbf{r}_1, \mathbf{r}_2, \mathbf{r}_{12}$  can be made by writing their expression in a simple configuration, in which the triangle lies in the  $xz$ -plane with  $\mathbf{d}_1$  pointing along the positive  $z$ -direction, and  $\mathbf{R} = 0$ . Then, a first rotation  $\mathcal{R}_z(\gamma)$  of an angle  $\gamma$  around the  $z$ -axis, a second rotation  $\mathcal{R}_y(\beta)$  of an angle  $\beta$  around the  $y$ -axis, and a translation along  $\mathbf{R}$  will bring the vectors to the most general configuration. In other words,

$$\begin{aligned} \mathbf{r}_1 &= \mathbf{R} + \mathcal{R}_y(\beta)\mathcal{R}_z(\gamma)\mathbf{r}'_1, \\ \mathbf{r}_{12} &= \mathcal{R}_y(\beta)\mathcal{R}_z(\gamma)\mathbf{r}'_{12}, \\ \mathbf{r}_2 &= \mathbf{r}_1 + \mathbf{r}_{12}, \end{aligned} \quad (5.2.60)$$

with

$$\mathbf{r}'_1 = \begin{bmatrix} 0 \\ 0 \\ d_1 \end{bmatrix}, \quad (5.2.61)$$

$$\mathbf{r}'_{12} = r_{12} \begin{bmatrix} \sin(\alpha) \\ 0 \\ -\cos(\alpha) \end{bmatrix}, \quad (5.2.62)$$

and the rotation matrixes are

$$\mathcal{R}_y(\beta) = \begin{bmatrix} \cos(\beta) & 0 & \sin(\beta) \\ 0 & 1 & 0 \\ -\sin(\beta) & 0 & \cos(\beta) \end{bmatrix}, \quad (5.2.63)$$

and

$$\mathcal{R}_z(\gamma) = \begin{bmatrix} \cos(\gamma) & -\sin(\gamma) & 0 \\ \sin(\gamma) & \cos(\gamma) & 0 \\ 0 & 0 & 1 \end{bmatrix}. \quad (5.2.64)$$

then

$$\mathbf{r}_1 = \begin{bmatrix} d_1 \sin(\beta) \\ 0 \\ R + d_1 \cos(\beta) \end{bmatrix}, \quad (5.2.65)$$

$$\mathbf{r}_{12} = \begin{bmatrix} r_{12} \cos(\beta) \cos(\gamma) \sin(\alpha) - r_{12} \sin(\beta) \cos(\alpha) \\ r_{12} \sin(\gamma) \sin(\alpha) \\ -r_{12} \sin(\beta) \cos(\gamma) \sin(\alpha) - r_{12} \cos(\alpha) \cos(\beta) \end{bmatrix}, \quad (5.2.66)$$

$$\mathbf{r}_2 = \begin{bmatrix} d_1 \sin(\beta) + r_{12} \cos(\beta) \cos(\gamma) \sin(\alpha) - r_{12} \sin(\beta) \cos(\alpha) \\ r_{12} \sin(\gamma) \sin(\alpha) \\ R + d_1 \cos(\beta) - r_{12} \sin(\beta) \cos(\gamma) \sin(\alpha) - r_{12} \cos(\alpha) \cos(\beta) \end{bmatrix}. \quad (5.2.67)$$

We also need  $\cos(\theta_{12})$ ,  $\zeta$  and  $\cos(\theta_\zeta)$ ,  $\theta_{12}$  being the angle between  $\mathbf{r}_1$  and  $\mathbf{r}_2$ ,  $\zeta = \mathbf{r}_p - \frac{\mathbf{r}_1 + \mathbf{r}_2}{A+2}$  the position of the proton with respect to the final nucleus, and  $\theta_\zeta$  the angle between  $\zeta$  and the  $z$ -axis:

$$\cos(\theta_{12}) = \frac{\mathbf{r}_1 \cdot \mathbf{r}_2}{r_1 r_2}, \quad (5.2.68)$$

and

$$\zeta = 3\mathbf{R} - \frac{A+3}{A+2}(\mathbf{r}_1 + \mathbf{r}_2), \quad (5.2.69)$$

where we have used (5.2.49).

For heavy ions, we find instead

$$\mathbf{R} = \frac{1}{m_a} (\mathbf{r}_{A1} + \mathbf{r}_{A2} + m_b \mathbf{r}_{Ab}), \quad (5.2.70)$$

$$\mathbf{d}_1 = \frac{1}{m_a} (m_b \mathbf{r}_{b2} - (m_b + 1) \mathbf{r}_{12}), \quad (5.2.71)$$

$$d_1 = \frac{1}{m_a} \sqrt{(m_b + 1)r_{12}^2 + m_b(m_b + 1)r_{b1}^2 - m_b r_{b2}^2}, \quad (5.2.72)$$

$$d_2 = \frac{1}{m_a} \sqrt{(m_b + 1)r_{12}^2 + m_b(m_b + 1)r_{b2}^2 - m_b r_{b1}^2}, \quad (5.2.73)$$

and

$$\zeta = \frac{m_a}{m_b} \mathbf{R} - \frac{m_B + m_b}{m_b m_B} (\mathbf{r}_{A1} + \mathbf{r}_{A2}). \quad (5.2.74)$$

The rest of the formulae are identical to the  $(t, p)$  ones. We list them for convenience,

$$\mathbf{r}_{A1} = \begin{bmatrix} d_1 \sin(\beta) \\ 0 \\ R + d_1 \cos(\beta) \end{bmatrix}, \quad (5.2.75)$$

$$\mathbf{r}_{A2} = \begin{bmatrix} d_1 \sin(\beta) + r_{12} \cos(\beta) \cos(\gamma) \sin(\alpha) - r_{12} \sin(\beta) \cos(\alpha) \\ r_{12} \sin(\gamma) \sin(\alpha) \\ R + d_1 \cos(\beta) - r_{12} \sin(\beta) \cos(\gamma) \sin(\alpha) - r_{12} \cos(\alpha) \cos(\beta) \end{bmatrix}. \quad (5.2.76)$$

We we also find

$$\mathbf{r}_{b1} = \frac{1}{m_b} (\mathbf{r}_{A2} + (m_b + 1) \mathbf{r}_{A1} - m_a \mathbf{R}), \quad (5.2.77)$$

and

$$\mathbf{r}_{b2} = \frac{1}{m_b} (\mathbf{r}_{A1} + (m_b + 1) \mathbf{r}_{A2} - m_a \mathbf{R}). \quad (5.2.78)$$

One can readily obtain

$$\cos \theta_{12} = \frac{r_{A1}^2 + r_{A2}^2 - r_{12}^2}{2r_{A1} r_{A2}}, \quad (5.2.79)$$

and

$$\cos \theta_i = \frac{r_{b1}^2 + r_{b2}^2 - r_{12}^2}{2r_{b1} r_{b2}}. \quad (5.2.80)$$

### 5.2.4 Matrix element for the transition amplitude (alternative derivation)

In what follows we work out an alternative derivation of  $T_{2N}^{1\text{step}}$ , more closely related to heavy ion reactions. Following Bayman and Chen (1982) it can be written as

$$\begin{aligned}
 T^{(1)}(\theta) = & 2 \frac{(4\pi)^{3/2}}{k_{Aa} k_{Bb}} \sum_{l_p j_p m_l j_p} i^{-l_p} \exp[i(\sigma_{l_p}^p + \sigma_{l_t}^t)] \sqrt{2l_t + 1} \\
 & \times \langle l_p m - m_p 1/2 m_p | j_p m \rangle \langle l_t 0 1/2 m_t | j_t m_t \rangle Y_{m-m_p}^{l_p}(\hat{\mathbf{k}}_{Bb}) \\
 & \times \sum_{\sigma_1 \sigma_2 \sigma_p} \int d\mathbf{r}_{Cc} d\mathbf{r}_{b1} d\mathbf{r}_{A2} [\psi^{j_f}(\mathbf{r}_{A1}, \sigma_1) \psi^{j_f}(\mathbf{r}_{A2}, \sigma_2)]_0^{0*} \\
 & \times v(r_{b1}) [\psi^{j_i}(\mathbf{r}_{b1}, \sigma_1) \psi^{j_i}(\mathbf{r}_{b2}, \sigma_2)]_0^0 \frac{g_{l_t j_t}(r_{Aa}) f_{l_p j_p}(r_{Bb})}{r_{Aa} r_{Bb}} \\
 & \times [Y^{l_t}(\hat{\mathbf{r}}_{Aa}) \chi(\sigma_p)]_{m_t}^{j_t} [Y^{l_p}(\hat{\mathbf{r}}_{Bb}) \chi(\sigma_p)]_m^{j_p*}. \tag{5.2.81}
 \end{aligned}$$

As shown above one can write,

$$\begin{aligned}
 & \sum_{\sigma_p} \langle l_p m - m_p 1/2 m_p | j_p m \rangle \langle l_t 0 1/2 m_t | j_t m_t \rangle [Y^{l_t}(\hat{\mathbf{r}}_{Aa}) \chi(\sigma_p)]_{m_t}^{j_t} [Y^{l_p}(\hat{\mathbf{r}}_{Bb}) \chi(\sigma_p)]_m^{j_p*} \\
 & = -\frac{\delta_{l_p, l_t} \delta_{j_p, j_t} \delta_{m, m_t}}{\sqrt{2l+1}} [Y^l(\hat{\mathbf{r}}_{Aa}) Y^l(\hat{\mathbf{r}}_{Bb})]_0^0 \begin{cases} \frac{l}{2l+1} & \text{if } m_t = m_p \\ -\frac{\sqrt{l(l+1)}}{2l+1} & \text{if } m_t = -m_p \end{cases} \tag{5.2.82}
 \end{aligned}$$

when  $j = l - 1/2$  and

$$\begin{aligned}
 & \sum_{\sigma_p} \langle l_p m - m_p 1/2 m_p | j_p m \rangle \langle l_t 0 1/2 m_t | j_t m_t \rangle [Y^{l_t}(\hat{\mathbf{r}}_{Aa}) \chi(\sigma_p)]_{m_t}^{j_t} [Y^{l_p}(\hat{\mathbf{r}}_{Bb}) \chi(\sigma_p)]_m^{j_p*} \\
 & = -\frac{\delta_{l_p, l_t} \delta_{j_p, j_t} \delta_{m, m_t}}{\sqrt{2l+1}} [Y^l(\hat{\mathbf{r}}_{Aa}) Y^l(\hat{\mathbf{r}}_{Bb})]_0^0 \begin{cases} \frac{l+1}{2l+1} & \text{if } m_t = m_p \\ \frac{\sqrt{l(l+1)}}{2l+1} & \text{if } m_t = -m_p \end{cases} \tag{5.2.83}
 \end{aligned}$$

if  $j = l + 1/2$ . One then gets

$$\begin{aligned}
 T^{(1)}(\mu = 0; \theta) = & 2 \frac{(4\pi)^{3/2}}{k_{Aa} k_{Bb}} \sum_l i^{-l} \frac{\exp[i(\sigma_l^p + \sigma_l^t)]}{2l+1} Y_{m_t - m_p}^l(\hat{\mathbf{k}}_{Bb}) \\
 & \times \sum_{\sigma_1 \sigma_2} \int \frac{d\mathbf{r}_{Cc} d\mathbf{r}_{b1} d\mathbf{r}_{A2}}{r_{Aa} r_{Bb}} [\psi^{j_f}(\mathbf{r}_{A1}, \sigma_1) \psi^{j_f}(\mathbf{r}_{A2}, \sigma_2)]_0^{0*} \\
 & \times v(r_{b1}) [\psi^{j_i}(\mathbf{r}_{b1}, \sigma_1) \psi^{j_i}(\mathbf{r}_{b2}, \sigma_2)]_0^0 [Y^l(\hat{\mathbf{r}}_{Aa}) Y^l(\hat{\mathbf{r}}_{Bb})]_0^0 \\
 & \times \left[ (f_{ll+1/2}(r_{Bb}) g_{ll+1/2}(r_{Aa})(l+1) + f_{ll-1/2}(r_{Bb}) g_{ll-1/2}(r_{Aa})l) \delta_{m_p, m_t} \right. \\
 & \left. + (f_{ll+1/2}(r_{Bb}) g_{ll+1/2}(r_{Aa}) \sqrt{l(l+1)} - f_{ll-1/2}(r_{Bb}) g_{ll-1/2}(r_{Aa}) \sqrt{l(l+1)}) \delta_{m_p, -m_t} \right]. \tag{5.2.84}
 \end{aligned}$$

Making use of the relations,

$$\begin{aligned}
 & [\psi^{j_f}(\mathbf{r}_{A1}, \sigma_1) \psi^{j_f}(\mathbf{r}_{A2}, \sigma_2)]_0^{0*} \\
 & = ((l_f \frac{1}{2})_{j_f} (l_f \frac{1}{2})_{j_f} | (l_f l_f)_0 (\frac{1}{2} \frac{1}{2})_0)_0 u_{l_f}(r_{A1}) u_{l_f}(r_{A2}) \\
 & \times [Y^{l_f}(\hat{\mathbf{r}}_{A1}) Y^{l_f}(\hat{\mathbf{r}}_{A2})]_0^{0*} [\chi(\sigma_1) \chi(\sigma_2)]_0^{0*} \\
 & = \sqrt{\frac{2j_f + 1}{2(2l_f + 1)}} u_{l_f}(r_{A1}) u_{l_f}(r_{A2}) \\
 & \times [Y^{l_f}(\hat{\mathbf{r}}_{A1}) Y^{l_f}(\hat{\mathbf{r}}_{A2})]_0^{0*} [\chi(\sigma_1) \chi(\sigma_2)]_0^{0*} \\
 & = \sqrt{\frac{2j_f + 1}{2}} \frac{u_{l_f}(r_{A1}) u_{l_f}(r_{A2})}{4\pi} P_{l_f}(\cos \omega_A) [\chi(\sigma_1) \chi(\sigma_2)]_0^{0*}, \tag{5.2.85}
 \end{aligned}$$

and

$$\begin{aligned}
 & [\psi^{j_i}(\mathbf{r}_{b1}, \sigma_1) \psi^{j_i}(\mathbf{r}_{b2}, \sigma_2)]_0^0 \\
 & = ((l_i \frac{1}{2})_{j_i} (l_i \frac{1}{2})_{j_i} | (l_i l_i)_0 (\frac{1}{2} \frac{1}{2})_0)_0 u_{l_i}(r_{b1}) u_{l_i}(r_{b2}) \\
 & \times [Y^{l_i}(\hat{\mathbf{r}}_{b1}) Y^{l_i}(\hat{\mathbf{r}}_{b2})]_0^0 [\chi(\sigma_1) \chi(\sigma_2)]_0^0 \\
 & = \sqrt{\frac{2j_i + 1}{2(2l_i + 1)}} u_{l_i}(r_{b1}) u_{l_i}(r_{b2}) \\
 & \times [Y^{l_i}(\hat{\mathbf{r}}_{b1}) Y^{l_i}(\hat{\mathbf{r}}_{b2})]_0^0 [\chi(\sigma_1) \chi(\sigma_2)]_0^0 \\
 & = \sqrt{\frac{2j_i + 1}{2}} \frac{u_{l_i}(r_{b1}) u_{l_i}(r_{b2})}{4\pi} P_{l_i}(\cos \omega_b) [\chi(\sigma_1) \chi(\sigma_2)]_0^0, \tag{5.2.86}
 \end{aligned}$$

where  $\omega_A$  is the angle between  $\mathbf{r}_{A1}$  and  $\mathbf{r}_{A2}$ , and  $\omega_b$  is the angle between  $\mathbf{r}_{b1}$  and  $\mathbf{r}_{b2}$ . Consequently

$$\begin{aligned} T^{(1)}(\theta) = & (4\pi)^{-3/2} \frac{\sqrt{(2j_i + 1)(2j_f + 1)}}{k_{Aa}k_{Bb}} \sum_l i^{-l} \frac{\exp[i(\sigma_l^p + \sigma_l^t)]}{\sqrt{2l + 1}} Y_m^l(\hat{\mathbf{k}}_{Bb}) \\ & \times \int \frac{d\mathbf{r}_{Cc} d\mathbf{r}_{b1} d\mathbf{r}_{A2}}{r_{Aa}r_{Bb}} P_{l_f}(\cos \omega_A) P_{l_i}(\cos \omega_b) P_l(\cos \omega_{if}) \\ & \times v(r_{b1}) u_{l_i}(r_{b1}) u_{l_i}(r_{b2}) u_{l_f}(r_{A1}) u_{l_f}(r_{A2}) \\ & \times [(f_{ll+1/2}(r_{Bb}) g_{ll+1/2}(r_{Aa})(l+1) + f_{ll-1/2}(r_{Bb}) g_{ll-1/2}(r_{Aa})l) \delta_{m_p, m_t} \\ & + (f_{ll+1/2}(r_{Bb}) g_{ll+1/2}(r_{Aa}) \sqrt{l(l+1)} - f_{ll-1/2}(r_{Bb}) g_{ll-1/2}(r_{Aa}) \sqrt{l(l+1)}) \delta_{m_p, -m_t}], \end{aligned} \quad (5.2.87)$$

where  $\omega_{if}$  is the angle between  $\mathbf{r}_{Aa}$  and  $\mathbf{r}_{Bb}$ . For heavy ions, we can consider that the optical potential does not have a spin-orbit term, and the distorted waves are independent of  $j$ . We thus have

$$\begin{aligned} T^{(1)}(\theta) = & (4\pi)^{-3/2} \frac{\sqrt{(2j_i + 1)(2j_f + 1)}}{k_{Aa}k_{Bb}} \sum_l i^{-l} \exp[i(\sigma_l^p + \sigma_l^t)] Y_0^l(\hat{\mathbf{k}}_{Bb}) \sqrt{2l + 1} \\ & \times \int \frac{d\mathbf{r}_{Cc} d\mathbf{r}_{b1} d\mathbf{r}_{A2}}{r_{Aa}r_{Bb}} P_{l_f}(\cos \omega_A) P_{l_i}(\cos \omega_b) P_l(\cos \omega_{if}) \\ & \times v(r_{b1}) u_{l_i}(r_{b1}) u_{l_i}(r_{b2}) u_{l_f}(r_{A1}) u_{l_f}(r_{A2}) f_l(r_{Bb}) g_l(r_{Aa}). \end{aligned} \quad (5.2.88)$$

Changing variables one obtains,

$$\begin{aligned} T^{(1)}(\theta) = & (4\pi)^{-1} \frac{\sqrt{(2j_i + 1)(2j_f + 1)}}{k_{Aa}k_{Bb}} \sum_l \exp[i(\sigma_l^p + \sigma_l^t)] P_l(\cos \theta) (2l + 1) \\ & \times \int dr_{1A} dr_{2A} dr_{Aa} d(\cos \beta) d(\cos \omega_A) d\gamma r_{1A}^2 r_{2A}^2 r_{Aa}^2 \\ & \times P_{l_f}(\cos \omega_A) P_{l_i}(\cos \omega_b) P_l(\cos \omega_{if}) v(r_{b1}) \\ & \times u_{l_i}(r_{b1}) u_{l_i}(r_{b2}) u_{l_f}(r_{A1}) u_{l_f}(r_{A2}) f_l(r_{Bb}) g_l(r_{Aa}). \end{aligned} \quad (5.2.89)$$

### 5.2.5 Coordinates used to derive Eq. (5.2.89)

We determine the relation between the integration variables in (5.2.87) and the coordinates needed to evaluate the quantities in the integrand. Noting that

$$\mathbf{r}_{Aa} = \frac{\mathbf{r}_{A1} + \mathbf{r}_{A2} + m_b \mathbf{r}_{Ab}}{m_b + 2}, \quad (5.2.90)$$

one has

$$\mathbf{r}_{b1} = \mathbf{r}_{bA} + \mathbf{r}_{A1} = \frac{(m_b + 1)\mathbf{r}_{A1} + \mathbf{r}_{A2} - (m_b + 2)\mathbf{r}_{Aa}}{m_b}, \quad (5.2.91)$$

$$\mathbf{r}_{b2} = \mathbf{r}_{bA} + \mathbf{r}_{A2} = \frac{(m_b + 1)\mathbf{r}_{A2} + \mathbf{r}_{A1} - (m_b + 2)\mathbf{r}_{Aa}}{m_b}, \quad (5.2.92)$$

and

$$\begin{aligned} \mathbf{r}_{Cc} &= \mathbf{r}_{CA} + \mathbf{r}_{A1} + \mathbf{r}_{1c} = -\frac{1}{m_A + 1}\mathbf{r}_{A2} + \mathbf{r}_{A1} - \frac{m_b}{m_b + 1}\mathbf{r}_{b1} \\ &= \frac{m_b + 2}{m_b + 1}\mathbf{r}_{Aa} - \frac{m_b + 2 + m_A}{(m_b + 1)(m_A + 1)}\mathbf{r}_{A2} \end{aligned} \quad (5.2.93)$$

Since,

$$\mathbf{r}_{AB} = \frac{\mathbf{r}_{A1} + \mathbf{r}_{A2}}{m_A + 2}, \quad (5.2.94)$$

one obtains

$$\mathbf{r}_{Bb} = \mathbf{r}_{BA} + \mathbf{r}_{Ab} = \frac{m_b + 2}{m_b}\mathbf{r}_{Aa} - \frac{m_A + m_b + 2}{(m_A + 2)m_b}(\mathbf{r}_{A1} + \mathbf{r}_{A2}). \quad (5.2.95)$$

Using the same rotations as those used in Section 5.2.3 one gets,

$$\mathbf{r}_{A1} = r_{A1} \begin{bmatrix} \sin \alpha \\ 0 \\ \cos \alpha \end{bmatrix}, \quad (5.2.96)$$

and

$$\mathbf{r}_{A2} = r_{A2} \begin{bmatrix} -\cos \alpha \cos \gamma \sin \omega_A + \sin \alpha \cos \omega_A \\ -\sin \gamma \sin \omega_A \\ \sin \alpha \cos \gamma \sin \omega_A + \cos \alpha \cos \omega_A \end{bmatrix}, \quad (5.2.97)$$

with

$$\cos \alpha = \frac{r_{A1}^2 - d_1^2 + r_{Aa}^2}{2r_{A1}r_{Aa}}, \quad (5.2.98)$$

and

$$d_1 = \sqrt{r_{A1}^2 - r_{Aa}^2 \sin^2 \beta} - r_{Aa} \cos \beta. \quad (5.2.99)$$

Note that though  $\beta, r_{1A}, r_{Aa}$  are independent integration variables, they have to fulfill the condition

$$r_{Aa} \sin \beta \leq r_{A1}, \quad \text{for } 0 \leq \beta \leq \pi. \quad (5.2.100)$$

The expression of the remaining quantities appearing in the integral are now straightforward,

$$\begin{aligned} r_{b1} &= m_b^{-1} |(m_b + 1)\mathbf{r}_{A1} + \mathbf{r}_{A2} - (m_b + 2)\mathbf{r}_{Aa}| \\ &= m_b^{-1} \left( (m_b + 2)^2 r_{Aa}^2 + (m_b + 1)^2 r_{A1}^2 + r_{A2}^2 \right. \\ &\quad \left. - 2(m_b + 2)(m_b + 1)\mathbf{r}_{Aa} \mathbf{r}_{A1} - 2(m_b + 2)\mathbf{r}_{Aa} \mathbf{r}_{A2} + 2(m_b + 1)\mathbf{r}_{A1} \mathbf{r}_{A2} \right)^{1/2}, \end{aligned} \quad (5.2.101)$$

$$\begin{aligned}
r_{b2} &= m_b^{-1} |(m_b + 1)\mathbf{r}_{A2} + \mathbf{r}_{A1} - (m_b + 2)\mathbf{r}_{Aa}| \\
&= m_b^{-1} \left( (m_b + 2)^2 r_{Aa}^2 + (m_b + 1)^2 r_{A2}^2 + r_{A1}^2 \right. \\
&\quad \left. - 2(m_b + 2)(m_b + 1)\mathbf{r}_{Aa} \mathbf{r}_{A2} - 2(m_b + 2)\mathbf{r}_{Aa} \mathbf{r}_{A1} + 2(m_b + 1)\mathbf{r}_{A2} \mathbf{r}_{A1} \right)^{1/2}, \\
\end{aligned} \tag{5.2.102}$$

$$\begin{aligned}
r_{Bb} &= \left| \frac{m_b + 2}{m_b} \mathbf{r}_{Aa} - \frac{m_A + m_b + 2}{(m_A + 2)m_b} (\mathbf{r}_{A1} + \mathbf{r}_{A2}) \right| \\
&= \left[ \left( \frac{m_b + 2}{m_b} \right)^2 r_{Aa}^2 + \left( \frac{m_A + m_b + 2}{(m_A + 2)m_b} \right)^2 (r_{A1}^2 + r_{A2}^2 + 2\mathbf{r}_{A1} \mathbf{r}_{A2}) \right. \\
&\quad \left. - 2 \frac{(m_b + 2)(m_A + m_b + 2)}{(m_A + 2)m_b^2} \mathbf{r}_{Aa} (\mathbf{r}_{A1} + \mathbf{r}_{A2}) \right]^{1/2}, \\
\end{aligned} \tag{5.2.103}$$

$$\begin{aligned}
r_{Cc} &= \left| \frac{m_b + 2}{m_b + 1} \mathbf{r}_{Aa} - \frac{m_b + 2 + m_A}{(m_b + 1)(m_A + 1)} \mathbf{r}_{A2} \right| \\
&= \left[ \left( \frac{m_a}{(m_a - 1)} \right)^2 r_{Aa}^2 + \left( \frac{m_A + m_a}{(m_A + 1)(m_a - 1)} \right)^2 r_{A2}^2 \right. \\
&\quad \left. - 2 \frac{m_A m_a + m_a^2}{(m_A + 1)(m_a - 1)^2} \mathbf{r}_{Aa} \mathbf{r}_{A2} \right]^{1/2}, \\
\end{aligned} \tag{5.2.104}$$

$$\cos \omega_b = \frac{\mathbf{r}_{b1} \mathbf{r}_{b2}}{r_{b1} r_{b2}}, \tag{5.2.105}$$

$$\cos \omega_{if} = \frac{\mathbf{r}_{Aa} \mathbf{r}_{Bb}}{r_{Aa} r_{Bb}}, \tag{5.2.106}$$

with

$$\mathbf{r}_{Aa} \mathbf{r}_{A1} = r_{Aa} r_{A1} \cos \alpha, \tag{5.2.107}$$

$$\mathbf{r}_{Aa} \mathbf{r}_{A2} = r_{Aa} r_{A2} (\sin \alpha \cos \gamma \sin \omega_A + \cos \alpha \cos \omega_A), \tag{5.2.108}$$

$$\mathbf{r}_{A1} \mathbf{r}_{A2} = r_{A1} r_{A2} \cos \omega_A. \tag{5.2.109}$$

### 5.2.6 Successive transfer

The successive two-neutron transfer amplitudes can be written as (Bayman and Chen (1982)):

$$\begin{aligned}
T_{succ}^{(2)}(\theta) = & \frac{4\mu_{Cc}}{\hbar^2} \sum_{\substack{\sigma_1 \sigma_2 \\ \sigma'_1 \sigma'_2 \\ KM}} \int d^3 r_{Cc} d^3 r_{b1} d^3 r_{A2} d^3 r'_{Cc} d^3 r'_{b1} d^3 r'_{A2} \chi^{(-)*}(\mathbf{k}_{Bb}, \mathbf{r}_{Bb}) \\
& \times \left[ \psi^{j_f}(\mathbf{r}_{A1}, \sigma_1) \psi^{j_f}(\mathbf{r}_{A2}, \sigma_2) \right]_0^{0*} v(r_{b1}) \left[ \psi^{j_f}(\mathbf{r}_{A2}, \sigma_2) \psi^{j_i}(\mathbf{r}_{b1}, \sigma_1) \right]_M^K \\
& \times G(\mathbf{r}_{Cc}, \mathbf{r}'_{Cc}) \left[ \psi^{j_f}(\mathbf{r}'_{A2}, \sigma'_2) \psi^{j_i}(\mathbf{r}'_{b1}, \sigma'_1) \right]_M^{K*} v(r'_{c2}) \\
& \times \left[ \psi^{j_i}(\mathbf{r}'_{b1}, \sigma'_1) \psi^{j_i}(\mathbf{r}'_{b2}, \sigma'_2) \right]_0^0 \chi^{(+)}(\mathbf{r}'_{Aa}). 
\end{aligned} \tag{5.2.110}$$

It is of notice that the time-reversal phase convention is used throughout. Expanding the Green function and the distorted waves in a basis of angular momentum eigenstate one can write,

$$\chi^{(-)*}(\mathbf{k}_{Bb}, \mathbf{r}_{Bb}) = \sum_{\tilde{l}} \frac{4\pi}{k_{Bb} r_{Bb}} i^{-\tilde{l}} e^{i\sigma_f^{\tilde{l}}} F_{\tilde{l}} \sum_m Y_m^{\tilde{l}}(\hat{r}_{Bb}) Y_m^{\tilde{l}*}(\hat{k}_{Bb}), \tag{5.2.111}$$

the sum over  $m$  being

$$\sum_m (-1)^{\tilde{l}-m} Y_m^{\tilde{l}}(\hat{r}_{Bb}) Y_{-m}^{\tilde{l}}(\hat{k}_{Bb}) = \sqrt{2\tilde{l}+1} \left[ Y^{\tilde{l}}(\hat{r}_{Bb}) Y^{\tilde{l}}(\hat{k}_{Bb}) \right]_0^0, \tag{5.2.112}$$

where we have used (5.D.2) and (5.D.18), so

$$\chi^{(-)*}(\mathbf{k}_{Bb}, \mathbf{r}_{Bb}) = \sum_{\tilde{l}} \sqrt{2\tilde{l}+1} \frac{4\pi}{k_{Bb} r_{Bb}} i^{-\tilde{l}} e^{i\sigma_f^{\tilde{l}}} F_{\tilde{l}}(r_{Bb}) \left[ Y^{\tilde{l}}(\hat{r}_{Bb}) Y^{\tilde{l}}(\hat{k}_{Bb}) \right]_0^0. \tag{5.2.113}$$

Similarly,

$$\chi^{(+)}(\mathbf{r}'_{Aa}) = \sum_l l! \sqrt{2l+1} \frac{4\pi}{k_{Aa} r'_{Aa}} e^{i\sigma_f^l} F_l(r'_{Aa}) \left[ Y^l(\hat{r}'_{Aa}) Y^l(\hat{k}_{Aa}) \right]_0^0 \tag{5.2.114}$$

where we have taken into account the choice  $\hat{k}_{Aa} \equiv \hat{z}$ . The Green function can be written as

$$G(\mathbf{r}_{Cc}, \mathbf{r}'_{Cc}) = i \sum_{l_c} \sqrt{2l_c+1} \frac{f_{l_c}(k_{Cc}, r_{<}) P_{l_c}(k_{Cc}, r_{>})}{k_{Cc} r_{Cc} r'_{Cc}} \left[ Y^{l_c}(\hat{r}_{Cc}) Y^{l_c}(\hat{r}'_{Cc}) \right]_0^0. \tag{5.2.115}$$

Finally

$$\begin{aligned}
T_{succ}^{(2)}(\theta) = & \frac{4\mu_{Cc}(4\pi)^2 i}{\hbar^2 k_{Aa} k_{Bb} k_{Cc}} \sum_{l,l_c,\tilde{l}} e^{i(\sigma_i^l + \sigma_f^{\tilde{l}})} i^{l-\tilde{l}} \sqrt{(2l+1)(2l_c+1)(2\tilde{l}+1)} \\
& \times \sum_{\substack{\sigma_1 \sigma_2 \\ \sigma'_1 \sigma'_2}} \int d^3 r_{Cc} d^3 r_{b1} d^3 r_{A2} d^3 r'_{Cc} d^3 r'_{b1} d^3 r'_{A2} v(r_{b1}) v(r'_{c2}) \left[ Y^{\tilde{l}}(\hat{r}_{Bb}) Y^{\tilde{l}}(\hat{k}_{Bb}) \right]_0^0 \\
& \times \left[ Y^l(\hat{r}'_{Aa}) Y^l(\hat{k}'_{Aa}) \right]_0^0 \left[ Y^{l_c}(\hat{r}_{Cc}) Y^{l_c}(\hat{r}'_{Cc}) \right]_0^0 \frac{F_l(r_{Bb})}{r_{Bb}} \frac{F_l(r'_{Aa})}{r'_{Aa}} \\
& \times \frac{f_{l_c}(k_{Cc}, r_<) P_{l_c}(k_{Cc}, r_>)}{r_{Cc} r'_{Cc}} \left[ \psi^{j_f}(\mathbf{r}_{A1}, \sigma_1) \psi^{j_f}(\mathbf{r}_{A2}, \sigma_2) \right]_0^{0*} \\
& \times \left[ \psi^{j_i}(\mathbf{r}'_{b1}, \sigma'_1) \psi^{j_i}(\mathbf{r}'_{b2}, \sigma'_2) \right]_0^0 \sum_{KM} \left[ \psi^{j_f}(\mathbf{r}_{A2}, \sigma_2) \psi^{j_i}(\mathbf{r}_{b1}, \sigma_1) \right]_M^K \\
& \times \left[ \psi^{j_f}(\mathbf{r}'_{A2}, \sigma'_2) \psi^{j_i}(\mathbf{r}'_{b1}, \sigma'_1) \right]_M^{K*}. 
\end{aligned} \tag{5.2.116}$$

Let us now perform the integration over  $\mathbf{r}_{A2}$ ,

$$\begin{aligned}
& \sum_{\sigma_1 \sigma_2} \int d\mathbf{r}_{A2} \left[ \psi^{j_f}(\mathbf{r}_{A1}, \sigma_1) \psi^{j_f}(\mathbf{r}_{A2}, \sigma_2) \right]_0^{0*} \left[ \psi^{j_f}(\mathbf{r}_{A2}, \sigma_2) \psi^{j_i}(\mathbf{r}_{b1}, \sigma_1) \right]_M^K \\
&= \sum_{\sigma_1 \sigma_2} (-1)^{1/2-\sigma_1+1/2-\sigma_2} \int d\mathbf{r}_{A2} \left[ \psi^{j_f}(\mathbf{r}_{A1}, -\sigma_1) \psi^{j_f}(\mathbf{r}_{A2}, -\sigma_2) \right]_0^0 \left[ \psi^{j_f}(\mathbf{r}_{A2}, \sigma_2) \psi^{j_i}(\mathbf{r}_{b1}, \sigma_1) \right]_M^K \\
&= - \sum_{\sigma_1 \sigma_2} (-1)^{1/2-\sigma_1+1/2-\sigma_2} \int d\mathbf{r}_{A2} \left[ \psi^{j_f}(\mathbf{r}_{A2}, -\sigma_2) \psi^{j_f}(\mathbf{r}_{A1}, -\sigma_1) \right]_0^0 \left[ \psi^{j_f}(\mathbf{r}_{A2}, \sigma_2) \psi^{j_i}(\mathbf{r}_{b1}, \sigma_1) \right]_M^K \\
&= -((j_f j_f)_0 (j_f j_i)_K | (j_f j_f)_0 (j_f j_i)_K)_K \sum_{\sigma_1 \sigma_2} (-1)^{1/2-\sigma_1+1/2-\sigma_2} \\
&\quad \times \int d\mathbf{r}_{A2} \left[ \psi^{j_f}(\mathbf{r}_{A2}, -\sigma_2) \psi^{j_f}(\mathbf{r}_{A2}, \sigma_2) \right]_0^0 \left[ \psi^{j_f}(\mathbf{r}_{A1}, -\sigma_1) \psi^{j_i}(\mathbf{r}_{b1}, \sigma_1) \right]_M^K \\
&= \frac{1}{2j_f + 1} \sqrt{2j_f + 1} ((l_f \frac{1}{2})_{j_f} (l_i \frac{1}{2})_{j_i} | (l_f l_i)_K (\frac{1}{2} \frac{1}{2})_0)_K \\
&\quad \times u_{l_f}(r_{A1}) u_{l_i}(r_{b1}) \left[ Y^{l_f}(\hat{r}_{A1}) Y^{l_i}(\hat{r}_{b1}) \right]_M^K \sum_{\sigma_1} (-1)^{1/2-\sigma_1} \left[ \chi^{1/2}(-\sigma_1) \chi^{1/2}(\sigma_1) \right]_0^0 \\
&= -\sqrt{\frac{2}{2j_f + 1}} ((l_f \frac{1}{2})_{j_f} (l_i \frac{1}{2})_{j_i} | (l_f l_i)_K (\frac{1}{2} \frac{1}{2})_0)_K \left[ Y^{l_f}(\hat{r}_{A1}) Y^{l_i}(\hat{r}_{b1}) \right]_M^K u_{l_f}(r_{A1}) u_{l_i}(r_{b1}),
\end{aligned} \tag{5.2.117}$$

where we have evaluated the 9j-symbol

$$((j_f j_f)_0 (j_f j_i)_K | (j_f j_f)_0 (j_f j_i)_K)_K = \frac{1}{2j_f + 1}, \tag{5.2.118}$$

as well as (5.D.19). We proceed in a similar way to evaluate the integral over  $\mathbf{r}'_{b1}$ ,

$$\begin{aligned}
& \sum_{\sigma'_1, \sigma'_2} \int d\mathbf{r}'_{b1} [\psi^{j_i}(\mathbf{r}'_{b1}, \sigma'_1) \psi^{j_i}(\mathbf{r}'_{b2}, \sigma'_2)]_0^0 [\psi^{j_f}(\mathbf{r}'_{A2}, \sigma'_2) \psi^{j_i}(\mathbf{r}'_{b1}, \sigma'_1)]_M^{K*} \\
&= -(-1)^{K-M} \sum_{\sigma'_1, \sigma'_2} \int d\mathbf{r}'_{b1} [\psi^{j_f}(\mathbf{r}'_{A2}, -\sigma'_2) \psi^{j_i}(\mathbf{r}'_{b1}, -\sigma'_1)]_{-M}^K \\
&\quad \times [\psi^{j_i}(\mathbf{r}'_{b2}, \sigma'_2) \psi^{j_i}(\mathbf{r}'_{b1}, \sigma'_1)]_0^0 (-1)^{1/2-\sigma'_1+1/2-\sigma'_2} \\
&= -(-1)^{K-M} ((j_f j_i)_K (j_i j_i)_0 (j_f j_i)_K (j_i j_i)_0)_K (-\sqrt{2j_i + 1}) \\
&\quad \times ((l_f \frac{1}{2})_{j_f} (l_i \frac{1}{2})_{j_i} | (l_f l_i)_K (\frac{1}{2} \frac{1}{2})_0)_K (-\sqrt{2}) u_{l_f}(r'_{A2}) u_{l_i}(r'_{b2}) [Y^{l_f}(\hat{r}'_{A2}) Y^{l_i}(\hat{r}'_{b2})]_{-M}^K \\
&= -\sqrt{\frac{2}{2j_i + 1}} ((l_f \frac{1}{2})_{j_f} (l_i \frac{1}{2})_{j_i} | (l_f l_i)_K (\frac{1}{2} \frac{1}{2})_0)_K [Y^{l_f}(\hat{r}'_{A2}) Y^{l_i}(\hat{r}'_{b2})]_M^{K*} u_{l_f}(r'_{A2}) u_{l_i}(r'_{b2}). \tag{5.2.119}
\end{aligned}$$

Setting the different elements together one obtains

$$\begin{aligned}
T_{succ}^{(2)}(\theta) &= \frac{4\mu_{Cc}(4\pi)^2 i}{\hbar^2 k_{Aa} k_{Bb} k_{Cc}} \frac{2}{\sqrt{(2j_i + 1)(2j_f + 1)}} \sum_{K,M} ((l_f \frac{1}{2})_{j_f} (l_i \frac{1}{2})_{j_i} | (l_f l_i)_K (\frac{1}{2} \frac{1}{2})_0)_K^2 \\
&\quad \times \sum_{l_c, \tilde{l}} e^{i(\sigma'_i + \sigma^{\tilde{l}})} \sqrt{(2l_c + 1)(2l + 1)(2\tilde{l} + 1)} t^{l-\tilde{l}} \\
&\quad \times \int d^3 r_{Cc} d^3 r_{b1} d^3 r'_{Cc} d^3 r'_{A2} v(r_{b1}) v(r'_{c2}) u_{l_f}(r_{A1}) u_{l_i}(r_{b1}) u_{l_f}(r'_{A2}) u_{l_i}(r'_{b2}) \\
&\quad \times [Y^{l_f}(\hat{r}'_{A2}) Y^{l_i}(\hat{r}'_{b2})]_M^{K*} [Y^{l_f}(\hat{r}_{A1}) Y^{l_i}(\hat{r}_{b1})]_M^K \frac{F_l(r'_{Aa}) F_{\tilde{l}}(r'_{Bb}) f_{l_c}(k_{Cc}, r_<) P_{l_c}(k_{Cc}, r_>)}{r'_{Aa} r_{Bb} r_{Cc} r'_{Cc}} \\
&\quad \times [Y^{\tilde{l}}(\hat{r}_{Bb}) Y^{\tilde{l}}(\hat{k}_{Bb})]_0^0 [Y^l(\hat{r}'_{Aa}) Y^l(\hat{k}_{Aa})]_0^0 [Y^{l_c}(\hat{r}_{Cc}) Y^{l_c}(\hat{r}'_{Cc})]_0^0. \tag{5.2.120}
\end{aligned}$$

We now proceed to write this expression in a more compact way. For this purpose one writes

$$\begin{aligned}
& [Y^{\tilde{l}}(\hat{r}_{Bb}) Y^{\tilde{l}}(\hat{k}_{Bb})]_0^0 [Y^l(\hat{r}'_{Aa}) Y^l(\hat{k}_{Aa})]_0^0 = \\
& ((l \tilde{l})_0 (\tilde{l} \tilde{l})_0 | (l \tilde{l})_0 (\tilde{l} \tilde{l})_0)_0 [Y^{\tilde{l}}(\hat{r}_{Bb}) Y^l(\hat{r}'_{Aa})]_0^0 [Y^l(\hat{k}_{Bb}) Y^l(\hat{k}_{Aa})]_0^0 \\
& = \frac{\delta_{\tilde{l}l}}{2l + 1} [Y^l(\hat{r}_{Bb}) Y^l(\hat{r}'_{Aa})]_0^0 [Y^l(\hat{k}_{Bb}) Y^l(\hat{k}_{Aa})]_0^0. \tag{5.2.121}
\end{aligned}$$

Taking into account the relations

$$[Y^l(\hat{k}_{Bb}) Y^l(\hat{k}_{Aa})]_0^0 = \frac{(-1)^l}{\sqrt{4\pi}} Y_0^l(\hat{k}_{Bb}) i^l, \tag{5.2.122}$$

and

$$\begin{aligned}
& \left[ Y^l(\hat{r}_{Bb}) Y^l(\hat{r}'_{Aa}) \right]_0^0 \left[ Y^{l_c}(\hat{r}_{Cc}) Y^{l_c}(\hat{r}'_{Cc}) \right]_0^0 = \\
& \quad ((ll)_0(l_c l_c)_0 | (ll)_K(l l_c)_K)_0 \left\{ \left[ Y^l(\hat{r}_{Bb}) Y^{l_c}(\hat{r}_{Cc}) \right]^K \left[ Y^l(\hat{r}'_{Aa}) Y^{l_c}(\hat{r}'_{Cc}) \right]^K \right\}_0^0 \\
& \quad = \sqrt{\frac{2K+1}{(2l+1)(2l_c+1)}} \\
& \quad \times \sum_{M'} \frac{(-1)^{K+M'}}{\sqrt{2K+1}} \left[ Y^l(\hat{r}_{Bb}) Y^{l_c}(\hat{r}_{Cc}) \right]_{-M'}^K \left[ Y^l(\hat{r}'_{Aa}) Y^{l_c}(\hat{r}'_{Cc}) \right]_{M'}^K \\
& \quad = \sqrt{\frac{1}{(2l+1)(2l_c+1)}} \\
& \quad \times \sum_{M'} \left[ Y^l(\hat{r}_{Bb}) Y^{l_c}(\hat{r}_{Cc}) \right]_{M'}^{K*} \left[ Y^l(\hat{r}'_{Aa}) Y^{l_c}(\hat{r}'_{Cc}) \right]_{M'}^K. 
\end{aligned} \tag{5.2.123}$$

It is of notice that the integrals

$$\int d\hat{r}_{Cc} d\hat{r}_{b1} \left[ Y^l(\hat{r}_{Bb}) Y^{l_c}(\hat{r}_{Cc}) \right]_M^{K*} \left[ Y^{l_f}(\hat{r}_{A1}) Y^{l_i}(\hat{r}_{b1}) \right]_M^K, \tag{5.2.124}$$

and

$$\int d\hat{r}'_{Cc} d\hat{r}'_{A2} \left[ Y^l(\hat{r}'_{Aa}) Y^{l_c}(\hat{r}'_{Cc}) \right]_M^K \left[ Y^{l_f}(\hat{r}'_{A2}) Y^{l_i}(\hat{r}'_{b2}) \right]_M^{K*}, \tag{5.2.125}$$

over the angular variables do not depend on  $M$ . Let us see why this is so with the help of (5.2.124),

$$\begin{aligned}
& \left[ Y^l(\hat{r}_{Bb}) Y^{l_c}(\hat{r}_{Cc}) \right]_M^{K*} \left[ Y^{l_f}(\hat{r}_{A1}) Y^{l_i}(\hat{r}_{b1}) \right]_M^K = (-1)^{K-M} \left[ Y^l(\hat{r}_{Bb}) Y^{l_c}(\hat{r}_{Cc}) \right]_{-M}^K \\
& \quad \times \left[ Y^{l_f}(\hat{r}_{A1}) Y^{l_i}(\hat{r}_{b1}) \right]_M^K = (-1)^{K-M} \sum_J \langle K \ K \ M \ - M | J \ 0 \rangle \\
& \quad \times \left\{ \left[ Y^l(\hat{r}_{Bb}) Y^{l_c}(\hat{r}_{Cc}) \right]^K \left[ Y^{l_f}(\hat{r}_{A1}) Y^{l_i}(\hat{r}_{b1}) \right]^K \right\}_0^J. 
\end{aligned} \tag{5.2.126}$$

After integration, only the term

$$\begin{aligned}
& (-1)^{K-M} \langle K \ K \ M \ - M | 0 \ 0 \rangle \left\{ \left[ Y^l(\hat{r}_{Bb}) Y^{l_c}(\hat{r}_{Cc}) \right]^K \left[ Y^{l_f}(\hat{r}_{A1}) Y^{l_i}(\hat{r}_{b1}) \right]^K \right\}_0^0 = . \\
& \quad \frac{1}{\sqrt{2K+1}} \left\{ \left[ Y^l(\hat{r}_{Bb}) Y^{l_c}(\hat{r}_{Cc}) \right]^K \left[ Y^{l_f}(\hat{r}_{A1}) Y^{l_i}(\hat{r}_{b1}) \right]^K \right\}_0^0 
\end{aligned} \tag{5.2.127}$$

corresponding to  $J = 0$  survives, which is indeed independent of  $M$ . We can thus omit the sum over  $M$  in (5.2.120) and multiply by  $(2K + 1)$ , obtaining

$$\begin{aligned} T_{succ}^{(2)}(\theta) &= \frac{64\mu_{Cc}(\pi)^{3/2}i}{\hbar^2 k_{Aa} k_{Bb} k_{Cc}} \frac{i^{-l}}{\sqrt{(2j_i + 1)(2j_f + 1)}} \\ &\times \sum_K (2K + 1) ((l_f \frac{1}{2})_{jf} (l_i \frac{1}{2})_{ji} | (l_f l_i)_K (\frac{1}{2} \frac{1}{2})_0)_K^2 \\ &\times \sum_{l_c, l} \frac{e^{i(\sigma_i^l + \sigma_f^l)}}{\sqrt{(2l + 1)}} Y_0^l(\hat{k}_{Bb}) S_{K, l, l_c}, \end{aligned} \quad (5.2.128)$$

where

$$\begin{aligned} S_{K, l, l_c} &= \int d^3 r_{Cc} d^3 r_{b1} v(r_{b1}) u_{l_f}(r_{A1}) u_{l_i}(r_{b1}) \frac{s_{K, l, l_c}(r_{Cc})}{r_{Cc}} \frac{F_l(r_{Bb})}{r_{Bb}} \\ &\times [Y^{l_f}(\hat{r}_{A1}) Y^{l_i}(\hat{r}_{b1})]_M^K [Y^{l_c}(\hat{r}_{Cc}) Y^l(\hat{r}_{Bb})]_M^{K*}, \end{aligned} \quad (5.2.129)$$

and

$$\begin{aligned} s_{K, l, l_c}(r_{Cc}) &= \int_{r_{Cc} \text{fixed}} d^3 r'_{Cc} d^3 r'_{A2} v(r'_{c2}) u_{l_f}(r'_{A2}) u_{l_i}(r'_{b2}) \frac{F_l(r'_{Aa})}{r'_{Aa}} \frac{f_l(k_{Cc}, r_{<}) P_{l_c}(k_{Cc}, r_{>})}{r'_{Cc}} \\ &\times [Y^{l_f}(\hat{r}'_{A2}) Y^{l_i}(\hat{r}'_{b2})]_M^{K*} [Y^{l_c}(\hat{r}'_{Cc}) Y^l(\hat{r}'_{Aa})]_M^K. \end{aligned} \quad (5.2.130)$$

It can be shown that the integrand in (5.2.129) is independent of  $M$ . Consequently, one can sum over  $M$  and divide by  $(2K + 1)$ , to get

$$\begin{aligned} \frac{1}{2K + 1} v(r_{b1}) u_{l_f}(r_{A1}) u_{l_i}(r_{b1}) \frac{s_{K, l, l_c}(r_{Cc})}{r_{Cc}} \frac{F_l(r_{Bb})}{r_{Bb}} \\ \times \sum_M [Y^{l_f}(\hat{r}_{A1}) Y^{l_i}(\hat{r}_{b1})]_M^K [Y^{l_c}(\hat{r}_{Cc}) Y^l(\hat{r}_{Bb})]_M^{K*}. \end{aligned} \quad (5.2.131)$$

This integrand is rotationally invariant (it is proportional to a  $T_M^L$  spherical tensor with  $L = 0, M = 0$ ), so one can evaluate it in the “standard” configuration in which  $\mathbf{r}_{Cc}$  is directed along the  $z$ -axis and multiply by  $8\pi^2$  (see Bayman and Chen (1982)), obtaining the final expression for  $S_{K, l, l_c}$ :

$$\begin{aligned} S_{K, l, l_c} &= \frac{4\pi^{3/2} \sqrt{2l_c + 1}}{2K + 1} i^{-l_c} \\ &\times \int r_{Cc}^2 dr_{Cc} r_{b1}^2 dr_{b1} \sin \theta d\theta v(r_{b1}) u_{l_f}(r_{A1}) u_{l_i}(r_{b1}) \\ &\times \frac{s_{K, l, l_c}(r_{Cc})}{r_{Cc}} \frac{F_l(r_{Bb})}{r_{Bb}} \\ &\times \sum_M \langle l_c 0 l M | K M \rangle [Y^{l_f}(\hat{r}_{A1}) Y^{l_i}(\theta + \pi, 0)]_M^K Y_M^{l*}(\hat{r}_{Bb}). \end{aligned} \quad (5.2.132)$$

Similarly, one has

$$\begin{aligned}
 s_{K,l,l_c}(r_{Cc}) &= \frac{4\pi^{3/2} \sqrt{2l_c + 1}}{2K + 1} i^{l_c} \\
 &\times \int r'_{Cc}^2 dr'_{Cc} r'^2_{A2} dr'_{A2} \sin \theta' d\theta' v(r'_{c2}) u_{l_f}(r'_{A2}) u_{l_i}(r'_{b2}) \\
 &\times \frac{F_l(r'_{Aa}) f_{l_c}(k_{Cc}, r_<) P_{l_c}(k_{Cc}, r_>)}{r'_{Aa} r'_{Cc}} \\
 &\times \sum_M \langle l_c 0 l M | K M \rangle [Y^{l_f}(\hat{r}'_{A2}) Y^{l_i}(\hat{r}'_{b2})]_M^{K*} Y_M^l(\hat{r}'_{Aa}). \tag{5.2.133}
 \end{aligned}$$

Introducing the further approximations  $\mathbf{r}_{A1} \approx \mathbf{r}_{C1}$  and  $\mathbf{r}_{b2} \approx \mathbf{r}_{c2}$ , one obtains the final expression

$$\begin{aligned}
 T_{succ}^{(2)}(\theta) &= \frac{1024\mu_{Cc}\pi^{9/2}i}{\hbar^2 k_{Aa} k_{Bb} k_{Cc}} \frac{1}{\sqrt{(2j_i+1)(2j_f+1)}} \\
 &\times \sum_K \frac{1}{2K+1} ((l_f \frac{1}{2})_{j_f} (l_i \frac{1}{2})_{j_i} | (l_f l_i)_K (\frac{1}{2} \frac{1}{2})_0)_K^2 \\
 &\times \sum_{l_c, l} e^{i(\sigma_i^l + \sigma_f^l)} \frac{(2l_c + 1)}{\sqrt{2l + 1}} Y_0^l(\hat{k}_{Bb}) S_{K,l,l_c}, \tag{5.2.134}
 \end{aligned}$$

with

$$\begin{aligned}
 S_{K,l,l_c} &= \int r_{Cc}^2 dr_{Cc} r_{b1}^2 dr_{b1} \sin \theta d\theta v(r_{b1}) u_{l_f}(r_{C1}) u_{l_i}(r_{b1}) \\
 &\times \frac{s_{K,l,l_c}(r_{Cc})}{r_{Cc}} \frac{F_l(r_{Bb})}{r_{Bb}} \\
 &\times \sum_M \langle l_c 0 l M | K M \rangle [Y^{l_f}(\hat{r}_{C1}) Y^{l_i}(\theta + \pi, 0)]_M^K Y_M^{l*}(\hat{r}_{Bb}), \tag{5.2.135}
 \end{aligned}$$

and

$$\begin{aligned}
 s_{K,l,l_c}(r_{Cc}) &= \int r'_{Cc}^2 dr'_{Cc} r'^2_{A2} dr'_{A2} \sin \theta' d\theta' v(r'_{c2}) u_{l_f}(r'_{A2}) u_{l_i}(r'_{c2}) \\
 &\times \frac{F_l(r'_{Aa})}{r'_{Aa}} \frac{f_{l_c}(k_{Cc}, r_<) P_{l_c}(k_{Cc}, r_>)}{r'_{Cc}} \\
 &\times \sum_M \langle l_c 0 l M | K M \rangle [Y^{l_f}(\hat{r}'_{A2}) Y^{l_i}(\hat{r}'_{c2})]_M^{K*} Y_M^l(\hat{r}'_{Aa}). \tag{5.2.136}
 \end{aligned}$$

### 5.2.7 Coordinates for the successive transfer

In the standard configuration in which the integrals (5.2.135) and (5.2.136) are to be evaluated, we have

$$\mathbf{r}_{Cc} = r_{Cc} \hat{\mathbf{z}}, \quad \mathbf{r}_{b1} = r_{b1}(-\cos \theta \hat{\mathbf{z}} - \sin \theta \hat{\mathbf{x}}). \tag{5.2.137}$$

Now,

$$\begin{aligned}\mathbf{r}_{C1} &= \mathbf{r}_{Cc} + \mathbf{r}_{c1} = \mathbf{r}_{Cc} + \frac{m_b}{m_b + 1} \mathbf{r}_{b1} \\ &= \left( r_{Cc} - \frac{m_b}{m_b + 1} r_{b1} \cos \theta \right) \hat{\mathbf{z}} - \frac{m_b}{m_b + 1} r_{b1} \sin \theta \hat{\mathbf{x}},\end{aligned}\quad (5.2.138)$$

and

$$\mathbf{r}_{Bb} = \mathbf{r}_{BC} + \mathbf{r}_{Cb} = -\frac{1}{m_B} \mathbf{r}_{C1} + \mathbf{r}_{Cb}. \quad (5.2.139)$$

Substituting the relation

$$\mathbf{r}_{Cb} = \mathbf{r}_{Cc} + \mathbf{r}_{cb} = \mathbf{r}_{Cc} - \frac{1}{m_b + 1} \mathbf{r}_{b1}, \quad (5.2.140)$$

in (5.2.139) one gets

$$\mathbf{r}_{Bb} = \left( \frac{m_B - 1}{m_B} r_{Cc} + \frac{m_b + m_B}{m_B(m_b + 1)} r_{b1} \cos \theta \right) \hat{\mathbf{z}} + \frac{m_b + m_B}{m_B(m_b + 1)} r_{b1} \sin \theta \hat{\mathbf{x}}. \quad (5.2.141)$$

The primed variables are arranged in a similar fashion,

$$\mathbf{r}'_{Cc} = r'_{Cc} \hat{\mathbf{z}}, \quad \mathbf{r}'_{A2} = r'_{A2} (-\cos \theta' \hat{\mathbf{z}} - \sin \theta' \hat{\mathbf{x}}). \quad (5.2.142)$$

Thus,

$$\mathbf{r}'_{c2} = \left( -r'_{Cc} - \frac{m_A}{m_A + 1} r'_{A2} \cos \theta' \right) \hat{\mathbf{z}} - \frac{m_A}{m_A + 1} r'_{A2} \sin \theta' \hat{\mathbf{x}}, \quad (5.2.143)$$

and

$$\mathbf{r}'_{Aa} = \left( \frac{m_a - 1}{m_a} r'_{Cc} - \frac{m_A + m_a}{m_a(m_A + 1)} r'_{A2} \cos \theta' \right) \hat{\mathbf{z}} - \frac{m_A + m_a}{m_a(m_A + 1)} r'_{A2} \sin \theta' \hat{\mathbf{x}}. \quad (5.2.144)$$

### 5.2.8 Simplifying the vector coupling

We will now turn our attention to the vector-coupled quantities in (5.2.135) and (5.2.136),

$$\sum_M \langle l_c 0 l M | K M \rangle \left[ Y^{l_f}(\hat{r}_{C1}) Y^{l_i}(\theta + \pi, 0) \right]_M^K Y_M^{l_*}(\hat{r}_{Bb}), \quad (5.2.145)$$

and

$$\sum_M \langle l_c 0 l M | K M \rangle \left[ Y^{l_f}(\hat{r}_{A2}) Y^{l_i}(\hat{r}'_{c2}) \right]_M^{K*} Y_M^l(\hat{r}'_{Aa}). \quad (5.2.146)$$

We can express them both as

$$\sum_M f(M), \quad (5.2.147)$$

where e.g. in the case of (5.2.145), one has

$$f(M) = \langle l_c 0 l M | K M \rangle \left[ Y_f^{l_f}(\hat{r}_{C1}) Y_i^{l_i}(\theta + \pi, 0) \right]_M^K Y_M^{l_*}(\hat{r}_{Bb}). \quad (5.2.148)$$

Note that all the vectors that come into play in the above expressions are in the  $(x, z)$ -plane. Consequently, the azimuthal angle  $\phi$  is always equal to zero. Under these circumstances and for time-reversed phases, ( $Y_M^{L*}(\theta, 0) = (-1)^L Y_M^L(\theta, 0)$ ) one has

$$f(-M) = (-1)^{l_c + l_f + l_i + l} f(M). \quad (5.2.149)$$

Consequently,

$$\begin{aligned} \sum_M \langle l_c 0 l M | K M \rangle f(M) &= \langle l_c 0 l 0 | K 0 \rangle f(0) \\ &+ \sum_{M>0} \langle l_c 0 l M | K M \rangle f(M) \left( 1 + (-1)^{l_c + l + l_i + l_f} \right). \end{aligned} \quad (5.2.150)$$

Consequently, in the case in which  $l_c + l + l_i + l_f$  is odd, we have only to evaluate the  $M = 0$  contribution. This consideration is useful to restrict the number of numerical operations needed to calculate the transition amplitude.

### 5.2.9 non-orthogonality term

We write the non-orthogonality contribution to the transition amplitude (see Bayman and Chen (1982)):

$$\begin{aligned} T_{NO}^{(2)}(\theta) = & 2 \sum_{\substack{\sigma_1 \sigma_2 \\ \sigma'_1 \sigma'_2 \\ KM}} \int d^3 r_{Cc} d^3 r_{b1} d^3 r_{A2} d^3 r'_{b1} d^3 r'_{A2} \chi^{(-)*}(\mathbf{k}_{Bb}, \mathbf{r}_{Bb}) \\ & \times \left[ \psi^{j_f}(\mathbf{r}_{A1}, \sigma_1) \psi^{j_f}(\mathbf{r}_{A2}, \sigma_2) \right]_0^{0*} v(r_{b1}) \left[ \psi^{j_f}(\mathbf{r}_{A2}, \sigma_2) \psi^{j_i}(\mathbf{r}_{b1}, \sigma_1) \right]_M^K \\ & \times \left[ \psi^{j_f}(\mathbf{r}'_{A2}, \sigma'_2) \psi^{j_i}(\mathbf{r}'_{b1}, \sigma'_1) \right]_M^{K*} \left[ \psi^{j_i}(\mathbf{r}'_{b1}, \sigma'_1) \psi^{j_i}(\mathbf{r}'_{b2}, \sigma'_2) \right]_0^0 \chi^{(+)}(\mathbf{r}'_{Aa}). \end{aligned} \quad (5.2.151)$$

This expression is equivalent to (5.2.110) if we make the replacement

$$\frac{2\mu_{Cc}}{\hbar^2} G(\mathbf{r}_{Cc}, \mathbf{r}'_{Cc}) v(r'_{A2}) \rightarrow \delta(\mathbf{r}_{Cc} - \mathbf{r}'_{Cc}). \quad (5.2.152)$$

Looking at the partial-wave expansions of  $G(\mathbf{r}_{Cc}, \mathbf{r}'_{Cc})$  and  $\delta(\mathbf{r}_{Cc} - \mathbf{r}'_{Cc})$  (see App. 5.D), we find that we can use the above expressions for the successive transfer with the replacement

$$i \frac{2\mu_{Cc}}{\hbar^2} \frac{f_{l_c}(k_{Cc}, r_<) P_{l_c}(k_{Cc}, r_>)}{k_{Cc}} \rightarrow \delta(r_{Cc} - r'_{Cc}). \quad (5.2.153)$$

We thus have

$$\begin{aligned} T_{2NT}^{NO} = & \frac{512\pi^{9/2}}{k_{Aa}k_{Bb}} \frac{1}{\sqrt{(2j_i+1)(2j_f+1)}} \\ & \times \sum_K ((l_f \frac{1}{2})_{j_f} (l_i \frac{1}{2})_{j_i} | (l_f l_i)_K (\frac{1}{2} \frac{1}{2})_0)_K^2 \\ & \times \sum_{l_c, l} e^{i(\sigma_i^l + \sigma_f^l)} \frac{(2l_c+1)}{\sqrt{2l+1}} Y_0^l(\hat{k}_{Bb}) S_{K,l,l_c}, \end{aligned} \quad (5.2.154)$$

with

$$\begin{aligned} S_{K,l,l_c} = & \int r_{Cc}^2 dr_{Cc} r_{b1}^2 dr_{b1} \sin \theta d\theta v(r_{b1}) u_{l_f}(r_{C1}) u_{l_i}(r_{b1}) \\ & \times \frac{s_{K,l,l_c}(r_{Cc})}{r_{Cc}} \frac{F_l(r_{Bb})}{r_{Bb}} \\ & \times \sum_M \langle l_c 0 l M | K M \rangle [Y^{l_f}(\hat{r}_{C1}) Y^{l_i}(\theta + \pi, 0)]_M^K Y_M^{l*}(\hat{r}_{Bb}), \end{aligned} \quad (5.2.155)$$

and

$$\begin{aligned} s_{K,l,l_c}(r_{Cc}) = & r_{Cc} \int dr'_{A2} r'^2_{A2} \sin \theta' d\theta' u_{l_f}(r'_{A2}) u_{l_i}(r'_{c2}) \frac{F_l(r'_{Aa})}{r'_{Aa}} \\ & \times \sum_M \langle l_c 0 l M | K M \rangle [Y^{l_f}(\hat{r}'_{A2}) Y^{l_i}(\hat{r}'_{c2})]_M^{K*} Y_M^l(\hat{r}'_{Aa}). \end{aligned} \quad (5.2.156)$$

### 5.2.10 Arbitrary orbital momentum transfer

We will now examine the case in which the two transferred nucleons carry an angular momentum  $\Lambda$  different from 0. Let us assume that two nucleons coupled to angular momentum  $\Lambda$  in the initial nucleus  $a$  are transferred into a final state of zero angular momentum in nucleus  $B$ . The transition amplitude is given by the integral

$$\begin{aligned} 2 \sum_{\sigma_1 \sigma_2} \int d\mathbf{r}_{cC} d\mathbf{r}_{A2} d\mathbf{r}_{b1} \chi^{(-)*}(\mathbf{r}_{bB}) [\psi^{j_f}(\mathbf{r}_{A1}, \sigma_1) \psi^{j_f}(\mathbf{r}_{A2}, \sigma_2)]_0^{0*} \\ \times v(r_{b1}) \Psi^{(+)}(\mathbf{r}_{aA}, \mathbf{r}_{b1}, \mathbf{r}_{b2}, \sigma_1, \sigma_2). \end{aligned} \quad (5.2.157)$$

If we neglect core excitations, the above expression is exact as long as  $\Psi^{(+)}(\mathbf{r}_{aA}, \mathbf{r}_{b1}, \mathbf{r}_{b2}, \sigma_1, \sigma_2)$  is the exact wavefunction. We can instead obtain an approximation for the transfer amplitude using

$$\begin{aligned} \Psi^{(+)}(\mathbf{r}_{aA}, \mathbf{r}_{b1}, \mathbf{r}_{b2}, \sigma_1, \sigma_2) \approx & \chi^{(+)}(\mathbf{r}_{aA}) [\psi^{j_{i1}}(\mathbf{r}_{b1}, \sigma_1) \psi^{j_{i2}}(\mathbf{r}_{b2}, \sigma_2)]_\mu^\Lambda \\ & + \sum_{K,M} \mathcal{U}_{K,M}(\mathbf{r}_{cC}) [\psi^{j_f}(\mathbf{r}_{A2}, \sigma_2) \psi^{j_{i1}}(\mathbf{r}_{b1}, \sigma_1)]_M^K \end{aligned} \quad (5.2.158)$$

as an approximation for the incoming state. The first term of (5.2.158) gives rise to the simultaneous amplitude, while from second one leads to both the successive and the non-orthogonality contributions. To extract the amplitude  $\mathcal{U}_{K,M}(\mathbf{r}_{cC})$ , we define  $f_{KM}(\mathbf{r}_{cC})$  as the scalar product

$$f_{KM}(\mathbf{r}_{cC}) = \left\langle \left[ \psi^{j_f}(\mathbf{r}_{A2}, \sigma_2) \psi^{j_{i1}}(\mathbf{r}_{b1}, \sigma_1) \right]_M^K \middle| \Psi^{(+)}(\mathbf{r}_{aA}, \mathbf{r}_{b1}, \mathbf{r}_{b2}, \sigma_1, \sigma_2) \right\rangle \quad (5.2.159)$$

for fixed  $\mathbf{r}_{cC}$ , which can be seen to obey the equation

$$\begin{aligned} & \left( \frac{\hbar^2}{2\mu_{cC}} k_{cC}^2 + \frac{\hbar^2}{2\mu_{cC}} \nabla_{r_{cC}}^2 - U(r_{cC}) \right) f_{KM}(\mathbf{r}_{cC}) \\ &= \left\langle \left[ \psi^{j_f}(\mathbf{r}_{A2}, \sigma_2) \psi^{j_{i1}}(\mathbf{r}_{b1}, \sigma_1) \right]_M^K \middle| v(r_{c2}) \middle| \Psi^{(+)}(\mathbf{r}_{aA}, \mathbf{r}_{b1}, \mathbf{r}_{b2}, \sigma_1, \sigma_2) \right\rangle. \end{aligned} \quad (5.2.160)$$

The solution can be written in terms of the Green function  $G(\mathbf{r}_{cC}, \mathbf{r}'_{cC})$  defined by

$$\left( \frac{\hbar^2}{2\mu_{cC}} k_{cC}^2 + \frac{\hbar^2}{2\mu_{cC}} \nabla_{r_{cC}}^2 - U(r_{cC}) \right) G(\mathbf{r}_{cC}, \mathbf{r}'_{cC}) = \frac{\hbar^2}{2\mu_{cC}} \delta(\mathbf{r}_{cC} - \mathbf{r}'_{cC}). \quad (5.2.161)$$

Thus,

$$\begin{aligned} f_{KM}(\mathbf{r}_{cC}) &= \frac{2\mu_{cC}}{\hbar^2} \int d\mathbf{r}'_{cC} G(\mathbf{r}_{cC}, \mathbf{r}'_{cC}) \left\langle \left[ \psi^{j_f}(\mathbf{r}'_{A2}, \sigma'_2) \psi^{j_{i1}}(\mathbf{r}'_{b1}, \sigma'_1) \right]_M^K \middle| v(r_{c2}) \middle| \Psi^{(+)}(\mathbf{r}'_{aA}, \mathbf{r}'_{b1}, \mathbf{r}'_{b2}, \sigma'_1, \sigma'_2) \right\rangle \\ &\approx \frac{2\mu_{cC}}{\hbar^2} \sum_{\sigma'_1 \sigma'_2} \int d\mathbf{r}'_{cC} d\mathbf{r}'_{A2} d\mathbf{r}'_{b1} G(\mathbf{r}_{cC}, \mathbf{r}'_{cC}) \left[ \psi^{j_f}(\mathbf{r}'_{A2}, \sigma'_2) \psi^{j_{i1}}(\mathbf{r}'_{b1}, \sigma'_1) \right]_M^{K*} \\ &\quad \times v(r'_{c2}) \chi^{(+)}(\mathbf{r}'_{aA}) \left[ \psi^{j_{i1}}(\mathbf{r}'_{b1}, \sigma'_1) \psi^{j_{i2}}(\mathbf{r}'_{b2}, \sigma'_2) \right]_\mu^\Lambda = \mathcal{U}_{K,M}(\mathbf{r}_{cC}) \\ &\quad + \left\langle \left[ \psi^{j_f}(\mathbf{r}'_{A2}, \sigma_2) \psi^{j_{i1}}(\mathbf{r}'_{b1}, \sigma_1) \right]_M^K \middle| \chi^{(+)}(\mathbf{r}'_{aA}) \left[ \psi^{j_{i1}}(\mathbf{r}'_{b1}, \sigma'_1) \psi^{j_{i2}}(\mathbf{r}'_{b2}, \sigma'_2) \right]_\mu^\Lambda \right\rangle. \end{aligned} \quad (5.2.162)$$

Therefore

$$\begin{aligned} \mathcal{U}_{K,M}(\mathbf{r}_{cC}) &= \frac{2\mu_{cC}}{\hbar^2} \sum_{\sigma'_1 \sigma'_2} \int d\mathbf{r}'_{cC} d\mathbf{r}'_{A2} d\mathbf{r}'_{b1} G(\mathbf{r}_{cC}, \mathbf{r}'_{cC}) \left[ \psi^{j_f}(\mathbf{r}'_{A2}, \sigma'_2) \psi^{j_{i1}}(\mathbf{r}'_{b1}, \sigma'_1) \right]_M^{K*} \\ &\quad \times v(r'_{c2}) \chi^{(+)}(\mathbf{r}'_{aA}) \left[ \psi^{j_{i1}}(\mathbf{r}'_{b1}, \sigma'_1) \psi^{j_{i2}}(\mathbf{r}'_{b2}, \sigma'_2) \right]_\mu^\Lambda \\ &\quad - \left\langle \left[ \psi^{j_f}(\mathbf{r}'_{A2}, \sigma_2) \psi^{j_{i1}}(\mathbf{r}'_{b1}, \sigma_1) \right]_M^K \middle| \chi^{(+)}(\mathbf{r}'_{aA}) \left[ \psi^{j_{i1}}(\mathbf{r}'_{b1}, \sigma'_1) \psi^{j_{i2}}(\mathbf{r}'_{b2}, \sigma'_2) \right]_\mu^\Lambda \right\rangle. \end{aligned} \quad (5.2.163)$$

When we substitute  $\mathcal{U}_{K,M}(\mathbf{r}_{cC})$  into (5.2.158) and (5.2.157), the first term gives rise to the successive amplitude for the two-particle transfer, while the second term is responsible for the non-orthogonal contribution.

### 5.2.11 Successive transfer contribution

We need to evaluate the integral

$$\begin{aligned} T_{succ}^{(2)}(\theta; \mu) = & \frac{4\mu_{cC}}{\hbar^2} \sum_{\sigma_1 \sigma_2} \sum_{KM} \int d\mathbf{r}_{cC} d\mathbf{r}_{A2} d\mathbf{r}_{b1} d\mathbf{r}'_{cC} d\mathbf{r}'_{A2} d\mathbf{r}'_{b1} [\psi^{j_f}(\mathbf{r}_{A1}, \sigma_1) \psi^{j_f}(\mathbf{r}_{A2}, \sigma_2)]_0^{0*} \\ & \times \chi^{(-)*}(\mathbf{r}_{bB}) G(\mathbf{r}_{cC}, \mathbf{r}'_{cC}) [\psi^{j_f}(\mathbf{r}'_{A2}, \sigma'_2) \psi^{j_{i1}}(\mathbf{r}'_{b1}, \sigma'_1)]_M^{K*} \chi^{(+)}(\mathbf{r}'_{aA}) v(r'_{c2}) v(r_{b1}) \\ & \times [\psi^{j_{i1}}(\mathbf{r}'_{b1}, \sigma'_1) \psi^{j_{i2}}(\mathbf{r}'_{b2}, \sigma'_2)]_\mu^K [\psi^{j_f}(\mathbf{r}_{A2}, \sigma_2) \psi^{j_{i1}}(\mathbf{r}_{b1}, \sigma_1)]_M^K, \end{aligned} \quad (5.2.164)$$

where we must substitute the Green function and the distorted waves by their partial wave expansions (see App. 5.E). The integral over  $\mathbf{r}'_{b1}$  is:

$$\begin{aligned} & \sum_{\sigma'_1} \int d\mathbf{r}'_{b1} [\psi^{j_f}(\mathbf{r}'_{A2}, \sigma'_2) \psi^{j_{i1}}(\mathbf{r}'_{b1}, \sigma'_1)]_M^{K*} [\psi^{j_{i1}}(\mathbf{r}'_{b1}, \sigma'_1) \psi^{j_{i2}}(\mathbf{r}'_{b2}, \sigma'_2)]_\mu^K \\ = & \sum_{\sigma'_1} \int d\mathbf{r}'_{b1} (-1)^{-M+j_f+j_{i1}-\sigma_1-\sigma_2} [\psi^{j_{i1}}(\mathbf{r}'_{b1}, -\sigma'_1) \psi^{j_f}(\mathbf{r}'_{A2}, -\sigma'_2)]_{-M}^K [\psi^{j_{i1}}(\mathbf{r}'_{b1}, \sigma'_1) \psi^{j_{i2}}(\mathbf{r}'_{b2}, \sigma'_2)]_\mu^K \\ = & \sum_{\sigma'_1} \int d\mathbf{r}'_{b1} (-1)^{-M+j_f+j_{i1}-\sigma_1-\sigma_2} \sum_P \langle K \Lambda - M \mu | P \mu - M \rangle ((j_{i1} j_f)_K (j_{i1} j_{i2})_\Lambda | (j_{i1} j_{i1})_0 (j_f j_{i2})_P)_P \\ & \times [\psi^{j_{i1}}(\mathbf{r}'_{b1}, -\sigma'_1) \psi^{j_{i1}}(\mathbf{r}'_{b1}, \sigma'_1)]_0^0 [\psi^{j_f}(\mathbf{r}'_{A2}, -\sigma'_2) \psi^{j_{i2}}(\mathbf{r}'_{b2}, \sigma'_2)]_{\mu-M}^P \\ = & (-1)^{-M+j_f+j_{i1}} \sqrt{2j_{i1} + 1} u_{l_f}(r_{A2}) u_{l_{i2}}(r'_{b2}) \sum_P \langle K \Lambda - M \mu | P \mu - M \rangle \\ & \times ((j_{i1} j_f)_K (j_{i1} j_{i2})_\Lambda | (j_{i1} j_{i1})_0 (j_f j_{i2})_P)_P ((l_f \frac{1}{2})_{j_f} (l_{i2} \frac{1}{2})_{j_{i2}} | (l_f l_{i2})_P (\frac{1}{2} \frac{1}{2})_0)_P \\ & \times [Y^{l_f}(\hat{\mathbf{r}}'_{A2}) Y^{l_{i2}}(\hat{\mathbf{r}}'_{b2})]_{\mu-M}^P u_{l_f}(r_{A2}) u_{l_{i2}}(r_{b2}). \end{aligned} \quad (5.2.165)$$

Integrating over  $\mathbf{r}_{A2}$  (see (5.2.117)) leads to,

$$\begin{aligned} & \sum_{\sigma_2} \int d\mathbf{r}_{A2} [\psi^{j_f}(\mathbf{r}_{A1}, \sigma_1) \psi^{j_f}(\mathbf{r}_{A2}, \sigma_2)]_0^{0*} [\psi^{j_f}(\mathbf{r}_{A2}, \sigma_2) \psi^{j_{i1}}(\mathbf{r}_{b1}, \sigma_1)]_M^K \\ = & - \sqrt{\frac{2}{2j_f + 1}} ((l_f \frac{1}{2})_{j_f} (l_{i1} \frac{1}{2})_{j_{i1}} | (l_f l_{i1})_K (\frac{1}{2} \frac{1}{2})_0)_K [Y^{l_f}(\hat{\mathbf{r}}_{A1}) Y^{l_{i1}}(\hat{\mathbf{r}}_{b1})]_M^K u_{l_f}(r_{A1}) u_{l_{i1}}(r_{b1}). \end{aligned} \quad (5.2.166)$$

Let us examine the term

$$\sum_M (-1)^M \langle K \Lambda - M \mu | P \mu - M \rangle [Y^{l_f}(\hat{\mathbf{r}}_{A1}) Y^{l_{i1}}(\hat{\mathbf{r}}_{b1})]_M^K [Y^{l_f}(\hat{\mathbf{r}}'_{A2}) Y^{l_{i2}}(\hat{\mathbf{r}}'_{b2})]_{\mu-M}^P. \quad (5.2.167)$$

Making use of the relation

$$\langle l_1 l_2 m_1 m_2 | L M_L \rangle = (-1)^{l_2-m_2} \sqrt{\frac{2L+1}{2l_1+1}} \langle L l_2 - M_L m_2 | l_1 - m_1 \rangle, \quad (5.2.168)$$

the expression (5.2.168) is equivalent to,

$$(-1)^K \sqrt{\frac{2P+1}{2\Lambda+1}} \left\{ \left[ Y^{l_f}(\hat{\mathbf{r}}'_{A2}) Y^{l_{i2}}(\hat{\mathbf{r}}'_{b2}) \right]^P \left[ Y^{l_f}(\hat{\mathbf{r}}_{A1}) Y^{l_{i1}}(\hat{\mathbf{r}}_{b1}) \right]^K \right\}_\mu^\Lambda. \quad (5.2.169)$$

We now recouple the term

$$\left[ Y^{l_a}(\hat{\mathbf{r}}'_{aA}) Y^{l_a}(\hat{\mathbf{k}}_{aA}) \right]_0^0 \left[ Y^{l_b}(\hat{\mathbf{r}}_{bB}) Y^{l_b}(\hat{\mathbf{k}}_{bB}) \right]_0^0, \quad (5.2.170)$$

arising from the partial wave expansion of the incoming and outgoing distorted waves to have,

$$((l_a l_a)_0 (l_b l_b)_0 | (l_a l_b)_\Lambda (l_a l_b)_\Lambda)_0 \left\{ \left[ Y^{l_a}(\hat{\mathbf{r}}'_{aA}) Y^{l_b}(\hat{\mathbf{r}}_{bB}) \right]^\Lambda \left[ Y^{l_a}(\hat{\mathbf{k}}_{aA}) Y^{l_b}(\hat{\mathbf{k}}_{bB}) \right]^\Lambda \right\}_0^0. \quad (5.2.171)$$

The only term which does not vanish upon integration is

$$\frac{(-1)^{\Lambda-\mu}}{\sqrt{(2l_a+1)(2l_b+1)}} \left[ Y^{l_a}(\hat{\mathbf{r}}'_{aA}) Y^{l_b}(\hat{\mathbf{r}}_{bB}) \right]_{-\mu}^\Lambda \left[ Y^{l_a}(\hat{\mathbf{k}}_{aA}) Y^{l_b}(\hat{\mathbf{k}}_{bB}) \right]_\mu^\Lambda. \quad (5.2.172)$$

Again, the only term surviving

$$\left\{ \left[ Y^{l_f}(\hat{\mathbf{r}}'_{A2}) Y^{l_{i2}}(\hat{\mathbf{r}}'_{b2}) \right]^P \left[ Y^{l_f}(\hat{\mathbf{r}}_{A1}) Y^{l_{i1}}(\hat{\mathbf{r}}_{b1}) \right]^K \right\}_\mu^\Lambda \left[ Y^{l_a}(\hat{\mathbf{r}}'_{aA}) Y^{l_b}(\hat{\mathbf{r}}_{bB}) \right]_{-\mu}^\Lambda \quad (5.2.173)$$

is

$$\frac{(-1)^{\Lambda+\mu}}{\sqrt{2\Lambda+1}} \left[ \left\{ \left[ Y^{l_f}(\hat{\mathbf{r}}'_{A2}) Y^{l_{i2}}(\hat{\mathbf{r}}'_{b2}) \right]^P \right. \right. \\ \left. \left. \left[ Y^{l_f}(\hat{\mathbf{r}}_{A1}) Y^{l_{i1}}(\hat{\mathbf{r}}_{b1}) \right]^K \right\}^\Lambda \left[ Y^{l_a}(\hat{\mathbf{r}}'_{aA}) Y^{l_b}(\hat{\mathbf{r}}_{bB}) \right]_\mu^\Lambda \right]_0^0. \quad (5.2.174)$$

We now couple this last term with the term  $\left[ Y^{l_c}(\hat{\mathbf{r}}'_{cC}) Y^{l_c}(\hat{\mathbf{r}}_{cC}) \right]_0^0$ , arising from the partial wave expansion of the Green function. That is,

$$\begin{aligned}
& \left[ \left\{ \left[ Y^{l_f}(\hat{\mathbf{r}}'_{A2}) Y^{l_{i2}}(\hat{\mathbf{r}}'_{b2}) \right]^P \left[ Y^{l_f}(\hat{\mathbf{r}}_{A1}) Y^{l_{i1}}(\hat{\mathbf{r}}_{b1}) \right]^K \right\}^\Lambda \left[ Y^{l_a}(\hat{\mathbf{r}}'_{aA}) Y^{l_b}(\hat{\mathbf{r}}_{bB}) \right]^\Lambda \right]_0^0 \left[ Y^{l_c}(\hat{\mathbf{r}}'_{cC}) Y^{l_c}(\hat{\mathbf{r}}_{cC}) \right]_0^0 \\
&= ((l_a l_b)_\Lambda (l_c l_c)_0 | (l_a l_c)_P (l_b l_c)_K)_\Lambda \left[ \left\{ \left[ Y^{l_f}(\hat{\mathbf{r}}'_{A2}) Y^{l_{i2}}(\hat{\mathbf{r}}'_{b2}) \right]^P \left[ Y^{l_f}(\hat{\mathbf{r}}_{A1}) Y^{l_{i1}}(\hat{\mathbf{r}}_{b1}) \right]^K \right\}^\Lambda \right. \\
&\quad \left. \left\{ \left[ Y^{l_a}(\hat{\mathbf{r}}'_{aA}) Y^{l_c}(\hat{\mathbf{r}}'_{cC}) \right]^P \left[ Y^{l_b}(\hat{\mathbf{r}}_{bB}) Y^{l_c}(\hat{\mathbf{r}}_{cC}) \right]^K \right\}^\Lambda \right]_0^0 = ((l_a l_b)_\Lambda (l_c l_c)_0 | (l_a l_c)_P (l_b l_c)_K)_\Lambda \\
&\quad \times ((PK)_\Lambda (PK)_\Lambda | (PP)_0 (KK)_0)_0 \left\{ \left[ Y^{l_f}(\hat{\mathbf{r}}'_{A2}) Y^{l_{i2}}(\hat{\mathbf{r}}'_{b2}) \right]^P \left[ Y^{l_a}(\hat{\mathbf{r}}'_{aA}) Y^{l_c}(\hat{\mathbf{r}}'_{cC}) \right]^P \right\}_0^0 \\
&\quad \times \left\{ \left[ Y^{l_f}(\hat{\mathbf{r}}_{A1}) Y^{l_{i1}}(\hat{\mathbf{r}}_{b1}) \right]^K \left[ Y^{l_b}(\hat{\mathbf{r}}_{bB}) Y^{l_c}(\hat{\mathbf{r}}_{cC}) \right]^K \right\}_0^0 = ((l_a l_b)_\Lambda (l_c l_c)_0 | (l_a l_c)_P (l_b l_c)_K)_\Lambda \\
&\quad \times \sqrt{\frac{2\Lambda + 1}{(2K+1)(2P+1)}} \left\{ \left[ Y^{l_f}(\hat{\mathbf{r}}'_{A2}) Y^{l_{i2}}(\hat{\mathbf{r}}'_{b2}) \right]^P \left[ Y^{l_a}(\hat{\mathbf{r}}'_{aA}) Y^{l_c}(\hat{\mathbf{r}}'_{cC}) \right]^P \right\}_0^0 \\
&\quad \times \left\{ \left[ Y^{l_f}(\hat{\mathbf{r}}_{A1}) Y^{l_{i1}}(\hat{\mathbf{r}}_{b1}) \right]^K \left[ Y^{l_b}(\hat{\mathbf{r}}_{bB}) Y^{l_c}(\hat{\mathbf{r}}_{cC}) \right]^K \right\}_0^0. \tag{5.2.175}
\end{aligned}$$

Collecting all the contributions (including the constants and phases arising from the partial wave expansion of the distorted waves and the Green function), we get

$$\begin{aligned}
T_{succ}^{(2)}(\theta; \mu) &= (-1)^{j_f + j_{i1}} \frac{2048\pi^5 \mu_{Cc}}{\hbar^2 k_{Aa} k_{Bb} k_{Cc}} \sqrt{\frac{(2j_{i1} + 1)}{(2\Lambda + 1)(2j_f + 1)}} \sum_{K,P} ((l_f \frac{1}{2})_{j_f} (l_{i2} \frac{1}{2})_{j_{i2}} | (l_f l_{i2})_P (\frac{1}{2} \frac{1}{2})_0)_P \\
&\quad \times ((l_f \frac{1}{2})_{j_f} (l_{i1} \frac{1}{2})_{j_{i1}} | (l_f l_{i1})_K (\frac{1}{2} \frac{1}{2})_0)_K ((j_{i1} j_f)_K (j_{i1} j_{i2})_\Lambda | (j_{i1} j_{i1})_0 (j_f j_{i2})_P)_P \\
&\quad \times \frac{(-1)^K}{(2K+1)\sqrt{2P+1}} \sum_{l_c, l_a, l_b} ((l_a l_b)_\Lambda (l_c l_c)_0 | (l_a l_c)_P (l_b l_c)_K)_\Lambda e^{i(\sigma_i^{l_a} + \sigma_f^{l_b})} i^{l_a - l_b} \\
&\quad \times (2l_c + 1)^{3/2} \left[ Y^{l_a}(\hat{\mathbf{k}}_{aA}) Y^{l_b}(\hat{\mathbf{k}}_{bB}) \right]_\mu^K S_{K,P,l_a,l_b,l_c}, \tag{5.2.176}
\end{aligned}$$

with (note that we have reduced the dimensionality of the integrals in the same fashion as for the  $L=0$ -angular momentum transfer calculation, see (5.2.132))

$$\begin{aligned}
S_{K,P,l_a,l_b,l_c} &= \int r_{Cc}^2 dr_{Cc} r_{b1}^2 dr_{b1} \sin \theta d\theta v(r_{b1}) u_{l_f}(r_{C1}) u_{l_i}(r_{b1}) \\
&\quad \times \frac{s_{P,l_a,l_c}(r_{Cc})}{r_{Cc}} \frac{F_{l_b}(r_{Bb})}{r_{Bb}} \\
&\quad \times \sum_M \langle l_c 0 l_b M | K M \rangle \left[ Y^{l_f}(\hat{r}_{C1}) Y^{l_{i1}}(\theta + \pi, 0) \right]_M^K Y_{-M}^{l_b}(\hat{r}_{Bb}), \tag{5.2.177}
\end{aligned}$$

and

$$\begin{aligned} s_{P,l_a,l_c}(r_{Cc}) &= \int r'_{Cc}^2 dr'_{Cc} r'^2_{A2} dr'_{A2} \sin \theta' d\theta' v(r'_{c2}) u_{l_f}(r'_{A2}) u_{l_i}(r'_{c2}) \\ &\times \frac{F_{l_a}(r'_{Aa}) f_{l_c}(k_{Cc}, r_<) P_{l_c}(k_{Cc}, r_>)}{r'_{Aa} r'_{Cc}} \\ &\times \sum_M \langle l_c 0 l_a M | P M \rangle \left[ Y^{l_f}(\hat{r}'_{A2}) Y^{l_{i2}}(\hat{r}'_{c2}) \right]_M^P Y^{l_a}_{-M}(\hat{r}'_{Aa}). \end{aligned} \quad (5.2.178)$$

We have evaluated the transition matrix element for a particular projection  $\mu$  of the initial angular momentum of the two transferred nucleons. If they are coupled to a core of angular momentum  $J_f$  to total angular momentum  $J_i, M_i$ , the fraction of the initial wavefunction with projection  $\mu$  is  $\langle \Lambda \mu J_f M_i - \mu | J_i M_i \rangle$ , and the cross section will be

$$\frac{d\sigma}{d\Omega}(\hat{\mathbf{k}}_{bB}) = \frac{k_{bB}}{k_{aA}} \frac{\mu_{aA}\mu_{bB}}{(2\pi\hbar^2)^2} \left| \sum_\mu \langle \Lambda \mu J_f M_i - \mu | J_i M_i \rangle T_{succ}^{(2)}(\theta; \mu) \right|^2. \quad (5.2.179)$$

For a non polarized incident beam,

$$\frac{d\sigma}{d\Omega}(\hat{\mathbf{k}}_{bB}) = \frac{k_{bB}}{k_{aA}} \frac{\mu_{aA}\mu_{bB}}{(2\pi\hbar^2)^2} \frac{1}{2J_i + 1} \sum_{M_i} \left| \sum_\mu \langle \Lambda \mu J_f M_i - \mu | J_i M_i \rangle T_{succ}^{(2)}(\theta; \mu) \right|^2. \quad (5.2.180)$$

This would be the differential cross section for a transition to a definite final state  $M_f$ . If we do not measure  $M_f$  we have to sum for all  $M_f$ ,

$$\frac{d\sigma}{d\Omega}(\hat{\mathbf{k}}_{bB}) = \frac{k_{bB}}{k_{aA}} \frac{\mu_{aA}\mu_{bB}}{(2\pi\hbar^2)^2} \frac{1}{2J_i + 1} \sum_\mu |T_{succ}^{(2)}(\theta; \mu)|^2 \sum_{M_i, M_f} |\langle \Lambda \mu J_f M_f | J_i M_i \rangle|^2. \quad (5.2.181)$$

The sum over  $M_i, M_f$  of the Clebsh–Gordan coefficients gives  $(2J_i + 1)/(2\Lambda + 1)$  (see Eq. (5.D.26)). One then gets,

$$\frac{d\sigma}{d\Omega}(\hat{\mathbf{k}}_{bB}) = \frac{k_{bB}}{k_{aA}} \frac{\mu_{aA}\mu_{bB}}{(2\pi\hbar^2)^2} \frac{1}{(2\Lambda + 1)} \sum_\mu |T_{succ}^{(2)}(\theta; \mu)|^2, \quad (5.2.182)$$

where one can write

$$\begin{aligned} T_{succ}^{(2)}(\theta; \mu) &= \sum_{l_a, l_b} C_{l_a, l_b} \left[ Y^{l_a}(\hat{\mathbf{k}}_{aA}) Y^{l_b}(\hat{\mathbf{k}}_{bB}) \right]_\mu^\Lambda \\ &= \sum_{l_a, l_b} C_{l_a, l_b} i^{l_a} \sqrt{\frac{2l_a + 1}{4\pi}} \langle l_a l_b 0 \mu | \Lambda \mu \rangle Y_\mu^{l_b}(\hat{\mathbf{k}}_{bB}). \end{aligned} \quad (5.2.183)$$

Note that (5.2.182) takes into account only the spins of the heavy nucleus. In a  $(t, p)$  or  $(p, t)$  reaction, we have to sum over the spins of the proton and of the triton

and divide by 2. If a spin-orbit term is present in the optical potential, the sum yields the combination of terms shown in Section (5.2.2),

$$\frac{d\sigma}{d\Omega}(\hat{\mathbf{k}}_{bB}) = \frac{k_B}{k_{aA}} \frac{\mu_{aA}\mu_{bB}}{(2\pi\hbar^2)^2} \frac{1}{2(2\Lambda+1)} \sum_{\mu} |A_{\mu}|^2 + |B_{\mu}|^2. \quad (5.2.184)$$

## Appendix 5.A ZPF and Pauli principle at the basis of medium polarization effects: self-energy, vertex corrections and induced interaction

In keeping with a central objective of the formulation of quantum mechanics, namely that the basic concepts on which it is based relate directly to experiment<sup>2</sup> (Heisenberg (1925)), elementary modes of nuclear excitation (single-particle, collective vibrations and rotations), are solidly anchored on observation (inelastic and Coulomb excitation, one- and two-particle transfer reactions). Of all quantal phenomena, zero point fluctuations (ZPF), closely connected with virtual states, are likely to be most representative of the essential difference existing between quantum and classical mechanics. In fact, ZPF are intimately connected with the complementary principle (Bohr (1928)), and thus with indeterminacy (Heisenberg (1927)) and non-commutative (Born and Jordan (1925), Born et al. (1926)) relations, and with the probabilistic interpretation (Born, 1926) of the (modulus squared) of the wavefunctions, solution of Schrödinger's or Dirac's equations (Schrödinger, E. (1926), Dirac (1930)). Pauli principle (Pauli, 1925) brings about

Figure 5.A.1: Nuclear field theory (NFT) diagrams describing renormalization processes associated with ZPF. For details cf. caption to Fig. 5.A.2.

essential modifications of the virtual fluctuations of the many-body system, modifications which are instrumental in the dressing and interweaving of the elementary modes of excitation (within the present context, see also Schrieffer (1964)).

In Fig. 5.A.1, NFT diagrams are given which correspond to the lowest order medium polarization effects renormalizing the properties of a particle-hole collective mode (wavy line), correlated particle-hole excitation which in the shell model basis corresponds to a linear combination of particle-hole excitations ((up-going)-(down-going) arrowed lines) calculated within the random phase approx-

---

<sup>2</sup>The abstract of this reference reads: “In this paper it will be attempted to secure foundations for a quantum theoretical mechanics which is exclusively based on relations between quantities which in principle are observables”. Within the present context, namely that of probing the nuclear structure (e.g. pairing correlations) with direct nuclear reactions, in particular Cooper pair transfer, one can hardly think of a better *incipit* for the introduction of elementary modes of excitation, modes which carry within them most of the correlations thus requiring for their theoretical treatment an effective field theory, like e.g. NFT to properly take into account the essential overcompleteness of the basis (non-orthogonality) as well as of Pauli violating processes.

Figure 5.A.2: Pauli effects associated (p-h) ZPF dressing a pairing vibrational (pair addition) mode (see inset I) in terms of self-energy (graphs (a)–(c); correlation (CO) and polarization (PO) diagrams, inset II) and vertex correction (graphs (d)–(f); induced particle-particle (pairing) interaction, ) processes (inset (III)), associated with phonon exchange (inset (IV)).

imation (RPA), and leading to the particle-vibration coupling vertex (formfactor and strength, i.e. transition density (solid dot), see inset (I), bottom). The action of an external field on the zero point fluctuations (ZPF) of the vacuum (inset (II)), forces a virtual process to become real, leading to a collective vibration by annihilating a (virtual, spontaneous) particle-hole excitation (backwards RPA amplitude) or, in the time ordered process, by creating a particle-hole excitation which eventually, through the particle-vibration coupling vertex, correlate into the collective (coherent) state (forwardgoing amplitudes). Now, oyster-like diagrams associated with the vacuum ZPF can occur at any time (see inset (III)). Because the texture of the vacuum is permeated by symmetry rules (while one can violate energy conservation in a virtual state one cannot violate e.g. angular momentum conservation or the Pauli principle), the process shown in the inset III ( $\alpha$ ) leads, through Pauli principle correcting processes (exchange of fermionic arrowed lines) to self-energy (inset III ( $\beta$ ), ( $\delta$ )) and vertex corrections (induced p-h interaction; inset III ( $\gamma$ ), ( $\varepsilon$ )) processes (phonon exchange, cf. inset (IV) of Fig. 5.A.2). The first ones are detailed in graphs (a)–(f), while the second ones in graphs (g)–(i). In keeping with the fact that the vibrational states can be viewed as a coherent state exhausting a consistent fraction of the EWSR (e.g. a Giant Resonance) for which the associated uncertainty relations in momentum and coordinate fulfills the absolute minimum consistent with quantum mechanics ( $\Delta\alpha_{\lambda\mu}\Delta\pi_{\lambda\mu} = \hbar/2$ ,  $\alpha_{\lambda\mu} = (\hbar\omega_{\lambda}/2C_{\lambda}^{1/2})(\Gamma_{\lambda\mu}^{\dagger} + \Gamma_{\lambda\mu})$  being the (harmonic) collective coordinate,  $\pi_{\lambda\mu}$  being the conjugate momentum, cf. e.g. Glauber (1969)), there is a strong cancellation between the contribution of self-energy and vertex correction diagrams (Bortignon and Broglia, 1981), implying small anharmonicities and long lifetimes ( $\Gamma/E \ll 1$ , where  $\Gamma$  is the width and  $E$  the centroid of the mode  $|\lambda\mu\rangle = \Gamma_{\lambda\mu}^{\dagger}|0\rangle$ ,  $(\hbar\omega_{\lambda}/2C_{\lambda})^{1/2}$  being the ZPF amplitude (cf. e.g. Brink, D. and Broglia (2005))).

## Appendix 5.B Coherence and effective formfactors

In what follows we shall work out a simplified derivation of the simultaneous two-nucleon transfer amplitude, within the framework of first order DWBA specially suited to discuss correlation aspects of pair transfer in general, and of the associated effective formfactors in particular.

We will concentrate on  $(t, p)$  reaction, namely reactions of the type  $A(\alpha, \beta)B$  where  $\alpha = \beta + 2$  and  $B = A + 2$ .

The intrinsic wave functions are in this case

$$\begin{aligned}\psi_\alpha &= \psi_{M_i}^{J_i}(\xi_A) \sum_{ss'_f} \left[ \chi^s(\sigma_\alpha) \chi^{s'_f}(\sigma_\beta) \right]_{M_{s_i}}^{s_i} \phi_t^{L=0} \left( \sum_{i<j} |\vec{r}_i - \vec{r}_j| \right) \\ &= \psi_{M_i}^{J_i}(\xi_A) \sum_{M_s M'_{s_f}} (s M'_s s'_f M'_{s_f} |s_i M_{s_i}) \chi_{M'_s}^s(\sigma_\alpha) \chi_{M'_{s_f}}^{s'_f}(\sigma_\beta) \\ &\quad \times \phi_t^{L=0} \left( \sum_{i<j} |\vec{r}_i - \vec{r}_j| \right)\end{aligned}\quad (5.B.1)$$

while

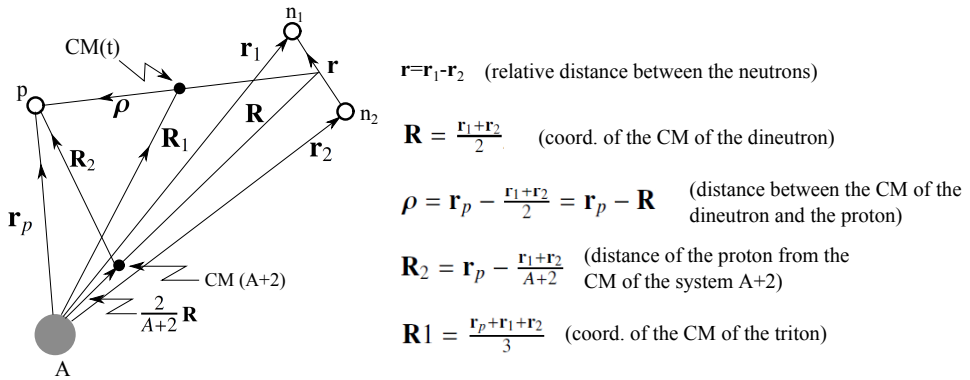


Figure 5.B.1: Coordinate system used in the calculation of the two–nucleon transfer amplitude.

$$\begin{aligned}\psi_\beta &= \psi_{M_f}^{J_f}(\xi_{A+2}) \chi_{M_{s_f}}^{s_f}(\sigma_\beta) \\ &= \sum_{\substack{n_1 l_1 j_1 \\ n_2 l_2 j_2}} B(n_1 l_1 j_1, n_2 l_2 j_2; J J'_i J_f) \left[ \phi^J(j_1 j_2) \phi^{J'_i}(\xi_A) \right]_{M_f}^{J_f} \\ &\quad \times \chi_{M_{s_f}}^{s_f}(\sigma_\beta)\end{aligned}\quad (5.B.2)$$

Making use of the above equation one can define the spectroscopic amplitude  $B$  as

$$\begin{aligned}B(n_1 l_1 j_1, n_2 l_2 j_2; J J'_i J_f) \\ = \left\langle \psi^{J_f}(\xi_{A+2}) \left[ \phi^J(j_1 j_2) \phi^{J_i}(\xi_A) \right]^{J_f} \right\rangle,\end{aligned}\quad (5.B.3)$$

where

$$\phi^J(j_1 j_2) = \frac{\left[ \phi_{j_1}(\vec{r}_1) \phi_{j_2}(\vec{r}_2) \right]^J - \left[ \phi_{j_1}(\vec{r}_2) \phi_{j_2}(\vec{r}_1) \right]^J}{\sqrt{1 + \delta(j_1, j_2)}},\quad (5.B.4)$$

is an antisymmetrized, normalized wave function of the two transferred particles. The function  $\chi_{M_s}^s(\sigma_\beta)$  appearing both in eq. (5.B.1) and (5.B.2) is the spin wave function of the proton while

$$\chi^s(\sigma_\alpha) = [\chi^{s_1}(\sigma_{n_1})\chi^{s_2}(\sigma_{n_2})]^s, \quad (5.B.5)$$

is the spin function of the two-neutron system.

A convenient description of the intrinsic degrees of freedom of the triton is obtained by using a wavefunction symmetric in the coordinates of all particles, i.e.

$$\begin{aligned} \phi_t^{L=0} \left( \sum_{i < j} |\vec{r}_i - \vec{r}_j| \right) &= N_t e^{[(r_1 - r_2)^2 + (r_1 - r_p)^2 + (r_2 - r_p)^2]} \\ &= \phi_{000}(\vec{r})\phi_{000}(\vec{\rho}), \end{aligned} \quad (5.B.6)$$

where

$$\phi_{000}(\vec{r}) = R_{nl}(v^{1/2}r)Y_{lm}(\hat{r}). \quad (5.B.7)$$

The coordinate  $\vec{\rho}$  is the radius vector which measures the distance between the center of mass of the dineutron and the proton, while the vector  $\vec{r}$  is the dineutron relative coordinate (cf. Fig. 5.B.1).

To obtain the DWBA cross section we have to calculate the integral

$$T(\theta) = \int d\xi_A d\vec{r}_1 d\vec{r}_2 d\vec{r}_p \chi_p^{(-)}(\vec{R}_2) \psi_\beta^*(\xi_{A+2}, \sigma_\beta) V_\beta \psi_\alpha(\xi_A, \sigma_\alpha, \sigma_\beta) \psi_t^{(+)}(\vec{R}_1) \quad (5.B.8)$$

where the final state effective interaction  $V_\beta(\rho)$  is assumed to depend only on the distance  $\rho$  between the center of mass of the di-neutron and of the proton. Instead of integrating over  $\xi_A, \vec{r}_1, \vec{r}_2$  and  $\vec{r}_p$  we would integrate over  $\xi_A, \vec{r}, \vec{r}'$  and  $\vec{r}_p$ . The Jacobian of the transformation is equal to 1, i.e.  $\partial(\vec{r}_1, \vec{r}_2)/\partial(\vec{r}, \vec{r}') = 1$ .

To carry out the integral (5.B.8) we transform the wave function (5.B.4) into center of mass and relative coordinates. If we assume that both  $\phi_{j_1}(\vec{r}_1)$  and  $\phi_{j_2}(\vec{r}_2)$  are harmonic oscillator wave functions (used as a basis to expand the Saxon-Woods single-particle wavefunctions), this transformation can be carried with the aid of the Moshinsky brackets. If  $|n_1 l_1, n_2 l_2; \lambda \mu\rangle$  is a complete system of wave functions in the harmonic oscillator basis, depending on  $\vec{r}_1$  and  $\vec{r}_2$  and  $|nl, NL; \lambda \mu\rangle$  is the corresponding one depending on  $\vec{r}$  and  $\vec{R}$ , we can write

$$\begin{aligned} |n_1 l_1, n_2 l_2; \lambda \mu\rangle &= \sum_{nlNL} |nl, NL; \lambda \mu\rangle \langle nl, NL; \lambda \mu| |n_1 l_1, n_2 l_2; \lambda \mu\rangle \\ &= \sum_{nlNL} |nl, NL; \lambda \mu\rangle \langle nl, NL; \lambda \mu| n_1 l_1, n_2 l_2; \lambda \rangle \end{aligned} \quad (5.B.9)$$

The labels  $n, l$  are the principal and angular momentum quantum numbers of the relative motion, while  $N, L$  are the corresponding ones corresponding to the

center of mass motion of the two-neutron system. Because of energy and parity conservation we have

$$\begin{aligned} 2n_1 + l_1 + 2n_2 + l_2 &= 2n + l + 2N + L \\ (-1)^{l_1+l_2} &= (-1)^{l+L}. \end{aligned} \quad (5.B.10)$$

The coefficients  $\langle nl, NL, L | n_1 l_1, n_2 l_2, L \rangle$  are tabulated and were first discussed by (Moshinsky, 1959)

With the help of eq. (5.B.9) we can write the wave function  $\psi_{M_f}^{J_f}(\xi_{A+2})$  as

$$\begin{aligned} \psi_{M_f}^{J_f}(\xi_{A+2}) &= \sum_{\substack{n_1 l_1 j_1 \\ n_2 l_2 j_2 \\ JJ_i}} B(n_1 l_1 j_1, n_2 l_2 j_2; JJ'_i J_f) [\phi^J(j_1 j_2) \phi^{J'_i}(\xi_A)]_{M_f}^{J_f} \\ &= \sum_{\substack{n_1 l_1 j_1 \\ n_2 l_2 j_2}} \sum_{JJ_i} B(n_1 l_1 j_1, n_2 l_2 j_2; JJ'_i J_f) \\ &\quad \times \sum_{M_J M'_{J_i}} \langle JM_J J'_i M_{J_i} | J_f M_{J_f} \rangle \psi_{M'_{J_i}}^{J'_i}(\xi_A) \\ &\quad \times \sum_{LS'} \langle S' LJ | j_1 j_2 J \rangle \sum_{M_L M'_S} \langle LM_L S' M'_S | JM_J \rangle \chi_{M'_S}^{S'}(\sigma_\alpha) \\ &\quad \times \sum_{nlN\Lambda} \langle nl, N\Lambda, L | n_1 l_1, n_2 l_2, L \rangle \\ &\quad \times \sum_{m_l M_\Lambda} \langle lm_l \Lambda M_\Lambda | LM_L \rangle \phi_{nlm_l}(\vec{r}) \phi_{N\Lambda M_\Lambda}(\vec{R}) \end{aligned} \quad (5.B.11)$$

Integration over  $\vec{r}$  gives

$$\langle \phi_{nlm_l}(\vec{r}) | \phi_{000}(\vec{r}) \rangle = \delta(l, 0) \delta(m_l, 0) \Omega_n \quad (5.B.12)$$

where

$$\Omega_n = \int R_{nl}(\nu_1^{1/2} r) R_{00}(\nu_2^{1/2} r) r^2 dr \quad (5.B.13)$$

Note that there is no selection rule in the principal quantum number  $n$ , as the potential in which the two neutrons move in the triton has a frequency  $\nu_2$  which is different from the one that the two neutrons are subjected to, when moving in the system  $A$  (non-orthogonality effect).

Integration over  $\xi_A$  and multiplication of the spin functions gives

$$\begin{aligned} (\psi_{M_{J_i}}^{J_i}, V'_\beta(\rho) \psi_{M'_{J_i}}^{J'_i}) &= \delta(J_i, J'_i) \delta(M_{J_i}, M_{J'_i}) V(\rho), \\ (\chi_{M_S}^S(\sigma_\alpha), \chi_{M'_S}^{S'}(\sigma_\alpha)) &= \delta(S, S') \delta(M_S, M_{S'}), \\ (\chi_{M_{S_f}}^{S_f}(\sigma_\beta), \chi_{M'_{S_f}}^{S'_f}(\sigma_\beta)) &= \delta(S_f, S'_f) \delta(M_{S_f}, M_{S'_f}). \end{aligned} \quad (5.B.14)$$

The integral (5.B.8) can then be written as

$$\begin{aligned}
T(\theta) = & \sum_{n_1 l_1 j_1} \sum_{JM_J} \sum_{nN} \sum_S B(n_1 l_1 j_1, n_2 l_2 j_2; JJ'_i J_f) \\
& \times \langle JM_J J_i M_{J_i} | J_f M_{J_f} \rangle \langle SLJ | j_1 j_2 J \rangle \\
& \times \langle LM_L S M_S | JM_J \rangle \langle n0, NL, L | n_1 l_1, n_2 l_2, L \rangle \\
& \times \langle S M_S S_f M_{S_f} | S_i M_{S_i} \rangle \Omega_n \\
& \times \int d\vec{R} d\vec{r}_p \chi_t^{(+)*}(\vec{R}_1) \phi_{NLM_L}^*(\vec{R}) V(\rho) \phi_{000}(\vec{\rho}) \chi_t^{(+)}(\vec{R}_1),
\end{aligned} \tag{5.B.15}$$

where we have approximated  $V'_\beta$  by an effective interaction depending on  $\rho = |\vec{\rho}|$ .

We now define the effective two-nucleon transfer form factor as

$$\begin{aligned}
u_{LSJ}^{j_i J_f}(R) = & \sum_{n_1 l_1 j_1} B(n_1 l_1 j_1, n_2 l_2 j_2; JJ_i J_f) \langle SLJ | j_1 j_2 J \rangle \\
& \langle n0, NL, L | n_1 l_1, n_2 l_2; L \rangle \Omega_n R_{nL}(R).
\end{aligned} \tag{5.B.16}$$

We can now rewrite eq. (5.B.15) as

$$\begin{aligned}
T(\theta) = & \sum_J \sum_L \sum_S (JM_J J_i M_{J_i} | J_f M_{J_f} ) (S M_S S_f M_{S_f} | S_i M_{S_i} ) (LM_L S M_S | JM_J ) \\
& \times \int d\vec{R} d\vec{r}_p \chi_p^{*(-)}(\vec{R}_2) u_{LSJ}^{j_i J_f}(R) Y_{LM_L}^* V(\rho) \phi_{000}(\vec{\rho}) \chi_t^{(+)}(\vec{R}_1).
\end{aligned} \tag{5.B.17}$$

Because the di-neutron has  $S = 0$ , we have that

$$(LM_L 00 | JM_J) = \delta(J, L) \delta(M_L, M_J), \tag{5.B.18}$$

and the summations over  $S$  and  $L$  disappear from eq. (5.B.17). Let us now make also here, as done in App. 4.F, Eq. (4.F.15) for one-particle transfer reactions, the zero range approximation, that is,

$$V(\rho) \phi_{000}(\vec{\rho}) = D_0 \delta(\vec{\rho}). \tag{5.B.19}$$

This means that the proton interacts with the center of mass of the di-neutron, only when they are at the same point in space. Within this approximation (cf. Fig. 5.B.1)

$$\begin{aligned}
\vec{R} = & \vec{R}_1 = \vec{r}, \\
\vec{R}_2 = & \frac{A}{A+2} \vec{R},
\end{aligned} \tag{5.B.20}$$

Then Eq. (5.B.15) can be written as

$$T = D_0 \sum_L (LM_L J_i M_{J_i} | J_f M_{J_f}) \\ \times \int d\vec{R} \chi_p^{*(-)} \left( \frac{A}{A+2} \vec{R} \right) u_L^{J_i J_f}(R) Y_{LM_L}^*(\hat{R}) \chi_t^{(+)}(\vec{R}) \quad (5.B.21)$$

From Eq. (5.B.21) it is seen that the change in parity implied by the reaction is given by  $\Delta\pi = (-1)^L$ . Consequently, the selection rules for  $(t, p)$  and  $(p, t)$  reactions in zero-range approximation are,

$$\begin{aligned} \Delta S &= 0 \\ \Delta J &= \Delta L = L \\ \Delta\pi &= (-1)^L \end{aligned} \quad (5.B.22)$$

i.e. only normal parity states are excited.

The integral appearing in Eq. (5.B.21) has the same structure as the DWBA integral appearing in Eq. (4.F.16) which was derived for the case of one-nucleon transfer reactions.

The difference between the two processes manifests itself through the different structure of the two form factors. While  $u_l(r)$  is a single-particle bound state wave function (cf. Eq. (4.F.1a)),  $u_L^{J_i J_f}$  is a coherent summation over the center of mass states of motion of the two transferred neutrons (see Eq. (5.B.16)). In other words, an effective quantity (function). It is of notice that this difference essentially vanishes, when one considers dressed particles resulting from the coupling to collective motion, and leading, among other things, to  $\omega$ -dependent effective masses. Examples of two-nucleon transfer form factors are given in Figs 5.B.2, 5.B.3 and 5.B.4.

### Appendix 5.C Relative importance of successive and simultaneous transfer and non-orthogonality corrections

In what follows we discuss the relative importance of successive and simultaneous two-neutron transfer and of non-orthogonality corrections associated with the reaction

$$\alpha \equiv a (= b + 2) + A \rightarrow b + B (= A + 2) \equiv \beta \quad (5.C.1)$$

in the limits of independent particles and of strongly correlated Cooper pairs, making use for simplicity of the semiclassical approximation (for details cf. Broglia and Winther (2004), Broglia and refs. therein), in which case the two-particle transfer differential cross section can be written as

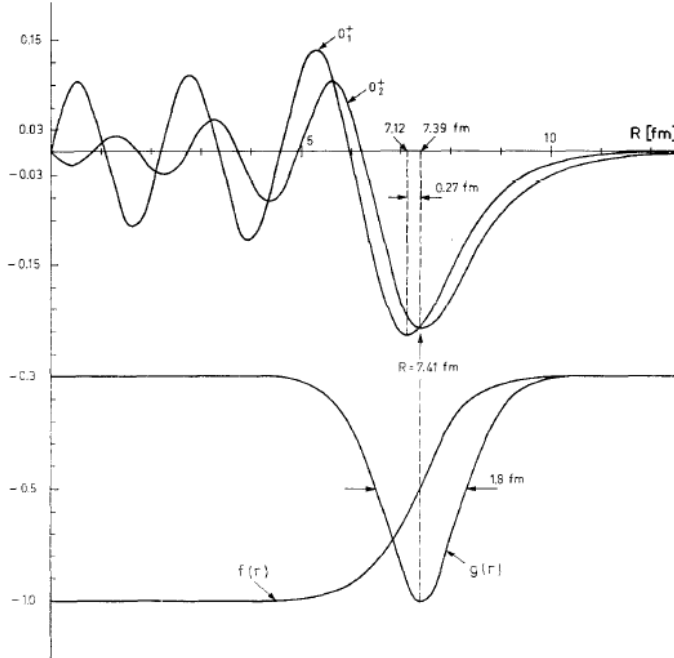


Figure 5.B.2: The upper part of the figure shows the modified formfactor for the  $^{206}\text{Pb}(t,p)^{208}\text{Pb}$  transition to the ground state ( $0_1^+$ ) and the pairing vibrational state ( $0_2^+$ ) at 4.87 MeV. Both curves are matched with appropriate Hankel functions. In the lower part the form factors of the real ( $f(r)$ ) and the imaginary ( $g(r)$ ) part of the optical potential used to calculate the differential cross sections (cf. Fig. 3.4.4), are given in the same scale for the radius. After Broglia and Riedel (1967).

$$\frac{d\sigma_{\alpha \rightarrow \beta}}{d\Omega} = P_{\alpha \rightarrow \beta}(t = +\infty) \sqrt{\left( \frac{d\sigma_\alpha}{d\Omega} \right)_{el}} \sqrt{\left( \frac{d\sigma_\beta}{d\Omega} \right)_{el}}, \quad (5.C.2)$$

where  $P$  is the absolute value squared of a quantum mechanical transition amplitude. It gives the probability that the system at  $t = +\infty$  is found in the final channel. The quantities  $(d\sigma/d\Omega)_{el}$  are the classical elastic cross sections in the center of mass system, calculated in terms of the deflection function, namely the functional relating the impact parameter and the scattering angle.

The transfer amplitude can be written as

$$a(t = +\infty) = a^{(1)}(\infty) - a^{(NO)}(\infty) + \tilde{a}^{(2)}(\infty), \quad (5.C.3)$$

where  $\tilde{a}^{(2)}(\infty)$  at  $t = +\infty$  labels the successive transfer amplitude expressed in the post-prior representation (see below). The simultaneous transfer amplitude is given by (see Fig. 5.C.1 (I))

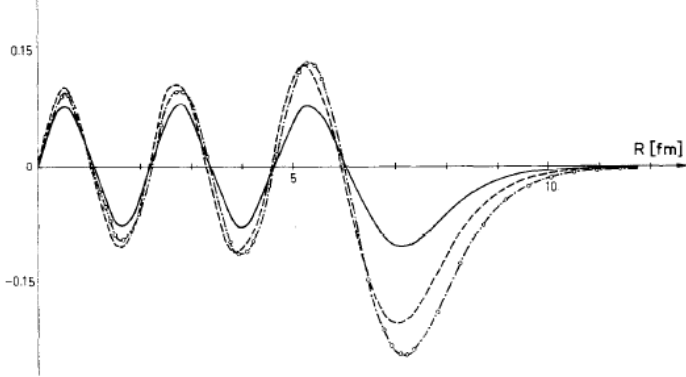


Figure 5.B.3: Modified formfactor for the transition to the ground state ( $^{206}\text{Pb}(t,\text{p})^{208}\text{Pb}(\text{gs})$ ; see Fig. 3.4.4 2A4) calculated in different spectroscopic models (pure shell-model configuration —, shell model plus pairing residual interaction ---, including ground state correlations -o-o-). After Broglia and Riedel (1967).

$$\begin{aligned}
 a^{(1)}(\infty) &= \frac{1}{i\hbar} \int_{-\infty}^{\infty} dt (\psi^b \psi^B, (V_{bB} - \langle V_{bB} \rangle) \psi^a \psi^A) \times \exp\left[\frac{i}{\hbar}(E^{bB} - E^{aA})t\right] \\
 &\approx \frac{2}{i\hbar} \int_{-\infty}^{\infty} dt \left( \phi^{B(A)}(S_{(2n)}^B; \vec{r}_{1A}, \vec{r}_{2A}), U(r_{1b}) e^{i(\sigma_1 + \sigma_2)} \phi^{a(b)}(S_{(2n)}^a; \vec{r}_{1b}, \vec{r}_{2b}) \right) \\
 &\quad \times \exp\left[\frac{i}{\hbar}(E^{bB} - E^{aA})t + \gamma(t)\right]
 \end{aligned} \tag{5.C.4}$$

where

$$\sigma_1 + \sigma_2 = \frac{1}{\hbar} \frac{m_n}{m_A} (m_{aA} \vec{v}_{aA}(t) + m_{bB} v_{bB}(t)) \cdot (\vec{r}_{1\alpha} - \vec{r}_{2\alpha}), \tag{5.C.5}$$

in keeping with the fact that  $\exp(i(\sigma_1 + \sigma_2))$  takes care of recoil effects (Galilean transformation associated with the mismatch between entrance and exit channels). The phase  $\gamma(t)$  is related with the effective  $Q$ -value of the reaction. In the above expression,  $\phi$  indicates an antisymmetrized, correlated two-particle (Cooper pair) wavefunction,  $S(2n)$  being the two-neutron separation energy (see Fig. 5.C.3),  $U(r_{1b})$  being the single particle potential generated by nucleus  $b$  ( $U(r) = \int d^3 r' \rho^b(r') v(|r - r'|)$ ). The contribution arising from non-orthogonality effects can be written as (see Fig. 5.C.1 (II))

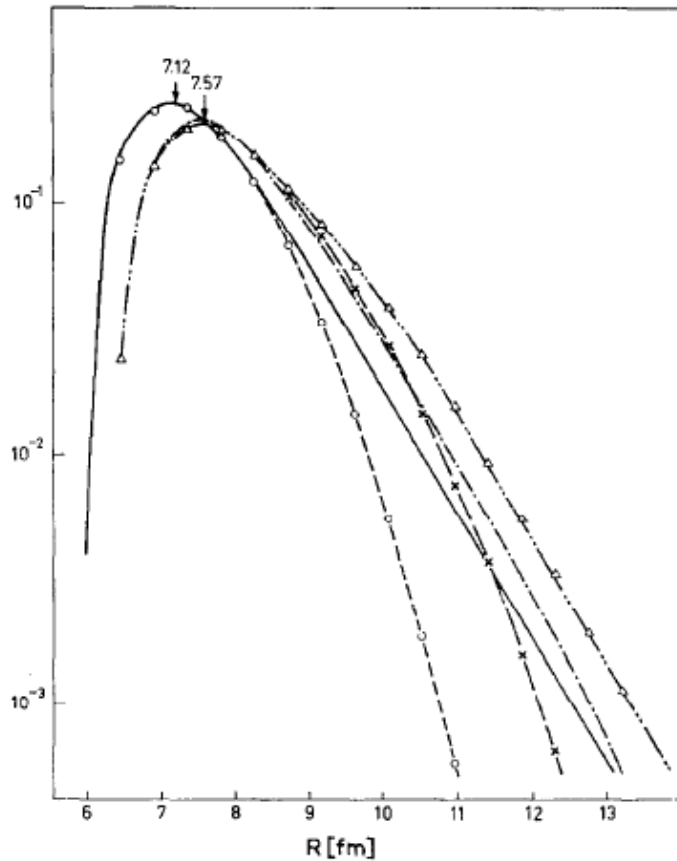


Figure 5.B.4: Asymptotic behavior of the modified formfactor for the  $^{206}(\text{t},\text{p})^{208}\text{Pb}(\text{gs})$  ground state transition for oscillator plus Hankel wave functions (continuous solid curve), oscillator wave functions alone (dash point dashed curve), and Saxon-Woods wave functions with a variety of asymptotic matchings (cf. Broglia and Riedel (1967)).

$$\begin{aligned}
 a^{(NO)}(\infty) &= \frac{1}{i\hbar} \int_{-\infty}^{\infty} dt (\psi^b \psi^B, (V_{bB} - \langle V_{bB} \rangle) \psi^f \psi^F) (\psi^f \psi^F, \psi^a \psi^A) \exp\left[\frac{i}{\hbar}(E^{bB} - E^{aA})t\right] \\
 &\approx \frac{2}{i\hbar} \int_{-\infty}^{\infty} \phi^{B(F)}(S_{(n)}^B, \vec{r}_{1A}), U(r_{1b}) e^{i\sigma_1} (\phi^{f(b)}(S^f(n), \vec{r}_{1b}) \\
 &\quad \times \phi^{F(A)}(S^F(n), \vec{r}_{2A}) e^{i\sigma_2} \phi^{a(f)}(S^a(n), \vec{r}_{2b})) \exp\left[\frac{i}{\hbar}(E^{bB} - E^{aA})t + \gamma(t)\right],
 \end{aligned} \tag{5.C.6}$$

the reaction channel  $f = (b+1) + F (= A+1)$  having been introduced, the quantity  $S(n)$  being the one-neutron separation energy (see Fig. 5.C.3). The summation

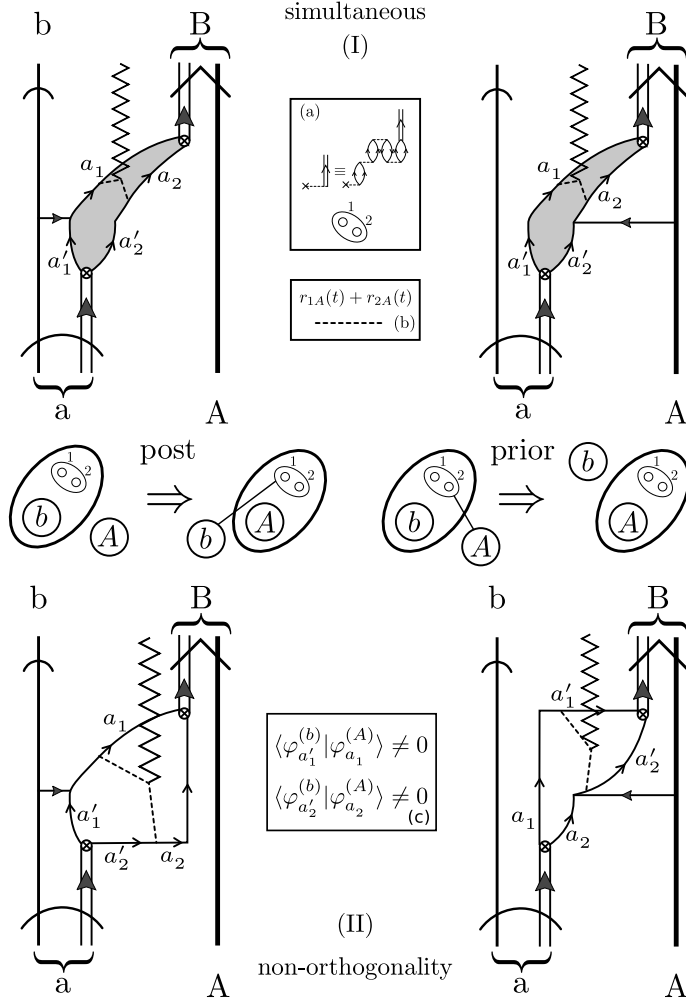


Figure 5.C.1: Graphical representation of simultaneous (I) and non-orthogonality (II) transfer processes. For details see text and cf. caption to Fig. 5.C.2.

over  $f(\equiv a'_1, a'_2)$  and  $F(\equiv a_1, a_2)$  involves a restricted number of states, namely the valence shells in nuclei  $B$  and  $a$ .

The successive transfer amplitude  $\tilde{a}_\infty^{(2)}$  written making use of the post-prior representation is equal to (see Fig. 5.C.2 (III))

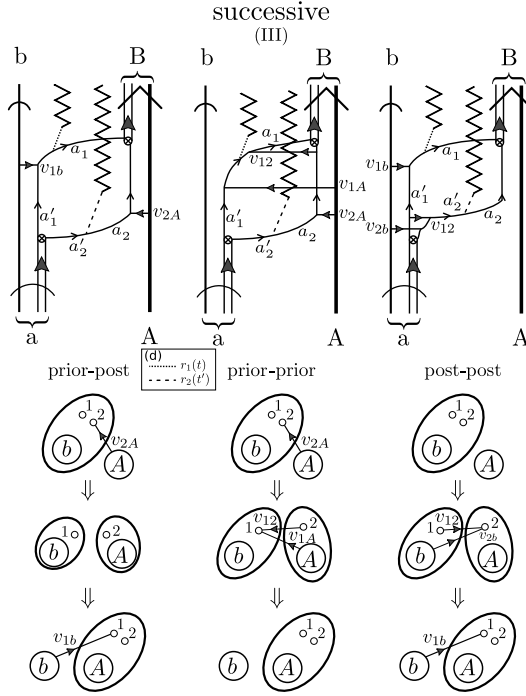


Figure 5.C.2: Graphical representation of the successive transfer of two nucleons. For details see text.

$$\begin{aligned}
 \tilde{a}^{(2)}(\infty) = & \frac{1}{i\hbar} \int_{-\infty}^{\infty} dt (\psi^b \psi^B, (V_{bB} - \langle V_{bB} \rangle) e^{i\sigma_1} \psi^f \psi^F) \\
 & \times \exp\left[\frac{i}{\hbar}(E^{bB} - E^{fF})t + \gamma_1(t)\right] \\
 & \times \frac{1}{i\hbar} \int_{-\infty}^t dt' (\psi^f \psi^F, (V_{fF} - \langle V_{fF} \rangle) e^{i\sigma_2} \psi^a \psi^A) \\
 & \times \exp\left[\frac{i}{\hbar}(E^{fF} - E^{aA})t' + \gamma_2(t)\right]. \tag{5.C.7}
 \end{aligned}$$

To gain insight into the relative importance of the three terms contributing to Eq. (5.C.3) we discuss two situations, namely, the independent-particle model and the strong-correlation limits.

Before doing so, let us describe in some detail the graphical description of the transfer amplitudes (5.C.4) (5.C.6) and (5.C.7) displayed in Figs. 5.C.1 and 5.C.2. It is of notice that the time arrow is assumed to point upwards: (I) Simultaneous transfer, in which one particle is transferred by the nucleon-nucleon interaction (note that  $U(r) = \int d^3r' \rho(r') v(|\vec{r} - \vec{r}'|)$ ) acting either in the entrance  $\alpha \equiv a + A$  channel (prior) or in the final  $\beta \equiv b + B$  channel (post), while the other particle follows suit making use of the particle-particle correlation (grey area) which binds the

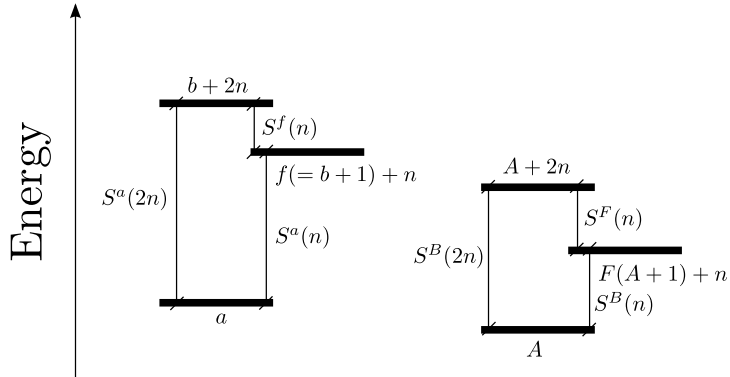


Figure 5.C.3: One- and two-neutron separation energies  $S(n)$  and  $S(2n)$  associated with the channels  $\alpha \equiv a (= b + 2) + A \rightarrow \gamma \equiv f (= b + 1) + F (= A + 1) \rightarrow \beta \equiv b + B (= A + 2)$ .

Cooper pair (see upper inset labelled (a)), represented by a solid arrow on a double line, to the projectile (curved arrowed lines) or to the target (opened arrowed lines). The above argument provides the explanation why when e.g.  $v_{1b}$  acts on one nucleon, the other nucleon also reacts instantaneously. In fact a Cooper pair displays generalized rigidy (emergent property in gauge space). A crossed open circle represents the particle-pair vibration coupling. The associated strength, together with an energy denominator, determines the amplitude  $X_{a'_1 a'_2}$  with which the pair mode (Cooper pair) is in the (time reversed) two particle configuration  $a'_1 a'_2$ . In the transfer process, the relative motion orbit changes, the readjustement of the corresponding trajectory mismatch being operated by a Galilean transformation induced by the operator  $(\exp\{\vec{k} \cdot (\vec{r}_{1A}(t) + \vec{r}_{2A}(t))\})$ . This phenomenon, known as recoil process, is represented by a jagged line which provides simultaneous information on the two transferred nucleons (single time appearing as argument of both single-particle coordinates  $r_1$  and  $r_2$ ; see inset labeled (b)). In other words, information on the coupling of structure and reaction modes. (II) Non-orthogonality contribution. While one of the nucleons of the Cooper pairs is transferred under the action of  $v$ , the other goes, uncorrelatedly over, profiting of the non-orthogonality of the associated single-particle wavefunctions (see inset (c)). In other words of the non-vanishing values of the overlaps, as shown in the inset. (III) Successive transfer. In this case, there are two time dependences associated with the acting of the nucleon-nucleon interaction twice (see inset (d)).

From a physical point of view the recoil-related coupling (jagged line) is similar to the one involved in the restoration of translational invariance violated by the shell-model potential  $U$ . This is done by including the effects of the collective field generated by a small displacement of the nucleus, giving rise to a coupling Hamiltonian proportional to the gradient of  $U$ . The spectrum of normal modes generated by such coupling contains a zero frequency mode, orthogonal to the additional nor-

mal modes which represent  $1^-$  states, displaying a divergent ZPF but a finite inertia equal to  $AM$ , result which testifies to translational invariance restoration (cf. Bohr, A. and Mottelson (1975) p. 445).

### 5.C.1 Independent particle limit

In the independent particle limit, the two transferred particles do not interact among themselves but for antisymmetrization. Thus, the separation energies fulfill the relations (see Fig. 5.C.3)

$$S^B(2n) = 2S^B(n) = 2S^F(n), \quad (5.C.8)$$

and

$$S^a(2n) = 2S^a(n) = 2S^f(n). \quad (5.C.9)$$

In this case

$$\phi^{B(A)}(S^B(2n), \vec{r}_{1A}, \vec{r}_{2A}) = \sum_{a_1 a_2} \phi_{a_1}^{B(F)}(S^B(n), \vec{r}_{1A}) \phi_{a_2}^{F(A)}(S^F(n), \vec{r}_{2A}), \quad (5.C.10)$$

and

$$\phi^{a(b)}(S^a(2n), \vec{r}_{1b}, \vec{r}_{2b}) = \sum_{a'_1 a'_2} \phi_{a'_1}^{a(f)}(S^a(n), \vec{r}_{1b}) \phi_{a'_2}^{f(b)}(S^f(n), \vec{r}_{2b}), \quad (5.C.11)$$

where  $(a_1, a_2) \equiv F$  and  $(a'_1, a'_2) \equiv f$  span, as mentioned above, shells in nuclei  $B$  and  $a$  respectively.

Inserting Eqs. (5.C.8–5.C.11) in Eq. (5.C.4) one can show that

$$a^{(1)}(\infty) = a^{(NO)}(\infty). \quad (5.C.12)$$

It can be further demonstrated that within the present approximation,  $\text{Im } \tilde{a}^{(2)} = 0$ , and that

$$\begin{aligned} \tilde{a}^{(2)}(\infty) &= \frac{1}{i\hbar} \int_{-\infty}^{\infty} dt (\psi^b \psi^B, (V_{bB} - < V_{bB} >) e^{i\sigma_1} \psi^f \psi^F) \\ &\quad \times \exp\left[\frac{i}{\hbar} (E^{bB} - E^{fF}) t + \gamma_1(t)\right] \\ &\quad \times \frac{1}{i\hbar} \int_{-\infty}^{\infty} dt' (\psi^f \psi^F, (V_{fF} - < V_{fF} >) e^{i\sigma_2} \psi^a \psi^A) \\ &\quad \times \exp\left[\frac{i}{\hbar} (E^{fF} - E^{aA}) t' + \gamma_2(t)\right]. \end{aligned} \quad (5.C.13)$$

The total absolute differential cross section (5.C.2), where  $P = |a(\infty)|^2 = |\tilde{a}^{(2)}|^2$ , is then equal to the product of two one-particle transfer cross sections (see Fig. 4.1.1), associated with the (virtual) reaction channels

$$\alpha \equiv a + A \rightarrow f + F \equiv \gamma, \quad (5.C.14)$$

and

$$\gamma \equiv f + F \rightarrow b + B \equiv \beta. \quad (5.C.15)$$

In fact, Eq.(5.C.13) involves no time ordering and consequently the two processes above are completely independent of each other. This result was expected because being  $v_{12} = 0$ , the transfer of one nucleon cannot influence, aside from selecting the initial state for the second step, the behaviour of the other nucleon.

### 5.C.2 Strong correlation (cluster) limit

The second limit to be considered is the one in which the correlation between the two nucleons is so strong that (see Fig. 5.C.3)

$$S^a(2n) \approx S^a(n) \gg S^f(n), \quad (5.C.16)$$

and

$$S^B(2n) \approx S^B(n) \gg S^F(n). \quad (5.C.17)$$

That is, the magnitude of the one-nucleon separation energy is strongly modified by the pair breaking.

There is a different, although equivalent way to express (5.C.3) which is more convenient to discuss the strong coupling limit. In fact, making use of the post-prior representation one can write

$$\begin{aligned} a^{(2)}(t) &= \tilde{a}^{(2)}(t) - a^{(NO)}(t) = \frac{1}{i\hbar} \int_{-\infty}^{\infty} dt (\psi^b \psi^B, (V_{bB} - \langle V_{bB} \rangle) e^{i\sigma_1} \psi^f \psi^F) \\ &\quad \times \exp[\frac{i}{\hbar} (E^{bB} - E^{fF}) t + \gamma_1(t)] \\ &\quad \times \frac{1}{i\hbar} \int_{-\infty}^t dt' (\psi^f \psi^F, (V_{aA} - \langle V_{aA} \rangle) \psi^a \psi^A) \\ &\quad \times \exp[\frac{i}{\hbar} (E^{fF} - E^{aA}) t' + \gamma_2(t')]. \end{aligned} \quad (5.C.18)$$

The relations (5.C.16), (5.C.17) imply

$$E^{fF} - E^{aA} = S^a(n) - S^F(n) \gg \frac{\hbar}{\tau}, \quad (5.C.19)$$

where  $\tau$  is the collision time. Consequently the real part of  $a^{(2)}(\infty)$  vanishes exponentially with the  $Q$ -value of the intermediate transition, while the imaginary part vanishes inversely proportional to this energy. One can thus write,

$$\text{Re } a^{(2)}(\infty) \approx 0, \quad (5.C.20)$$

and

$$\begin{aligned} a^{(2)}(\infty) &\approx \frac{1}{i\hbar} \frac{\tau}{\langle E^{fF} \rangle - E^{bB}} \sum_{fF} (\psi^b \psi^B, (V_{bB} - \langle V_{bB} \rangle) \psi^f \psi^F)_{t=0} \\ &\quad \times (\psi^f \psi^F, (V_{aA} - \langle V_{aA} \rangle) \psi^a \psi^A)_{t=0}, \end{aligned} \quad (5.C.21)$$

where one has utilized the fact that  $E^{bB} \approx E^{aA}$ . For  $v_{12} \rightarrow \infty$ , ( $\langle E^{fF} \rangle - E^{bB} \rightarrow \infty$ ) and, consequently,

$$\lim_{v_{12} \rightarrow \infty} a^{(2)}(\infty) = 0. \quad (5.C.22)$$

Thus the total two-nucleon transfer amplitude is equal, in the strong coupling limit, to the amplitude  $a^{(1)}(\infty)$ .

Summing up, only when successive transfer and non-orthogonal corrections are included in the description of the two-nucleon transfer process, does one obtain a consistent description of the process, which correctly converges to the weak and strong correlation limiting values.

## Appendix 5.D Spherical harmonics and angular momenta

With Condon–Shortley phases

$$Y_m^l(\hat{z}) = \delta_{m,0} \sqrt{\frac{2l+1}{4\pi}}, \quad Y_m^{l*}(\hat{r}) = (-1)^m Y_{-m}^l(\hat{r}). \quad (5.D.1)$$

Time-reversed phases consist in multiplying Condon–Shortley phases with a factor  $i^l$ , so

$$Y_m^l(\hat{z}) = \delta_{m,0} i^l \sqrt{\frac{2l+1}{4\pi}}, \quad Y_m^{l*}(\hat{r}) = (-1)^{l-m} Y_{-m}^l(\hat{r}). \quad (5.D.2)$$

With this phase convention, the relation with the associated Legendre polynomials includes an extra  $i^l$  factor with respect to the Condon–Shortley phase,

$$Y_m^l(\theta, \phi) = i^l \sqrt{\frac{2l+1}{4\pi} \frac{(l-m)!}{(l+m)!}} P_l^m(\cos \theta) e^{im\phi}. \quad (5.D.3)$$

### 5.D.1 addition theorem

The addition theorem for the spherical harmonics states that

$$P_l(\cos \theta_{12}) = \frac{4\pi}{2l+1} \sum_m Y_m^l(\mathbf{r}_1) Y_m^{l*}(\mathbf{r}_2), \quad (5.D.4)$$

where  $\theta_{12}$  is the angle between the vectors  $\mathbf{r}_1$  and  $\mathbf{r}_2$ . This result is independent of the phase convention. With *time-reversed phases*,

$$P_l(\cos \theta_{12}) = \frac{4\pi}{\sqrt{2l+1}} [Y^l(\hat{\mathbf{r}}_1) Y^l(\hat{\mathbf{r}}_2)]_0^0. \quad (5.D.5)$$

With *Condon–Shortley phases*,

$$P_l(\cos \theta_{12}) = (-1)^l \frac{4\pi}{\sqrt{2l+1}} [Y^l(\hat{\mathbf{r}}_1) Y^l(\hat{\mathbf{r}}_2)]_0^0. \quad (5.D.6)$$

### 5.D.2 expansion of the delta function

The Dirac delta function can be expanded in multipoles, yielding

$$\begin{aligned}\delta(\mathbf{r}_2 - \mathbf{r}_1) &= \sum_l \delta(r_1 - r_2) \frac{2l+1}{4\pi r_1^2} P_l(\cos \theta_{12}) \\ &= \sum_l \delta(r_1 - r_2) \frac{1}{r_1^2} \sum_m Y_m^l(\mathbf{r}_1) Y_m^{l*}(\mathbf{r}_2).\end{aligned}\quad (5.D.7)$$

This result is independent of the phase convention. With *time-reversed phases*,

$$\delta(\mathbf{r}_2 - \mathbf{r}_1) = \sum_l \delta(r_1 - r_2) \frac{\sqrt{2l+1}}{r_1^2} [Y^l(\hat{\mathbf{r}}_1) Y^l(\hat{\mathbf{r}}_2)]_0^0. \quad (5.D.8)$$

### 5.D.3 coupling and complex conjugation

If  $\Psi_{M_1}^{I_1*} = (-1)^{I_1-M_1} \Psi_{-M_1}^{I_1}$  and  $\Phi_{M_2}^{I_2*} = (-1)^{I_2-M_2} \Phi_{-M_2}^{I_2}$ , as it happens to be the case for spherical harmonics with time-reversed phases, then

$$\begin{aligned}[\Psi^{I_1} \Phi^{I_2}]_M^{I*} &= \sum_{\substack{M_1 M_2 \\ (M_1 + M_2 = M)}} \langle I_1 I_2 M_1 M_2 | IM \rangle \Psi_{M_1}^{I_1*} \Phi_{M_2}^{I_2*} \\ &= \sum_{\substack{M_1 M_2 \\ (M_1 + M_2 = M)}} (-1)^{I-M_1-M_2} \langle I_1 I_2 - M_1 - M_2 | I - M \rangle \Psi_{-M_1}^{I_1} \Phi_{-M_2}^{I_2} \\ &= (-1)^{I-M} \sum_{\substack{M_1 M_2 \\ (M_1 + M_2 = M)}} \langle I_1 I_2 - M_1 - M_2 | I - M \rangle \Psi_{-M_1}^{I_1} \Phi_{-M_2}^{I_2} \\ &= (-1)^{I-M} [\Psi^{I_1} \Phi^{I_2}]_{-M}^I,\end{aligned}\quad (5.D.9)$$

where we have used (5.D.23).

Let us care now about the spinor functions  $\chi_m^{1/2}(\sigma)$ , which have the form

$$\chi^{1/2}(\sigma = 1/2) = \begin{bmatrix} 1 \\ 0 \end{bmatrix}, \quad \chi^{1/2}(\sigma = -1/2) = \begin{bmatrix} 0 \\ 1 \end{bmatrix}, \quad (5.D.10)$$

or

$$\chi_m^{1/2}(\sigma) = \delta_{m,\sigma}. \quad (5.D.11)$$

Thus,  $\chi_m^{1/2*}(\sigma) = \chi_m^{1/2}(-\sigma) = \delta_{m,\sigma}$ , but we can also write

$$\chi_m^{1/2*}(\sigma) = (-1)^{1/2-m+1/2-\sigma} \chi_{-m}^{1/2}(-\sigma). \quad (5.D.12)$$

This trick enable us to write

$$[Y^l(\hat{\mathbf{r}}) \chi^{1/2}(\sigma)]_M^{J*} = (-1)^{1/2-\sigma+J-M} [Y^l(\hat{\mathbf{r}}) \chi^{1/2}(-\sigma)]_{-M}^J, \quad (5.D.13)$$

which can be derived in a similar way as (5.D.9).

### 5.D.4 angular momenta coupling

Relation between Clebsh–Gordan and  $3j$  coefficients:

$$\langle j_1 \ j_2 \ m_1 \ m_2 | JM \rangle = (-1)^{j_1 - j_2 + M} \sqrt{2J+1} \begin{Bmatrix} j_1 & j_2 & J \\ m_1 & m_2 & -M \end{Bmatrix}. \quad (5.D.14)$$

Relation between Wigner and  $9j$  coefficients:

$$((j_1 j_2)_{j_{12}} (j_3 j_4)_{j_{34}} | (j_1 j_3)_{j_{13}} (j_2 j_4)_{j_{24}})_j = \sqrt{(2j_{12} + 1)(2j_{13} + 1)(2j_{24} + 1)(2j_{34} + 1)} \begin{Bmatrix} j_1 & j_2 & j_{12} \\ j_3 & j_4 & j_{34} \\ j_{13} & j_{24} & j \end{Bmatrix}. \quad (5.D.15)$$

### 5.D.5 integrals

Let us now prove

$$\int d\Omega [Y^l(\hat{r}) Y^l(\hat{r})]_M^I = \delta_{M,0} \delta_{I,0} \sqrt{2l+1}. \quad (5.D.16)$$

$$\begin{aligned} \int d\Omega [Y^l(\hat{r}) Y^l(\hat{r})]_M^I &= \sum_{\substack{m_1, m_2 \\ (m_1 + m_2 = M)}} \langle l \ l \ m_1 \ m_2 | IM \rangle \int d\Omega Y_{m_1}^l(\hat{r}) Y_{m_2}^l(\hat{r}) \\ &= \sum_{\substack{m_1, m_2 \\ (m_1 + m_2 = M)}} (-1)^{l+m_1} \langle l \ l - m_1 \ m_2 | IM \rangle \int d\Omega Y_{m_1}^{l*}(\hat{r}) Y_{m_2}^l(\hat{r}) \\ &= \delta_{M,0} \sum_m (-1)^{l+m} \langle l \ l - m \ m | I0 \rangle \\ &= \delta_{M,0} \sqrt{2l+1} \sum_m \langle l \ l - m \ m | I0 \rangle \langle l \ l - m \ m | 00 \rangle \\ &= \delta_{M,0} \delta_{I,0} \sqrt{2l+1}, \end{aligned} \quad (5.D.17)$$

where we have used

$$\langle l \ l - m \ m | 0 \ 0 \rangle = \frac{(-1)^{l+m}}{\sqrt{2l+1}} \quad (5.D.18)$$

Let us now prove

$$\sum_{\sigma} \int d\Omega (-1)^{1/2-\sigma} [\Psi^j(\hat{r}, -\sigma) \Psi^j(\hat{r}, \sigma)]_M^I = -\delta_{M,0} \delta_{I,0} \sqrt{2j+1}. \quad (5.D.19)$$

$$\begin{aligned}
& \sum_{\sigma} \int d\Omega (-1)^{1/2-\sigma} [\Psi^j(\hat{r}, -\sigma) \Psi^j(\hat{r}, \sigma)]_M^I \\
&= \sum_{\substack{m_1, m_2 \\ (m_1+m_2=M)}} \langle j \ j \ m_1 \ m_2 | IM \rangle \sum_{\sigma} \int d\Omega \Psi_{m_1}^j(\hat{r}, -\sigma) \Psi_{m_2}^j(\hat{r}, \sigma) \\
&= \sum_{\substack{m_1, m_2 \\ (m_1+m_2=M)}} \langle j \ j \ m_1 \ m_2 | IM \rangle \sum_{\sigma} (-1)^{j+m_1} \int d\Omega \Psi_{-m_1}^{j*}(\hat{r}, \sigma) \Psi_{m_2}^j(\hat{r}, \sigma) \\
&= \sum_{\substack{m_1, m_2 \\ (m_1+m_2=M)}} \langle j \ j \ m_1 \ m_2 | IM \rangle (-1)^{j+m_1} \delta_{-m_1, m_2} \\
&= \delta_{M,0} \sum_m (-1)^{j+m} \langle j \ j \ m \ -m | I0 \rangle \\
&= -\delta_{M,0} \sqrt{2j+1} \sum_m (-1)^{j+m} \langle j \ j \ m \ -m | I0 \rangle \langle j \ j \ m \ -m | 00 \rangle \\
&= -\delta_{M,0} \delta_{I,0} \sqrt{2j+1}.
\end{aligned} \tag{5.D.20}$$

### 5.D.6 symmetry properties

Note also another useful property

$$[\Psi^{I_1} \Psi^{I_2}]_M^I = (-1)^{I_1+I_2-I} [\Psi^{I_2} \Psi^{I_1}]_M^I, \tag{5.D.21}$$

by virtue of the symmetry property of the Clebsh-Gordan coefficients

$$\langle I_1 \ I_2 \ m_1 \ m_2 | IM \rangle = (-1)^{I_1+I_2-I} \langle I_2 \ I_1 \ m_2 \ m_1 | IM \rangle. \tag{5.D.22}$$

Here's another symmetry property of the Clebsh-Gordan coefficients

$$\langle I_1 \ I_2 \ m_1 \ m_2 | IM \rangle = (-1)^{I_1+I_2-I} \langle I_1 \ I_2 \ -m_2 \ -m_1 | I-M \rangle. \tag{5.D.23}$$

Another one, which can be derived from the simpler properties of 3*j*-symbols

$$\langle I_1 \ I_2 \ m_1 \ m_2 | IM \rangle = (-1)^{I_1-m_1} \sqrt{\frac{2I+1}{2I_2+1}} \langle I_1 \ I \ m_1 \ -M | I_2 m_2 \rangle. \tag{5.D.24}$$

Let us use this last property to calculate sums of the type

$$\sum_{m_1, m_3} |\langle I_1 \ I_2 \ m_1 \ m_2 | I_3 m_3 \rangle|^2. \tag{5.D.25}$$

Using (5.D.24), we have

$$\begin{aligned}
& \sum_{m_1, m_3} |\langle I_1 \ I_2 \ m_1 \ m_2 | I_3 m_3 \rangle|^2 = \\
& \quad \frac{2I_3+1}{2I_2+1} \sum_{m_1, m_3} |\langle I_1 \ I_3 \ m_1 \ -m_3 | I_2 m_2 \rangle|^2 = \frac{2I_3+1}{2I_2+1},
\end{aligned} \tag{5.D.26}$$

since

$$\sum_{m_1, m_3} |\langle I_1 I_3 m_1 - m_3 | I_2 m_2 \rangle|^2 = \sum_{m_1, m_3} |\langle I_1 I_3 m_1 m_3 | I_2 m_2 \rangle|^2 = 1. \quad (5.D.27)$$

## Appendix 5.E distorted waves

Let us have a closer look at the partial wave expansion of the distorted waves

$$\chi^{(+)}(\mathbf{k}, \mathbf{r}) = \sum_l \frac{4\pi}{kr} i^l e^{i\sigma l} F_l \sum_m Y_m^l(\hat{r}) Y_m^{l*}(\hat{k}). \quad (5.E.1)$$

Notice the very important fact that *this definition is independent of the phase convention*, since the  $l$ -dependent phase is multiplied by its complex conjugate.

$$\chi^{(-)}(\mathbf{k}, \mathbf{r}) = \chi^{(+)*}(-\mathbf{k}, \mathbf{r}) = \sum_l \frac{4\pi}{kr} i^{-l} e^{-i\sigma l} F_l^* \sum_m Y_m^{l*}(\hat{r}) Y_m^l(-\hat{k}). \quad (5.E.2)$$

As  $Y_m^l(-\hat{k}) = (-1)^l Y_m^l(\hat{k})$ , we have

$$\chi^{(-)}(\mathbf{k}, \mathbf{r}) = \sum_l \frac{4\pi}{kr} i^l e^{-i\sigma l} F_l^* \sum_m Y_m^{l*}(\hat{r}) Y_m^l(\hat{k}), \quad (5.E.3)$$

which is also independent of the phase convention. With time-reversed phase convention

$$\chi^{(+)}(\mathbf{k}, \mathbf{r}) = \sum_l \frac{4\pi}{kr} i^l \sqrt{2l+1} e^{i\sigma l} F_l [Y^l(\hat{r}) Y^l(\hat{k})]_0^0, \quad (5.E.4)$$

while with Condon–Shortley phase convention we get an extra  $(-1)^l$  factor:

$$\chi^{(+)}(\mathbf{k}, \mathbf{r}) = \sum_l \frac{4\pi}{kr} i^{-l} \sqrt{2l+1} e^{i\sigma l} F_l [Y^l(\hat{r}) Y^l(\hat{k})]_0^0. \quad (5.E.5)$$

The partial-wave expansion of the Green function  $G(\mathbf{r}, \mathbf{r}')$  is

$$G(\mathbf{r}, \mathbf{r}') = i \sum_l \frac{f_l(k, r_<) P_l(k, r_>)}{krr'} \sum_m Y_m^l(\hat{r}) Y_m^{l*}(\hat{r}'), \quad (5.E.6)$$

where  $f_l(k, r_<)$  and  $P_l(k, r_>)$  are the regular and the irregular solutions of the homogeneous problem respectively. With *time-reversed* phase convention

$$G(\mathbf{r}, \mathbf{r}') = i \sum_l \sqrt{2l+1} \frac{f_l(k, r_<) P_l(k, r_>)}{krr'} [Y^l(\hat{r}) Y^l(\hat{r}')]_0^0. \quad (5.E.7)$$

## Appendix 5.F hole states and time reversal

Let us consider the state  $|jm\rangle^{-1}$  obtained by removing a  $\psi_{jm}$  single-particle state from a  $J = 0$  closed shell  $|0\rangle$ . The antisymmetrized product state

$$\sum_m \mathcal{A}\{\psi_{jm}|(jm)^{-1}\} \propto |0\rangle \quad (5.F.1)$$

is clearly proportional to  $|0\rangle$ . This gives us the transformation rules of  $|jm\rangle^{-1}$  under rotations, which must be such that, when multiplied by a  $j, m$  spherical tensor and summed over  $m$ , yields a  $j = 0$  tensor. It can be seen that these properties imply that  $|jm\rangle^{-1}$  transforms like  $(-1)^{j-m} T_{j-m}$ ,  $T_{j-m}$  being a spherical tensor. It also follows that the hole state  $|j\bar{m}\rangle^{-1}$  transforms like a  $j, m$  spherical tensor if  $\psi_{j\bar{m}}$  is defined as the  $\mathcal{R}$ -conjugate to  $\psi_{jm}$  by the relation

$$\psi_{j\bar{m}} \equiv (-1)^{j+m} \psi_{j-m}. \quad (5.F.2)$$

In other words, with the latter definition a *hole state* transforms under rotations with the right phase. We will now show that  $\mathcal{R}$ -conjugation is equivalent to a rotation of spin and spatial coordinates through an angle  $-\pi$  about the  $y$ -axis:

$$e^{i\pi J_y} \psi_{jm} = (-1)^{j+m} \psi_{j-m} \equiv \psi_{j\bar{m}}. \quad (5.F.3)$$

Let us begin by calculating  $e^{i\pi L_y} Y_l^m$ . The rotation matrix about the  $y$ -axis is

$$R_y(\theta) = \begin{pmatrix} \cos(\theta) & 0 & \sin(\theta) \\ 0 & 1 & 0 \\ -\sin(\theta) & 0 & \cos(\theta) \end{pmatrix}, \quad (5.F.4)$$

so for  $R_y(-\pi)$  we get

$$R_y(-\pi) = \begin{pmatrix} -1 & 0 & 0 \\ 0 & 1 & 0 \\ 0 & 0 & -1 \end{pmatrix}. \quad (5.F.5)$$

When applied to the generic direction  $(\sin(\theta) \cos(\phi), \sin(\theta) \sin(\phi), \cos(\theta))$ , we obtain  $(-\sin(\theta) \cos(\phi), \sin(\theta) \sin(\phi), -\cos(\theta))$ , which corresponds to making the substitutions

$$\theta \rightarrow \pi - \theta, \quad \phi \rightarrow \pi - \phi. \quad (5.F.6)$$

When we substitute these angular transformations in the spherical harmonic  $Y_l^m(\theta, \phi)$ , we obtain the rotated  $Y_l^m(\theta, \phi)$ :

$$e^{i\pi L_y} Y_l^m = (-1)^{l+m} Y_l^{-m}. \quad (5.F.7)$$

Let us now turn our attention to the spin coordinates rotation  $e^{i\pi s_y} \chi_m$ . The rotation matrix in spin space is

$$\begin{pmatrix} \cos(\theta/2) & -\sin(\theta/2) \\ \sin(\theta/2) & \cos(\theta/2) \end{pmatrix}, \quad (5.F.8)$$

which, for  $\theta = -\pi$  is

$$\begin{pmatrix} 0 & 1 \\ -1 & 0 \end{pmatrix}. \quad (5.F.9)$$

Applying it to the spinors, we find the rule

$$e^{i\pi s_y} \chi_m = (-1)^{1/2+m} \chi_{-m}, \quad (5.F.10)$$

so

$$\begin{aligned} e^{i\pi J_y} \psi_{jm} &= \sum_{m_l m_s} \langle l m_l 1/2 m_s | j m \rangle e^{i\pi L_y} Y_l^{m_l} e^{i\pi s_y} \chi_{m_s} \\ &= \sum_{m_l m_s} (-1)^{1/2+m_s+l+m_l} \langle l m_l 1/2 m_s | j m \rangle Y_l^{-m_l} \chi_{-m_s} \\ &= \sum_{m_l m_s} (-1)^{1+m-j+2l} \langle l -m_l 1/2 -m_s | j -m \rangle Y_l^{-m_l} \chi_{-m_s} \\ &= (-1)^{m+j} \psi_{j-m} \equiv \psi_{j\bar{m}}, \end{aligned} \quad (5.F.11)$$

where we have used  $(-1)^{1+m-j+2l} = -(-1)^{m-j} = (-1)^{m+j}$ , as  $j, m$  are always half-integers and  $l$  is always an integer.

We now turn our attention to the time reversal operation, which amounts to the transformations

$$\mathbf{r} \rightarrow \mathbf{r}, \quad \mathbf{p} \rightarrow -\mathbf{p}. \quad (5.F.12)$$

This is enough to define the operator of time reversal of a spinless particle (see Messiah). In the position representation, in which  $\mathbf{r}$  is real and  $\mathbf{p}$  pure imaginary, this (unitary antilinear) operator is the complex conjugation operator.

As angular momentum  $\mathbf{l} = \mathbf{r} \times \mathbf{p}$  changes sign under time reversal, so does spin:

$$\mathbf{s} \rightarrow -\mathbf{s}, \quad (5.F.13)$$

which, along with (5.F.12), completes the set of rules that define the time reversal operation on a particle with spin. In the representation of eigenstates of  $\mathbf{s}^2$  and  $s_z$ , complex conjugation alone changes only the sign of  $s_y$ , so an additional rotation of  $-\pi$  around the  $y$ -axis is necessary to change the sign of  $s_x, s_z$  and implement the transformation (5.F.13). If we call  $K$  the time-reversal operator, we have

$$K\psi_{jm} = e^{i\pi s_y} \psi_{jm}^*. \quad (5.F.14)$$

This is completely general and independent of the phase convention. It only depends on the fact that we have used the  $\mathbf{r}$  representation for the spatial wave function and the representation of the eigenstates of  $\mathbf{s}^2$  and  $s_z$  for the spin part. *If we use time-reversal phases for the spherical harmonics (see (5.D.2)),*

$$Y_m^{l*} = (-1)^{l+m} Y_{-m}^l = e^{i\pi L_y} Y_m^l. \quad (5.F.15)$$

So we can write

$$K\psi_{jm} = e^{i\pi J_y} \psi_{jm} = \psi_{j\bar{m}}. \quad (5.F.16)$$

Note again that this last expression is valid only if we use time-reversal phases for the spherical harmonics. Only in this case time-reversal coincides with  $\mathcal{R}$ -conjugation and hole states.

In BCS theory, the quasiparticles are defined in terms of linear combinations of particles and holes. With time-reversal phases, holes are equivalent to time-reversed states, and we get the definitions

$$\begin{aligned} a_\nu^\dagger &= u_\nu a_\nu^\dagger - v_\nu a_{\bar{\nu}} & a_\nu^\dagger &= u_\nu a_\nu^\dagger + v_\nu a_{\bar{\nu}} \\ a_{\bar{\nu}}^\dagger &= u_\nu a_{\bar{\nu}}^\dagger + v_\nu a_\nu & a_{\bar{\nu}}^\dagger &= u_\nu a_{\bar{\nu}}^\dagger - v_\nu a_\nu \\ a_\nu &= u_\nu a_\nu - v_\nu a_{\bar{\nu}}^\dagger & a_\nu &= u_\nu a_\nu + v_\nu a_{\bar{\nu}}^\dagger \\ a_{\bar{\nu}} &= u_\nu a_{\bar{\nu}} + v_\nu a_\nu^\dagger & a_{\bar{\nu}} &= u_\nu a_{\bar{\nu}} - v_\nu a_\nu^\dagger \end{aligned} \quad (5.F.17)$$

## Appendix 5.G Spectroscopic amplitudes in the BCS approximation

The creation operator of a pair of fermions coupled to  $J, M$  can be expressed in second quantization as

$$P^\dagger(j_1, j_2, JM) = N \sum_m \langle j_1 m j_2 M - m | J M \rangle a_{j_1 m}^\dagger a_{j_2 M-m}^\dagger, \quad (5.G.1)$$

where  $N$  is a normalization constant. To determine it, we write the wave function resulting from the action of (5.G.1) on the vacuum

$$\begin{aligned} \Psi &= P^\dagger(j_1, j_2, JM)|0\rangle = \frac{N}{\sqrt{2}} \sum_m \langle j_1 m j_2 M - m | J M \rangle \\ &\times (\phi_{j_1 m}(\mathbf{r}_1) \phi_{j_2 M-m}(\mathbf{r}_2) - \phi_{j_2 M-m}(\mathbf{r}_1) \phi_{j_1 m}(\mathbf{r}_2)). \end{aligned} \quad (5.G.2)$$

The norm is

$$\begin{aligned} |\Psi|^2 &= \frac{N^2}{2} \sum_{mm'} \langle j_1 m j_2 M - m | J M \rangle \langle j_1 m' j_2 M - m' | J M \rangle \\ &\times (\phi_{j_1 m}(\mathbf{r}_1) \phi_{j_2 M-m}(\mathbf{r}_2) - \phi_{j_2 M-m}(\mathbf{r}_1) \phi_{j_1 m}(\mathbf{r}_2)) \\ &\times (\phi_{j_1 m'}(\mathbf{r}_1) \phi_{j_2 M-m'}(\mathbf{r}_2) - \phi_{j_2 M-m'}(\mathbf{r}_1) \phi_{j_1 m'}(\mathbf{r}_2)). \end{aligned} \quad (5.G.3)$$

Integrating we get

$$\begin{aligned}
1 &= \frac{N^2}{2} \sum_{mm'} \langle j_1 m j_2 M - m | J M \rangle \langle j_1 m' j_2 M - m' | J M \rangle \\
&\quad \times (2\delta_{m,m'} - 2\delta_{j_1,j_2}\delta_{m,M-m'}) \\
&= N^2 \left( \sum_m \langle j_1 m j_2 M - m | J M \rangle^2 \right. \\
&\quad \left. - \delta_{j_1,j_2} \sum_m \langle j_1 m j_2 M - m | J M \rangle \langle j_1 M - m j_2 m | J M \rangle \right) \\
&= N^2 (1 - \delta_{j_1,j_2}(-1)^{2j-J}),
\end{aligned} \tag{5.G.4}$$

where we have used the closure condition for Clebsh–Gordan coefficients and (5.D.22), and  $\delta_{j_1,j_2}$  must be interpreted as a  $\delta$  function regarding all the quantum numbers but the magnetic one. We see that two fermions with identical quantum numbers (but the magnetic one) *cannot couple to  $J$  odd*. If  $J$  is even, the normalization constant is

$$N = \frac{1}{\sqrt{1 + \delta_{j_1,j_2}}}. \tag{5.G.5}$$

To sum up,

$$P^\dagger(j_1, j_2, JM) = \frac{1}{\sqrt{1 + \delta_{j_1,j_2}}} \sum_m \langle j_1 m j_2 M - m | J M \rangle a_{j_1 m}^\dagger a_{j_2 M - m}^\dagger. \tag{5.G.6}$$

The spectroscopic amplitude for finding in a  $A + 2, J_f, M_f$  nucleus a couple of nucleons with quantum numbers  $j_1, j_2$  coupled to  $J$  on top of a  $A, J_i$  nucleus is

$$B(J, j_1, j_2) = \sum_{M, M_i} \langle J_i M_i JM | J_f M_f \rangle \langle \Psi_{J_f M_f} | P^\dagger(j_1, j_2, JM) | \Psi_{J_i M_i} \rangle. \tag{5.G.7}$$

This is completely general. It depends on the structure model only through the way the  $A + 2$  and  $A$  nuclei are treated. We now want to turn our attention to the expression of  $B(J, j_1, j_2)$  in the BCS approximation when both the  $A + 2$  and the  $A$  are  $0^+$ , zero-quasiparticle ground states. In order to do this, we write (5.G.6) in terms of quasiparticle operators using (5.F.17)<sup>3</sup>:

$$\begin{aligned}
P^\dagger(j_1, j_2, JM) &= \frac{1}{\sqrt{1 + \delta_{j_1,j_2}}} \sum_{m_1, m_2} \langle j_1 m_1 j_2 m_2 | J M \rangle \left( U_{j_1} U_{j_2} \alpha_{j_1 m_1}^\dagger \alpha_{j_2 m_2}^\dagger \right. \\
&\quad + (-1)^{j_1+j_2-M} V_{j_1} V_{j_2} \alpha_{j_1-m_1} \alpha_{j_2-m_2} \\
&\quad + (-1)^{j_2-m_2} U_{j_1} V_{j_2} \alpha_{j_1 m_1}^\dagger \alpha_{j_2-m_2} \\
&\quad - (-1)^{j_1-m_1} V_{j_1} U_{j_2} \alpha_{j_2 m_2}^\dagger \alpha_{j_1-m_1} \\
&\quad \left. + (-1)^{j_1-m_1} V_{j_1} U_{j_2} \delta_{j_1 j_2} \delta_{-m_1 m_2} \right).
\end{aligned} \tag{5.G.8}$$

---

<sup>3</sup>In what follows, we use the phase convention  $\alpha_{j\bar{m}}=(-1)^{j-m}\alpha_{j-m}$  instead of  $\alpha_{j\bar{m}}=(-1)^{j+m}\alpha_{j-m}$ , consistent with (5.F.2). Had we stick to the definition (5.F.2), the amplitude  $B(0, j, j)$  calculated below would have a minus sign, which would not have any physical consequence.

If both nuclei are in zero-quasiparticle states, the only term that survives is the last one in the above expression, and (5.G.7) becomes (see also Sect. 2.4.2 and equation 2.1.8).

$$\begin{aligned}
 B_j = B(j^2(0)) &= \frac{1}{\sqrt{2}} \sum_m \langle j \ m \ j - m | 0 \ 0 \rangle (-1)^{j-m} V_j U_j \\
 &= \frac{1}{\sqrt{2}} \sum_m \frac{(-1)^{j-m}}{\sqrt{(2j+1)}} (-1)^{j-m} V_j U_j \\
 &= \frac{1}{\sqrt{2}} \sum_m \frac{1}{\sqrt{(2j+1)}} V_j U_j.
 \end{aligned} \tag{5.G.9}$$

After carrying out the summation one finds,

$$B_j = B(j^2(0)) = \sqrt{j+1/2} V_j U_j. \tag{5.G.10}$$

Note that in this final expression  $V_j$  refers to the  $A$  nucleus, while  $U_j$  is related to the  $A + 2$  nucleus. In practice, it does not make a big difference to calculate both for the same nucleus.

## Appendix 5.H Derivation of two-nucleon transfer transition amplitudes including recoil, non-orthogonality and successive transfer.

In the present Appendix we reproduce with the permission of the author the first (manuscript) page (cf. Fig. 5.H.1) of what, arguably, was the first complete derivation (Bayman (1970)(unpublished)) of the different contributions needed to calculate absolute two-nucleon transfer cross sections in a systematic way (cf. Bayman (1971) and Bayman and Chen (1982)). Within this context we refer to Broglia, R.A. et al. (1973) and Potel, G. et al. (2013) in particular Fig. 10 of this reference.

## Bibliography

- B. F. Bayman. Finite-range calculation of the two-neutron transfer reaction. *Phys. Rev. Lett.*, 25:1768, 1970.
- B. F. Bayman. Finite-range calculation of the two-neutron transfer reaction. *Nuclear Physics A*, 168:1, 1971.
- B. F. Bayman and J. Chen. One-step and two-step contributions to two-nucleon transfer reactions. *Phys. Rev. C*, 26:1509, 1982.
- B. F. Bayman and A. Kallio. Relative-angular-momentum-zero part of two-nucleon wave functions. *Phys. Rev.*, 156:1121, 1967.

$\downarrow \rightarrow$

$$A + a \xrightarrow{(b+n_1+n_2)} C + c \xrightarrow{(A+n_2)} b + B \xrightarrow{(A+n_1+n_2)}$$

We need

$$2 \sum_{\sigma_1 \sigma_2} \int d^3 \vec{r}_{C_c} d^3 \vec{r}_{b_1} d^3 \vec{r}_{A_2} \left[ \Psi^{j_{f_2}}(\vec{r}_{A_1}, \sigma_1) \Psi^{j_{f_2}}(\vec{r}_{A_2}, \sigma_2) \right]_M^* \chi_f^{(-)}(\vec{r}_{Bb}) U(r_{b_1}) \Psi^{(+)}(\vec{r}_{C_c})$$

$$H = H_C + H_c - \frac{\hbar^2}{2\mu_{C_c}} \nabla_{\vec{r}_{C_c}}^2 + U(r_{C_c}) + V(r_{c_2}), \quad (E - H) \Psi^{(+)} = 0 = [E - H]$$

Let  $f_{K_H}(\vec{r}_{C_c}) = \langle \Psi^{j_{f_2}}(\vec{r}_{A_2}, \sigma_2) \Psi^{j_i}(\vec{r}_{b_1}, \sigma_1) \rangle_M^K | \Psi^{(+)}(\vec{r}_{A_2}, \sigma_2, \vec{r}_{b_1}; \vec{r}_{C_c}) \rangle_{fixed}$

$$f_{K_H}(\vec{r}_{C_c}) = \frac{2\mu_{C_c}}{\hbar^2} \int d^3 \vec{r}'_{C_c} G(\vec{r}_{C_c}, \vec{r}'_{C_c}) \langle [\Psi^{j_{f_2}}(\vec{r}'_{A_2}, \sigma'_2) \Psi^{j_i}(\vec{r}'_{b_1}, \sigma'_1)]_M^K | V(r'_{c_2}) | \Psi \rangle_{fixed}$$

$$\approx \frac{2\mu_{C_c}}{\hbar^2} \sum_{\sigma'_1 \sigma'_2} \int d^3 \vec{r}'_{C_c} d^3 \vec{r}'_{A_2} d^3 \vec{r}'_{b_1} G(\vec{r}_{C_c}, \vec{r}'_{C_c}) \left[ \Psi^{j_{f_2}}(\vec{r}'_{A_2}, \sigma'_2) \Psi^{j_i}(\vec{r}'_{b_1}, \sigma'_1) \right]_M^K V(r'_{c_2}) \chi_f^{(+)}(\vec{r}'_{A_2})$$

$$\times \left[ \Psi^{j_i}(\vec{r}'_{b_1}, \sigma'_1) \Psi^{j_i}(\vec{r}'_{b_1}) \right]_o \rangle + u_{K_H}$$

$$= \langle \Psi^{j_{f_2}}(\vec{r}'_{A_2}, \sigma'_2) \Psi^{j_i}(\vec{r}'_{b_1}, \sigma'_1) \rangle_M^K | \chi_f^{(+)}(\vec{r}'_{A_2}) \langle \Psi^{j_i}(\vec{r}'_{b_1}, \sigma'_1) \Psi^{j_i}(\vec{r}'_{b_1}) \rangle_o \rangle + u_{K_H}$$

Thus  $u_{K_H}(\vec{r}_{C_c}) = \frac{2\mu_{C_c}}{\hbar^2} \sum_{\sigma'_1 \sigma'_2} \int d^3 \vec{r}'_{C_c} d^3 \vec{r}'_{A_2} d^3 \vec{r}'_{b_1} G(\vec{r}_{C_c}, \vec{r}'_{C_c}) \left[ \Psi^{j_{f_2}}(\vec{r}'_{A_2}, \sigma'_2) \Psi^{j_i}(\vec{r}'_{b_1}, \sigma'_1) \right]_M^K \chi_f^{(+)}(\vec{r}'_{A_2}) V(r'_{c_2})$

4  
↓

Figure 5.H.1: First manuscript page of Ben Bayman's derivation of the two-nucleon transfer reaction amplitude, in second order DWBA approximation.

- N. Bohr. The quantum postulate and the recent development of atomic theory. *Nature*, 121:580, 1928.
- Bohr, A. and B. R. Mottelson. *Nuclear Structure, Vol.II*. Benjamin, New York, 1975.
- M. Born. Zur Quantenmechanik der Stoßvorgänge. *Zeitschr.f. Phys.*, 37:863, 1926.
- M. Born and Jordan. Zur quantenmechanik. *Zeitschr. Phys.*, 34:858, 1925.
- M. Born, Jordan, and W. Heisenberg. Zur Quantenmechanik II. *Zeitschr. Phys.*, 35:557, 1926.
- P. F. Bortignon and R. A. Broglia. Role of the nuclear surface in an unified description of the damping of single-particle states and giant resonances. *Nucl. Phys. A*, 371:405, 1981.
- Brink, D. and R. A. Broglia. *Nuclear Superfluidity*. Cambridge University Press, Cambridge, 2005.
- R. Broglia and A. Winther. *Heavy Ion Reactions*. Westview Press, Boulder, CO., 2004.
- R. A. Broglia. Heavy ion reaction, notes of lectures delivered during the academic years 1974–1976 at SUNY, Stony Brook at Brookhaven National Laboratory, and at Niels Bohr Institute, unpublished.
- R. A. Broglia and C. Riedel. Pairing vibration and particle-hole states excited in the reaction  $^{206}\text{Pb}(\text{t}, \text{p})^{208}\text{Pb}$ . *Nucl. Phys.*, 92:145, 1967.
- Broglia, R.A., O. Hansen, and C. Riedel. Two-neutron transfer reactions and the pairing model. *Advances in Nuclear Physics*, 6:287, 1973. URL [www.mi.infn.it/~vigezzi/BHR/BrogliaHansenRiedel.pdf](http://www.mi.infn.it/~vigezzi/BHR/BrogliaHansenRiedel.pdf).
- P. A. M. Dirac. *The principles of quantum mechanics*. Oxford University Press, London, 1930.
- R. J. Glauber. In R. J. Glauber, editor, *International School of Physics “Enrico Fermi” Course XLII on Quantum Optics*, page 15, Academic Press, 1969. New York.
- W. Heisenberg. Über quantentheoretische umdeutung kinematischer und mechanischer beziehungen. *Z. Phys.*, 33:879, 1925.
- W. Heisenberg. Über der anschaulichen inhalt der quantentheoretischen kinematik und mechanik. *Z. Phys.*, 43:172, 1927.
- M. Moshinsky. Transformation brackets for harmonic oscillator functions. *Nucl. Phys.*, 13:104, 1959.

- B. Mottelson. Selected topics in the theory of collective phenomena in nuclei. In G. Racah, editor, *International School of Physics “Enrico Fermi” Course XV, Nuclear Spectroscopy*, page 44, New York, 1962. Academic Press.
- W. Pauli. Zur quantenmechanik ii. *Zeitschr. Phys.*, 31:625, 1925.
- Potel, G., A. Idini, F. Barranco, E. Vigezzi, and R. A. Broglia. Cooper pair transfer in nuclei. *Rep. Prog. Phys.*, 76:106301, 2013.
- J. Schrieffer. *Superconductivity*. Benjamin, New York, 1964.
- Schrödinger, E. Quantisierung als eigenwertproblem. *Annalen der Phys.*, 384:273, 1926.
- Y. C. Tang and R. C. Herndon. Form factors of  $^3\text{H}$  and  $^4\text{He}$  with repulsive–core potentials. *Phys. Lett.*, 18:42, 1965.



## Chapter 6

# Nuclear Structure with two-nucleon transfer

In what follows, we apply the formalism worked out in the previous chapter with the help of software developed to calculate absolute two-particle transfer differential cross sections, associated with reactions induced by both light and heavy ions (cf. App. 6.D COOPER, ONE). A number of examples are treated with special detail. Namely, two-particle transfer in light pairing vibrational nuclei, including the halo unstable nucleus  $^{11}\text{Li}$ , in superfluid medium heavy nuclei lying along the stability valley (Sn-isotopes) and in heavy closed shell systems (Pb). In this last case both for light and heavy ion projectiles.

### 6.1 The $^1\text{H}(^{11}\text{Li}, ^9\text{Li})^3\text{H}$ reaction: evidence for phonon mediated pairing

We start by discussing the analysis of the two-neutron pickup reaction  $^1\text{H}(^{11}\text{Li}, ^9\text{Li})^3\text{H}$  (Tanihata, I. et al., 2008). Particular attention is paid to the excitation of the  $1/2^-$  first excited state of  $^9\text{Li}$  lying at 2.69 MeV (cf. Figs. 6.1.1 and 6.1.2). To assess the direct character of the  $1/2^-$  excitation process, the importance of inelastic (cf. Appendix 1E de la introducción inelastic scattering) and knockout (cf. Ch.4) channels were considered and found to be small (see App. 6.B). The results thus provide evidence for a new mechanism of pairing correlations in nuclei: pigmy resonance mediated pairing interaction (Barranco, F. et al. (2001), see also App. 6.A), which strongly renormalizes the bare,  $NN^{-1}S_0$  interaction (Potel et al., 2010). This is but a particular embodiment of phonon mediated pairing interaction found throughout in nuclei (cf. e.g. Barranco et al. (1999); Gori et al. (2004) cf. also Brink, D. and Broglia (2005)). The main difference between light halo exotic nuclei and medium heavy superfluid nuclei lying along the valley of stability is the role fluctuations play in dressing particles (quasiparticles) and in renormalizing their properties (mass, charge, etc.) and their interactions. In fact, in the case of e.g. Sn

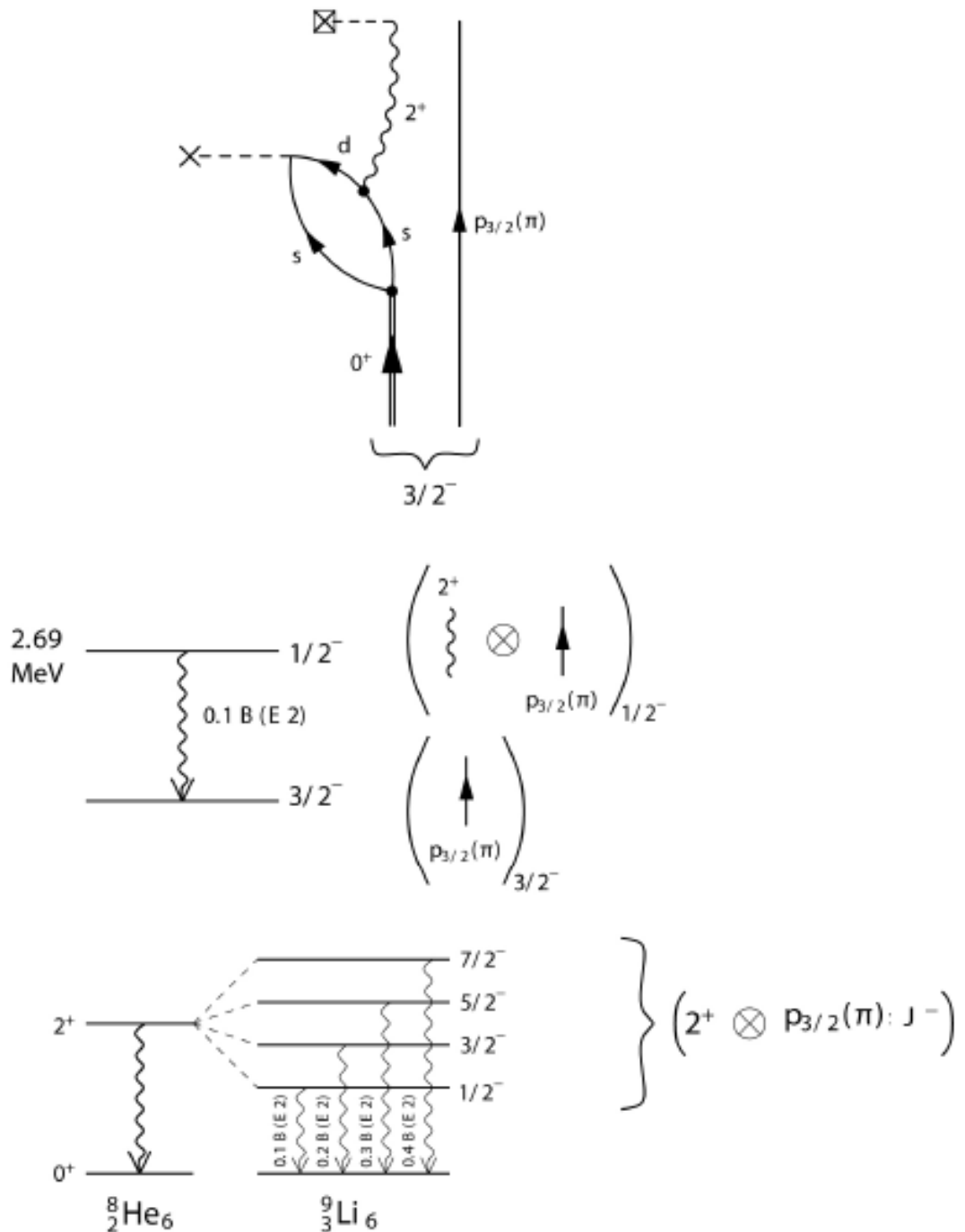


Figure 6.1.1: *Gedanken* (two-particle transfer) coincidence experiments aimed at better individuating the couplings involved in the neutron halo Cooper pair correlations in  $^{11}\text{Li}$  and of the  $1/2^-$  first excited state of  $^{9}\text{Li}$  populated in the  $^1\text{H}(^{11}\text{Li}, ^9\text{Li})^3\text{H}$  reaction (Barranco, F. et al. (2001); Potel et al. (2010)). From Potel et al. (2014).

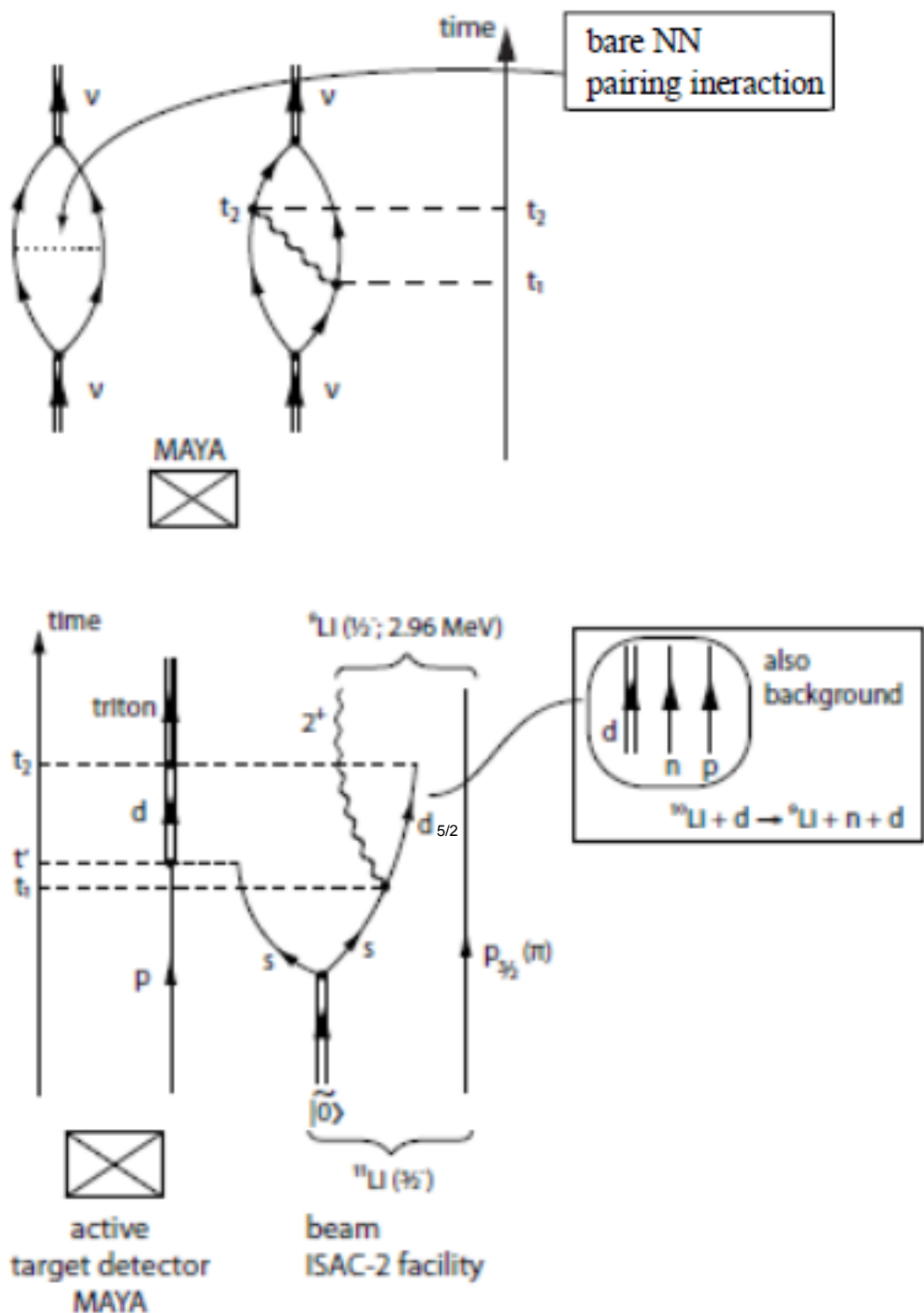


Figure 6.1.2: Schematic representation of the bare nucleon-nucleon and phonon induced pairing correlations (upper part) NFT diagrams, and of the population of the first, excited state of  ${}^9\text{Li}(1/2^-; 2.69 \text{ MeV})$ , in the TRIUMF experiment reported in ref. Tanihata, I. et al. (2008).

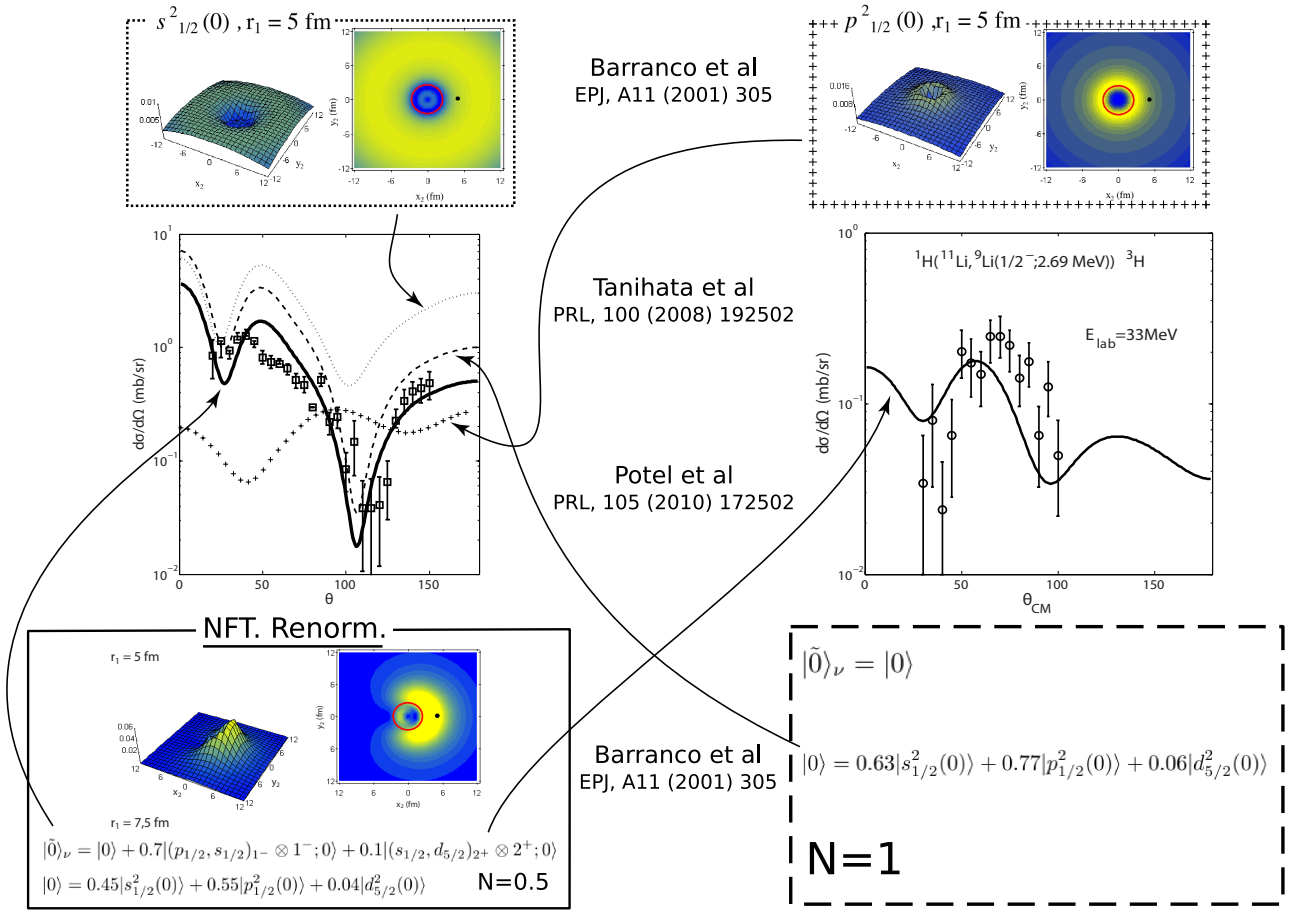


Figure 6.1.3: Absolute, two-nucleon transfer differential cross section associated with the ground state and the first excited state of  ${}^9\text{Li}$ , excited in the reaction  ${}^1\text{H}({}^{11}\text{Li}, {}^9\text{Li}) {}^3\text{H}$  (Tanihata, I. et al., 2008) in comparison with the predicted differential cross sections (Potel et al., 2010) calculated making use of spectroscopic amplitudes and Cooper pair wavefunctions calculated in NFT.

isotopes, mean field effects are dominant, while in the case of halo exotic nuclei renormalization effects can be as large as mean field ones.

### 6.1.1 Structure

Within the scenario presented in Chapter 2 (App. 2.6) and Chapter 4 (Sect. 4.2.2) the wavefunction describing the structure of the halo neutrons in the ground state of  $^{11}\text{Li}$  (the  $p_{3/2}$  proton being assumed to act only as a spectator) can be written as

$$|0\rangle_v = |0\rangle + \alpha|(p_{1/2}, s_{1/2})_{1^-} \otimes 1^-; 0\rangle + \beta|(s_{1/2}, d_{5/2})_{2^+} \otimes 2^+; 0\rangle, \quad (6.1.1)$$

with

$$\alpha = 0.7, \quad \text{and} \quad \beta = 0.1, \quad (6.1.2)$$

and

$$|0\rangle = 0.45|s_{1/2}^2(0)\rangle + 0.55|p_{1/2}^2(0)\rangle + 0.04|d_{5/2}^2(0)\rangle, \quad (6.1.3)$$

$|1^-\rangle$  and  $|2^+\rangle$  being the (RPA) states describing the dipole pigmy resonance of  $^{11}\text{Li}$  and the quadrupole vibration of the core. While these states are virtual excitations which, exchanged between the two neutrons bind them to the Fermi surface provided by the  $^9\text{Li}$  core, they can be forced to become real with the help of the specific probe of Cooper pairs in nuclei, namely two-particle transfer reactions (Figs. 6.1.2 and 6.1.3).

$^{11}\text{Li}(p, t)^9\text{Li}$												
	$V$	$W$	$V_{so}$	$W_d$	$r_1$	$a_1$	$r_2$	$a_2$	$r_3$	$a_3$	$r_4$	$a_4$
$p, {}^{11}\text{Li}^d)$	63.62	0.33	5.69	8.9	1.12	0.68	1.12	0.52	0.89	0.59	1.31	0.52
$d, {}^{10}\text{Li}^b)$	90.76	1.6	3.56	10.58	1.15	0.75	1.35	0.64	0.97	1.01	1.4	0.66
$t, {}^9\text{Li}^c)$	152.47	12.59	1.9	12.08	1.04	0.72	1.23	0.72	0.53	0.24	1.03	0.83

Table 6.1.1: Optical potentials (cf. Tanihata, I. et al. (2008)) used in the calculation of the absolute differential cross sections displayed in Fig. 6.1.3.

We are then in presence of a paradigmatic nuclear embodiment of Cooper's model which is at the basis of BCS theory: a single weakly bound neutron pair on top of the Fermi surface of the  $^9\text{Li}$  core. But the analogy goes beyond these aspects, and covers also the very nature of the interaction acting between Cooper pair partners. Due to the the high polarizability of the system under study and of the small overlap of halo and core single particle wavefunctions, most of the Cooper pair correlation energy stems, according to NFT, from the exchange of collective vibrations, the role of the strongly screened bare interaction being, in this case, minor and subcritical (see App. 2.6). In other words, we are in the presence of a new realization of Cooper's model in which a totally novel Bardeen–Pines–Frölich–like phonon induced interaction is generated by a self induced collective vibration of the nuclear medium. In connection with (6.1.1), it is revealing that,

the two final states excited in the inverse kinematics, two-neutron pick up reaction  ${}^1\text{H}({}^{11}\text{Li}, {}^9\text{Li}){}^3\text{H}$  are, the  $|3/2^- \text{gs}({}^9\text{Li})\rangle$  and the first excited  $|1/2^-, 2.69\text{MeV}\rangle$  Tanihata, I. et al. (2008). In fact, the associated absolute differential cross sections probe, within the NFT scenario, the  $|0\rangle$  and the  $|(s_{1/2}, d_{5/2})_{2^+} \otimes 2^+; 0\rangle$  component of the Cooper pair wavefunction respectively, (Fig. 6.1.2 cf. also Figs 4.2.5 and 4.2.6; cf. also Figs. 6.1.3 and 2.6.3 1F3). They were calculated making use of modified formfactors worked out (cf. App. 6.C) making use of the spectroscopic amplitudes given in Eqs. (6.1.1–6.1.3) and of the optical potentials collected in Table 6.1.1 and are compared with the experimental findings in Fig. 6.1.3. Theory reproduces the absolute two-particle differential cross section within experimental errors. But, more important, it provides a general picture of the physics behind the workings of halo pair addition modes.

### 6.1.2 Reaction

Because second order calculations of inelastic, break up and final state interaction channels, which in principle can provide alternative routes for the population of the  $|1/2^-, 2.69\text{MeV}\rangle$  (see Fig. 6.B.1) state to that predicted by the wavefunction (6.1.1) ( $\beta$  component), lead to absolute cross sections which are smaller by few orders of magnitude than that shown in Fig. 6.1.3 (see Figs. 6.B.2, 6.B.3, as well as Table 6.B.1, Potel et al. (2010)), one can posit that quadrupole core polarization effects in  $|\text{gs}({}^{11}\text{Li})\rangle$  is essential to account for the observation of the  $|1/2^-, 2.69\text{ MeV}\rangle$  state, thus providing direct evidence for phonon mediated pairing in nuclei.

The reason why in the case of  ${}^{11}\text{Li}$  evidence for phonon mediated pairing is, arguably, inescapable, is connected with the fact that reaching the limits of stability associated with drip line nuclei, the system also reaches to situations in which medium polarization effects become overwhelming. In fact, one is, in such cases confronted with elementary modes of nuclear excitation in which dynamic fluctuation effects are as important as static, mean field effects. Within this context we refer to parity inversion (cf. Figs. 2.6.3 and 4.2.4). Nuclear Field Theory within the Bloch–Horowitz (Dyson) set up which allows one to sum to infinite order little convergent processes are specially suited to study these systems (cf. e.g. Barranco, F. et al. (2001) and Gori et al. (2004)). From these studies it emerges a possible new elementary mode of excitation, namely pair addition halo vibration, of which  $|\text{gs}({}^{11}\text{Li})\rangle$  state is a concrete embodiment. They are associated with a novel mechanism for stabilizing Cooper pairs, which arises from a (dynamical) breakup of gauge invariance (cf. App 6.A). Their most distinctive feature, namely that of carrying on top of it a (dipole) pigmy resonance at a relative excitation energy of about 1 MeV, a necessary although not sufficient condition for this new mode to exist, can be instrumental for its characterization. While in the case of Li it constitutes the ground state, in other nuclei it may be an excited state which could be observed in a combined  $L = 0$ , and  $L = 1$ , two-particle transfer reaction to excited states, or in terms of  $E1$  decay of the pigmy resonance built on top of it. Within this context, it is an open question whether one could expect to find a realization of such a halo

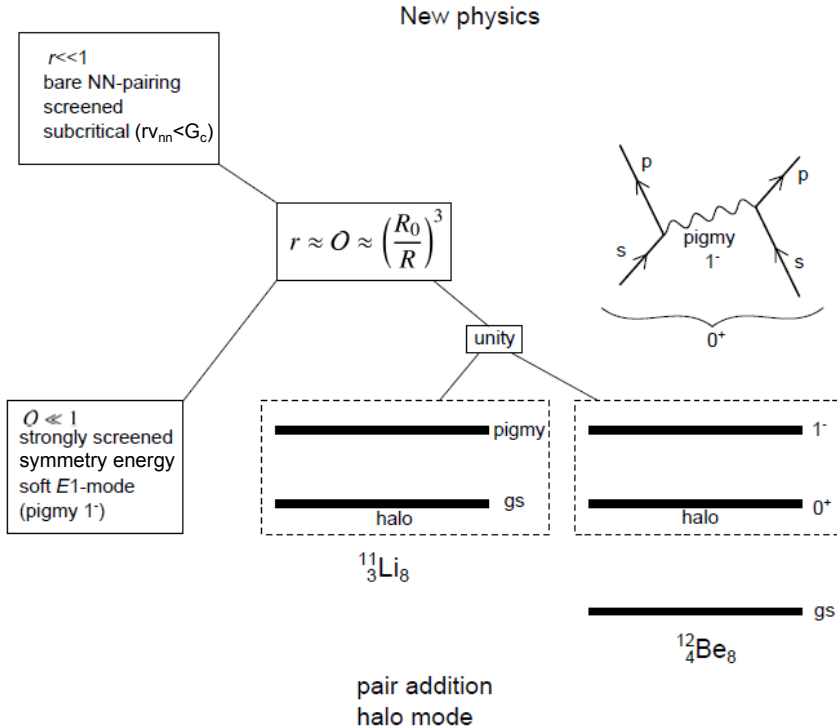


Figure 6.1.4: Schematic representation of a possible realization of halo pair addition mode in terms of the first excited  $0^+$  state (2.24 MeV) of  $^{12}\text{Be}$  (for details see App. 2.6).

pair addition mode in, for example, the first excited state of  $^{12}\text{Be}$  (see Fig. 6.1.4).

Pairing elementary modes of excitation based on  $s_{1/2}$  and  $p_{1/2}$  states at threshold have been found to lead, within the framework of a bare, short range, pairing interaction scheme to halo anti-pairing effects (cf. Bennaceur, K. et al. (2000), cf. also Hamamoto and Mottelson (2003), Hamamoto, I. and Mottelson (2004)). The fact that the separation energy of the halo neutrons (halo Cooper pair) of  $^{11}\text{Li}(\text{gs})$  is  $\approx 400\text{keV}$ , testifies to the fact that the anti-halo pairing effect is, in this case, overwhelmed by (dynamical) medium polarization effects.

Within this context it is of notice that, again, the interweaving of the different elementary modes of nuclear excitation, pairing and pigmy resonances in the present case, condition reaction studies, let alone the possibility to study (pigmy) giant resonances built on excited states, and to provide a novel test of the Brink-Axel hypothesis which is at the basis of the statistical description of photon decay from hot (compound) nuclei (cf. Brink (1955); cf. also Bortignon, P.F. et al. (1998), Bertsch, G. F. and Broglia (1986) and references therein).

Before concluding this section we provide in Fig. 6.1.5 examples of pairing vibrational states based on  $^9_3\text{Li}_6$ ,  $^{10}_4\text{Be}_6$ ,  $^{48}_{20}\text{Ca}_{28}$  and  $^{208}_{82}\text{Pb}_{126}$ ,  $N = 6$ ,  $N = 28$

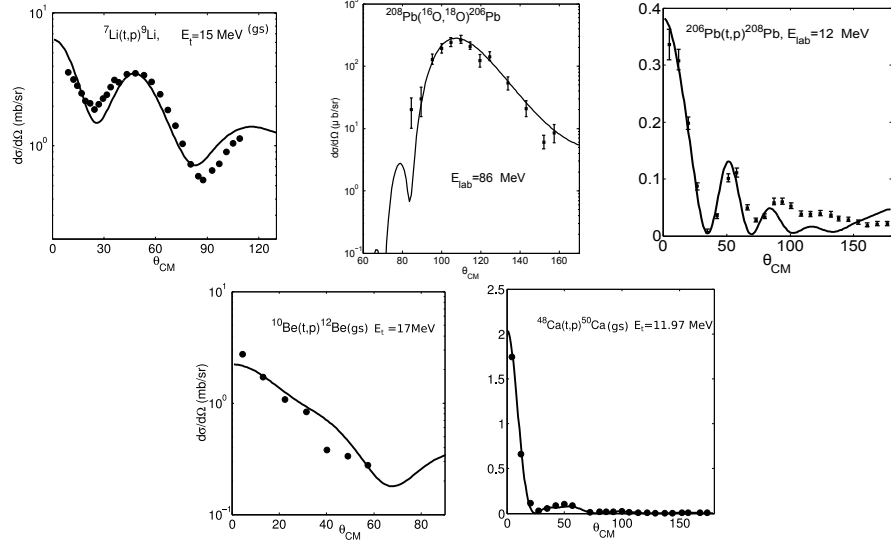


Figure 6.1.5: Absolute two-particle transfer differential cross sections for a number of reactions. Making use of spectroscopic amplitudes calculated as described in App. 2.5 in the particular case of  $N = 126$  (Pb),  $N = 48$  (Ca), and  $N = 6$  (Li,Be), of global optical parameters and of the software COOPER, the absolute differential cross sections were calculated and are displayed in comparison with the experimental data (after Potel, G. et al. (2013a)).

and  $N = 126$  neutron closed shell systems. The fact that among the  $(p,t)$  and  $(t,p)$  absolute differential cross sections one also finds the  $^{208}\text{Pb}(^{16}\text{O},^{18}\text{O})^{206}\text{Pb}(\text{gs})$  absolute differential cross section is in keeping with the fact that the formalism to treat both light and heavy ions two-nucleon transfer reactions and their connection is well known (cf. Broglia and Winther (2004), Bayman and Chen (1982) and Thompson (1988) and references therein) and rather homogeneous (cf. Potel, G. et al. (2013b)). Thus, it has been implemented in the software COOPER as a standard option (cf. App. 6.D).

## 6.2 Pairing rotational band with two-nucleon transfer: Sn-isotopes

Nuclear superfluidity can be studied at profit in terms of the mean field, (cf. also Sect. 2.4.2) BCS diagonalization of the pairing Hamiltonian, namely,

$$H = H_{sp} + V_p, \quad (6.2.1)$$

where

$$H_{sp} = \sum_{\nu} (\epsilon_{\nu} - \lambda) a_{\nu}^{\dagger} a_{\nu}, \quad (6.2.2)$$

while

$$V_p = -\Delta(P^+ + P) - \frac{\Delta^2}{G}, \quad (6.2.3)$$

and

$$\Delta = G\alpha_0, \quad (6.2.4)$$

is the pairing gap ( $\Delta \approx 12 \text{ MeV}/\sqrt{A}$ ),  $G$  ( $\approx 25 \text{ MeV}/A$ ) being the pairing coupling constant (Bohr, A. and Mottelson, 1975), and

$$P^+ = \sum_{\nu>0} P_\nu^+ = \sum_{\nu>0} a_\nu^+ a_{\bar{\nu}}^+, \quad (6.2.5)$$

$$P = \sum_{\nu>0} a_{\bar{\nu}} a_\nu, \quad (6.2.6)$$

are the pair addition and pair removal operators,  $a_\nu$  and  $a_\nu^+$  being single-particle creation and annihilation operators, ( $\nu\bar{\nu}$ ) labeling pairs of time reversal states.

The BCS ground state wavefunction describing the most favorable configuration of pairs to profit from the pairing interaction, can be written in terms of the product of the occupancy probabilities  $h_\nu$  for individual pairs,

$$|BCS\rangle = \prod_{\nu>0} ((1 - h_\nu)^{1/2} + h_\nu^{1/2} a_\nu^+ a_{\bar{\nu}}^+) |0\rangle, \quad (6.2.7)$$

where  $|0\rangle$  is the fermion vacuum (Schrieffer (1964); Schrieffer, J. R. (1973)).

Superfluidity is tantamount to the existence of a finite average value of the operators (6.2.5), (6.2.6) in this state, that is, to a finite value of the order parameter

$$\alpha_0 = \langle BCS | P^+ | BCS \rangle = \langle BCS | P | BCS \rangle^*, \quad (6.2.8)$$

which is equivalent to Cooper pair condensation. In fact,  $\alpha_0$  gives a measure of the number of correlated pairs in the BCS ground state which in the nuclear case is few units ( $< 10$ ). While the pairing gap (6.2.4) is an important quantity relating theory with experiment,  $\alpha_0$  provides the specific measure of superfluidity. In fact, the matrix elements of the pairing interaction may vanish for specific regions of space, or in the case of specific pairs of time reversal orbits, but this does not necessarily imply a vanishing of the order parameter  $\alpha_0$ , nor the obliteration of superfluidity.

In keeping with the fact that Cooper pair tunneling is proportional to  $|\alpha_0|^2$ , this quantity plays also the role of a ( $L = 0$ ) two-nucleon transfer sum rule, sum rule which is essentially exhausted by the superfluid nuclear  $|BCS\rangle$  ground state (see Fig. 2.1.3).

### 6.2.1 Fluctuations

The BCS solution of the pairing Hamiltonian was recasted by Bogoljubov (1958) and Valatin (1958) in terms of quasiparticles,

$$a_\nu^+ = U_\nu a_\nu^+ - V_\nu a_{\bar{\nu}}, \quad (6.2.9)$$

linear transformation inducing the rotation in  $(a^+, a)$ -space which diagonalizes the Hamiltonian (6.2.1).

The variational parameters  $U_\nu, V_\nu$  appearing in the above relation indicate that  $a_\nu^+$  acting on  $|0\rangle$  creates a particle in the state  $|\nu\rangle$  which is empty with a probability  $U_\nu^2 (\equiv (1 - h_\nu) = (1 + (\epsilon_\nu - \lambda)/E_\nu)/2)$ , and annihilates a particle in the time reversal state  $|\bar{\nu}\rangle$  (creates a hole) which is occupied with probability  $V_\nu^2 (\equiv h_\nu = (1 - (\epsilon_\nu - \lambda)/E_\nu)/2)$ . Thus,

$$|BCS\rangle = \Pi_{\nu>0} (U_\nu + V_\nu a_\nu^+ a_{\bar{\nu}}^+) |0\rangle, \quad (6.2.10)$$

is the quasiparticle vacuum, as  $|BCS\rangle \sim \Pi_\nu \alpha_\nu |0\rangle$ , the order parameter being

$$\alpha_0 = \sum_{\nu>0} U_\nu V_\nu. \quad (6.2.11)$$

In Table 6.2.1 we collect the spectroscopic amplitudes associated with the reactions  $^{A+2}\text{Sn}(p,t)^A\text{Sn}$ , for  $A$  in the interval 112–126. Making use of these results and of global optical parameters (see Table 6.2.2), the absolute differential cross section  $^{A+2}\text{Sn}(p,t)^A\text{Sn(gs)}$  were calculated. They are shown in Fig. 6.2.1 in comparison with the data.

## 6.2.2 Pairing rotations

	$^{112}\text{Sn}$	$^{114}\text{Sn}$	$^{116}\text{Sn}$	$^{118}\text{Sn}$	$^{120}\text{Sn}$	$^{122}\text{Sn}$	$^{124}\text{Sn}$
$1d_{5/2}$	0.664	0.594	0.393	0.471	0.439	0.394	0.352
$0g_{7/2}$	0.958	0.852	0.542	0.255	0.591	0.504	0.439
$2s_{1/2}$	0.446	0.477	0.442	0.487	0.451	0.413	0.364
$1d_{3/2}$	0.542	0.590	0.695	0.706	0.696	0.651	0.582
$0h_{11/2}$	0.686	0.720	1.062	0.969	1.095	1.175	1.222

Table 6.2.1: Two-nucleon transfer spectroscopic amplitudes  $\langle BCS(A)|P_\nu|BCS(A+2)\rangle = \sqrt{(2j_\nu + 1)/2} U_\nu(A) V_\nu(A+2)$ , associated with the reactions connecting the ground states (members of a pairing rotational band) of two superfluid Sn-nuclei  $^{A+2}\text{Sn}(p,t)^A\text{Sn(gs)}$  (Potel, G. et al. (2013a)).

The phase of the ground state BCS wavefunction may be chosen so that  $U_\nu = |U_\nu| = U'_\nu$  is real and  $V_\nu = V'_\nu e^{2i\phi}$  ( $V'_\nu \equiv |V_\nu|$ ). Thus (Schrieffer, J. R., 1973),

$$\begin{aligned} |BCS(\phi)\rangle_{\mathcal{K}} &= \Pi_{\nu>0} (U'_\nu + V'_\nu e^{-2i\phi} a_\nu^+ a_{\bar{\nu}}^+) |0\rangle = \Pi_{\nu>0} (U'_\nu + V'_\nu a_\nu^{'-} a_{\bar{\nu}}^{'-}) |0\rangle \\ &= |BCS(\phi = 0)\rangle_{\mathcal{K}'}, \end{aligned} \quad (6.2.12)$$

where  $a_\nu^{'-} = e^{-i\phi} a_\nu^+$  and  $a_{\bar{\nu}}^{'-} = e^{-i\phi} a_{\bar{\nu}}^+$ . This is in keeping with the fact that  $a_\nu^+$  and  $a_{\bar{\nu}}^+$  are single-particle creation operators which under gauge transformations (rotations in the 2D-gauge space of angle  $\phi$ ) induced by the operator  $G(\phi) = e^{-i\hat{N}(\phi)}$  and connecting the intrinsic and the laboratory frames of reference  $\mathcal{K}'$  and  $\mathcal{K}$  respectively, behave according to  $a_\nu^{'-} = G(\phi) a_\nu^+ G^{-1}(\phi) = e^{-i\phi} a_\nu^+$  and  $a_{\bar{\nu}}^{'-} = G(\phi) a_{\bar{\nu}}^+ G^{-1}(\phi) =$

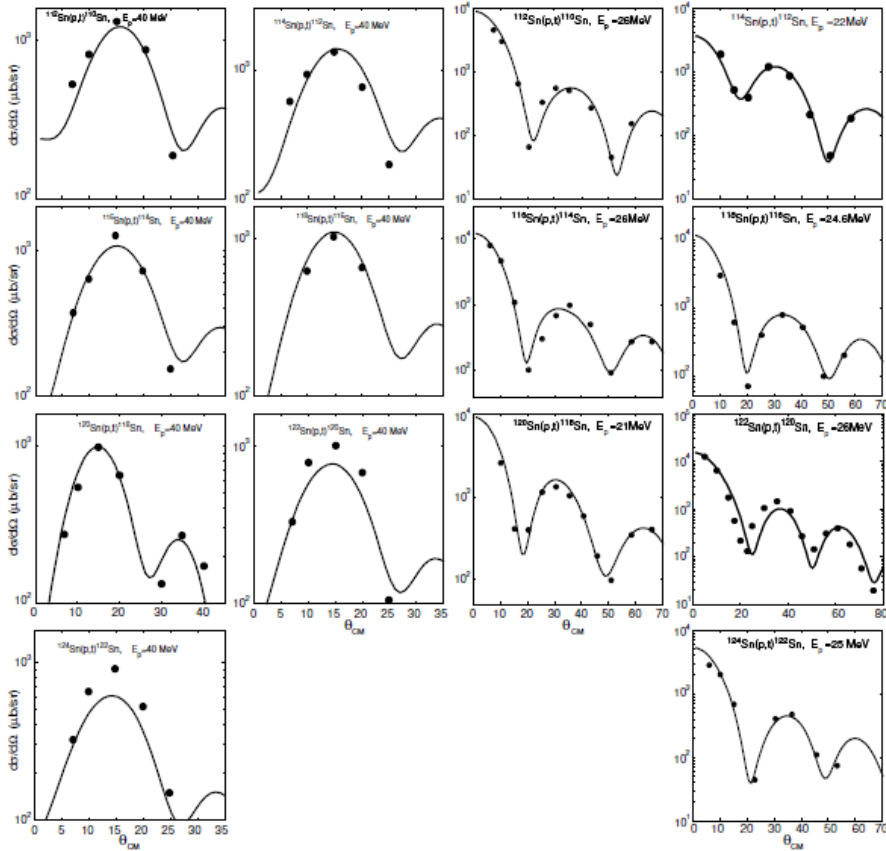


Figure 6.2.1: Predicted (Potel, G. et al. (2013a,b)) absolute differential  $^{A+2}\text{Sn}(p, t)^A\text{Sn}(\text{gs})$  cross sections for bombarding energies  $E_p=40$  MeV (in the two left columns) and  $21 \text{ MeV} \leq E_p \leq 26$  MeV (in the two right columns) in comparison with the experimental data (Bassani et al. (1965), Guazzoni, P. et al. (1999), Guazzoni, P. et al. (2004), Guazzoni, P. et al. (2006), Guazzoni, P. et al. (2008), Guazzoni, P. et al. (2011), Guazzoni, P. et al. (2012)).

${}^A\text{Sn}(p,t){}^{A-2}\text{Sn}$												
	$V$	$W$	$V_{so}$	$W_d$	$r_1$	$a_1$	$r_2$	$a_2$	$r_3$	$a_3$	$r_4$	$a_4$
$p, {}^A\text{Sn}^a)$	50	5	3	6	1.35	0.65	1.2	0.5	1.25	0.7	1.3	0.6
$d, {}^{A-1}\text{Sn}^b)$	78.53	12	3.62	10.5	1.1	0.6	1.3	0.5	0.97	0.9	1.3	0.61
$t, {}^{A-2}\text{Sn}^a)$	176	20	8	8	1.14	0.6	1.3	0.5	1.1	0.8	1.3	0.6

Table 6.2.2: Optical potentials used in the calculations of the absolute differential cross sections displayed in Fig. 6.2.1.

$e^{-i\phi}a_\nu^+$ , a consequence of the fact that  $\hat{N}$  is the number operator and that  $[\hat{N}, a_\nu^+] = a_\nu^+$ .

The fact that the mean field ground state ( $|BCS(\phi)\rangle_{\mathcal{K}}$ ) is a product of operators - one for each pair state - acting on the vacuum, implies that (6.2.12) represents an ensemble of ground state wavefunctions averaged over systems with ... $N-2, N, N+2$ ... even number of particles. In fact, (6.2.12) can also be written in the form

$$\begin{aligned} |BCS\rangle_{\mathcal{K}} = (\Pi_{\nu>0} U'_\nu) (1 + \dots + \frac{e^{-(N-2)i\phi}}{\binom{N-2}{2}!} \left( \sum_{\nu>0} c_\nu a_\nu^+ a_\nu^+ \right)^{\frac{N-2}{2}} + \frac{e^{-Ni\phi}}{\binom{N}{2}!} \left( \sum_{\nu>0} c_\nu a_\nu^+ a_\nu^+ \right)^{\frac{N}{2}} \\ + \frac{e^{-(N+2)i\phi}}{\binom{N+2}{2}!} \left( \sum_{\nu>0} c_\nu a_\nu^+ a_\nu^+ \right)^{\frac{N+2}{2}} + \dots) |0\rangle, \end{aligned} \quad (6.2.13)$$

where  $c_\nu = V'_\nu / U'_\nu$ .

Adjusting the Lagrange multiplier  $\lambda$  (chemical potential, see Eqs. (6.2.9, 6.2.10) and associated text), one can ensure that the mean number of fermions has the desired value  $N_0$ . Summing up, the BCS ground state is a wavepacket in the number of particles. In other words, it is a deformed state in gauge space defining a privileged orientation in this space, and thus an intrinsic coordinate system  $\mathcal{K}'$  (Anderson, 1958; Bohr, 1964; Bès,D. R. and Broglia, 1966). The magnitude of this deformation is measured by  $\alpha_0$ , a quantity whose modulus squared value is connected with the absolute value of the two-nucleon transfer cross section. A further element, if it was still the need, which testifies that two-nucleon transfer is specific to probe pairing in nuclei.

### 6.2.3 Pairing vibrations in superfluid nuclei

All the above arguments, point to a static picture of nuclear superfluidity which results from BCS theory. This is quite natural, as one is dealing with a mean field approximation. The situation is radically changed taking into account the interaction acting among the Cooper pairs (quasiparticles) which has been neglected until now, that is the term  $-G(P^+ - \alpha_0)(P - \alpha_0)$  left out in the mean field (BCS) approximation leading to (6.2.3). This interaction can essentially be written as (for details

see e.g. Brink, D. and Broglia (2005) Apps. G, I and J and references therein)

$$H_{\text{residual}} = H'_p + H''_p, \quad (6.2.14)$$

where

$$H'_p = -\frac{G}{4} \left( \sum_{\nu>0} (U_\nu^2 - V_\nu^2)(P_\nu^+ + P_\nu^-) \right)^2, \quad (6.2.15)$$

and

$$H''_p = \frac{G}{4} \left( \sum_{\nu>0} (P^+ - P^-) \right)^2. \quad (6.2.16)$$

The term  $H'_p$  gives rise to vibrations of the pairing gap which (virtually) change particle number in  $\pm 2$  units. The energy of these pairing vibrations cannot be lower than  $2\Delta$ . They are, as a rule, little collective, corresponding essentially to almost pure two-quasiparticle excitations (see excited  $0^+$  states of Fig. 2.1.3).

The term  $H''_p$  leads to a solution of particular interest, displaying exactly zero energy, thus being degenerate with the ground state. The associated wavefunction is proportional to the particle number operator and thus to the gauge operator inducing an infinitesimal rotation in gauge space. The fluctuations associated with this zero frequency mode diverge, although the Hamiltonian defines a finite inertia. A proper inclusion of these fluctuations (of the orientation angle  $\phi$  in gauge space) restores gauge invariance in the  $|BCS(\phi)\rangle_K$  state leading to states with fixed particle number

$$|N_0\rangle \sim \int_0^{2\pi} d\phi e^{iN_0\phi} |BCS(\phi)\rangle_K \sim \left( \sum_{\nu>0} c_\nu a_\nu^+ a_\nu^- \right)^{N_0/2} |0\rangle. \quad (6.2.17)$$

These are the members of the pairing rotational band, e.g. the ground states of the superfluid Sn-isotope nuclei. These states provide the nuclear embodiment of Schrieffer's ensemble of ground state wavefunctions which is at the basis of the BCS theory of superconductivity. An example of such a rotational band is provided by the ground states of the Sn-isotopes (cf. Fig. 2.1.3). Making use of COOPER, namely of an implementation of two-nucleon transfer second order DWBA which includes successive and simultaneous transfer, properly corrected from non-orthogonality contributions, of the spectroscopic amplitudes collected in Table 6.2.1 (see also Table 2.4.1), and of global optical parameters from the literature (see Table 6.2.2), the two-nucleon transfer absolute differential cross sections associated with the Sn-isotopes rotational band have been calculated. They are compared with the experimental findings in Fig. 6.2.1 (cf. also Fig. 2.2.1 and Potel, G. et al. (2013a,b)).

Summing up, a collective solution always comes at frequency  $\nu = 0$ . Proper inclusion of the associated divergent ZPF of the  $\nu = 0$  modes restores symmetry by projecting the solution onto the laboratory frame of reference, where measurements can be carried out and thus, symmetries are to be respected. Within his context, it

is observed that the  $\omega = 0$  ( $E = h\nu = \hbar\omega$ ) solution of  $H_p''$  finds its counterpart in the  $\omega = 0$  solution of  $H_D$  (cf. Eq. (2.6.6)). In the first case it restores gauge invariance, the associated collective modes being pairing rotational bands. In the second it restores translational invariance, the associated collective modes being, in the case of a single nucleus of mass number  $A$ , the GDR and the uniform translation of the nucleus as a whole with inertia  $AM$ . In the case of a direct reaction, for example of the two-nucleon transfer process  $a(= b + 2) + A \rightarrow b + B(= A + 2)$ , the collective modes are the GDR of the different nuclei involved (**structure**), and the continuous evolution of the relative motion (with varying reduced masses let alone the uniform motion of the CM) of the reacting nuclei, for each partial wave (quantal) or impact parameter (semiclassical), from the initial (to the intermediate  $f(= b + 1) + F(= A + 1)$ ), to the final channel (**reaction**). This continuity reflects the constrain  $H = H_a + H_A = H_f + H_F = H_b + H_B$ , which, in e.g. the semiclassical approximation is implemented by second order diagonalization of the operators  $\exp(\sigma_1 + \sigma_2)$  (recoil) and  $\exp(i/\hbar\gamma(t))$  ( $Q$ -value) (cf. App. 5.C, Eq. 5.C.4). In quantum mechanics (second order DWBA), it is implemented by diagonalizing  $v_{np}$  to second order perturbation, in terms of partial wave expansions of the wavefunctions of relative motion associated with the variety of channels involved in the reaction process (cf. Figs. 3.1.1 and 3.1.2), as well as the NFT diagrams displayed in Figs. 5.C.1 and 5.C.2 (jaggy line)). It is, of course, the concrete (microscopic) implementation of structure (cf. Eqs. 6.1.1–6.1.3 ( $^{11}\text{Li}$ ) and Table 6.2.1 (Sn-isotopes)) and reaction (cf. the equation given in Figs. (3.1.1) and (3.1.2) at the basis of the software COOPER, plus global optical potentials), which eventually allows to compare theory with experiment in terms of absolute cross sections (Fig. 6.B.2 ( $^{11}\text{Li}(p, t)^9\text{Li}(\text{gs})$ ) and Fig. 4.2.1 ( $^{A+2}\text{Sn}(p, t)^A\text{Sn}(\text{gs})$ )), which eventually validates or less, the soundness of the chain of concepts: spontaneous symmetry breaking  $\rightarrow$  restoration  $\rightarrow$  emergent properties, as a valid tool to individuate collective modes in particular, and new physics in general.

We note that in the above examples namely  $^{11}\text{Li}$  and Sn-isotopes, one is talking about dynamical ( $\omega \approx 0$ ; 380 keV) and static ( $\omega = 0$ ) breaking of gauge invariance respectively essentially on equal footing. Arguably, one is allowed to do so in keeping with the central role fluctuations in general and pairing vibrations in particular, play in atomic nuclei around closed shells, specially around the  $N = 6$  magic number.

### 6.3 BCS-like nucleon–nucleon correlation (Cooper pair)

The specific probe to quantitative test how much BCS-like correlated are two nucleons (nucleon holes) moving on top of the Fermi surface (in the Fermi sea) and interacting through an attractive pairing force, nuclear embodiment of a Cooper pair and known as pair addition (pair removal) modes (Bohr, A. and Mottelson (1975), Bès, D. R. and Broglia (1966)), is through two-nucleon transfer processes, e.g. through a  $(p, t)$  ( $a(t, p)$ ) reaction, like e.g.  $^1\text{H}(^{11}\text{Li}, ^9\text{Li}(\text{gs}))^3\text{H}$  and  $(^{206}\text{Pb}(t, p)^{208}\text{Pb})$ .

Let us start discussing the second one. In Fig. 3.4.4 we show the predictions of the pairing vibrational model in comparison with the experimental data (Bjergaard, J. H. et al. (1966)). The calculations were carried out making use of the software COOPER and of the spectroscopic amplitudes collected in Tables 2.5.2 and 2.5.3, and corresponding to the RPA,  $X$ - and  $Y$ - amplitudes associated with  $^{208}\text{Pb}$  pair removal mode, i.e. describing the ground state of  $^{206}\text{Pb}$  (two holes interacting via a pairing force of constant matrix element, and allowed to move in the single-particle valence orbitals; cf. Table 2.4.1). The global optical parameters for the proton and the triton were taken from the experimental paper, while those of the deuteron channel needed in COOPER to work out the successive transfer amplitude was taken from (An and Cai (2006)). Theory (RPA) provides an overall account of the observations ( $\sigma = 0.52\text{mb}$  to be compared with the experimental finding  $0.68 \pm 0.24\text{ mb}$ ).

The large cross section, also for the pair addition mode, that is, associated with the population of the two-phonon ( $2p - 2h$ ) pairing vibrational state of  $^{208}\text{Pb}$  ( $0^+$ ; 4.95 MeV) was interpreted in Bertsch, G. F. et al. (1967) in terms of the angular correlation between the two fermions (holes) displayed in figure 7 of this reference (cf. also Figs. 2.4 and 2.5 Brink, D. and Broglia (2005)). By plotting the modulus square of the two-hole wavefunction as a function of one coordinate leaving the other fixed (both lying on the  $z$ -axis) it was shown that while  $j^2(0)$  displays a symmetric distribution for  $\Omega_{12} = 0^\circ$  and  $180^\circ$ , the correlated state displays an angular enhancement at  $\Omega_{12} = 0^\circ$ , radially peaked on the nuclear surface.

The fact that in the analysis of Broglia and Riedel (1967) only simultaneous transfer was considered, corroborated the connection between pairing collectivity, closeness of the two nucleons and thus the large cross sections. A further corroboration seems to emerge from the fact that TD (neglect of ground state correlations), let alone the pure two-hole configuration  $|p_{1/2}^{-2}(0)\rangle$  gives rise to cross sections which are smaller than that predicted by the full correlated state (Fig. 3.4.4). Now, as can be seen from the inset of this figure, most of the absolute cross section arises from successive transfer, a sobering result. Within this context, let us now comment on the reaction  $^1\text{H}(^{11}\text{Li}, ^9\text{Li(gs)})^3\text{H}$ . As seen from the  $|\Psi(\mathbf{r}_1, \mathbf{r}_2)|^2$  plots of the halo Cooper pair wavefunction displayed in Figs. 2.6.3 and 6.1.3, the correlation between the two pairing interacting neutrons is evident. Similarly the lack of correlation of the pure, angular momentum coupled configurations  $|s_{1/2}^2(0)\rangle$  and  $|p_{1/2}^2(0)\rangle$ . Now, the theoretical results reported in Fig. 6.1.3 calculated making use of the NFT results (6.1.1)–(6.1.3) and the optical potentials of Tanihata, I. et al. (2008) (those of An and Cai (2006) for the deuteron channel) reproduced the observations within the experimental findings. Again in this case, most of the absolute two-nucleon transfer differential cross section is connected with successive transfer (cf. Figs. 6.B.2 and 6.B.3). But not only this. While in the present case the absolute cross section associated with the pure  $|p_{1/2}^2(0)\rangle$  configuration is about an order of magnitude smaller than that associated with the full wavefunction (and thus also experiment), as observed in connection with  $^{206}\text{Pb}(t, p)^{208}\text{Pb(gs)}$ , that as-

sociated with the  $|s_{1/2}^2(0)\rangle$  pure configuration overpredicts the data by an order of magnitude. This is in spite of the fact that, as seen from the left, top corner of the two-dimensional plot of this configuration (Fig. 6.1.3), the two nucleons are as far as they can be from each other. This result is due to the fact that the  $p_{1/2}^2(0)$  is a cold configuration (small  $S = 0$  component) while  $s_{1/2}^2(0)$  is a hot one (large  $S = 0$  component) (cf.e.g. Broglia, R. A. et al. (1972) and refs. therein). Furthermore, the fact that the density associated with the two halo neutrons is much lower than that associated with the core nucleons, implies that in average, they are further away from each other than nucleons in a “normal” ( $R_0 = 1.2A^{1/3}$  fm-like) nucleus (cf. Sect. 3.2 Eqs. 3.2.21–3.2.27). This fact allows them to lower their relative momentum, without for that loosing their coherence, nor the associated conspicuous ability to tunnel as a single entity (absolute  $(p, t)$  cross section). In fact  $\sigma(^{11}\text{Li}(p, t)^9\text{Li(gs)}) \approx 5.7 \pm 0.9$  mb (cf. Fig. 6.B.2), to be compared to  $\sigma(^{206}\text{Pb}(t, p)^{208}\text{Pb(gs)}) \approx 0.68 \pm 0.24$  mb.

Summing up, the two halo neutrons of  $^{11}\text{Li}$  are likely to provide a paradigm of nuclear Cooper pairs: delicate (soap bubble like) extended objects with low relative momentum behaving in tunneling processes as an entity, in keeping with their unique emergent property: generalized gauge rigidity, equally present in collective pairing vibrational (dynamic) as pairing rotational situations (within this context cf. also Apps. 6.G, 6.H and 6.I).

One can conclude this Section by stating that its title could as well having been: “prejudices revisited”. Prejudices that the senior author of this monograph have helped to foster for a long time.

## Appendix 6.A Bootstrap particle–phonon mechanism to spontaneously break gauge invariance

In this Appendix we discuss a gedanken experiment, aimed at clarifying the bootstrap pairing mechanism resulting in the binding of the neutron halo of  $^{11}\text{Li}$ .

### 6.A.1 Gedanken eksperiment

Let us assume that one shines a low-energy neutron beam on a  $^9\text{Li}$  target. If these neutrons felt only the associated single-particle mean field, they will go by essentially as fast as they came in. However, part of the time pairs of these neutrons will bound themselves in presence of phonon (bosonic) excitations of quadrupole and of (pygmy) dipole character, produced also by the field the two neutron create themselves. The first of these collective modes is associated with vibrations of the (even)  $^8\text{He}$  core, the second resulting from the sloshing back and forth of the strongly non-local field of two (passing by) neutrons of the beam, together with the neutrons, and against the protons, of the core. Such possibility implies that, for a short time, of the order of the traversal time, the two (unbound) neutrons will move in a gas of virtual bosonic excitations, also made out of dipole pigmy reso-

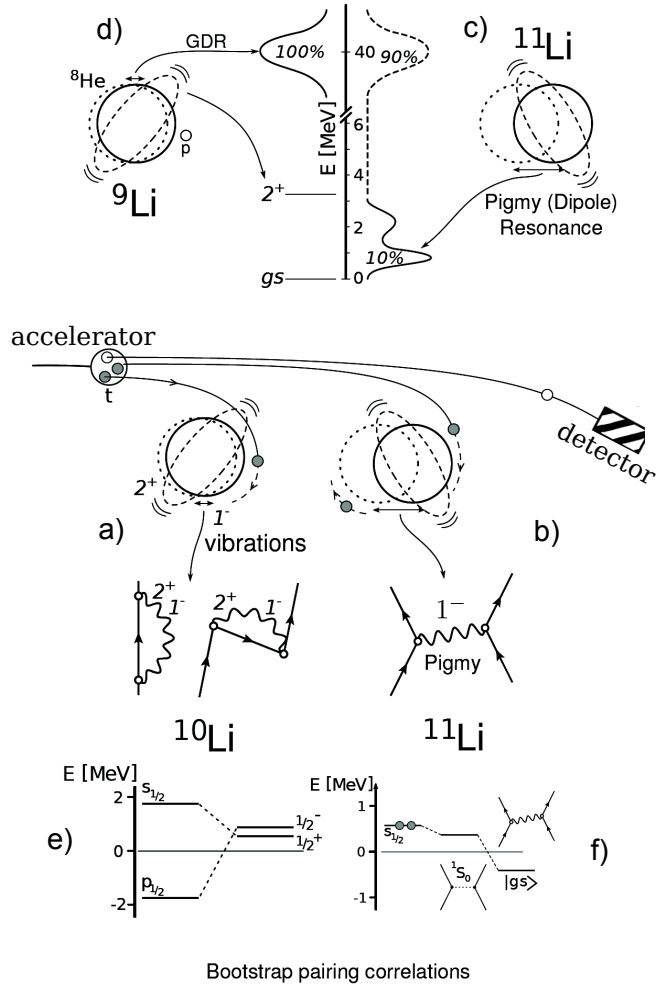


Figure 6.A.1: Schematic representation of the collective quadrupole and dipole response of lithium isotopes, and of a  $(t, p)$  reaction (in the text one reasons in terms of flux of low energy neutrons) in which two neutrons are transferred to  $^{9}\text{Li}$  (see also Fig. 6.1.3).

nances. Consequently, they can get dressed becoming heavier (lighter), as well as getting correlated by exchanging these bosonic collective vibrations. The first phenomenon is associated, as discussed above, with phononic backflow (Pauli principle upflow) leading to  $^{10}\text{Li}$ -like quasi-bound ( $s$ -wave) and resonant ( $p$ -wave) dressed single-particle states displaying parity inversion. The second phenomenon, mediated by phonon exchange between halo neutrons, contributes in a major way to the glue which binds the neutron halo Cooper pair to the  $^{9}\text{Li}$  core. Within the above scenario, one can posit that the  $^{11}\text{Li}$  dipole pigmy resonance can hardly be

viewed but in symbiosis with the  ${}^9\text{Li}$  halo neutron pair addition mode. The above described bootstrap phonon-exchange mechanism can be viewed as a novel microscopic embodiment of the Bardeen–Pines–Frölich-like processes to spontaneously break gauge invariance<sup>1</sup>.

To conclude, let us comment on Fig. 6.A.1. As said above, (a) the dressing of single-particle levels by collective vibrations and (b) the renormalization of the bare  $NN$ -interaction, in particular of the pairing interaction, through the exchange of these modes between nucleons moving in time reversal states lying close to the Fermi energy, play a central role in nuclear structure. In particular, in the case of the single Cooper pair system  ${}^{11}\text{Li}$ , most of the glue is provided by the exchange of the pigmy resonance, namely a low-lying isovector dipole vibration. The pigmy resonance (c) is a chunk of the GDR of the core  ${}^9\text{Li}$  (d) and arises from radial inhomogeneous damping. This mode is intimately related to the spontaneous symmetry breaking of space homogeneity associated with the fact that the center of mass of a finite system like the atomic nucleus, specifies a privileged position in space. While  ${}^9\text{Li}_6$  is bound,  ${}^9\text{Li}_7$  is not. (e) through renormalization processes, the  $p_{1/2}$  bound state is shifted to higher energies from that predicted by a standard mean field potential, while the  $s_{1/2}$  continuum state is lowered to an energy close, below that of the  $p_{1/2}$  state. (f) While the screened bare pairing interaction is subcritical, the exchange of vibrations between the halo neutrons is able to, weakly, bind the system.

## Appendix 6.B Table 1 PRL

The  $1/2^-$  (2.69 MeV) first excited state of  ${}^9\text{Li}$  can in principle, not only be populated through a two-particle transfer process, but also through a break up process in which one (see Fig. 6.B.1(f)), or both neutrons (see Fig. 6.B.1(g)) are forced into the continuum for then eventually one of them to fall into the  $1p_{3/2}$  orbital of  ${}^9\text{Li}$  and excite the quadrupole vibration of the core (Potel et al. (2010)), in keeping with the fact that the main RPA amplitude of this state is precisely  $X(1p_{3/2}^{-1}, 1p_{1/2})(\approx 1)$  (cf. ref Barranco, F. et al. (2001)). The remaining channel populating the first excited state of  ${}^9\text{Li}$  is associated with an inelastic process (see Fig. 6.B.1(h)): two-particle transfer to the ground state of  ${}^9\text{Li}$  and Final State (inelastic scattering) Interaction (FSI) between the outgoing triton and  ${}^9\text{Li}$  in its ground state, resulting in the inelastic excitation of the  $1/2^-$  state.

Making use of the wavefunctions of Barranco, F. et al. (2001) and of a software developed on purpose to take into account microscopically all the different processes mentioned above, that is 9 different reaction channels (cf. caption to Table 6.B.1) and continuum states up to 50 MeV of excitation energy, the corresponding transfer amplitudes and associated probabilities  $p_l$  were calculated.

---

<sup>1</sup>Bootstrapping or booting. The term is often attributed to Rudolf Erich Raspe's story The surprising Adventures of Baron Münchhausen, where the main character pulls himself out of a swamp by his hair. Early 19th century USA: "pull oneself over a fence by one's bootstraps"

In Table 6.B.1 are displayed the probabilities  $p_l = |S_l^{(c)}|^2$  associated with each of the processes discussed above, where the amplitude  $S_l^{(c)}$  is related to the total cross section associated with each of the channels  $c$  by the expression (Satchler, 1980; Landau and Lifshitz, 1981)

$$\sigma_c = \frac{\pi}{k^2} \sum_l (2l+1) |S_l^{(c)}|^2, \quad (6.B.1)$$

$k$  being the wave number of the relative motion between the reacting nuclei.

In keeping with the small values of  $p_l$ , in what follows we take into account the interference between the contributions associated with the different reaction paths making use of second order perturbation theory, instead of a coupled channel treatment (cf. e.g. Ascuitto and Glendenning (1969) Tamura, T. et al. (1970) Khoa and von Oertzen (2004) Keeley et al. (2007) Thompson (1988)). In particular in the case of the  $1/2^-$  (2.69 MeV) first excited state of  ${}^9\text{Li}$ ,

$$\frac{d\sigma}{d\Omega}(\theta) = \frac{\mu^2}{16\pi^3\hbar^4} \left| \sum_l (2l+1) P_l(\theta) \sum_{c=2}^5 T_l^{(c)} \right|^2, \quad (6.B.2)$$

where  $\mu$  is the reduced mass and  $T_l^{(c)}$  are the transition matrix elements (in the DWBA Satchler (1980)) associated with the different channels and for each partial wave.

Making use of all the elements discussed above, multistep transfer (see e.g. Bayman and Chen (1982), Igarashi et al. (1991), Bayman and Feng (1973) as well as Broglia and Winther (2004)), breakup and inelastic channels were calculated, and the results displayed in Figs. 6.B.2 and 6.B.3 and in Table 6.B.1. Theory provides an overall account of the experimental findings. In particular, in connection with the  $1/2^-$  state, this result essentially emerges from cancellations and coherence effects taking place between the three terms contributing to the multistep two-particle transfer cross section (see Fig. 6.B.3), tuned by the nuclear structure amplitudes associated with the process shown in Fig. 6.B.1 (e) as well as Eqs. (6.1.1)–(6.1.3). In fact, and as shown in Figs. 6.B.2 and 6.B.3, the contributions of break up processes and inelastic (Figs. 6.B.1(f),(g) and (h) respectively) to the population of the  $1/2^-$  (2.69 MeV) first excited state of  ${}^9\text{Li}$  are negligible as compared with the process depicted in Fig. 6.B.1(e). In the case of the breakup channel (Figs. 6.B.1(f) and 6.B.1(g)) this is a consequence of the low bombarding energy of the  ${}^{11}\text{Li}$  beam (inverse kinematics), combined with the small overlap between continuum (resonant) neutron  $p_{1/2}$  wavefunctions and bound state wavefunctions. In the case of the inelastic process (Fig. 6.B.1(h)), it is again a consequence of the relative low bombarding energy. In fact, the adiabaticity parameters  $\xi_C, \xi_N$  (see eqs. (IV.12) and (IV.14) of ref. Broglia and Winther (2004)) associated with Coulomb excitation and inelastic excitation in the  $t+{}^9\text{Li}$  channel are larger than 1, implying an adiabatic cutoff. In other words, the quadrupole mode is essentially only polarized during the reaction but not excited. The situation is quite different

$l \backslash c$	<b>1</b>	<b>2</b>	<b>3</b>	<b>4</b>	<b>5</b>
$l$	$4.35 \times 10^{-3}$	$1.79 \times 10^{-4}$	$4.81 \times 10^{-6}$	$2.90 \times 10^{-11}$	$3.79 \times 10^{-8}$
0	$3.50 \times 10^{-3}$	$9.31 \times 10^{-4}$	$1.47 \times 10^{-5}$	$1.87 \times 10^{-9}$	$1.09 \times 10^{-6}$
1	$7.50 \times 10^{-4}$	$8.00 \times 10^{-5}$	$2.45 \times 10^{-5}$	$1.25 \times 10^{-8}$	$1.21 \times 10^{-6}$
2	$6.12 \times 10^{-4}$	$9.81 \times 10^{-5}$	$1.51 \times 10^{-6}$	$6.50 \times 10^{-10}$	$2.20 \times 10^{-7}$
3	$1.10 \times 10^{-4}$	$1.18 \times 10^{-5}$	$2.21 \times 10^{-7}$	$4.80 \times 10^{-11}$	$1.46 \times 10^{-8}$
4	$3.65 \times 10^{-5}$	$2.16 \times 10^{-7}$	$7.42 \times 10^{-9}$	$6.69 \times 10^{-13}$	$9.63 \times 10^{-10}$
5	$1.35 \times 10^{-5}$	$6.05 \times 10^{-8}$	$2.88 \times 10^{-10}$	$8.04 \times 10^{-15}$	$1.08 \times 10^{-11}$
6	$4.93 \times 10^{-6}$	$7.78 \times 10^{-8}$	$6.01 \times 10^{-11}$	$4.05 \times 10^{-16}$	$5.26 \times 10^{-13}$
7	$2.43 \times 10^{-6}$	$2.62 \times 10^{-8}$	$7.4 \times 10^{-12}$	$1.26 \times 10^{-17}$	$9.70 \times 10^{-11}$

Table 6.B.1: Probabilities  $p_l$  associated with the processes described in the text for each partial wave  $l$ . The different channels are labeled by a channel number  $c$  equal to: **1**, multistep transfer to the  ${}^9\text{Li}$  ground state (Fig. 6.B.1(d)); **2**, multistep transfer (Fig. 6.B.1(e)) to the first excited  ${}^9\text{Li}$  state, **3**, breakup (Fig. 6.B.1(f)), **4**, breakup (Fig. 6.B.1(g)), and **5** inelastic processes (Fig. 6.B.1(h)) involved in the population of the  $1/2^-$  (2.69 MeV) first excited state of  ${}^9\text{Li}$ . Of notice that the probabilities displayed in columns **1** and **2** result from the (coherent) sum of three amplitudes namely those associated with successive, simultaneous and non-orthogonality transfer channels (see also Fig. 6.B.3) after Potel et al. (2010).

in the case of the intervening of the virtual processes displayed in Fig. 6.B.1 (b) and (c) leading to the population of the  $1/2^-$  state displayed in Fig. 6.B.1 (e). Being those off-the-energy shell processes, energy is not conserved, and adiabaticity gets profoundly modified.

## Appendix 6.C Modified formfactor associated with the reactions $^1H(^{11}Li, ^9Li(gs))^3H$ and $^1H(^{11}Li, ^9Li(1/2^-); 2.69 \text{ MeV})^3H$ state

## Appendix 6.D Software

In this Appendix we provide a brief description of the numerical methods implemented in the code written to evaluate the differential cross sections. The two-nucleon transfer differential cross section is given by Eq. (5.1.4), so the principal task consist in calculating the transfer amplitudes  $T^{(1)}(\theta)$ ,  $T_{succ}^{(2)}(\theta)$  and  $T_{NO}^{(2)}(\theta)$  described in Eqs. 5.1.5a–5.1.5c, by numerically evaluating the corresponding integrals. The dimensionality of the integrals can be reduced by expanding in partial waves (eigenfunctions of the angular momentum operator) the distorted waves and wavefunctions present in the corresponding integrands. The resulting expressions are Eqs. (5.2.36) and (5.2.37) for  $T^{(1)}(\theta)$ , Eqs. (5.2.128), (5.2.129) and (5.2.130) for  $T_{succ}^{(2)}(\theta)$ , and Eqs. (5.2.154), (5.2.155) and (5.2.156) for  $T_{NO}^{(2)}(\theta)$ . The integrals are computed numerically with the method of Gaussian quadratures.

The one-dimensional (radial) functions appearing in the integrands are defined in a spatial grid up to a given maximum radius  $r_{max}$ . The bound state wavefunctions are obtained by numerical integration of the radial Schrödinger equation for a Woods–Saxon potential with a spin–orbit term. The parameters defining the shape of the potential are given as an input, while the depth is adjusted to reproduce the binding energy of the state under consideration. The resulting potential corresponding to the final (initial) nucleon bound state stands also for the interaction potential featured in the integrand in the prior (post) representation. The distorted waves are obtained by integrating the radial Schrödinger equation with positive energy from  $r = 0$  to  $r_{max}$ , and matching the solution with the corresponding Coulomb wave function at a given  $r = r_{match}$ , big enough to lie outside of the range of the nuclear interaction. The Woods–Saxon optical potentials used to obtain the distorted waves consist on a real Coulomb term, a real and imaginary volume terms, an imaginary surface term, and a real and imaginary spin orbit terms. The parameters needed to specify all those terms are given as an input.

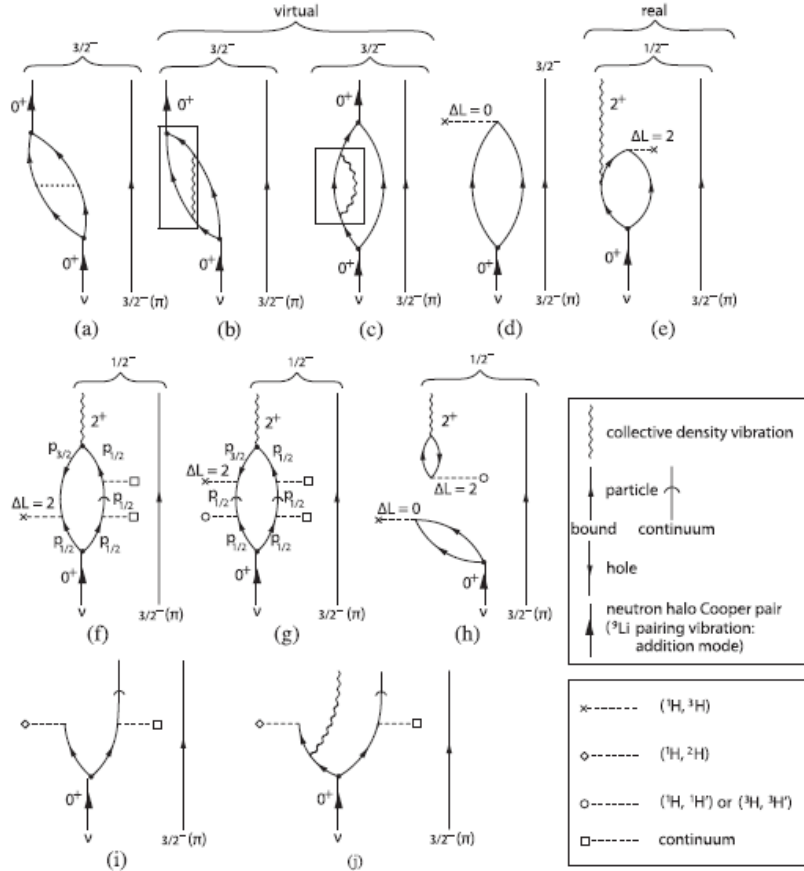


Figure 6.B.1: Representative Nuclear Field Theory–Feynman diagrams associated with correlation process ((a),(b),(c)) and with one– and two–particle pick–up reactions ((i),(j) and (d),(e) respectively) of the halo neutrons of  $^{11}\text{Li}$  (Cooper pair, indicated in terms of a double arrowed line). Also shown are the possible diagrams associated with other channels (breakup and inelastic) populating the  $1/2^-$  (2.69 MeV) state: f) one of the halo neutrons is picked up (the other one going into the continuum, i.e. breaking up from the  $^9\text{Li}$  core) together with a neutron from the  $p_{3/2}$  orbital of the  $^9\text{Li}$  core leading eventually to the excitation of the  $1/2^-$  final state ( $2^+$  density mode (wavy line) coupled to the  $p_{3/2}(\pi)$ ), g) the proton field acting once breaks the Cooper pair forcing one of the halo neutrons to populate a  $p_{1/2}$  continuum state (the other one follows suit), while acting for the second time picks up one of the neutrons moving in the continuum and another one from those moving in the  $p_{3/2}$  orbital of  $^9\text{Li}$  eventually leaving the core in the quadrupole mode of excitation. In (h) the two-step transfer to the  $^9\text{Li}$  ground state plus the inelastic final channel process exciting the  $(2^+ \otimes p_{3/2}(\pi))_{1/2^-}$  state is shown. After Potel et al. (2010).

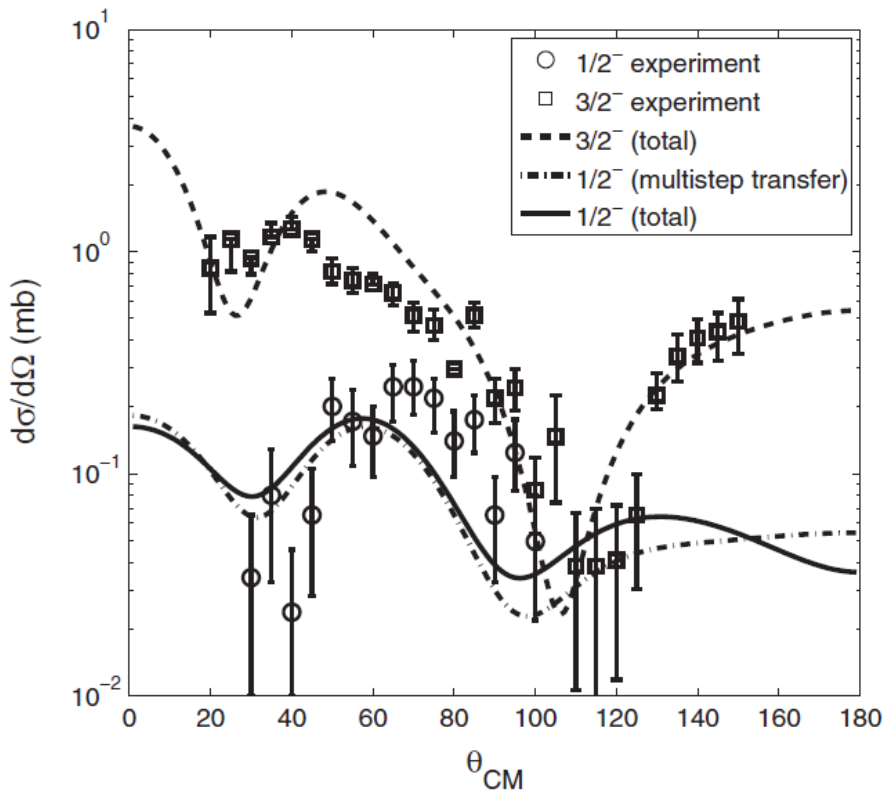


Figure 6.B.2: Experimental (Tanihata, I. et al. (2008)) and theoretical differential cross sections (including multistep transfer as well as breakup and inelastic channels, Potel et al. (2010)). of the  ${}^1\text{H}({}^{11}\text{Li}, {}^9\text{Li}){}^3\text{H}$  reaction populating the ground state ( $3/2^-$ ) and the first excited state ( $1/2^-$ ; 2.69 MeV) of  ${}^9\text{Li}$ . Also shown (dash-dotted curve) is the differential cross section associated with this state but taking into account only multistep transfer. The optical potentials used are from (Tanihata, I. et al., 2008; An and Cai, 2006). The absolute cross sections associated with the ground state ( $3/2^-$ ) is predicted to be 6.1 mb ( $6.7 \pm 0.9$  mb) while that corresponding to the first excited state ( $1/2^-$ ; 2.69 MeV) being 0.7 mb ( $1.0 \pm 0.36$  mb).

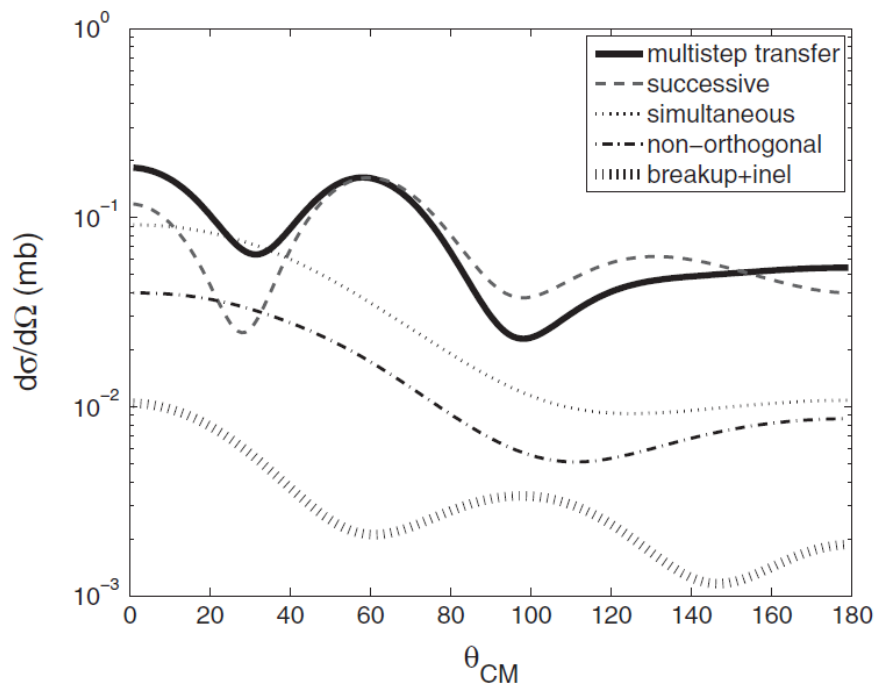


Figure 6.B.3: Successive, simultaneous and non-orthogonality contributions (prior representation) to the  ${}^1\text{H}({}^{11}\text{Li}, {}^9\text{Li}){}^3\text{H}$  differential cross section associated with the population of the  $1/2^-$  state of  ${}^9\text{Li}$ , displayed in Fig. 6.B.2. Also shown is the (coherent) sum of the breakup ( $c = 3$  and 4) and inelastic ( $c = 5$ ) channel contributions.

## Appendix 6.E Articulo Belyaev Pairing vibrational band based on $N = 6$ .

## Appendix 6.F Simple estimates revisited.

## Appendix 6.G Statistics.

Let us consider two identical particles moving in a one-dimensional harmonic oscillator. Let us assume that one is in the ground state and the other is in the first excited state. According to the superposition principle

$$\Phi(x_1, x_2) = \lambda\phi_1(x_1)\phi_0(x_2) + \mu\phi_0(x_1)\phi_1(x_2). \quad (6.G.1)$$

Let us calculate the correlation of these particles, that is, the quantity

$$C = \frac{\langle x_1 x_2 \rangle - \langle x_1 \rangle \langle x_2 \rangle}{\sqrt{(\langle x_1^2 \rangle - \langle x_1 \rangle^2)(\langle x_2^2 \rangle - \langle x_2 \rangle^2)}} \quad (6.G.2)$$

Let us start with

$$\begin{aligned} \langle x_1 x_2 \rangle &= \int dx_1 dx_2 (\lambda^* \phi_1^*(x_1) \phi_0^*(x_2) + \mu^* \phi_0^*(x_1) \phi_1^*(x_2)) \\ &\quad \times (x_1 x_2) (\lambda \phi_1(x_1) \phi_0(x_2) + \mu \phi_0(x_1) \phi_1(x_2)) \\ &= |\lambda|^2 \langle \phi_1 | x_1 | \phi_1 \rangle \langle \phi_0 | x_2 | \phi_0 \rangle + \lambda^* \mu \langle \phi_1 | x_1 | \phi_0 \rangle \langle \phi_0 | x_2 | \phi_1 \rangle \\ &\quad + \lambda \mu^* \langle \phi_0 | x_1 | \phi_1 \rangle \langle \phi_1 | x_2 | \phi_0 \rangle + |\mu|^2 \langle \phi_0 | x_1 | \phi_0 \rangle \langle \phi_1 | x_1 | \phi_1 \rangle \langle \phi_0 | x_1 | \phi_0 \rangle \langle \phi_1 | x_1 | \phi_1 \rangle \end{aligned} \quad (6.G.3)$$

In keeping with the fact that

$$\langle \phi_1 | x | \phi_1 \rangle = \langle \phi_0 | x | \phi_0 \rangle = 0, \quad (6.G.4)$$

and

$$\langle \phi_0 | x | \phi_1 \rangle = \langle \phi_1 | x | \phi_0 \rangle = \sqrt{\frac{\hbar\omega}{2C}}, \quad (6.G.5)$$

one obtains

$$\langle x_1 x_2 \rangle = \left( \frac{\hbar\omega}{2C} \right) \Re(\lambda^* \mu). \quad (6.G.6)$$

And

$$\sqrt{-} = \left( \frac{\hbar\omega}{2C} \right), \quad (6.G.7)$$

for the denominator of Eq. (6.G.2). From the above results the correlation function between particle 1 and 2 is

$$C = \frac{2C}{\hbar\omega} \langle x_1 x_2 \rangle = 2\Re(\lambda^* \mu) = \begin{cases} 1 & (\lambda = +\mu = \frac{1}{\sqrt{2}}) \\ -1 & (\lambda = -\mu = \frac{1}{\sqrt{2}}) \end{cases} \quad (6.G.8)$$

It is of notice that, in quantum mechanics, average values imply the mean outcome of a large number of experiments. In this case, of the (simultaneous) measure of the position of the two particles (cf. Basdevant and Dalibard (2005)).

## Appendix 6.H Correlation length and quantality parameter.

The correlation length can be defined as

$$\xi = \frac{\hbar v_F}{2\Delta} \approx \frac{\hbar^2}{m} \frac{k_F}{2\Delta} \quad (6.H.1)$$

where the Fermi momentum in the case of stable nuclei lying along the stability valley is

$$k_F \approx 1.36 \text{ fm}^{-1}. \quad (6.H.2)$$

Thus,

$$\xi = 20 \text{ MeV fm}^2 \times \frac{1.36}{\Delta} \text{ fm}^{-1} \approx \frac{27}{\Delta} \text{ fm}, \quad (6.H.3)$$

and,

$$\xi \approx 27 \text{ fm}, \quad (\Delta \approx 1 \text{ MeV}). \quad (6.H.4)$$

Let us now define,

$$k_F \approx \frac{a}{\xi} = 1.36 \text{ fm}^{-1} \quad (6.H.5)$$

obtaining,

$$a \approx 37; \quad k_F \approx \frac{37}{\xi}. \quad (6.H.6)$$

One can then write,

$$1 = \left( \frac{\hbar^2}{m\xi^2} \right) \left( \frac{1}{2\Delta} \right) 37 = q \times 37, \quad (6.H.7)$$

where the quantality parameter is, in the present case,

$$q \approx 0.03. \quad (6.H.8)$$

That is, the two partner nucleons are, in the Cooper pair, rigidly anchored.

We now consider  $^{11}\text{Li}$ , and calculate  $k_F$  (neutrons) with the help of the Thomas–Fermi model,

$$k_F = \left( 3\pi^2 \frac{8}{\frac{4\pi}{3}(4.58)^3} \right)^{1/3} \text{fm}^{-1} \approx \frac{(18\pi)^{1/3}}{4.58} \text{fm}^{-1} \approx 0.84 \text{ fm}^{-1}. \quad (6.\text{H}.9)$$

The correlation length is,

$$\xi \approx \frac{\hbar^2}{m} \frac{k_F}{2E_{corr}} \approx 20 \text{ MeV fm}^{-1} \approx 42 \text{ fm}, \quad (6.\text{H}.10)$$

and

$$k_F = \frac{a}{\xi} \approx \frac{a}{42 \text{ fm}} = 0.84 \text{ fm}^{-1}; \quad a \approx 35; \quad k_F = \frac{35}{\xi}, \quad (6.\text{H}.11)$$

leading to

$$1 = \left( \frac{\hbar^2}{m\xi^2} \right) \left( \frac{1}{2E_{corr}} \right) 35 = q \times 35, \quad (6.\text{H}.12)$$

and of the resulting quantity parameter,

$$q \approx 0.03. \quad (6.\text{H}.13)$$

It is of notice that this result is but an alternative embodiment of the relation (3.3.8). Now, one could argue that both (3.3.8) and (6.H.13) (as well as (6.H.8) for stable nuclei), are just a manifestation of (6.G.8). That there is more to it is forcefully expressed by the fact that, selecting  $|s_{1/2}^2(0)\rangle$  ( $|p_{1/2}^2(0)\rangle$ ) as the Cooper pair of  $^{11}\text{Li}$  leads to absolute two-particle transfer cross sections which are about one order of magnitude larger (smaller) than the observed cross section (see Fig. 6.1.3). The fact that the NFT result (6.1.1)–(6.1.3) with its unusual pigmy binding and parity inversion clothing mechanism reproduces observations within experimental errors, underscores the central role played by structure on Cooper pair tunneling, through the emergent property of generalized pairing rigidity.

Summing up pairing, both bare  $NN$ – and long range induced interaction changes the statistics of the elementary modes from fermionic to bosonic and, at the same time, the value of the quantality parameter from  $q \approx 1$  to  $q \ll 1$  (delocalized  $\rightarrow$  rigidly anchored to the Cooper pair) thus leading to a generalized gauge rigidity, the detailed renormalizing and dressing mechanisms ultimately deciding on the soundness and applicability of the description under discussion. The fact that in working out the reaction mechanism one uses, for practical reasons, a single-particle basis (second order DWBA corrected by non-orthogonality), reconstructing the interweaving of these particles with the collective modes in term of sums over virtual states, does not alter the physics embodied in the NFT solutions. Rather, it provides its confirmation (Fig. 6.1.3).

## Appendix 6.I $k$ -mass in $^{11}\text{Li}$ and Pauli principle.

### Bibliography

- H. An and C. Cai. Global deuteron optical model potential for the energy range up to 183 MeV. *Phys. Rev. C*, 73:054605, 2006.
- P. W. Anderson. Random-phase approximation in the theory of superconductivity. *Phys. Rev. Lett.*, 112:1900, 1958.
- R. J. Asciutto and N. K. Glendenning. Inelastic processes in particle transfer reactions. *Physical Review*, 181:1396, 1969.
- F. Barranco, R. A. Broglia, G. Gori, E. Vigezzi, P. F. Bortignon, and J. Terasaki. Surface vibrations and the pairing interaction in nuclei. *Phys. Rev. Lett.*, 83: 2147, 1999.
- Barranco, F., P. F. Bortignon, R. A. Broglia, G. Colò, and E. Vigezzi. The halo of the exotic nucleus  $^{11}\text{Li}$ : a single Cooper pair. *Europ. Phys. J. A*, 11:385, 2001.
- J. L. Basdevant and J. Dalibard. *Quantum Mechanics*. Springer, Berlin, 2005.
- G. Bassani, N. M. Hintz, C. D. Kavaloski, J. R. Maxwell, and G. M. Reynolds. ( $p, t$ ) Ground-State  $L = 0$  Transitions in the Even Isotopes of Sn and Cd at 40 MeV,  $N = 62$  to 64. *Phys. Rev.*, 139:B830, 1965.
- B. F. Bayman and J. Chen. One-step and two-step contributions to two-nucleon transfer reactions. *Phys. Rev. C*, 26:1509, 1982.
- B. F. Bayman and B. H. Feng. Monte Carlo calculations of two-neutron transfer cross sections. *Nuclear Physics A*, 205:513, 1973.
- Bennaceur, K., J. Dobaczewski, and M. Ploszajczak. Pairing anti-halo effect. *Physics Letters B*, 496:154, 2000.
- Bertsch, G. F. and R. A. Broglia. Giant resonances in hot nuclei. *Physics Today*, 39 (8):44, 1986.
- Bertsch, G. F., R. A. Broglia, and C. Riedel. Qualitative description of nuclear collectivity. *Nucl. Phys. A*, 91:123, 1967.
- Bès,D. R. and R. A. Broglia. Pairing vibrations. *Nucl. Phys.*, 80:289, 1966.
- Bjerregaard, J. H., O. Hansen, Nathan, and S. Hinds. States of  $^{208}\text{Pb}$  from double triton stripping. *Nucl. Phys.*, 89:337, 1966.
- N. Bogoljubov. On a new method in the theory of superconductivity. *Il Nuovo Cimento*, 7:794, 1958.

- A. Bohr. In *Comptes Rendus du Congrès International de Physique Nucléaire*, volume 1, page 487. Centre National de la Recherche Scientifique, 1964.
- Bohr, A. and B. R. Mottelson. *Nuclear Structure, Vol.II*. Benjamin, New York, 1975.
- Bortignon, P.F., A. Bracco, and R. Broglia. *Giant Resonances*. Harwood Academic Publishers, Amsterdam, 1998.
- D. M. Brink. *PhD Thesis*. Oxford University, 1955.
- Brink, D. and R. A. Broglia. *Nuclear Superfluidity*. Cambridge University Press, Cambridge, 2005.
- R. Broglia and A. Winther. *Heavy Ion Reactions*. Westview Press, Boulder, CO., 2004.
- R. A. Broglia and C. Riedel. Pairing vibration and particle-hole states excited in the reaction  $^{206}\text{Pb}(t, p)^{208}\text{Pb}$ . *Nucl. Phys.*, 92:145, 1967.
- Broglia, R. A., C. Riedel, and T. Udagawa. Sum rules and two-particle units in the analysis of two-neutron transfer reactions. *Nuclear Physics A*, 184:23, 1972.
- G. Gori, F. Barranco, E. Vigezzi, and R. A. Broglia. Parity inversion and breakdown of shell closure in Be isotopes. *Phys. Rev. C*, 69:041302, 2004.
- Guazzoni, P., M. Jaskola, L. Zetta, A. Covello, A. Gargano, Y. Eisermann, G. Graw, R. Hertenberger, A. Metz, F. Nuoffer, and G. Staudt. Level structure of  $^{120}\text{Sn}$ : High resolution ( $p, t$ ) reaction and shell model description. *Phys. Rev. C*, 60: 054603, 1999.
- Guazzoni, P., L. Zetta, A. Covello, A. Gargano, G. Graw, R. Hertenberger, H.-F. Wirth, and M. Jaskola. High-resolution study of the  $^{116}\text{Sn}(p, t)$  reaction and shell model structure of  $^{114}\text{Sn}$ . *Phys. Rev. C*, 69:024619, 2004.
- Guazzoni, P., L. Zetta, A. Covello, A. Gargano, B. F. Bayman, G. Graw, R. Hertenberger, H.-F. Wirth, and M. Jaskola. Spectroscopy of  $^{110}\text{Sn}$  via the high-resolution  $^{112}\text{Sn}(p, t)^{110}\text{Sn}$  reaction. *Phys. Rev. C*, 74:054605, 2006.
- Guazzoni, P., L. Zetta, A. Covello, A. Gargano, B. F. Bayman, T. Faestermann, G. Graw, R. Hertenberger, H.-F. Wirth, and M. Jaskola.  $^{118}\text{Sn}$  levels studied by the  $^{120}\text{Sn}(p, t)$  reaction: High-resolution measurements, shell model, and distorted-wave Born approximation calculations. *Phys. Rev. C*, 78:064608, 2008.
- Guazzoni, P., L. Zetta, A. Covello, A. Gargano, B. F. Bayman, T. Faestermann, G. Graw, R. Hertenberger, H.-F. Wirth, and M. Jaskola. High-resolution measurement of the  $^{118,124}\text{Sn}(p, t)^{116,122}$  reactions: Shell-model and microscopic

- distorted-wave Born approximation calculations. *Phys. Rev. C*, 83:044614, 2011.
- Guazzoni, P., L. Zetta, A. Covello, A. Gargano, B. F. Bayman, G. Graw, R. Hertenberger, H. F. Wirth, T. Faestermann, and M. Jaskola. High resolution spectroscopy of  $^{112}\text{Sn}$  through the  $^{114}\text{Sn}(p,t)^{112}\text{Sn}$  reaction. *Phys. Rev. C*, 85:054609, 2012.
- I. Hamamoto and B. R. Mottelson. Pair correlation in neutron drip line nuclei. *Phys. Rev. C*, 68:034312, 2003.
- Hamamoto, I. and B. R. Mottelson. Weakly bound  $s_{1/2}$  neutrons in the many-body pair correlation of neutron drip line nuclei. *Phys. Rev. C*, 69:064302, 2004.
- M. Igarashi, K. Kubo, and K. Yagi. Two–nucleon transfer mechanisms. *Phys. Rep.*, 199:1, 1991.
- N. Keeley, R. Raabe, N. Alamanos, and J.-L. Sida. Fusion and direct reactions of halo nuclei at energies around the Coulomb barrier. *Prog. Nucl. Part. Phys.*, 59: 579, 2007.
- D. T. Khoa and W. von Oertzen. Di-neutron elastic transfer in the  $^4\text{He}(^6\text{He}, ^6\text{He})^4\text{He}$  reaction. *Physics Letters B*, 595:193, 2004.
- L. Landau and L. Lifshitz. *Quantum Mechanics, 3rd ed.* Butterworth-Heinemann, 1981.
- G. Potel, F. Barranco, E. Vigezzi, and R. A. Broglia. Evidence for phonon mediated pairing interaction in the halo of the nucleus  $^{11}\text{Li}$ . *Phys. Rev. Lett.*, 105:172502, 2010.
- G. Potel, A. Idini, F. Barranco, E. Vigezzi, and R. A. Broglia. Nuclear Field Theory predictions for  $^{11}\text{Li}$  and  $^{12}\text{Be}$ : shedding light on the origin of pairing in nuclei. *Yad. Fiz.*, *in press*: arXiv:1210.5085 [nucl-th], 2014.
- Potel, G., A. Idini, F. Barranco, E. Vigezzi, and R. A. Broglia. Cooper pair transfer in nuclei. *Rep. Prog. Phys.*, 76:106301, 2013a.
- Potel, G., A. Idini, F. Barranco, E. Vigezzi, and R. A. Broglia. Quantitative study of coherent pairing modes with two–neutron transfer: Sn isotopes. *Phys. Rev. C*, 87:054321, 2013b.
- G. Satchler. *Introduction to Nuclear Reactions*. Mc Millan, New York, 1980.
- J. Schrieffer. *Superconductivity*. Benjamin, New York, 1964.
- Schrieffer, J. R. Macroscopic quantum phenomena from pairing in superconductors. *Physics Today*, 26 (7):23, 1973.

- Tamura, T., D. R. Bès, R. A. Broglia, and S. Landowne. Coupled-channel born-approximation calculation of two-nucleon transfer reactions in deformed nuclei. *Physical Review Letters*, 25:1507, 1970.
- Tanikawa, I., M. Alcorta, D. Bandyopadhyay, R. Bieri, L. Buchmann, B. Davids, N. Galinski, D. Howell, W. Mills, S. Mythili, R. Openshaw, E. Padilla-Rodal, G. Ruprecht, G. Sheffer, A. C. Shotter, M. Trinczek, P. Walden, H. Savajols, T. Roger, M. Caamano, W. Mittig, P. Roussel-Chomaz, R. Kanungo, A. Gallant, M. Notani, G. Savard, and I. J. Thompson. Measurement of the two-halo neutron transfer reaction  $^1\text{H}(^{11}\text{Li}, ^9\text{Li})^3\text{H}$  at 3A MeV. *Phys. Rev. Lett.*, 100:192502, 2008.
- I. J. Thompson. Coupled reaction channels calculations in nuclear physics. *Computer Physics Reports*, 7(4):167, 1988.
- J. Valatin. Comments on the theory of superconductivity. *Il Nuovo Cimento*, 7: 843, 1958.



# **Bibliography**